THE UNIVERSITY OF QUEENSLAND

AUSTRALIA

Evolution and migration of Cenozoic Australia: Precision $^{40}Ar/^{39}Ar$ geochronology, geochemistry and paleomagnetic data from east Australian Cenozoic magmas

Isabelle Mari Jones

Bachelor of Science (Honours 2A)

A thesis submitted for the degree of Doctor of Philosophy at

The University of Queensland in 2018

School of Earth and Environmental Sciences

Abstract

A belt of Cenozoic mafic volcanoes in eastern Australia spans >2000 km and encompasses >90 million years. The volcanic record of this belt links Cenozoic plate motion, tectonic reshuffling in the SW Pacific, and east Australian mantle geodynamics. These links are examined in this study based on new paleomagnetic data from >560 samples from six key time periods, new $^{40}Ar/^{39}Ar$ geochronology from 65 samples, and major element, trace element, and radiogenic isotope results from 62 samples of Cenozoic east Australian mafic rocks.

North-to-south age progression of some east Australian volcanic provinces is consistent with hotspot magmatism during the northward movement of Australia away from Antarctica. Other provinces are non-age-progressive, however, leading to a traditional two-fold division between east Australian "central volcanoes" (age-progressive) and "lava-fields" (non-age-progressive). However, animated reconstructions indicate that volcanism is protracted and concurrent in both central volcanoes and lava-fields. Furthermore, new geochemical results indicate that the compositions of the groups are virtually identical: major element, trace element, and radiogenic isotope data suggest generation of both groups below the garnet stability field, and modelling shows that all provinces were likely generated from various degrees of melting of a source similar to the Australian garnet-amphibole lherzolite. The combination of age-progressive and non-age-progressive mafic magmatism (which overlapped spatially, temporally, and in terms of geochemical composition) is consistent with a model wherein both multiple plumes and edge-drive convection along the stepped lithosphere of eastern Australia, accompanied by shear-driven upwelling, contributed to the formation of the Cenozoic volcanic belt.

Paleomagnetic and high-resolution $^{40}Ar/^{39}Ar$ data from the east Australian volcanoes were used to create a new Australian Cenozoic apparent polar wander path (APWP). The new APWP includes a longitudinal excursion at ~25 Ma that corresponds with tectonic collisions in the SW Pacific. Spreading rates between Australia and Antarctica indicate a substantial decrease in plate speed during the late Oligocene, which was larger in the east (10 km/My^2) than the west (2 km/My^2). The period of reduced plate velocity between 30 and 24 Ma, the discrepancy in half-spreading rates, an eastward offset in the Tasmantid seamounts, the high volume, eruption rates, and intense crustal assimilation at the Tweed province; as well as the divergence of the APWP, correspond to approximately 10º of plate rotation relative to the synthetic reference pole of the global moving hotspot reference frame.

Declaration by author

This thesis is composed of my original work, and contains no material previously published or written by another person except where due reference has been made in the text. I have clearly stated the contribution by others to jointly-authored works that I have included in my thesis.

I have clearly stated the contribution of others to my thesis as a whole, including statistical assistance, survey design, data analysis, significant technical procedures, professional editorial advice, and any other original research work used or reported in my thesis. The content of my thesis is the result of work I have carried out since the commencement of my research higher degree candidature and does not include a substantial part of work that has been submitted to qualify for the award of any other degree or diploma in any university or other tertiary institution. I have clearly stated which parts of my thesis, if any, have been submitted to qualify for another award.

I acknowledge that an electronic copy of my thesis must be lodged with the University Library and, subject to the policy and procedures of The University of Queensland, the thesis be made available for research and study in accordance with the Copyright Act 1968 unless a period of embargo has been approved by the Dean of the Graduate School.

I acknowledge that copyright of all material contained in my thesis resides with the copyright holder(s) of that material. Where appropriate I have obtained copyright permission from the copyright holder to reproduce material in this thesis.

Publications during candidature

Journal papers

1. Jones, I., and Verdel, C. (2015). Basalt distribution and volume estimates of Cenozoic volcanism in the Bowen Basin region of eastern Australia: Implications for a waning mantle plume. *Australian Journal of Earth Sciences*, *62*(2), 255-263.

2. Verdel and Jones (2016) Tertiary Volcanic Fields of Eastern Australia: Regional Characteristics and Implications for Coal Quality and Mining. ACARP Project C22023 report.

3. Jones, I., Verdel, C., Crossingham, T., and Vasconcelos, P. (2017). Animated reconstructions of the Late Cretaceous to Cenozoic northward migration of Australia, and implications for the generation of east Australian mafic magmatism. *Geosphere*, *13*(2), 460-481.

Conference attendance

1. Jones and Verdel (2015) An animated reconstruction of the Australian Plate over the last 100 million years. Specialist Group in Tectonics and Structural Geology (SGTSG) conference, Geoscience Australia.

2. Jones, Verdel and Wilding (2016) Geochemistry of mafic magmatism in the Bowen Basin, Australia: A re-evaluation of lava-fields and central volcanoes. Goldschmidt Abstracts, 2016.

Publications included in this thesis

Publication 1: Jones, I., and Verdel, C., (2015) Basalt distribution and volume estimates for Cenozoic volcanism in the Bowen Basin region of eastern Australia: Implications for a waning mantle plume. Australian Journal of Earth Sciences – Included as Chapter 2

Contributor	Statement of contribution
Author Isabelle Jones (Candidate)	Designed experiments (90%) Wrote the paper (100%) Edited the paper (70%)
Author Dr. Charles Verdel	Designed experiments (10%) Edited paper (30%)

Publication 2: Jones, I., Verdel, C., Crossingham, T., and Vasconcelos, P. (2017). Animated reconstructions of the Late Cretaceous to Cenozoic northward migration of Australia, and implications for the generation of east Australian mafic magmatism. Geosphere, GES01405-1. – Included as Chapter 4

Contributor	Statement of contribution
Author Isabelle Jones (Candidate)	Ran the experiments (95%) Processed and interpreted data (90%) Wrote the paper (100%) Edited the paper (70%)
Author Dr Charles Verdel	Edited the paper (20%)
Author Tracey Crossingham	Processed and interpreted data - assisted with processing of data in table 3.1 (10%) Edited the paper (5%)
Author Professor Paulo Vasconcelos	Ran experiments - assisted with programming of samples (5%) Edited the paper (5%)

Contributions by others to the thesis

This research was conducted under the supervision of Dr. Charles Verdel (Principal advisor) and Professor Paulo Vasconcelos (associate). Major research funding was provided by an Australian Coal Association Research Program (ACARP) grant (C22023) to Dr. Charles Verdel, Dr. Kurt Knesel and Professor Paulo Vasconcelos. Scientific research permits (Take, use, keep or interfere with cultural or natural resources for scientific purposes) granted by the Department of Environment and Heritage Protection, Queensland (licence: WITK15117214) and the Office of Environment and Heritage Protection, New South Wales (licence: SL101471).

Technical assistance and advice were provided by Ms. Sarah Slotznik (Paleomagnetism techniques), Dr. Ai Nguyen (ICP-MS procedures and analysis), Ms. Marietjie Mostert (ICP-OES and ICP-MS procedures and analysis), Dr. David Thiede ($^{40}Ar/^{39}Ar$ geochronology) and Dr. Gang Xia (sample preparation procedures).

Paleomagnetic analysis would not have been possible without the technical expertise of Ms. Sarah Slotznik, Mr. Isaac Hilburn and Professor Joseph Kirschvink. Technical expertise in $^{40}Ar/^{39}Ar$ geochronology was provided by Dr. David Thiede, Professor Paulo Vasconcelos and Ms. Tracey Crossingham. Dr. Teresa Ubide provided assistance with geochemical data interpretations.

The chapters of this thesis benefited from editing and suggestions by Dr. Charles Verdel, Professor Paulo Vasconcelos and Dr. Teresa Ubide. Chapters submitted for publication benefitted from suggestions by reviewers by the peer-review system.

Statement of parts of the thesis submitted to qualify for the award of another degree

The basalt isopach map (Chapter Two, page 20 paragraph 1) was included in BSc Honours, University of Queensland 2013, degree awarded 19 December 2013. The content has since been substantially changed since submission of the thesis, new data added, new model parameters used and the interpretation has changed.

Acknowledgements

I would like to dedicate this thesis to the people who supported me both emotionally, financially and occasionally physically during the course of this thesis. First, I would like to thank the RHD support staff of both the old School of Earth Sciences and the newly formed School of Earth and Environmental Sciences, for their assistance and support over the course of my PhD. Secondly, I would like to thank my field partners for their hard work and assistance in equipment operation and the long hours we all spent driving to collect them; Llyam White, Anannya Mazumder, Oliver Turner and Bradley Wilding. I would also like to thank Dr Gang Xia, Dr Wei Zhou and Dr Faye Liu for technical assistance with laboratory equipment. I would like to thank my family and friends for their continued support of me during my research. Lastly, I would like to thank my reviewers Dr. Terry Spell and Dr. Rhodri Davies for their comments and critique of the thesis.

I would like to acknowledge the Australian Federal Government for financial support in the form of the Research Training Program (RTP) scholarship, and the Australian Coal Research Program (ACARP) for funding part of the geochemical analysis (Project C22023).

Individually I would like to thank first Tracey Crossingham for endless discussion of results, reading over my terrible writing, our 24/7 field cohabitation, and all the pizza-and-rage parties we celebrated: where I would be without you. Secondly, I would like to thank Jacqueline Wong, for our discussions regarding project backgrounds and tectonic models, reading over some of my early drafts, and the overwhelming amount of caffeine we have consumed together. Thirdly, Dr Marietjie Mostert and Dr Ai Duc Nyugen for training me in the correct preparation procedure, machine operation, and data reduction for major and trace elements and radiogenic isotopic ratios. Fourth, I would also like to thank Dr. Joseph Kirschvink, Sarah Slotznik and Isaac Hilburn for both allowing me to use their paleomagnetics laboratory and all the subsequent assistance with data reduction and interpretation. Fifth, I would like to thank Paulo Vasconcelos for his assistance with data interpretation and project design for some of the chapters.

Finally, I would like to thank my primary supervisor Dr. Charles Verdel, without whom this thesis would not exist. I would like to thank him for reading over and editing my writing, supporting my research financially and emotionally, and just generally being there when I needed help.

Keywords

East Australia, Cenozoic magmatism, $^{40}Ar/^{39}Ar$ geochronology, radiogenic isotope geochemistry, paleomagnetism, plate reconstructions, trace element geochemistry, apparent polar wander paths

Australian and New Zealand Standard Research Classifications (ANZSRC)

ANZSRC code: 040303, Geochronology (30%)

ANZSRC code: 040304, Igneous and Metamorphic Petrology (40%)

ANZSRC code: 040406, Magnetism and Palaeomagnetism (30%)

Fields of Research (FoR) Classification

FoR code: 0402, Geochemistry (40%)

FoR code: 0403, Geology (30%)

FoR code: 0404, Geophysics (30%)

Contents

Abstract ii
Declaration by author iii
Publications during candidature iv
Publications included in this thesis iv
Contributions by others to the thesis vi
Statement of parts of the thesis submitted to qualify for the award of another degree vi
Acknowledgements vii
Keywords viii
Australian and New Zealand Standard Research Classifications (ANZSRC) viii
Fields of Research (FoR) Classification viii
Abbreviations xviii
Chapter 1: Introduction 1
1.1 Introduction 2
1.2 Aims of the thesis 2
1.3 Background 3
1.3.1 Geological background 3
1.3.2 Paleomagnetism and plate motion 4
1.3.3 Current APWP 7
1.3.4 The pitfalls of previous APWP reconstructions 7
1.3.5 The origin of lava-field provinces 9
1.4 Thesis Overview 11
Chapter 2: Basalt distribution and volume estimates of Cenozoic volcanism in eastern Australia: Implications for a waning mantle plume 14
2.1 Introduction 15
2.1.1 Geological context 15
2.1.2 Characteristics of east Australian Cenozoic magmatism 16
2.2 Methodology 19
2.2.1 Drill hole correlation and data interpolation 19
2.2.2 Isopach map and thickness estimates 20
2.3 Discussion 21
2.3.1 Spatial trends in volumes of the central volcanoes 21
2.3.2 Spatial trends in eruption rates 23
2.3.3 Comparison with geophysical data 25
2.4 Conclusions 27

Chapter 3: $^{40}Ar/^{39}Ar$ geochronology of Cenozoic mafic magmatism in Queensland and New South Wales 29

3.1 Introduction 30

3.2 $^{40}Ar/^{39}Ar$ Geochronology Methodology 30

3.3 Results 32

3.3.1 McBride province 32

3.3.2 Peak Range 32

3.3.3 Springsure 33

3.3.4 Bauhinia 34

3.3.5 Monto 35

3.3.6 Mitchell 35

3.3.7 Policeman's Knob 36

3.3.8 Tweed 36

3.3.9 Ebor 36

3.3.10 Warrumbungles 37

3.3.11 Barrington 38

3.3.12 Canobolas 39

3.4 Discussion 40

3.4.1 Timing of east Australian Cenozoic volcanism 40

Chapter 4: Animated reconstructions of the Late Cretaceous to Cenozoic northward migration of Australia, and implications for the generation of east Australian mafic magmatism 64

4.1 Introduction 65

4.2 Geological Background 67

4.2.1 Cenozoic Volcanism in Eastern Australia 67

4.2.2 Collisional tectonics in the SW Pacific during the Cenozoic 71

4.3 Methods 74

4.3.1 Geochronology Compilation 74

4.3.2 $^{40}Ar/^{39}Ar$ Geochronology 75

4.3.3 Animated Reconstruction 75

4.4 Results 76

4.4.1 $^{40}Ar/^{39}Ar$ Geochronology 76

4.4.2 Animated Reconstruction 77

4.5 Discussion 78

4.5.1 Comparison of Paleomagnetic APWPs to the Global Moving Hotspot Reference Frame 78

4.5.2 Age-Progressive and Rift-Related Late Cretaceous-Cenozoic Mafic Volcanism in Eastern Australia 80

4.5.3 Edge Driven Convection as a Mechanism for Volcanic Activity in Eastern Australia 83

4.5.4 Longitudinal Offset of the Tasmantid and Lord Howe Seamount Chains 84

4.5.5 A Period of Reduced Northward Motion of Australia During the Late Oligocene to Early Miocene 87

4.6 Conclusions 88

Chapter 5: Evidence of a common source component for east Australian Cenozoic magmatism 90

5.1 Introduction 91

5.2 Geological Background 92

5.2.1 Classification of central volcanoes 92

5.2.2 Classification of lava-fields 96

5.2.3 Uncertainties in the central volcano vs. lava-field classification 97

5.3 Materials and methods 98

5.3.1 Sample collection, cleaning, and preparation 98

5.3.2 Geochemical Analyses 98

5.3.3 Major element analysis 99

5.3.4 Trace element analysis 99

5.3.5 Radiogenic isotopes 100

5.4 Results 100

5.4.1 Geochemical analyses 100

5.4.2 Principal component analysis 109

5.5 Discussion 109

5.5.1 Geochemical variations in Central Queensland volcanic provinces 109

5.5.2 Principal component analysis 115

5.5.3 Similarities in the source and depth of melting 116

5.5.4 Tectonic-magmatic relationships 122

5.6 Conclusions 124

Chapter 6: An updated Australian Cenozoic apparent polar wander path 133

6.1 Introduction 134

6.2 East Australian volcanic provinces 136

6.3 Methodology 138
6.3.1 Paleomagnetic analysis 138
6.3.2 Paleopole calculation 139
6.4 Results 150
6.4.1 Undara 150
6.4.2 Peak Range, Moranbah, and the Gemini Mountains 150
6.4.3 Policeman's Knob 151
6.4.4 Springsure 152
6.4.5 Mitchell 153
6.4.6 Tweed 153
6.4.7 Ebor 154
6.4.8 Warrumbungles 155
6.4.9 Barrington 156
6.4.10 Canobolas 156
6.4.11 Combined paleopoles 157
6.5 Discussion 157
6.5.1 Magnetostratigraphy 157
6.5.2 An updated Australian Cenozoic apparent polar wander path 159
6.5.3 Plate velocities and the global moving hotspot reference frame 161
6.5.4 Implications for "paleomagnetic dating" 162
6.5.5 Improving the paleopoles 164
6.5.6 Cenozoic plate rotation 164
6.5.7 Comparison with the Indian APWP 165
6.6 Conclusions 167
Chapter 7: Conclusions 172
7.1 $^{40}Ar/^{39}Ar$ dating, geochemistry and plate reconstructions 173
7.2 Plate motion and volcanic province distribution 174
7.2.1 The updated APWP 174
7.2.2 Plate rotation, reduced velocity and patterns of volcanism 175
7.2.3 Tectonics and volcanism in the SW Pacific during the Cenozoic 176
7.3 Conclusions 176
7.4 Future Work 177
References 179

9 Appendix A: Sample locality 212
10 Appendix B: $^{40}Ar/^{39}$ Ar Numerical data 214
11 Appendix C: Accuracy and precision data from geochemical analysis 270
11.1 Major element precision calculations from repeat analysis 270
11.2 Major element accuracy calculations from repeat analysis 273
11.3 Trace element precision calculations from repeat analysis 275
11.4 Trace element accuracy calculations from repeat analysis 277
11.5 Isotope element precision calculations from repeat analysis 283
11.6 Isotope element accuracy calculations from repeat analysis 284
12 Appendix D – Paleomagnetic Zerdfeld results 286
12.1 Barrington 286
12.2 Ebor 301
12.3 Canobolas 321
12.4 Springsure 333
12.5 Peak Range 360
12.6 Tweed 378
12.7 Warrumbungles 390
12.8 Undara 405
12.9 Policeman's knob 422
12.10 Mitchell 425

List of Figures

Figure 1.1: Location and age ranges of the stepped lithosphere, seamount chains, central volcanoes and lava-fields of east Australia. Primary age ranges from Johnson et al. (1989) and Vasconcelos et al. (2008). Stepped lithosphere after Fishwick et al. (2008) and Rawlinson et al. (2017).....6

Figure 1.2: Cenozoic apparent polar wander paths of Australia after a) Wellman et al. (1969), b) Embleton and McElhinny (1982), c) Idnurm (1985) and d) Musgrave (1989). 9

Figure 2.1: Location of central volcanoes and lava-fields in eastern Australia. Age ranges after Wellman and McDougall (1974), Johnson et al. (1989) and Vasconcelos et al. (2008). 18

Figure 2.2: Basalt thickness variation across the Bowen Basin. Isopach map was generated using a kriging model to determine likely isograd distribution based on the distance between all points. 22

Figure 2.3: Latitudinal variation in basalt volume and eruption rate for the eastern Australian central volcanoes. a) Variation of volume (filled squares) and eruption rate (unfilled triangles) with latitude. Nandewar and Warrumbungles are represented by grey symbols. 24

Figure 2.4: Distribution of isopachs against (a) aerial magnetics and (b) Bouger gravity survey for the Bowen Basin, Queensland. 26

Figure 3.1: Location of samples selected for geochronological analysis. This includes samples used for geochemistry as well as paleomagnetism. 31

Figure 3.2: $^{40}Ar/^{39}Ar$ geochronology results for samples from the McBride province (Undara) 41

Figure 3.3: $^{40}Ar/^{39}Ar$ geochronology results for samples from the Peak Range province 42

Figure 3.4: $^{40}Ar/^{39}Ar$ geochronology results for samples from the Springsure province 45

Figure 3.5: $^{40}Ar/^{39}Ar$ geochronology results for samples from the Bauhinia province 50

Figure 3.6: $^{40}Ar/^{39}Ar$ geochronology results for samples from the Monto province 51

Figure 3.7: $^{40}Ar/^{39}Ar$ geochronology results for samples from the Mitchell province 51

Figure 3.8: $^{40}Ar/^{39}Ar$ geochronology results for samples from the Policeman's Knob (Hoy province) 51

Figure 3.9: $^{40}Ar/^{39}Ar$ geochronology results for samples from the Tweed province.....52

Figure 3.10: $^{40}Ar/^{39}Ar$ geochronology results for samples from the Ebor province.....53

Figure 3.11: $^{40}Ar/^{39}Ar$ geochronology results for samples from the Warrumbungles province55

Figure 3.12: $^{40}Ar/^{39}Ar$ geochronology results for samples from the Barrington province 57

Figure 3.13: $^{40}Ar/^{39}Ar$ geochronology results for samples from the Canobolas province.....59

Figure 4.1: Map of Eastern Australia showing onshore (central volcanoes and lava-fields) and offshore (Tasmantid and Lord Howe Rise seamount chains) volcanic provinces. 66

Figure 4.2: A simplified tectonic map of the SW Pacific. 68

Figure 4.3: Australian Cenozoic apparent polar wander paths after a) Idnurm (1985), using primarily sedimentary basins and laterites; and b) Embleton and McElhinny (1982), using igneous rocks and laterites. 69
Figure 4.4: Simplified reconstructions of collision between PNG and the composite terranes after a) Pigram and Davies (1987) showing late Oligiocene through Miocene collision and b) early Oligocene through early Miocene accretion of composite terranes after Davies et al. (1997). 70
Figure 4.5: Location of samples taken from the Peak Range, Springsure, Bauhinia and Monto provinces. 73
Figure 4.6: Representative thin sections in plane polarised light (PPL) and crossed polarised light (XPL) for a) Springsure (IJS08b), b) Bauhinia (CIB) and c) Monto (AA2). 78
Figure 4.7: Comparison of the longitudinal, linear and GMHRF models using apparent polar wander paths. 79
Figure 4.8: Reconstruction of an arbitrarily chosen point through time based on the GMHRF, linear and longitudinal models looking at a) the geographical location and b) age-latitude relationship. 85
Figure 4.9: Longitudinal migration of Australia using modified reconstruction path based on work by Embleton and McElhinny (1982; open squares) and the rotation model after Seton et al. (2012; closed diamonds).....86
Figure 4.10: Apparent latitude of Stradbroke over time. Modified after Knesel et al. (2008).88
Figure 5.1: Map of Eastern Australia, showing the location and age of volcanic provinces and step in lithospheric thickness (*Fishwick et al.* 2008; *Rawlinson et al.* 2017).....93
Figure 5.2: Age vs. latitude relationship for volcanic provinces in east Australia. 94
Figure 5.3: Location of samples selected for geochemical study. 95
Figure 5.4: Photomicrographs (left- plan poles; right-crossed poles) of representative examples from volcanic provinces: 101
Figure 5.5: Major element compositions of volcanic rocks from the east Australian Cenozoic volcanic zone by a) Total Alkali vs. Silica diagram (Le Bas et al., 1986); and b) Major and trace element harker diagrams for both central volcanoes and lava-fields.....103
Figure 5.6: Chondrite-normalised REE diagrams in order of decreasing age. 105
Figure 5.7: Primitive mantle-normalised multi-element diagrams in order of decreasing age.106
Figure 6.1: Previous reconstructed APWPs using a) basaltic paleomagnetic data (Wellman et al. 1969); b) a sliding window, best fit estimate after basaltic and lateritic paleomagnetic data (Embleton and McElhinny 1982); c) lateritic and sedimentary paleomagnetic data (Idnurm 1985); and d) a least-squares regression best fit model of lateritic and sedimentary paleomagnetic data using basaltic paleopoles as anchor points (Musgrave, 1989). 135

Figure 6.2: Location of Cenozoic age basaltic provinces in eastern Australia with selected provinces for paleomagnetic study. 137
Figure 6.3: Site-mean directions and rockmagnetic results of Undara volcano, north Queensland. 140
Figure 6.4: Site-mean directions and rockmagnetic results of Peak Range, central Queensland 141
Figure 6.5: Site-mean directions and rockmagnetic results of Policeman's Knob, central Queensland 142
Figure 6.6: Site-mean directions and rockmagnetic results of Springsure, central Queensland143
Figure 6.7: Site-mean directions and rockmagnetic results of Mitchell, central Queensland.144
Figure 6.8: Site-mean directions and rockmagnetic results of Tweed, south-east Queensland.145
Figure 6.9: Site-mean directions and rockmagnetic results of Ebor, New South Wales 146
Figure 6.10: Site-mean directions and rockmagnetic results of Warrumbungles, New South Wales. 147
Figure 6.11: Site-mean directions and rockmagnetic results of Barrington, New South Wales.148
Figure 6.12: Site-mean directions and rockmagnetic results of Canobolas, New South Wales.149
Figure 6.13: Dispersion estimates for poles calculated from east Australian Cenozoic magmas. 160
Figure 6.14: A) A new APWP for the Australian plate in the Cenozoic, using paleomagnetic data collected from a series over volcanic provinces. B) Comparison of the new APWP with Embleton 1981 (dashed line), Embleton and McElhinny (1982; Black) and the GMHRF (Doubrovine 2012). C) The relative latitude of a fixed point (-27˚N, 152˚E) when moved in the GMHRF (purple line) and new APWP (red line) reference frames. The GMHRF is taken every 10 Ma, while the new APWP is taken every 5 Ma. 163
Figure 6.15: Improved paleopoles after the addition of data from Wellman et al. (1969) and Wellman (1975). 164
Figure 6.16: a) Half spreading rate on the Australian plate after Cande and Stock, (2004) and Cohen, (2007); b) relative rate of velocity change over the Cenozoic. 166
Figure 6.17: Comparison between the improved APWP (purple) and the Indian APWP (red; Besse and Courtillot, 2002). The Indian plate has been rotated to the Australian plate through the African plate circuit (Doubrovine et al. 2012). 167

List of Tables

Table 2.1: Ordinary kriging model parameters and outputs used in constructing the isopach map. 28

Table 2.2: Volume estimates for central volcanoes in the western Bowen Basin. Volcanoes are ordered north to south. 28

Table 3.1: $^{40}Ar/^{39}Ar$ geochronology results of mafic and felsic samples from east Australian Cenozoic magmatic provinces 60

Table 5.1: Major element analysis of mafic samples from Cenozoic volcanic provinces in eastern Australia. 126

Table 5.2: Trace element analysis of mafic samples from Cenozoic volcanic provinces in eastern Australia. 128

Table 5.3: Radiogenic isotopic ratios of mafic samples from Cenozoic volcanic provinces in eastern Australia. 132

Table 6.1: Site-mean flow directions for paleomagnetic samples collected from east Australian Cenozoic volcanoes.....168

Table 6.2: Calculated paleopoles collected from east Australian Cenozoic volcanoes. 171

Table 6.3: Improved paleopoles for Australia by combining the data from this study with data from Wellman and McElhinny (1969) and Wellman (1975). 171

Abbreviations

AF – Alternating field demagnetisation

AFC – Assimilation fractional crystallisation

APWP – Apparent polar wander path

ARM – Anhysteretic remanent magnetism

ChRM – Characteristic remanent magnetism

CRM – Chemical remanent magnetism

DRM – Detrital remanent magnetism

EDC – Edge driven convection

EMI – Enriched mantle 1

EMII – Enriched mantle 2

FOZO – Focal Zone

GAP – Gradient of acquisition plot

GMHRF – Global moving hotspot reference frame

HIMU – High μ

HREE – Heavy Rare Earth Element

ICP-OES – Inductively Coupled Plasma Optical Emission Spectrometer

ICP-MS – Inductively Coupled Plasma Mass Spectrometer

IRM – Isothermal remanent magnetism

LREE – Light Rare Earth Element

MAD – Mean Angle of Deviation

MD – Multi-domain grains

MDF – Mean destructive field

MORB – Mid-ocean ridge basalt

MPTS – Magnetic Polarity time scale

MSWD – Means squared weighted deviation

NHRL – Northern Hemisphere reference line

NRM – Natural remanent magnetism

NVP – Newer Volcanic Province

OIB – Ocean Island Basalt

OJP – Ontong Java Plateau

OVP – Older Volcanic Province

PCA – Principal component analysis

PHEM – Primitive helium enriched mantle

PM – Primitive mantle

PNG – Papuan New Guinea

PSD – Pseudo-single domain grains

RSD – Relative standard deviation

SCLM – Subcontinental lithospheric mantle

SD – Single domain grains

Chapter 1: Introduction

1.1 Introduction

Eastern Australia is currently a passive margin, and, as such, it is commonly considered a region of little tectonic activity. One of the most prominent topographic features of the region is a >2000 km-long belt of dominantly mafic volcanoes that stretches from northern Queensland to Tasmania (*Johnson,* 1989). These volcanoes, which began to form in the Late Cretaceous during the opening of the Tasman and Coral Seas (*O'Reilly and Zhang,* 1995; *Gaina et al.,* 2006), and which continued to erupt until the Holocene, are a record of Cenozoic tectonic activity in eastern Australia, and they reflect a complex interplay between mantle dynamics and plate motion. Because of their extended life-spans, exposure above the surrounding landscape, and the general absence of structural deformation, the volcanic provinces are ideal targets for geochemical and paleomagnetic analyses. Cenozoic volcanism has been reasonably well-studied in much of Australia, but many questions remain about the distribution, geochemistry, and origin of the east Australian Cenozoic volcanoes. In recent years, $^{40}Ar/^{39}Ar$ geochronological studies of lava flows from apparently age-progressive volcanoes in eastern Australia have been used to reconstruct the velocity of the Australian plate over the time interval from 34 to 10 Ma (*Knesel et al.,* 2008; *Cohen et al.,* 2013). However, no recent detailed study of plate motion has been attempted based on paleomagnetic data from the volcanoes. This thesis therefore examines links between mantle processes and plate motion through the use of geochemistry, $^{40}Ar/^{39}Ar$ geochronology, and paleomagnetism.

1.2 Aims of the thesis

This thesis aims to examine the evolution of the Australian plate throughout Cenozoic, with regards to magmatism and motion. The thesis comprises of three main parts: 1) physical change and landscaping features of the Cenozoic; 2) development of temporally unconstrained lava provinces in East Australia; and 3) motion of the Australian plate. The physical change and land scaping features are summarised in chapter 2. This includes the change in volume and average basalt output over time. Chapter 3 comprises a revised definition of some lava-field and central volcanic provinces, as well as a possible source for the mid-Miocene Bowen Basin lava-field provinces.

The first aim of this thesis is to examine spatial and temporal changes in the volumes of basalt erupted from the eastern Australian volcanoes. Specifically, the volumes of basalt in the Bowen Basin region of eastern Australia are re-evaluated based on a compilation of topographic and subsurface data. Results from this part of the project shed light on the Cretaceous and early Cenozoic topographic relief of eastern Australia, and the newly-calculated volumes are combined with previous

geochronological results to determine the eruption rates of individual volcanoes, as well as long-term and along-strike changes in eruption rate.

The second aim of the thesis is to use geochemical data to examine the sources of volcanism in eastern Australia. Volcanic provinces in the Bowen Basin region, in particular, have been largely unstudied. A key hypothesis related to this part of the project is that Bowen Basin lava-fields were formed as a result of melting in the upper mantle due to proximity to a mantle plume. This hypothesis was tested by examining major element, trace element, and radiogenic isotope data from Oligocene to Holocene basalts from volcanic provinces in Queensland.

The final aim is to examine the Cenozoic motion of the Australian plate, particularly with regard to the development of east Australian volcanism. Plate motion was assessed via paleomagnetic data and plate reconstructions. New, high-resolution paleomagnetic data were acquired from east Australian volcanoes to reconstruct the Cenozoic motion of Australia. These data were compared against, and combined with, suitable older paleomagnetic data from across the continent. The combined dataset is used to evaluate potential changes in plate motion that may be manifest in the distribution of the east Australian Cenozoic volcanoes.

1.3 Background

1.3.1 Geological background

The northward migration of the Australian plate away from Antarctica began during Cenozoic time (e.g., *Duncan and McDougall,* 1989; *Hall,* 2002). At approximately 70 Ma, mafic volcanism was initiated in eastern Australia, and it continued until the Holocene. Age-progressive volcanism (the "central volcanoes" of eastern Australia) was initiated on land at 34 Ma and continued until ~6 Ma (Fig. 1.1; *Wellman and McDougall,* 1974a; *Cohen et al.,* 2007; *Knesel et al.,* 2008; *Vasconcelos et al.,* 2008; *Sutherland et al.,* 2012). The central volcano tracks are assumed to represent the surface manifestation of separate mantle plumes (*Wellman and McDougall,* 1974a; *Cohen et al.,* 2007; *Knesel et al.,* 2008; *Sutherland et al.,* 2012; *Davies et al.,* 2015); columns of hot material fixed relative to the plate that rise from a thermal-boundary layer, such as the core-mantle boundary, and form chains of volcanic provinces that progressively become younger in the direction opposite to plate motion (*Condie,* 2001; *Montelli et al.,* 2006). The central volcanoes are believed to track the motion of the Australian plate as it drifted northward (*Wellman and McDougall,* 1974a; *Knesel et al.,* 2008), and form between two and seven recognised hotspot tracks, though it is generally assumed that there are only two distinct tracks: a track that runs from Hillsborough, through the Bowen Basin to Macedon

in Victoria (the Cosgrove track; *Davies et al.,* 2015) and a coastal track that initiates at Fraser Island and continues down through Tweed and New South Wales. The central volcanoes of the Cosgrove track experience a significant hiatus after the eruption of the Buckland volcano, arising again in NSW as the leucitite suite (*Davies et al.,* 2015). The change from bimodal volcanism to leucitites is believed to result from geochemical change as the plume passed under a section of thicker lithosphere (*Davies et al.,* 2015). In addition to the age-progressive central volcanoes, non-age-progressive and putatively unrelated mafic "lava-fields" were also erupted along eastern Australia throughout the Cenozoic Era. Since the initial division of the volcanic provinces into the groups of central volcanoes and lava-fields, there have been many attempts to constrain their origin, but, particularly in the case of lava-fields, the origins are poorly constrained. A key previous suggestion is that relatively young lava-fields are related to small-scale convection in the upper mantle, while the oldest lava-field magmatism was related to rifting in the Tasman Basin and opening of the Tasman Sea (*Zhang and O'Reilly,* 1995).

1.3.2 Paleomagnetism and plate motion

Ancient plate motion can be revealed by both geochronological studies of hotspot tracks, as well as paleomagnetic studies aimed at constructing apparent polar wander paths (APWPs). Advances in data handling, equipment, analysis and magnetic cleaning techniques have led to improved paleomagnetic results and APWPs. Perhaps most importantly, the now widely employed principal component analysis (*Kirschvink,* 1980) of step-wise demagnetisation and low temperature cleaning has allowed for the removal of low stability and secondary magnetic acquisition from final vector calculations.

Different versions of an Australian Cenozoic APWP has been constructed using several techniques in the past. An early attempt by Le Pichon and Heirtzler (1968) combined remanent magnetism of the Indian Ocean with heat flow observations to determine migration rates and paths of continental Australia. This research suggested that the Australian continent split off from Antarctica at ~36 Ma and began to migrate northward. A similar study was conducted by McKenzie and Sclater (1971), but these early approaches were only useful for gross tectonic reconstructions. Subsequent studies, which utilised paleomagnetic data from the continent itself, revealed more details of plate motion. Wellman et al. (1969) used paleomagnetic results from volcanic rocks to reconstruct the Cenozoic motion of the Australian plate (Fig. 1.2a). A later APWP from Embleton (1981), which was based on paleomagnetic data from basalt in eastern Australia, suggested a "jagged" pattern of plate motion, including a notable westward "kink" during mid-Miocene time. Importantly, the kink occurs within the same timeframe as the docking of the Ontong Java plateau with the Solomon Islands, which has been linked to reduced speed of the Australian plate and the eastward excursion of the Tasman

seamount chains between 26 and 23 Ma (*Knesel et al.,* 2008). This APWP was later discarded, however, because it is not in agreement with the migration pattern of India (*Klootwijk and Peirce,* 1979). A revised Australian Cenozoic APWP was proposed by Embleton and McElhinny (1982) using a 17 point digital filter that greatly diminished the relatively jagged migration path, although this filter did not eliminate the westward excursion of the plate (Fig. 1.2b). This excursion may, however, be an artefact related to incomplete time averaging that did not account for paleosecular variation of the earth's magnetic field. The greatest downfalls of the previous Australian Cenozoic APWPs that are based on results from volcanic rocks are (1) possible incomplete time averaging and a lack of appreciation for paleosecular variation; and (2) geochronology inaccuracies inherent to the K-Ar dating method (e.g., excess Ar and Ar loss). It should be noted, however, that the apparent westward migration of the plate at 25 Ma coincides with the docking of the Ontong Java plateau, a reduction in plate velocity and the eastward excursion of the Tasman seamount chains between 26 and 23 Ma (*Knesel et al.,* 2008). An additional APWP was proposed by Idnurm (1985) based on paleomagnetic data from sedimentary rocks and laterites. This APWP relies on data from several basins, such as the Carnarvon and Perth Basins, and also includes several previous datasets. The Idnurm (1985) APWP is much smoother and more linear than previous models (Fig. 1.2c). However, paleomagnetic data from laterites are complicated because of the protracted history of crystallisation of magnetic phases in weathering profiles, and, for the same reason, radiometric dating of laterites is also complicated. Furthermore, paleomagnetic results from sediments can suffer from inclination shallowing, and the ages of sedimentary rocks may be only loosely constrained by faunal assemblages. Another issue with the APWP of Idnurm (1985) is the lack of sufficient sampling to account for within site variation: only one to two samples were demagnetised per site, thereby violating the Van der Voo (1990) pole selection criteria. The Australian Cenozoic APWPs proposed by both Embleton and McElhinny (1982) and Idnurm (1985) were subsequently disputed by Musgrave (1989), who undertook a comparison of paleomagnetic results from basalts, laterites, and sediments (Fig. 1.2d). His analysis produced a more linear migratory pattern that better agreed with the APWP of India. However, this APWP was later disputed by Idnurm (1990), who claimed that the statistical method employed was subject to question, as the data were treated in an unorthodox "ad hoc" manner and poles were excluded from the study without clear reason. In 1994, Idnurm included more paloemagnetic data from the Bowens Creek Formation in the Otway Basin. The new paleomagnetic data formed a late Eocene (~36.5 Ma) pole and was added to the APWP that he proposed in 1986. Despite the addition of more data, the APWP remained largely unchanged and still included a significant gap between 26 and 2.9 Ma (*Idnurm,* 1994).

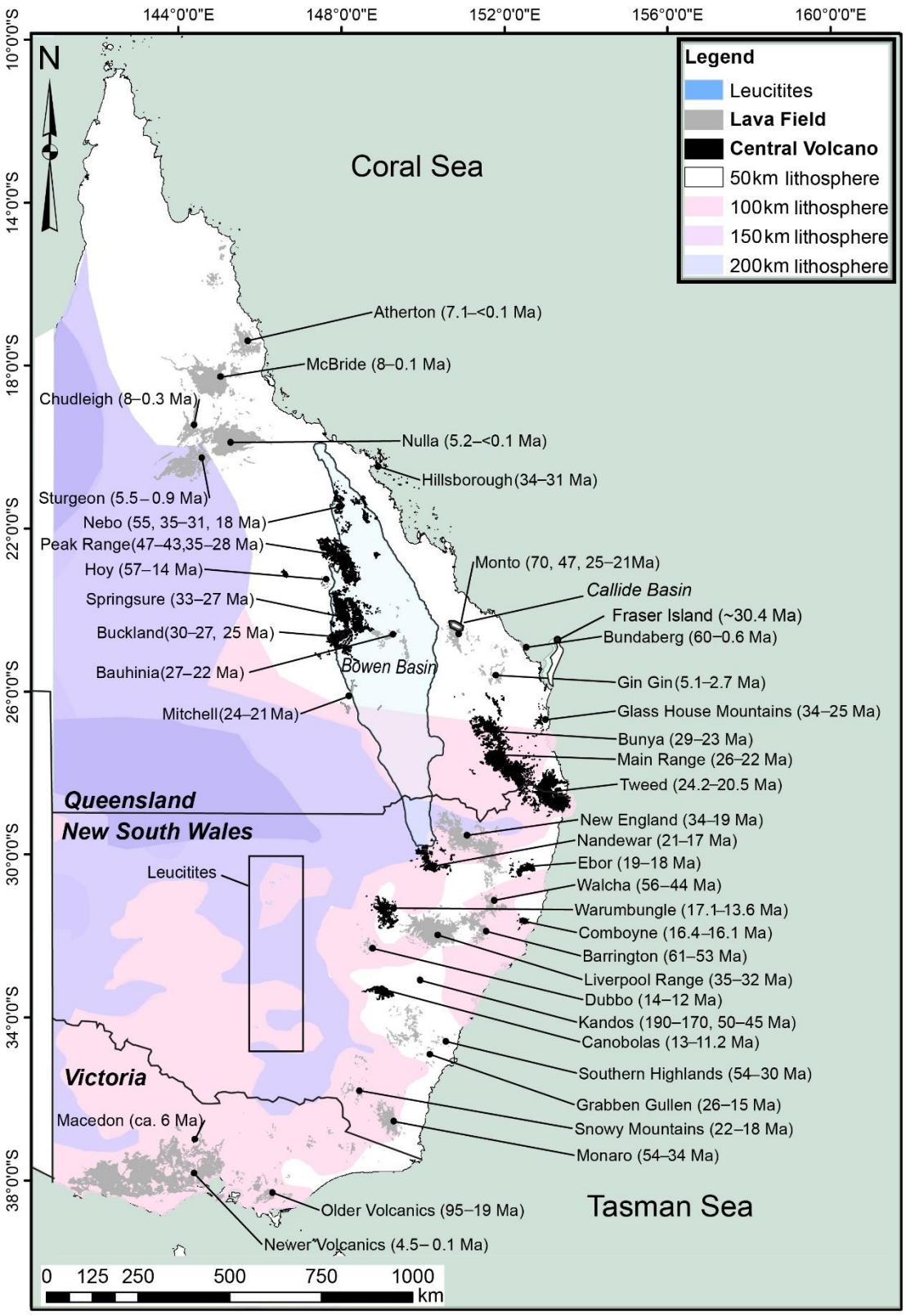

Figure 1.1: Location and age ranges of the stepped lithosphere, seamount chains, central volcanoes and lava-fields of east Australia. Primary age ranges from Johnson et al. (1989) and Vasconcelos et al. (2008). Stepped lithosphere after Fishwick et al. (2008) and Rawlinson et al. (2017).

1.3.3 Current APWP

The currently favoured Cenozoic APWP for Australia is the sediment- and laterite-based APWP of Idnurm (1985). Previous paleomagnetic results from volcanic rocks have been completely excluded from this "preferred" path because they deviate from it. The deviation has been explained previously as a failure of the volcanic-based results to eliminate polar wander by time averaging, as the volcanic provinces were erupted episodically. The limitations of the current APWP are that it (1) assumes that the migration of Australia and India was congruous throughout the Cenozoic Era; (2) averages paleo-pole positions for large durations due to uncertainties in the timing of ferromagnetic mineral formation; and (3) does not agree with migration paths based on the timing of age-progressive volcanism.

1.3.4 The pitfalls of previous APWP reconstructions

Many of the disparities between the various Australian Cenozoic APWPs mentioned above can be traced to the mode of primary magnetic acquisition of different rock types. Primary magnetism is typically acquired through either detrital remanent magnetism (DRM), which is characteristic of sedimentary rocks, or through thermo-remanent magnetism (TRM). Primary magnetism of igneous rocks is usually defined by TRM, where cooling occurs in the presence of a magnetic field from above the Curie temperature of 858˚K (*Butler*, 2004). Due to the complex process of diagenesis, including bioturbation, compaction, precipitation of new ferromagnetic minerals, and natural demagnetisation, DRM is generally not as well understood as TRM (*Butler,* 2004; *Vasconcelos et al.*, 2008). Secondary magnetic overprinting is often carried by chemical remanent magnetism (CRM), formed during the alteration of magnetic minerals through weathering, and is dominant in lateritic profiles. Some of the previous Australian Cenozoic APWPs, including the "preferred" APWP of Idnurm (1985), relied primarily on DRM and CRM. For this reason, it is possible that some previous sediment- and laterite-based paleomagnetic results from Australia reflect magnetic overprints (*Vasconcelos et al.,* 2008). A potential effect is intense smoothing of the Cenozoic paleomagnetic record, if primary and secondary remanences are mixed (*Vasconcelos et al.,* 2008). The use of paleomagnetic data from basalt, which has TRM as a primary carrier, has its own issues. Whereas DRM can produce an over-averaged record, TRM from basalt comprises "snap-shots" of the magnetic field. If volcanic flows are erupted in quick succession, such that they do not capture paleosecular variation, individual sites do not represent independent samples of the paleo-geomagnetic field (*Butler,* 2004). Unfortunately, it is not clear from Wellman et al. (1969) or Wellman (1975) how many independent sites and samples were collected from each volcano. This omission left later studies to question the validity of poles constructed from the east Australian Cenozoic volcanoes, claiming that the jagged nature of the

APWP may reflect either insufficient sampling of secular variation or the contribution of non-dipole fields (*Embleton,* 1981; *Embleton and McElhinney*, 1982; *Idnurm,* 1985; *Musgrave,* 1989). To account for paleosecular variation, the paleomagnetic poles that are calculated in this thesis use approximately ten site-mean virtual geomagnetic poles (VGPs) from each of ten volcanic provinces, and each VGP consists of three to ten samples.

In addition, previous Australian Cenozoic APWPs may not have accounted for the effects of viscous remanent magnetism (VRM). VRM is an additional magnetic field, acquired by continued exposure to a magnetic or null field. Typically, thermal relaxation and the acquisition of VRM occurs on a scale of 10^9 years. However, thermal activation of magnetic minerals can distort paleomagnetic vectors by causing a magnetic relaxation effect in multi-domain crystals (>10 μm). The magnetic relaxation, causing a decay of remanent magnetism, allows for the acquisition of VRM. Multi-domain crystals >200 nm are particularly susceptible to the effects of VRM. Low intensity alternating-field (AF) and thermal demagnetisation can remove this "softer" acquired magnetism. Red-beds are particularly known for having hard, strong VRM overprints (*Creer,* 1957; *Dunlop,* 2007) due to the prevalence of hematite (*Dunlop and Stirling,* 1977). Low-temperature cycling of rocks in liquid nitrogen can remove acquired magnetism (*Ozima et al.,* 1964; *Merrill,* 1970), and has been proven to be effective at removing VRM from multi-domain crystals (*Dunlop and Özdemir,* 2001). Previous Australian Cenozoic APWPs used either AF cleaning or thermal cleaning, but none employed low-temperature liquid nitrogen cycling, raising the possibility that these paleomagnetic results may have been highly affected by VRM. Samples analysed for paleomagnetism in this thesis were all cycled through low-temperature liquid nitrogen and AF cleaning procedures before thermal or full AF demagnetisation was attempted.

Possibly the largest issue with previously constructed Cenozoic APWPs of Australia is the reliance on either secondary dating methods, such as faunal counts, or K-Ar dating as calibration poles. While the K-Ar method was the most suitable dating technique of the time, more recent geochronological studies indicate that many of the K-Ar results may be age overestimates due to excess argon. If this is the case, then the location of the poles defined by K-Ar dating, and any poles calibrated using these poles, are inaccurate. A comparison of newer $^{40}Ar/^{39}Ar$ results with the previous K-Ar dates indicates differences of 2 My, on average, though in some instances the differences are as great as 10 My. To construct a more accurate path, improved high-resolution dating techniques ($^{40}Ar/^{39}Ar$ geochronology) were employed in this project.

1.3.5 The origin of lava-field provinces

Lava-fields are a set of dispersed volcanic provinces in east Australia that range in composition from alkaline to tholeiitic and in age from Late Cretaceous to late Cenozoic (Fig. 1.1; e.g., *Ewart,* 1985). The youngest lava-field was active as little as 100,000 years ago (Fig. 1.1), but peak activity was between 55 and 34 Ma (*Wellman and McDougall,* 1974, *Ewart et al.* 1976). Unlike the central volcanoes, which form an age-progressive chain, lava-field volcanoes have no clear temporal or spatial patterns.

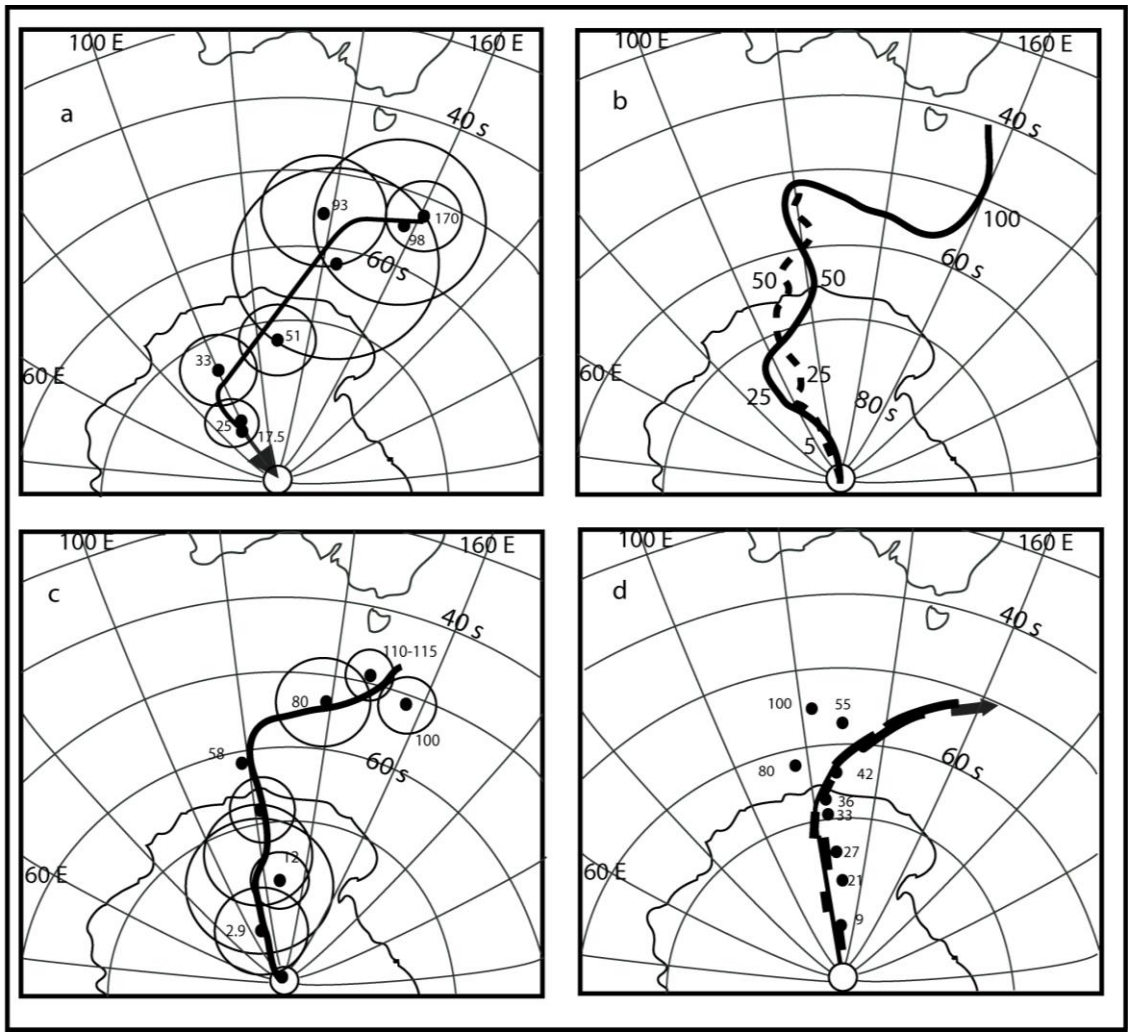

Figure 1.2: Cenozoic apparent polar wander paths of Australia after a) Wellman et al. (1969), b) Embleton and McElhinny (1982), c) Idnurm (1985) and d) Musgrave (1989).

The origin of the lava-fields has been frequently debated. Geochemical and geochronological data from some lava-fields such as Hoy and Monaro (Fig. 1.1) suggest that they formed in response to rifting, leading to a more general interpretation that lava-field magmatism was related to the Late Cretaceous to mid-Paleogene opening of the Tasman and Coral Seas (*Ewart et al.*, 1988, *Skae* 1998, *Cohen et al.,* 2007). The most comprehensive previous study of lava-field geochemistry was

undertaken by O'Reilly and Zhang (1995) in which they selected seven Cenozoic volcanic centres from across eastern Australia. The study divided them into three groups: provinces related to rift-magmatism (e.g. the Older Volcanics); those ascribed to lithosphere-plume interaction (the Newer Volcanics); and provinces related to localised melting by a changing stress-regime in a weakened lithosphere (North Queensland). A model proposed by O'Reilly and Zhang (1995) suggested a plume swath originating from an elongated region of mantle upwelling, resulting in dispersed volcanism with no spatial or temporal relationship. The plume swath may be linked to opening in the Tasman and Coral Seas, or the Late Cretaceous to early Eocene break-up of Gondwana (*O'Reilly and Zhang,* 1995). Later studies linked large scale features of the asthenospheric mantle, and the encroachment of the Indian MORB (IMORB) asthenosphere by Pacific MORB (PMORB), with the age and geographic location of lava-field provinces (*Zhang et al.,* 1999).

An alternate model for magma generation of the Newer Volcanics province was proposed by Demidjuk et al. (2007) and supported by the works of Holt et al. (2013) and Davies and Rawlinson (2014). The study focused on Quaternary basaltic rocks from South Australia and employed U disequilibrium ratios and geodynamic constraints as a means of describing ascent rate and mantle flow patterns. The results suggested upwelling of the mantle triggered by edge driven convection (EDC) as the source of the South Australia volcanic province (*Demidjuk et al.,* 2007), as opposed to interaction with a mantle plume (*O'Reilly and Zhang,* 1995). EDC relies on steep variations in lithospheric thickness forming areas where hydrostatic pressure gradients can be generated. The pressure gradients are created when hot, cycling asthenosphere is sharply juxtaposed against cooler lithosphere, creating a series of downwellings with associated upwellings if plate speeds are sufficient (*Farrington et al.,* 2010). Where EDC is accompanied by shear-driven upwelling (SDU; shear flow caused by the relative motion between the lithosphere and asthenosphere; *Conrad,* 2011), convection is focused in these relatively thin sections of lithosphere rather than occurring on all steps, at all times. EDC cells are expected to produce i) fast seismic waves speeds in the upper mantle, ii) upwellings elongated parallel to the direction of plate travel if the cell is perpendicular to motion (and vis versa; *Vogt,* 1991; *Foulger et al.,* 2001; *King,* 2004), iii) scattered and sporadic patterns of volcanism on moving plates (*Geldmacher et al.,* 2005; *Farrington et al.,* 2010) and iv) long eruption hiatus' and extended periods of volcanism at single centres (*Geldmacher et al.,* 2005). Holt et al. (2013) combined thermodynamic modelling and geochemical analysis to determine melt generation parameters. They found that the melts were likely generated from decompression melting in the upper asthenosphere (2-4 GPa). Additionally, Davies and Rawlinson (2014), and later Rawlinson et al. (2017), used combined surface-wave tomography and geodynamic modelling of the complex lithospheric structure to show that the source of the Newer Volcanic province was an isolated EDC

cell restricted to the upper mantle and focused by shear-driven upwelling. Furthermore, the work of Rawlinson et al. (2017) showed another isolated cavity of upwelling beneath much of central New South Wales.

While these interpretations likely have overall merit, the ages and locations of some lava-fields suggest that it may be an overgeneralization. As one example, relatively young (<8 Ma) lava-field volcanism in the McBride province of northern Queensland formed tens of millions of years after seafloor spreading in the Tasman and Coral Seas had ceased (*Wellman and McDougall*, 1974a; *Davies and Rawlinson,* 2014). While it has been suggested that their formation is linked to the changing stress-regime, little evidence has been provided to support this claim. However, models involving EDC, such as those for the Newer Volcanics (*Demidjuk et al.,* 2007; *Davies and Rawlinson,* 2014), could plausibly explain the location of the North Queensland lava-fields as they may overlie relatively thin lithosphere (*Fishwick et al.,* 2008). As another example, the Bauhinia, Mitchell, and Monto lava-field provinces of east-central Queensland are spatially and temporally related to the hotspot track of the age-progressive central volcanoes (*Vasconcelos et al.*, 2008). Unfortunately, very little geochemical data have been collected from these late Oligocene to early Miocene lava-field provinces in the Bowen Basin. Alternative explanations for magmatism in these two examples include EDC, a mechanism that has been proposed for particularly young lava-field volcanism in the Newer and Older Volcanic provinces of Victoria (*Demidjuk et al.,* 2007; *Davies and Rawlinson,* 2014) and which may also be applicable to young volcanism in the McBride province of north Queensland, and deep plume interactions, which may have generated localised lithospheric melting and subsequent volcanism in the Bauhinia-Mitchell-Monto region.

1.4 Thesis Overview

The morphological characteristics of some central volcanoes and lava-fields are explored in Chapter 2. The foundation of this chapter was undertaken during my Honours research at the University of Queensland in 2013. The initial database of drill-core measurements was collected and a base interpolation of the isopach map was created in 2013, and additional data were added during the course of my PhD. Drillhole data were compiled and analysed by krigging using the ARCMAP data interpolation tool to examine subsurface geology. The isopach map indicates that not only did the Bowen Basin region volcanoes have greater volumes than previously believed, but they also infill subsurface channels. Results from this part of the project reveal a north-to-south decrease in both eruption rate and volume, a finding that is consistent with northward motion of eastern Australia over a waning mantle plume.

Based on the overall pattern of decreasing volcanism, samples were selected from several Cenozoic volcanic provinces for $^{40}Ar/^{39}Ar$ geochronology to assess the reliability of previous K-Ar geochronology (Chapter 3). Based on new $^{40}Ar/^{39}Ar$ results, it appears that the ages of volcanism in many provinces was more restricted than K-Ar results had suggested. Furthermore, the results indicate that provinces with protracted eruption histories are composed of several restricted periods of activity.

In Chapter 4, I examine the correlation between volcanism and plate motion and evaluate previous Cenozoic APWPs. A large database of geochronological data (including K-Ar, U-Pb and $^{40}Ar/^{39}Ar$) was combined with various APWPs. The results show that there is only a limited overall relationship between the northward migration of Australia and volcanic activity on the continent. However, the reconstructions did indicate that a previous APWP based on paleomagnetic data from basaltic volcanoes coincides with previous estimates of plate velocity based solely on $^{40}Ar/^{39}Ar$ results from age-progressive volcanoes (*Knesel et al.*, 2008).

Additionally, I used geochemical data to examine source depths and compositions of lava-fields and central volcanoes (Chapter 5). Using major and trace element data, along with radiogenic isotope data, I found that the source, type of melting, and depth of melting of many of the volcanic provinces are the same irrespective of age, location, or province type (i.e., lava-field or central volcano). The geochemical results have led to a conceptual framework for east Australian volcanism, in which much of the variation could be described by residence time in the crust and assimilation of heterogeneous lithospheric mantle as it rose from the asthenosphere.

Finally, in Chapter 6 I combine new $^{40}Ar/^{39}Ar$ and paleomagnetic data from east Australian volcanoes to formulate a new Australian Cenozoic APWP. The new APWP is similar to both the older APWPs that were based on basaltic data, as well as the global moving hotspot reference frame (GMHRF; *Doubrovine et al.*, 2012). The new APWP also recreates the periods of slow plate velocity predicted by $^{40}Ar/^{39}Ar$ geochronology of age-progressive volcanoes (*Knesel et al.*, 2008). The new APWP was compared to the Indian APWP and was found to be a reasonable match after 25 Ma. The Indian APWP also includes a westward offset.

Chapter 7 is a summary of findings and outlines areas of future research. I was involved in all stages of paleomagnetic, geochemical, and paleomagnetic analyses, including both field- and lab-work. In the Ar Geochronology Lab at UQ I was assisted by Paulo Vasconcelos and David Thiede. I programmed the sample run steps, evaluated background levels on the mass spectrometer and

calculated the discrimination data for each of my runs. Once the regression was completed, I constrained the age and assessed the effects of excess argon and loss of argon by weathering by inspected all step-heating spectra, isochron diagrams and age-probability plots, refitting the isotope evolutions where appropriate. In the UQ Geochemistry Lab I was assisted by Marietjie Mostert and Ai Duc Nguyen; and in the Caltech Paleomagnetics Lab I was assisted by Joseph Kirschvink, Isaac Hilburn and Sarah Slotznik. All programming and data regression of paleomagnetic samples were conducted by performed by myself using the PMAG program by Craig Jones.

Appendix A has the locality information for all samples analysed in the study. Appendix B contains the $^{40}Ar/^{39}Ar$ geochronology analytical results. Appendix C contains all accuracy and precision measurements calculated by the standards and replicates for the major and trace elements and radiogenic isotopes. Appendix D contains all Zijderfeld demagnetisation diagrams from every paleomagnetic sample. Included with the thesis are two animation files (supplemental files 1 and 2).

Chapter 2: Basalt distribution and volume estimates of Cenozoic volcanism in eastern Australia: Implications for a waning mantle plume

Isabelle Jones and Charles Verdel,

School of Earth Sciences, University of Queensland, Brisbane, QLD, Australia

This chapter was published in Australia Journal of Earth Sciences and is reproduced here with permission of the Geological Society of Australia.

Jones, I., and Verdel, C. (2015). Basalt distribution and volume estimates of Cenozoic volcanism in the Bowen Basin region of eastern Australia: Implications for a waning mantle plume. *Australian Journal of Earth Sciences, 62*(2), 255-263.

2.1 Introduction

The large, shield volcanoes of the Cenozoic volcanic provinces extend along the east coast of Australia and represent, in some places, up to 4000 km^3 of eruptive material and extremely high eruption rates (*Wellman and McDougall,* 1974). The volume of Cenozoic volcanism in eastern Australia (Fig. 2.1) has been estimated previously from the outcrop extent of basalts, but drill holes and more recent studies (e.g. *Sutherland et al.* 1977) have subsequently revealed subsurface volcanic flows with a cumulative thickness of up to 60 m. The magnitude of Cenozoic magmatism is therefore greater than previously thought, especially in the central volcanoes, necessitating a re-evaluation of basalt distribution and estimates of eruptive volumes. The central volcanoes are typically considered hotspot related, though tomographic imaging of a zone of anomalous slow seismic velocity in the mid-mantle indicated no obvious underlying tails extending to the core-mantle boundary (*Montelli et al.,* 2006). These hotspot tracks are localised to the easternmost and thinnest part of the Australian continent, implying that lithospheric structure was a key factor in their emplacement (Fig 2.1; *Fishwick et al.,* 2008; *Rawlinson et al.,* 2017). The northern portion of the track, the focus of this chapter, is located along the edge of the Bowen Basin in eastern Queensland and extends from Hillsborough in the north to Buckland in the south (*Wellman and McDougall,* 1974a). Particularly large volumes of eruptive material from some of the volcanic provinces (for example, the Tweed and Peak Range areas) have been correlated with significant slowdowns in the motion of the Australian Plate (*Knesel et al.,* 2008; *Cohen et al.,* 2013). However, the distribution of basalts has been under-constrained previously because prior estimates of the volumes of these volcanoes were based only on their surficial exposure (*Wellman,* 1971; *Wellman and McDougall,* 1974a; *Duncan and McDougall,* 1989). Coal deposits are located within proximity of several volcanic provinces, and coal resource drilling has revealed basalts buried in the shallow subsurface, suggesting that previous volume estimates were likely underestimates.

2.1.1 Geological context

Subduction along the Australian Plate to the north and sea-floor spreading between Australia and Antarctica to the south drove the Cenozoic northward migration of Australia (e.g. *Duncan and McDougall,* 1989; *Hall,* 2002). Intraplate basaltic magmas were first erupted along the eastern margin of Australia at ca 90 Ma, and volcanism continued until <1 Ma (Fig. 2.1; *Wellman and McDougall,* 1974; *Vasconcelos et al.,* 2008). East Australian volcanic provinces that have no clear time–space progression have been referred to as lava-fields (*Wellman and McDougall,* 1974a). These include the earliest magmatism in the east Australian belt and are associated with the onset of rifting in the Tasman Sea (*Johnson et al.,* 1989).

Initial eruption of the lava-field volcanoes was followed by formation of the central volcanic provinces (*Wellman and McDougall,* 1974a), which are believed to be related to the northward migration of the Australian Plate over at least two fixed thermal anomalies in the underlying mantle (*Wellman and McDougall,* 1974; *Sutherland et al.,* 2012). Some studies suggest that these basalts are related to a mantle plume or plumes because several volcanoes in the chain have plume-like geochemical compositions (*Ewart and Chappell,* 1989). These Cenozoic "hot-spot" volcanoes were first erupted at Hillsborough *ca* 34 Ma (Cosgrove track) and Fraiser Island *ca* 32 Ma (coastal track) and become progressively younger to the south, terminating at Macedon (6 Ma) in Victoria and Canobolas (10 Ma) in NSW, respectively (*Wellman and McDougall,* 1974a; *Cohen et al.,* 2007; *Davies et al.,* 2015). Inclusion of the Frasier Island volcano and the Bunya volcano within the coastal central volcanic track provides geochronological support in favour of a multiple plume model because these volcanoes imply a coastal age progression comparable to inland volcanism. More recent volcanism, such as the northern Queensland McBride (8 to <0.1 Ma) and Victorian Newer Volcanic (<5 Ma) provinces, is associated with the lava-fields, although the exact sources of volcanism in these provinces are not well constrained. The Newer Volcanic province has been related to mantle upwelling beneath the continent, rather than directly to a plume (*Demidjuk et al.,* 2007; *Davies and Rawlinson,* 2014). It has been shown, however, that the passage of the inland plume to the east of the Newer Volcanics province may have acted as a catalyst for volcanism (*Davies et al.,* 2015; *Rawlinson et al.,* 2017).

2.1.2 Characteristics of east Australian Cenozoic magmatism

The two distinct Cenozoic magmatic provinces recognised in Queensland (central volcanoes and lava-fields) can be distinguished based on spatial and geochemical characteristics (*Wellman and McDougall,* 1974a; *Ewart et al.,* 1976; *Ewart et al.,* 1977; *Ewart,* 1981; *Ewart,* 1982; *Ewart,* 1985; *Ewart et al.,* 1988; *Ewart and Chappell,* 1989). The central volcanoes are bimodal shield volcanoes that were erupted inland across the western margin of the Bowen Basin and along the coastal margin from Fraser Island to Canobolas, and represent the largest volumes of extrusive material per central vent (Fig. 2.1; Wellman and McDougall 1974). The central volcanoes of the Bowen Basin region begin at Nebo and form a chain that extends south through Peak Range, Springsure, and Buckland (Fig. 2.1). The Peak Range and Tweed volcanic provinces are composed of multiple volcanic structures and large volumes that may be associated with a reduction in plate velocity (*Knesel et al.,* 2008; *Cohen et al.,* 2013). The spatial pattern of the time-progressive central volcanoes suggests links with the Cenozoic motion of the Australian Plate. Plate velocity during formation of some of the central volcanoes was, on average, 65 ± 3 mm/yr, although velocity varied significantly with time (*Knesel et al.,* 2008). For example, during emplacement of the Tweed and Peak Range volcanic

provinces (Fig. 2.1), plate velocity was 20 ± 10 and 22 ± 5 mm/yr, respectively (*Cohen et al.,* 2013). Excluding the period of slow plate motion that occurred during formation of the Tweed volcanic province, the volume of volcanism along the central volcano chain diminishes to the south, as elaborated below.

In contrast with the central volcanoes described above, east Australian lava-fields are primarily alkaline to tholeiitic basalts that have no time–space correlation between individual provinces. These volcanoes were most active between 55 and 34 Ma (*Cohen et al.,* 2007), and most basalt from the lava-fields tend to have geochemical characteristics reflecting contributions from the lithospheric mantle. While basalts from areas such as Bauhinia have ages that are closely associated with eruption of central volcanoes (*Sutherland et al.,* 1989a), other lava-fields have geochemical compositions that suggest a relationship with rifting and opening of the Tasman Sea (*O'Reilly and Zhang,* 1995). The lava fields are typically not shield volcanoes and do not produce as voluminous eruptions. They are, however, often comprised of multiple eruptive events, scoria cones and smaller shield structures. Drilling programs from the Bowen Basin have also shown lava fields to consist of many subsurface flows and infilling of incised channels.

Wellman (1971) estimated the extrusive volumes of east Australian volcanism using a simple conical model that utilised outcrop extent of the volcanoes and assumed that marginal erosion occurred. He noted that the volume of volcanic material at Peak Range (860 km3) was significantly greater than volcanoes to the south; for example, volcanic volumes at Springsure, Warrumbungle and Ebor are approximately 360, 400 and 300 km3, respectively (*Wellman,* 1971). The volumes of preserved lavas or pyroclastics from any volcano are less than the overall original volume of material, which may include volumetrically significant ash blankets that are quickly eroded. As such, volume estimates based on preserved volcanic material are clearly minimum estimates of the amount of material that was originally erupted.

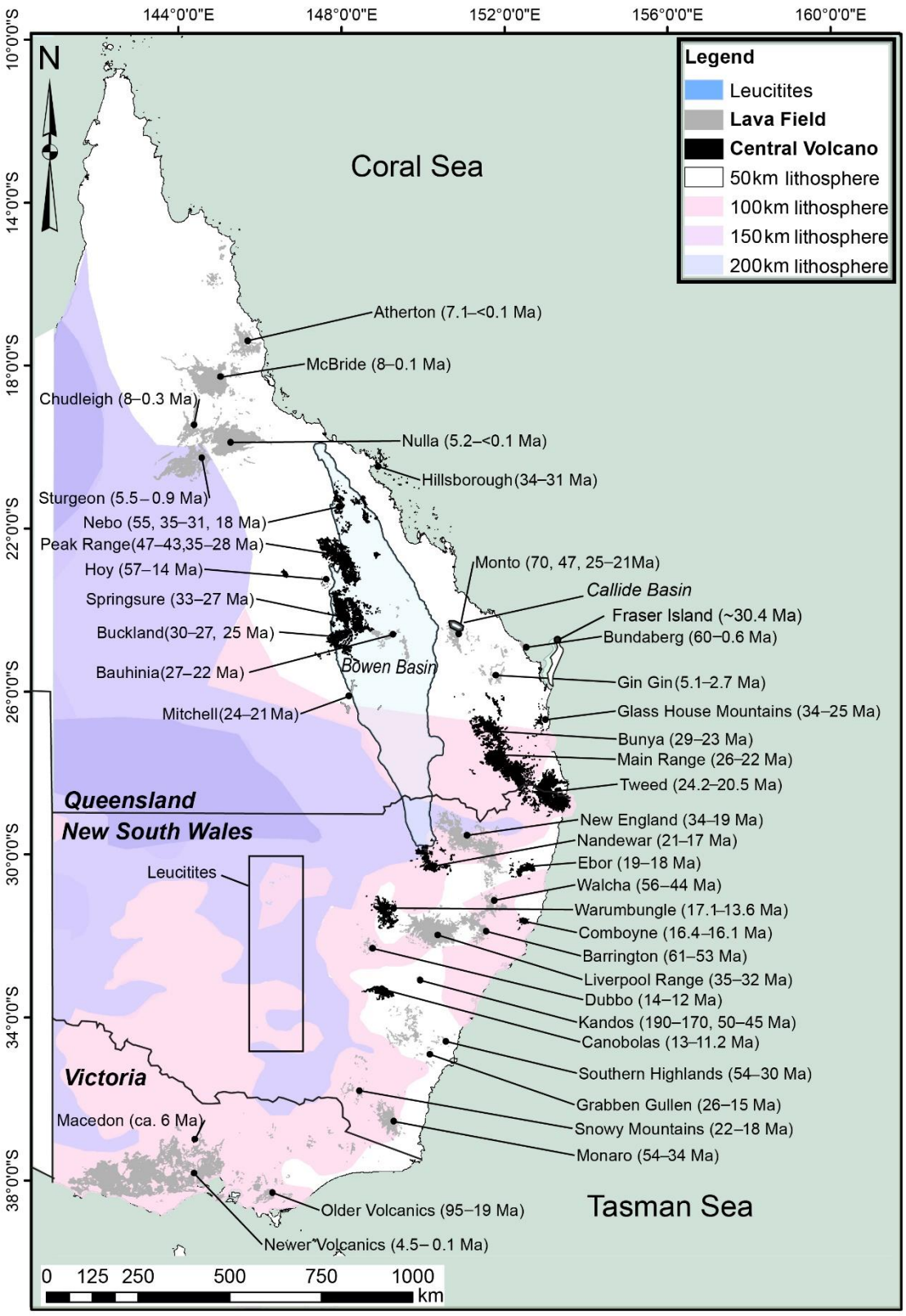

Figure 2.1: Location of central volcanoes and lava-fields in eastern Australia. Age ranges after Wellman and McDougall (1974), Johnson et al. (1989) and Vasconcelos et al. (2008). Stepped lithosphere after Fishwick et al. (2008) and Rawlinson et al. (2017).

2.2 Methodology

2.2.1 Drill hole correlation and data interpolation

Drill hole data were collected from approximately 30 sites across eastern Australia and compiled into a single dataset comprising over 150 000 individual drill hole logs. Due to confidentiality agreements, the exact locations of these drill holes cannot be shown, nor can the mines be named in this paper. However, the location of all active coal mines in the Bowen Basin, including those that donated data, are shown in Fig. 2.2. The volcanic provinces examined during this project are either within the Bowen or Callide basins; all other comparisons are made using previously published data. Drill hole logs include the depth and thickness of basalts that overlie coal deposits in the Bowen Basin, as well as lithological information. In most cases the drill hole logs do not distinguish Cenozoic basalts from older basalts. To account for this uncertainty, drill holes were added to the database only if they correspond with known Cenozoic basalt outcrops or if the age of the basalts, or the depth of the Cenozoic base, were distinguished in mine and resource reports. The drill hole logs described the weathering and physical properties of basalts, including interpretations about whether igneous rocks were intrusive or extrusive. The exclusion of intrusive units permitted us to draw a distinction between the most likely thicknesses of the basalts and the effects of vertical intrusions. Intercalated sandstones were not included in the thickness estimates. Data were restricted, for the most part, to the east of the volcanic chain in the Peak Range province. Approximate thicknesses of the Springsure, Hoy, Peak Range and Buckland volcanoes were estimated from field and drill hole elevation data and from thickness measurements reported in Sutherland et al. (1989b). The combined drill hole dataset was analysed using the ARCGIS Geostatistical Analyst function and plotted as an isopach map. A spherical kriging model was used to estimate thickness because it is the best linear unbiased estimator that can be used to interpolate between dispersed points (*Srinivasan et al.,* 2010). The use of ordinary kriging produced the most realistic distribution of basalt thickness based on field observations and the general geometric model of shield volcanoes (*Winter,* 2010). The kriging model provides an approximate distribution of basalts on both sides of the volcanic chain based on patterns observed in the basin. Using the current subsurface extent of the basalts and estimated sequence thickness, basalt volumes were estimated using a simple conical volume calculation in a manner similar to prior studies (*Wellman and McDougall,* 1974a). Like Wellman and McDougall (1974a), the estimates assume that: (1) the volcanoes have conical geometries, as is typical for shield volcanoes (*Winter,* 2010); and (2) while erosion has occurred, it is not substantial. Owing primarily to erosion since the time of eruption, the estimates are viewed as minimum estimates of eruptive volume.

2.2.2 Isopach map and thickness estimates

A basalt isopach map derived from drill hole data (Fig. 2.2) illustrates variation in the thickness of Cenozoic basalts across a portion of eastern Australia. The model parameters are reported in Table 2.1. The error associated with the model is 25%, with a nugget of ~188. The model produced spatial patterns that reflect field observations in the basin and demonstrates the likely distribution of basalts in the area. Several subsurface basaltic bodies along the eastern margin of the Bowen Basin, which are covered by soil and other sediments to a depth of ~5 m, were revealed from drill hole data. These basalt flows have an average thickness of approximately 40 m. The central volcanoes have low pyramid geometries, typical of volcanoes with thick flows beneath the plugs of the volcanic chain and thinner dispersed flows on the flanks (*Winter*, 2010). The isopach map illustrates that thickness generally decreases toward the southern end of the volcanic chain. Peak Range has the thickest volcanic sequence (~390 m), and thickness progressively decreases toward Springsure and Buckland. Hoy has lava sequences that range in thickness from roughly 70 to 100 m. Basalts in the Callide region are relatively fairly flat-lying sheets that, in places, have filled pre-existing channels.

The isopach map illustrates that the thicknesses of flow sequences from individual volcanoes may be variable. Thicknesses of flows vary, on average, from 5 to 30 m. Basalt-filled paleochannels around Peak Range vary in depth from 30 to 60 m (average depth of about 40 m) and deepen toward the NE. Channel basalts were also drilled down to 136+ m depth from the Wodehouse N.S.3 bore in the south of the Nebo province (*Sutherland et al.* 1977). Similar channel infilling is observed in both the Callide Basin and the Bunya region, near the Tweed volcanic province. Channels in these areas are as deep as 60 m and 220 m, respectively, and deepen toward the east.

Eruptive volumes of the Springsure, Peak Range, and Buckland volcanic provinces were estimated based on an assumption of conical geometry. The heights of the volcanoes were estimated from drill hole thickness data and published values, and the heights are assumed to be the maximum basalt sequence thickness in each area (*Sutherland et al.*, 1989b; *Waltenburg*, 2006). The radius of each volcano was estimated from the basalt isopach map. The estimated eruptive volumes of the Peak Range, Springsure and Buckland volcanic provinces are approximately 2600 km^3, 1460 km^3 and 850 km^3, respectively (Table 2.2).

The three subsurface basalts that infill channels to the west of Peak Range each have a volume of approximately 0.08 km^3 (Fig. 2.2). This estimate is based on a half conical volume to account for the shape of the channels. These basalts may be part of the central volcano, but their exact provenance is

unclear. This volume is a minimum estimate because the full lateral extents of the channels are not constrained in the dataset.

2.3 Discussion

2.3.1 Spatial trends in volumes of the central volcanoes

The basalt isopach map (Fig. 2.2) reveals that the thickest basaltic flows are beneath the central volcanoes in the Bowen Basin, indicating that large volumes of magma were generated in these locations when they resided above an inferred mantle plume. Lavas are intercalated with sediments, suggesting intermittent hiatuses of basalt eruption and the existence of proximal lake or river systems during volcanism. There is a progressive southward decrease in thickness and eruptive volume, from 389 m and 2607 km^3 at Peak Range, to 330 m and 1460 km^3 at Springsure, to 300 m and 849 km^3 at Buckland (Table 2.2). Volume estimates from Hillsborough and Nebo (*Stephenson et al.* 1980) have not been included because the extents of the original volcano are unclear. The large volume of magmatism at Peak Range is consistent with a recent study (*Cohen et al.* 2013) suggesting that the motion of the Australian Plate during the Peak Range eruption was slower than during the eruptive periods at Springsure and Buckland.

A similar decrease in plate velocity and resultant increase in magma generation is believed to have occurred during eruption of the Tweed volcanic province, as suggested by $^{40}Ar/^{39}Ar$ geochronological studies (*Knesel et al.* 2008). Other factors beyond plate motion may have influenced the size and volume of the volcano, as well as the eruption rate. Pre-existing weaknesses within the crust, such as from thermal sag, crustal thinning or faulting, may have impacted the volume of extruded material. A waning plume tail or changes in the physical conditions of the magma chamber may also affect the volume of lava extruded. However, given that there are no obvious structural differences between Peak Range, Springsure and Buckland (all are located along the same basin margin), I suggest that the overall southward decrease in volume and thickness is related to a waning mantle plume (*Condie,* 2001; *Montelli et al.,* 2006).

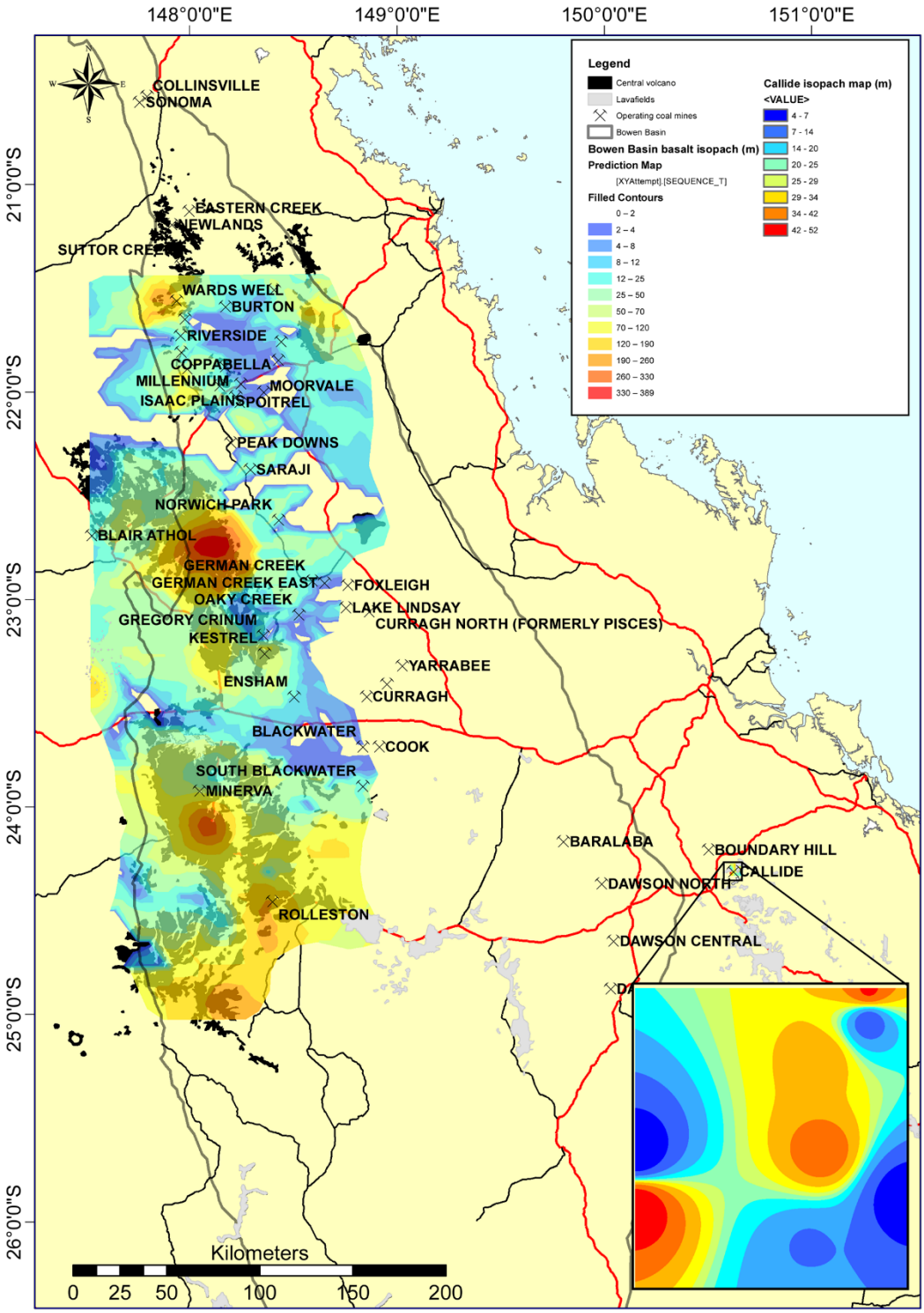

Figure 2.2: Basalt thickness variation across the Bowen Basin. Isopach map was generated using a kriging model to determine likely isograd distribution based on the distance between all points. Geological unit data provided by Raymond et al. (2012). Cross-hatching refers to all operating coal mines within the Bowen Basin. The smaller inset map represents the isopach distribution for the Monto province basalts of the Callide mine, in the Callide Basin.

The eruptive volumes for the central volcanoes are not consistent with previous volume estimates of 800 km^3 for Peak Range and 360 km^3 for Springsure (*Wellman*, 1971). The discrepancy stems from

different estimates of radii of the central volcanoes, which are larger in the present study owing to incorporation of subsurface basalts. Although the volumes themselves are different, the significantly larger volume of Peak Range compared with Springsure is consistent with the trend noted by Wellman (1971).

While the study is principally concerned with the central volcanoes, I also note that lava-field basalts vary in thickness and extent within individual provinces. This variation likely arises because the thickest basalt accumulations are located within wide incised channels that may have originally formed in Cretaceous time. The formation of these channels may be related to a Cretaceous period of uplift and erosion of the Bowen Basin region (*Raza et al.*, 2009).

2.3.2 Spatial trends in eruption rates

Using the volumes above and the mean timespan between the oldest and youngest eruptions as determined by earlier studies (*Wellman and McDougall*, 1974a; *Duncan and McDougall*, 1989), I derived estimates of average eruption rates for various central volcanoes in the Bowen Basin (Fig. 2.3). Peak Range was active for approximately 7.8 Ma (35.2 to 27.4 Ma), suggesting an overall eruption rate of 334 km3/Ma. Springsure was active for approximately 5.8 Ma (32.8 to 27 Ma; *Webb and McDougall*, 1967), corresponding with an average eruption rate of 251 km^3/Ma. Because these eruption rate estimates do not take into account hiatuses or the eruption time of individual units, they are best viewed as estimates of overall eruption rate. Accumulations of sandstone between basalt flows in some drill holes imply significant eruption hiatuses of some Bowen Basin volcanoes. Indeed, previous estimates of the eruption rate of the Buckland volcano (*Waltenburg*, 2006) suggest two periods of volcanic activity separated by a large hiatus. Eruption rate during the first period (30.5 to 29.8 Ma) was 108 km^3/Ma and then climbed to 900 km^3/Ma during a second, short-lived period of volcanism from 27.6 to 27.3 Ma (*Waltenburg*, 2006), although the errors of these ages are relatively large (±1 and 0.8 Ma, respectively). The higher rate of volcanism during the second phase may be a result of changing thermal patterns and magma inflow from the chamber beneath. Based on volume estimates from this study, the average eruption rate of the Buckland volcano was 265 km^3/Ma, about 20% less than an overall eruption rate derived from the findings of Waltenburg (2006). As no detailed eruption history exists for either Springsure or Peak Range, it is difficult to compare eruption rates between these volcanoes.

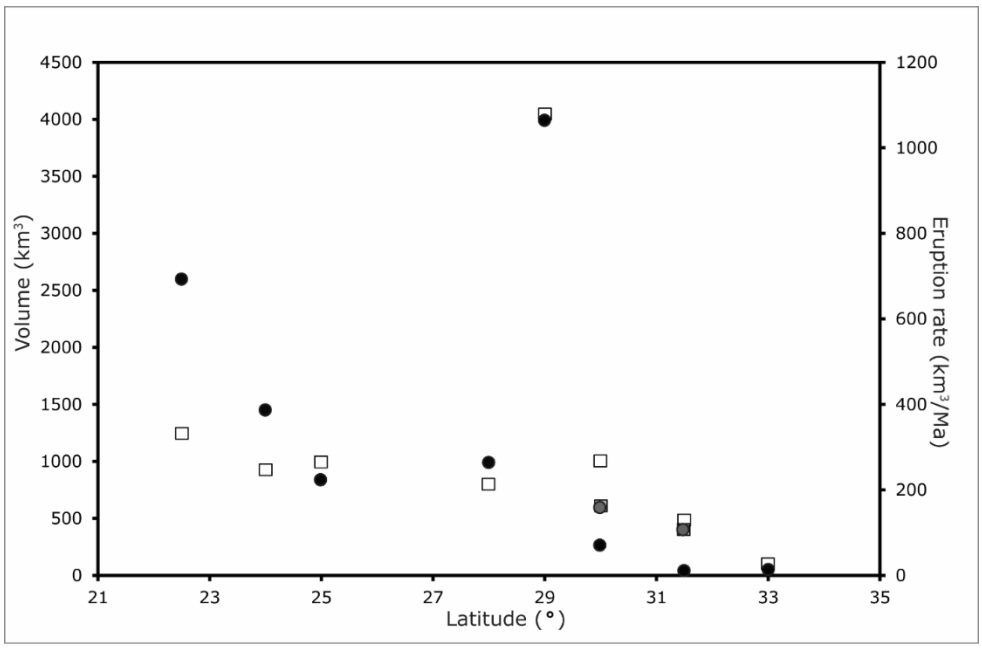

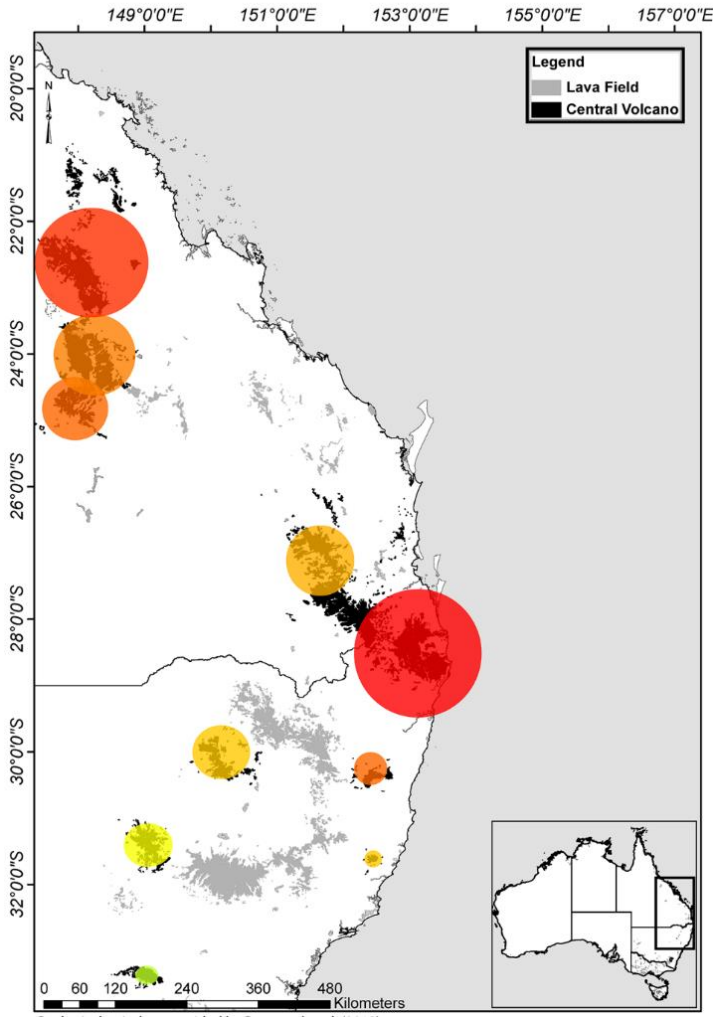

Figure 2.3: Latitudinal variation in basalt volume and eruption rate for the eastern Australian central volcanoes. a) Variation of volume (filled circles) and eruption rate (unfilled squares) with latitude. Nandewar and Warrumbungles are represented by grey symbols. b) Map of east Australian volcanoes. The size and colour of the circles represent volume and eruption rate, respectively,

of volcanic provinces. Larger circles with warmer colours indicate high volumes and eruption rates.

Average eruption rate estimates for central volcanoes in NSW calculated in this study using reported volumes and eruption periods are used for comparison (*Duncan and McDougall*, 1989; *Ashley et al.*, 1995). Eruption rates decrease south of the Tweed volcanic province, which had an average eruption rate of 1081 km^3/Ma. Eruption rates at Nandewar, Ebor, Warrumbungles, Comboyne and Canobolas were 166, 270, 114, 133 and 27.7 km^3/Ma, respectively (Fig. 2.3). As stated earlier, discrepancy between the surficial and subsurface basalts calls into question previous volume estimates from the coastal track because these estimates do not take into account subsurface information. While additional drilling in the future may facilitate more accurate volume estimates in these areas, the overall decreasing trend in volume is likely to hold true, much as it did in the northern section.

The southward-diminishing trend in eruption rates following the major pulses at Peak Range and Tweed is consistent with the waning plume hypothesis (*Condie*, 2001). Moreover, these findings, in conjunction with previous geochronology data, allow us to quantify the rate at which eruption rate decreased from north to south along the east Australian central volcanic chain over the time period from roughly 30 to 10 Ma. With the exception of the Tweed volcanic province, which is clearly an outlier in terms of both volume and eruption rate (Fig. 2.3; *Cohen et al.*, 2013), eruption rate estimates define a relatively linear decrease in eruption rate of ~15 km^3/Ma^2 from 30 to 10 Ma. The anomalous pulse of magmatism from 24–20 Ma during formation of the Tweed volcanic province has previously been related to a slowdown in the motion of the Australian Plate (*Knesel et al.*, 2008; *Cohen et al.*, 2013). For this reason, Peak Range was included in the estimate, while Tweed was not.

It is also possible that the change in the melt volumes is related to variations in lithospheric thickness, as has been proposed for the Cosgrove track (Davies et al. 2015), without the necessity for a wane in plume strength. While this is certainly possible for parts of the Cosgrove track, lithospheric thickness estimates from coastal NSW are not significantly thicker than the lithosphere in Central Queensland yet that pattern of waning magmatism is still maintained. Similarly, thickness below the Central Queensland track does not vary substantially and for this reason does not explain why volumes decrease from Peak Range to Buckland.

2.3.3 Comparison with geophysical data

The basalt isopach map was compared with regional magnetic and gravity surveys to determine if magnetic or gravity data could assist in predicting basalt thickness in the Bowen Basin (Fig. 2.4). Comparison of the isopach map with regional aeromagnetic data from Queensland suggests that

magnetic data are not particularly useful for estimating the sizes of volcanoes in this region. The magnetic data reveal the singular pipes and intrusive complexes of the volcanoes but do not accurately image the true extent or thickness of eruptive material. Furthermore, the magnetic anomalies may reflect magnetic reversals, which would exhibit negative magnetic signals (*Monroe and Wicander*, 2011), however it may be difficult to distinguish the negative anomaly of the basalts from the surrounding non-magnetic sediments. Gravity data more accurately reveal the lateral extents of the volcanoes, but these data are not useful for revealing basalt in regions of relatively thin flows. The inability to accurately model the distribution of basalts with gravity data may be due to the fairly dispersed gravity stations employed in the study or by possible interference from underlying coal, which has a negative gravity anomaly that may diminish the density signal of the basalts. In short, neither geophysical tool is particularly effective in predicting basalt thickness distributions for basalts across the Bowen Basin.

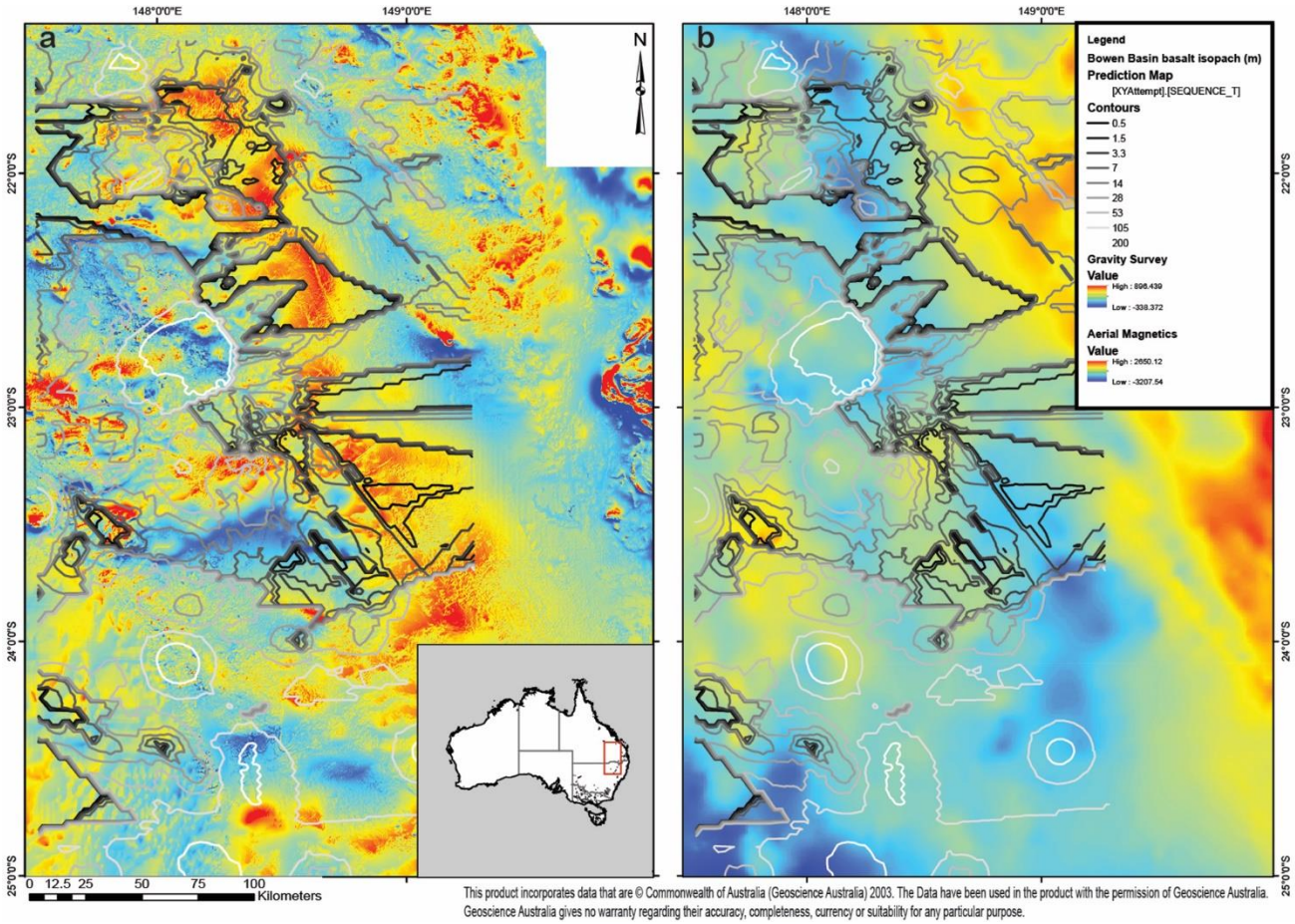

Figure 2.4: Distribution of isopachs against (a) aerial magnetics and (b) Bouger gravity survey for the Bowen Basin, Queensland. Note that warmer colours equate to higher anomalies. Geophysical data has been adapted for use by addition of secondary datasets as overlays. Geophysical data is copyrighted by Geoscience Australia (2014), are under the Creative Commons Attribution 3.0 Australia license (http://creativecommons.org/licenses/by/3.0/au/legalcode) and are available for download from the Geophysical Archive Data Delivery System (GADDS) database. Magnetics data is part of the AWAGS

Radiometrics and Magnetics Project; Magnetic Anomaly Map of Australia, 5th edition, 1:5 million scale, 2010.

2.4 Conclusions

The geometric properties of Cenozoic volcanic rocks in the Bowen Basin region can be summarised as follows.

1. Central volcanoes are large, conical shield volcanoes. The thickness of these volcanoes (which vary in height from 300 to ~389 m) decreases to the south. Volcanic provinces of the Bowen Basin region decrease in eruptive volume from approximately 2600 km^3 in the north to 850 km^3 in the south, a pattern that may reflect waning plume magmatism.
2. With the exception of the Tweed volcanic province, eruption rates of central volcanoes decrease overall from north to south. The average eruption rates for the Peak Range, Springsure, and Buckland volcanic provinces were 372, 251, and 265 km^3/Ma, respectively. Eruption rates for Tweed, Nandewar, Ebor, Warrumbungle, Comboyne, and Canobolas volcanic provinces were 1081, 166, 270, 114, 133, and 27.7 km^3/Ma, respectively. Like the southward decrease in volume, this pattern suggests waning plume activity.
3. Some Cenozoic magmas fill wide Cretaceous channels that deepen toward the NE. In the Bowen and Callide basins, the depths of these channels typically reach approximately 60 m, although some are over 100 m deep. In the Bunya region, these valleys can be up to 220 m deep. Interlayered sediments within basalt flows are likely related to eruption hiatuses. These sediments are particularly notable at the Peak Range volcano, where individual sediment layers are up to 5 m thick.
4. Lava-fields have variable thickness profiles based on their location and size. The lava-fields tend to fill incised channels, as seen in the Callide Basin. Thicknesses of lava-field basalt flows can range from 5 to 56 m in the Callide region, with cumulative volumes of 0.66 km^3.
5. Basalt extent cannot be accurately predicted using aerial magnetic or gravity surveys in the Bowen Basin, as neither exploratory tool illustrates the full extent of basalts.

Table 2.1: Ordinary kriging model parameters and outputs used in constructing the isopach map.

Method	Kriging
Type	Ordinary
Output type	Prediction
Searching neighbourhood	Standard
Neighbours to include	5
Include at least	2
Sector type	Four and 45 degrees
Major semiaxis	19,472.290
Minor semiaxis	19,472.290
Angle	0
Variogram	Semivariogram
Number of lags	14
Lag size	1000
Nuggest	188.85
Measurement error %	25
Model type	Gaussian
Range	19,472.290
Aniostropy	No
Partial sill	497.794

Table 2.2: Volume estimates for central volcanoes in the western Bowen Basin. Volcanoes are ordered north to south.

Location	**Height (km)**	**Radius (km)**	**Volume (km^3)**
Peak Range	0.389	80	2607
Springsure	0.33	65	1460
Buckland	0.3	52	849

Chapter 3: $^{40}Ar/^{39}Ar$ geochronology of Cenozoic mafic magmatism in Queensland and New South Wales

3.1 Introduction

Geochronology of mafic volcanic rocks in eastern Australia is a critical component in our understanding of the Cenozoic evolution of the Australian continent. Previous studies have utilised K-Ar (e.g. *Wellman and McDougall,* 1974a and 1974b; *Sutherland,* 1991; *Sharp,* 2004; *Grey and McDougall,* 2009) and $^{40}Ar/^{39}Ar$ (e.g. *Ashley et al.,* 1995a; *Cohen et al.,* 2007; *Knesel et al.,* 2008; *Matchan and Phillips,* 2011; *Cohen et al.,* 2013; *Sutherland et al.* 2014) geochronology to quantify both the eruption histories of these volcanoes, as well as the motion of the Australian plate. While extensive K-Ar dating has been utilised for all of the volcanic provinces (e.g. *Wellman and McDougall,* 1974a and 1974b; *Sutherland,* 1991; *Sharp,* 2004; *Grey and McDougall,* 2009), $^{40}Ar/^{39}Ar$ geochronology has only been extensively applied to the central volcanoes (*Ashley et al.,* 2005; *Cohen et al.,* 2007; *Cohen et al.,* 2013), and many of these studies are restricted to silicic volcanism within the central volcanic provinces (*Cohen et al.,* 2007; *Knesel et al.,* 2008; *Cohen et al.,* 2013). Geochronological data from many of the lava-fields, as well as the mafic flows from the central volcanoes, are therefore limited. In this chapter, I discuss new $^{40}Ar/^{39}Ar$ results and compare them to previous literature. The ages and durations of volcanic periods from each of the volcanic provinces are compared at the end of this chapter to assess relationships between volcanic provinces and overall peak magmatic activity.

3.2 $^{40}Ar/^{39}Ar$ Geochronology Methodology

Fifty-nine mafic samples from the Peak Range (7 samples), Springsure (17 samples), Bauhinia (4 samples), Monto (1 sample), Mitchell (1 sample), Hoy (1 sample), Tweed (1 sample), McBride (4 samples), Ebor (8 samples), Warrumbungles (6 samples), Barrington (7 samples) and Canobolas (2 samples) volcanic provinces, as well as four evolved samples from Peak Range were selected for $^{40}Ar/^{39}Ar$ geochronology (Fig. 3.1; Appendix A). The samples were collected from roadcuts and other outcrops. Samples were crushed in a tungsten-carbide percussion mill, and ~1 mm^3 whole-rock fragments were selected. The chips were cleaned using distilled water and ethanol in an ultrasonic bath, and five fragments from each sample were hand-picked under a binocular microscope and loaded into a 21-pit aluminium disk, as per Vasconcelos et al. (2002). GA1550 (biotite; 98.79 ± 0.96; *Renne et al.,* 1998) and sanidine from the Fish Canyon Tuff (age of 28.201±0.04 Ma; *Kuiper et al.,* 2008) were also loaded as secondary standards. The disks were irradiated for 14 hrs in the CLICIT facility TRIGA-type reactor at Oregon State University. Samples were allowed at least six months to decay before one whole-rock aliquot from each sample was analysed on a MAP 215-50 mass spectrometer in the University of Queensland Argon Geochronology in Earth Sciences Laboratory (UQ-AGES).

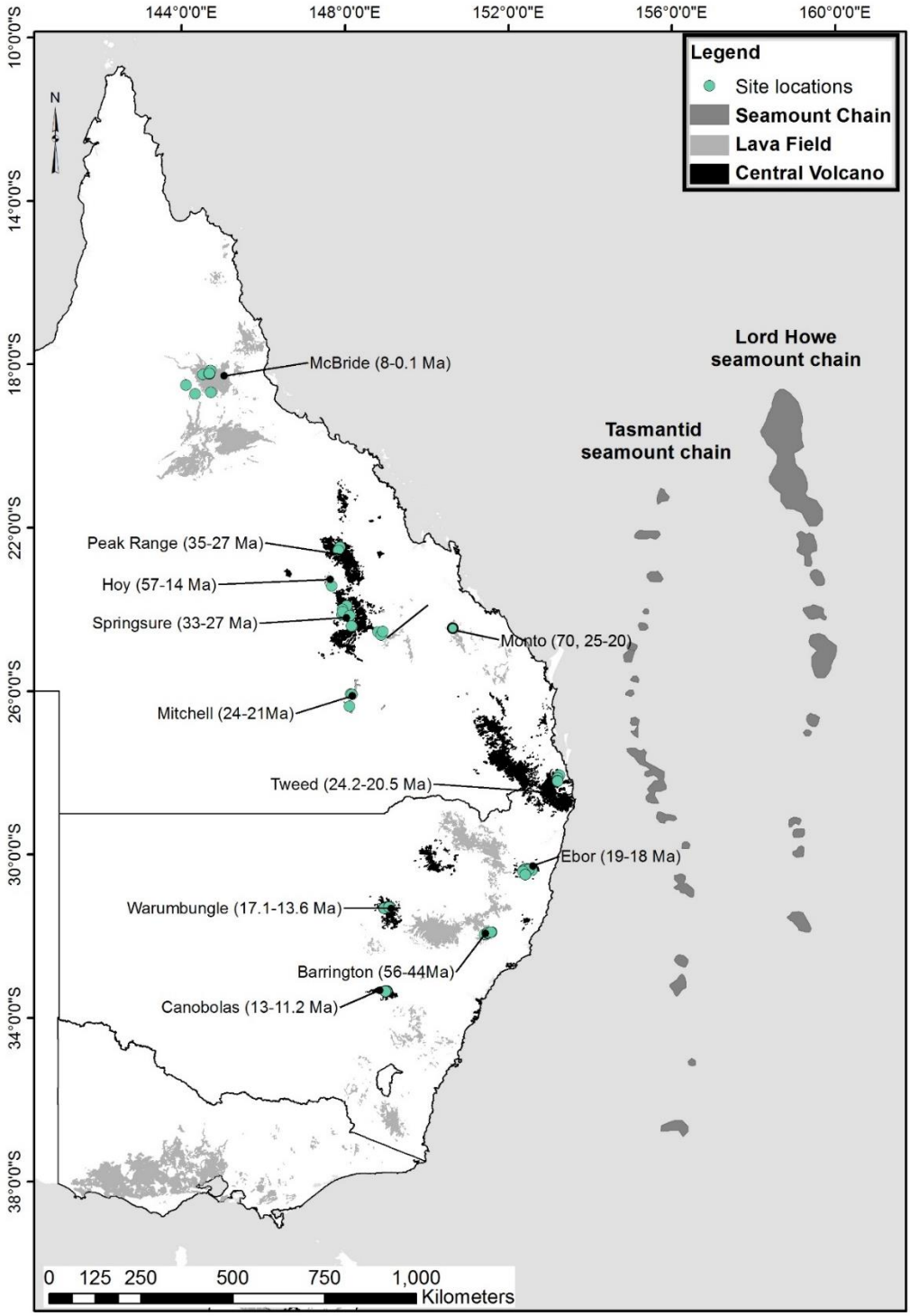

Figure 3.1: Location of samples selected for geochronological analysis. This includes samples used for geochemistry as well as paleomagnetism.

For some samples, a second aliquot was analysed to check reproducibility, or in instances where the initial aliquot did not produce a plateau. Samples were continuously heated with an Ar-ion laser with a defocused beam, as outlined in Vasconcelos (1999) and Vasconcelos et al. (2002), and the released gas was passed through a single cryocooled trap and three getter pumps. A full-system air-pipettes and three blanks were analysed between each sample to measure the baseline and check for machine

contamination. To constrain the accuracy of the $^{40}Ar/^{39}Ar$ results of the whole-rock aliquots, two grains of GA1550 biotite from each irradiation disk were also analysed by the incremental-heating method. The J-factor was calculated from 15 sanidine crystals using the total fusion method (*Vasconcelos et al.,* 2002). The results were corrected for mass discrimination, irradiation (J-factor), atmospheric contamination, and nucleogenic interferences using the MassSpec 8.03 for Mac program. Full run data are presented in Appendix B.

3.3 Results

3.3.1 McBride province

The McBride province is one of the six relatively young volcanic provinces of northern Queensland (Fig. 3.1). The province is made up of several small volcanic shields and scoria cones (*Johnson et al.*, 1989), including the Undara volcano and its associated lava tubes, as well as Kalkarney Crater. Flows in the McBride province are typically primitive basalts that infill older drainage systems in the north (*Johnson et al.,* 1989). Recent dating from the Undara volcano has revealed ages as young as 0.06 Ma (*Cohen et al.,* 2017).

Four sites from the McBride province were selected for $^{40}Ar/^{39}Ar$ geochronology: one from the lower section of Kalkarney Crater (KC3) and three from road cuts around Undara (samples UR1 through UR3). The samples produced an age range between 0.41 and 0.09 Ma (Table 3.1). The plateau ages are within error of ages produced by isochrons, and there is no evidence of significant excess argon or argon loss (Fig. 3.2). The preferred ages, defined by the combined isochrons for samples KC3, UR1, UR2 and UR3, are 0.41±0.11, 0.09±0.15, 0.257±0.076 and 0.36±0.19 Ma, respectively. The McBride province therefore includes volcanism as young as ~0.1 Ma, in agreement with recent geochronology from the Undara lava tubes (*Cohen et al.,* 2017). Samples from the base of the previously undated Kalkarney Crater produced an age of 0.4 Ma. Although samples UR1 and UR3 were collected from roadcuts in areas where previous K-Ar results indicated ~2 Ma old flows, the new samples produced the same, young age as the Undara volcano, implying that these samples represent an extension of Undara.

3.3.2 Peak Range

The Peak Range province is the largest central volcano in central Queensland, and the second most extensive in Australia (*Wellman and McDougall*, 1974; *Johnson*, 1989). The province has a diameter of 80 km and is located south of Nebo on the western margin of the Bowen Basin (Fig. 3.1). Flows spread out in the subsurface and infill channels that were incised during Cretaceous time (*Jones and*

Verdel, 2015; Chapter 2). Volcanism is bi-modal, as is typical of the central volcanoes, with the more evolved samples representing the youngest extrusive material (*Cohen et al.*, 2013). Previous $^{40}Ar/^{39}Ar$ dating from the Peak Range volcano was primarily focused on silicic volcanism (*Cohen*, 2007; *Cohen et al.*, 2013).

$^{40}Ar/^{39}Ar$ data from the Peak Range province were collected from four samples in the Moranbah region (Table 3.1; Fig. 3.3). These samples produced a range of ages from 34.25 to 30.14 Ma. Only single aliquots from samples M01 and GM1 produced plateaus, which are within error of the isochron ages. All isochron ages were within error of the plateau and ideogram age, and the $^{40}Ar/^{39}Ar$ intercept was within the present atmospheric argon ratio, so the isochron ages are considered the most reliable. On this basis, the preferred ages for samples M01, GM01, GM02, and GM03 are 34.25±0.98, 30.15±0.19, 30.86±0.32, and 30.41±0.28 Ma, respectively. An additional seven samples from road cuts around the Peak Range province were also analysed (Figs. 3.3.3 and 3.3.4). These samples yield two main clusters of ages: samples PR01a, PR02, PR05, and PR07 produced ages of 26.0±0.2 Ma, 33.3±0.4 Ma, 31.6±0.3 Ma, and 34.7±0.4 Ma, respectively, while samples PR04, PR08, and PR09 produced significantly older ages of 47.2±0.5 Ma, 44.7 ±0.4 Ma, and 45.0±0.3 Ma, respectively. The older ages correspond with a result obtained by Cohen (2007) from the Peak Range province, and they are evidence of an early period of volcanism in the Peak Range province. Excluding the anomalously old, as well as the anomalously young, ages from the Peak Range volcano, the age range for this volcano is approximately 34.7 to 28.6 Ma. The resultant duration ~6 Myr is consistent with the average period of activity for Cenozoic volcanism (3-5 Myr; *Wellman and McDougall*, 1974a), though it is not consistent with the duration of volcanism in central volcanoes specifically (1-3 Myr; *Wellman and McDougall*, 1974a; i.e. Springsure [discussed below]; Buckland [*Waltenburg*, 2006]).

3.3.3 Springsure

The Springsure shield is of bi-modal composition and covers a diameter of approximately 100 km (Fig. 3.1). Extensive erosion of the region has removed much of the original shield geometry and exposed a large number of vents and pipes (*Johnson*, 1989). As there are few extensive sections of exposed flows, many previous studies of the Springsure region do not have stratigraphic control (e.g. *Wellman and McDougall*, 1974a; *Ewart*, 1982). However, Mount Catherine is one such exposed section of flows: it includes eleven mapped flows on the southern edge of the Springsure volcano (*Johnson et al.*, 1989). The flows are between 1 and 3 m-thick and are composed, primarily, of alkaline basalt. As the flows are easily defined, a series of samples were collected for geochronological and paleomagnetic analysis through the section.

Five samples from Mount Catherine in the Springsure province have $^{40}Ar/^{39}Ar$ ages from 28 to 27 Ma (Fig. 3.48; Table 3.1). Stratigraphically lower samples (MC8 and 9) are intercalated with sedimentary beds up to 2 m-thick. The preferred $^{40}Ar/^{39}Ar$ ages from the Mount Catherine samples are defined by the combined isochrons. The preferred ages for samples MC1, MC5, MC6, MC8 and MC9 are 27.02±0.24, 27.92±0.2, 27.89±0.18, 28.41±0.47 and 27.47±0.2 Ma, respectively. The preferred age for sample MC2 is the plateau age of 27.8±0.2 Ma. The isochron does not indicate the presence of excess atmosphere in this sample, but the isochron is outside of both the ideogram and plateau ages, so in this case it was not used.

An additional eleven samples from roadcuts around the Springsure province produced a restricted age range of 27.8±0.3 to 28.2±0.2 Ma. The combined isochron is also the preferred age for these samples (Fig. 3.4). Sample IJS07 showed signs of extensive alteration, with initial $^{40}Ar/^{36}Ar$ outside the range of the present atmospheric ratio (298.56±0.31; *Lee et al.,* 2006; Table 3.1). Samples IJS08b, IJS11b, CVLF01, and CIK produced well-constrained combined isochrons of 28.0±0.4 Ma, 27.8±0.3 Ma, 28.2±0.3 Ma, and 28.2±0.2 Ma, respectively. A single grain isochron is the preferred age for sample CIS. The combined isochron of CIS exceeds the present atmospheric ratio, but the second fragment produced an isochron with no excess Ar and an age of 28.0±0.3 Ma. Samples MHV04, MHV05, MHV06, MHV07, and MHV10 produced isochron ages of 27.99±0.13, 27.27±0.5, 27.84±0.12, 28.45±0.14, and 27.92±0.14 Ma, respectively.

The age range from all 16 samples from the Springsure province is 27.02 to 28.45 Ma, a duration of ~1.4 Myr. Although older flows may exist in the subsurface, it is likely that many of the relatively old K-Ar ages reported from Springsure by previous studies (e.g. Wellman and McDougall, 1974) were the result of excess argon.

3.3.4 Bauhinia

The Bauhinia province, which is classified as a lava-field, is located in the Bowen Basin region and occurs as a series of isolated exposures (Fig. 3.1; *Johnson et al.,* 1989). The province shares a boundary with the Springsure volcano. Lava flows of the Bauhinia province infill incised channels and are of basaltic composition (*Johnson et al.,* 1989). The Bauhinia province is an ideal candidate for $^{40}Ar/^{39}Ar$ geochronology because it is spatially associated with Springsure, yet has remained undated.

Four samples from the Bauhinia province produced isochron ages of 22.5±1.8 Ma, 28.0±0.3 Ma, 27.0±2.8 Ma, and 26.8±0.3 Ma, respectively, an overall age range of 22.5 to 28 Ma (Fig. 3.5; Table

3.1). Only one fragment from sample TRLF05 (27.8±1.5 Ma), and neither fragment from TRLF01, produced a plateau age. The relatively large errors from these samples are likely due to alteration. The age range of the Bauhinia province overlaps with the period of activity in the adjacent Springsure province. Given the close proximity between the provinces and the overlap in age, it is possible the two provinces have the same source.

3.3.5 Monto

The Monto province is located near the towns of Monto and Callide, roughly 400 km east of the Bauhinia province (Fig. 3.1). Lava piles of the Monto province form long, channel-filling basalts, and K-Ar dating indicates >50 million years of activity, though peak activity was during the Oligocene (*Johnson et al.,* 1989). Only one sample from the Monto province was analysed in this study, from which the combined isochron yielded the most reliable age. The single sample from Monto, collected from the Callide mine (AA2), produced an age of 29.0±0.3 Ma, though the $^{40}Ar/^{36}Ar$ intercept (330±11) exceeds the present atmospheric ratio (Fig. 3.6; Table 3.1). The high $^{40}Ar/^{36}Ar$ intercept may be related to the slight disagreement between the two plateau ages: 29.1±0.4 Ma and 30.2±0.4 Ma. As the plateau age of the second grain includes the low temperature steps, which seem to include atmospheric argon, the preferred age is from a single grain isochron, which produced an age of 29.1±0.4 Ma and an $^{40}Ar/^{36}Ar$ intercept at 296±13.

3.3.6 Mitchell

The Mitchell province is composed of a series of discontinuous, mafic flows that fill incised channels in the region below the Buckland province volcano (Fig. 3.1). The lava sequences in the region are typically 30 to 80 m-thick and are dominated by tholeiitic basalts (*Sutherland et al.*, 1989). One sample was dated from the Mitchell province. It was collected at Kilmorey Falls and produced an isochron age of 24.2±1.1 Ma (Fig. 3.7; Table 3.1). The analysed aliquot showed signs of argon loss at low temperatures, similar to previous dating from the region (*Cohen*, 2007). The aliquot did not produce a plateau, but the isochron age is within error of the ideogram and integrated ages. 24 Ma is the youngest age from the Mitchell province determined by $^{40}Ar/^{39}Ar$ geochronology, and it is within the age range of the nearby Buckland Volcano. The close proximity to Buckland, and the correspondence with younger volcanism around the Buckland region, implies that, much like the Bauhinia province, the Mitchell province may be closely related to an adjacent central volcano.

3.3.7 Policeman's Knob

Policeman's Knob is an isolated volcanic plug within the Hoy province (Fig. 3.1). The plug is of basaltic composition and displays columnar jointing. Previous dating (*Cohen*, 2007) produced an age of 66.8 Ma. A single sample was dated from Policeman's Knob, and it produced an $^{40}Ar/^{39}Ar$ isochron age of 53.3±8.9 (Fig. 3.8; Table 3.1). The error on the $^{40}Ar/^{39}Ar$ intercept is exceptionally large, which would account for the significant error in the age. It is likely that significant excess argon is the result of secondary alteration of the sample.

3.3.8 Tweed

The Tweed shield volcano is the largest central volcano in Australia (Fig. 3.1). It is over 1.2 km-thick, underlain by a basement high, and when first erupted would have covered an area of approximately 7800 km^2. It has the highest eruption rate (1081 km^3/Myr; *Jones and Verdel,* 2015) of all central volcanoes. K-Ar dating of the volcanic sequence suggested an approximate age range of ~23.7 to 20.5 Ma, a duration of 3.2 Myr (*Webb et al.,* 1967; *Wellman and McDougall,* 1974a). However, previous $^{40}Ar/^{39}Ar$ dating at the Tweed shield volcano indicated a shorter period of volcanic activity, from ~24.3 to 23.1 Ma. A single sample from the Tweed shield volcano (a sample from the Beechmont Basalt) was dated in this study (Fig. 3.9; Table 3.1). The isochron from this sample has an age of 24.11±0.2 Ma, though it reveals significant excess argon.

The relative short eruptive period implied by $^{40}Ar/^{39}Ar$ results from the Tweed volcano would increase the eruption rate to 3300 km^3/Myr, and it seems to be at odds with the average duration of magmatic activity in older central volcanoes. These duration estimates are largely based on K-Ar ages, however.

3.3.9 Ebor

The Ebor shield volcano is located south of the Tweed central volcano, and it covers an area of 480 km^2 (Fig. 3.1; *Cohen,* 2007). The shield is heavily eroded by the retreat of the New England plateau escarpment, which it overlies (*Duggan,* 1989). The sequence is approximately 400 m-thick at its thickest near Point Lookout on the northern side, from which many of the samples dated in this study were collected. Previous $^{40}Ar/^{39}Ar$ geochronology results were recalculated by Cohen (2007; after *Ashley et al.,* 1995) to the new Fish Canyon standards (28.02 ± 0.09 Ma; *Renne et al.,* 1998), producing an age range of 19.8 to 19.25 Ma.

Eight whole rock and one plagioclase sample from Ebor were selected for $^{40}Ar/^{39}Ar$ geochronology, and a secondary plagioclase aliquot was analysed for sample EB14. The combined isochrons are the

preferred ages (Fig. 3.10; Table 3.1). Samples EB1, EB5, EB8, EB11, EB13, and EB20 produced well-constrained isochrons with ages of 19.78±0.11, 20.39±0.09, 20.1±0.08, 20.23±0.11, 20.34±0.2, and 19.8±0.08 Ma, respectively. The plateau ages consisted of 50-80% of the total gas and were within error of the isochron ages. Only one aliquot from samples EB5 and EB20 produced a plateau, so the single isochron is preferred for these samples. Whole-rock aliquots from samples EB3 and EB14 produced isochron ages of 19.78±0.11 and 19.7±0.13 Ma, respectively. Two plagioclase phenocrysts from EB14 were analysed, producing a combined isochron age (18.0±1.1 Ma) that is significantly younger than the whole rock age, a result that could arise from a later alteration event, or reheating, of the sample after eruption.

Combined with previous argon dating from some of the oldest flows in the Ebor volcano, the volcano had an overall period of activity from ~20.4 to 19.25 Ma. Results suggest eruptions occurred at intervals of 10^5 years for slightly more than 1 Myr. This duration estimate is substantially shorter than for many other volcanoes in eastern Australia, though the short eruption period is consistent with the Tweed shield volcano to the north (*Cohen et al.,* 2007).

3.3.10 Warrumbungles

The Warrumbungles volcanic province is located south of the Nandewar volcano and to the west of the New South Wales central highlands (Fig. 3.1). It is contemporaneous with the Comboyne shield volcano to the east of the highlands and the Great Dividing Range (*Wellman and McDougall,* 1974b; *Johnson et al.,* 1989; *Cohen,* 2007). As with all central volcanoes, volcanism is bi-modal, and extensive erosion has exposed the more silicic plugs (*Wellman and McDougall,* 1974b; *Johnson et al.,* 1989). Mafic units are primarily alkaline basaltic rocks, and, as in the central volcanoes of the Bowen Basin, they are intercalated with sediments (*Duggan et al.,* 1993). Silicic volcanism is dominated by mugearite to trachyte compositions, and although rhyolites are present in the area, they are considered to be part of an older volcanic stage (*Johnson et al.,* 1989). Previous $^{40}Ar/^{39}Ar$ geochronological dating has shown the volcanic sequence was erupted over a period of ~2.6 Myr, similar to other central volcanoes in New South Wales (*Cohen et al.,* 2007).

Six relatively fresh samples from the Warrumbungles province were selected for analysis by $^{40}Ar/^{39}Ar$ geochronology, and the results cluster near 16 Ma (Table 3.1). Three samples were collected from the Observatory Road section (W1, W4, W6), and three are from the Mount Exmouth section (W11-14; Fig. 3.11). Sample plateaus were within error of the isochron ages, and there is no evidence of significant recoil or argon loss at high temperature steps. The preferred ages for samples W1, W6, W11, W13, and W14 are 15.95±0.08, 16.14±0.06, 14.76±0.64, 16.31±0.06 and 16.25±0.08 Ma,

respectively. Both plagioclase phenocrysts and whole rock grains were dated from sample W4. Plagioclase from the W11 site was also analysed. The age of the W11 plagioclase is younger than the whole rock age (16.02 Ma; *Crossingham,* 2017), likely arising from a secondary period of alteration of plagioclase. The combined isochron for the two plagioclase phenocrysts (16.211±0.05 Ma) from sample W4 were significantly older than the corresponding whole rock age (15.9±0.066 Ma), implying relatively long residence time of the magma.

Sample W11 from the Warrumbungles, which produced an age of 16.02 Ma, is stratigraphically below sample W10, which was collected from the peak of the volcano and has an age of ~15.8 Ma (*Crossingham,* 2017). The overall age range of the Mount Exmouth section of the Warrumbungles is 16.3 to 15.8 Ma. Compared to the ages from Siding Spring Mountain Road (*Cohen,* 2007; this study), the Mount Exmouth section is coeval with the Mount Woorut section (*Cohen,* 2007), though only a short part of the section is exposed. The relatively short period of activity of the Warrumbungles province implies an average eruption rate of 192 km^3/Myr, significantly higher than the average eruption rate when K-Ar dates are used (*Jones and Verdel,* 2015). The discrepancy is likely due to the effects of argon loss and excess argon in previous K-Ar results.

3.3.11 Barrington

The Barrington province consists of a large shield volcano complex, spreading out atop the Barrington Plateau, which has been substantially eroded by a prominent drainage pattern (Fig. 3.1; *Pain,* 1982). K-Ar dating has constrained the age of the volcano to approximately 50 Ma, though many of the basalts are weathered to some degree (*Wellman and McDougall,* 1974b; *Pain,* 1982). Lavas are typically of basaltic composition, and can be up to 30 m-thick (*Johnson,* 1989). The province overlies a large fault system (*Galloway,* 1967) and the Barrington syncline, though deformation appears to have preceded eruption of the volcanic province (*Pain,* 1982). The Barrington province is one of the many lava-fields that have not previously been analysed with $^{40}Ar/^{39}Ar$ geochronology.

Seven samples from the Barrington province produced an $^{40}Ar/^{39}Ar$ age range from ~59 to 56 Ma (Fig. 3.12; Table 3.1), substantially older than K-Ar results from the same region (*Wellman et al.,* 1969; *Wellman and McDougall,* 1974). Isochron results were generally within error of their corresponding step-heating plateaus. Aliquots that produced plateaus show no signs of significant recoil or argon loss in high temperature steps, and plateaus included between 50 and 80% of the total gas released. Samples that did not produce plateaus have a progressive step-down, indicative of ^{39}Ar recoil. Samples BRT1, BRT3, BRT5, and BRT10 produced well-constrained isochrons with ages of 55.84±0.76, 56.55±0.49, 58.5±0.47 and 58.99±0.58 Ma, respectively. The step-heating plateau

(58.2±0.47 Ma) is the preferred age for sample BRT6, and the preferred age of BRT2 is the ideogram age of 56.82±0.24 Ma. Sample BRT7 show signs of minor excess argon, so the preferred age is from the isochron, 57.1±1.2 Ma. Sample BRT9 is well beyond this age range and did not produce a plateau due to the continuously stepped-down pattern. The isochron produces an age of 52.7±2.4 Ma, more similar to K-Ar ages obtained by Wellman et al. (1969). However, many of the samples suffer from argon recoil or loss in early temperature steps, which may account for the younger K-Ar ages. If the age for BRT9 is excluded, the new results indicate a relatively short period of volcanism from ~59 to 56 Ma.

3.3.12 Canobolas

The Canobolas volcano is the youngest of the New South Wales central volcanic provinces (Fig. 3.1). The volcanic rocks of the Canobolas province are typically more evolved than other provinces (*Middlemost,* 1981), ranging from trachyte in the central complex to hawaiite on the outer edges, with no flows exhibiting primitive compositions (Mg# >65). Subsidence has juxtaposed many rocks of different ages adjacent to each other (*Johnson et al.,* 1989). The province has an approximate volume of 50 km^3 and covers an area of 825 km^2. Older geochronology produced a restricted age range of ~13.2 to 11.2 Ma (*Wellman and McDougall,* 1974b; *Cohen,* 2007; *Cohen et al.,* 2007).

Two sites from the Canobolas province were selected for $^{40}Ar/^{39}Ar$ geochronology. A single whole-rock specimen was selected from Ca6, and both whole-rock and plagioclase phenocrysts were dated from Ca3, producing an age range from 11.23 to 11.65 Ma (Fig. 3.13; Table 3.1). All analyses produced well-constrained plateaus that were within error of their isochron ages. The discrepancy between the plagioclase phenocryst (11.23±0.25 Ma) and the whole rock age from sample Ca3 (11.55±0.051 Ma) could be explained by subsequent partial alteration of plagioclase phenocrysts after initial cooling.

The age range from Canobolas is consistent with $^{40}Ar/^{39}Ar$ results reported by Cohen et al. (2007). As was pointed out by Cohen (2007), these results do not include lower parts of the volcanic stratigraphy, so they may not reflect the full extent of volcanism. However, even including the younger K-Ar ages, the volcanic history is reasonably short (~2 Myr) and similar to the eruption durations of the neighbouring Warrumbungles volcano.

3.4 Discussion

3.4.1 Timing of east Australian Cenozoic volcanism

The results summarised above indicate that if only the constraints from $^{40}Ar/^{39}Ar$ are considered, many of the east Australian volcanoes had greater eruption rates than were calculated in chapter 2. For example, the Tweed shield is one of the more well-constrained central volcanic provinces in terms of $^{40}Ar/^{39}Ar$ geochronology, but inclusion of K-Ar results from Tweed doubles its duration (*Johnson et al.*, 1989). Eruption rate estimates from Tweed thus vary from ~1080 km^3/Myr (K-Ar ages included) to 3300 km^3/Myr (only $^{40}Ar/^{39}Ar$ ages included).

Samples collected from stratigraphic sections indicate relatively short eruption durations, typically 1 to 3 Myr. The restricted periods of activity are at odds with previous age estimates based on K-Ar geochronology (typical durations of 3 to 5 Ma; *Wellman and McDougall*, 1974a). For example, $^{40}Ar/^{39}Ar$ results from a stratigraphic section in the Ebor volcano suggests eruption of a flow every 10^5 years, a finding that is supported by magnetic polarity changes between some flows. Even the volcanoes with the longest total periods of activity (Peak Range and Barrington) are characterised by multiple, short-lived phases of volcanism that are separated by hiatuses of approximately 5 Myr. The restricted nature of volcanic activity, particularly in the shorter-lived provinces, and the prevalence of atmospheric argon in many samples suggests that previous, highly dispersed K-Ar ages are likely to be inaccurate due to excess argon. This finding underpins the need for more $^{40}Ar/^{39}Ar$ geochronology of mafic flows from all volcanic centres along the eastern margin of Australia.

This chapter forms some of the analytical basis on which the following chapters are based. This is particularly true of the chapter pertaining to paleomagnetism, because accurate and precise geochronology is a necessity for a well-constrained apparent polar wander path. The relatively consistent interval of eruption of individual flows (10^5 years) over time intervals of order 10^6 years facilitates well-defined age constraints on paleopoles calculated in chapter 6. Additionally, the overall age range of the sampled volcanoes, which spans from the Paleocene (Barrington province) to Quaternary (McBride province), and includes volcanoes with intermediate ages of Paleocene to Eocene (Policeman's Knob), Eocene to Oligocene (Peak Range), Oligocene (Springsure, Monto, Mitchell, and Tweed), Oligocene to Miocene (Bauhinia), and Miocene (Ebor, Warrumbungles, and Canoblas), is the basis for utilising paleomagnetic data from them to reconstruct the Cenozoic motion of Australia.

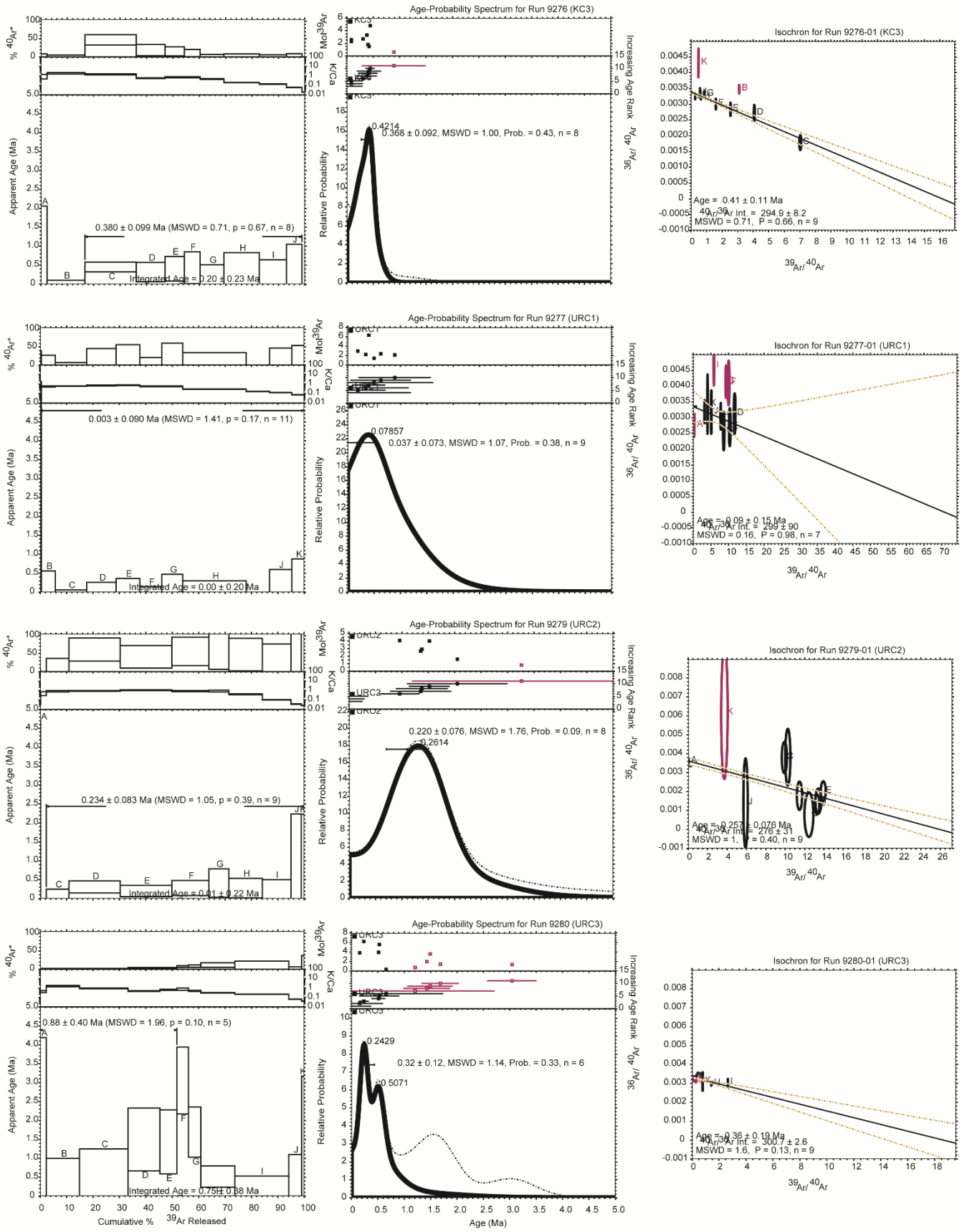

Figure 3.2: $^{40}Ar/^{39}Ar$ geochronology results for samples from the McBride province (Undara)

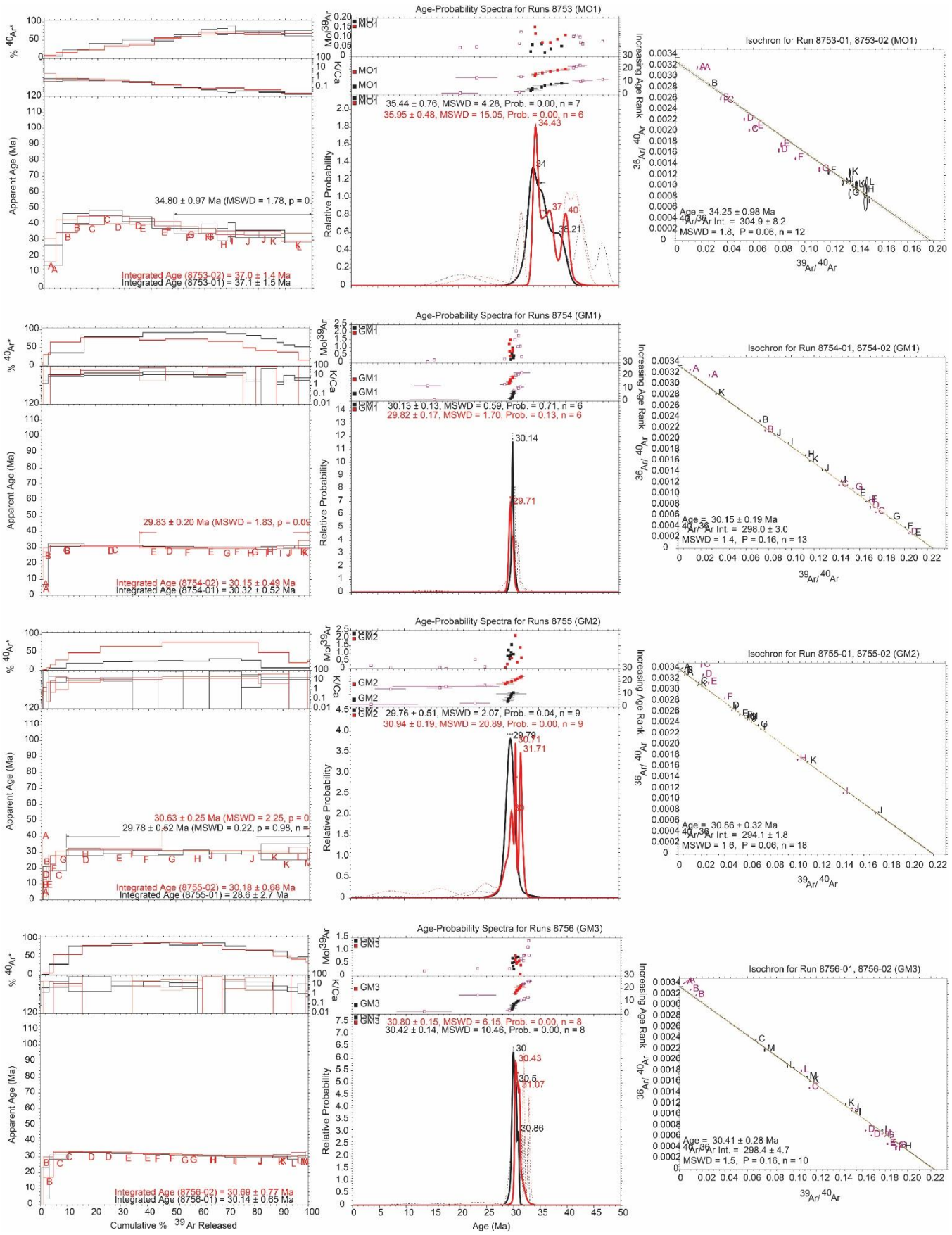

Figure 3.3: $^{40}Ar/^{39}Ar$ geochronology results for samples from the Peak Range province

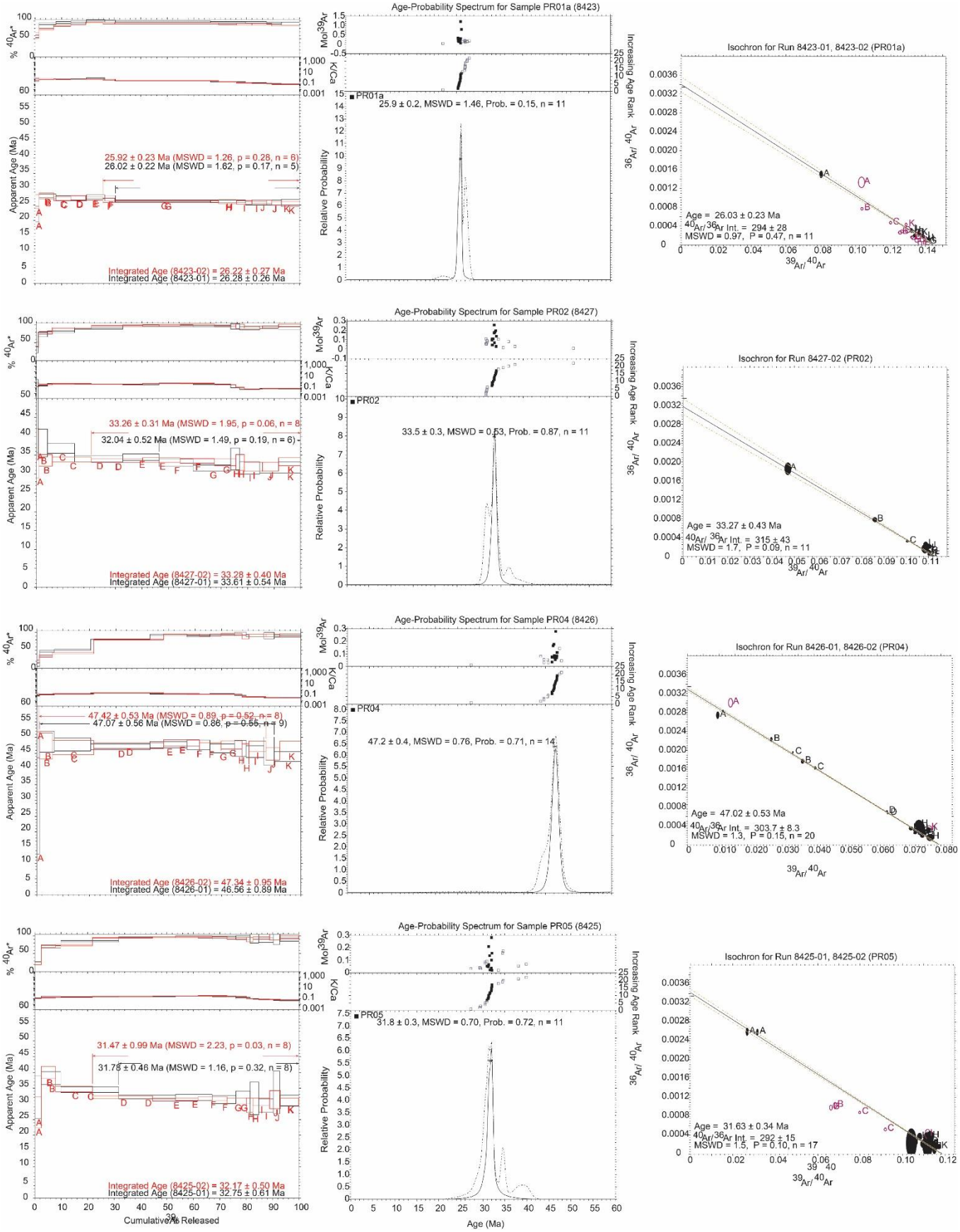

Figure 3.3 cont.: $^{40}Ar/^{39}Ar$ geochronology results for samples from the Peak Range province

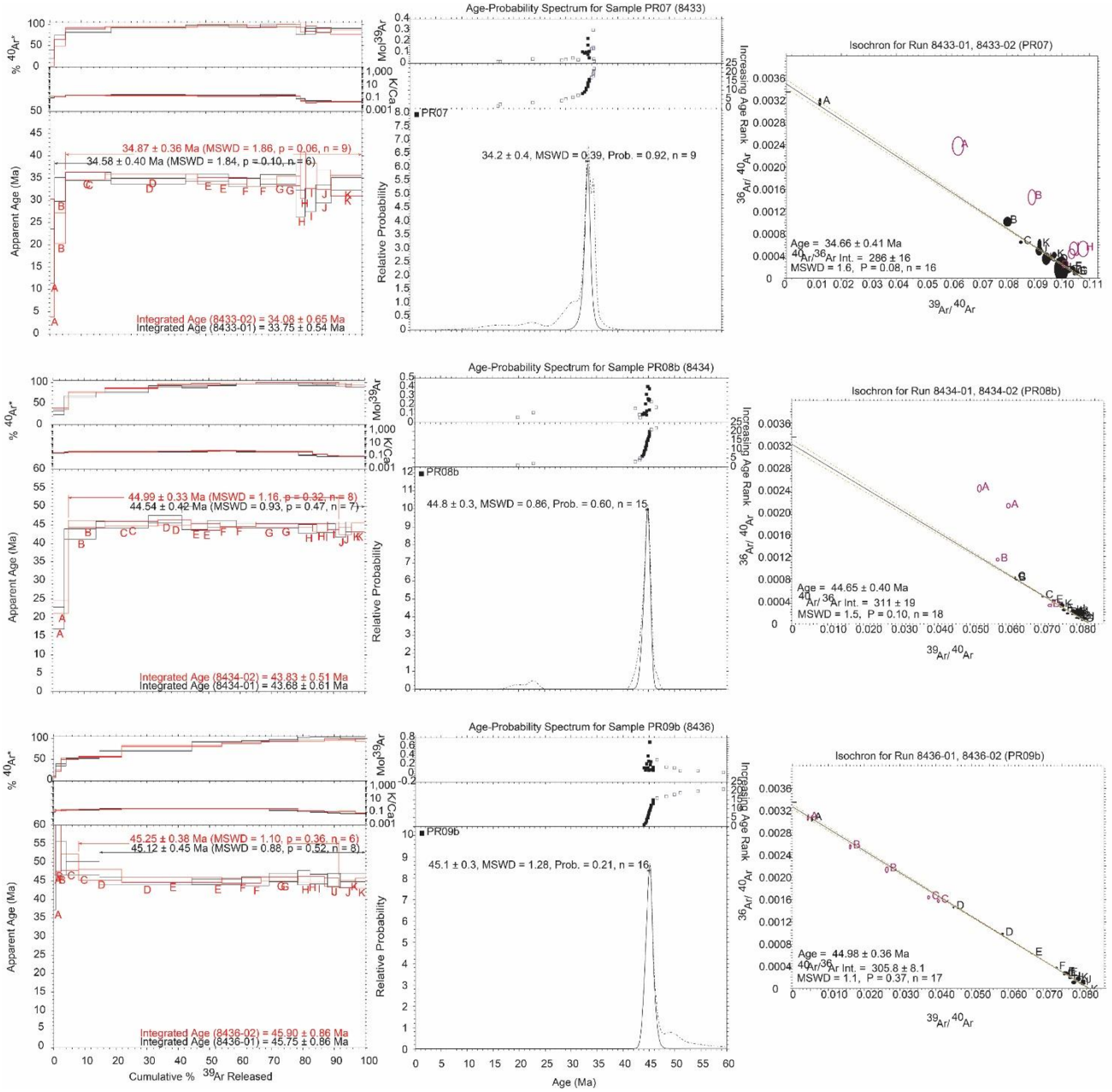

Figure 3.3 cont.: $^{40}Ar/^{39}Ar$ geochronology results for samples from the Peak Range province

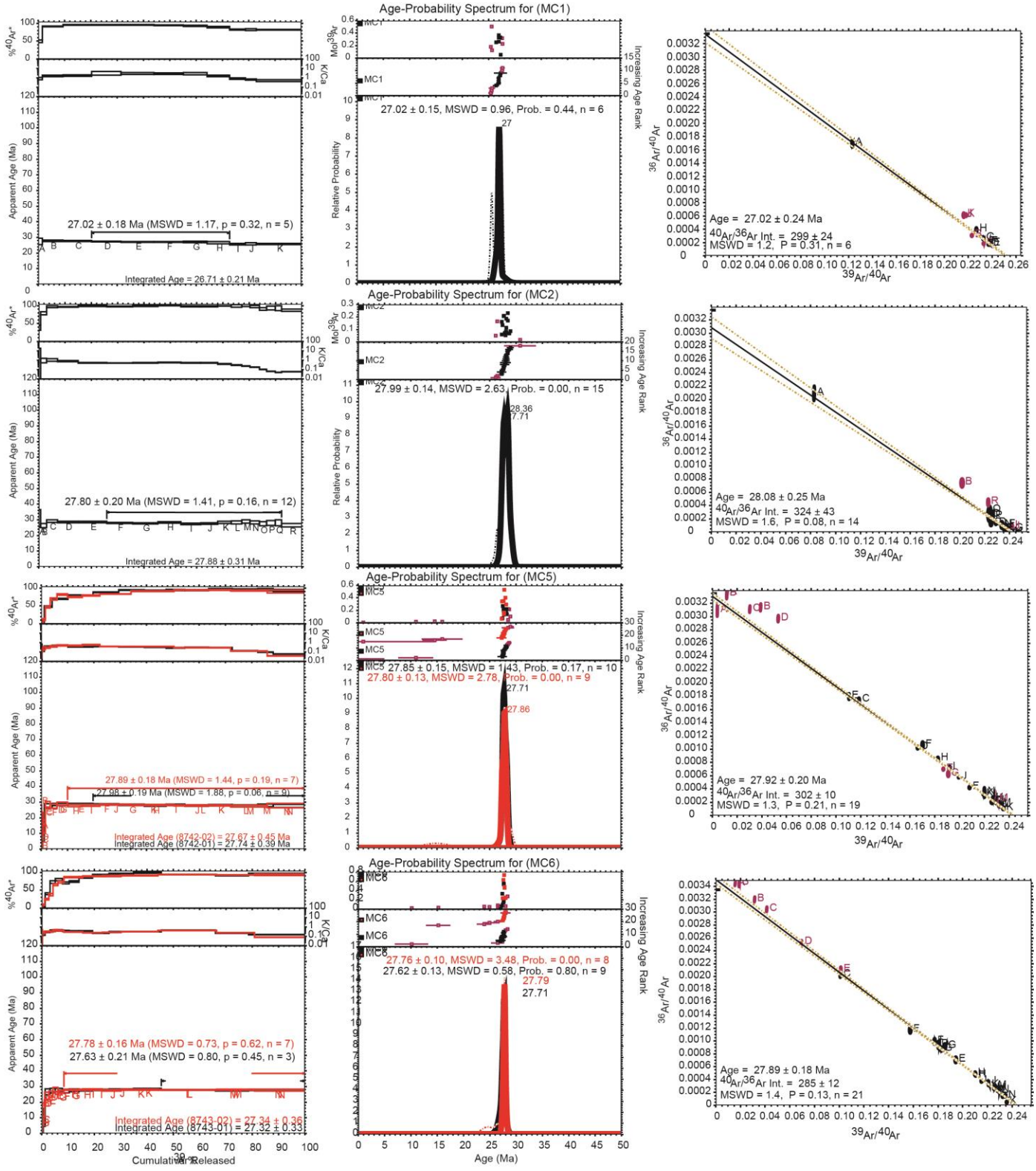

Figure 3.4: $^{40}Ar/^{39}Ar$ geochronology results for samples from the Springsure province

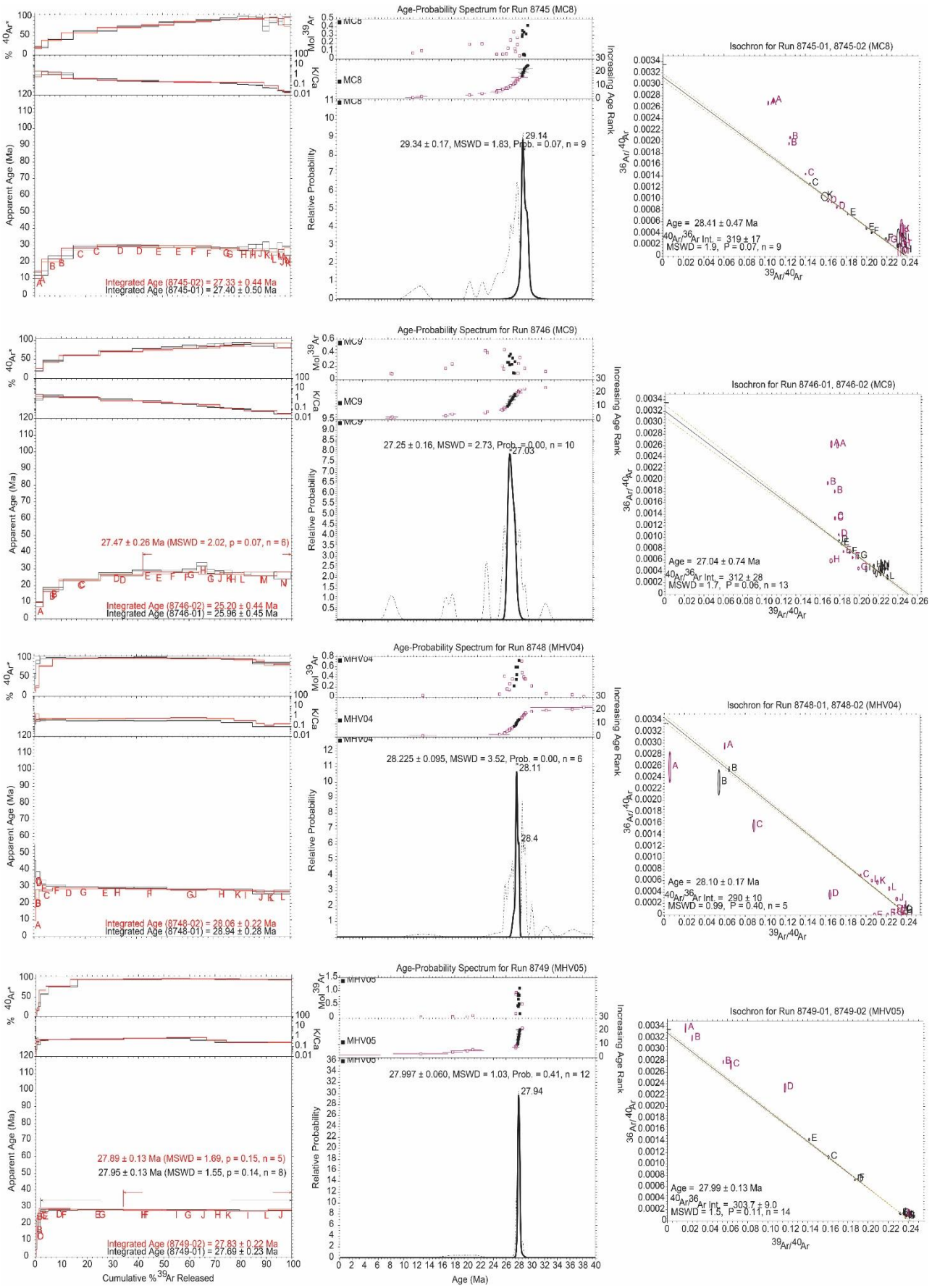

Figure 3.4 cont.: $^{40}Ar/^{39}Ar$ geochronology results for samples from the Springsure province

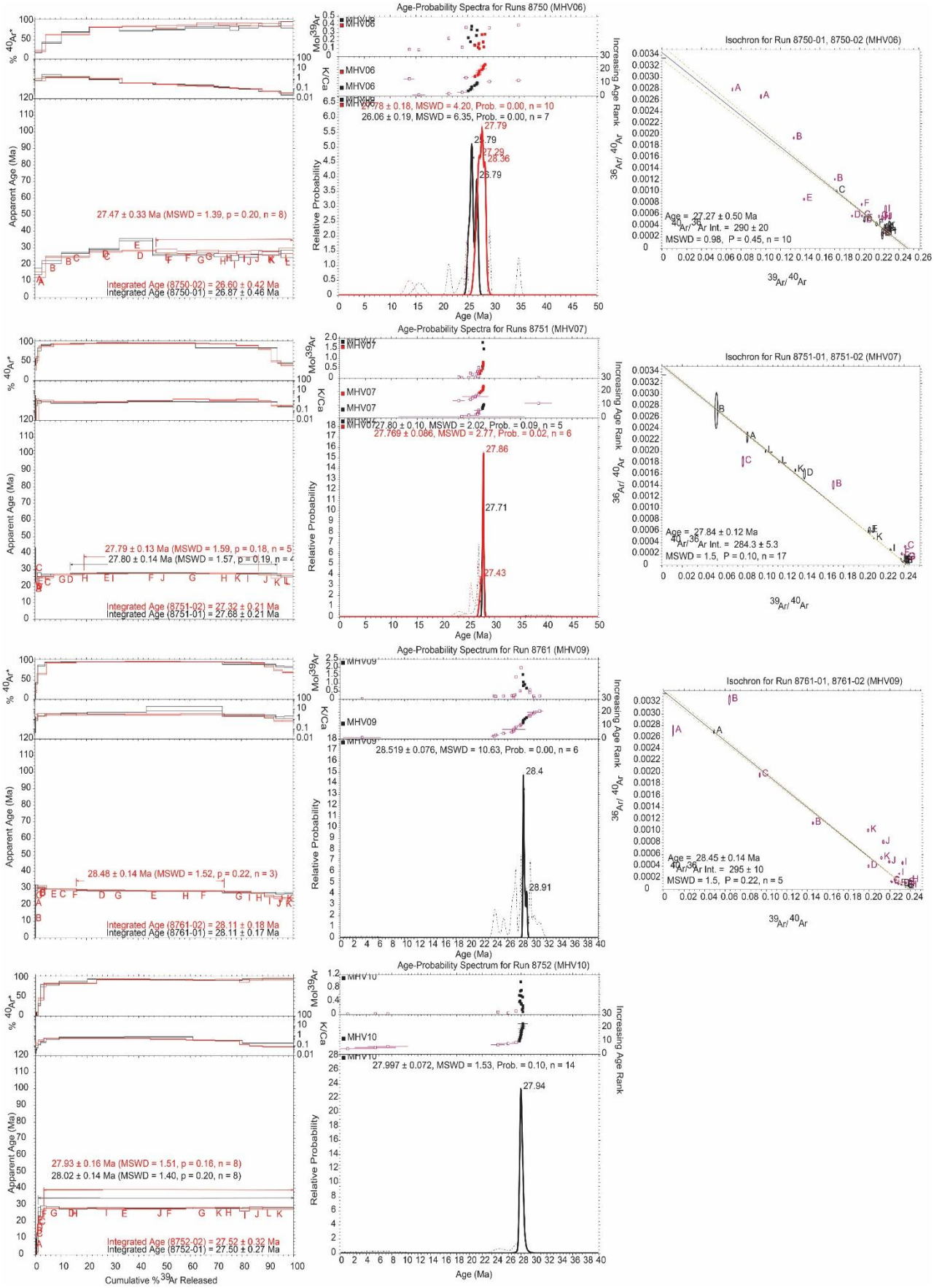

Figure 3.4 cont.: $^{40}Ar/^{39}Ar$ geochronology results for samples from the Springsure province

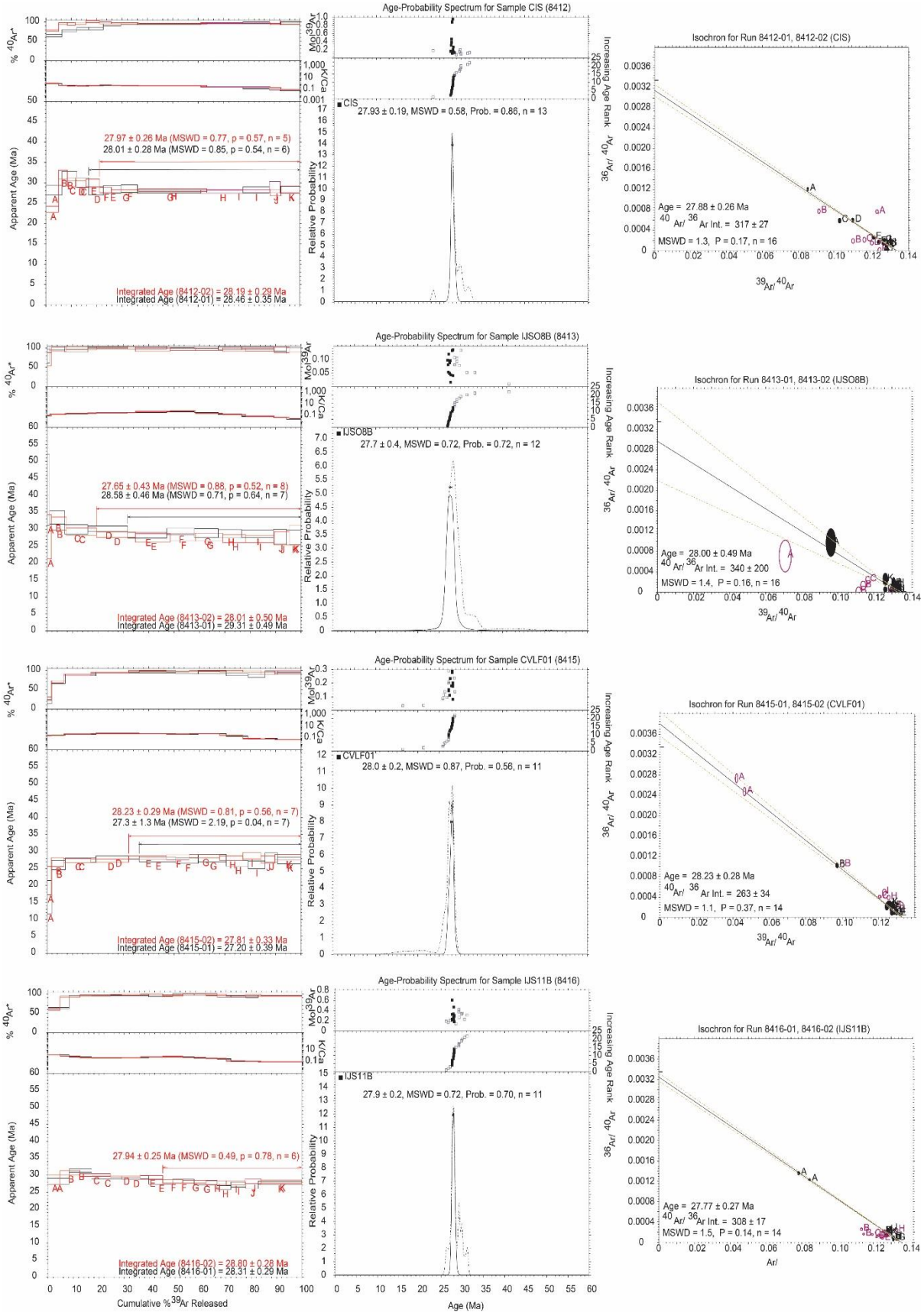

Figure 3.4 cont.: $^{40}Ar/^{39}Ar$ geochronology results for samples from the Springsure province

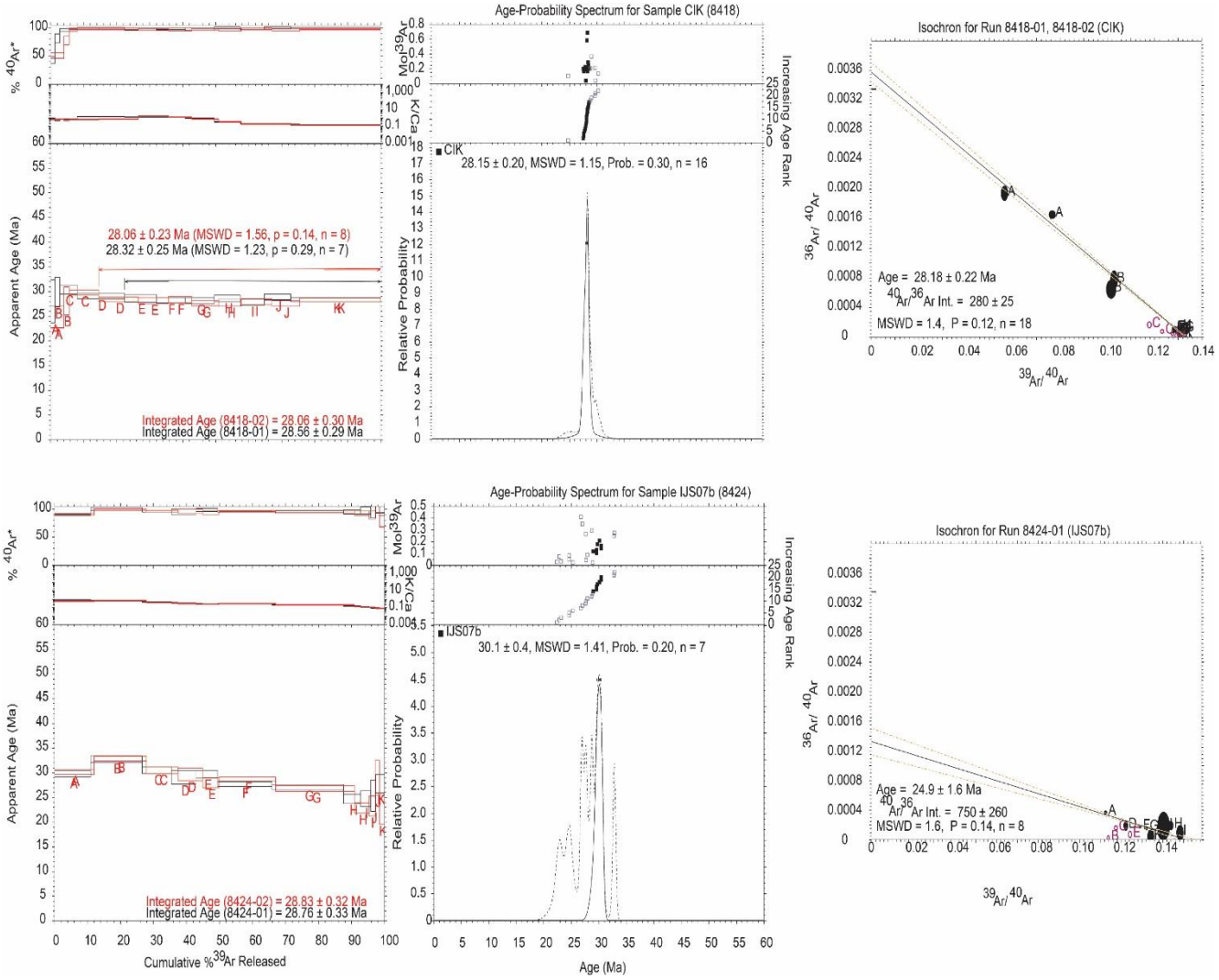

Figure 3.4 cont.: $^{40}Ar/^{39}Ar$ geochronology results for samples from the Springsure province

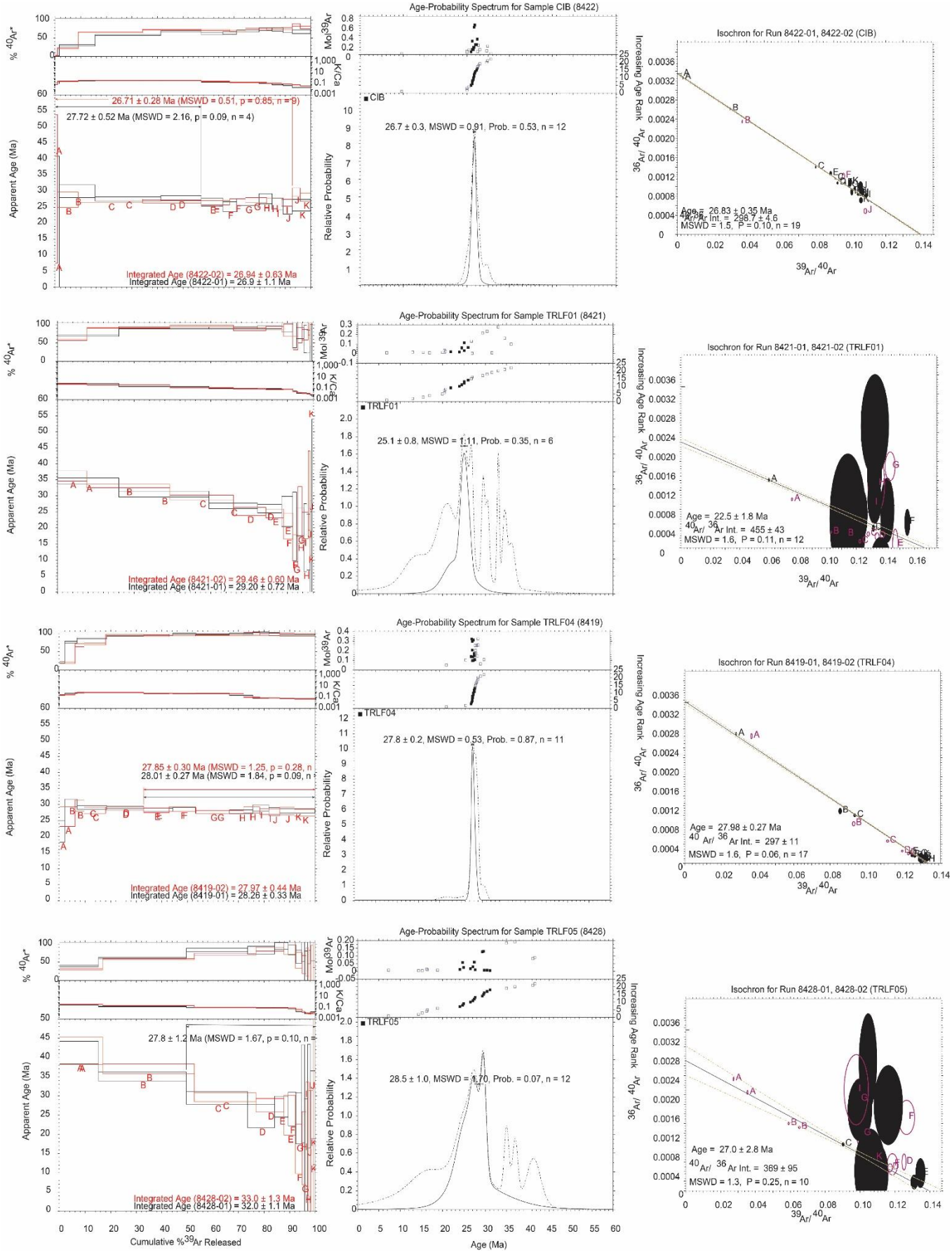

Figure 3.5: $^{40}Ar/^{39}Ar$ geochronology results for samples from the Bauhinia province

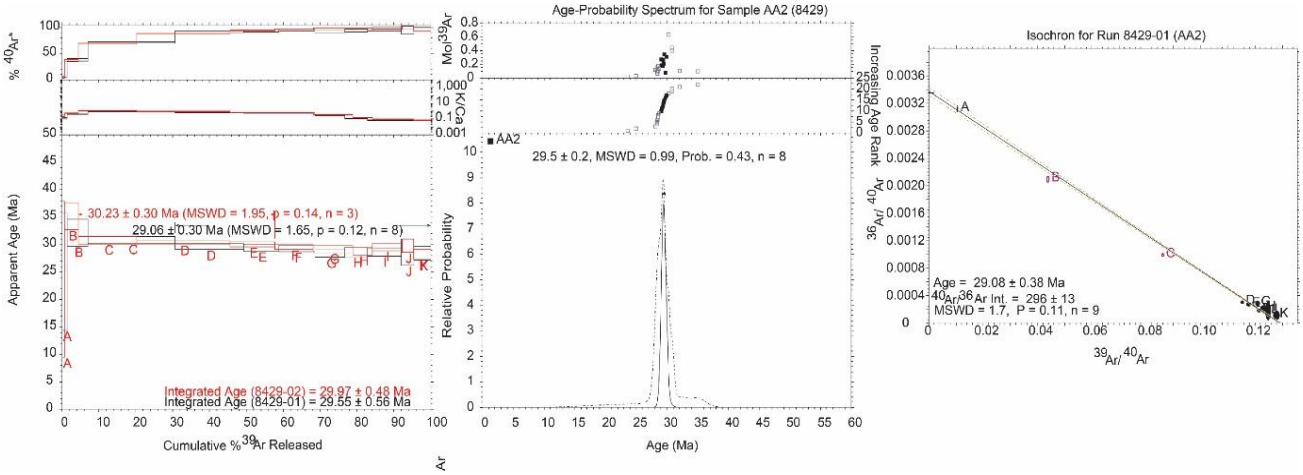

Figure 3.6: $^{40}Ar/^{39}Ar$ geochronology results for samples from the Monto province

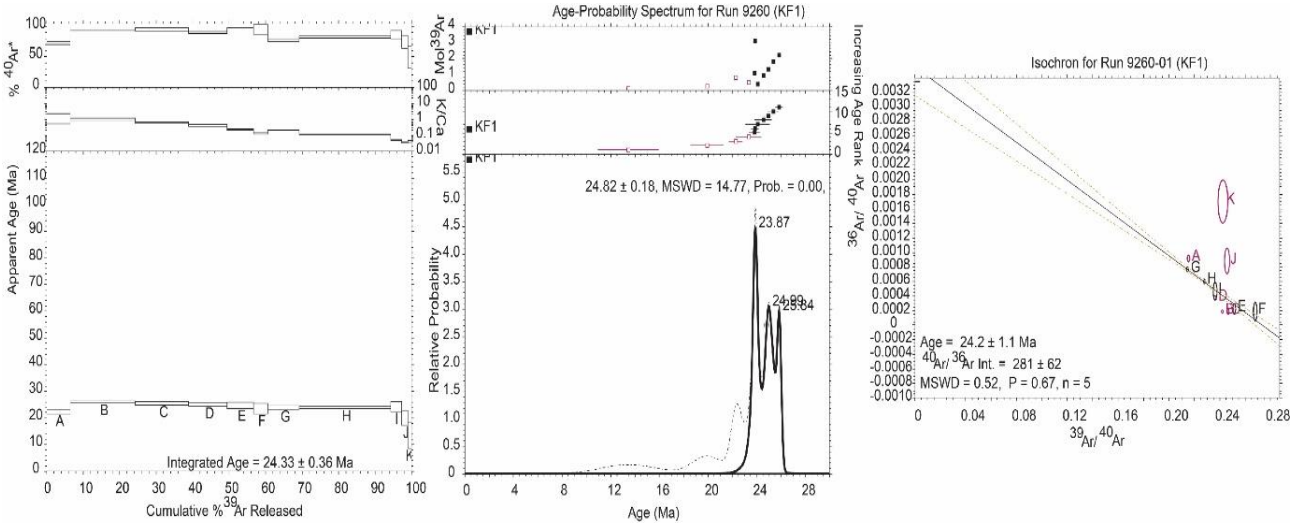

Figure 3.7: $^{40}Ar/^{39}Ar$ geochronology results for samples from the Mitchell province

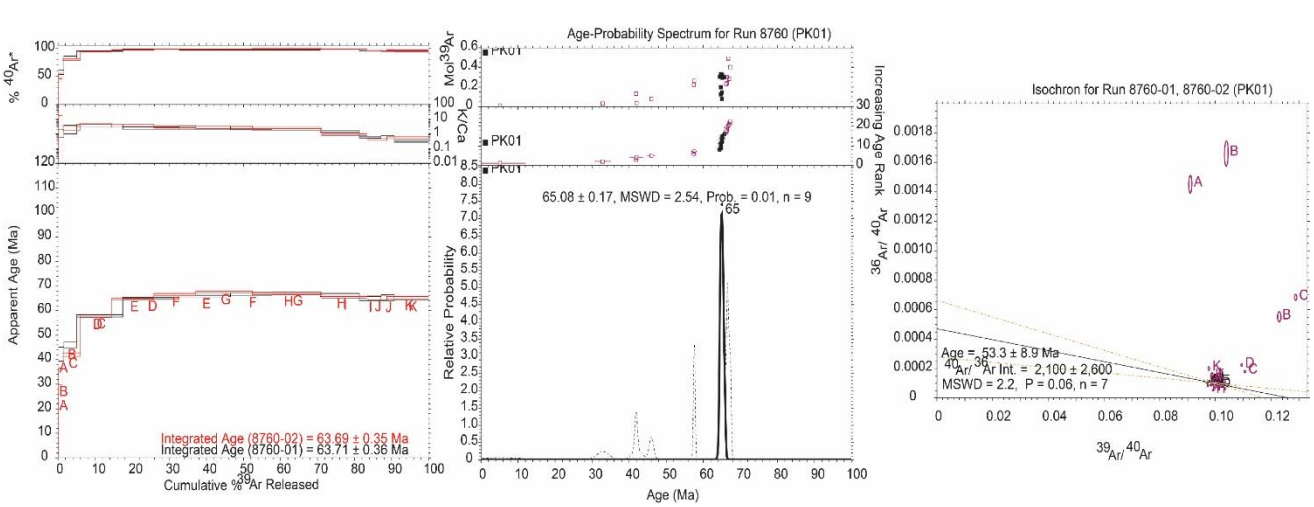

Figure 3.8: $^{40}Ar/^{39}Ar$ geochronology results for samples from the Policeman's Knob (Hoy province)

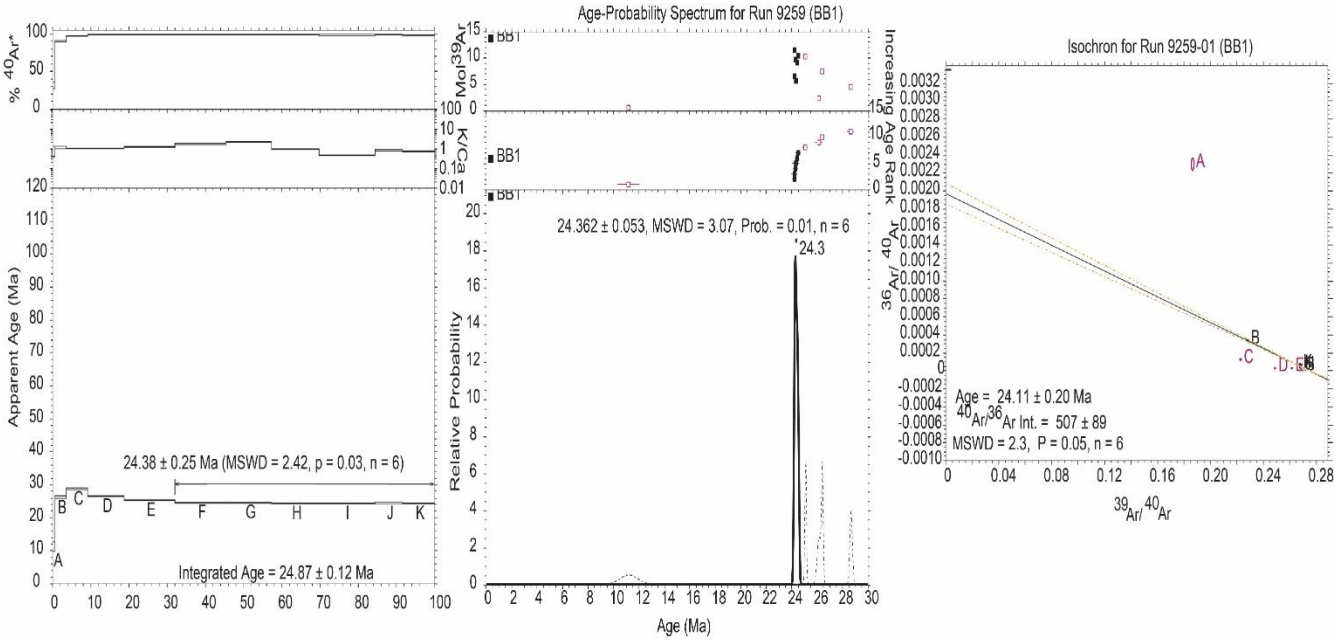

Figure 3.9: $^{40}Ar/^{39}Ar$ geochronology results for samples from the Tweed province

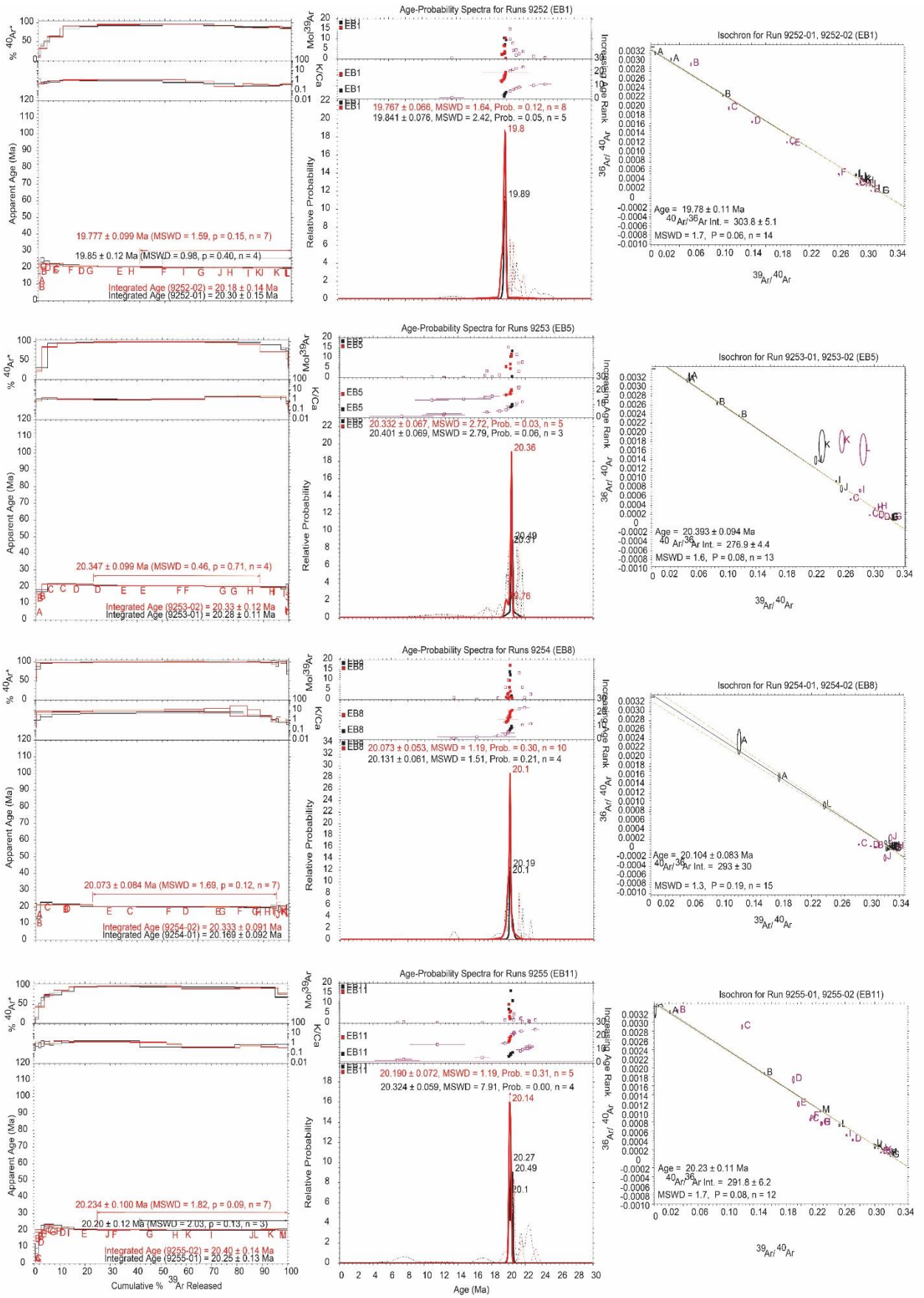

Figure 3.10: $^{40}Ar/^{39}Ar$ geochronology results for samples from the Ebor province

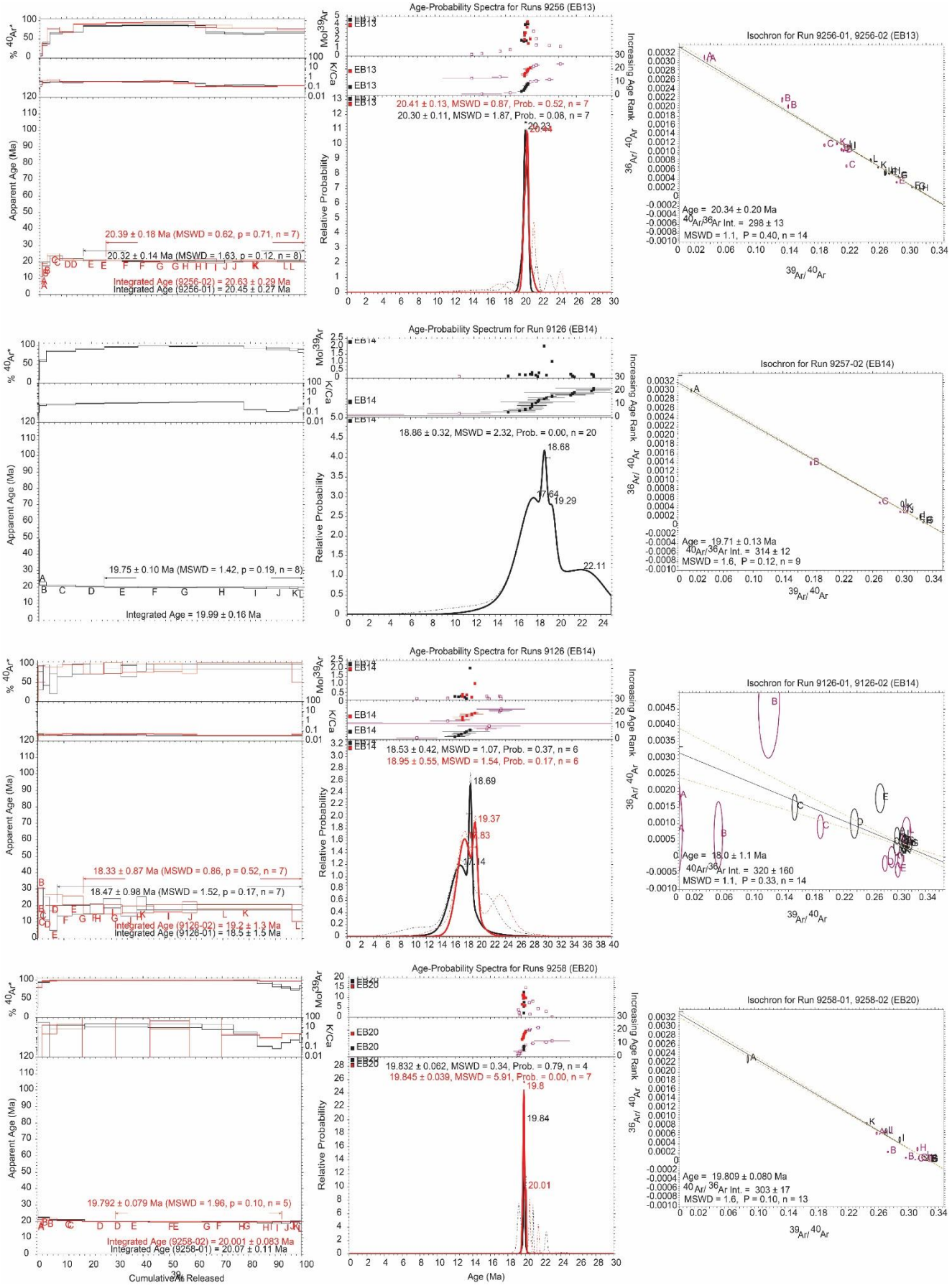

Figure 3.10 cont.: $^{40}Ar/^{39}Ar$ geochronology results for samples from the Ebor province

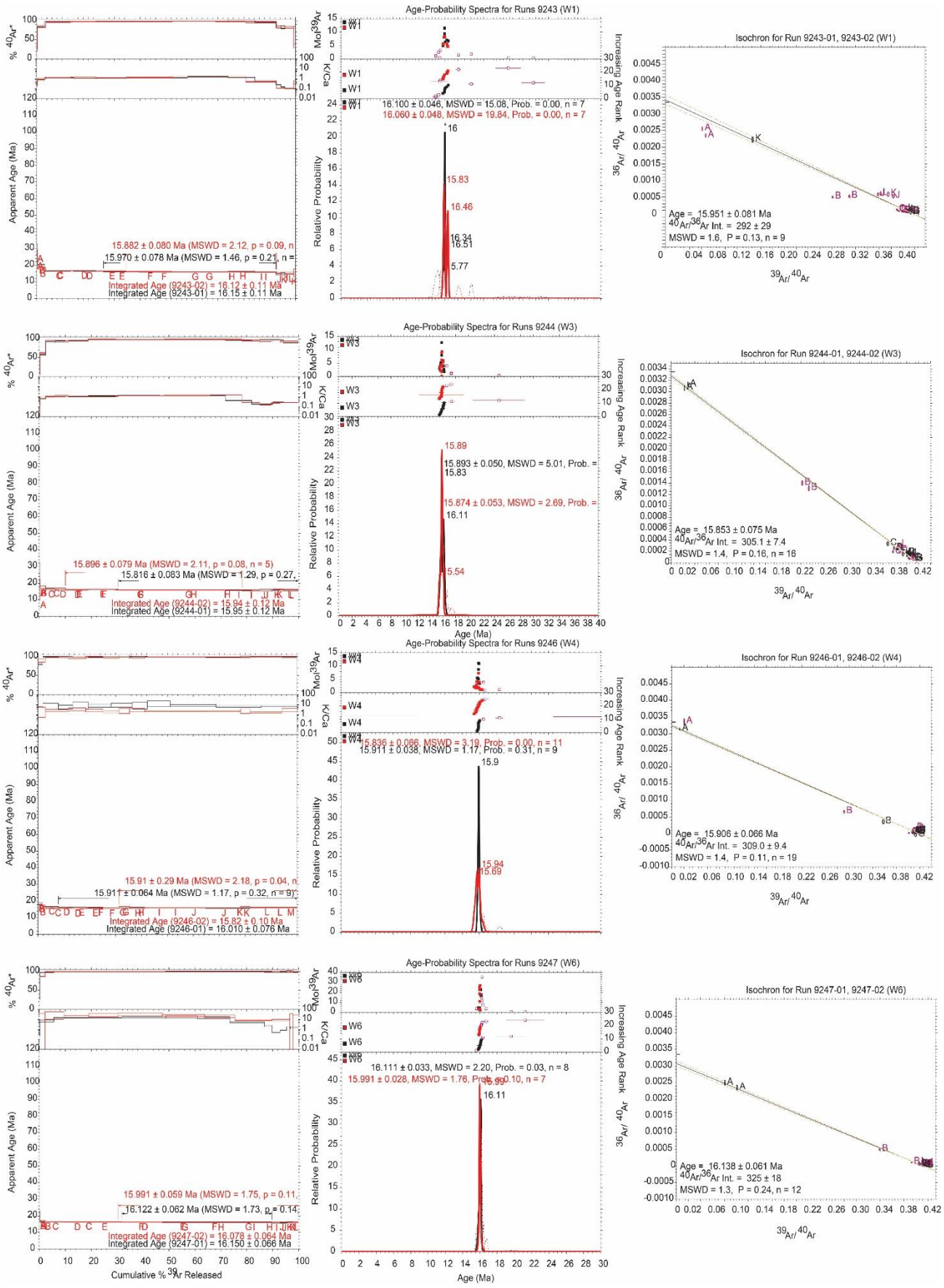

Figure 3.11: $^{40}Ar/^{39}Ar$ geochronology results for samples from the Warrumbungles province

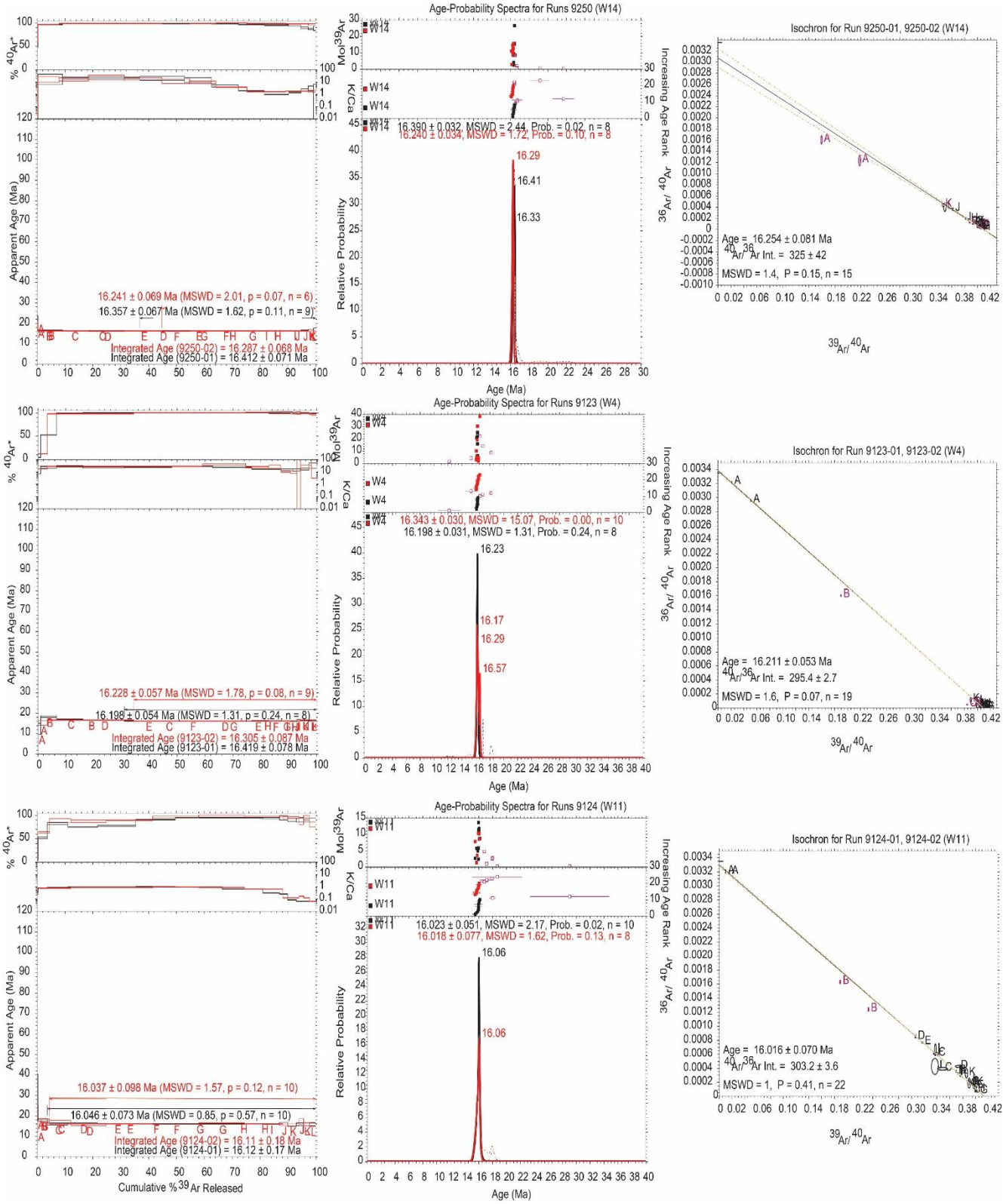

Figure 3.11 cont.: $^{40}Ar/^{39}Ar$ geochronology results for samples from the Warrumbungles province

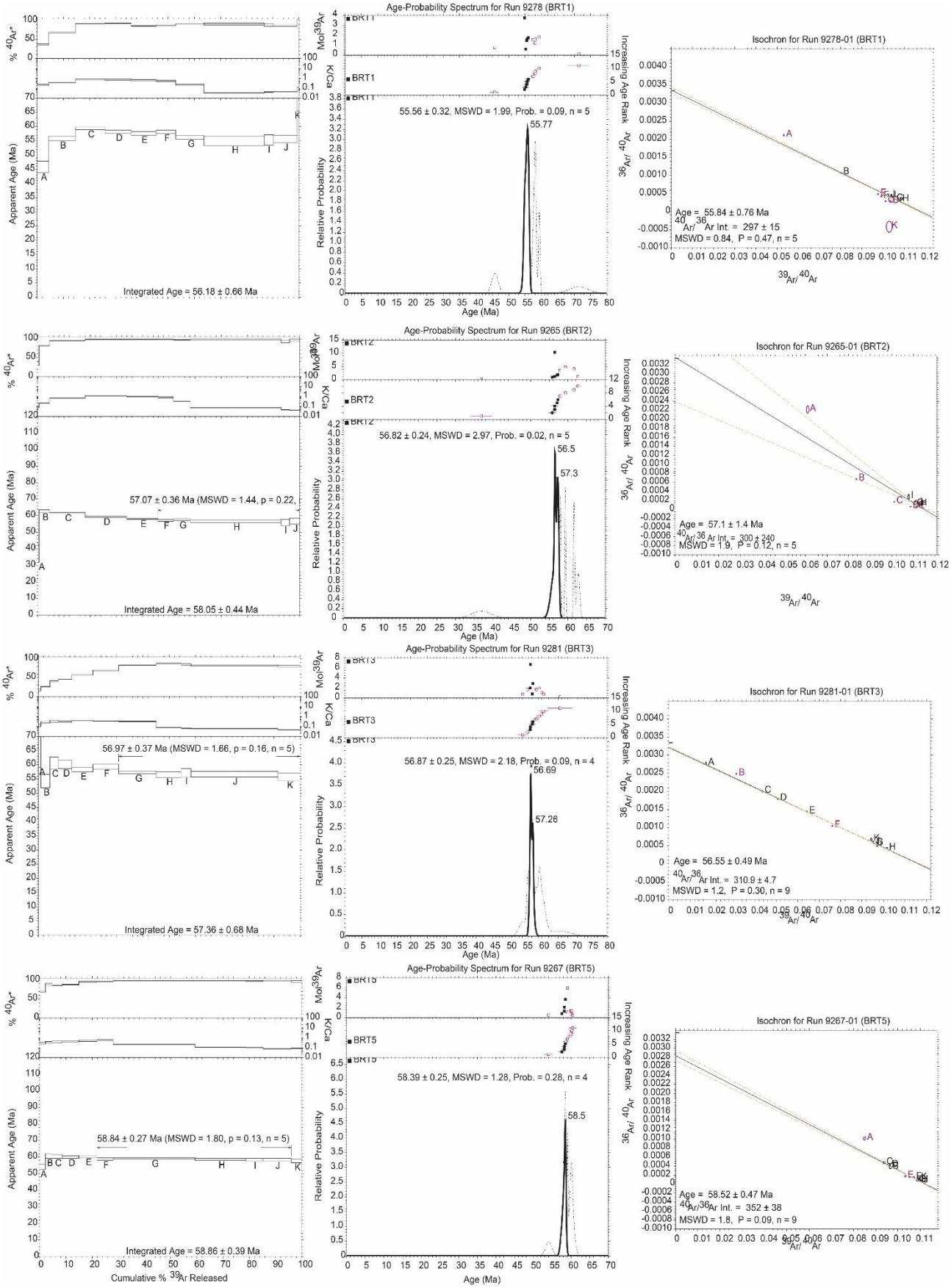

Figure 3.12: $^{40}Ar/^{39}Ar$ geochronology results for samples from the Barrington province

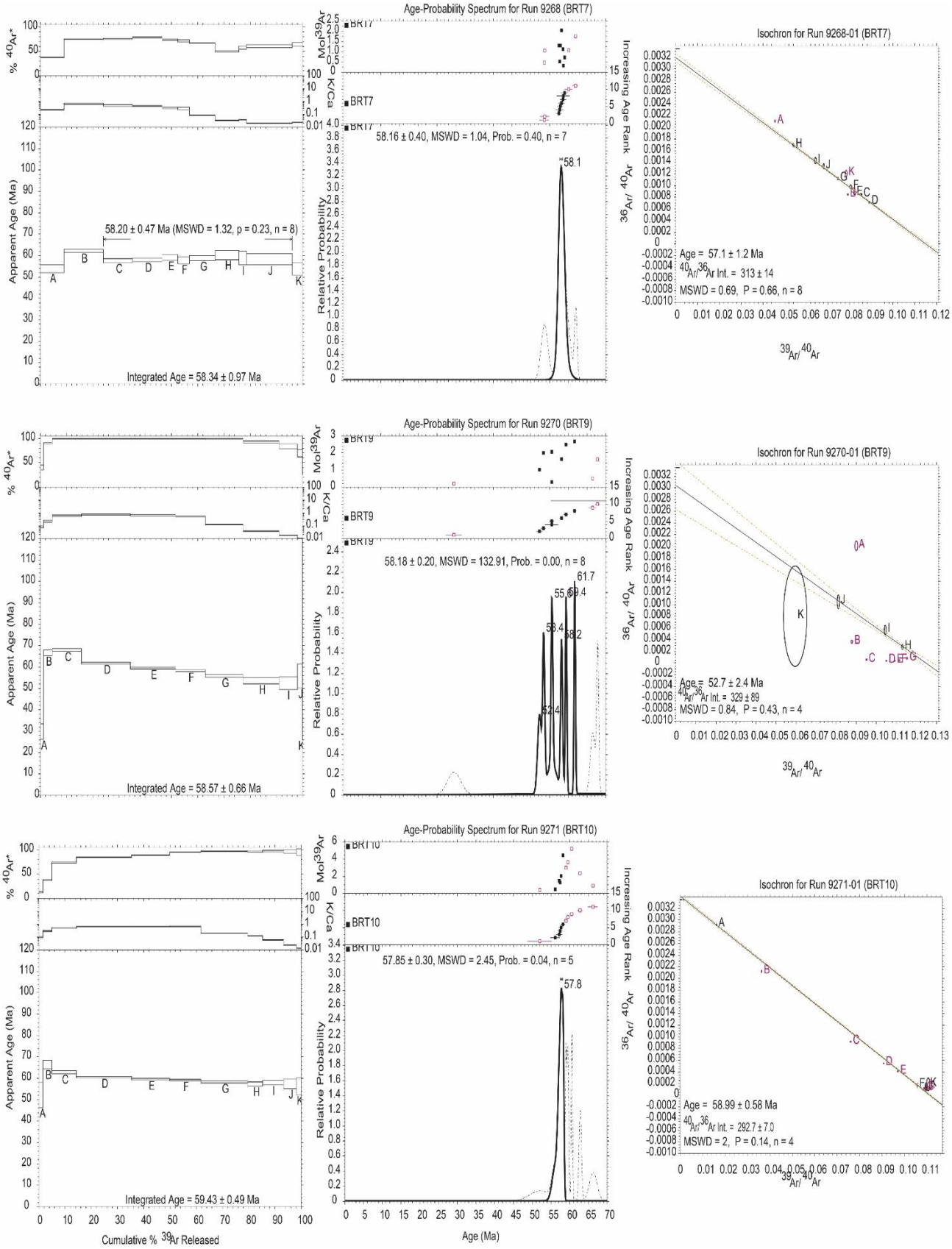

Figure 3.12 cont.: $^{40}Ar/^{39}Ar$ geochronology results for samples from the Barrington province

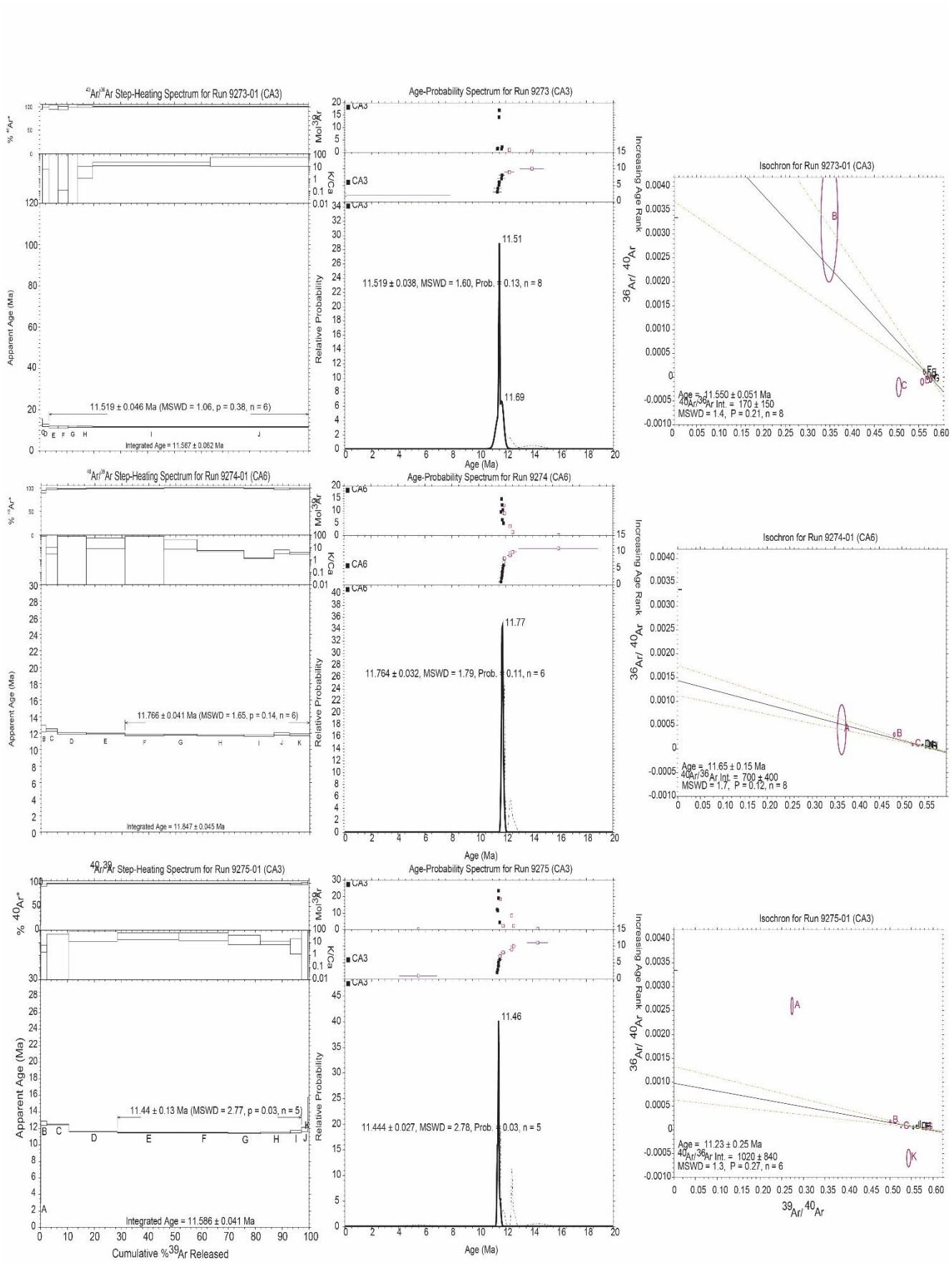

Figure 3.13: $^{40}Ar/^{39}Ar$ geochronology results for samples from the Canobolas province

Table 3.1: $^{40}Ar/^{39}Ar$ geochronology results of mafic and felsic samples from east Australian Cenozoic magmatic provinces

Sample	Location	Run No.	Run ID	Steps	Plateau steps (% gas)	Plateau Age[a]	Integrated age	Ideogram[b]	Combined Isochron age[c]	40Ar/36Ar intercept	Comment
MC1	Mount Catherine, Springsure	137	8739-01	11	D-K	27.02±0.18	26.71±0.21	27.02±0.15	**27.02±0.24**	299±24	
MC2	Mount Catherine, Springsure	137	8740-02	18	F-Q	**27.8±0.2**	27.88±0.31	27.99±0.14	**27.04±0.74**	312±28	
MC5	Mount Catherine, Springsure	137	8742-01	14	F-N	27.98±0.19	27.74±0.39	27.821±0.097	**27.92±0.2**	302±10	Ar-loss
		137	8742-02	14	H-N	27.89±0.18	27.67±0.45				Ar-loss
MC6	Mount Catherine, Springsure	137	8743-01	14	L-N	27.63±0.21	27.32±0.33	27.713±0.078	**27.89±0.18**	285±12	Ar-loss
		137	8743-02	14	H-N	27.78±0.16	27.34±0.36				Ar-loss
MC8	Mount Catherine, Springsure	137	8745-01	14			27.33±0.44	29.35±0.25	**28.41±0.47**	319±17	Ar-loss
		137	8745-02	14			27.4±0.5				Ar-loss
MC9	Mount Catherine, Springsure	137	8746-01	14			25.96±0.45	27.25±0.16	**28.08±0.25**	324±43	Ar-loss
		137	8746-02	14	E-N	**27.47±0.26**	25.2±0.44				Ar-loss
MHV04	Springsure	137	8748-01	14			28.94±0.28	28.225±0.095	**28.10±0.17**	290±10	Recoil
		137	8748-02	14			28.06±0.22				Ar loss
MHV05	Springsure	137	8749-01	12	C-L	27.95±0.13	27.69±0.23	27.997±0.06	**27.99±0.13**	303.7±9	Ar loss
		137	8749-02	12	H-L	27.89±0.13	27.83±0.22				Ar loss
MHV06	Springsure	137	8750-01	12			26.87±0.46	26.9±0.22	**27.27±0.5**	290±20	
		137	8750-02	12	E-L	27.47±0.33	26.6±0.42				Two gas reservoirs appear to have been tapped.
MHV07	Springsure	137	8751-01	12	E-H	27.8±0.14	27.68±0.21	27.781±0.065	**27.84±0.12**	284.3±5.3	
		137	8751-02	12	E-I	27.79±0.13	27.32±0.21				
MHV09	Springsure	137	8761-01	11			28.11±0.17	28.519±0.076	**28.45±0.14**	295±10	
		137	8761-02	11	D-F	28.48±0.14	28.11±0.18				Recoil
MHV10	Springsure	137	8752-01	12	G-L	28.02±0.14	27.50±0.27	27.997±0.072	**27.92±0.14**	295±10	
		137	8752-02	10		27.93±0.16	27.52±0.32				
M01	Moranbah road cutting, Peak Range	137	8753-01	12	F-L	34.8±0.97	37.1±1.5	35.44±0.76	**34.25±0.98**	304.9±8.2	Recoil
		137	8753-02	11			37.0±1.4	35.95±0.48			
GM1	Near Gemini Mountains, Peak Range	137	8754-01	11			30.32±0.49	30.051±0.099	**30.15±0.19**	298±3	
		137	8754-02	11	E-K	29.83±0.2	30.32±0.52				
GM2	Near Gemini Mountains, Peak Range	137	8755-01	13	D-K	29.78±0.52	28.6±2.7	29.82±0.37	**30.86±0.32**	294±1.8	
		137	8755-02	11	I-L	30.63±0.25	30.18±0.68				

GM3	Near Gemini Mountains, Peak Range		137	8756-01	13			30.14±0.65	30.41±0.13	**30.41±0.28**	298.4±4.7	Recoil
			137	8756-02	13			30.69±0.77				
PK01	Policeman's Knob, Hoy		137	8760-01	11			63.69±0.35	65.08±0.17	**53.3±8.9**	2100±2600	Significant excess argon
			137	8760-02	11			63.71±0.36				
KF1	Kilmorey Falls, Mitchell		143	9260-01	11			24.33±0.36	24.82±0.18	**24.2±1.1**	281±62	
KC3	Kalkarney Crator, McBride		143	9276-01	11	C-J	0.38±0.099	0.2±0.23	0.368±0.092	**0.41±0.11**	294.9±8.2	
UR1	Kalkarney Crator, McBride		143	9277-01	11	B-K	0.003±0.09	0±0.2	0.037±0.073	**0.09±0.15**	299±90	
UR2	Road cutting, McBride		143	9279-01	11	C-K	0.234±0.083	0.01±0.22	0.229±0.076	**0.257±0.076**	276±31	
UR3	Road cutting, McBride		143	9280-01	11	A-E	0.88±0.4	0.75±0.38	0.36±0.12	**0.36±0.19**	300.7±2.6	Two gas reservoirs appear to have been tapped.
W1	Siding Spring road, Warrumbungles	143		9243-01	12	E-I	15.970±0.078	16.12±0.11	15.93±0.04	**15.95±0.08**	292±29	Recoil
			143	9243-02	11	F-I	15.882±0.08	16.15±0.11				Recoil
W3	Siding Spring road, Warrumbungles		143	9244-01	12	G-L	15.816±0.083	15.94±0.12	15.865±0.04	**15.85±0.075**	305.1±7.4	
			143	9244-02	12	D-I	15.896±0.079	15.95±0.12				
W4	Siding Spring road, Warrumbungles		143	9246-01	13	D-L	15.911±0.064	16.01±0.076	15.902±0.033	**15.9±0.066**	309±9.4	
			143	9246-02	12	G-M	15.91±0.29	15.82±0.1				
W4	Siding Spring road, Warrumbungles		143	9123-01	12	C-K	16.198±0.054	16.419±0.078	16.211±0.024	**16.211±0.05**	295±2.7	
			143	9123-02	11	E-L	16.228±0.057	16.305±0.087				
W6	Siding Spring road, Warrumbungles		143	9247-01	12	D-H	16.122±0.062	16.150±0.066	16.02±0.024	**16.14±0.06**	325±18	
			143	9247-02	12	F-L	15.991±0.059	16.078±0.064				
W11	Mt Exmouth, Warrumbungles		143	9249-01	12	C-L	14.2±1.1	14.9±1.7	15.41±0.24	**14.76±0.64**	281±23	
			143	9249-02	11	D-J	14.69±0.69	14.9±1.4				
W11	Mt Exmouth, Warrumbungles		143	9124-01	12	C-L	16.046±0.073	16.12±0.17	16.033±0.043	**16.02±0.07**	303±3.6	
			143	9124-02	11	C-L	16.037±0.098	16.11±0.18				
W13	Mt Exmouth, Warrumbungles				12	B-D	16.34±0.09	16.22±0.08	16.32±0.06	16.31±0.06	340±30	
					12	C-K	16.33±0.08	16.49±0.09				Recoil?
W14	Mt Exmouth, Warrumbungles	143		9250-01	12	D-L	16.357±0.067	16.412±0.071	16.347±0.026	**16.25±0.08**	325±42	
			143	9250-02	11	F-K	16.241±0.069	16.287±0.068				
EB1	Ebor		143	9252-01	12	G-L	19.85±0.12	20.30±0.15	19.799±0.05	**19.78±0.11**	303.8±5.1	Recoil
			143	9252-02	12	H-L	19.777±0.099	20.18±0.14				
EB3	Ebor		143	9264-01	11			20.08±0.11	20.188±0.057	**19.78±0.11**	303.8±5.1	
EB5	Ebor		143	9253-01	12			20.28±0.11	20.375±0.048	**20.39±0.09**	376.9±4.4	
			143	9253-02	11	E-H	20.347±0.099	20.33±0.12				

EB8	Ebor	143	9254-01	12			20.169±0.092	20.068±0.037	**20.1±0.08**	293±30	Recoil
		143	9254-02	12	C-J	20.073±0.084	20.333±0.091				
EB11	Ebor	143	9255-01	12	K-M	20.234±0.1	20.4±0.14	20.226±0.05	**20.23±0.11**	291.8±6.2	Recoil
		143	9255-02	13	F-L	20.2±0.12	20.25±0.13				Recoil
EB13	Ebor	143	9256-01	12	E-L	20.32±0.14	20.45±0.27	20.359±0.084	**20.34±0.2**	298±13	Recoil
		143	9256-02	12	F-L	20.39±0.18	20.63±0.29				Recoil
EB14	Ebor	143	9257-01	12	E-L	19.75±0.1	19.99±0.16	19.7±0.12	**19.7±0.13**	314±12	
EB14	Ebor	143	9126-01	12	E-K	18.47±0.98	19.2±1.3	19.755±0.076	**18.0±1.1**	320±160	
		143	9126-02	12	F-L	18.33±0.87	18.5±1.5				
EB20	Ebor	143	9258-01	12			20.07±0.11	19.812±0.035	**19.8±0.08**	303±17	
		143	9258-02	11	E-I	19.792±0.079	20.001±0.083				
BB1	Beechmont basalt, Tweed	143	9259-01	11	F-K	24.38±0.25	24.87±0.12	24.362±0.053	**24.11±0.2**	507±89	Significant excess argon
BRT1	Barrington Tops	143	9278-01	11			56.18±0.66	55.56±0.32	**55.84±0.76**	297±15	Recoil
BRT2	Barrington Tops	143	9265-01	11	F-J	57.07±0.38	58.05±0.44	56.82±0.24	**57.1±1.4**	300±240	
BRT3	Barrington Tops	143	9281-01	11	G-K	56.97±0.37	57.36±0.68	56.87±0.25	**56.55±0.49**	310.9±4.7	
BRT5	Barrington Tops	143	9267-01	11	F-J	58.84±0.27	58.86±0.39	58.39±0.25	**58.5±0.47**	352±38	
BRT7	Barrington Tops	143	9268-01	11	C-J	58.2±0.47	58.34±0.97	58.16±0.4	**57.1±1.2**	313±14	
BRT9	Barrington Tops	143	9270-01	11			58.57±0.66	52.7±2.3	**52.7±2.4**	329±89	Recoil
BRT10	Barrington Tops	143	9271-01	11			59.43±0.49	57.85±0.3	**58.99±0.58**	292.7±7	Recoil
CA3	Canobolas	143	9273-01	10	E-J	11.519±0.046	11.567±0.062	11.519±0.038	**11.55±0.051**	170±150	
CA3	Canobolas	143	9275-01	11	E-I	11.44±0.13	11.586±0.041	11.444±0.027	**11.23±0.25**	1020±840	Significant excess argon within error
CA6	Canobolas	143	9274-01	11	F-K	11.766±0.041	11.847±0.045	11.764±0.032	**11.65±0.15**	700±400	Significant excess argon within error
IJS07	Springsure	129	8424-01	11			28.8± 0.3	30.1± 0.4	**24.9±1.6***	**750 ± 260**	Significant excess argon
		129	8424-02	11			28.8±0.3	30.1± 0.4	**24.9±1.6***	**750 ± 260**	Significant excess argon
								27.7±0.4	**28±0.4**	**340 ± 200**	Significant excess argon within error
IJS08	Springsure	129	8413-01	11	E-K (68.3)	28.6±0.5	28.3±0.3				
		129	8413-02	11	D-K (80.5)	27.6±0.4	28.8±0.3	27.7±0.4	**28±0.4**	**340 ± 200**	Significant excess argon within error
								27.9±0.2	**27.7 ± 0.27**	**308 ± 17**	
IJS11B	Springsure	129	8416-01	11			29.3±0.5				
		129	8416-02	11	F-K (54.8)	27.9±0.3	28±0.5	27.9±0.2	**27.7 ± 0.27**	**308 ± 17**	
								28.0±0.2	**28.23±0.28**	**263 ± 34**	
CVLF01	Springsure	129	8415-01	11	C-G (63.6)	27.8±0.4	27.2±0.4				
		129	8415-02	11	E-K (67.7)	26.2±0.3	27.8±0.3	28.0±0.2	**28.23±0.28**	**263 ± 34**	
								27.93±0.18	**27.95±0.31***	**303 ± 24**	
CIS	Springsure	129	8412-01	11	D-K (62.2)	28±0.3	28.3±0.3				
		129	8412-02	11	F-K (54)	27.9±0.2	28.1±0.3	27.93±0.18	**27.95±0.31***	**303 ± 24**	
								28.15±0.2	**28.18±0.22**	**280 ± 25**	
CIK	Springsure	129	8418-01	11	E-K (77.5)	28.3±0.3	28.6±0.3				
		129	8418-02	11	D-K (85.3)	28.1±0.3	28.1±0.3	28.15±0.2	**28.18±0.22**	**280 ± 25**	
								26.7±0.3	**26.83±0.35**	**298.7 ± 4.6**	
CIB	Bauhinia	129	8422-01	11	C-E (57.2)	27.4±0.6	26.9±1.1				

		129	8422-02	11	A-I (92.8)	26.7±0.3	26.9±0.6	26.7±0.3 25.1±0.8	**26.83±0.35** **22.5±1.8**	**298.7 ± 4.6** **445 ± 43**	Significant excess argon
TRLF01	Bauhinia	129	8421-01	11			29.2±0.7				
		129	8421-02	11			29.5±0.6				
TRLF04	Bauhinia	129	8419-01	11	E-K (67.1)	28±0.3	28.3±0.3	27.8±0.2	**27.98±0.27**	**297 ± 11**	
		129	8419-02	11	E-K (67)	27.9±0.3	28±0.4	27.8±0.2 28.5±1	**27.98±0.27** **27±2.8**	**297 ± 11** **369 ± 95**	
TRLF05	Bauhinia	129	8428-01	11	C-K (50.3)	27.8±1.5	32±1.1				
		129	8428-02	11			33±1.3	28.5±1 25.9±0.2	**27±2.8** **26.03±0.23**	**369 ± 95** **294 ± 28**	
PR01	Peak Range	129	8423-01	11	G-K (69.5)	26±0.3	26.3±0.3				
		129	8423-02	11	F-K (74.4)	25.9±0.3	26.2±0.3	25.9±0.2 33.5±0.3	**26.03±0.23** **33.27±0.4***	**294 ± 28** **315 ± 43**	
PR02	Peak Range	129	8427-01	11	F-K (53.4)	32±0.6	33.6±0.5				
		129	8427-02	11	D-K (79)	33.3±0.4	33.3±0.4	33.5±0.3 47.2±0.4	**33.27±0.4*** **47.02 ±0.53**	**315 ± 43** **303.7 ± 8.3**	
PR04	Peak Range	129	8426-01	11	B-J (88.7)	47.1±0.6	46.6±0.9				
		129	8426-02	11	B-I (85.8)	47.4±0.5	47.3±1	47.2±0.4 31.8±0.3	**47.02 ±0.53** **31.63±0.34**	**303.7 ± 8.3** **292 ± 15**	
PR05	Peak Range	129	8425-01	11	D-K (68.2)	31.8±0.5	32.8±0.6				
		129	8425-02	11	D-K (78.1)	31.5±0.4	32.2±0.5	31.8±0.3 34.2±0.4	**31.63±0.34** **34.66±0.41**	**292 ± 15** **286 ± 16**	
PR07	Peak Range	129	8433-01	11	B-G (77.4)	34.6±0.5	33.7±0.5				
		129	8433-02	11	C-K (95)	34.9±0.5	34.1±0.7	34.2±0.4 44.8±0.3	**34.66±0.41** **44.65±0.4**	**286 ± 16** **311 ± 19**	
PR08	Peak Range	129	8434-01	11	E-K (58.6)	44.5±0.4	43.7±0.6				
		129	8434-02	11	B-I (86.9)	45±0.3	43.8±0.5	44.8±0.3 45.1±0.30	**44.65±0.4** **44.98±0.36**	**311 ± 19** **313 ± 6**	
PR09	Peak Range	129	8436-01	11	D-K (85.3)	45.1±0.5	45.8±0.9				
		129	8436-02	11	D-I (83.6)	45.3±0.4	45.8±0.9	45.1±0.30 29.5±0.2	**44.98±0.36** **29.08±0.38***	**313 ± 6** **296 ± 13**	
AA2	Monto	129	8429-01	11	D-K (69.3)	29.1±0.4	29.5±0.6				
		129	8429-02	11	C-E (53.3)	30.2±0.4	30±0.4	29.5±0.2	**29.08±0.38***	**296 ± 13**	

a) For the purposes of this study, a plateau age is defined as 3 or more consecutive steps, in which at least 50% of the total 39Ar was released, and overlap of ages within the 95% confidence interval (Fleck et al., 1977). Errors are calculated based on the mean weight by inverse variance and include errors in irradiation correction factors and J. All plateau definitions use error-overlap (2σ).

b) The Ideogram is an age-probability plot where age is given by the weighted mean of both grains. The error is given to 2σ, and is based on the standard error of the probability mean.

c) Isochron ages are measured at the 95% confidence level (2σ). Isochron age errors do not include the uncertainty in the potassium decay constant, however cover errors in irradiation correction factors and J. Where two grains were analysed, the isochron includes their combined ages.

* Isochron from single grains

Chapter 4: Animated reconstructions of the Late Cretaceous to Cenozoic northward migration of Australia, and implications for the generation of east Australian mafic magmatism

This chapter was published in Geosphere and is reproduced here with permission of the Geological Society of America under their fair use guidelines:

'An author has the right to use his or her article or a portion of the article in a thesis or dissertation without requesting permission from GSA, provided the bibliographic citation and the GSA copyright credit line are given on the appropriate pages.'

https://www.geosociety.org/GSA/Publications/Info_Services/Copyright/GSA/Pubs/guide/copyright.aspx#fair

Jones, I., Verdel, C., Crossingham, T., and Vasconcelos, P. (2017). Animated reconstructions of the Late Cretaceous to Cenozoic northward migration of Australia, and implications for the generation of east Australian mafic magmatism. *Geosphere*, *13*(2), 460-481.

4.1 Introduction

The generation of basalts is frequently ascribed to the processes of rifting and hotspot activity (e.g., *Wilson,* 1963; *White and McKenzie,* 1989). The Late Cretaceous through Cenozoic magmatic history of eastern Australia is potentially somewhat unique in that it includes periods of what have been previously described as both rift- and hotspot-related basaltic magmatism that overlapped in time and space (Fig. 4.1; e.g., *Wellman and McDougall,* 1974a; *Cohen et al.,* 2007; *Vasconcelos et al.,* 2008). Cenozoic "rift-related" mafic volcanism in eastern Australia has been attributed to the Paleogene opening of the Tasman and Coral Seas (Fig. 4.2; *O'Reilly and Zhang,* 1995). In apparent contrast, a series of on- and off-shore, age-progressive, bimodal shield volcanoes that decrease, at least in part, in both age and volume to the south were attributed in chapter 2 to the northward motion of Australia over stationary and irregularly active (but primarily waning) mantle plumes (e.g., *Wellman and McDougall,* 1974a; *Cohen et al.,* 2007; *Sutherland et al.,* 2012*; Jones and Verdel,* 2015). Detailed $^{40}Ar/^{39}Ar$ geochronological studies of these age-progressive volcanoes have previously been used to quantify plate velocity and, in doing so, have revealed Cenozoic periods of anomalously slow plate motion (*Knesel et al.,* 2008; *Cohen et al.,* 2013). In particular, an apparent late Oligocene to early Miocene period of significant plate slowdown has previously been linked to docking of the Ontong Java Plateau (OJP; Fig. 4.2) with the Solomon Islands (*Knesel et al.,* 2008).

Several previous studies have used paleomagnetic data to reconstruct the Cenozoic motion of Australia. From these studies, two general types of apparent polar wander paths (APWPs) have emerged: a "linear" path (i.e., an APWP with latitudinal changes but little variation in longitude; Fig. 4.3a; *Idnurm,* 1985; *Musgrave,* 1989) and a competing "longitudinal" path that includes significant variation in longitude (Fig. 4.3b; *Embleton and McElhinny,* 1982). The linear APWP is largely based on paleomagnetic data from sedimentary basins and laterites, and it is consistent with the northward trajectory of India (*Idnurm,* 1985). However, paleomagnetic data from sedimentary and lateritic profiles can suffer from inclination-shallowing and (particularly in the case of laterites) a complex history of inheritance and crystallisation of magnetic minerals that could result in over-smoothing of APWPs (*Butler,* 2004; *Vasconcelos et al.,* 2008). In contrast, the longitudinal APWP is based largely on paleomagnetic data from a combination of basalts and laterites (*Embleton and McElhinny,* 1982). The longitudinal APWP includes a significant westward diversion during Miocene time (Fig. 4.3b), a potential artefact that could have arisen from the failure of some previous paleomagnetic studies to

account for paleosecular variation of the Earth's magnetic field (*Idnurm*, 1985). Alternatively, this diversion in the APWP may be accurate, and it may correspond with the eastward offset of the Lord Howe and Tasmantid seamount chains (Fig. 4.1), as well as the initial "soft-docking" of the OJP with the Solomon Islands (*Knesel et al.*, 2008).

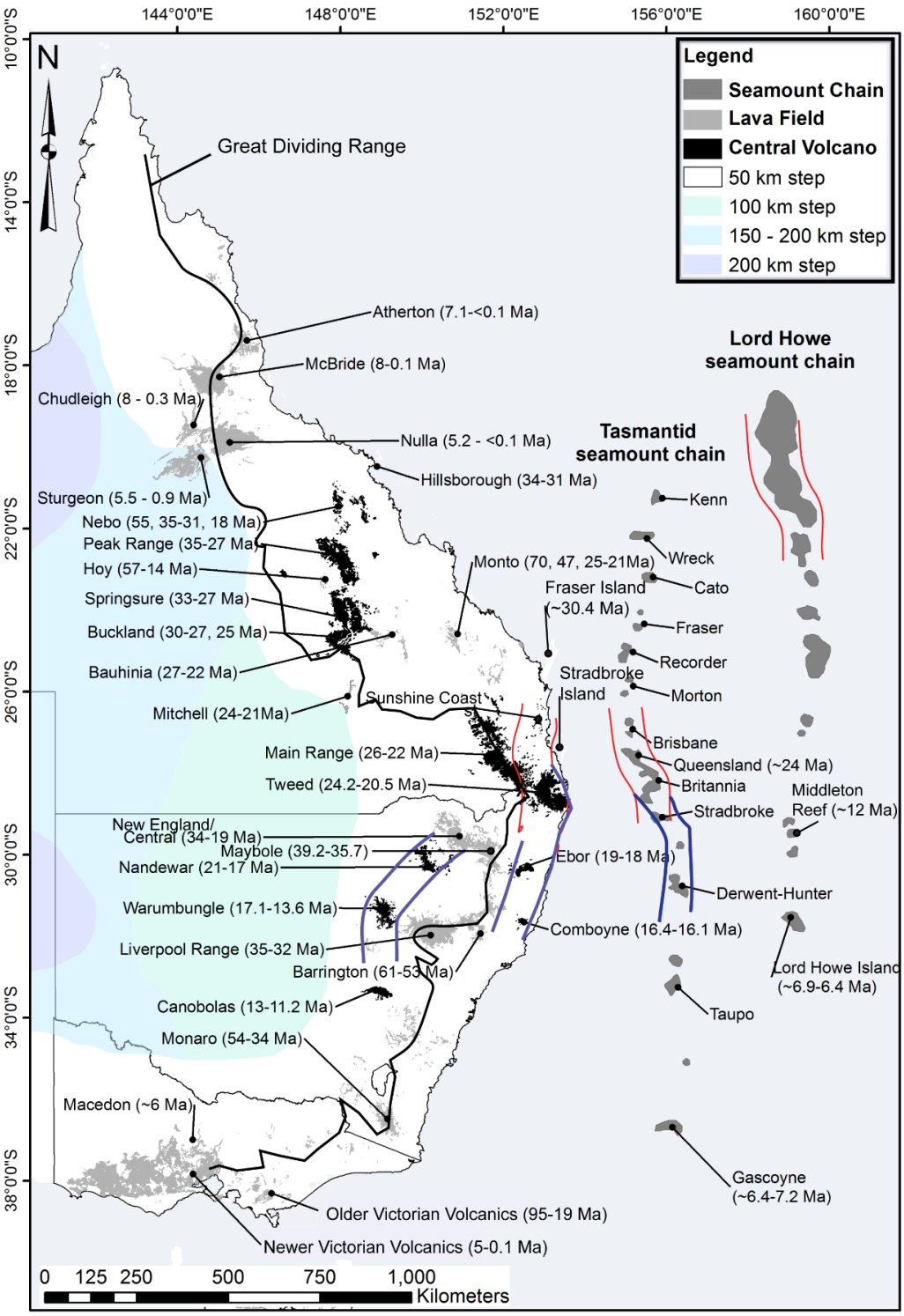

Figure 4.1: Map of Eastern Australia showing onshore (central volcanoes and lava-fields) and offshore (Tasmantid and Lord Howe Rise seamount chains) volcanic provinces. Red boundaries

indicate apparent 25 Ma kink (Knesel et al., 2008), while blue boundaries represent apparent change in plume pattern after slowdown period. Age ranges from Duncan and McDougall (1989) and Vasconcelos et al. (2008), using both K-Ar and Ar/Ar. Stepped lithospheric boundary after Fishwick et al. 2008. Geological unit data after Raymond et al. (2012).

The generation of east Australian Cenozoic basalts, as well as the conflicting APWPs of the Australian Plate described above, are thus fundamental components of the overall Cenozoic tectonic history of Australia and the SW Pacific. Cenozoic plate reconstructions are therefore powerful tools for clarifying the relationship between tectonic and magmatic events that shaped the Australian continent, Papua New Guinea (PNG), the Solomon Islands, the OJP, and the Tasman and Coral Seas (Fig. 4.2). In this study, I use a combination of plate reconstructions and $^{40}Ar/^{39}Ar$ geochronology to test both the competing Cenozoic APWPs and the relationship of volcanism to plate motion. I used G-PLATES to create two Late Cretaceous through Cenozoic plate reconstructions that correspond with the linear and longitudinal APWPs. I assessed these two reconstructions, and thus the APWPs on which they are founded, by evaluating whether they reproduce two key geologic and tectonic observations: (1) an eastward offset in the Lord Howe and Tasmantid seamount chains (*Knesel et al.,* 2008); and (2) a reduction in the velocity of Australia between 26 and 23 Ma, which coincides with anomalously high volume and eruption rates of the Tweed shield volcano (Fig. 4.1; e.g., *Knesel et al.,* 2008; *Cohen et al.,* 2013). Additionally, I evaluate the agreement between these APWPs and the global moving hotspot reference frame model of Doubrovine et al. (2012).

4.2 Geological Background

4.2.1 Cenozoic Volcanism in Eastern Australia

The key attribute used to distinguish the two primary groups of Cenozoic volcanism in east Australia is that central volcanoes, although dominantly basaltic, include a component of felsic flows and/or intrusions, whereas lava-fields are nearly entirely basaltic, with a few exceptions of limited felsic flows (*Wellman and McDougall,* 1974a; *Sutherland et al.,* 2014). It is the age progression of the central volcanoes, forming a series of N-S chains of bimodal shield volcanoes along the east coast of Australia, that defines the northward motion of the Australian plate (Fig. 4.1; *Wellman and McDougall, 1974a,* 1974b; *Sutherland et al.*, 2012; *Davies et al.,* 2015). The volcanic tracks run parallel down the east coast of Australia, though the inland track at the latitude of Buckland appears to end at ~27 Ma (Fig. 4.1; e.g., *Wellman and McDougall,* 1974a; *Sutherland et al.,* 2012). It is suggested that the track resurfaces in central NSW as a

series of leucite-bearing basaltic provinces of Miocene age, and it continues south through Victoria to the Bass Strait (*Sutherland*, 1981; *Cohen et al.*, 2008; *Davies et al.*, 2015).

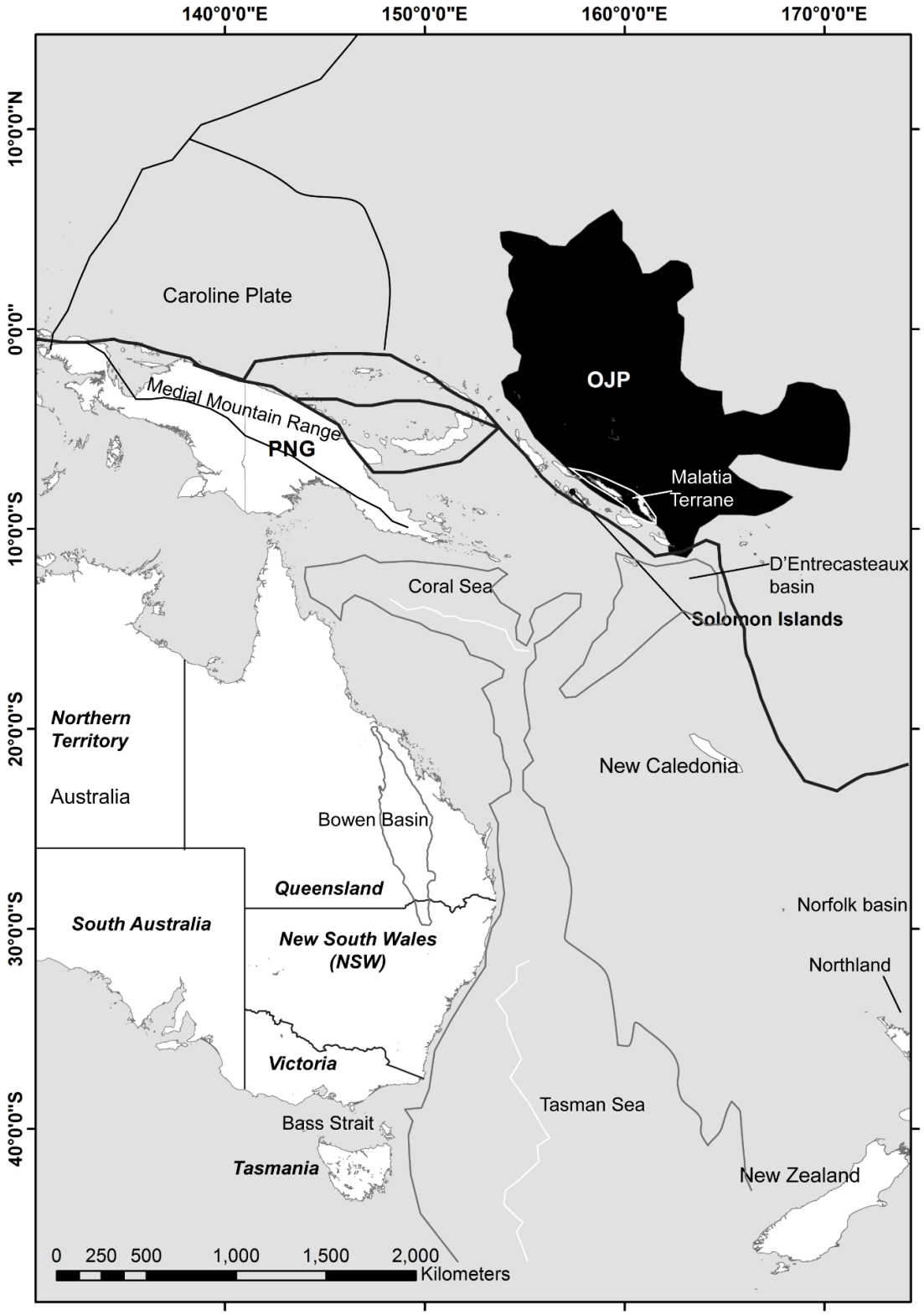

Figure 4.2: A simplified tectonic map of the SW Pacific.

Approximately 500 km east of Buckland, a second, "coastal track" of central volcanoes is exposed at Fraser Island (Fig. 4.1), which is characterised by 30.4±0.2 Ma mafic magmatism. The coastal track continues south from Fraser Island through New South Wales, although the number of tracks involved is debatable (*Sutherland et al.*, 2012). The youngest exposure of any central volcano is the ~6 Ma Macedon-Trentham province in Victoria (Fig. 4.1; *Sutherland et al.*, 2014). Based on $^{40}Ar/^{39}Ar$ ages of the final felsic products erupted from each central volcano, the overall N-S chains form age-progressive tracks that become younger to the south (*Cohen et al.*, 2013). The age progression of the central volcanoes is mirrored by the offshore Tasmantid and Lord Howe seamount chains (Fig. 4.1), and all of the east Australian volcanic tracks have been previously ascribed to the Cenozoic northward passage of the Australian Plate over multiple stationary thermal anomalies (*Wellman and McDougall*, 1974a; *McDougall and Duncan*, 1988; *Cohen et al.*, 2007; *Sutherland et al.*, 2012; *Davies et al.*, 2015).

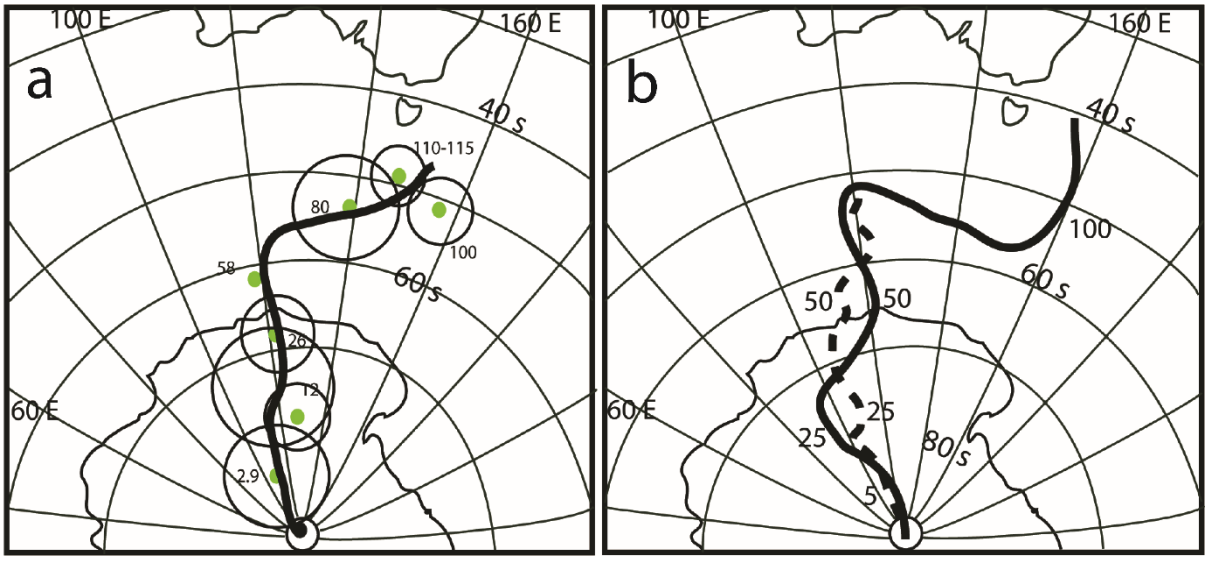

Figure 4.3: Australian Cenozoic apparent polar wander paths after a) Idnurm (1985), using primarily sedimentary basins and laterites; and b) Embleton and McElhinny (1982), using igneous rocks and laterites. Solid line is data prior to digital smoothing, and dashed represents the final product that I here use in the reconstruction.

Lava-fields are generally considered to contrast with central volcanoes in that lava-fields are not bimodal, shield-building, or age-progressive, but nevertheless they often overlap temporally with central volcanoes or are adjacent to central volcanoes (*Wellman and McDougall*, 1974a and 1974b; *Cohen et al.*, 2007). These previously described distinctions notwithstanding, several lava-fields include evolved lithologies ranging from trachytes (Newer

Victorian Volcanics) and maugerites (e.g., Liverpool, Walcha and New England) to phonolites (McBride and Maybole [part of New England]). Additionally, some lava-fields (e.g., Barrington) are remnants of shield volcanoes (*Johnson et al.*, 1989). The onset of volcanism in the lava fields is roughly coeval with rifting between Australia and Antarctica (95 Ma; *Cande and Mutter, 1982*; *Sayers et al.*, 2001) and the opening of the Tasman Sea (84 Ma; Fig. 4.2; *O'Reilly and Zhang,* 1995; *Gaina et al.*, 1998b; *Sutherland et al.*, 2012). However, many lava-field provinces were active long after rifting of those ocean basins ceased (e.g., the North Queensland lava-fields erupted from ~8 Ma to Recent; Fig. 4.1; *Wyatt and Webb*, 1970; *Griffin and McDougall*, 1975; *Stephenson et al.*, 1980). Previous explanations for lava-field generation include decompression melting associated with rifting, as well as the ascent of diapers and mafic underplating from an anomalously hot asthenosphere (*Johnson et al.* 1989). However, no conclusive evidence of Cenozoic underplating has been recognised (*Johnson et al.* 1989), and neither of these explanations accounts for the absence of conjugate magmatism in eastern Gondwana rifted fragments that now lie to the east of the Coral and Tasman Seas.

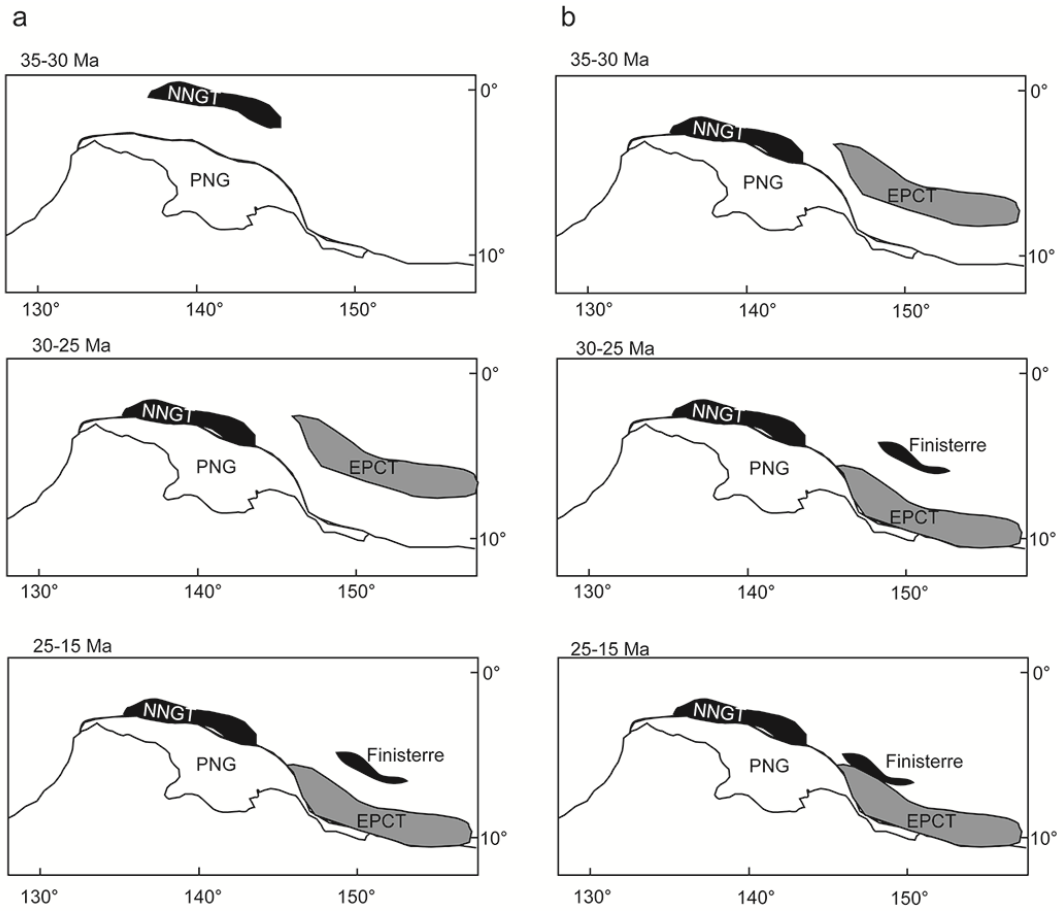

Figure 4.4: Simplified reconstructions of collision between PNG and the composite terranes after a) Pigram and Davies (1987) showing late Oligiocene through Miocene collision and b) early Oligocene through early Miocene accretion of composite terranes after Davies et al. (1997).

Distances are approximate. NNGT = North New Guinea Terranes and EPCT = East Papua composite terrane.

A series of lava-fields extend in an east-west alignment between the inland and coastal central volcanic chains in the region between Buckland and Main Range (Fig. 4.1). The spatial and temporal association of these particular lava-fields with the neighbouring central volcanoes blurs the distinctions between "rift-related" and "plume-related" magmatism in eastern Australia. In this study I contribute new $^{40}Ar/^{39}Ar$ data from the largest of these lava-fields (Bauhinia and Monto; Fig. 4.1), as well as from basalts of the nearby, but putatively distinct, central volcanoes of Peak Range and Springsure (Fig. 4.1). Similar lava-field provinces, such as the western portion of the New England (formally Central) Province, exhibit no time-space correlation, but they do share isotopic characteristics with nearby central volcanoes (*Vickery et al.,* 2007) and have since been included in some depictions of age-progressive tracks (*Sutherland et al.* 2012).

4.2.2 Collisional tectonics in the SW Pacific during the Cenozoic

4.2.2.1 Docking of the Ontong Java Plateau with the Solomon Islands

The past motion of the OJP may be directly relevant to the Cenozoic motion of the Australian Plate and the distribution of some of the east Australian central volcanoes (e.g., *Knesel et al.,* 2008). The OJP lies to the north of the Solomon Islands (Fig. 4.2) and was originally part of the larger Ontong Java-Manihiki-Hikurangi Plateau (e.g., *Taylor,* 2006). Break-up of this earlier plateau and subsequent NW drift of the OJP to its current position occurred during the Cretaceous and Cenozoic (*Taylor,* 2006), although the timing of its collision with the Solomon Islands remains contentious (e.g., *Yan and Kroenke,* 1993; *Petterson et al.,* 1999; *Mann and Taira,* 2004; *Holm et al.,* 2016). A hiatus of arc magmatism in the Solomon Islands suggests that docking of the OJP and subsequent blocking of the subduction zone occurred between 25 and 20 Ma (*Petterson et al.,* 1999), leading to subduction on the northern side of the OJP by 12 Ma (*Yan and Kroenke,* 1993). Plate reconstructions coupled with an eruption hiatus in the Solomon Islands arc suggest early Miocene docking (*Yan and Kroenke,* 1993; *Hall,* 2002), but, because the original extent of OJP is unknown, it is possible that its leading edge was subducted before 20 Ma (*Hall,* 2002; *Holm et al.,* 2013). However, other studies have concluded that there was no cessation in subduction (and hence no contact between the Solomon Islands and OJP) until ~5 Ma (e.g., *Mann and Taira,* 2004). Even accounting for subduction of the leading edge

of the OJP, paleomagnetic evidence from both the OJP and the accreted Malaita terrane at the Solomon Islands constrains the collision to ~20 Ma (*Musgrave*, 2013), and there is no substantial geological evidence of a ~25-20 Ma collision in the Solomon Islands (*Mann and Taira*, 2004; *Holm et al.* 2013; *Musgrave,* 2013).

4.2.2.2 Collision of Papua New Guinea with the Medial Mountains subduction zone and the New Guinea Composite Terranes

Changes in the Cenozoic motion of Australia may have also been related to interactions between PNG and tectonic elements to the north. During the early Miocene, the PNG-Australian plate boundary terminated where the Medial Mountain System is currently located (Fig. 4.2; *Hamilton,* 1979). To the north of the boundary was a north-dipping Medial Mountains subduction zone and an active island arc system. A complex history of oblique continent-arc collisions is recorded on the New Guinea peninsula, including several collisions in the Eocene, Oligocene, and perhaps early Miocene (*Hall,* 2002; *Baldwin et al.,* 2012). The timing and number of continent-arc collisions are matters of debate: some studies have suggested that composite terranes were formed before collision, while other studies argue for separate collisional events for each arc (Fig. 4.4; *van Ufford and Cloos,* 2005; *Baldwin et al.,* 2012). For simplicity, I consider the collision of the composite terranes, rather than individual arcs. The Sepik Terrane accreted in the early Oligocene (Hill and Hall, 2003), and the Philippines-Halmahera arc accreted in the late Oligocene (~25 Ma; *Hill and Hall,* 2003). These terranes form part of what I refer to as the North New Guinea Terranes (Fig. 4.4; *Pigram and Davies,* 1987; *Crowhurst et al.,* 1996; *Davies,* 2012; and *Holm,* 2013). During the late Oligocene to middle Miocene, the continental crust of PNG collided with the East Papua Composite Terrane (*Pigram and Davies,* 1987) and a series of Paleogene island arcs (*Jaques and Robinson,* 1977; *Gaina and Müller,* 2007; *Davies,* 2012). The timing of the Finnisterre Arc collision is possibly the most contentious. Some studies suggest a single collision at ~5 Ma (*Abbott et al.,* 1994), while other studies propose two separate collisional events: the collision of the Finnisterre Arc with PNG in the middle Miocene, and a subsequent Pliocene collision between the Finnisterre Arc and Bismark Arc (*Pigram and Davies,* 1987). Collision of PNG with these exotic terranes progressively led to cessation and subsequent reversal of the subduction zone (*Jaques and Robinson,* 1977; *Baldwin et al.,* 2012).

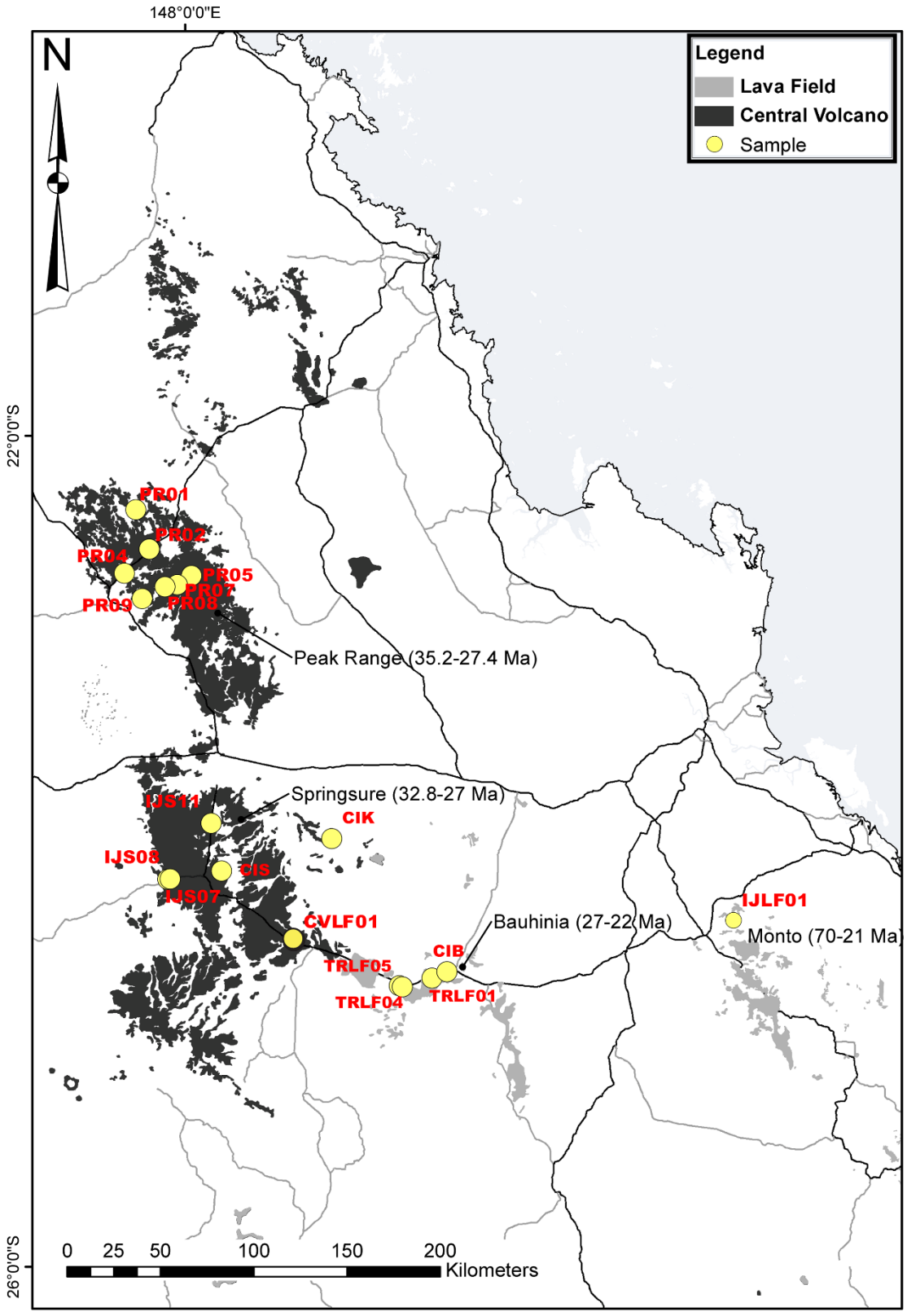

Figure 4.5: Location of samples taken from the Peak Range, Springsure, Bauhinia and Monto provinces.

4.2.2.3 *Slab tearing and detachment at the Loyalty arc*

The detachment of the Loyalty slab may have also affected the pattern of Cenozoic mafic magmatism in eastern Australia (*Sutherland et al.,* 2012; *Cohen et al.,* 2013). Previous studies have described an extinct northeast- to east-dipping subduction zone to the north of New Caledonia (e.g., *Schellart et al.,* 2006; *Schellart et al.,* 2009). The subduction zone extended from the transform boundary at d'Entrecasteaux past New Caledonia to Northland (Fig. 4.2). During the late Eocene-early Oligocene, a series of ophiolites and terranes were obducted onto New Caledonia (*Aitchison et al.,* 1995), followed by obduction onto Northland between 24 and 21 Ma (*Mortimer et al.,* 2003). Toward the end of the subduction period, sub-horizontal tearing of the slab is believed to have taken place, resulting in slab detachment at 30 Ma in the north and 24 Ma in the south (*Schellart et al.,* 2009). Detachment of the slab induced magmatism along the subduction zone, resulting in volcanism in the Norfolk Basin, New Caledonia, and Northland (*Schellart et al.,* 2009).

The timing of proposed slab tearing roughly coincides with a major period of Cenozoic volcanic activity in eastern Australia. Sutherland et al., (2012) suggested that east Australian volcanism was related to perturbed mantle flow from progressive tearing of the slab during detachment. They argued that opening of a slab window during detachment could cause asthenospheric mantle convective swells and related volcanism. Cohen et al., (2013) came to a different conclusion, arguing that greater plate velocities during the Oligocene could be due to the initiation of slab tearing between 29 and 28 Ma.

4.3 Methods

4.3.1 Geochronology Compilation

In order to include east Australian volcanism in the tectonic reconstructions, I compiled a dataset of previous geochronological results from east Australian central volcanoes and lava-fields, largely compiled by Vasconcelos et al., (2008). I incorporated additional published U-Pb (*Sutherland et al.,* 2012; *Sutherland et al.,* 2014), K-Ar (*Wyborn and Owen*, 1986; *Grey and McDougall,* 2009) and $^{40}Ar/^{39}Ar$ geochronology results (*Matchan and Phillips,* 2011; *Cohen et al.,* 2013*; Sutherland et al.,* 2014) and, as described in detail below, I added new $^{40}Ar/^{39}Ar$ data from four key east Australian volcanic provinces (Peak Range, Springsure, Bauhinia, and Monto; Fig. 4.5). U-Pb ages that were in agreement with corresponding zircon fission track and K-Ar ages from the same volcanoes were included in the dataset, unless the

authors noted Pb contamination, loss of Pb, or if there was evidence of zircon inheritance (*Sutherland and Fanning*, 2001). K-Ar data were used only when there were insufficient $^{40}Ar/^{39}Ar$ results for comparison. K-Ar data that were considered unreliable by the original authors were excluded, as were K-Ar results that did not agree with $^{40}Ar/^{39}Ar$ ages from the same formation or sample, particularly if argon loss, recoil, or excess argon had been identified by the authors.

4.3.2 $^{40}Ar/^{39}Ar$ Geochronology

Eighteen mafic samples from the Peak Range (7 samples), Springsure (6 samples), Bauhinia (4 samples), and Monto (1 sample) volcanic provinces were selected for $^{40}Ar/^{39}Ar$ geochronology (Fig. 4.5). The samples were collected from roadcuts and other outcrops in an approximately east-west transect across the Bowen Basin. Samples were crushed in a tungsten-carbide percussion mill, and whole-rock crushed fragments (~1 mm^3) were cleaned using distilled water and ethanol in an ultrasonic bath and hand-picked under a binocular microscope. Approximately five fragments from each sample were loaded into a 21-pit aluminium disk, as per Vasconcelos et al. (2002). Sanidine from the Fish Canyon Tuff (age of 28.201±0.04 Ma; *Kuiper et al.,* 2008) and GM1550 (biotite; 98.79 ± 0.96; *Renne et al.,* 1998) were also loaded as secondary standards. The disks were irradiated for 14 hrs in the CLICIT facility TRIGA-type reactor at Oregon State University. Two whole-rock aliquots were analysed for each sample on a MAP 215-50 mass spectrometer in the University of Queensland Argon Geochronology in Earth Sciences Laboratory (UQ-AGES). Samples were continuously heated with an Ar-ion laser with a defocused beam, as outlined in Vasconcelos (1999) and Vasconcelos et al. (2002). To constrain the accuracy of the $^{40}Ar/^{39}Ar$ results of the whole rock aliquots, two grains of GA1550 biotite from each irradiation disk were also analysed by the incremental-heating method. Additional details of the $^{40}Ar/^{39}Ar$ procedure are available in Chapter 3.

4.3.3 Animated Reconstruction

Two animated reconstructions were created using G-PLATES software (version 1.5.0). The "linear" reconstruction used the base reconstruction rotation file compiled by Seton et al. (2012), which consists of a database of the last 200 million years of rotation. Continents within the region, the Cenozoic volcanic provinces, the New Guinea composite terranes, and the OJP were digitised in their present day locations, linked to the overall rotation of their respective

tectonic plates, and reconstructed to their previous positions. Active central volcanoes are shown in orange in these reconstructions, and lava-fields are shown in blue. Inactive provinces change to black. Red dots signify the locations and approximate ages of dated samples and give an idea of overall volcanic activity. The PNG terranes remain dark blue until their contact with continental New Guinea. Magnetic anomaly lines change from red to green as they increase in age, and inactive rift-zones are blue. While the initial positions of the North New Guinea Terranes and East Papua Composite Terrane are unknown, the collisional timing of these terranes with PNG is well-constrained (*Pigram and Davies,* 1987; *Davies,* 2012). Both terranes have been reconstructed relative to the Caroline Plate (Fig. 4.2; *Gaina and Müller,* 2007), but their reconstruction is only approximate (*Pigram and Davies,* 1987; *Hill and Hall,* 2003; *Davies,* 2012).

A second reconstruction, the "longitudinal" reconstruction, was created using a paleomagnetic path for the Australian continent after 60 Ma based on data produced and compiled by Embleton and McElhinny (1982) after Wellman et al. (1969), Rahman (1971), and Wellman (1975). The model included virtual geomagnetic poles (VGPs) at 4.5, 15, 22, 25, 30, 50 and 60 Ma. The 15, 25, 30, 50, and 60 Ma poles are from a corrected lateritic profile (*Embleton,* 1981). A plate reconstruction pole was generated using these VGPs. To prevent the violation of relative plate boundaries that are assumed fixed, the reconstruction tree was arranged so that all other plates move relative to Australia.

4.4 Results

4.4.1 $^{40}Ar/^{39}Ar$ Geochronology

The samples selected for $^{40}Ar/^{39}Ar$ geochronology contained euhedral to subhedral olivine (15-30%), clinopyroxene (5-10%), and plagioclase (10-20%) phenocrysts in a groundmass (30-60%) of olivine, clinopyroxene, and plagioclase ± orthopyroxene (Fig. 4.6). In several samples, olivine was altered to iddingsite, and plagioclase was altered to sericite. Because olivine and clinopyroxene phenocrysts are sparse in these samples, their influence on the $^{40}Ar/^{39}Ar$ results was minimal. The results of the 34 whole-rock analyses discussed in this chapter are presented in Chapter 3.

4.4.1.1 Peak Range

The Peak Range province yields two main clusters of ages: samples PR01a, PR02, PR05, and PR07 produced ages of 26.0±0.2 Ma, 33.3±0.4 Ma, 31.6±0.3 Ma, and 34.7±0.4 Ma, respectively, while samples PR04, PR08, and PR09 produced significantly older ages of 47.2±0.5 Ma, 44.7 ±0.4 Ma, and 45.0±0.3 Ma, respectively.

4.4.1.2 Springsure

Six samples from Springsure were analysed, producing a restricted age range of 27.8 ± 0.3 to 28.2 ±0.2 Ma. Samples IJS08b, IJS11b, CVLF01, and CIK produced well-constrained combined isochrons of 28.0±0.4 Ma, 27.8±0.3 Ma, 28.2±0.3 Ma, and 28.2±0.2 Ma, respectively. A single grain isochron is the preferred age for sample CIS, with an age of 28.0±0.3 Ma.

4.4.1.3 Bauhinia and Monto

Four samples from the Bauhinia province and one from the Monto province were analysed, and the combined isochrons yield the most reliable ages for these samples. Of the samples from the Bauhinia region, TRLF01, TRLF04, TRLF05, and CIB produced isochrons with ages of 22.5±1.8 Ma, 28.0±0.3 Ma, 27.0±2.8 Ma, and 26.8±0.3 Ma, respectively, an overall range from ~23 to 28 Ma. Samples TRLF01 and TRLF05 produced combined isochron ages of 22.5±1.8 Ma and 27.0±2.8 Ma, respectively.

The preferred age is from the single isochron from Monto (AA2), produces an age of 29.1±0.4 Ma and an $^{40}Ar/^{36}Ar$ intercept at 296±13.

4.4.2 Animated Reconstruction

The new $^{40}Ar/^{39}Ar$ results were added to the geochronology data compilation and incorporated into the two reconstructions. The reconstructions show alternate versions of the northward migration of the Australian Plate during the last 100 million years (Supplemental File 1[1] and 2[2]). The most notable difference between the "linear" and "longitudinal" paths is between 50 and 14 Ma. While in the linear path the longitude of the Australian continent has been similar over the last 100 My to the present-day longitude, in the longitudinal path Australia was farther to the east prior to 22-25 Ma, before diverting west and subsequently continuing on a northward trajectory (Fig. 4.3).

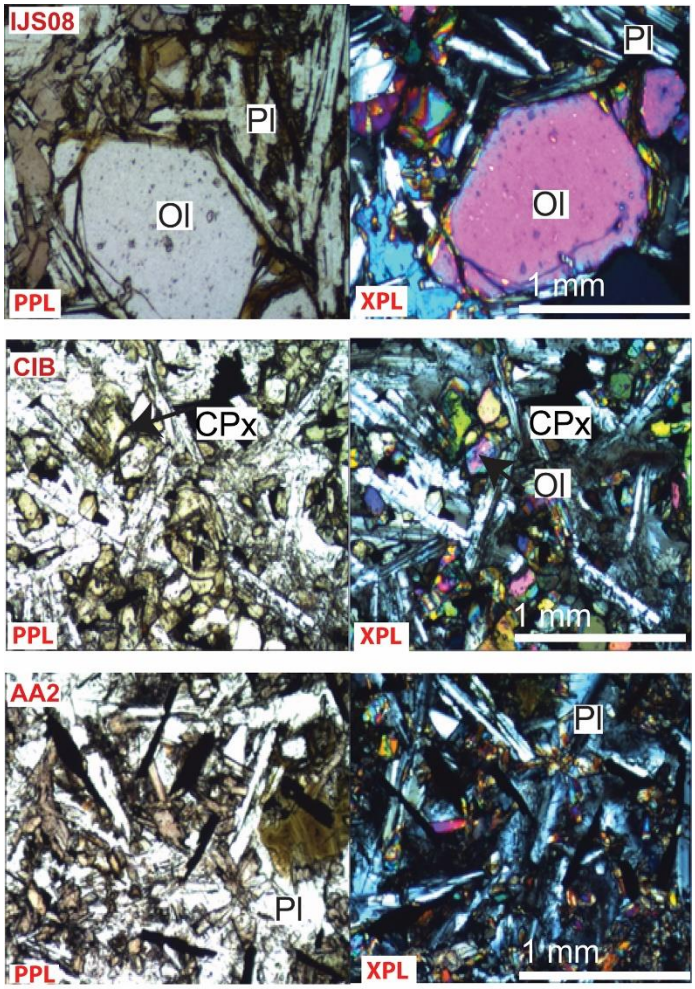

Figure 4.6: Representative thin sections in plane polarised light (PPL) and crossed polarised light (XPL) for a) Springsure (IJS08b), b) Bauhinia (CIB) and c) Monto (AA2). Ol = olivine, cpx = clinopyroxene and Pl = plagioclase.

4.5 Discussion

4.5.1 Comparison of Paleomagnetic APWPs to the Global Moving Hotspot Reference Frame

An inherent shortcoming of paleomagnetic poles is that they do not constrain absolute longitude (e.g., *Butler,* 2004), but plate motions described relative to the mantle can resolve longitudinal position (*Müller et al.,* 1993). The global moving hotspot reference frame (GMHRF) uses the position of seamount chains, which are considered to be the surface expression of plumes, to determine a best-fit rotation relative to their hotspot source. The motion of plates is approximated by fitting the age progression of the seamounts to their geometry.

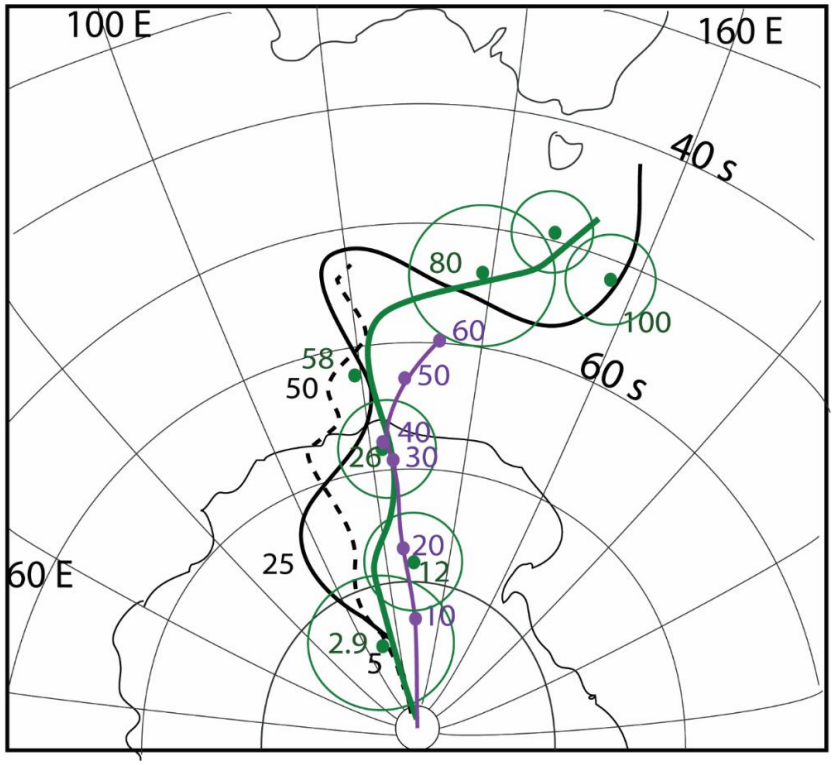

Figure 4.7: Comparison of the longitudinal, linear and GMHRF models using apparent polar wander paths.

Many studies have used only hotspots from a single hemisphere (e.g., *O'Neill et al., 2005*; *Torsvik et al.*, 2008), which may not represent the entirety of the mantle, but Doubrovine et al. (2012) produced a multi-plate, multi-hemisphere GMHRF model that compares well with other hotspot reference frame models (e.g., *O'Neill et al.,* 2005; *Torsvik et al.,* 2008). I utilise the Doubrovine et al. (2012) model below because it is more likely to represent the entire mantle, rather than just the northern hemisphere.

I compared the "linear" APWP of Idnurm (1985), the "longitudinal" APWP of Embleton and McElhinny (1982), and synthetic VGPs derived from the GMHRF model of Doubrovine et al. (2012; Fig. 4.7). I used the APWP of Idnurm (1985) instead of the linear model used in Seton et al. (2012) because the goal is to compare only the APWPs. The latitude of the 60 Ma pole from the GMHRF (-59.9°) is slightly more similar to the 60 Ma pole from the longitudinal APWP (-58.6°) than the linear APWP (-61.7°). At 30 Ma, the latitude from the linear APWP more closely matches the GMHRF, though the latitudes from the longitudinal model are better matches to the GMHRF from 20 Ma onward. Notably, the pronounced apparent shift in longitude at 20 Ma in the longitudinal APWP is not obvious in the GMHRF, which includes a

slight change in longitude (<0.4˚) at that time, but otherwise the temporal resolution of the GMHRF is too coarse to resolve subtle shifts in plate motion. Although the longitudes of the synthetic paleopoles from the GMHRF are more similar to those of the linear APWP, the linear APWP and GMHRF have significantly different age-latitude relationships. For this reason, the longitudinal APWP seems to be a slightly closer match to the GMHRF, though, as noted above, the temporal resolution of the GMHRF is too coarse for detailed comparison with some of the most important and characteristic features of the longitudinal APWP.

As another way of comparing the various estimates for the Cenozoic motion of Australia, the northward component of Cenozoic velocity of the Australian plate was approximated by reconstructing the geographical position of an arbitrary point (27°S 150°E) at 10 Myr increments back to 60 Ma using the GMHRF, the linear APWP, and the longitudinal APWP (Fig. 4.8). Model errors were calculated after Doubrovine et al. (2012). Northward plate velocity was relatively slow from 60 to 40 Ma in each of the three models, although the northward velocity of Australia during this period based on the longitudinal APWP (~40 mm/yr) is closer to the velocity predicted by the GMHRF (~30 mm/yr) than is the linear APWP (~15 mm/yr). The GMHRF model indicates an increase in northward plate velocity to ~60 mm/yr after ~40 Ma that remains virtually constant. The longitudinal and linear APWPs also indicate a marked increase in velocity to ~60 mm/yr and ~45 mm/yr, respectively, at ~40 Ma. According to the longitudinal APWP, plate velocity decreased between 30 and 20 Ma to ~30 mm/yr, before resuming relatively fast northward velocity of approximately ~55 mm/yr. Unlike the GMHRF and the longitudinal APWP, which produce plate velocities similar to modern rates (~60 to 70 mm/yr; *Tregoning*, 2002; *DeMets et al.*, 2010), the linear APWP indicates extremely fast plate velocities of ~100 mm/yr from 10 Ma onward. Based on the overall fit of the GMHRF synthetic VGPs to the APWPs and the approximate relative plate speeds, I find that the GMHRF is more similar to the longitudinal APWP than the "linear" APWP.

4.5.2 Age-Progressive and Rift-Related Late Cretaceous-Cenozoic Mafic Volcanism in Eastern Australia

Our animated reconstructions illustrate the temporal and spatial development of east Australian Late Cretaceous to Cenozoic mafic magmatism in the context of the tectonic history of the SW Pacific. The animations show that there was relatively limited east Australian volcanism from Cretaceous to mid Cenozoic time, including during the initial rifting of the Tasman and Coral

Seas. Magmatism became widespread along much of eastern Australia during the latest Eocene to Oligocene, peaking during the late Oligocene to earliest Miocene. At ~20 Ma (early Miocene) volcanism dissipated in NE Australia, though it continued along the SE coast. By the middle to late Miocene (~10 Ma), SE Australian volcanism had largely ceased as well, such that there was little volcanic activity occurring in eastern Australia at that time. Volcanism was rejuvenated during Pliocene time in the Newer Volcanics Province of SE Australia, as well as the North Queensland lava-fields in NE Australia.

As noted above, the relationship between central volcanoes and lava-fields is particularly acute in the region separating the inland and coastal central volcanic chains. In this region, $^{40}Ar/^{39}Ar$ ages from the Peak Range province, which is part of the Crosgrove volcanic track, fall into two groups. Four relatively young samples (PR01a, PR02, PR05, and PR07) range in age from approximately 26 to 35 Ma, which is consistent with previous geochronological results from the region (*Cohen,* 2007). Results from this young group suggest several distinct flows in the Peak Range volcano and peak activity between ~30 and 35 Ma, although a relatively young age of 26 Ma (sample PR01a) was obtained from the northern margin of the Peak Range volcano. In fact, the 26 Ma basalt post-dates the late stage felsic eruption used to define the age progression of the inland volcanic track, and it is consistent with relatively young ages from the adjacent Nebo province (~21 Ma; *Sutherland et al.,* 1977). The other group, which consists of samples PR04, PR08, and PR09 from the north-western margin of the Peak Range province, is significantly older (44.65±0.4 to 47.2±0.5 Ma). These mid-Eocene ages coincide with a prior $^{40}Ar/^{39}Ar$ result from the same area (*Cohen,* 2007) but are older than many previously published results from Peak Range (*Duncan and McDougall,* 1989). The age range of the older group is also far outside the proposed 34 to 6 Ma timeframe for the overall passage of eastern Australia over a stationary plume (*Cohen et al.,* 2007). $^{40}Ar/^{39}Ar$ results from this old group of Peak Range basalts therefore imply that either some Peak Range "hotspot-related" magmas were produced far earlier than previously described, or the Peak Range central volcano overlies an earlier lava-field. The relatively long duration of volcanism of Peak Range may, itself, constitute evidence that magmatism there originated from multiple processes (*Wellman and McDougall,* 1974a). These results imply a complex history of eruption of the Peak Range volcano that is difficult to reconcile with simple northward passage over a fixed plume source. The animations were used to investigate the relationship between eruption of the lava-fields and rifting in the Tasman and Coral Seas. Volcanic activity in the lava-field provinces spans

from the Late Cretaceous to Holocene, with periods of peak activity at 90 Ma (*Embleton et al.,* 1985), 60-40 Ma (e.g., *Duncan and McDougall,* 1989), 34-15 Ma (e.g., *Wellman and McDougall,* 1974a; *Vickery et al.,* 2007), and 5 Ma to Recent (e.g., *Henley and Webb,* 1990; *Grey and McDougall,* 2009). From 34 to 6 Ma, mafic volcanism was widespread in eastern Australia but was not restricted to the central volcanoes. Many provinces, including the Monaro, Older Victorian Volcanics, New England, Liverpool, Hoy, and the Tasmanian provinces, were active during this period but were distinctly unrelated to age-progressive volcanism. Peak activity of the relatively old (60-40 Ma) lava-fields of Monaro, Hoy, Monto, the Older Victorian Volcanics, and Barrington (*Duncan and McDougall,* 1989) correspond with the opening of the Tasman and Coral Seas (73 to 52 Ma; *Gaina et al.,* 1998a, 1998b), a temporal relationship that is consistent with previous suggestions that the lava-fields are vaguely related to Tasman and Coral Sea rifting (*Ewart et al.,* 1988; *O'Reilly and Zhang,* 1995). However, at the time of their eruption, the reconstruction places the distance between the spreading ridge in the Tasman and Coral Seas and the aforementioned volcanoes at over 200 km (*White and McKenzie,* 1989; *van den Bogaard,* 2013). In many examples from around the world, the inception of rifting is associated with volcanism in close proximity to either side of the rift (e.g., *White et al.,* 1987; *White and McKenzie,* 1989; *Franke,* 2013), but, in the case of Tasman and Coral Sea rifting, volcanism was restricted to the east Australian coast at considerable distance to the rift. The lack of correspondence between the onset of rifting in the Tasman and Coral Seas and eruption of the lava-fields raises some doubts about whether lava-fields are truly "rift-related". Furthermore, subsequent Oligocene to Miocene (34-15 Ma) lava-field magmatism, such as at Central/Doughboy, Liverpool, Bauhinia, Monto, and Mitchell, as well as the later pulses of volcanic activity in the Hoy and Monto provinces, occurred long after the cessation of rifting, and at a considerable distance to spreading ridges in the Tasman and Coral Seas (*Wellman and McDougall,* 1974a; *McDougall and Roksandic,* 1974; *Vickery et al.,* 2007). Eruption of these lava-fields was broadly coincident, however, with the period of the age-progressive volcanism of the central volcanoes. As explained in more detail below, an alternative interpretation is that eruption of the lava-fields was related to edge driven convection (EDC). Formation of the present day continental margin of eastern Australia via the opening of the Tasman and Coral Seas may have been a necessary condition for east Australian EDC, and, in that respect, eruption of the lava-fields might be considered tangentially "rift-related." I find little evidence linking their eruption directly with rifting, however.

The distribution of new $^{40}Ar/^{39}Ar$ ages from Peak Range, Springsure, Bauhinia, and Monto illustrates a close temporal relationship in the region between central volcanoes and lava-fields. Volcanic activity at Peak Range, a central volcano, occurred during three periods (47 to 44 Ma, 35 to 28, and a pulse at 26 Ma), though, as noted above, the older period may be more accurately described as lava-field volcanism. $^{40}Ar/^{39}Ar$ results from mafic and felsic parts of the nearby Springsure central volcano indicate activity from at least 29 to 27 Ma, a timeframe that overlaps with both the second phase of volcanism at Peak Range, as well as eruption of the adjacent Buckland central volcano (Fig. 4.1; *Cohen et al.,* 2007). Immediately to the east of Springsure, the data reveal a protracted history of volcanism at the Bauhinia lava-field between 28 and 23 Ma, and, farther to the east, the Monto lava-field was erupting at 29 Ma. In other words, during a time interval from roughly 30 to 25 Ma, there was both central volcano and lava-field basaltic magmatism occurring within a small region of SE Queensland. Given that these provinces are largely coeval, geographically adjacent, and seem to grade into each other, I find it doubtful that there is a substantive difference in origin, in this region, between central volcanoes and neighbouring lava-fields. An implication of this conclusion is that previous clear-cut distinctions between "plume-related central volcanoes" and "rift-related lava-fields" are likely inaccurate. Perhaps a more plausible scenario is one in which there were parts of eastern Australia, the Bauhinia region being a leading example, where the generation of Cenozoic basaltic magmatism of the lava-fields and central volcanoes were intrinsically linked.

4.5.3 Edge Driven Convection as a Mechanism for Volcanic Activity in Eastern Australia

The most prominent alternative to the traditional plume-related and rift-related models of east Australian Cenozoic basaltic magmatism is EDC, which refers to convective cells of magma that arise from a lateral thermal gradient across a large change in lithospheric thickness (*King and Anderson,* 1998). EDC is generally believed to form at boundaries between hot, asthenospheric mantle and cold, lithospheric mantle. The juxtaposition forms a region of convective melting that circulates against the "edge" of the contact at sufficient plate speeds (*Farrington et al.,* 2010). The sporadic eruption pattern of Late Cretaceous to Cenozoic mafic magmas in eastern Australia, which includes a broad and irregular distribution of volcanism, multiple late-stage eruptions (e.g., a pulse of magmatism at Peak Range [26 Ma; this study] and Nebo [~20 Ma; *Sutherland et al.,* 1977]), and eruption interruptions (*Jones and Verdel,*

2015), deviates significantly from a classic plume model (e.g., *Wilson,* 1969). A useful analogue for east Australian mafic magmatism might be the Canary Islands seamount province, where older volcanism was dominant in the south, both older and younger volcanism occurred in the middle, and rocks of intermediate age are found in the north (*van den Bogaard,* 2013). The pattern of sporadic volcanism at the Canary Islands seamount province, which nevertheless forms a broad age progression, has been attributed to plume interaction with an EDC cell (*Geldmacher et al.,* 2005).

In the case of eastern Australia, EDC may arise from steps in lithospheric thickness. Farrington et al. (2010) concluded that at current plate velocities, the temperature variation and shear-flows at the east Australian stepped lithospheric boundary are within the expected range to support EDC. In fact, EDC has been proposed as a mechanism for formation of the lava-fields of the Victorian and South Australian Newer Volcanics Province (*Demidjuk et al.,* 2007; *Holt et al.,* 2013; *Davies and Rawlinson,* 2014). Importantly, while moderately high sub-lithospheric heat flow along eastern Australia is consistent with EDC, the absence of north to south gradients in heat flow is difficult to reconcile with proposed Cenozoic passage of eastern Australia over mantle plumes (*Hasterok and Gard,* 2016), though, given the depth and age of the plume or plumes, heat flow would not necessarily be identifiable at the surface. I suggest that, similar to the Canary Islands, EDC may have played an important role in producing the Late Cretaceous to Cenozoic mafic magmatism in eastern Australia. EDC is less likely, however, to account for the age progression of the off-shore Tasmantid and Lord Howe seamount chains, as discussed below.

4.5.4 Longitudinal Offset of the Tasmantid and Lord Howe Seamount Chains

The Lord Howe and Tasmantid seamount chains are thought to have formed as a result of the northward migration of the Australian plate over stationary hotspots (Fig. 4.1; e.g., *Wellman and McDougall,* 1974a), and both seamount chains have east-west offsets. Geochronology and robust regression models based on Cenozoic plate velocities place both offsets between 23 and 26 Ma, during a period of anomalously slow plate velocity discussed below (*Knesel et al.,* 2008), although $^{40}Ar/^{39}Ar$ dating of Middleton Reef in the Lord Howe seamounts (*Mortimer et al.,* 2010) is approximately 2 Ma older than that predicted by robust regression plate models (*Sutherland et al.,* 2012).

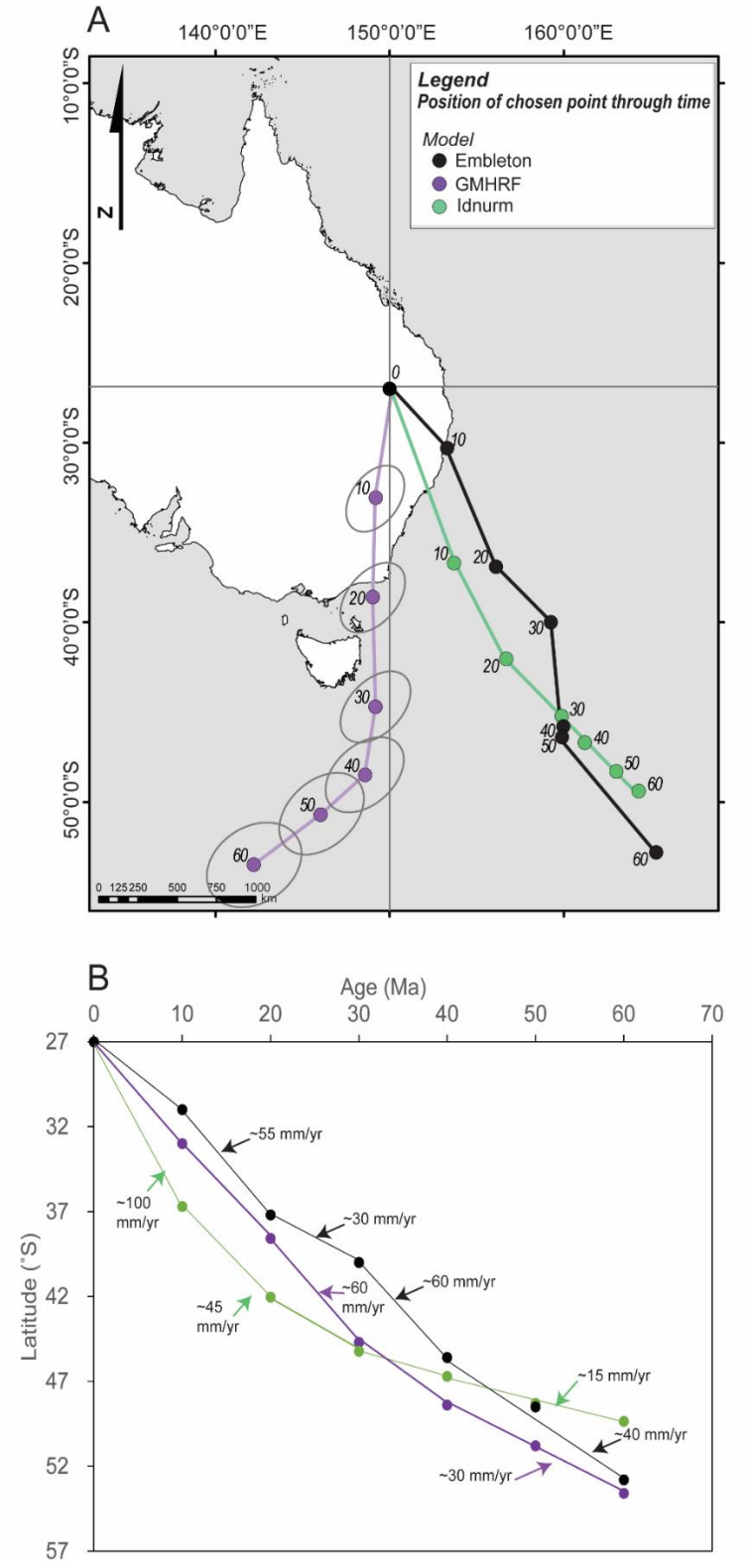

Figure 4.8: Reconstruction of an arbitrarily chosen point through time based on the GMHRF, linear and longitudinal models looking at a) the geographical location and b) age-latitude relationship.

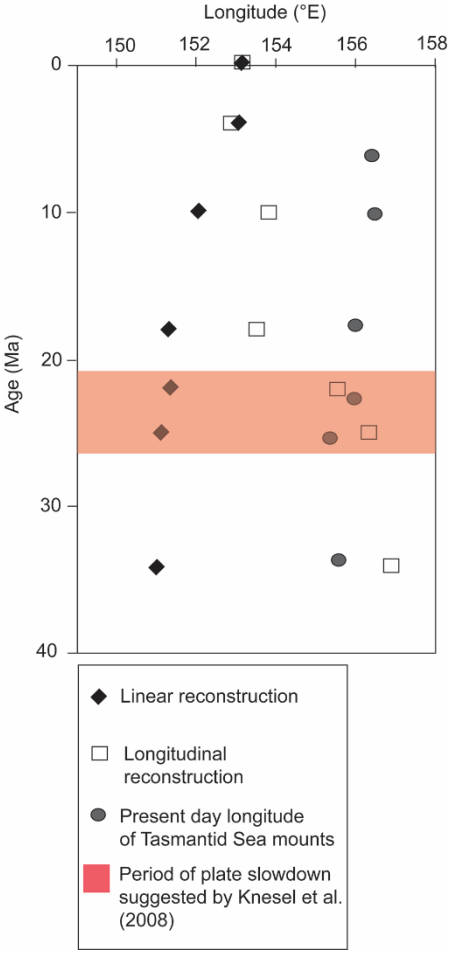

Figure 4.9: Longitudinal migration of Australia using modified reconstruction path based on work by Embleton and McElhinny (1982; open squares) and the rotation model after Seton et al. (2012; closed diamonds). Present day longitude of the the Tasmantid Sea Mounts are also shown for comparison (closed circles).

Importantly, these offsets coincide with a westward divergence of the Australian Plate between 25 and 22 Ma in the longitudinal APWP (Fig. 4.9). There is no such early Miocene divergence in the linear reconstruction, so, in the case of this criterion, the longitudinal reconstruction is more closely aligned with readily observable physical features. A westward bend in age-progressive tracks is also present onshore after 17 Ma, implying an additional change in plate motion, although it is not evident in either reconstruction. It is likely that the precision of the APWP is insufficient to reflect this subtle shift in plate motion, which may be artificially intensified between Nandewar and Canobolas by proximity to the Great Dividing Range (Fig. 4.1).

An alternative explanation for the offset in the off-shore volcanic chains is that they could be related to the structure of the east Australian lithosphere, as opposed to changes in plate motion

(*Fishwick et al.*, 2008). However, while offsets in the on-shore and Tasmantid chains (Fig. 4.1) may correspond with a bend in the stepped-lithospheric boundary of eastern Australia (*Fishwick et al.*, 2008), the offset in the Lord Howe seamounts does not (*Knesel et al.*, 2008). Therefore, a stepped lithosphere probably did not produce the same pattern of volcanism in both the Tasmantid and Lord Howe chains, nor could such a pattern be produced by purely northward motion of Australia, as illustrated in the linear reconstruction. Movement of the plumes themselves is a possibility, although this explanation would require that both the Lord Howe and Tasmantid plumes shifted simultaneously and abruptly between 26 and 23 Ma (*Knesel et al.*, 2008).

4.5.5 A Period of Reduced Northward Motion of Australia During the Late Oligocene to Early Miocene

I used the two reconstructions to evaluate the Cenozoic motion of a point in eastern Australia, which was somewhat arbitrarily chosen as Stradbroke Island (Fig. 4.1). The past latitude of Stradbroke Island is significantly different in the two reconstructions and, from this difference, I estimated changes in the magnitude of the Cenozoic velocity of eastern Australia (Fig. 4.10). For the longitudinal reconstruction, there is a reduction in the north-component of velocity to about 30 mm/yr between 26 and 22 Ma. According to the linear reconstruction there is no late Oligocene to early Miocene reduction in plate velocity, although there is a reduction in the north-component of velocity from 61.9 mm/yr to 42.5 mm/yr after 21 Ma. I then compared these velocity estimates with similar estimates from Knesel et al. (2008) and Cohen et al. (2013), and I found correspondence with the estimates of the longitudinal reconstruction (Fig. 4.10). This correspondence is significant because it highlights agreement between two independent estimates of the Cenozoic motion of Australia: the longitudinal reconstruction is fundamentally based on the paleomagnetic data of Embleton and McElhinny (1982), while the estimate of Knesel et al. (2008) and Cohen et al. (2013) is based purely on high resolution $^{40}Ar/^{39}Ar$ geochronology from a number of east Australian central volcanoes.

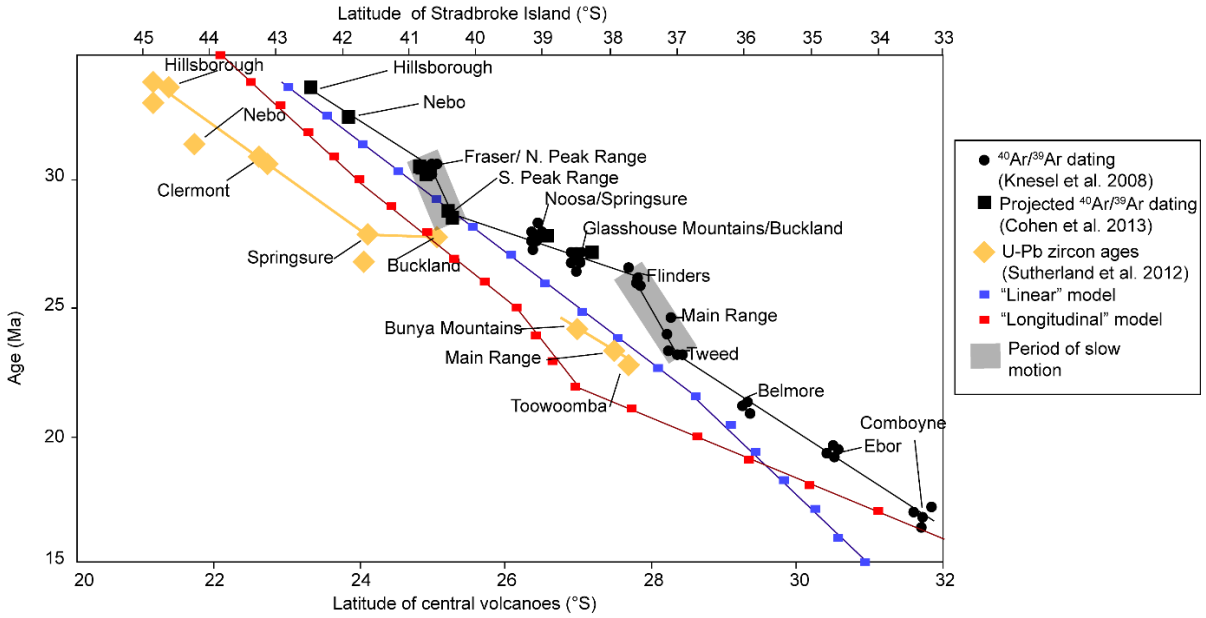

Figure 4.10: Apparent latitude of Stradbroke over time. Modified after Knesel et al. (2008). Red squares indicate artefacts created by VGP plate reconstructions, representing very little latitudinal motion between 25 and 22 Ma. Grey area marks apparent period of low plate velocity after Knesel et al. (2008).

As described above, there are two likely causes for the late Oligocene to early Miocene slowdown of the Australian plate and contemporaneous shift in plate trajectory: "soft docking" of the OJP and the Solomon Islands, and collision of PNG with the East Papuan Composite Terrane. Although the longitudinal reconstruction seems to illustrate the effects on the Australian Plate of one or both of these collisions, it is not possible to distinguish the respective effects of the two because they were essentially coeval. Likewise, the results do not bear directly on the possible existence of detached slabs and slab windows beneath the Loyalty Arc during mid Cenozoic time (*Sutherland et al.*, 2012), though the general lack of a clear age progression in the overall Cenozoic volcanism in eastern Australia argues against an interpretation that links on-shore volcanism with tectonic interactions in the Loyalty Arc region.

4.6 Conclusions

Two competing, Late Cretaceous-Cenozoic reconstructions of the motion of Australia illustrate several key points relevant to the overall tectonic development of the SW Pacific. First, while the temporal resolution of the Cenozoic GMHRF (*Doubrovine et al.*, 2012) is not sufficient to resolve an apparent late Oligocene-early Miocene slowdown or offset in the motion of

Australia, the apparent latitudes and plate speeds for Australia before 40 Ma and after 30 Ma based on the GMHRF are more consistent with the "longitudinal" APWP of Embleton and McElhinny (1982). Second, this APWP, which incorporates paleomagnetic data from Cenozoic volcanic rocks of the Australian continent, includes a westward shift of the Australian Plate at 26-22 Ma. The westward divergence coincides with a longitudinal offset in the Tasmantid and Lord Howe seamount chains. The "linear" APWP of Idnurm, (1985) and Musgrave (1989), which includes no significant longitudinal movement, does not account for the offset in the seamount chains. Finally, the longitudinal APWP includes a late Oligocene to early Miocene period of reduced northward velocity of Australia that is detectable from high-resolution geochronology of age-progressive volcanoes in eastern Australia (*Knesel et al.,* 2008). Therefore, comparison of the linear and longitudinal reconstructions suggests that, on balance, the longitudinal reconstruction is more compatible with observable geological features in the SW Pacific.

Finally, on-shore, east Australian, age-progressive volcanism, which has been used previously as a basis for reconstructing the Cenozoic motion of Australia, seems to reflect a complex interplay between magmatic processes. I find no clear spatial or temporal distinctions between lava-fields and central volcanoes, and no obvious correlations between even the oldest lava-fields and the opening of the Tasman and Coral Seas. The widespread distribution of Cenozoic volcanism in eastern Australia, eruption hiatuses at individual volcanoes, and late-stage volcanism are not simply explained by a framework consisting of clearly distinct, "plume-related" and "rift-related" Cenozoic volcanoes. This period of east Australian magmatism is more likely fundamentally related to EDC arising from the stepped structure of the east Australian lithosphere.

SUPPLEMENTARY FILES

[1] Supplementary file 1: Animated reconstruction showing the last 100 My of motion of the Australian plate using base reconstruction file of Seton et al. (2012). Approximate position of New Guinea composite terrains after Davies et al. (1997).

[2] Supplementary file 2: Animated reconstruction showing the last 100 My of motion of the Australian plate using paleomagnetic VGP's calculated by Embleton and McElhinney (1982). Approximate position of New Guinea composite terrains after Davies et al. (1997)

Chapter 5: Evidence of a common source component for east Australian Cenozoic magmatism

5.1 Introduction

A series of Cenozoic volcanic provinces form a prominent topographical feature that stretches for >2000 km along the east Australian margin (*Wellman and McDougall,* 1974a; *Cohen et al.,* 2007; *Sutherland et al.,* 2012). While Cenozoic mafic volcanoes have been subdivided into plume and non-plume related magmatism, neither geochronological nor geometric classifications offer a distinct means of differentiating the two. These volcanic provinces are restricted almost exclusively to relatively thin lithosphere (<50 km) that lies to the east of a step in lithospheric thickness (Fig. 5.1; *Davies et al.,* 2015, *Fishwick et al.,* 2008). Large pulses of magmatism occurred in eastern Australia during Eocene time as the Tasman and Coral Seas opened (*O'Reilly and Zhang,* 1995; *Sutherland et al.,* 2012), and magmatism continued until <1 Ma (*Sutherland et al.,* 2014).

In broad terms, the overall phase of widespread Cenozoic mafic volcanism in eastern Australia has traditionally been linked to two processes: hotspot magmatism (which has been proposed as the source of the east Australian age-progressive "central volcanoes") and rift-related magmatism accompanying the opening of the Tasman and Coral Seas (proposed as the source of east Australian non-age-progressive "lava-fields;" Fig. 5.1; *Wellman and McDougall,* 1974a; *O'Reilly and Zhang,* 1995; *Cohen et al.,* 2007; *Sutherland et al.,* 2012). As discussed in Chapter 4, a key difference (and indeed, perhaps the only substantive difference) between central volcanoes and lava-fields is that the central volcanoes form age-progressive tracks (Fig. 5.2; *Wellman and McDougall,* 1974a). Variations of the broad explanations for east Australian Cenozoic mafic magmatism include a combination of multiple mantle plumes and extension-related melts (*Wellman and McDougall,* 1974a; *Sutherland et al.,* 1993; *Davies et al.,* 2015), edge-driven convection (*Demidjuk et al.,* 2007; *Davies and Rawlinson,* 2014), and asthenospheric convection related to slab tearing along the Loyalty Arc (*Sutherland et al.,* 2012). Two observations that seem at odds with these traditional classifications and interpretations are that (1) as shown in Chapter 4, some lava-fields, particularly those from the southern Bowen Basin region of eastern Queensland, are far too young to be directly related to opening of the Tasman and Coral Seas (*Hall,* 2002; *Jones et al.,* 2017), and (2) many of the lava-fields are spatially and temporally associated with central volcanic provinces (Fig. 5.1; *Zhang and O'Reilly* 1997; *Cohen et al.,* 2007). Additionally, although distinctions between east Australian lava-fields and central volcanoes were originally rationalised on the basis of lithological and geomorphological criteria (*Wellman and McDougall,* 1974a), these criteria are

neither consistent nor robust (i.e., some volcanic provinces that are frequently described as lava-fields have attributes of central volcanoes, and vice versa; *Jones et al.*, 2017). In an effort to clarify these distinctions and relationships, I use major element, trace element, and radiogenic isotope (Sr, Nd, Pb, and Hf) data to re-examine the differences between east Australian central volcanoes and lava-fields, including potential differences in their source characteristics. Based on my findings, I formulate a new working hypothesis for Cenozoic mafic magmatism in eastern Australia.

5.2 Geological Background

5.2.1 Classification of central volcanoes

5.2.1.1 Geometry and time-space relationships

The central volcanoes were originally defined as a series of shield volcanoes, erupted from well-defined central vent areas, that were distinguished based on the presence of both mafic and felsic flows and intrusions, that were later used to define age-progressive tracks (*Wellman and McDougall,* 1974a). The central volcanic cones of these provinces are surrounded by an apron of mafic flows that can be up to 1 km above the surrounding landscape, and many of these flows extend >100 km from the central vents with an active duration of 1 to 3 Myr (*Wellman and McDougall,* 1974a). The number and extent of central volcanic tracks are contentious, but three main onshore tracks have been proposed: (1) the Cosgrove track, which passes through central Queensland and leucitite provinces, ultimately terminating at Macedon (*Davies et al.*, 2015); (2) the inland track, which extends from Main Range south to Canobolas; and (3) the coastal track, which extends from Fraser Island to Comboyne (Fig. 5.1), though geochemical data is primarily restricted to the Cosgrove track.

5.2.1.2 Geochemistry

The geochemical characteristics of central volcanoes are typically described as "plume-like" (*Ewart and Chappell,* 1989). Mafic rocks from the central volcanoes typically have alkaline ocean island basalt (OIB) compositions, although sub-alkaline rocks are not uncommon (*Johnson et al.,* 1989). Central volcanoes usually include a continuous range of compositions from basalt to trachyte or rhyolite, formed by fractional crystallisation of magma stalled in the mid to upper crust with variable degrees of crustal assimilation (*Ewart et al.,* 1985; *Ewart,* 1985). The isotopic composition of central volcanoes indicates a primitive mantle (PM) source component (*Ewart et al.,* 1985).

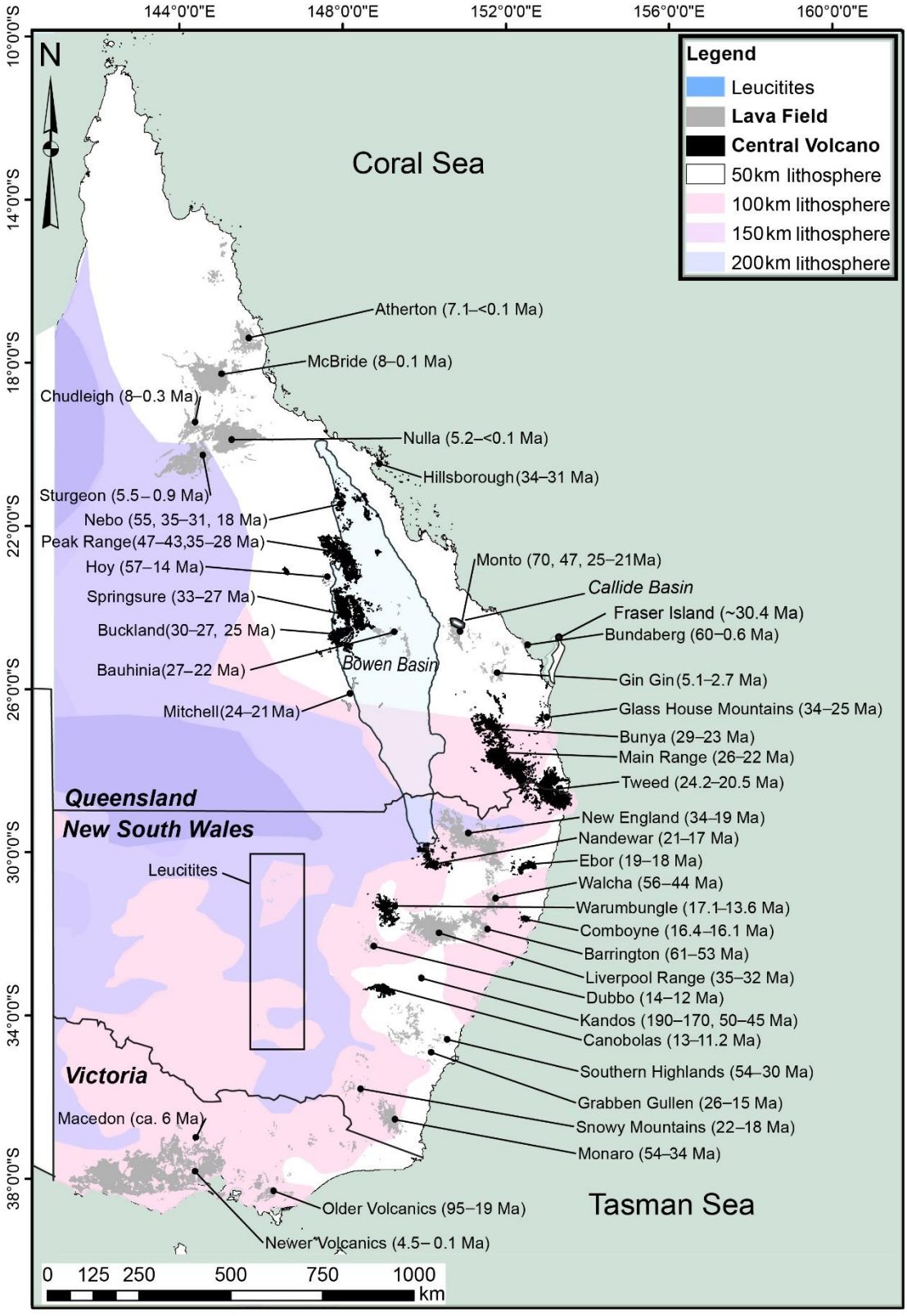

Figure 5.1: Map of Eastern Australia, showing the location and age of volcanic provinces and step in lithospheric thickness (*Fishwick et al.* 2008; *Rawlinson et al.* 2017). Ages after Johnson et al. (1989) and Vasconcelos et al. (2008).

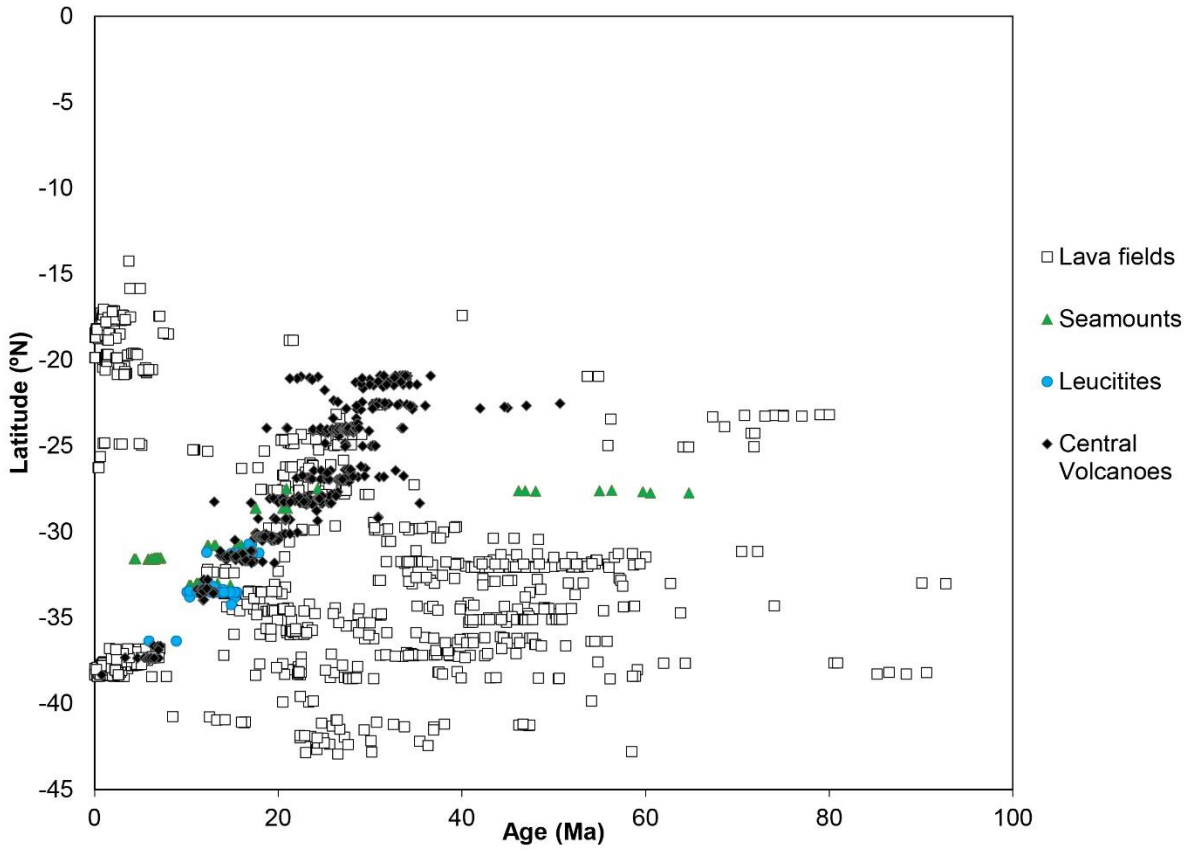

Figure 5.2: Age vs. latitude relationship for volcanic provinces in east Australia. Age data after Jones et al. 2017 (Chapter 3 and 4) and references therein.

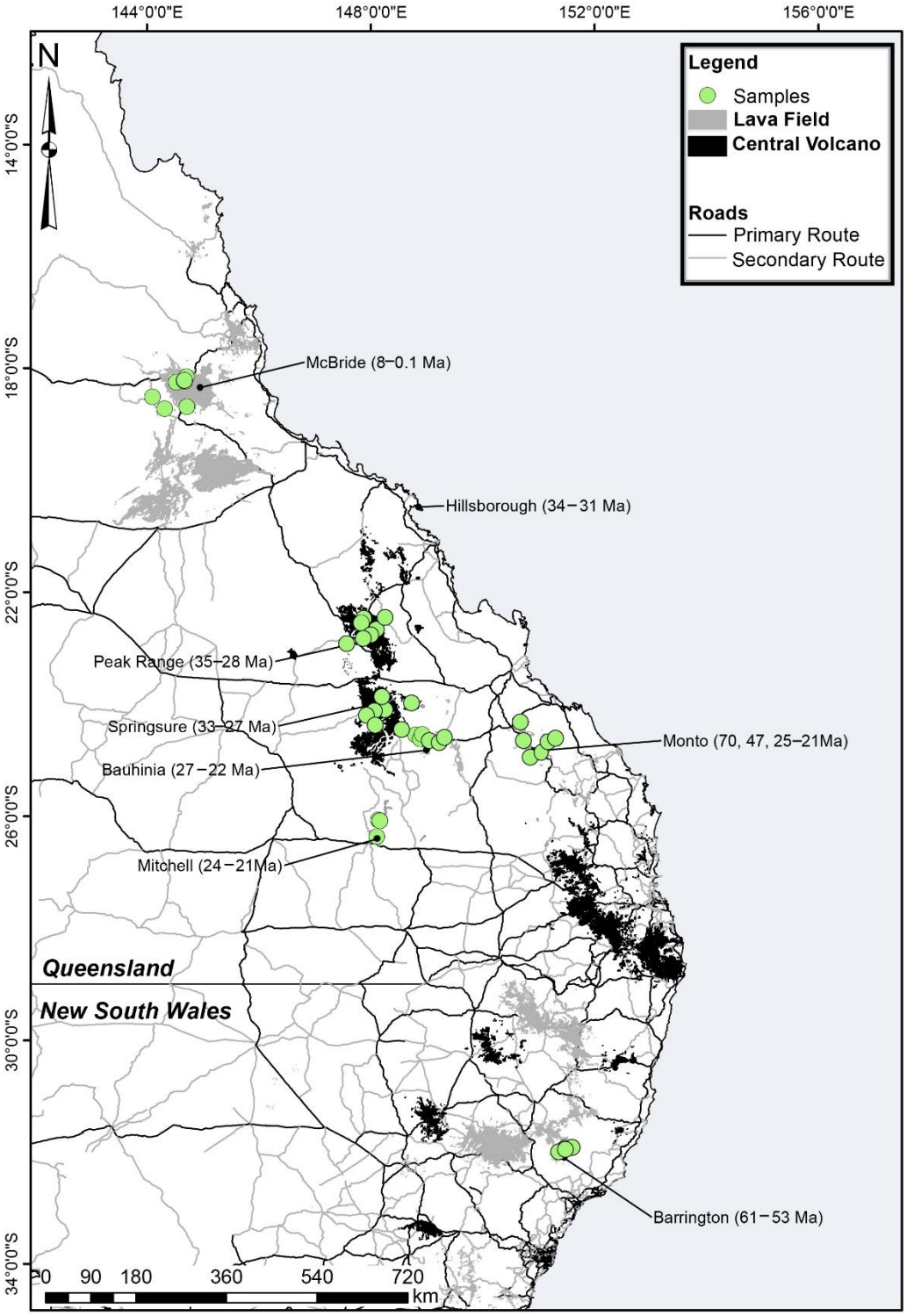

Figure 5.3: Location of samples selected for geochemical study.

5.2.2 Classification of lava-fields

5.2.2.1 Geometry and age distribution

East Australian lava-fields are defined as extensive fields or piles of volcanic rocks (up to 1 km-thick) that are composed of basaltic lavas fed through dyke and pipe swarms, many of which carry mantle and crustal xenoliths (*Wellman and McDougall,* 1974a; *Johnson et al.,* 1989). These provinces generally do not form shield volcanoes (a key distinction with central volcanoes). Unlike central volcanoes, lava-fields are not age-progressive (Fig. 5.2). Instead, lava-fields occur as isolated provinces that range in age from 90 Ma (Victorian Older Volcanics; *McKenzie et al.,* 1984; *Henley and Webb*, 1990) to <1 Ma (Victorian Newer Volcanics - *Grey and McDougall,* 2009; North Queensland – *Zhang et al.,* 2001; *Cohen et al.,* 2017), although they were most active between 55 and 34 Ma (*Wellman and McDougall,* 1974; *Ewart et al.,* 1976). Single volcanic provinces were typically active for <6 Myr, and lava-fields that were active for >10 Myr consist of several volcanic centres (*Wellman and McDougall,* 1974a*).*

The generation of east Australian lava-fields has been linked to the opening of the Tasman Sea, which may have caused destabilisation of the asthenosphere and generation of small upwellings that underplate the crust (*Lister and Etheridge,* 1989; *O'Reilly and Zhang,* 1995). Some studies have linked the younger lava-field volcanism in Victoria and South Australia to edge-driven convection (*Demidjuk et al.,* 2007; *Davies and Rawlinson,* 2014). The three-dimensional structure of the sub-continental lithospheric mantle beneath the Newer Volcanics province (*Davies and Rawlinson,* 2014), combined with longer ascension and residence times in South Australia (*Demidjuk et al.,* 2007), could support the formation of a large convective cell driven by the temperature gradient at a stepped boundary. The Newer Volcanics province is similar in both age and geometry to Oligocene-Holocene volcanism in northern Queensland (Fig. 5.1), but no link between these provinces has been suggested previously.

5.2.2.2 Geochemistry

Lava-fields are isolated, silica undersaturated alkaline to tholeiitic basalt provinces (*Ewart,* 1985). Upper lithospheric mantle affinities from some lava-fields in New South Wales have been cited as evidence in support of a rift-related source (*Ewart et al.,* 1988; *O'Reilly and Zhang,* 1995; *Skae,* 1998,). However, OIB-type lava-fields from central New South Wales, including Kandos, Oberon, Grabben Gullen, and Monaro (Fig. 5.1), have trace element and

isotopic compositions similar to central volcanoes (*O'Reilly and Zhang,* 1995). The Dubbo, Barrington, and Southern Highlands provinces are reasonably distinct and are believed to incorporate, or derive from, the subcontinental lithospheric mantle (SCLM; *O'Reilly and Zhang,* 1995). The Newer Volcanic Province, which is related to a complex mixture of magma source components, including EMI to EMII signatures, has trace element compositions similar to OIB-type magmas (e.g. *Van Otterloo et al.,* 2014). Similarly, the lava-fields of north Queensland have a subduction-modified SCLM source component (*O'Reilly and Zhang,* 1995; *Zhang et al.,* 2001). While previous studies of lava-fields in central New South Wales and northern Queensland have been substantial, the source characteristics and geochemistry of lava-fields from the Bowen Basin region have been largely ignored previously.

5.2.3 Uncertainties in the central volcano vs. lava-field classification

The criteria used to classify east Australian Cenozoic magmatism are reasonably strict and well-defined (*Johnson et al.,* 1989), but these criteria have frequently been relaxed when categorising various magmatic provinces. For example, despite the fact that east Australian lava-fields are, by definition, exclusively basaltic, several provinces that have been described as lava-fields include variably evolved lithologies that range from mugearites (Liverpool, Walcha and New England) to phonolites (Dubbo, McBride and Maybole) and trachytes (Dubbo and Newer Victorian Volcanics; *Sutherland et al.,* 2014). Finally, several lava-fields have been classified as such purely by virtue of lacking silicic volcanism. However, these lava-fields, most notably those in the Bowen Basin region, are both spatially and temporally associated with adjacent central volcanoes.

In addition to inconsistencies in usage of the "lava-field" and "central volcano" terminology, the individual provinces frequently have much more complicated histories than is suggested by studies that, for example, examine time-space relationships of east Australian mafic magmatism. For example, the Peak Range province (a nominal central volcano) has at least two centralised vent areas (north and south Peak Range) and was formed during three periods of volcanic activity: a series of eruptions in the early Eocene (47-43 Ma), a main period of activity in the late Eocene to early Oligocene (35-31 Ma), and an anomalous period of activity in the late Oligocene (25 Ma) that is significantly younger than the overall period of magmatism ascribed to the central volcanoes (*Jones et al.,* 2017).

5.3 Materials and methods

5.3.1 Sample collection, cleaning, and preparation

The geochemical data described in this paper are a subset from a suite of 62 samples along an east-west transect that extends from the Springsure region in the west to the Monto region in the east (Fig. 5.3). The location of the transect was selected because it intersects both central volcanos and lava-field provinces. Twenty-nine basalt samples were collected along the transect, which intersects the Bauhinia (11 samples) and Monto (1 sample) lava-field provinces. Seventeen basaltic samples were collected from the Springsure volcano. An additional five basaltic Monto samples held by the UQ collection (collected by Ben Cohen in 2007) were analysed, as well as eleven samples from the Mitchell province. Seven samples were collected from the Peak Range province. A further set of six basaltic samples was collected from the Barrington province (NSW), and four basaltic samples were collected from the McBride province (north Queensland; Fig. 5.3).

Thin sections of all the samples, prepared in the Sample Preparation Laboratory in the School of Earth Sciences, University of Queensland (UQ), were examined to determine mineralogical assemblages, suitability for geochemical analysis, and to assist with rock classification. Fifty-four fresh, geographically distributed samples were selected for geochemical analysis. These samples were crushed into chips using a jaw crusher, and the chips were separated into fresh samples and samples with weathered or altered faces. The fresh samples were cleaned in distilled water in an ultrasonic bath at 5-minute intervals to remove contaminants until no fine particles were released. The samples were then washed in acetone for approximately 10 minutes and left to dry. Following the cleaning process, the samples were pulverised using an agate ball mill.

5.3.2 Geochemical Analyses

Each sample was subdivided into two subsamples for major element, trace element, and radiogenic isotope analyses. USGS samples BHVO2 (*Wilson,* 1997a), AGV2 (*Wilson,* 1997c), BCR-2 (*Wilson,* 1997b), and W2 (*Gladney and Roelandts,* 1988) were used as secondary reference materials (SRM) in all runs and suggest accuracy of <10% for most samples and elements. Based on results from duplicate analysis of the SRM, the analytical precision was typically <3%. Major element, trace element, and radiogenic isotope results are presented in

Table 5.1 to 5.3, respectively. Detailed accuracy and precision calculations are supplied in the supporting information (Appendix C).

5.3.3 Major element analysis

100 mg of material were fused with 400 mg of lithium metaborate at 1000˚C, using a Katanax K2 Prime Automatic Fluxer, in a platinum crucible, cooled, and dissolved in 100 mL of a HNO_3 solution. Blanks were also prepared to assess possible contamination during analysis. Duplicates of samples IJS06, 08b and IJLF01 were analysed to evaluate reproducibility. Aliquots were analysed with a Perkin Elmer Optima 8300DV Inductively-Coupled Plasma Optical Emission Spectrometer (ICP-OES) at the Environmental Geochemistry Laboratory in the UQ School of Earth Sciences. Standards JB-2, BHVO-2, JA2, JR3, JGR3, and JB-3 were used as calibration standards in run 1-3, and W2, BHV02, and a serial dilution multi-element standard was used for run 4 (Dataset S1). Standards, duplicates, blanks, and samples were all prepared in the same manner. A small aliquot (~4 g) was heated in an oven at 100˚C and then 1000˚C for an hour. The samples were weighed before and after to determine loss on ignition (LOI).

5.3.4 Trace element analysis

Approximately 0.1 g of each sample was dissolved in a 4 mL solution of HF-HNO_3 (10:1) in Teflon beakers following the method of Eggins et al. (1997). The beakers were placed on a hotplate overnight at 140°C. Once dissolved, the solution was transferred into a 10 mL tube, and the solid residues in the aliquots were air-dried at 80-90°C and refluxed with 1 mL 6N HNO_3. Following reflux, the aliquots were again dried, and 2 ml of concentrated HNO_3 was added to ensure complete dissolution. A standard solution was added, and the removed liquid samples were returned to the Teflon beaker. Ultrapure H_2O was added to dilute the aliquots to 1:1000. The aliquots were then placed into 10 mL ICP tubes and reweighed before they were analysed. JB-2, BHVO-2, JA2, JR3, JGR3, and JB-3 were used for run 1-3 and W2, while BHV02 and a serial dilution multi-element standard (run 4) were used for calibration. Trace element concentrations were determined with an Agilent 7900 Inductively-Coupled Plasma Mass Spectrometer (ICP-MS) in the Radiogenic Isotope Facility within the UQ School of Earth Sciences. Trace element concentrations of some samples from Springsure and Bauhinia were measured with the Thermo X series 2 ICP-MS.

5.3.5 Radiogenic isotopes

Samples were selected for radiogenic isotope analysis based on multi-element and crustal contamination diagrams. Samples with low levels of crustal contamination were preferentially chosen for isotope analysis to ensure isotopic ratios would reflect source compositions. Radiogenic isotope analyses were conducted at the UQ Radiogenic Isotope Facility. Pb, Nd, Hf, and Sr isotopes were separated by stack Sr-spec, Thru-spec, LN-spec, and Hf-spec resin columns using a streamlined column chemistry procedure (*Miková and Denková*, 2007). Sr, Pb and Nd isotopes were analysed automatically in static and dynamic mode on a Nu Plasma Multi-Collector Inductively Coupled Plasma-Mass Spectrometer (MC-ICP-MS). Nd isotopes were corrected for differential mass fractionation by normalizing the raw data to $^{146}Nd/^{144}Nd = 0.7219$. Laboratory based Nd Metal and Hf standards were used to monitor detector efficiency drift. Pb isotope aliquots were doped with 4 ppb thallium with a $^{205}Tl/^{203}Tl$ ratio of 0.23875 and fractionation corrected. Sr isotope aliquots used $^{86}Sr/^{88}Sr = 0.1194$ for exponential mass fractionation corrections. SRM-987 (Sr standard) and SRM-981 (Pb standard) were used to monitor detector efficiency drift during the analysis.

5.4 Results

5.4.1 Geochemical analyses

5.4.1.1 Barrington

The Barrington samples are primarily aphanitic to microporphyrictic melanocratic basalts to basanites (Figs. 5.4a-b and 5.5). Some samples include olivine-rich xenoliths. Samples consist, primarily, of olivine (20-30 vol%), clinopyroxene (15-20 vol%), plagioclase (50-60 vol%), and opaque phases (10 vol%). Microphenocrysts are small euhedral to subhedral olivine (up to 10 vol%) and clinopyroxene crystals (up to 20 vol%) up to 0.5 mm, with minor occurrences of euhedral plagioclase up to 1 mm-long. The groundmass generally consists of plagioclase, olivine, and minor clinopyroxene. However, sample BRT2 has a groundmass consisting, primarily, of devitrified glass with minor plagioclase, opaque phases and clinopyroxene.

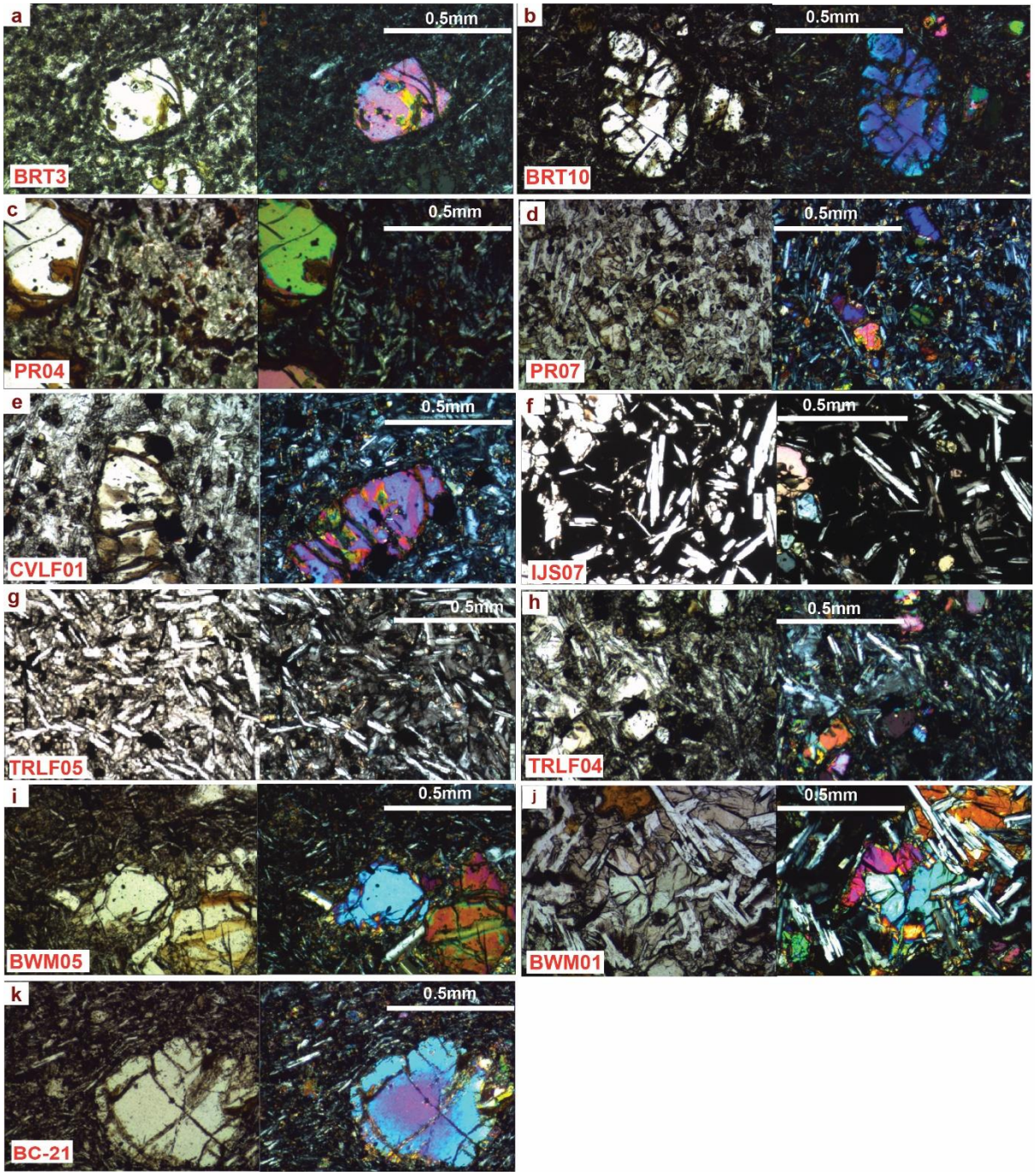

Figure 5.4: Photomicrographs (left- plan poles; right-crossed poles) of representative examples from volcanic provinces: Barrington (BRT3 and BRT10), Peak Range (PR04 and PR07), Springsure (CVLF01 and IJS07), Bauhinia (TRLF05 and TRLF04), Mitchell (BWM04 and BWM01) and Monto (BC-21).

The Barrington samples range in MgO from 8.8 to 12.9 wt%. Harker diagrams between major elements and MgO indicate little variation of major element concentrations with increasing MgO content (Fig. 5.5). Plots of incompatible elements vs. Th show generally increasing trends, implying fractional crystallisation (Fig. 5.5). The high Th concentrations in Barrington

samples, relative to the other volcanic provinces, suggest significant crustal assimilation. Normalised rare earth element (REE) diagrams show general enrichments of LREE over HREE and primitive mantle (Fig. 5.6; *Sun and McDonough*, 1989). Normalised La/Lu ratios range between 13.1 and 26.4, defining an OIB-type pattern (Fig. 5.6). Multi-element spidergrams also illustrate a pattern similar to OIB magmatism, although they include a significant negative K anomaly (Fig. 5.7). The Barrington samples also have substantial positive Sr, Pb and Th anomalies. The samples range in Sr and Nd isotopic ratios from 0.703218 to 0.703357 and 0.512910 to 0.512889, respectively, and cluster around the EMI (enriched mantle I) mantle compositional array (Fig. 5.8).

5.4.1.2 Peak Range

Samples from the Peak Range province are typically aphanitic to microporphyritic alkali basalts to trachy-basalts (Figs. 5.4c-d, and 5.5). They consist of plagioclase (45 vol%), olivine (25%), clinopyroxene (15%), devitrified glass (10%), and minor opaque phases (5%). Plagioclase occurs both in the groundmass (35%) and as euhedral to anhedral phenocryst laths (10 %) that are typically <0.5 mm but up to 1 mm in length in sample PR04. Olivine phenocrysts (10 %) are subhedral to anhedral and less than 0.5 mm, with minor alteration to iddingsite. Groundmass olivine comprises 15% of the sample. Clinopyroxene is found primarily in the groundmass (10%), with minor occurrences as subhedral phenocrysts (5%). The opaque phases are typically titanomagnetite and ilmenite.

MgO from the Peak Range samples ranges from 7.09 to 10.17 wt%. Major elements plotted against MgO define two main clusters. The higher MgO cluster is typically associated with higher CaO and TiO_2, and lower Al_2O_3, SiO_2 and Na_2O than the lower cluster (Fig. 5.5), suggesting fractionation of clinopyroxene. The clusters are not correlated with age. Normalised REE diagrams show LREE enrichment and relative HREE depletion, similar to OIB-type magmatism ([La/Lu]N 4.9 to 14.3; Fig. 5.6). All multi-element spidergrams have OIB-type trends and have positive Sr, Pb, and Ba anomalies (Fig. 5.7). Samples from the older generation of flows have a negative K anomaly that is absent in younger samples. The Peak Range samples cluster along the EMI array with possible contributions from EMII (Fig 5.8), with Sr, Nd and Hf isotopic ratios of 0.704483 to 0.703304, 0.512958 to 0.512652, and 0.283039 to 0.282826, respectively.

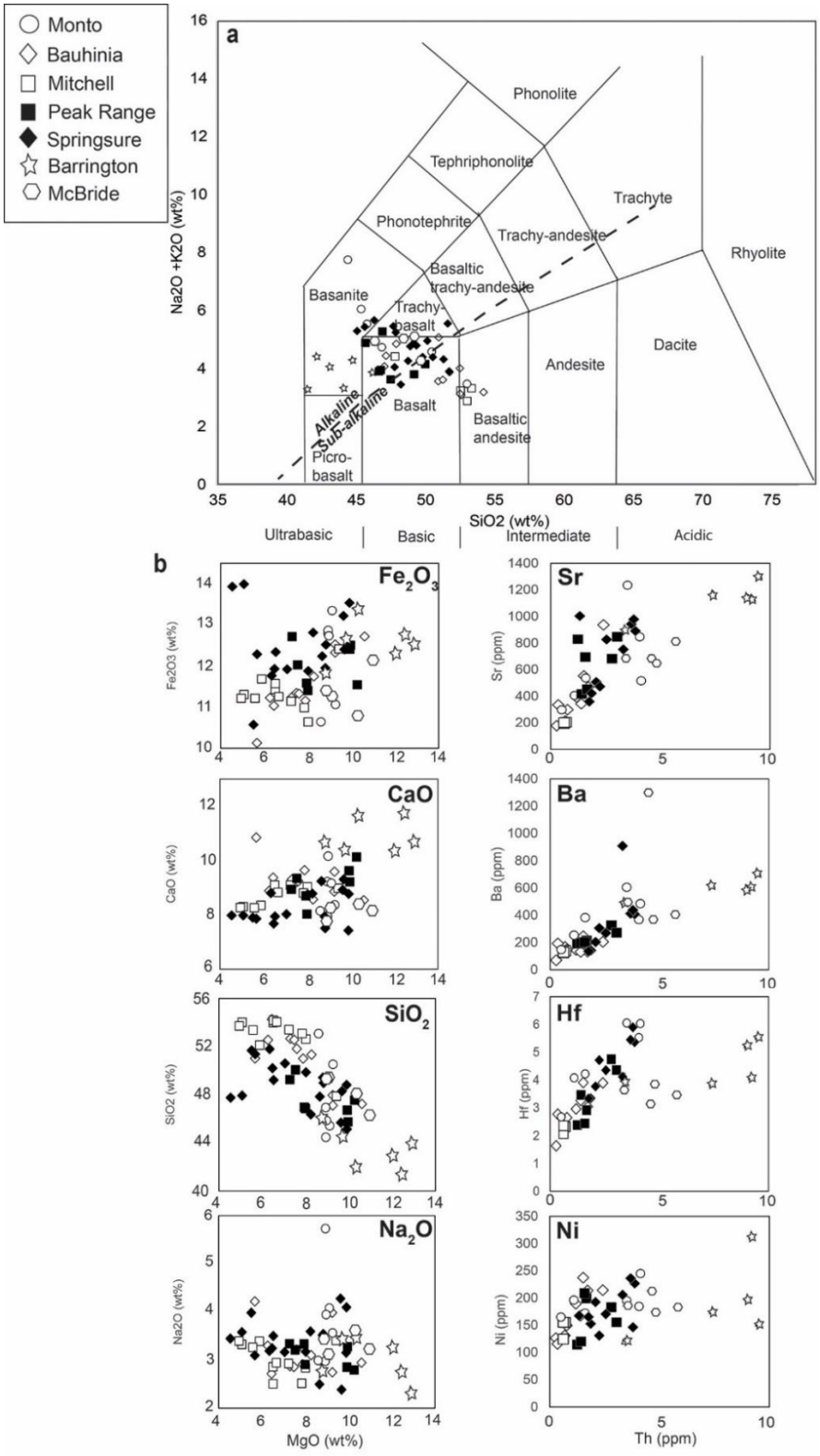

Figure 5.5: Major element compositions of volcanic rocks from the east Australian Cenozoic volcanic zone by a) Total Alkali vs. Silica diagram (*Le Bas et al.*, 1986; anhydrous basis); and b) Major and trace element harker diagrams for both central volcanoes (black) and lava-fields (hollow).

5.4.1.3 Springsure

Springsure samples are melanocratic, aphanitic to porphyritic, basalts to trachybasalts (Figs. 5.4e-f and 5.5). The groundmass is primarily composed of euhedral plagioclase (30-40%) and olivine (10-20%), with minor opaque phases (10-15%) and clinopyroxene (10-15%). Phenocrysts are large (up to 0.5 mm), euhedral to subhedral olivine (up to 10-15%), with less frequent plagioclase (up to 5%) and clinopyroxene (up to 5%). Clinopyroxene is often altered. Opaque phases are commonly titano-magnetite, and less frequently magnetite and ilmenite. Olivine crystals commonly have minor alteration to iddingsite. Plagioclase laths surrounding amygdales are sericitised in large reaction halos. Some samples, particularly the younger ones, have a large component of devitrified glass.

The Springsure samples have MgO ranging from 4.41 to 8.45 wt%. Major elements plotted against MgO show a general decrease in SiO_2 with increasing MgO (Fig. 5.5) and weak correlations with other elements. However, the data are reasonably dispersed. Positive trends are observed in plots of Hf, Nd and Zr vs. Th (Fig. 5.5). Normalised REE patterns indicate LREE enrichment and HREE depletion ([La/Lu]N 7.2 to 33.6; Fig. 5.6), producing a steep gradient that is reminiscent of OIB-type magmatism, as are spidergrams from these samples (Fig. 5.7). The REE gradients become steeper with decreasing age. Radiogenic isotope ratios cluster around the PHEM source, along the EMI mantle array (Fig. 5.8) with Sr, Nd, and Hf isotopic ratios of 0.704083 to 0.703884, 0.512797 to 0.512768, and 0.282966 to 0.282891, respectively.

5.4.1.4 Bauhinia

The Bauhinia samples are melanocratic, aphanitic to porphyritic, alkali to hawaiite basalts (Figs. 5.4g-h and 5.5). Their groundmass contains significant proportions of olivine and plagioclase. Olivine (up to 15 vol.%) and plagioclase (up to 20%) are the main phenocrysts phases, up to 0.5 mm in size, with minor, usually altered, clinopyroxene (up to 5%). Plagioclase has albite twinning and accounts for approximately 60% of the samples, with 40% in the groundmass and up to 20% as euhedral to subhedral phenocryst phases. Opaque phases (10%) include subhedral titano-magnetite and ilmenite. The youngest Bauhinia sample (CIB), collected from the volcano plug, is coarser grained than other samples and has more clinopyroxene in both the groundmass (20%) and as a phenocryst phase (up to 10%). Samples BWB2 and BWB6 are similar in composition and texture. All samples include a component of devitrified glass.

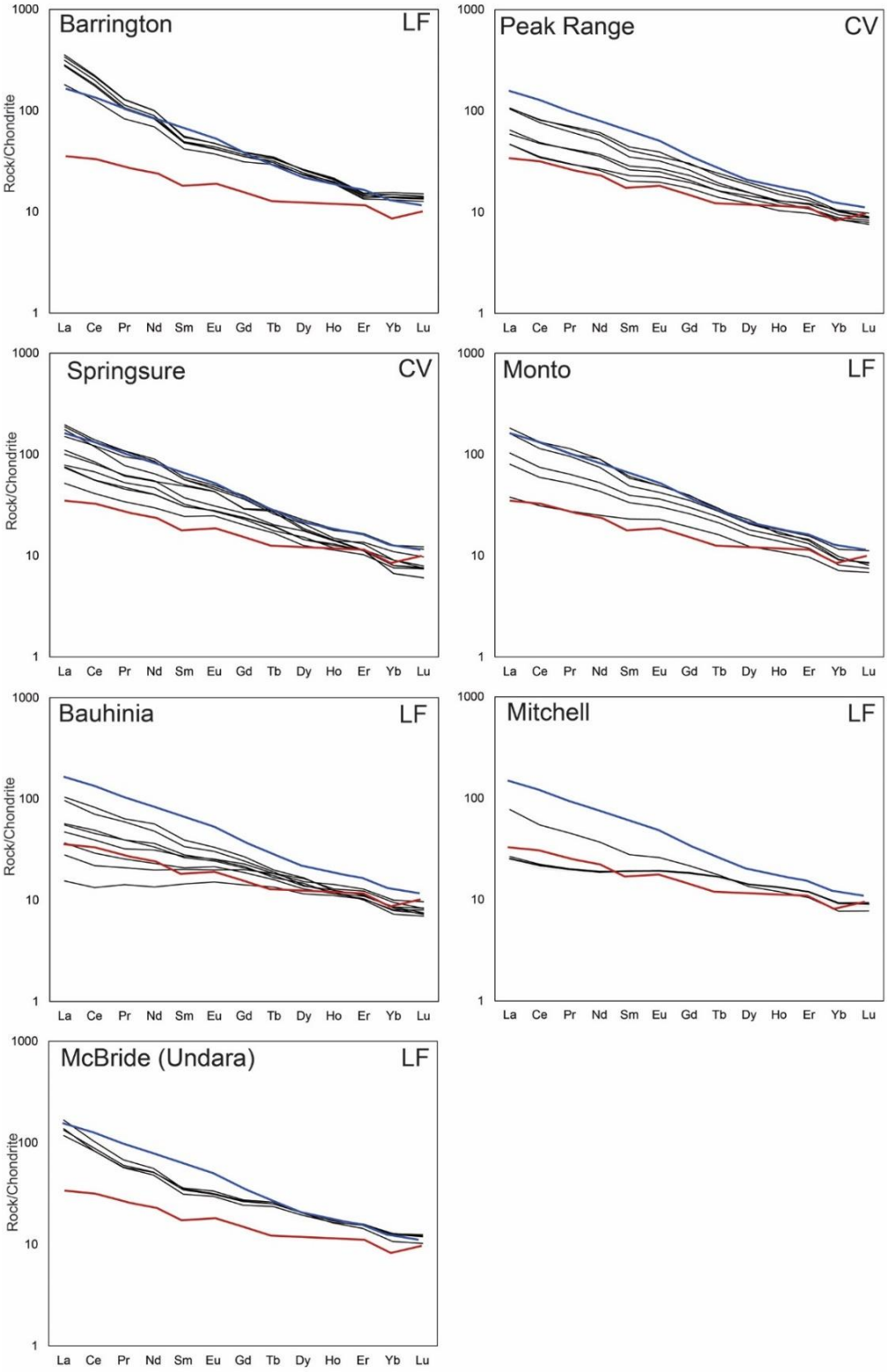

Figure 5.6: Chondrite-normalised REE diagrams in order of decreasing age. Samples were filtered such that only samples with MgO >7 wt% were selected. Normalisation factors after Sun and McDonough (1989). OIB (blue; *Sun and McDonough,* 1989) and lower crust (red; *Rudnick and Fountain,* 1995) are included for comparison. LF: lava-field; CV: central volcano.

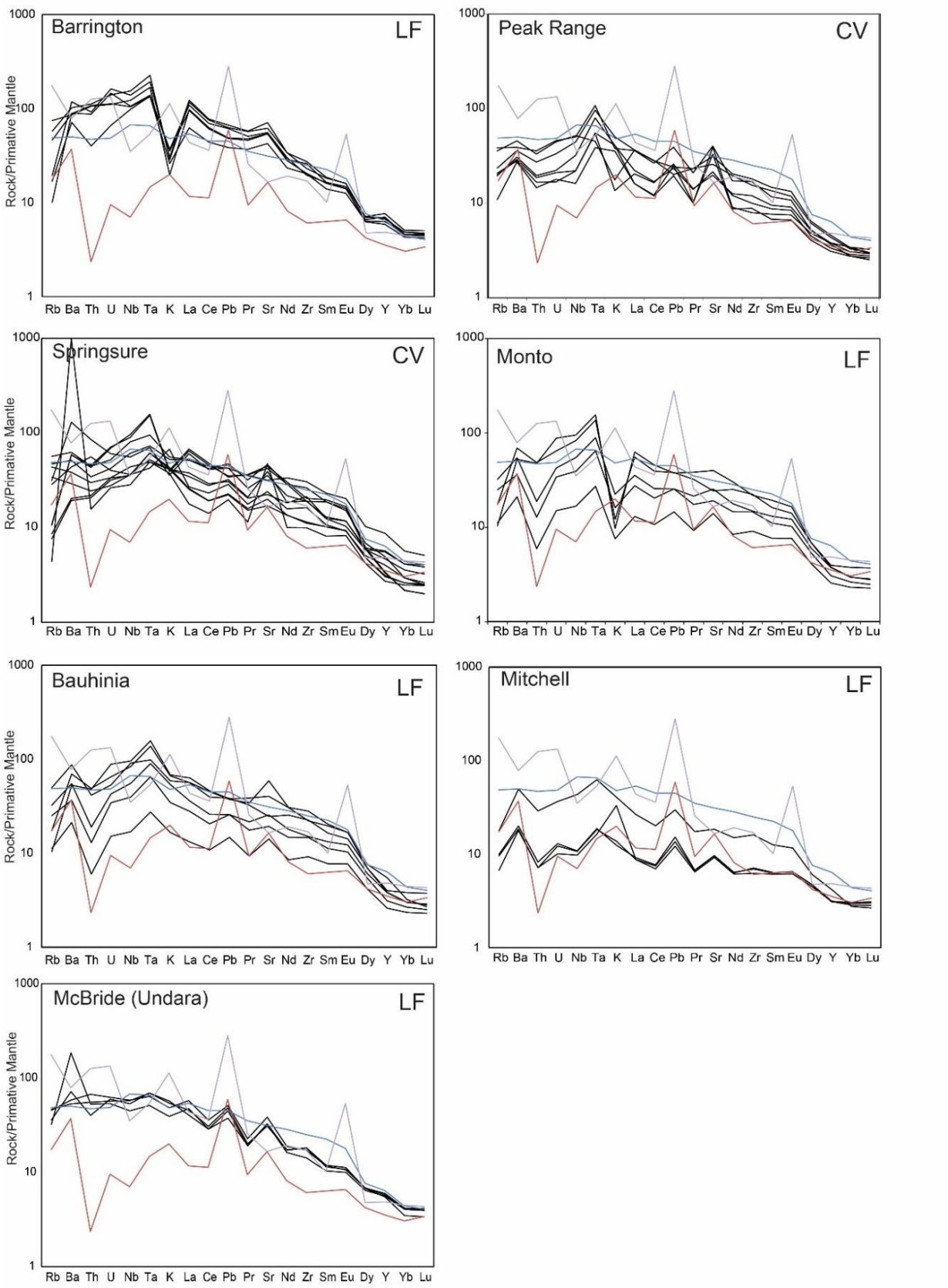

Figure 5.7: Primitive mantle-normalised multi-element diagrams in order of decreasing age. Samples were filtered such that only samples with MgO >7 wt% were selected. Normalisation factors after Sun and McDonough (1989). OIB (blue; *Sun and McDonough*, 1989), Upper-crust

(purple; *Rudnick and Fountain*., 1995) and lower crust (red; *Rudnick and Fountain*, 1995) are included for comparison. LF: lava-field; CV: central volcano.

MgO from the Bauhinia samples ranges from 5.64 to 10.36 wt%. Plots of major elements against MgO show a general increase of TiO_2 and Fe_2O_3, and decreases in SiO_2 and CaO, with increasing MgO. A comparison between Hf, Nd and Zr vs. Th show generally increasing trends (Fig. 5.5). Normalised REE diagrams indicate two trends: OIB-type (steep gradient) and E-MORB-type (flat gradient; $[La/Lu]_N$ 2 to 14.9; Fig. 5.6). Spidergrams of Bauhinia samples indicate enrichment of Ba, Pb, Sr, and K relative to primitive mantle (Fig. 5.7), although one sample shows a slight negative K anomaly. The Bauhinia samples have isotopic compositions that extend between the PHEM and HIMU source components, along the EMI array (Fig. 5.8). The samples have Sr, Nd, and Hf isotopic ratios of 0.703574 to 0.703451, 0.513016 to 0.512905, and 0.283117 to 0.282993, respectively.

5.4.1.5 Mitchell

Samples from the Mitchell province are typically aphanitic to porphyritic melanocratic alkali to hawaiite basalts (Figs. 5.4i-j and 5.5). The samples range from very fine to fine-grained, with minor euhedral to subhedral phenocrysts consisting primarily of clinopyroxene (up to 10%), plagioclase (up to 15%), and olivine (up to 5%) that are usually <0.5 mm, but up to 1 mm in some instances. The groundmass generally consists of plagioclase (60%), with lesser amounts of olivine (15%) and clinopyroxene (10%). Opaque phases (5%) are typically euhedral titanomagnetite. Sample BMW1 has interstitial clinopyroxene, with olivine as a phenocryst phase. Sample BWM5 includes a significant component of devitrified glass in the groundmass.

MgO from the Mitchell province ranges from 4.89 to 9.17 wt% (Fig. 5.5). Harker diagrams show general decrease in TiO_2, Fe_2O_3, K_2O and SiO_2 and increasing CaO content with increasing MgO, although correlations are poor due to high data dispersal. Comparison of Hf, Nd and Zr concentrations vs. Th show generally increasing trends within the range of other provinces (Fig. 5.5). Normalised REE gradients are reasonably flat, but are still more similar to OIB than to E-MORB ($[La/Lu]_N$ 2.9 to 10.4; Fig. 5.6). Multi-element spidergrams are similar to OIB (Fig. 5.7). Isotopic compositions are along the EMI compositional field (Fig. 5.8). Samples have Sr, Nd, and Hf isotopic ratios of 0.70372 to 0.70409, 0.51286 to 0.51292, and 0.28300 to 0.28303, respectively.

5.4.1.6 Monto

The Monto samples are very fine to fine-grained aphanitic to microporphyritic alkali basalts (Fig. 5.4k). Olivine phenocrysts (up to 10%) are commonly weathered to iddingsite and are <0.5mm in size. The groundmass contains plagioclase (50 %), clinopyroxene (15%) and minor olivine (5-10 %). The main phenocrysts are clinopyroxene (up to 5 %) and plagioclase (up to 15 %) that are marginally altered to sericite. Opaque phases are typically magnetite and ilmenite and account for approximately 3% of the total volume. MgO ranges from 8.49 to 9.17 wt%. Mg# is low (<45) for all samples.

The Monto sample have little variation in MgO content, but significant variation in other major elements such as SiO_2, CaO_2 and Al_2O_3. Hf, Nd and Zr and positively correlated with Th (Fig. 5.5). Both normalised REE and spidergrams are distinctly OIB-like, and all samples have positive Pb, Sr, and Ba anomalies, as well as a negative K anomaly ($[La/Lu]_N$ 5.7 to 22.4; Figs. 5.6 and 5.7). Isotopic compositions lie on a mixing array between EMI and HIMU (Fig. 5.8). Samples have Sr, Nd, and Hf isotopic ratios of 0.70298 to 0.70398, 0.51270 to 0.51299, and 0.28274 to 0.28306, respectively.

5.4.1.7 Undara (McBride)

The Undara samples are aphanitic to microporphyritic basalts to trachy-basalts. The groundmass of the samples consists of euhedral to anhedral plagioclase laths (50%), olivine (25%), clinopyroxene (20%), and opaque phases (5%). Euhedral to anhedral plagioclase and olivine (<1 mm) are the main phenocryst phases, with minor clinopyroxene. The plagioclase in some samples is altered to sericite or replaced with calcite. Opaque phases are primarily titanomagnetite, with minor ilmenite and hematite.

MgO of the Undara samples ranges from 8.88 to 11 wt% and has little correlation with other major elements (Fig. 5.5). Increasing trends are observed between incompatible elements and Th show (Fig. 5.5). Normalised REE diagrams suggest OIB-type magmatism, with LREE enrichment over HREE ([La/Lu]N 11.4 to 13.9; Fig. 5.6), as do the multi-element spidergrams (Fig. 5.7). The samples have Ba, Sr, and Pb enrichments relative to OIB. Isotopic compositions lie on an array from EMI to EMII (enriched mantle II; Fig. 5.8). The samples have Sr and Nd isotopic ratios of 0.704634 to 0.703900 and 0.512696 to 0.512933, respectively.

5.4.2 Principal component analysis

In an effort to quantify geochemical differences between volcanic provinces, I employed multivariant statistics in the form of a principal component analysis (PCA) using the PAST free software (*Hammer et al.,* 2001) of a suite of trace element ratios and radiogenic isotope data (e.g. *Ubide et al.,* 2014), including previously published compositions (North Queensland basalts – *Zhang et al.,* 2001; Nebo – *Sutherland,* 2003; New South Wales basalts – *O'Reilly and Zhang,* 1995; *Zhang et al.,* 1999; Newer Volcanics Province – *Price et al.,* 1997; *McBride et al.* 2001; *Demidjuk et al.,* 2007; *Van Otterloo et al.* 2014; Macedon - *Paul et al.,* 2005; Older Volcanics Province – *Price et al.,* 2014) together with my new data described in preceding sections. Samples were filtered such that only samples with MgO >7 wt% were selected for analysis, to avoid the complication of extensive fractional crystallisation affecting the analysis. PCA reduces initial variables (elemental concentrations) into principal components ordered such that those that account for the highest variability are the main components (*Joliffe,* 2002).

5.5 Discussion

5.5.1 Geochemical variations in Central Queensland volcanic provinces

5.5.1.1 Undara

Samples from the Undara Volcano, part of the McBride province, illustrate relatively low degrees of crustal contamination (Fig. 5.9A) and indicate steep OIB-type REE depletion gradients (Fig. 5.6), with high $[La/Lu]_N$ (11.4 to 13.9) and $[La/Yb]_N$ ratios. The relative enrichment of LREE over the HREE is indicative of melting in the garnet stability field (1.6 – 1.7 GPa; 55 km; *O'Reilly and Griffin,* 1996; *Fishwick et al.* 2008; *Van Otterloo et al.* 2014). Since Tb is (1) more incompatible in garnet than Yb, and (2) unaffected by melting of phlogopite (*Yang et al.,* 2003), high Tb/Yb (>0.3; $[Tb/Yb]_N \geq 1.4$) implies melting at or below the garnet stability field (*Jicha et al.,* 2009). In the case of Undara, primitive mantle normalised Tb/Yb places melting below the garnet stability field. Using the model of Wood (2004), I calculate the melting pressure and depth of the most primitive sample to be 1.9 GPa, which corresponds to a depth of 60 to 70 km. Based on the location of the lithosphere-asthenosphere boundary, initial melt generation must have occurred in the asthenosphere (>55 km; *Fishwick et al.,* 2008).

Multi-element spidergrams also indicate OIB-type magmatism (Fig. 5.7). High Ba concentration is accompanied by anomalously high Pb and Sr concentrations, and Nb/U, Ce/Pb,

Th/Ta and Rb/Cs are all anomalously high for OIB-type magmas. The anomalies are likely, therefore, related to crustal contamination rather than a feature of the source of melting. Similar to the Barrington province, samples from Undara contain unusually high Th concentrations relative to the other volcanic provinces, suggesting that crustal contamination might have played a major role. These samples are also more enriched in compatible elements than all other provinces, which could be a result of a marginally higher olivine content or the more primitive composition.

Pb, Sr and Nd isotope ratios cluster along the EMI array, with excursions towards EMII (Fig. 5.8). The samples extend from the I-MORB array towards the P-MORB mantle field along the Northern Hemisphere Reference Line (NHRL), contrary to suggestions made by the work of O'Reilly and Zhang (1995).

5.5.1.2 Peak Range

While geochemical data from the Peak Range province are restricted, there is no significant distinction in major element, trace element, or source components for different age groups in the province. Incompatible elements, such as Hf, Nd and Zr, plotted against Th show generally increasing trends, which may imply fractional crystallisation (Fig. 5.5). Anomalous Sr concentration values could be accounted for by minor crustal contamination, supported by the examination of select trace element ratios that extend toward the lower crust (Fig. 5.9A). Excluding one 47 Ma sample, REE diagrams from Peak Range indicate decreasing degrees of melting over time (Fig. 5.6). The presence of a negative K anomaly in the older samples, which is lessened or absent in younger rocks, reflects an unmelted K-bearing hydrous phase in the source (Fig. 5.7). The progressive change over time implies that the magmas were generated from the same magma chamber rather than two different volcanoes. Similarly, all samples fall along the EMI source array (Fig. 5.8). Models of the generation of these melts imply deep melting ($[La/Lu]_N$ 4.9 to 14.2; $[Tb/Yb]_N$ 1.6 to 2.4), with the most primitive samples originating from approximately 1.6 GPa (using the method of *Wood* 2004), which coincides with the garnet stability field and base of the lithosphere in Australia (*O'Reilly and Griffin*, 1996). A recalculation of the trace and major element abundances to the "primary melt" (Mg# 70; *Van Otterloo et al.*, 2014), indicates formation of the parental melt at pressures of 2 GPa, well into the asthenosphere.

Magmatism at Peak Range occurred for over 10 My, which is far longer than the average activity of central volcanoes (1-3 Myr; *Wellman and McDougall,* 1974a; *Cohen et al.,* 2007). The Peak Range volcanic province is at odds with a simple plume model for east Australian mafic magmatism. Peak Range includes three periods of volcanic activity: a pulse of magmatism at 47 to 45 Ma, a pulse between 35 and 31 Ma, and a final pulse at 25 Ma (*Jones et al.,* 2017). If Peak Range volcanism was plume-related, either the plume was active far longer than previously suggested, or plume-related volcanic rocks overlie an older lava-field.

5.5.1.3 Springsure

Trace element ratios show that there is little to no significant crustal contamination in the Springsure province, as all samples are within the mantle range (Fig. 5.9A; *Hoffman et al.,* 1986). $[Tb/Yb]_N$ ratios for samples from the Springsure province (1.8 to 4.3) imply a depth of melting below the garnet stability field. The gradual decrease of $[La/Lu]_N$ ratios with decreasing age (9.9 to 33.9) reflects an increase in melting fraction over the life of the volcano. The change in REE ratios correlates with the decreased pressure of melting calculated for these samples. Approximate degree of melting is around 5-10% for the most primitive samples. Melting pressures in Springsure samples are between 1.6 and 0.8 GPa, though this includes the lower intrusive rocks of the Springsure province. The oldest primitive sample from the extrusive samples (Mg# 59.3) produces a pressure of 1.2 GPa, well above the garnet stability field, though both multi-element spidergrams and REE diagrams indicate a source enriched in garnet. The modelled primary melt composition at Mg#70 supports melting at depths of 2 GPa, close to the garnet stability field and within range of the asthenosphere.

Both trace element and isotopic ratios indicate generation from an EMI type source in the asthenosphere, and a change in melting rates as the magmas ascended. The enrichment of Ba, Pb, and Sr relative to neighbouring elements is likely a result of variable degrees of crustal assimilation. Despite enrichment of Pb and Sr relative to the primitive mantle (Fig 5.7; *Sun and McDonough,* 1989), crustal contamination is minimal (Fig. 5.9), implying a short time of residence within the crust.

5.5.1.4 Bauhinia

Trace element ratios (Nb/U, Ce/Pb and Th/Ta) from the Bauhinia province indicate low to moderate degrees of crustal contamination (Fig. 5.9A). Multi-element spidergrams show

variable enrichment of Pb, Sr and Ba, consistent with upper-crustal assimilation. Modelling suggests that the basalts could be formed by approximately 10% melting of an enriched MORB source. $[Tb/Yb]_N$ values of 1.7 to 2.7 imply melting from the garnet stability field up to shallow depths. The pressure of formation places generation of melting at 1.6 to 0.02 GPa in the upper mantle, consistent with the increase in melt proportion indicated by the change in REE gradient ($[La/Lu]_N$ 2 to 15.1; Fig. 5.6). Melting occurred in an EMI-type source in the asthenosphere. As the Mg# (65.3) are not sufficient to imply primary melt, regression modelling of compositions back to Mg70 indicates melting pressures of 2.9 GPa.

5.5.1.5 Mitchell

Samples from the Mitchell province have a typical OIB-type multi-element spidergram pattern. Enrichment of Sr, Ba and Pb are typical of contamination by upper-crustal material, supported by the range of Nb/U, Ce/Pb and Th/Ta values which extend toward the composition of upper crust (Fig. 5.9A). $[La/Lu]_N$ values (2.9 to 10.4) progressively decrease between samples, but the most primitive (Mg# 63.2) samples indicate melting of a source rich in garnet ($[Tb/Yb]_N$ 1.8 to 2.3). The patterns range from OIB to EMORB, similar to the Bauhinia province farther to the north, which may reflect an increase in melt proportion over time. However, pressures of formation of these samples are between 1.2 and 0.1 GPa, far above the garnet transition zone.

As this is the case, it is likely these samples are more evolved than the parental melt. As the samples are not primitive enough to represent primary melts, the Mg#70 composition suggests that melting at pressures of 2 GPa would be sufficient to produce a parental magma with these source compositions.

Isotopic ratios place the samples from the Mitchell province along the EMI-type array, similar to the nearby Bauhinia and Springsure provinces within the Dupal lead anomaly zone. Finally, based on geochemical, geographic, and geochronological similarities, I conclude that the lava-fields of the Bowen Basin region are essentially indistinguishable from neighbouring central volcanoes.

5.5.1.6 Monto

Melting in the Monto province produced OIB-type multi-element spidergrams, with enrichment of Sr and Pb relative to primitive mantle. The enrichment of Sr and Pb are consistent with the spread of samples toward the upper crust in Nb/U, Ce/Pb and Th/Ta

discrimination diagrams (Fig. 5.9A). Modelling of primitive mantle-normalised U to Pb diagrams imply, however, that crustal contamination does not substantially alter the mantle chemistry of the samples (Fig. 5.9B). K-depletion is apparent in some samples, evidence of incomplete melting of a K-rich phase, such as phlogopite, in the source (Fig. 5.7). The presence of the K anomaly in only some samples may be a sign of changing melt conditions of the source over time.

$[La/Lu]_N$ values imply the presence of a residual garnet phase in the source (5.5 to 22.6). Depth of melting is constrained to below the garnet stability field ($[Tb/Yb]_N$ 2.3 to 3.3) and at pressures of 2.2 GPa (using the method of Wood [2004]), well into the asthenosphere (>80 km). These samples were generated from an EMI type source, similar to other volcanic provinces in the Bowen Basin.

5.5.1.7 The Barrington province

Th/Ta and Ce/Pb vs. Nb/U diagrams (Fig. 5.9A) suggest that samples from Barrington are affected by minor amounts of lower crustal contamination. Primitive mantle-normalised Pb vs. U correlations in filtered samples (MgO >7wt%; Fig. 5.9B) support the role of crustal contamination in Barrington, which has U concentrations that exceed even upper crust values (*Rudnick and Fountain*, 1995) that are not matched by high Pb. An AFC mixing array between average OIB and upper or lower crust indicates that the composition of the Barrington province is consistent with up to 5% assimilation of the lower crust. Bulk distribution modelling also indicates that fractionation was dominated by olivine, plagioclase, and clinopyroxene (Fig. 5.9B).

Multi-element spidergrams show not only enriched Pb and Sr, indicative of crustal contamination, but also a negative K anomaly similar to the Monto province. The combination of the negative K anomaly, steep REE gradients and the high $[La/Lu]_N$ values (13.2 to 26.6) imply melting in a source that included both garnet and amphibole. $[Tb/Yb]_N$ values are 2 to 2.6, and constrain the source depth to the garnet stability field ($[Tb/Yb]_N \geq 1.4$). Modelled pressures are between 1.95 to 0.8 GPa, placing melt generation in the asthenosphere. Radiogenic isotopic ratios indicate an EMI-type source, with an I-MORB component (208/204Pb v. 206/204Pb) close to the Dupal array.

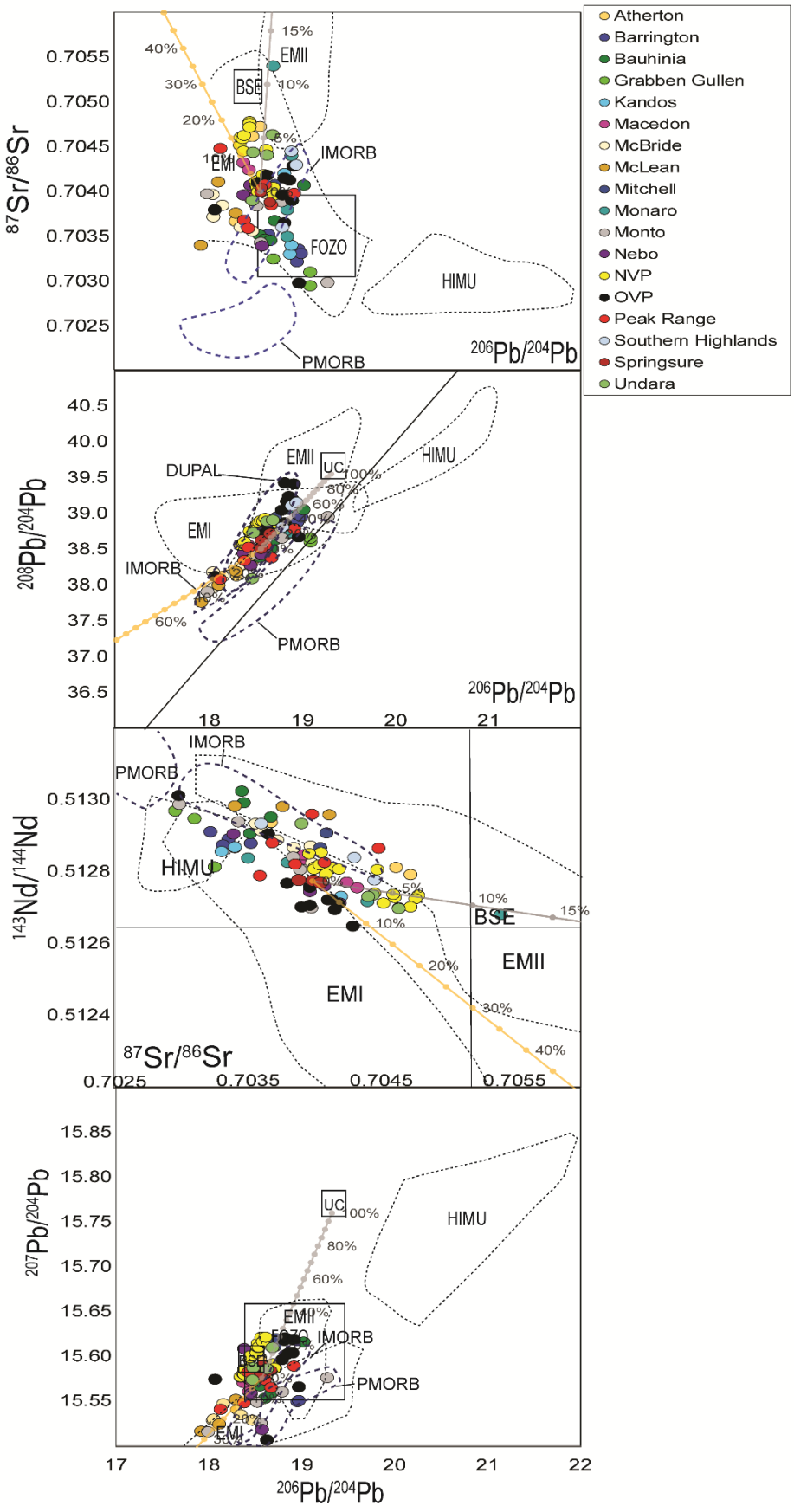

Figure 5.8: Filtered samples (MgO >7%) plotted on radiogenic isotope source component diagrams. Lines of mixing between the most primitive sample (CIK) and the upper (grey line)

and lower (yellow line) crusts are included. Mantle source components downloaded using the GEOROC database (Geochemistry of Rocks of the Oceans and Continents, http://georoc.mpch-mainz.gwdg.De) EMI – Pitcairn-Gambier, Gough and Tristan Du Cunha (*Gast, Tilton and Hedge,* 1964; *Sun Shen-su,* 1980; *Woodhead and McCulloch,* 1989; *La Roex et al.,* 1990; *Class and La Roex,* 2008; *Willbold and Stracke,* 2010; *Garapic et al.,* 2015), EMII –Samoan Islands (*Workman et al.,* 2004; *Jackson et al.,* 2007; 2010; 2014) and HIMU – St. Helena (*Sun Shen-su,* 1980; *Willbold and Stracke,* 2010; *Salters et al.,* 2011) field plotted for comparison. FOZO (*Winter,* 2010) included for reference. Samples are displayed by classification as either central volcanoes (black) or lava-fields (grey). NSW sample fields after O'Reilly and Zhang (1995, 1999; Grabben Gullen, Southern Highlands, Kandos) and North Queensland (Atherton, McBride, McLean) after Zhang et al. (2001).

5.5.2 Principal component analysis

The criteria described by Wellman and McDougall (1974a) for classifying east Australian mafic provinces were based on field observations and simple geochemistry. While the classification criteria have since been relaxed to accommodate newer data (*Johnson et al.,* 1989), many provinces still fail to meet these criteria. Furthermore, REE, multi-element, and source component diagrams (Figs. 5.6, 5.7 and 5.8) do not indicate significant differences between central volcanoes and lava-fields. While the central volcanoes do appear to have a more restricted range, this likely because there are fewer mafic data from central volcanic provinces (four provinces) relative to the lava-fields (twelve provinces).

Principal component analysis of new and previous trace element and radiogenic isotopic ratios highlights geochemical distinctions between provinces that are otherwise obscured in the trace element and radiogenic isotope data. The full list of available data was first subjected to the screening process (MgO >7wt%; Mg# >60). Trace element ratios were then calculated for all remaining data and used to compare differences in source characteristics and melting. The ratios were selected to represent depth and degree of melting (Tb/Yb, La/Lu, La/Yb), source characteristics (Rb/Ba, Ti/Zr) or crustal contamination (Ba/Y, Sr/Y, Nb/Th, K/Nb). Provinces were then grouped in four different ways. First, the samples were grouped by geographical region (Fig. 5.10a) and by their approximate age (Fig. 5.10b). Then the provinces were grouped into central volcano, lava-field, or "miscellaneous" categories (Fig. 5.10c). The "miscellaneous" category consists of provinces that include variably evolved magmas but were not classified as central volcanoes. Finally, provinces were compared provincially. The results

indicated compositional overlap between both central volcanoes and lava-fields, and little to no influence of age, location or provinciality (Fig. 5.11).

PCA of trace element ratios illustrates significant overlap between different provinces regardless of type, age, location and provinciality. PCA shows that most of the geochemical variability along PC1 is related to crustal contamination, and therefore much of the geochemical variation between and within provinces along the PC1 axis may arise from crustal assimilation. The elements that control PC2 (La/Yb etc.) are more representative of the mantle and the limited variability along the axis indicates generation from a similar source. PCA of the trace element ratio dataset suggests three groups when compared on a provincial level: (1) a group composed of central volcanoes, young lava-fields, and the miscellaneous group; (2) the Barrington province; and (3) the Newer Volcanics Province/Macedon Volcano (Fig. 5.11; *McBride et al.,* 2001; *Paul et al.,* 2005; *Van Otterloo et al.,* 2014). PCA shows that most of the geochemical variability along PC1 may be related to crustal contamination (K/Nb, Sr/Y, Ba/Y ect.), though La/Sm and La/Yb are also constituents of PC1, while PC2 is dominantly mantle derived ratios (Nb/Th, Ti/Zr, Tb/Yb, Rb/Ba).

PCA of isotopic data revealed that Pb isotopes are the most variable between and within provinces (Fig. 5.11). PC1 was dominated by Sr, Nd and 208Pb isotope ratios, while PC2 was dominantly the variation of 206Pb isotope ratios. The amount of variation in Nd or Sr isotopes is consistent with the expected variation of the EMI field. The majority of samples clustered around the origin.

5.5.3 Similarities in the source and depth of melting

The depth and source of melting of lava-fields and central volcanoes are important for understanding the potential differences between volcanic provinces. In order to assess source characteristics, only samples with MgO >7%, limited crustal contamination and with no olivine accumulation from each province are discussed below. The degree and effects of crustal contamination were assessed using primitive mantle normalised Th/Ta and Ce/Pb vs. Nb/U diagrams (Fig. 5.9A). The samples most affected by crustal contamination are from McBride, Macedon and Barrington, which extend toward the lower crust field and have isotopic signatures between the EMI and EMII mantle components. Primitive mantle-normalised Pb vs U correlations in filtered samples (MgO >7wt%; Fig. 5.9B) support major crustal

contamination in McBride, Macedon and Barrington, which has the highest Th concentrations in my dataset. Barrington has U concentrations that exceed even upper crust values (*Rudnick and Fountain*, 1995). Assimilation-fractional crystallisation modelling indicates mixing of approximately 5 to 15% of upper crust with average OIB composition in the Macedon province, followed by plagioclase-controlled fractionation (Fig. 5.9B).

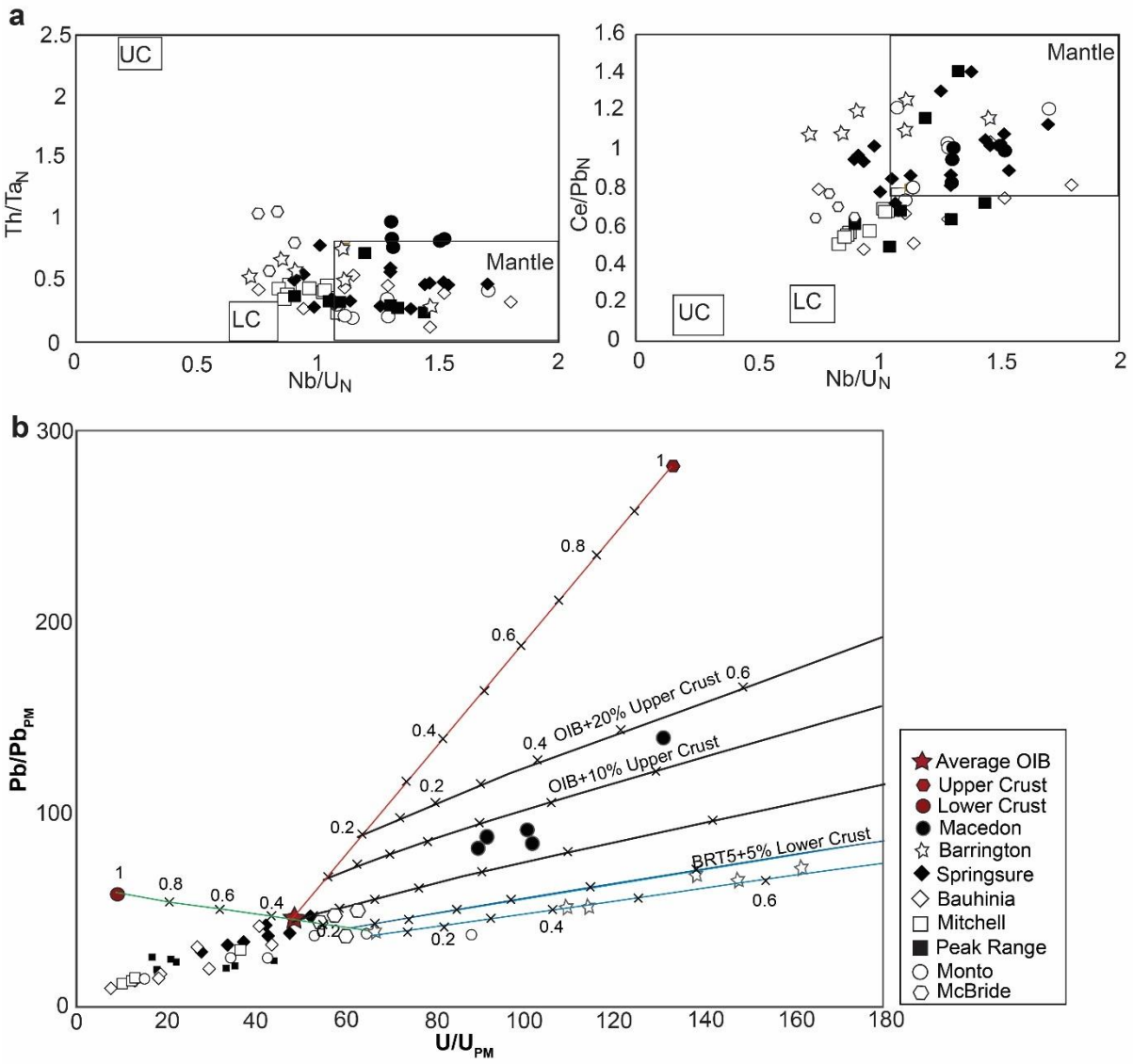

Figure 5.9: a) Crustal contamination diagrams of all samples using primitive mantle (*Sun and McDonough*, 1989) normalised Th/Ta and Ce/Pb against Nb/U. Lava-fields with significant crustal assimilation are plotted in grey. Nb/U and Ce/Pb mantle values from Hofmann et al. (1986) and crustal values from Rudnick and Fountain (1995). Th/Ta values from Condie (1994). b) Primitive mantle normalised trace element discrimination diagrams from filtered samples (>7wt% MgO). Average OIB is plotted for comparison. Average upper crust (*Rudnick and Fountain*, 2008) values were mixed with average OIB composition (*Sun and McDonough*, 1989) in 10% increments (red line) and fractionated using a simple Rayleigh fractionation equation

(black lines). The least fractionated sample from Barrington was used as the starting composition, mixed with average lower crust (green line; *Rudnick and Fountain,* 2008) and fractionated (blue lines).

Both lava-field and central volcano samples have fractionated REE normalised patterns (Fig. 5.6), where high $[Tb/Yb]_N$ varying from 1.6 to 4.3 suggest melt generation at the garnet stability field (>55 km; *Van Otterloo et al.,* 2014). Multi-element spider diagram patterns are in overall agreement with enriched mantle sources, with an OIB-type signature (Fig. 5.7). $[La/Yb]_N$, and $[La/Lu]_N$ indicate a change in the degree of melting between samples in all provinces (Table 2; *Serrano et al.,* 2011). A plot of $[Tb/Yb]_N$ vs. $[La/Yb]_N$ of the most primitive samples from each province illustrates the distribution of assumed melt depth and degree of melting (Fig. 5.12A) compared with melting curves produced by melting of garnet-amphibole peridotite and spinel-amphibole peridotite with a source similar to either the east Australian amphibole lherzolite (*O'Reilly and Griffin,* 1988) or the primitive mantle (PM; *Sun and McDonough,* 1989). The models use the melting proportions of Mayer et al. (2013) and modal mineralogy after Van Otterloo et al. (2014). Displacement of values to the right of the garnet PM curve would imply an enriched source, but not as enriched as the Australian average garnet-amphibole lherzolite suite (*O'Reilly and Griffin,* 1988). Most provinces exhibit moderate to low (<15% to <5%) degrees of melting (Fig. 5.12A). Geochemical data from the Springsure, Peak Range, and Bauhinia provinces, coupled with previous $^{40}Ar/^{39}Ar$ results (*Jones et al.,* 2017), indicate an overall decrease in the degree of melting with time, a pattern that reflects progressive fractionation and extraction of melts from single magma chambers.

First-order modelling of melt generation indicates low degrees of garnet-lherzolite melting in the most primitive samples from both central volcanoes and lava-fields at pressures from 1.2 to 2.3 GPa (Fig. 5.12B). As the model relies on anhydrous melting the samples follow the dry-peridotite solidus. However, as the solidus is not intersected by the Australian geotherm, melting must have occurred in the presence of water. While the temperatures are not reflective of melting temperatures, studies that have used this model have shown agreement between these modelled pressures and those produced by pMelts (*Van Otterloo et al.,* 2014). Most sites, with the exception of Mitchell and Springsure (1.2 GPa), had peak melting pressures below the garnet stability field (>1.6 GPa; *Van Otterloo et al.,* 2014). Regression modelling of samples from Mitchell, which were not sufficiently primitive enough (Mg#63.2) to represent source composition (<Mg#65), to composition Mg#70 indicated possible melting of the source at 2

GPa. The modelled melting pressures combined with steep REE gradients suggest that samples from both central volcanoes and lava-fields have source components generated from the garnet stability field. Samples from some of the lava-field and central volcanic provinces (e.g. Nebo – *Sutherland,* 2003; Macedon – *Paul et al.*, 2005) have a deep negative K anomaly (Fig. 5.7), indicating the presence of an unmelted K-rich phase (such as amphibole or phlogopite) in the lithosphere, indicative of metasomatism (*Van Otterloo et al.,* 2014). Trace element ratios have been shown to be able to distinguish whether a mantle source bears phlogopite (Ba/Rb <20, Rb/Sr >0.1) or amphibole (Ba/Rb >50, Rb/Sr <0.006; *Furman and Graham,* 1999). Given the prevalence of low Rb/Sr (<0.1) values, which would suggest amphibole, accompanied by low Ba/Rb (<20) and a negative correlation with Nb/Th characteristic of phlogopite (*Furman and Graham,* 1999) for the most primitive samples, it is likely that both are present in the source. Interestingly, as the east Australian volcanic provinces become younger, the negative K anomaly appears to be replaced with a positive Ba anomaly, suggesting that an initially residual metasomatic phase may become increasingly incorporated into the melts.

By combining new geochemical data with previous results from across eastern Australia, I have been able to examine regional-scale differences in the source components of Cenozoic magmatic provinces. A combination of PCA and modelling using radiogenic isotopes and trace element data from lava-fields and central volcanoes reveals no systematic differences in their source components and no significant variation not attributable to natural variation in EMI-type lavas (Fig. 5.11). The combined dataset suggests that all of the provinces are characterised by OIB-type magmatism falling along an EMI type array. Many of the slight geochemical variations of these provinces are attributable to different depths of equilibrium melting or crustal assimilation processes (Figs. 5.9 and 5.10). This finding implies a common source for the entirety of the east Australian Cenozoic volcanism. Such a long-lived, 2000 km-long belt of volcanic activity sourced from the same region of the mantle is unique by global standards (e.g., *Davies et al.,* 2015), and the common source component of lava-fields and central volcanoes is unaccounted for in previous explanations of east Australian Cenozoic mafic magmatism.

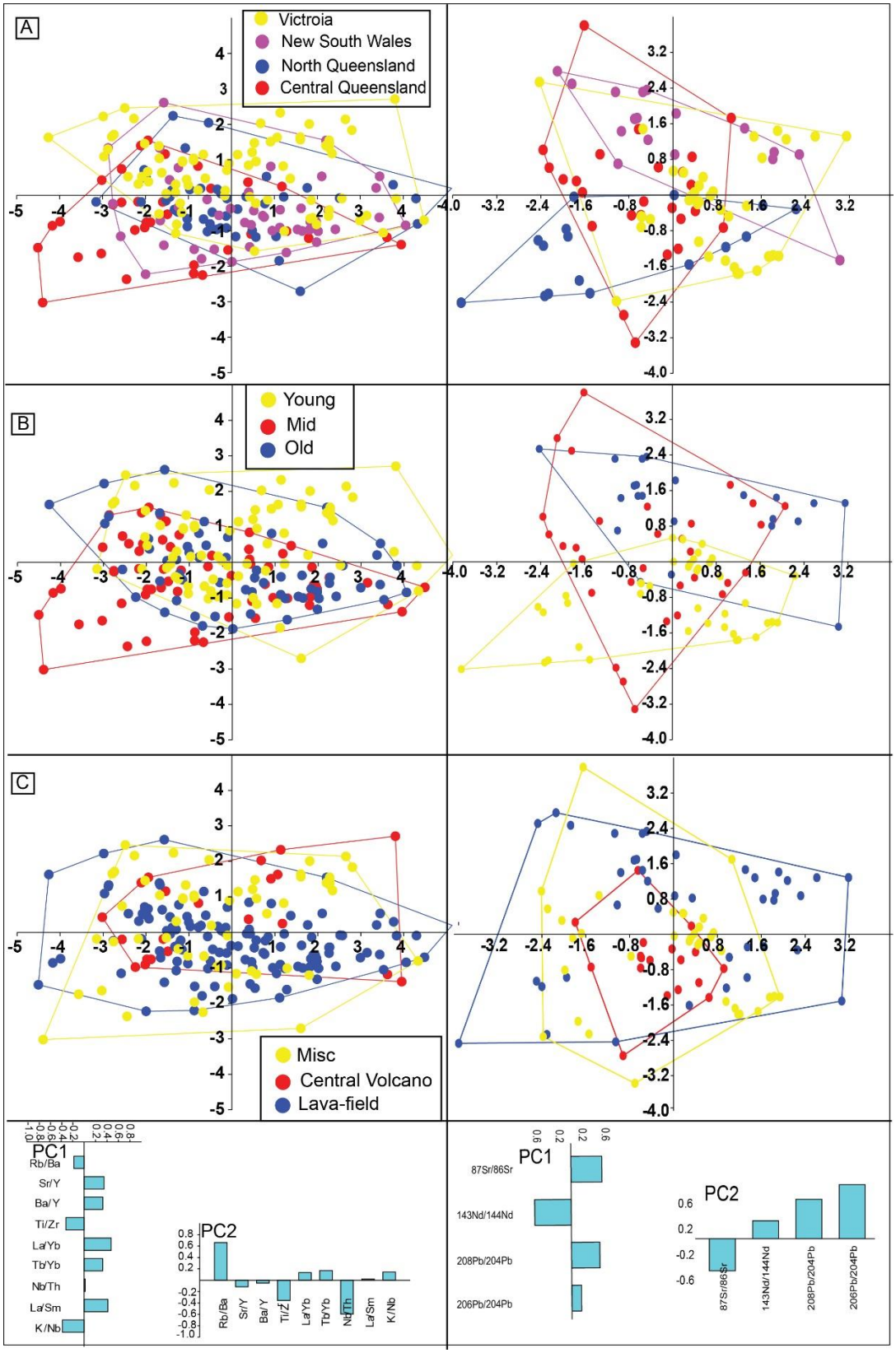

Figure 5.10: Principal component analyses of compiled whole rock trace element dataset. Polygon groups: a) region, b) age and c) type category.

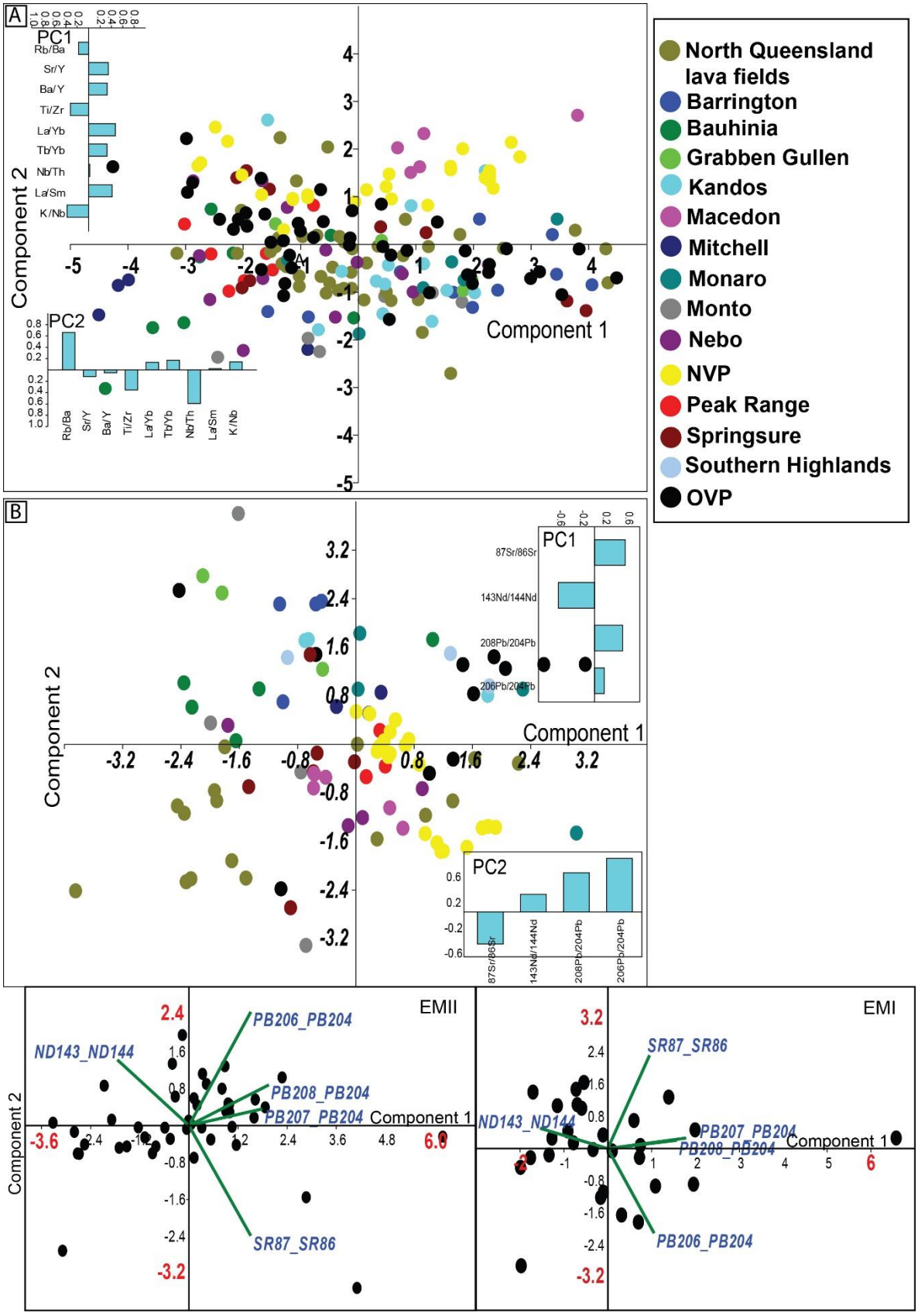

Figure 5.11: Principal component analyses of the compiled whole rock trace element and radiogenic isotope ratio dataset. Relative variation of EMI and EMII type volcanoes included for comparison.

5.5.4 Tectonic-magmatic relationships

Peak Range in particular is at odds with the "plume" model. The Peak Range volcanic province includes three periods of volcanic activity: a pulse of magmatism at 47 to 45 Ma, a pulse between 35 and 31 Ma, and a final pulse at 25 Ma (*Jones et al.*, 2017; Chapter 3 and 4). This age distribution indicates significant activity outside of the main phase used to define the overall age progression of central volcanoes. If Peak Range volcanism was plume-related, either the plume was active far longer than previously suggested, or plume-related volcanic rocks overlie an older lava-field.

While geochemical data from the Peak Range province are very restricted, there is no significant distinction in major element, trace element, or source components from the Peak Range province. Excluding one 47 Ma sample, REE diagrams from Peak Range indicate decreasing degrees of melting over time, similar to both the Springsure and Bauhinia provinces. If the geochemistry data are indistinct, it is not possible to distinguish between the age groups. The progressive change over time implies that the magmas are generated from the same static magma chamber rather than two different volcanoes. As such either magmatism occurred for over 10 Ma, which is far longer than the average activity of central volcanoes (1-3 Myr; *Wellman and McDougall,* 1974a; *Cohen et al.,* 2007), or there was no plume activity beneath the Peak Range volcano.

All provinces have a strong predilection toward I-MORB and the Dupal anomaly, at odds with the time-space correlation suggested previously (*Zhang et al.,* 1999). The reconstruction of Zhang et al. (1999) indicates that all volcanism in Victoria should be sourced from the P-MORB mantle, however neither the Newer Volcanics, Older Volcanics or Macedon have P-MORB-type signatures. Some provinces do include samples that extend from the Dupal anomaly to P-MORB (both Graben Gullen samples, along with one sample each from Peak Range, OVP, Monto and Undara) but no strong correlation can be made between age, location and the underlying asthenospheric mantle geochemistry. The roll of SCLM assimilation, and provinciality, has been explored in Zhang et al. (2001), who showed that some provincial differences between different localities in east Australian may arise from incorporation of heterogeneous lithospheric mantle.

The data suggest that the central volcanoes of central Queensland and many of the lava-fields in both Queensland and New South Wales originated from a common source. Recent work has

concluded that the pattern of north-to-south lithospheric mantle heat flow does not support a deep mantle plume origin (*Hasterok and Gard*, 2016) and the slow-seismic wave anomaly located in the Bass Strait and concurrent with the predicted present location of the Crosgrove plume can only be tracked to the mid-asthenosphere (*Montelli et al.* 2006). An alternative hypothesis is generation of magmas by edge-driven convection, which can explain the sporadic distribution of east Australian mafic magmatism and is supported both by the presence of a stepped lithosphere and abnormally fast shear flow in the asthenosphere (*Conrad et al.,* 2010; 2011). Localisation of an EDC cell is facilitated by the presence of shear-driven upwelling (SDU) in the asthenosphere, which has been shown to focus the effects of EDC to lithospheric steps where flow is away from the thicker lithosphere (*Davies and Rawlinson,* 2014). However, edge-driven convection in the lithospheric or asthenospheric mantle alone cannot explain the age progression in many central volcanoes.

Recent and more detailed tomography from Victoria and New South Wales show at least two domains of relatively thin lithosphere (*Rawlinson et al.,* 2017). The two domains, C1 and C2, show clear evidence of upwelling in both the NVP (C1) and beneath the NSW lava-fields and central volcanoes, though these cavities are believed to predate them (*Rawlinson et al.,* 2017). The upwelling in C1 is believed to be a result of the passage of the Australian plume to the east and the focalisation effect of SDU, though this does not apply to central NSW and no suggestion as to the mechanism behind initiation has been made where volcanism predates the passage of the plume. As there is no detailed tomography from Queensland, it is unclear whether such a cavity exists underneath the Bowen Basin lava-fields, however the observations from NVP provinces are consistent with the geochemical and geochronological results from the Bowen Basin. However, these observations cannot explain the young volcanism in North Queensland that is not associated with plume volcanism (*Zhang et al.,* 2001) and the mechanism by which the volcanism was initiated, nor does it explain the geochemical similarities and overlap between all provinces in eastern Australia addressed in this study. All Cenozoic provinces are, however, related to variations in lithospheric structure that has the potential to isolate convective cells (*Rawlinson et al.,* 2017), and abnormally fast shear flow in the asthenosphere (*Conrad et al.,* 2011), implying that all volcanism is likely related to EDC, plume volcanism or a combination of both.

The conclusions drawn from the geochemical data in this chapter are 1) no systematic variation of geochemical patterns by either age, locality or type, 2) all provinces appear to be sourced

from an EMI type source, where provinciality can be explained by assimilation of SCLM or crust, and 3) there is an agreement between the geochemical data and the link between plume volcanism and EDC that are supported by the models of lithospheric structure after Rawlinson et al. (2017).

5.6 Conclusions

Although east Australian central volcanoes and lava-fields have long been viewed as distinctly separate groups, my new geochemical data indicate there is no systematic geochemical distinction between these Cenozoic volcanic provinces. Based on a combination of new isotopic and elemental data and previous results, I conclude that all east Australian Cenozoic mafic magmas share a common source. Geochemical data from the east Australian Cenozoic mafic magmas typically cluster around the FOZO mantle reservoir and along the EMI array, and first-order melting models indicate a similar degree and depth of equilibrium melting for central volcanoes and lava-fields. Smaller variations toward EMII signatures are evident in some provinces, and my statistical analysis of trace element data relates them to crustal assimilation. I also observed differences in the degree of source melting in long-lived provinces. I propose that all east Australian Cenozoic volcanic provinces are the result of melting of a common EMI-type source, trapped in areas of low lithospheric thickness. It is likely that magmatism was generated from the interplay of mantle plumes and EDC that tap the same EMI source.

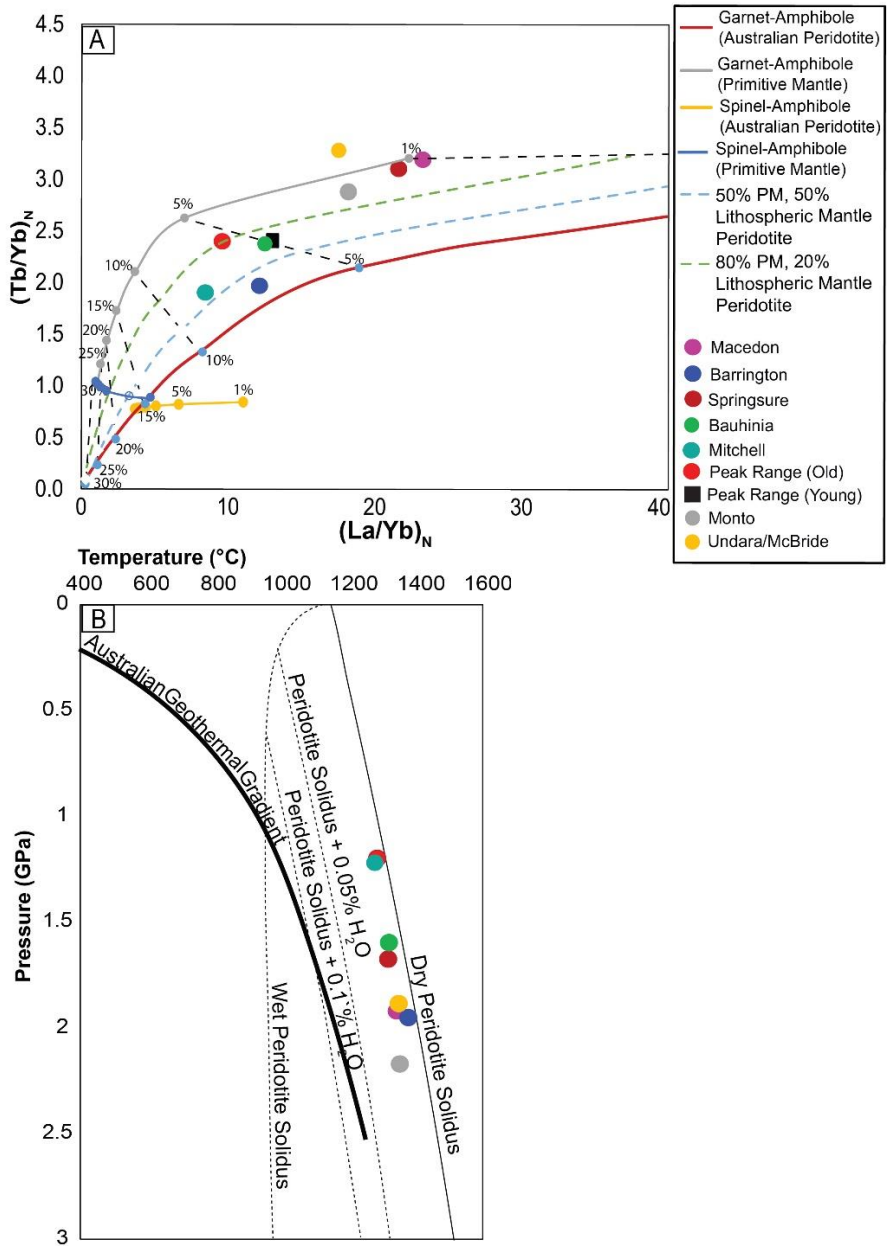

Figure 5.12: a) Melt generation models for the most primitive east Australian Cenozoic magmas. Melting was modelled using simple non-modal batch melting, assuming melting proportions of ol:opx:cpx:grnt:amph at 0.05:0.15:0.25:0.3:0.25 (modal mineralogy 58:30:10:2:1) and ol:opx:cpx:spn:amph 0.08:0.25:0.27:0.1:0.3 (modal mineralogy 50:25:10:3:12) for garnet and spinel lherzolite, respectively (*Van Otterloo et al.*, 2014). Source melting compositions were primitive mantle (*Sun and McDonough et al.*, 1989), average Australian lherzolite and average Australian spinel lherzolite (*O'Reilly and Griffin*, 1988). Samples are displayed by classification as either central volcanoes (black) or lava-fields (hollow). b) Estimated anyhydrous melting temperature and depth of east Australian volcanism using method of Wood (2004). As the East Australian geotherm does not intersect the dry peridotite solidus, melting must occur in the presence of water. Pressures between method of Wood (2004) and Tb/Yb are reasonably consistent.

Table 5.1: Major element analysis of mafic samples from Cenozoic volcanic provinces in eastern Australia.

Province	Sample	SiO2	TiO2	Al2O3	Fe2O3	MnO	MgO	CaO	Na2O	K2O	P2O5	Total	Mg#
Barrington	*BRT1*	44.53	2.52	14.51	12.68	0.18	9.73	10.39	3.42	0.86	1.18	100.00	63.4
	BRT3	42.89	2.30	15.00	12.31	0.18	12.02	10.35	3.27	0.78	0.90	100.00	68.9
	BRT5	46.05	2.33	15.47	11.84	0.18	8.82	10.67	2.78	1.11	0.75	100.00	62.7
	BRT6	42.02	2.12	14.76	13.40	0.20	10.35	11.65	3.48	0.91	1.09	100.00	63.6
	BRT8	41.34	2.30	14.63	12.77	0.19	12.46	11.76	2.73	0.59	1.23	100.00	68.8
	BRT10	43.90	2.22	13.61	12.53	0.18	12.91	10.69	2.30	1.07	0.59	100.00	70.0
Bauhinia	*CIB*	47.96	1.79	14.43	12.33	0.21	9.25	8.86	3.98	0.89	0.31	100.00	62.9
	TRLF01	51.00	1.73	14.49	11.16	0.19	7.88	9.64	2.91	0.67	0.32	100.00	61.5
	TRLF04	47.11	2.15	14.46	12.53	0.20	9.26	9.59	2.75	1.35	0.61	100.00	62.6
	TRLF05	51.02	1.87	14.87	10.13	0.17	5.67	10.85	4.22	0.87	0.33	100.00	55.9
	BWB01	54.27	1.46	13.93	11.04	0.15	6.44	9.37	2.72	0.49	0.15	100.00	56.9
	BWB02	52.65	1.24	14.94	11.26	0.16	7.30	9.30	2.87	0.23	0.04	100.00	59.4
	BWB03	52.57	1.58	14.46	11.35	0.15	7.47	9.18	2.86	0.29	0.09	100.00	59.8
	BWB04	51.82	1.66	14.13	11.33	0.15	7.59	9.23	3.22	0.68	0.19	100.00	60.3
	BWB05	51.33	1.83	14.25	11.75	0.16	8.27	8.57	3.10	0.53	0.22	100.00	61.4
	BWB06	52.55	1.95	14.69	11.23	0.14	6.26	8.89	3.30	0.73	0.26	100.00	55.8
	BWB07	47.23	2.03	13.79	12.72	0.17	10.60	8.54	2.95	1.51	0.47	100.00	65.3
McBride	*UBA3*	49.45	1.55	15.49	11.27	0.16	9.08	8.26	3.09	1.19	0.46	100.00	64.6
	UPW4	49	1.71	15.49	11.4	0.16	8.88	7.8	3.433	1.64	0.48	100.00	63.8
	UR1	48.1	1.66	15.13	10.77	0.15	10.3	8.4	3.548	1.47	0.44	100.00	68.5
	UR3	46.3	2.14	14.54	12.15	0.25	11	8.15	3.221	1.73	0.56	100.00	67.2
Mitchell	*BWM01*	52.11	1.93	15.12	11.69	0.13	5.88	8.35	3.39	1.07	0.33	100.00	53.2
	BWM02	53.40	1.57	14.00	11.14	0.15	7.23	9.09	2.93	0.41	0.08	100.00	59.5
	BWM03	47.88	1.77	14.48	12.42	0.17	9.43	8.98	3.41	1.02	0.45	100.00	63.2
	BWM04	54.01	2.15	14.04	11.31	0.13	5.07	8.30	3.33	1.23	0.43	100.00	50.4
	BWM05	53.71	2.15	14.62	11.22	0.13	4.94	8.26	3.40	1.14	0.43	100.00	49.9
	BWM06	53.36	2.14	14.38	11.22	0.13	5.58	8.25	3.26	1.23	0.44	100.00	52.9
	BWM07	52.61	1.50	14.74	10.64	0.14	8.01	9.03	2.84	0.42	0.07	100.00	63.0
	BWM08	53.99	1.71	13.75	11.43	0.16	6.51	8.93	2.86	0.56	0.10	100.00	56.3
	BWM09	54.19	1.65	13.70	11.57	0.15	6.51	9.10	2.51	0.54	0.08	100.00	56.0
	BWM10	54.04	1.64	13.89	11.26	0.15	6.66	8.82	2.94	0.51	0.07	100.00	57.2
	BWM11	53.09	1.50	14.68	10.99	0.14	7.84	8.80	2.52	0.38	0.07	100.00	61.7
Monto	*IJLF01*	46.93	3.07	13.16	12.79	0.23	8.93	9.22	2.98	1.78	0.91	100.00	61.2
	BC21	45.42	2.69	13.33	13.35	0.23	9.12	9.16	4.08	1.99	0.64	100.00	60.7
	BC24	50.52	1.99	13.66	11.07	0.15	9.27	8.37	3.56	1.04	0.38	100.00	65.5
	BC25 (wet)	53.07	1.63	14.06	10.64	0.19	8.60	8.14	2.99	0.50	0.17	100.00	64.6
	BC27	44.46	2.40	13.98	12.87	0.19	8.93	7.95	5.73	2.04	1.45	100.00	61.1
	BC28	45.85	2.48	13.49	12.74	0.18	8.97	10.16	3.94	1.61	0.58	100.00	61.4
Peak Range	*PRO1a*	45.74	3.00	13.88	12.51	0.17	9.96	9.22	3.27	1.63	0.62	100.00	64.3
	PRO2b	46.72	2.64	13.97	12.41	0.17	9.93	9.62	2.85	1.07	0.62	100.00	64.4
	PRO4	49.25	1.54	16.03	12.72	0.16	7.28	8.94	3.34	0.48	0.26	100.00	56.4
	PRO5	50.07	1.84	14.55	12.03	0.15	7.53	9.34	3.21	0.96	0.32	100.00	58.6
	PRO7	47.55	1.76	14.68	11.55	0.16	10.27	10.13	2.79	0.85	0.26	100.00	66.8
	PRO8b	46.96	2.20	16.55	11.59	0.17	7.95	8.70	3.33	1.96	0.58	100.00	60.8

	PRO9b	46.85	1.59	19.76	11.41	0.15	8.00	8.02	2.91	1.06	0.26	100.00	61.3
Rolleston Mine	*RM2*	48.8	1.77	14.88	12.42	0.18	9.89	7.42	3.153	1.13	0.34	100.00	64.3
	RM4a	45.7	2.34	13.41	13.22	0.18	9.63	8.92	4.276	1.18	1.17	100.00	62.2
	RM4b	49.4	1.88	14.53	11.96	0.15	8.8	7.94	3.513	1.3	0.52	100.00	62.5
	RM5a	45.1	2.37	13.59	13.54	0.18	9.91	8.77	4.096	1.22	1.19	100.00	62.3
	RM5b	49	1.96	14.85	12.52	0.16	8.83	7.51	3.541	1.24	0.41	100.00	61.5
Springsure	*CIK*	46.37	2.89	14.17	12.81	0.21	8.24	8.78	3.59	2.09	0.84	100.00	59.3
	CIS	50.20	2.95	14.93	11.93	0.20	6.47	7.68	3.24	1.73	0.66	100.00	55.1
	IJS06	47.75	3.19	16.16	13.93	0.19	4.54	7.98	3.45	2.03	0.78	100.00	42.4
	IJS07B	51.68	2.54	15.42	10.58	0.15	5.51	7.89	3.98	1.59	0.67	100.00	54.1
	IJS08B	49.86	1.79	14.74	11.88	0.19	8.02	8.75	3.17	1.24	0.36	100.00	60.4
	IJS11	47.92	3.12	15.02	13.99	0.23	5.07	7.98	3.58	1.69	1.40	100.00	45.0
	CVLF01	47.84	1.91	15.34	12.24	0.22	8.66	9.24	2.50	1.57	0.48	100.00	61.5
	MC1	49.2	2.51	15.93	12.34	0.13	6.52	7.94	3.5	1.39	0.51	100.00	54.5
	MC2	51.37	2.44	15.44	12.29	0.16	5.67	7.85	3.10	1.24	0.44	100.00	51.1
	MC5	48.29	1.91	14.25	12.41	0.19	9.68	9.31	2.39	1.08	0.51	100.00	63.8
	MC6	50.60	2.17	15.25	11.92	0.15	7.05	8.02	3.17	1.24	0.42	100.00	57.2
	MC8	51.79	1.76	15.14	11.77	0.14	6.34	8.80	3.19	0.73	0.35	100.00	54.9

Table 5.2: Trace element analysis of mafic samples from Cenozoic volcanic provinces in eastern Australia.

Sample	Sc	Ti	V	Cr	Co	Ni	Cu	Zn	Ga	Rb	Sr	Y	Zr	Nb
BRT1	84	15135	213	210	48	154	87	100	21	36	1304	31	306	110
BRT5	59	13777	229	252	44	121	69	108	18	11	895	28	227	70
BRT6	51	13981	216	263	51	177	86	105	18	6	1173	27	219	76
BRT8	44	12735	244	268	52	218	63	113	20	12	1493	31	258	99
BRT3	108	13789	257	301	53	200	83	126	22	47	1147	35	291	87
BRT10	88	13314	224	418	56	313	60	100	19	29	1136	32	228	74
CIB	20	10703	198	362	50	214	61	137	20	13	470	18	143	22
TRLF01	21	10373	196	311	47	190	65	118	20	14	393	19	133	20
TRLF04	20	12863	217	327	54	214	71	127	20	18	936	19	198	38
TRLF05	18	11214	180	204	42	119	64	150	21	13	453	20	126	17
BWB1	13	8729	156	206	39	134	53	96	16	7	274	15	81	11
BWB2	3	7461	150	241	37	126	32	83	14	1	178	12	55	5
BWB3	4	9477	146	188	36	131	50	94	15	3	214	16	79	8
BWB4	4	9972	138	243	38	150	46	86	15	7	299	13	98	14
BWB5	5	10970	132	232	36	168	35	86	15	8	343	14	129	16
BWB6	3	11687	136	170	35	116	50	98	16	9	335	14	103	15
BWB7	3	12189	132	292	39	237	49	92	15	14	553	12	161	34
UBA3	94	9298	156	260	46	214	51	96	18	20	686	26	160	29
UPW4	102	10274	167	256	45	176	49	101	19	30	657	27	203	37
UR1	97	9934	161	254	43	183	47	100	19	29	815	28	192	37
UR3	96	12832	178	261	52	185	46	194	20	23	693	26	205	34
BWM1	3	11559	116	140	34	105	43	107	16	13	316	13	129	20
BWM2	3	9415	129	177	32	125	42	86	14	4	195	14	70	7
BWB3b	4	10605	137	252	39	165	45	93	16	10	432	13	128	31
BWM4	13	12875	134	154	30	64	45	113	21	11	390	19	180	27
BWM5	9	12890	136	148	30	59	45	111	21	13	383	19	182	27
BWM6	12	12823	137	158	32	71	45	112	21	12	402	19	187	28
BWM7	3	8989	136	209	38	156	46	89	15	6	202	14	80	8
BWM8	3	10260	149	192	37	135	55	100	15	7	194	16	88	8
BWM9	3	9894	139	187	37	143	51	89	14	6	186	14	82	8
BWM10	5	9825	144	186	37	136	54	89	15	7	192	16	84	8
BWM11	4	8973	135	209	38	155	48	90	15	6	204	14	78	8
BC21	11	18402	127	240	37	245	43	81	16	11	515	18	251	59
BC24	2	16105	141	269	37	196	46	91	16	16	405	14	164	28
BC25	2	11940	111	261	34	165	32	86	15	7	297	12	102	12
BC27	7	9794	102	233	34	185	36	102	18	7	846	17	246	68
BC28	3	14405	148	244	42	172	48	150	17	20	537	17	167	39
IJLF01	16	14878	218	300	47	195	53	136	22	31	1235	25	312	65
PRO1a	23	18015	184	188	50	183	38	105	20	23	683	22	200	38
PRO-2b	24	15823	194	240	47	192	53	92	19	15	544	20	173	32
PRO-4	24	9252	175	203	41	115	48	94	17	7	828	17	89	12
PRO-5	21	11031	150	204	42	120	42	123	18	13	417	17	134	16
PRO-7	26	10539	190	453	48	200	64	164	16	12	452	15	112	23
PRO-8b	18	13216	147	153	40	156	23	143	19	24	847	17	189	36
PRO-9b	19	9540	132	152	36	209	85	100	14	13	695	14	99	16
RM2	11	10590	155	200	42	167	53	87	17	3	1003	12	112	20

RM4a	9	14008	139	252	45	227	121	114	19	7	891	15	213	64
RM4b	11	11242	151	174	42	153	71	91	17	5	422	14	125	25
RM5A	10	14195	150	264	48	236	53	119	21	7	943	15	228	68
RM5B	12	11776	154	178	44	165	69	100	17	5	359	14	128	26
IJS06	16	17302	206	21	40	40	40	150	25	30	1004	29	323	45
IJS07B	16	17715	171	224	41	145	46	141	24	28	787	18	320	45
IJS08B	22	19120	214	286	49	193	65	124	20	22	507	18	182	26
IJS11	19	15232	208	82	43	63	56	166	25	30	671	40	343	43
CVLF01	22	10722	230	287	47	171	47	106	19	28	826	21	215	31
CIK	17	18688	209	212	47	146	54	139	23	36	979	23	296	57
CIS	17	11475	205	138	39	87	40	159	23	28	889	26	322	52
MC1	66	15045	176	270	38	155	26	128	21	19	602	30	258	26
MC2	25	14656	179	234	49	159	34	122	20	16	541	24	237	25
MC5	67	11444	196	285	50	206	55	132	18	20	752	25	213	40
MC6	47	13026	181	213	42	131	34	118	20	18	473	26	238	26
MC8	22	10522	189	192	47	138	58	129	21	16	494	22	181	20
Sample	***Sn***	***Cs***	***Ba***	***La***	***Ce***	***Pr***	***Nd***	***Sm***	***Eu***	***Gd***	***Tb***	***Dy***	***Ho***	***Er***
BRT1	2.0		714	80	134	11.9	46	8.3	2.7	8	1.3	6.3	1.13	2.33
BRT5	1.6		498	43	78	7.7	32	6.2	2.1	6	1.1	5.8	1.09	2.28
BRT6	1.6		623	75	123	10.6	41	7.3	2.4	7	1.1	5.7	1.04	2.14
BRT8	1.7		825	84	137	12.0	46	8.1	2.7	8	1.2	6.3	1.16	2.40
BRT3	2.0		601	67	111	9.9	39	7.3	2.5	7.3	1.2	6.4	1.18	2.46
BRT10	1.9		616	65	108	9.6	38	7.1	2.4	7.0	1.1	6.0	1.06	2.21
CIB	1.3	0.5	132	13	30	3.6	17	4	1.4	4.3	0.6	3.6	0.63	1.75
TRLF01	1.2	0.2	146	11	24	3.0	14	4	1.4	4.5	0.7	4.0	0.70	1.97
TRLF04	1.5	0.3	205	25	51	5.9	26	6	1.9	5.4	0.7	4.1	0.68	1.81
TRLF05	1.1	0.1	192	10	24	3.0	15	4	1.6	4.8	0.7	4.1	0.72	1.96
BWB1	0.9	0.2	120	7	15	2.2	10	3.0	1.1	3.5	0.6	3.2	0.66	1.73
BWB2	0.7	0.1	70	4	8	1.3	6	2.1	0.9	2.8	0.5	2.8	0.61	1.64
BWB3	1.1	0.1	167	7	13	1.9	9	3.0	1.1	4.0	0.7	3.7	0.78	2.06
BWB4	1.1	0.1	149	9	18	2.4	11	3.1	1.2	3.7	0.6	3.2	0.63	1.65
BWB5	1.4	0.3	132	13	28	3.7	15	3.9	1.4	4.1	0.6	3.4	0.69	1.79
BWB6	1.1	0.1	193	9	20	2.7	12	3.7	1.4	4.3	0.7	3.6	0.71	1.79
BWB7	1.5	0.3	246	23	43	5.5	22	5.0	1.7	4.9	0.7	3.4	0.65	1.61
UBA3	1.2		###	33	51	5.3	22	5.9	2.0	5	0.9	4.7	0.90	2.47
UPW4	1.5		374	32	55	5.6	24	6.5	2.1	5	0.9	5.0	0.94	2.54
UR1	1.4		409	40	64	6.3	26	6.7	2.2	5.3	0.9	5.0	0.93	2.53
UR3	1.6		503	28	51	5.3	23	6.8	2.3	5.4	0.9	5.0	0.89	2.30
BWM1	1.4	0.3	202	13	26	3.3	14	3.7	1.4	4.1	0.6	3.2	0.63	1.60
BWM2	1.0	0.1	125	6	12	1.8	8	2.7	1.0	3.5	0.6	3.3	0.68	1.80
BWB3b	1.3	0.3	194	18	33	4.2	17	4.1	1.5	4.3	0.6	3.3	0.65	1.67
BWM4	1.8	0.2	346	18	36	4.8	20	5.6	2.0	6.0	0.9	4.5	0.83	2.00
BWM5	1.9	0.3	263	18	36	4.9	21	5.6	2.0	6.2	0.9	4.6	0.84	2.04
BWM6	2.0	0.3	416	19	37	4.9	21	5.7	2.0	6.1	0.9	4.6	0.85	2.05
BWM7	1.0	0.2	129	6	13	1.8	9	2.8	1.1	3.6	0.6	3.5	0.72	1.91
BWM8	1.0	0.2	97	7	14	2.0	9	3.1	1.2	4.0	0.7	3.8	0.79	2.08
BWM9	1.0	0.2	128	6	13	1.9	9	2.9	1.1	3.8	0.6	3.5	0.74	1.96
BWM10	1.0	0.2	85	6	14	2.0	9	3.1	1.1	3.9	0.6	3.7	0.77	2.01
BWM11	1.0	0.2	140	6	14	1.9	9	2.8	1.1	3.7	0.6	3.5	0.72	1.91
BC21	2.0	0.1	485	38	70	8.9	34	7.2	2.4	7.0	1.0	5.1	0.99	2.51

BC24	1.6	0.2	254	19	36	4.8	20	4.9	1.7	5.2	0.8	4.0	0.76	1.90
BC25	1.0	0.1	147	9	19	2.6	11	3.4	1.3	3.8	0.6	3.0	0.60	1.55
BC27	2.0	0.1	368	43	81	10.6	41	8.6	2.8	7.8	1.1	5.1	0.93	2.25
BC28	1.8	0.3	382	25	46	5.9	24	5.8	2.1	6.0	0.9	4.4	0.86	2.10
IJLF01	2.1	0.3	605	38	80	9.4	41	9	2.8	7.9	1.0	5.6	0.90	2.32
PRO1a	1.8	0.6	326	25	50	6.6	28	6.5	2.2	5.9	0.9	4.8	0.88	2.22
PRO-2b	1.5	0.2	250	25	50	6.4	27	6.0	2.0	6.1	0.8	4.5	0.82	2.08
PRO-4	1.1	0.1	190	11	21	2.8	12	3.4	1.3	3.9	0.6	3.5	0.70	1.95
PRO-5	1.2	0.2	196	14	29	3.9	17	4.2	1.5	4.6	0.7	3.8	0.71	1.90
PRO-7	1.2	0.2	215	15	30	3.9	16	3.9	1.4	4.1	0.6	3.3	0.64	1.73
PRO-8b	1.5	0.4	272	25	47	5.8	23	5.2	1.8	5.2	0.7	3.8	0.68	1.73
PRO-9b	1.1	0.6	203	11	22	2.8	12	3.0	1.1	3.4	0.5	3.0	0.57	1.56
RM2	1.4	0.2	###	12	25	3.2	14	3.6	1.4	4.0	0.6	3.1	0.62	1.63
RM4a	2.0	0.1	408	44	81	10.0	39	8.3	2.7	7.5	1.0	4.4	0.77	1.79
RM4b	1.4	0.1	142	18	34	4.4	18	4.5	1.6	4.7	0.7	3.5	0.69	1.79
RM5A	2.0	0.1	412	46	86	10.1	41	8.8	2.8	7.8	1.0	4.5	0.78	1.81
RM5B	1.7	0.2	135	17	34	4.2	18	4.5	1.6	4.7	0.7	3.5	0.71	1.79
IJS06	2.2	0.2	266	31	68	8.1	36	8	2.5	7.6	1.0	5.9	1.01	2.75
IJS07B	2.0	0.4	291	31	67	8.0	36	8	2.4	6.8	0.8	4.4	0.66	1.60
IJS08B	1.3	0.1	204	19	41	4.9	21	5	1.5	4.6	0.6	3.7	0.65	1.82
IJS11	2.0	0.3	360	35	79	9.9	46	10	3.4	9.8	1.3	7.6	1.31	3.63
CVLF01	1.5	0.2	269	24	49	5.8	25	6	1.7	5.2	0.7	4.3	0.76	2.17
CIK	2.1	0.5	438	36	75	8.8	39	8	2.6	7.2	0.9	5.1	0.81	2.08
CIS	2.1	0.3	360	34	74	8.7	38	8	2.6	7.4	1.0	5.5	0.91	2.37
MC1	2.0		358	27	54	6.2	28	8.3	2.8	7	1.1	6.0	1.06	2.81
MC2	1.7		309	22	46	5.4	25	7.5	2.5	6	1.0	5.4	0.98	2.58
MC5	2.0		908	42	73	7.2	29	7.4	2.4	6	1.0	5.3	0.97	2.62
MC6	1.7		306	26	52	5.7	25	7.2	2.4	6	1.0	5.5	1.01	2.64
MC8	2		199	19	43	6	24	6	1.9	6.0	0.8	4.5	0.77	2.23

Sample	***Tm***	***Yb***	***Lu***	***Hf***	***Ta***	***Tl***	***Pb***	***Th***	***U***
BRT1	0.40	2.21	0.33	5.6	9.2	0.1	4.4	9.5	2.9
BRT5	0.40	2.39	0.35	4.2	5.6	0.0	2.7	3.4	1.4
BRT6	0.37	2.11	0.31	3.9	5.7	0.0	4.3	7.4	3.1
BRT8	0.41	2.39	0.34	4.4	7.9	0.0	4.7	7.8	3.4
BRT3	0.43	2.50	0.37	5.3	6.9	0.0	3.5	9.0	2.3
BRT10	0.38	2.26	0.34	4.1	5.5	0.0	3.4	9.2	2.4
CIB	0.21	1.38	0.18	3.0	1.5	0.0	2.2	1.7	0.6
TRLF01	0.23	1.53	0.20	3.0	1.4	0.0	1.2	1.2	0.4
TRLF04	0.20	1.35	0.18	3.9	2.5	0.0	3.0	2.4	0.9
TRLF05	0.23	1.49	0.19	2.8	1.1	0.0	1.1	0.7	0.3
BWB1	0.24	1.37	0.20	2.2	1.0	0.0	0.9	1.0	0.3
BWB2	0.23	1.29	0.20	1.6	0.5	0.0	0.7	0.3	0.2
BWB3	0.28	1.62	0.24	2.4	0.8	0.0	1.0	0.7	0.3
BWB4	0.22	1.27	0.18	2.6	1.3	0.0	1.1	0.8	0.4
BWB5	0.24	1.38	0.21	3.3	1.6	0.2	1.4	1.4	0.6
BWB6	0.24	1.33	0.19	2.8	1.3	0.0	0.8	0.3	0.3
BWB7	0.21	1.17	0.17	3.9	3.3	0.0	2.3	1.5	0.9
UBA3	0.33	2.01	0.29	3.1	2.1	0.1	3.2	10.3	1.1
UPW4	0.35	2.06	0.30	3.8	2.9	0.1	3.4	10.7	1.2

UR1	0.36	2.05	0.31	3.5	2.6	0.1	3.7	13.1	1.3
UR3	0.31	1.72	0.25	3.9	2.9	0.1	2.7	7.6	1.3
BWM1	0.20	1.16	0.17	3.4	1.9	0.0	1.4	1.0	0.5
BWM2	0.25	1.42	0.21	2.1	0.7	0.0	0.9	0.6	0.2
BWB3b	0.22	1.24	0.19	3.1	2.6	0.0	1.4	1.3	0.7
BWM4	0.25	1.37	0.20	4.8	2.5	0.1	2.1	2.5	0.8
BWM5	0.26	1.41	0.20	4.9	2.6	0.1	2.1	2.2	0.8
BWM6	0.26	1.41	0.20	4.9	2.6	0.1	2.2	2.3	0.8
BWM7	0.26	1.48	0.22	2.4	0.8	0.0	1.0	0.6	0.3
BWM8	0.29	1.61	0.24	2.6	0.8	0.0	5.0	0.6	0.3
BWM9	0.27	1.48	0.22	2.4	0.8	0.0	1.0	0.6	0.3
BWM10	0.27	1.59	0.24	2.5	0.8	0.0	1.0	0.8	0.3
BWM11	0.26	1.49	0.23	2.3	0.8	0.0	1.1	0.7	0.3
BC21	0.33	1.86	0.28	6.0	5.6	0.1	2.7	4.1	1.4
BC24	0.25	1.30	0.18	4.1	2.7	0.0	1.8	1.1	0.7
BC25	0.20	1.15	0.17	2.7	1.1	0.1	1.0	0.5	0.3
BC27	0.28	1.47	0.21	5.5	6.4	0.0	2.7	4.1	1.8
BC28	0.27	1.46	0.21	4.2	3.7	0.0	1.8	1.6	0.9
IJLF01	0.25	1.58	0.20	6.1	4.0	0.0	3	3.5	1.1
PRO1a	0.27	1.66	0.22	4.7	1.9	0.0	1.7	2.8	0.9
PRO-2b	0.27	1.62	0.22	4.2	4.0	0.0	1.4	2.3	0.7
PRO-4	0.26	1.69	0.24	2.4	1.6	0.0	1.4	1.2	0.4
PRO-5	0.25	1.51	0.22	3.5	2.2	0.0	1.8	1.4	0.4
PRO-7	0.22	1.41	0.20	2.9	3.3	0.0	1.7	1.7	0.5
PRO-8b	0.23	1.36	0.19	4.4	4.4	0.1	2.8	3.0	1.0
PRO-9b	0.21	1.35	0.20	2.4	2.3	0.0	1.8	1.6	0.4
RM2	0.22	1.22	0.18	3.0	2.0	0.0	1.4	1.3	0.6
RM4a	0.21	1.08	0.15	5.4	6.3	0.0	2.5	3.9	1.5
RM4b	0.23	1.29	0.19	3.3	2.5	0.0	1.6	1.9	0.7
RM5A	0.21	1.07	0.15	5.5	6.5	0.0	2.4	3.7	1.5
RM5B	0.23	1.29	0.18	3.3	2.5	0.0	1.6	1.8	0.7
IJS06	0.32	2.13	0.28	6.4	3.0	0.0	2	3.0	0.8
IJS07B	0.16	1.04	0.13	6.4	3.1	0.1	3	3.1	0.9
IJS08B	0.22	1.45	0.20	3.8	1.7	0.1	2	2.1	0.6
IJS11	0.42	2.80	0.38	6.5	3.0	0.1	3	2.9	0.9
CVLF01	0.26	1.76	0.24	4.4	2.0	0.0	2	2.5	0.7
CIK	0.23	1.45	0.18	5.9	3.9	0.1	3	3.8	1.1
CIS	0.26	1.72	0.22	6.5	3.5	0.1	3	3.6	1.0
MC1	0.35	2.03	0.30	5.0	2.2	0.0	2.3	5.6	0.8
MC2	0.34	1.91	0.27	4.8	2.1	0.0	1.8	2.5	0.7
MC5	0.36	2.03	0.30	4.1	2.9	0.0	3.0	7.3	1.3
MC6	0.35	2.03	0.29	4.7	2.1	0.0	2.2	4.8	0.8
MC8	0.28	1.81	0.27	4.3	1.2	0.4	0.7	1.9	0.7

Table 5.3: Radiogenic isotopic ratios of mafic samples from Cenozoic volcanic provinces in eastern Australia.

Location	Sample	87Sr/ 86Sr	143Nd/ 144Nd	176Hf/ 177Hf	208Pb/ 204Pb	207Pb/ 204Pb	206Pb/ 204Pb	208Pb/ 206Pb	207Pb/ 206Pb	EHf	ENd
Monto											
	BC25	0.70398	0.51270	0.28274	37.90145	15.51503	17.99823	2.10606	0.86200	-1.580	1.162
	IJLF-01	0.70389	0.51280	0.28288	38.65346	15.55988	18.79492	2.05627	0.82789	3.371	3.249
	BC24	0.70384	0.51284	0.28294	38.41486	15.54831	18.52727	2.07370	0.83921	5.349	3.938
	BC28	0.70343	0.51294	0.28303	38.42198	15.52465	18.56878	2.06940	0.83607	8.546	5.831
	BC27	0.70298	0.51299	0.28306	38.94947	15.57552	19.28324	2.02009	0.80773	9.788	6.793
Bauhinia											
	BWB03	0.70367	0.51295	0.28306	38.62684	15.58610	18.72047	2.06357	0.83258	9.826	7.192
	BWB04	0.70407	0.51282	0.28297	39.05044	15.61500	19.02701	2.05255	0.82064	6.653	4.568
	BWB05	0.70345	0.51302	0.28313	38.50743	15.55878	18.67612	2.06211	0.83309	12.161	8.590
	BWB06	0.70361	0.51289	0.28297	38.44542	15.56985	18.61054	2.06600	0.83662	6.557	6.031
	CIB	0.70357		0.28299	38.33853	15.56809	18.49317	2.07275	0.84184	7.341	-
	TRLF-01	0.70347	0.51299	0.28312	38.45390	15.55252	18.61181	2.06544	0.83555	11.757	7.953
	TRLF-04	0.70352	0.51290	0.28301	38.38477	15.56650	18.55606	2.06822	0.83888	7.900	6.329
	TRLF-05	0.70345	0.51302	-	38.25870	15.54423	18.43917	2.07448	0.84299	-	8.492
Mitchell											
	BWM01	0.70372	0.51292	0.28301	38.51807	15.58349	18.66898	2.06346	0.83471	8.031	6.507
	BWM02	0.70404	0.51286	0.28303	38.95451	15.61878	18.72874	2.08015	0.83395	8.806	5.510
	BWM07	0.70409	0.51291	0.28300	38.77013	15.61057	18.71816	2.07150	0.83399	7.666	6.315
Springsure											
	IJS-07B	0.70397	0.51280	0.28295	38.73506	15.58688	18.71075	2.06988	0.83305	5.967	4.175
	IJS08B	0.70404	0.51277	0.28293	38.61913	15.58916	18.57717	2.07856	0.83920	5.199	3.670
	IJS-11	0.70408	0.51279	0.28297	38.58805	15.57765	18.55871	2.07888	0.83938	6.393	4.089
	CVLF-01	0.70388	0.51278	0.28294	38.70952	15.58336	18.66677	2.07335	0.83481	5.521	3.807
	CIK	0.70399	0.51277	0.28289	38.50176	15.57658	18.56722	2.07322	0.83894	3.752	3.790
Peak Range											
	PR01A	0.70385	0.51282	0.28293	38.37553	15.56482	18.68079	2.05393	0.83321	5.273	4.641
	PR02	0.70330	-	0.28300	38.62422	15.55854	18.78423	2.05588	0.82830	7.709	-
	PR04	0.70408	0.51282	0.28297	38.55410	15.57340	18.61162	2.07108	0.83675	6.488	5.021
	PR05	0.70448	0.51286	0.28301	38.08033	15.54014	18.13375	2.09962	0.85696	7.994	5.587
	PR07B	0.70368	0.51288	0.28300	38.33702	15.54783	18.38775	2.08452	0.84557	7.630	5.905
	PR08	0.70359	0.51279	0.28294	38.51745	15.58157	18.43339	2.08919	0.84529	5.318	4.281
	PR09B	0.70398	0.51296	0.28304	38.78050	15.58826	18.92713	2.04859	0.82361	8.992	7.594
Barrington											
	BRT3	0.70322	0.51291	-	38.87465	15.54865	18.95876	2.05123	0.82013	-	-
	BRT10	0.70336	0.51289	-	38.97366	15.55008	18.97302	2.05495	0.81960	-	-
McBride											
	UBA3	0.70463	0.51270	-	38.90571	15.60902	18.69637	2.08174	0.83486	-	-
	UPW4	0.70444	0.51273	-	38.72786	15.58630	18.48736	2.09565	0.84309	-	-
	UR1	0.70440	0.51273	-	38.88989	15.58506	18.63437	2.08786	0.83637	-	-
	UR3	0.70390	0.51293	-	38.08810	15.57316	18.47574	2.06195	0.84289	-	-

Chapter 6: An updated Australian Cenozoic apparent polar wander path

6.1 Introduction

Cenozoic paleomagnetic records from Australia have been insufficient for accurate plate reconstructions. A number of previous studies have utilised paleomagnetic results to reconstruct the motion of Australia during the Cretaceous to Cenozoic break-up of Gondwana. The first of these attempts (*Le Pichon and Heirtzler*, 1968) examined magnetic anomalies in the Indian Ocean and focused on the remanent magnetism of the ocean floor as a means to track the Indian, Australian, and Antarctic Plates during continental break-up. A Cenozoic apparent polar wander path (APWP) based on data from east Australian volcanic rocks (*Wellman et al.,* 1969) included a late Miocene bend that was attributed to true polar wander (Fig. 6.1a). Embleton and McElhinny (1982) later produced a more "jagged" APWP using paleomagnetic poles derived from a combination of volcanic and lateritic profiles that relied on K-Ar geochronology of two calibration poles (Fig. 6.1b). This model was refined using a filter that greatly smoothed the jagged migration pattern, but which nevertheless preserved an apparent westward divergence of Australian plate motion during late Oligocene to early Miocene time. Later, the jagged APWP was ascribed by Idnurm (1985) to a failure to eliminate paleosecular variation in previous paleomagnetic studies. Idnurm (1985) advocated the use of paleomagnetic results from sedimentary basins and lateritic profiles, which produced a smoother and significantly more linear APWP (Fig. 6.1c). Musgrave (1989) subsequently utilised a weighted least-squares regression of paleomagnetic poles (Fig. 6.1d) that were included in both Idnurm (1985) and Embleton and McElhinny (1982) to produce an APWP that was largely linear, but this APWP was later rejected by Idnurm (1990) on the grounds that the statistical method was unorthodox and the exclusion of data was "ad-hoc."

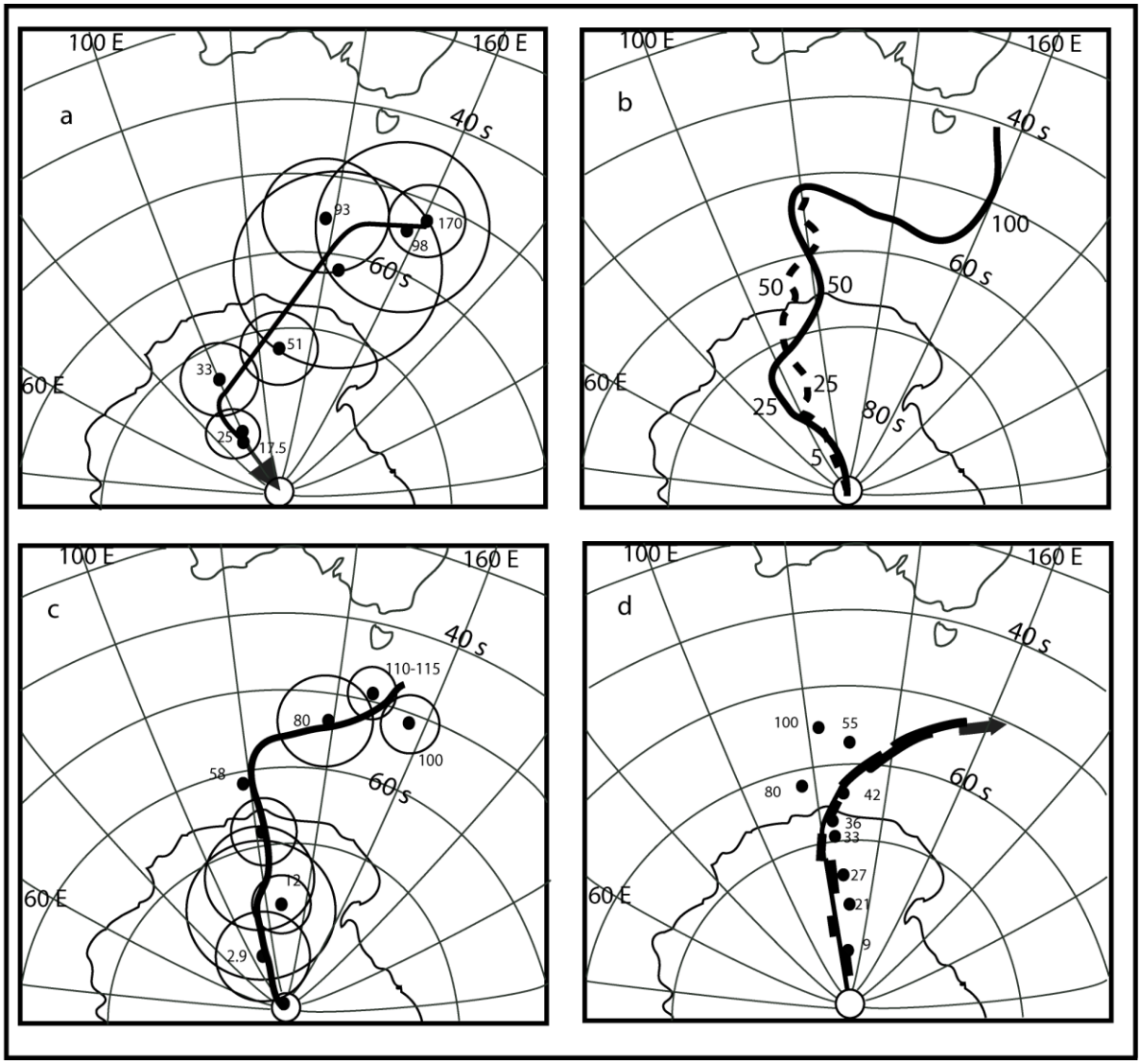

Figure 6.1: Previous reconstructed APWPs using a) basaltic paleomagnetic data (*Wellman et al.*, 1969); b) a sliding window, best fit estimate after basaltic and lateritic paleomagnetic data (*Embleton and McElhinny*, 1982); c) lateritic and sedimentary paleomagnetic data (*Idnurm*, 1985); and d) a least-squares regression best fit model of lateritic and sedimentary paleomagnetic data using basaltic paleopoles as anchor points (*Musgrave*, 1989).

Evaluation of the previous Australian APWPs reveals a number of potential complications. First, several previous paleomagnetic studies may not have accounted for paleosecular variation, and they may have had insufficient sample density (e.g. *Wellman et al.*, 1969; *Wellman*, 1975; *Embleton and McElhinny*, 1982). Second, radiometric dating was either entirely absent from some previous studies (as in the sedimentary and lateritic profiles; *Idnurm*, 1985) or reliant on the K-Ar method, which fails to account for excess Ar or Ar loss (e.g., *McDougall and Harrison*, 1999). Third, detrital remanent magnetisation (DRM), which is the

basis for paleomagnetic poles from studies of sedimentary rocks, can be strongly affected by diagenesis and other post-depositional processes such as compaction, bioturbation, and the precipitation and alteration of ferromagnetic minerals (*Butler,* 2004). Additionally, the protracted history of crystallisation and growth of ferro- and ferrimagnetic minerals during weathering in lateritic profiles greatly complicates paleomagnetic results from those profiles (*Butler,* 2004). To overcome many, perhaps all, of these complicating factors, this chapter describes the combination of high precision $^{40}Ar/^{39}Ar$ geochronology (Chapter 3) and new paleomagnetic data from east Australian volcanic rocks to re-evaluate the Cenozoic motion of Australia. The reconstructed APWP clarifies links between plate motion and observable geographic offsets in several on- and off-shore volcanic tracks in eastern Australia and the Tasman Sea.

6.2 East Australian volcanic provinces

The volcanic provinces included in this chapter stretch from the north coast of Queensland to central New South Wales and consist of a variety of rock types (Fig. 6.2). Compositions range from aphanitic basalts, vesicular basalts, and basanites, to glassy and spherulitic rhyolite (*Johnson et al.,* 1989). Ages of the various provinces included in this chapter span from the late Cretaceous to Holocene, and some of the provinces seem to be hot-spot related (*Wellman and McDougall,* 1974a; *Knesel et al.,* 2008; *Vasconcelos et al.,* 2008). Previous geochronology results suggest an average period of activity at each province of approximately 5 Myr, although activity at some was <1 Myr (*Vasconcelos et al.,* 2008; *Cohen et al.,* 2013; *Cohen et al.,* 2017; *Oostingh et al.,* 2017). Periods of activity >5 Myr are believed to represent multiple, overlapping provinces (*Wellman and McDougall,* 1974a and 1974b). Younger volcanic provinces have shorter, but more numerous, volcanic episodes and are composed of many smaller scoria cones and vents (*Wellman and McDougall,* 1974a; *Cohen et al.,* 2017; *Oostingh et al.,* 2017).

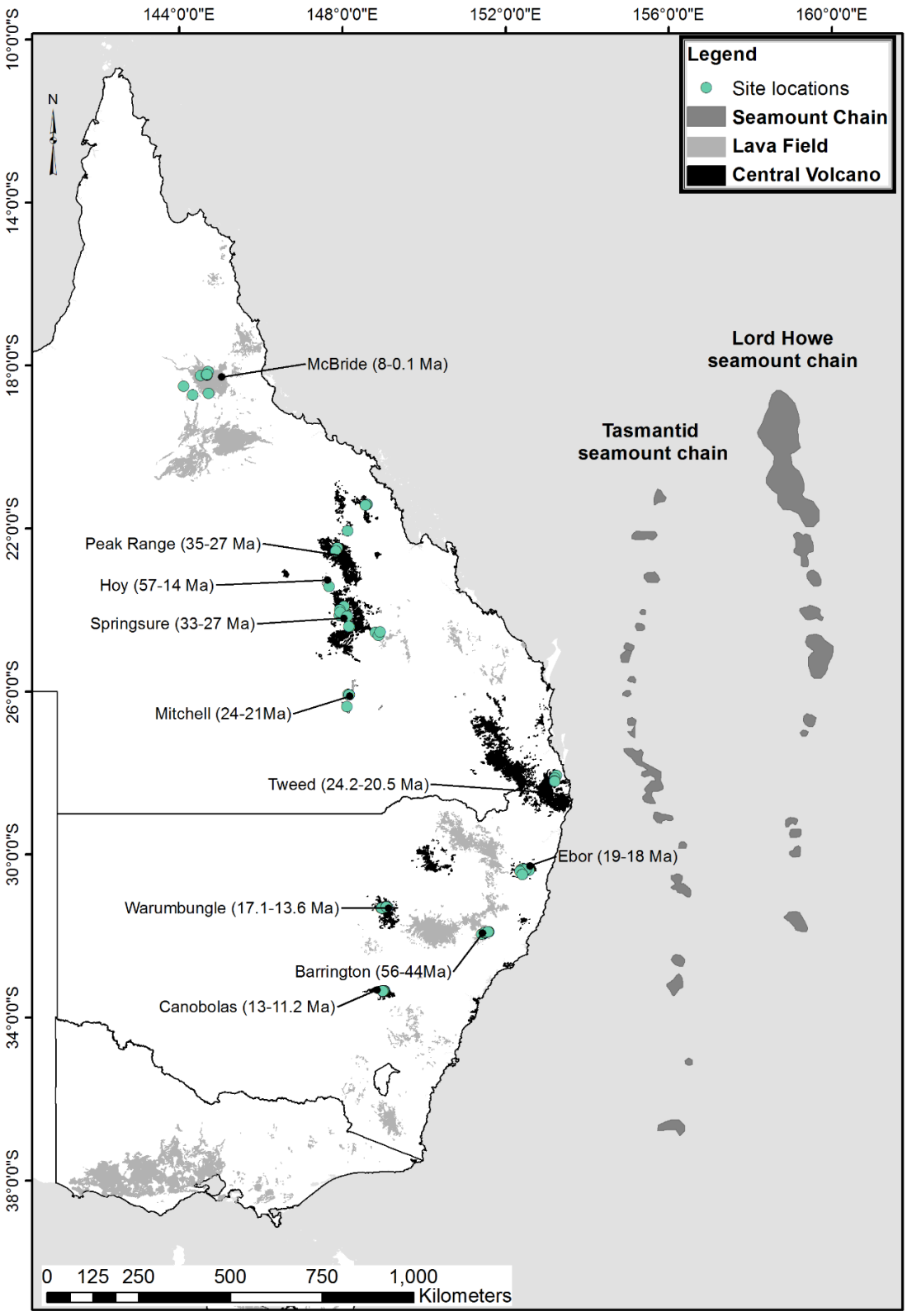

Figure 6.2: Location of Cenozoic age basaltic provinces in eastern Australia with selected provinces for paleomagnetic study. Geological unit data after Raymond et al. 2012, ages after Jones et al. (2017) and references therein.

6.3 Methodology

6.3.1 Paleomagnetic analysis

Approximately 560 oriented samples were collected from nine volcanic provinces in eastern Australia (3 to 10 samples from approximately 10 sites per province; Fig. 6.2). A subset of samples from each province was demagnetised using both thermal and alternating field (AF) techniques, and the remaining samples were demagnetised only with AF in the Paleomagnetics and Biomagnetics Laboratory at the Caltech Division of Geological and Planetary Sciences. Each specimen was twice cooled to -173°C and allowed to return to room temperature in a μ-metal shield over the course of an hour and remeasured to ensure viscous components were removed. The specimens were further "cleaned" using low intensity AF up to 7.5 mT. Two or three samples from each site were selected for a paired study. A specimen from each of these samples was demagnetised with thermal techniques up to 605˚C. A second specimen was demagnetised with AF up to 90 or 113 mT. The final resultant vector of each specimen was compared to evaluate the effectiveness of AF demagnetisation. The remaining samples were demagnetised using AF in a peak field of 90 to 120 mT using a Superconducting Technology, Inc. cryogenic moment magnetometer with a 2G Enterprises 60-liter, cryocooled dewar, electronics and computer-controlled sample changer, and a 2G/Applied Physics AF demagnetizer. Thermal demagnetisation was conducted with a magnetically shielded furnace. Resultant characteristic remanent magnetism (ChRM) directions were determined by principal component analysis of Zijderveld diagrams (*Kirschvink,* 1980). Each resultant direction was used to calculate individual site (volcanic flow) mean directions using PaleoMag software (*Jones,* 2002). Results are summarised in Table 6.1 and Zijderveld diagrams for each sample are located in Appendix D. Samples with high mean angle of deviation (MAD) scores (>10) were not included in site-mean calculations.

Four rock magnetic tests were used to determine grain type and approximate size. IRM Gradient of Acquisition Plot (GAP) diagrams (*Kruiver et al.,* 2001) were used to estimate the coercivity of magnetic minerals in the analysed samples. "Soft" magnetic minerals, such as magnetite or titanomagnetite, have lower coercivities and relatively broad distributions. "Hard" magnetic minerals, such as hematite or goethite, have higher coercivity indexes. Soft ferromagnetic mineral (likely pseudo-single domain or multi-domain magnetite) have peak coercivity of ≤20 mT ($\log B_{1/2}$ = 1.3; *Kruiver et al.,* 2001; *Abrajevitch et al.,* 2009). Higher coercivity of roughly 70 to 90 mT ($\log B_{1/2}$ = 1.8-2) are likely titanomagnetite grains (*Spassov*

et al., 2003). Coercivities on the order of 100 mT to 1 T indicate hematite ($logB_{1/2} = 3$), and ≥2-3 T is likely goethite ($logB_{1/2} \geq 3.5$; *Kruiver et al.,* 2001; *Abrajevitch et al.*, 2009). Second, Lowrie-Fuller tests (*Johnson et al.,* 1975) were used to determine the size of the dominant magnetic grains. When ARM (anhysteristic remanent magnetism) is greater than IRM (isothermal remanent magnetism), the grainsize is single domain (SD; <200 nm) or pseudo-single domain (PSD; >200 nm), and the opposite result is indicative of multi-domain (MD) grains. Roughly equivalent ARM and IRM suggest mixtures of grainsize. Third, the Cisowski test (*Cisowski,* 1981) examines interactions between magnetic grains. Values closer to the Chiton teeth magnetite line indicate stronger interactions between magnetic grains. Finally, Fuller tests (*Fuller et al.,* 1988) were used to examine the difference between natural remanent magnetism (NRM) and IRM acquisition. When NRM differs from IRM by more than two orders of magnitude, the suggestion is that magnetism is from chemical remanent magnetism (CRM), rather than thermal remanent magnetism (TRM).

6.3.2 Paleopole calculation

Time-averaged paleopoles were calculated using site mean virtual geomagnetic poles (VGPs) by combining geochronology and paleomagnetic results. Mean flow directions from provinces with shared age ranges were used to calculate the mean paleopole position. Sites were excluded from the calculation if they were poorly constrained ($\alpha95>20$) or were >40˚ away from the mean pole. Of the 91 sites from which samples were originally collected, 14 site mean directions that shared the same age and same direction were combined, forming six sites. Of the remaining 83 sites, 14 sites did not produce coherent site mean directions, reducing the number of sites to 69. Of these, 16 sites produced intermediate reversal directions. The sites were weighted based primarily on $1/\alpha95_n$ (Table 6.2), although, for fringe poles (>30˚ from the mean pole), the weighting was reduced and redistributed to more coherent poles. The dispersion both before and after weighting was calculated as an indication of sufficient sampling of the magnetic field to account for paleosecular variation. Where calculated dispersion was within error of expected dispersion, the poles were considered to account for paleosecular variation.

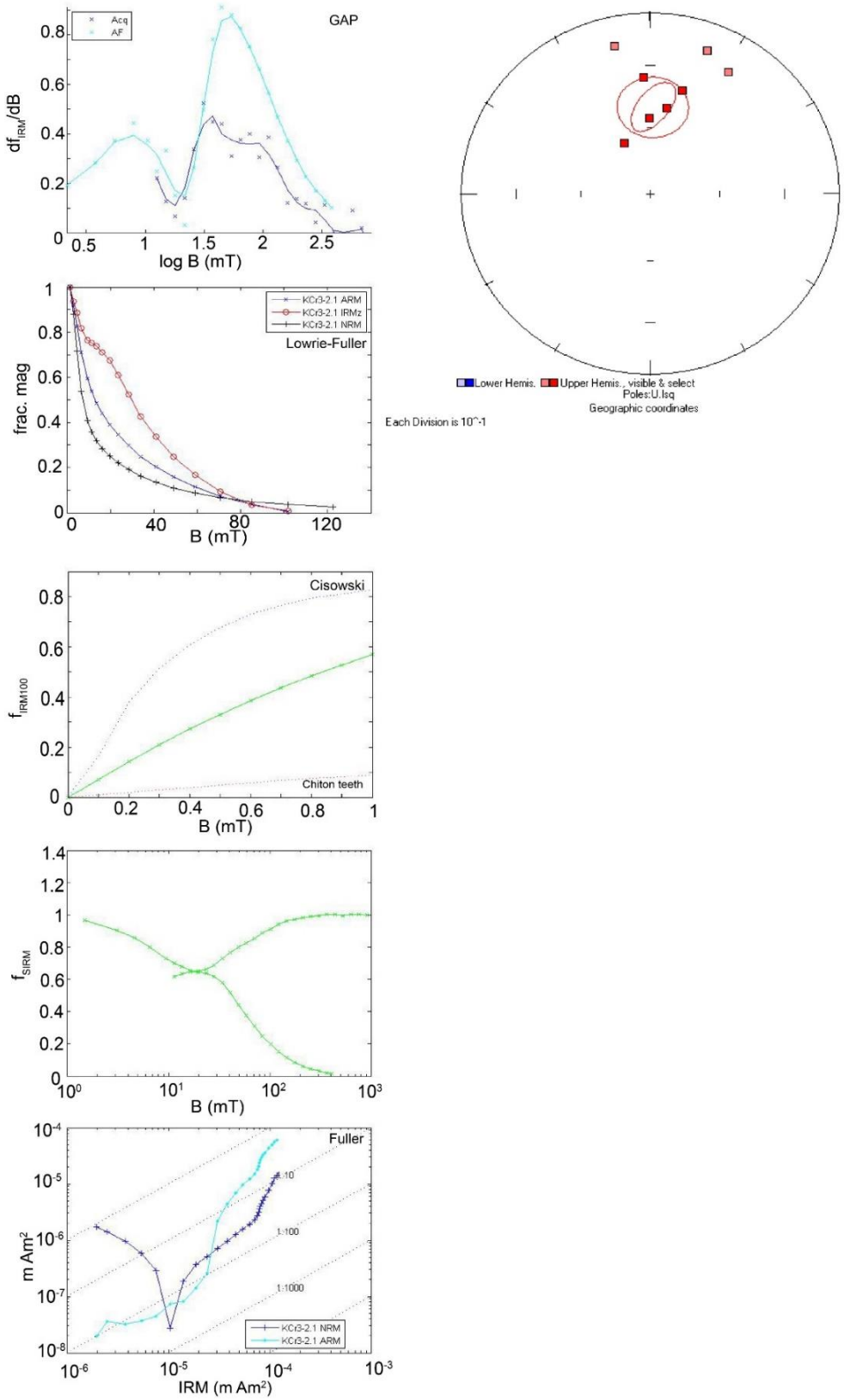

Figure 6.3: Site-mean directions and rockmagnetic results of Undara volcano (KC3), north Queensland.

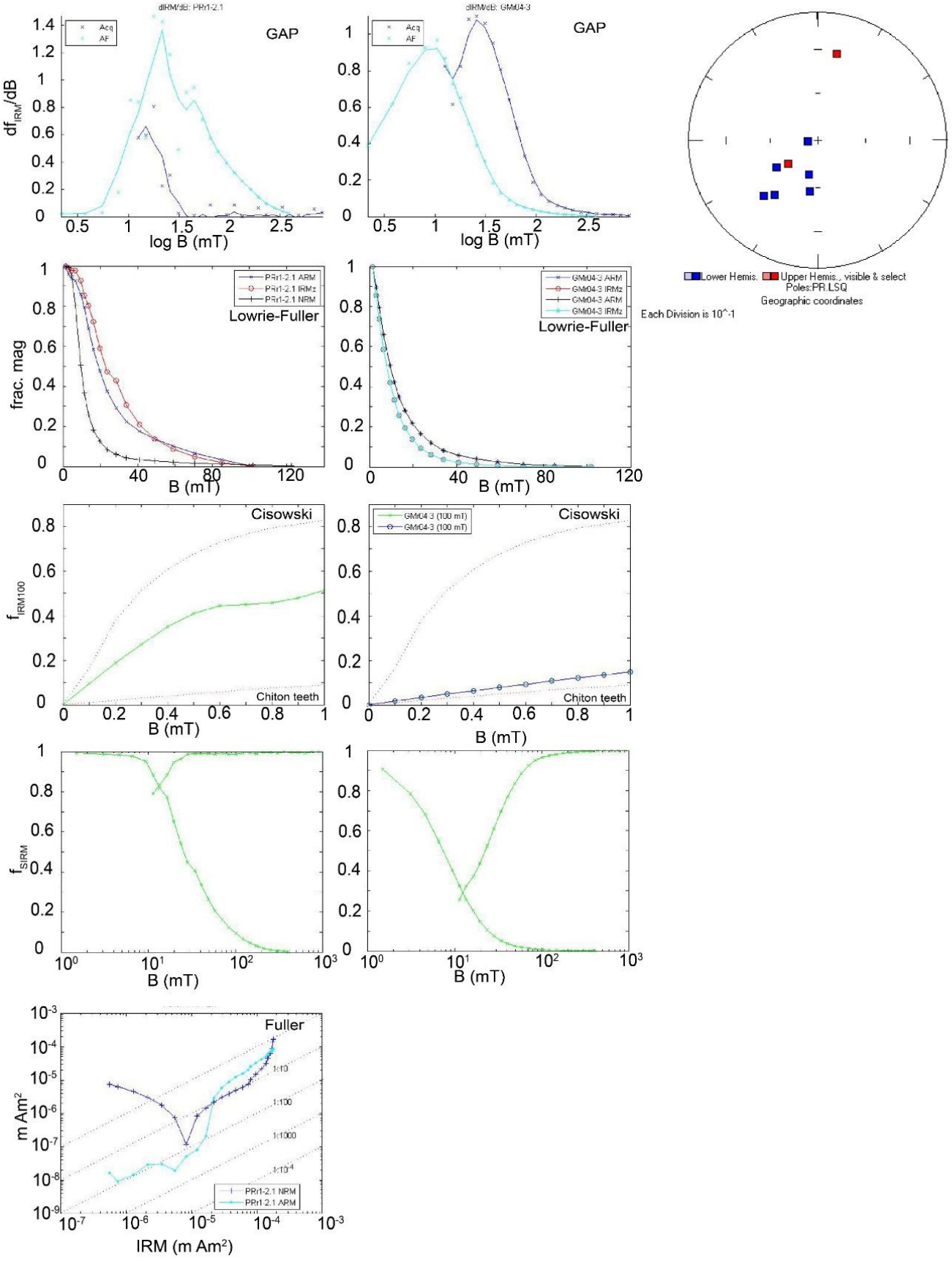

Figure 6.4: Site-mean directions and rockmagnetic results of Peak Range (Left- PR1; Right - GM4, central Queensland

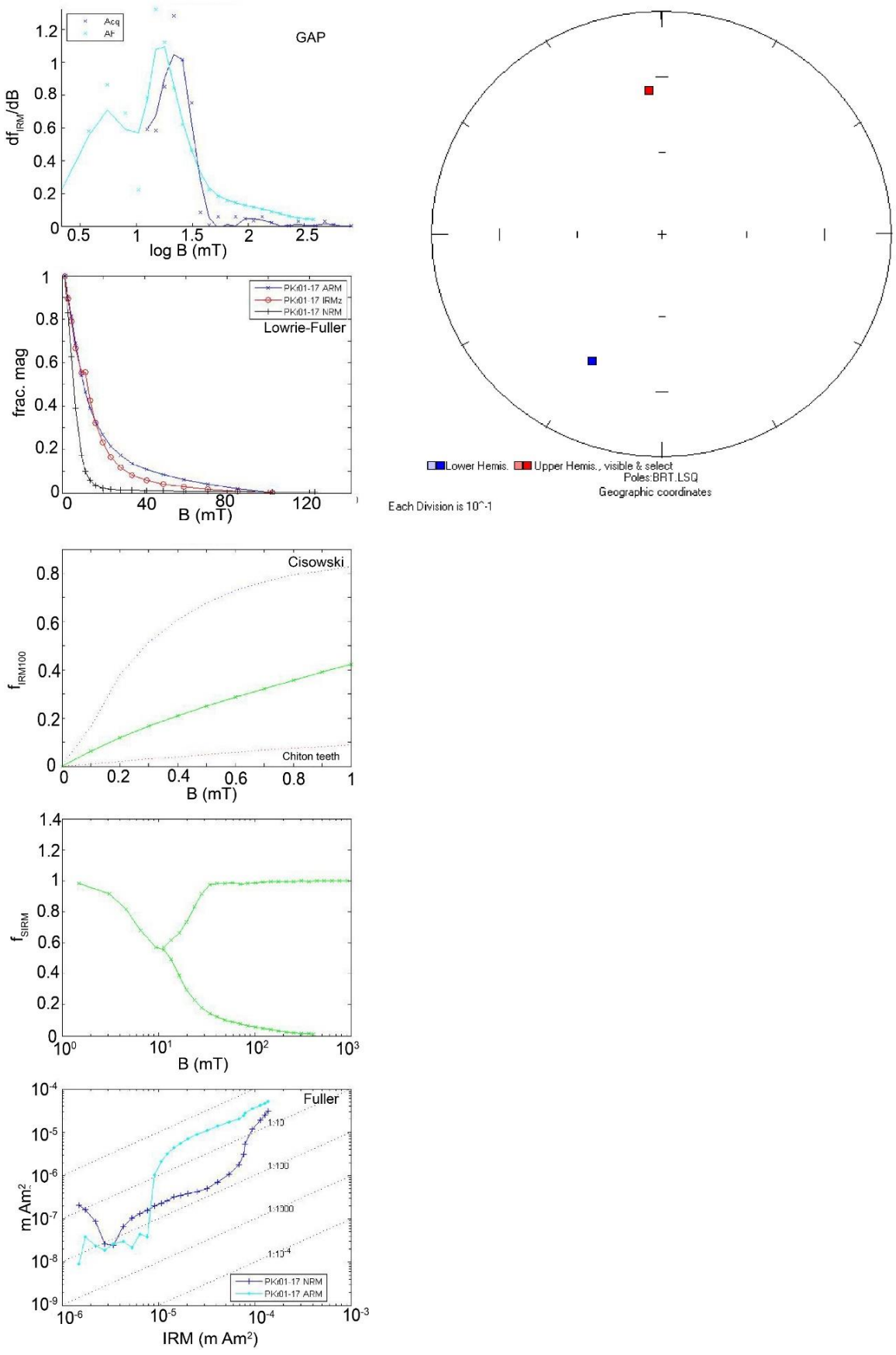

Figure 6.5: Site-mean directions and rockmagnetic results of Policeman's Knob (PK01-17), central Queensland

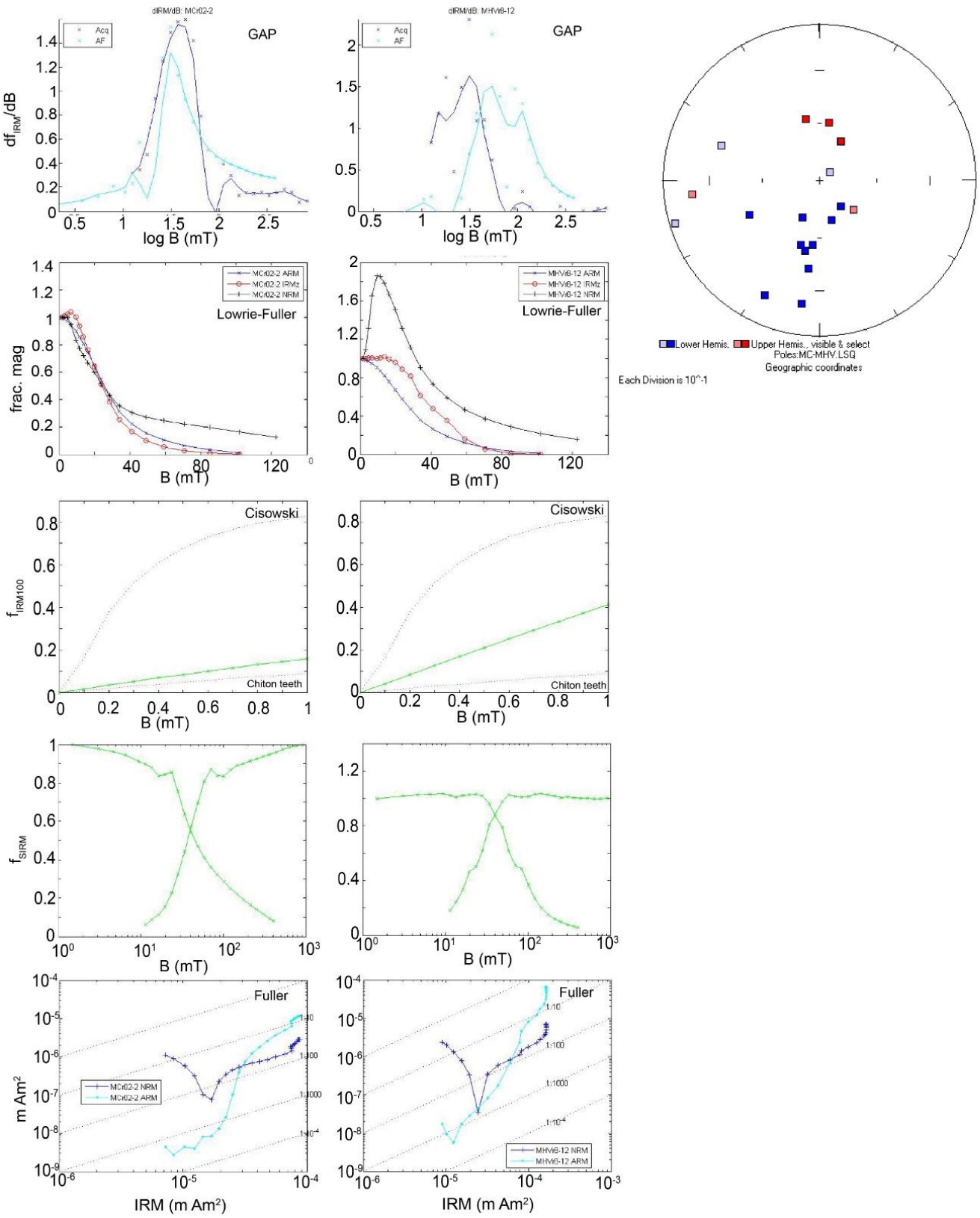

Figure 6.6: Site-mean directions and rockmagnetic results of Springsure (left – MC2; right – MHV6), central Queensland

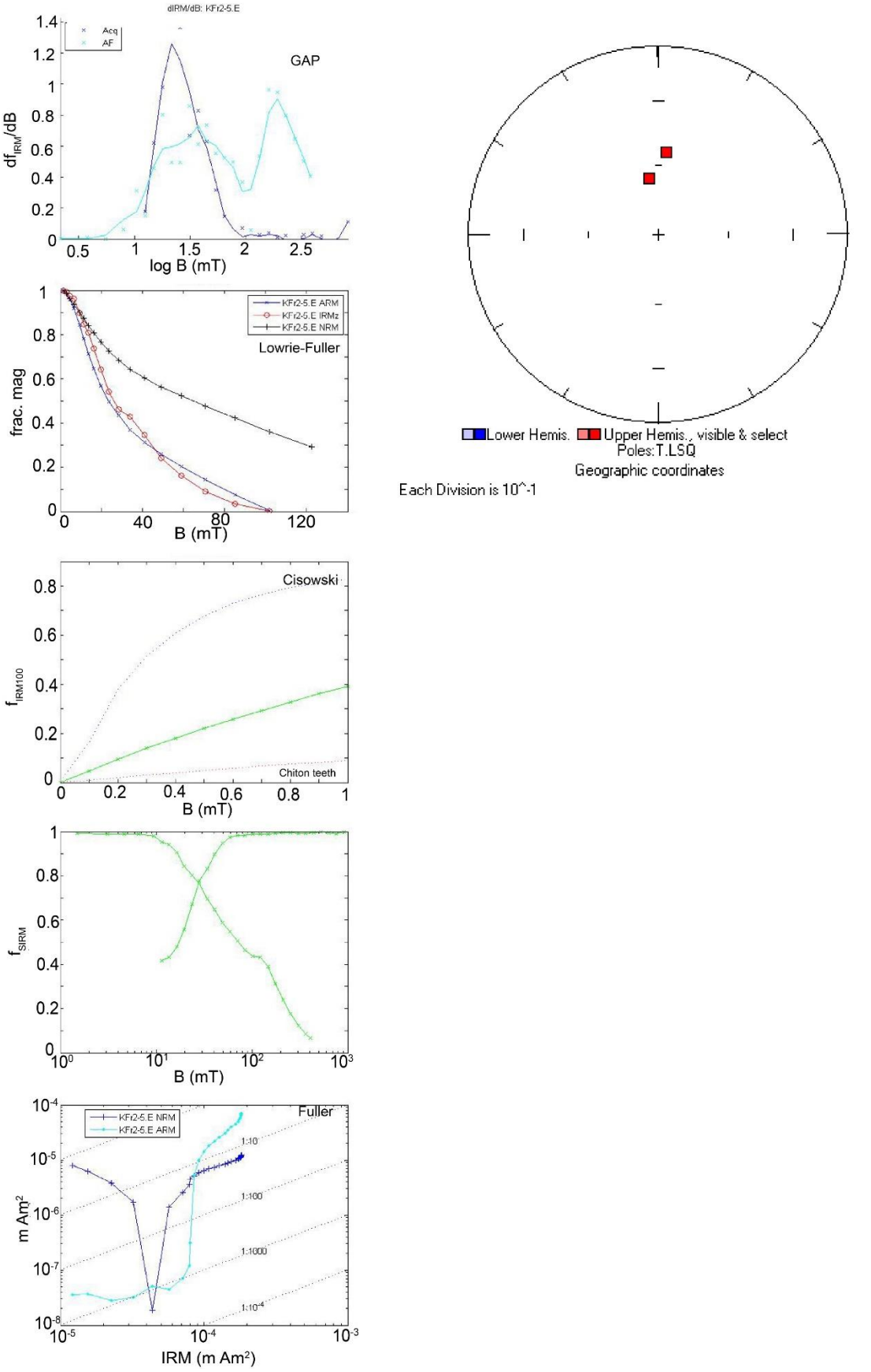

Figure 6.7: Site-mean directions and rockmagnetic results of Mitchell (KF2), central Queensland.

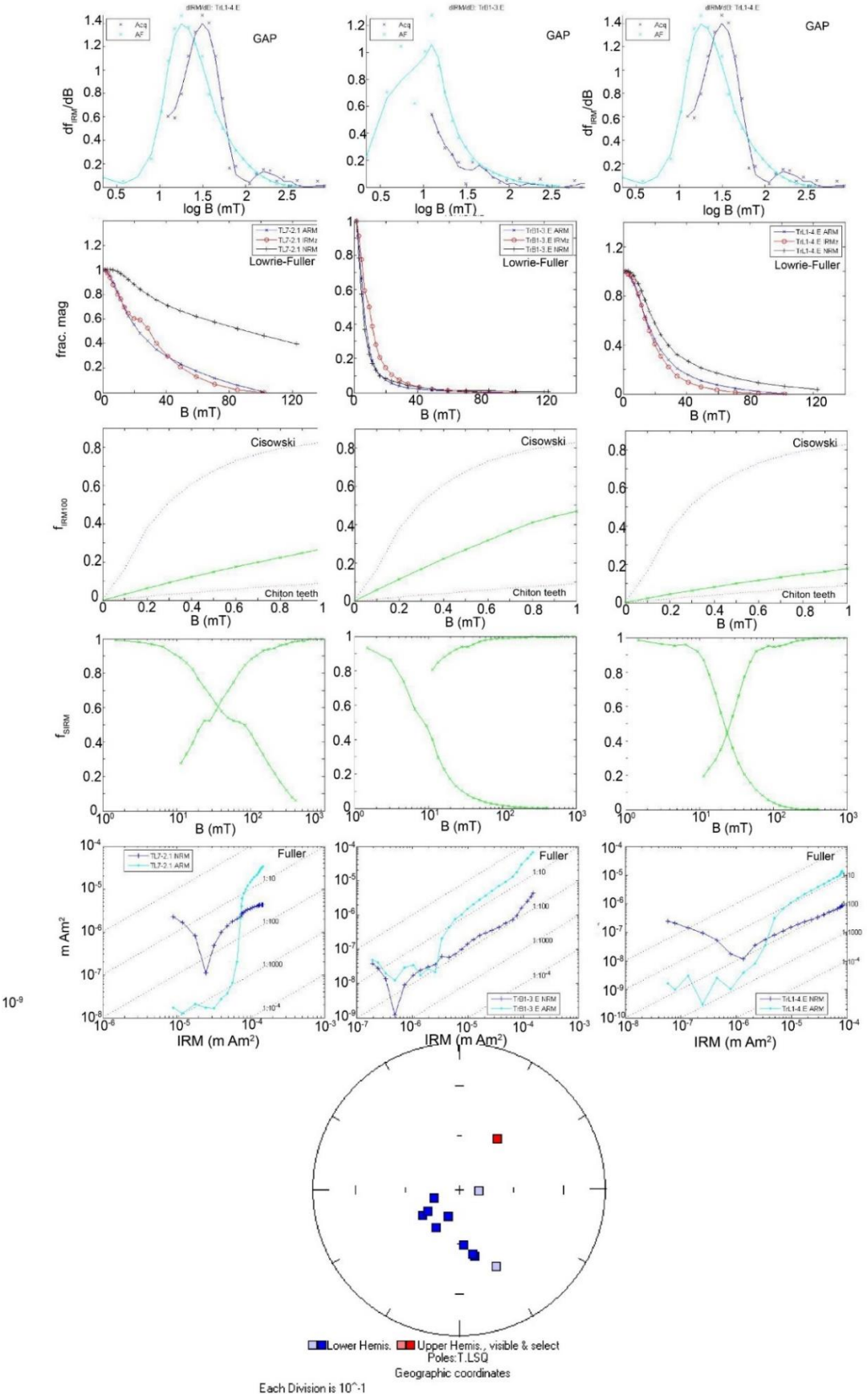

Figure 6.8: Site-mean directions and rockmagnetic results of Tweed (left – TL7; middle – TB1; right – TL1), south-east Queensland.

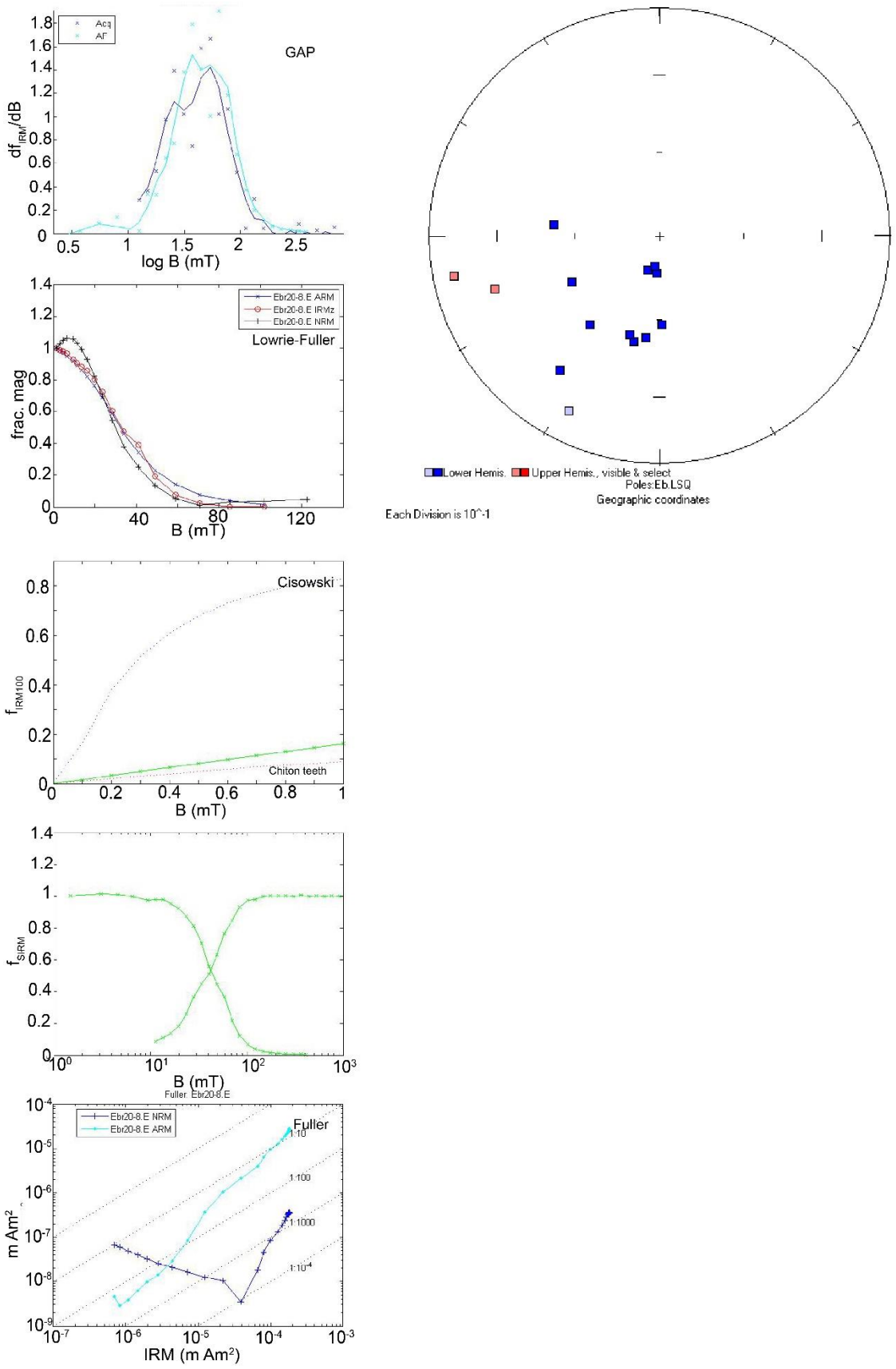

Figure 6.9: Site-mean directions and rockmagnetic results of Ebor (EB20), New South Wales

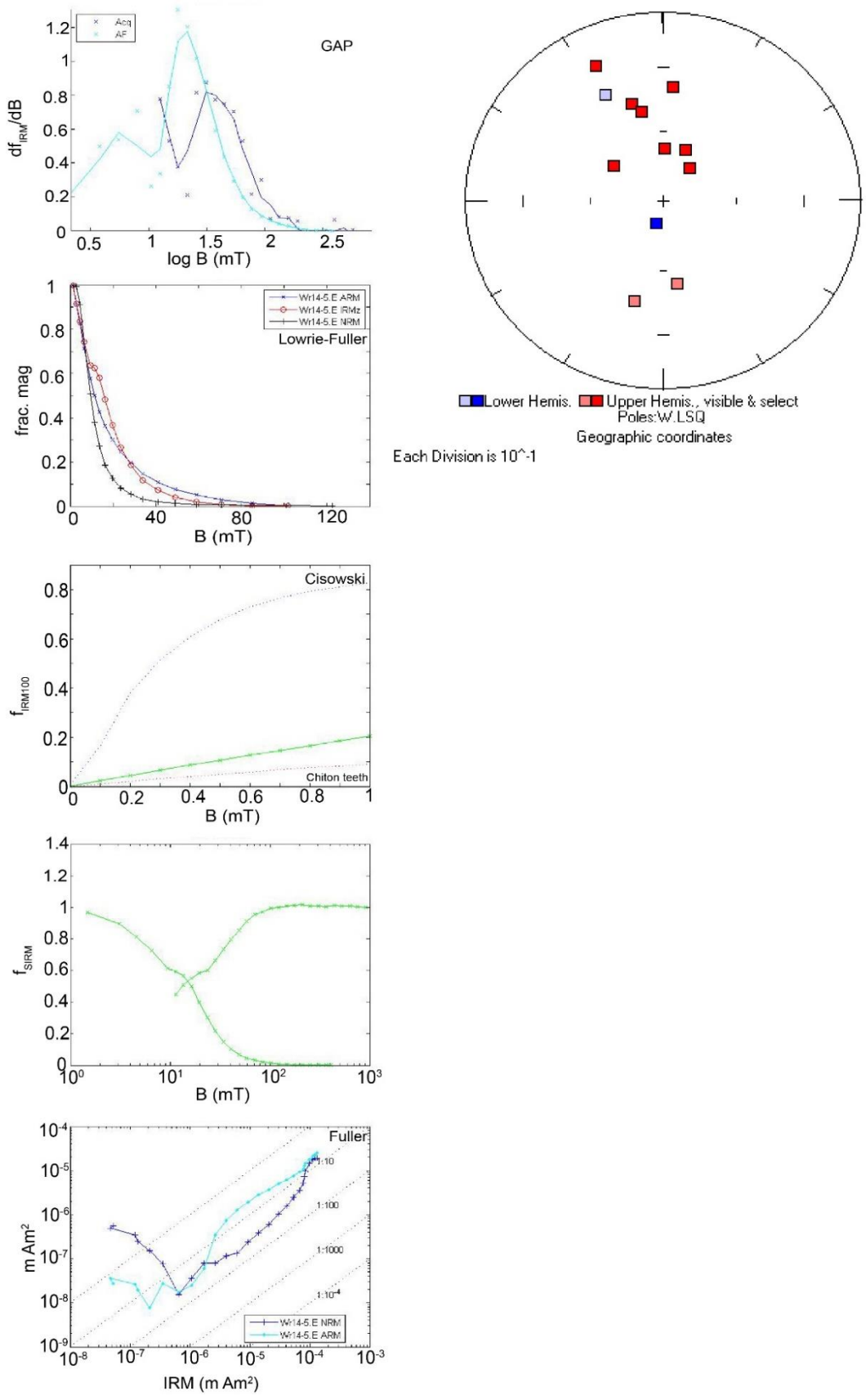

Figure 6.10: Site-mean directions and rockmagnetic results of Warrumbungles (W14), New South Wales.

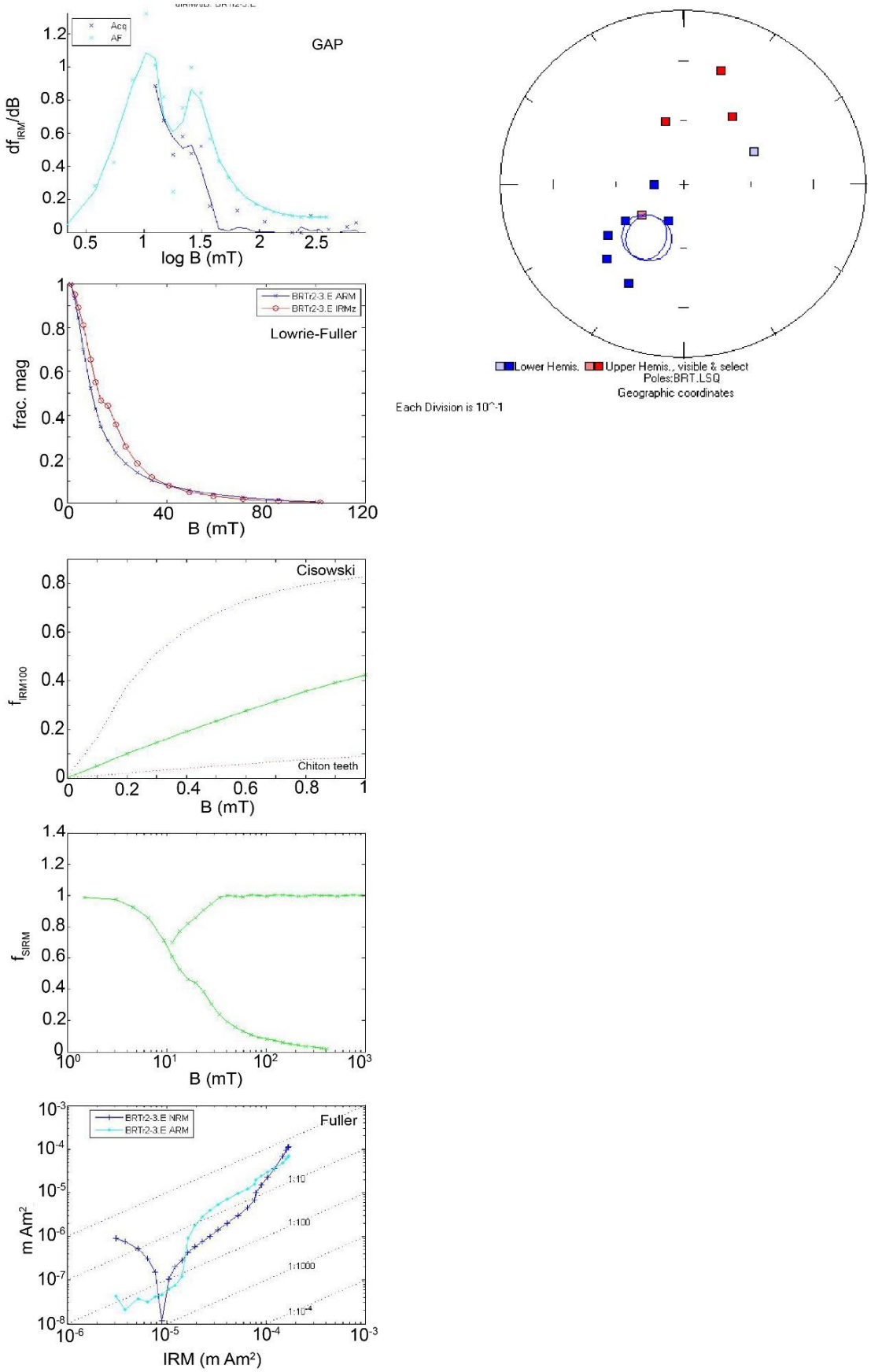

Figure 6.11: Site-mean directions and rockmagnetic results of Barrington (BRT2), New South Wales.

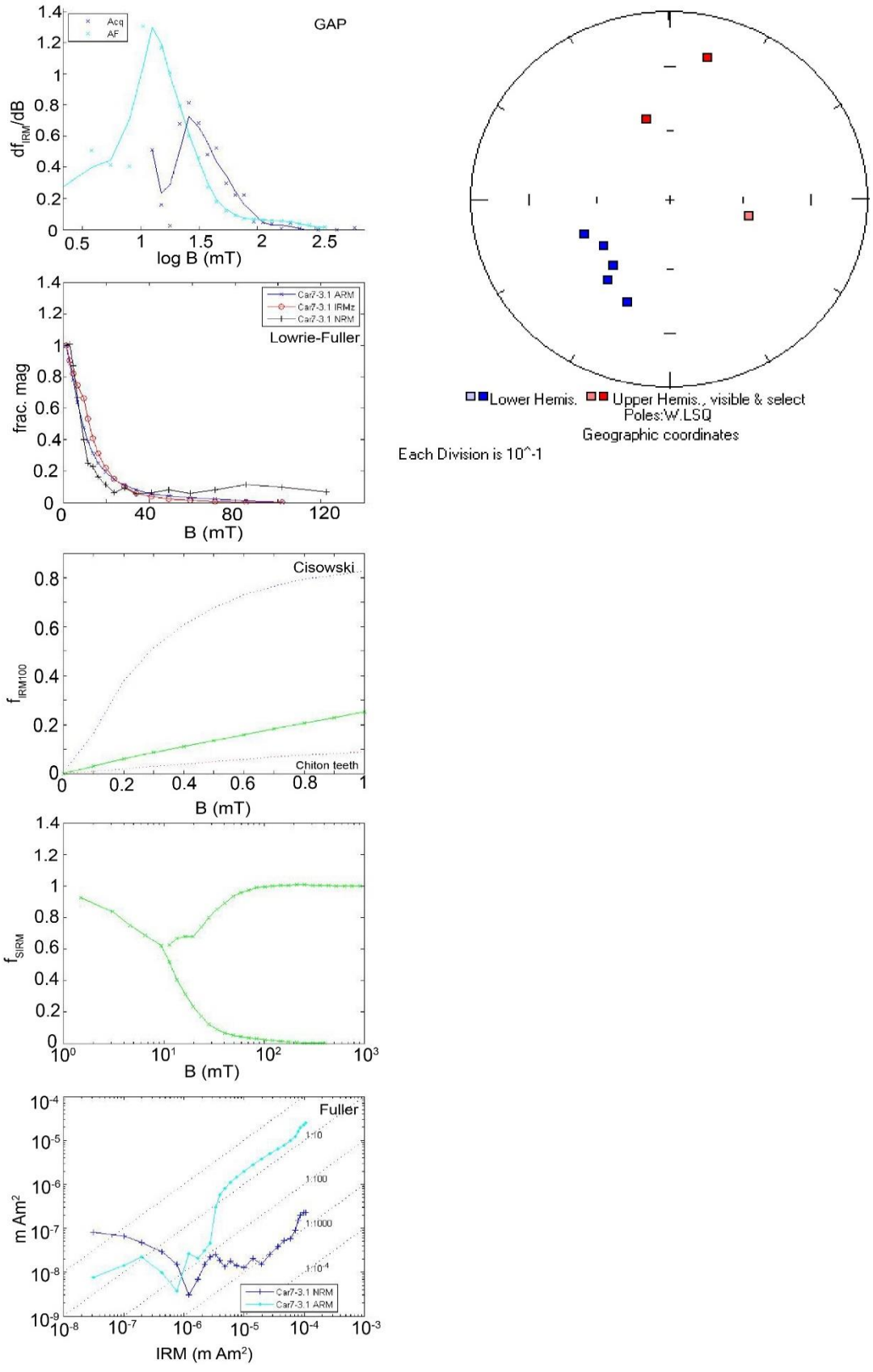

Figure 6.12: Site-mean directions and rockmagnetic results of Canobolas (Ca7), New South Wales.

6.4 Results

$^{40}Ar/^{39}Ar$ data were collected from ten volcanic provinces along the eastern coast of Australia than span 60 million years (Table 3.1; Chapter 3). The preferred ages from these samples were the $^{40}Ar/^{39}Ar$ isochrons, which were within error of the plateau ages (Chapter 3). $^{40}Ar/^{39}Ar$ results generally reveal restricted periods (1 to 2 My) of activity in each province, with a period of major eruptions of 10^5 y and large hiatuses of up to 6 Myr.

6.4.1 Undara

The Undara volcano, part of the McBride province, was selected to represent the modern pole and act as a northern counter to the Victorian 2 Ma pole (*Opdyke and Musgrave,* 2014). The Victorian results are also dominated by the modern geomagnetic field. Rock magnetic studies of a site from the Undara volcano indicate a mix of magnetic carriers (Fig. 6.3). A component at ~90 mT is prominent in the Kalkarny Crator sample, indicating the predominence of titanomagnetic as the magnetic carrier (Fig. 6.3). Secondary magnetite is indicated by a lower field component (<20 mT). The Lowrie-Fuller test indicates a dominance of MD titanomagnetite and minimal interaction between grains with a mean destructive field (MDF_{ARM}) of 13 mT and 44.7 mT (MDF_{IRM}). Saturation is acquired at ~120 mT, and the sample has an R value of 0.64. The original Fuller classification diagram shows two orders of magnitude difference between NRM and IRM acquisition, indicating that magnetisation is primary (Fig. 6.3).

Paleomagnetic data were collected from eight sites in the Undara province that have an average age of ~0.2 Ma. The site-mean directions are reported in Table 6.2. Of the eight sites, three did not produce coherent site-mean directions. Sites UR1 and UR2 were combined to form a single pole, as were UBA3 and UPW4. All sites were normal polarity (Fig. 6.3), although one site produced intermediate polarity and was not included in further pole calculations. The pole dispersion estimate is lower (16.4) than the modern dispersion, but it is within error of expected dispersion (*McFadden et al.,* 1991). An average pole was calculated for 0.2 Ma and is located at -84.7ºN 131.3ºE.

6.4.2 Peak Range, Moranbah, and the Gemini Mountains

Rock magnetic studies were conducted on one mafic and one evolved sample from the Peak Range province (Fig. 6.4). Peak Range has a major peak at ~20 mT, indicative of magnetite. A

secondary peak is evident at ~70 mT, implying the presence of a titanomagnetite component. The sample has mixed grainsize from MD at low field and either SD or PSD at higher field strengths. There is low to moderate interaction between grains and a mean destructive field of 18.9 mT (MDF_{ARM}) and 25.9 mT (MDF_{IRM}), with saturation at 40 mT. The Fuller test shows, at most, an order of magnitude difference between the NRM and IRM acquisition.

Sixty samples were collected from nine sites within the Peak Range province, and they produced stable magnetic directions (Table 6.1). The samples that were thermally demagnetised lost magnetisation between 500 and 600 ˚C. The Peak Range province sites can be divided into three age ranges: an Eocene group (G1; 47 to 45 Ma), a mid-Oligocene group (G2; 35 to 30 Ma), and a late-Oligocene group. The oldest of the Eocene sites has normal polarity, while the other two sites are reversed. The mid-Oligocene group is entirely reversed polarity (Fig. 6.4). Samples from site PR01 were highly scattered. The mid-Oligocene poles from the Gemini Mountains region were combined with the Springsure province to produce the 29 Ma pole, and the older mid-Oligocene poles form a poorly-constrained pole at ~34 Ma of -62.4ºN 116.3ºE (A95 = 23.1º).

6.4.3 Policeman's Knob

Rock magnetic acquisition studies were conducted on a sample from the outer rim of the Policeman's Knob plug (Fig. 6.5). The main magnetic carrier has peak coercivity at 30 mT, indicating magnetite, and a secondary peak at 90 mT. SD or PSD grains are the primary carriers, though a small component of MD grains are present. Grain interaction is relatively strong. Saturation was achieved at 20 mT, and the mean destructive field is 10.5 mT (MDF_{ARM}) and 13.6 mT (MDF_{IRM}). The difference between NRM and IRM acquisition is, at most, two orders of magnitude, indicating that the NRM is primary and derived from TRM rather than CRM.

Thirty paleomagnetic samples were collected from a transect across the surface of the ~64 Ma Policeman's Knob plug (*Cohen,* 2007). Samples treated with thermal demagnetisation lost magnetisation between 220˚C and 280˚C. IRM and ARM acquisition curves indicate titanomagnetite as the primary magnetic carrier. Previous thin-section and SEM studies revealed a prevalence of MD titanomagnetite (*Cohen,* 2007). Samples showed a progressive change from reverse to normal polarity from the periphery of the plug to the interior (Fig. 6.5).

When intermediate polarities are removed, the site passes an intermediate reversal test (Table 6.2; Fig. 6.5), although the reversal is incomplete.

6.4.4 Springsure

Rock magnetic experiments were conducted on samples from two sites within the Springsure province (Fig. 6.6). One sample was a relatively fresh basalt from the Mount Catherine section. Grainsize from this sample was mixed, although the Lowrie-Fuller test indicates a dominance of SD or PSD grains over MD grains. Grain interaction is strong. The GAP classification has a peak coercivity at ~60 mT, which is indicative of titanomagnetite. A second peak at ~300 mT could indicate the presence of a hard-coercivity mineral such as hematite. The Fuller test indicates TRM as the primary source of magnetism, likely acquired during formation. The mean destructive field was 25.6 mt (MDF_{ARM}) and 45.9 mt (MDF_{IRM}), with saturation occurring at 1 T. The second sample was a weathered basalt from a road cut near Mt. Zamia. This sample has mixed grainsize and a predominance of MD grains that are moderately interactive. Most of the magnetism from this sample appears to be carried by titanomagnetite and hematite, with a small component from goethite. Re-acquisition indicates that titanomagnetite is the primary carrier in most cases, with a mean destructive field of 27 mT (MDF_{ARM}) and 77.4 mT (MDF_{IRM}), reaching saturation at 70 mT. Despite alteration, the Fuller test indicates that the magnetisation is primary and likely acquired through TRM rather than chemical processes.

Sixteen paleomagnetic sites were collected from the Springsure province. MAD values were low, and stable directions consisted of five or more steps. Some sites show minor involvement of hematite and goethite, although magnetisation was lost between 450 ˚C and 585 ˚C. Four sites had normal polarity, and eight had reversed polarity (Fig. 6.6). The distribution of sites passes the reversals test (angle between the means of 3°), with a critical angle of 12.09° (95% confidence). The 28 Ma pole (-71ºN, 113ºE, dm=5.51, dp=9.07) was created by combining sites from the Springsure and Peak Range provinces, which have overlapping age ranges. Dispersion was 19.3, within error of the expected value of 20.16 for rocks produced at a latitude of 38°S (*McFadden et al.*, 1991).

6.4.5 Mitchell

Magnetite and hematite are the primary carriers from samples in the Mitchell province, although acquisition indicates that some of the magnetisation may be secondary from CRM during hematite formation (Fig. 6.7). Grainsize was mixed between MD and either SD or PSD magnetisation, with moderate to strong grain interaction. The NRM to IRM difference is typically two orders of magnitude, although differences were up to four orders of magnitude for some acquisitions. This result is concordant with the strong hematite component recognised through the IRM decay curves. Saturation of the field occurs at ~100 mT, and the mean destructive field is 23.6 mT (MDF_{ARM}) and 74 mT (MDF_{IRM}).

Two sites and a total of 12 samples were selected from the Mitchell province. The sites have an age of ~22 Ma. Both sites indicate two distinct poles (Fig. 6.7), with directions of 5.6, -53.8 (a95 6.5) and 350.6, -65.3 (a95 8.6). The sites were combined with the Tweed pole to construct the final 24 Ma pole.

6.4.6 Tweed

At Tweed, 60 samples were collected from 12 sites that erupted over a restricted period from 24 to 23 Ma (*Cohen et al.,* 2007). Rock magnetic experiments were conducted on three different rock types from the Tweed province (Fig. 6.8). The first was a basalt sample from below the Binna Burra rhyolite. This sample exhibited a resistance to AF demagnetisation, but lost magnetism at the unblocking temperature of magnetite (580 to 590°C), although both trajectories produced the same resultant vector direction. The Lowrie-Fuller diagram indicates a mixed grainsize between SD/PSD and MD carriers, although the SD/PSD grains appear to dominate and are strongly interactive. IRM decay curves, shown as GAP diagrams, indicate primary magnetisation through both magnetite and hematite components. Thin-sections show no significant signs of hematite, although it does show what appears to be alteration of magnetite to hematite, forming what may be maghemite. While the presence of maghemite indicates chemical weathering, and thus acquisition of CRM, maghemite is known to produce magnetism in the same direction as TRM (*Heider and Dunlop,* 1987; *Özdemir and Dunlop,* 1989; *Nishitani and Kono,* 1989). The Fuller test shows a difference between IRM and NRM acquisition of approximately two orders of magnetite. The mean destructive field is 22.8 mT (MDF_{ARM}) and 85 mT (MDF_{IRM}). The second sample is from the Beechmont Basalt, the oldest unit in the sequence. The Lowrie-Fuller test indicates the predominance of MD grains that are

moderately interacting. The GAP diagram indicates the presence of magnetite as the primary carrier of magnetisation, with minor occurrence of hematite. The difference in the Fuller test is two orders of magnitude, which is characteristic of primary TRM acquisition. The mean destructive fields were 6 mT and 9.8 mT. The final sample is from the rhyolite flow of the Tweed shield volcano. The Lowrie-Fuller test indicates a predominance of SD or PSD grains that strongly interact. IRM decay GAP diagrams indicate the main magnetic carrier is magnetite or titanomagnetite, with a mean difference between NRM and IRM of two orders of magnitude. The mean destructive field was 17.9 mT (MDF_{ARM}) and 22 mT (MDF_{IRM}; Fig. 6.8a).

Eleven sites (53 samples) from the Tweed volcano produced stable directions (Fig. 6.8b; Table 6.2). Sites LNP3, LNP8, and TS4 did not produce stable site-mean directions, and site TS6 was of intermediate polarity and was therefore excluded from the study. Samples LNP6 and 7 were combined to create the TL6-7 pole. Samples from site LNP7 did not respond to AF and lost magnetisation between 500 ˚C and 585 ˚C. Samples from sites TS3 and TS5, which are primarily composed of obsidian, produced stable site mean directions. All sites, with the exception of BB1, had reversed polarity (Fig. 6.8). The sites pass a C quality reversals test, with a critical angle of 16.89˚. Sites from the Tweed, Mitchell, and Peak Range provinces were combined to create the 23.5 Ma pole, at -73.40°N, 127.60°E (dm = 3.66, dp = 7.49). The poles for the Tweed province produced a dispersion estimate of 19.4, which is within error of the expected dispersion (*McFadden et al.,* 1991).

6.4.7 Ebor

Fourteen sites were selected from the Ebor province for paleomagnetic study, seven from a stratigraphic profile at Point Lookout and seven from roadcuts along the Dorrigo highway (Fig. 6.2). A single site, from the lower section of Ebor, was selected for a rock magnetism study (Fig. 6.9). The main magnetic carrier in the Ebor suite is titanomagnetite (~70 mT). The grain size is mixed between MD and SD/PSD that are strongly interacting. The Fuller test indicates a difference of three to four orders of magnitude between the NRM and IRM acquisition. This result implies that, in this sample, the magnetisation may come from CRM rather than TRM. When the CRM was acquired is unknown, though Australia was known to suffer from deep weathering at ~20 Ma. The mean destructive fields are 32.5 mT (MDF_{ARM}) and 45.3 mT (MDF_{IRM}).

Ten paleomagnetic sites from Ebor produced stable mean directions after demagnetisation (Table 6.2). All stable sites, with the exception of EB1, had reverse polarity (Fig. 6.9). Two sites, EB1 and EB11, produced intermediate directions. IRM and ARM studies indicate a derivative of the magnetite mineral group, possibly titanomagnetite, as the main magnetic carrier. The Ebor province was used to create the 19 Ma pole -74.6ºN, 117.5ºE (dm =3.8, dp =7.46). Site dispersion (19.7) was within error of the expected dispersion (*McFadden et al.*, 1991), implying sufficient sampling to account for paleosecular variation.

6.4.8 Warrumbungles

Samples were collected from eleven sites within the Warrumbungles province. Six sites were collected from the Siding Spring Road, part of the Mount Woorut sequence, and five sites were collected from the Mount Exmouth section. The main magnetic carriers from these samples are titanomagnetite and magnetite (given by the GAP diagram), which the Lowrie-Fuller test indicates are of mixed grain size (Fig. 6.10). The magnetic grains are strongly interactive (Cisowski test), though the two orders of magnitude difference between the NRM and IRM acquisition implies that the primary magnetism is from TRM, rather than CRM. The mean destructive fields are 11.4 mT (MDF_{ARM}) and 16.9 mT (MDF_{IRM}), with saturation occurring around 120 mT. This is supported by SEM-EDS analysis of the samples (Fig. 6.10b).

Ten sites from the Warrumbungles province produced coherent site mean directions, although only seven sites produced stable magnetic site mean directions (Table 6.2). Samples did not produce enough reverse directions to satisfy a reversals test as, apart from W10 and 11, all sites were normal polarity (Fig. 6.10c). Flows from the Warrumbungles volcano have both normal and reverse polarity, though the reverse polarity sites are intermediate and do not satisfy the reversals test. Geochronology results from sites W2, W3, W7, W10, and W11 are included in Crossingham (2017). Lower flows are normal polarity, coinciding with chron C5cn (17.1 to 15.97 Ma), and higher, reverse polarity flows coincide with chron C5br (15.16-15.97 Ma). Intermediate reversals, such as at sites W6 (16.8 (?) Ma) and 14 (16.1±0.1 (?) Ma), are located close to a boundary of polarity change. The 14 Ma pole is located at -80.10, 108.40 (dm=7.2, dp=8.5) and was created using the Warrumbungles and Canobolas VGPs.

6.4.9 Barrington

A relatively extended period of magmatic activity, and fresh exposures along roadcuts and deep incisions, make the Barrington province a good target for paleomagnetic analysis. Previous studies have included samples from around the Barrington province, resulting in a pole around 50 Ma, although new geochronology results indicate that previous age determinations were underestimates.

One site from Barrington was selected for rock magnetism studies (Fig. 6.11). The primary carrier of magnetism is MD magnetite, although the Lowrie-Fuller test indicates mixed grainsizes that are moderately interactive. The Fuller test shows a two order of magnitude difference between IRM and NRM acquisition, indicative of TRM as the primary magnetisation. The mean destructive fields are 9.9 mT (MDF_{ARM}) and 15 mT (MDF_{IRM}).

Paleomagnetic data were collected from ten sites at Barrington, totalling 64 samples. Seven sites produced coherent site mean directions, with a combined total of 35 samples (Table 6.2). Sites were primarily normal polarity and pass an indeterminate reversals test, likely due to the few viable reversal directions (Fig. 6.11). Rock magnetic results indicate magnetite as the primary carrier (Fig. 6.11). Results from the Barrington province were combined with the older population of Peak Range and Policeman's Knob to create a 60 Ma pole at -55.41, 104.55 (dm = 8.58, dp = 10.86).

6.4.10 Canobolas

The Canoblas samples produced too few useable directions to construct a coherent pole. The rock magnetism study indicated that MDmagnetite is the main magnetitic carrier in the Canobolas section, although the Lowrie-Fuller test shows mixed grainsize (Fig. 6.12). The mixed grains are strongly interacting, and the Fuller test shows that magnetism in this particular site may be from CRM, rather than TRM. This is not wholly unexpected, as poles from this site are inconsistent with poles from the slightly older volcanoes to the north. The mean destructive field is 9 mT and 12.5 mT, and saturation is achieved by 80 mT.

Of the nine sites from Canoblas, only five produced coherent site-mean VGPs (Table 6.2). Of these, only three sites were not of intermediate polarity (Fig. 6.12). These sites were combined with data from the Warrumbungles to improve the overall accuracy of the 13 Ma pole.

6.4.11 Combined paleopoles

Of the 69 sites that produced stable, coherent directions, 53 produced non-intermediate polarity directions. Paleo-poles are summarised in Table 6.2. Paleomagnetic data from the Barrington province were combined with results from the older parts of Peak Range and Policeman's Knob to create a 55 Ma pole at -57°N, 95°E (dm = 8.58, dp = 10.86). A pole for 35 Ma was calculated using late Eocene to early Oligocene sites from the Peak Range province (-62.5°N, 116.3°E) though this pole was poorly constrained (A95>20). The 30 Ma pole (-71°N, 113°E, dm=5.51, dp=9.07) was created by combining sites from Springsure, the Gemini Mountains, and Peak Range. Sites from the Tweed, Mitchell and Peak Range provinces were combined to create the 23.5 Ma pole at -73.4°N, 128°E (dm=3.66, dp=7.49). The Ebor province was used to create the 20 Ma pole -74.6°N, 116°E (dm=3.8, dp=7.46). The 14 Ma pole is located at -80.10°N, 108.40°E (dm=7.2, dp=8.5) and was created using the Warrumbungles and Canobolas VGPs. With the exception of the Barrington province, all other provinces produced dispersion estimates that were within error of the expected dispersion for poles (*McFadden et al.,* 1991; Fig. 6.13). Dispersion in the 55 Ma pole was high (27.8) for these samples, implying other factors that were unaccounted for, such as successive eruptive periods or re-magnetisation. The 0.5 Ma pole is located at -84.7°N, 131.3°E and is dominated by the modern geomagnetic field.

6.5 Discussion

6.5.1 Magnetostratigraphy

All magnetostratigraphy is compared to the Cenozoic Magnetic Polarity Time Scale (MPTS) after Ogg (2012). Comparison between the paleomagnetic results, geochronology, and the MPTS of Cande and Kent (1995), rather than the astrologically correlated MPTS, do not agree and imply complete structural overturning of the Ebor volcano. As this is most certainly not the case, and the results are in accordance with rocks of similar age in North America, the MPTS of Ogg (2012) was used as comparison and agrees readily with the chrons described here.

6.5.1.1 Barrington

The lowermost and uppermost flows from the Barrington province have reversed polarity. Mid-volcanic flows BRT1, BRT2 and BRT3 are normal polarity and, while not a perfect correlation with either Ogg (2012) or Cande and Kent (1995), coincide with chron C24n.1. Flow BRT5

coincides with chron C25r, while flows BRT7 and BRT2 coincide with chron C24r. The site BRT10 has reverse polarity, and geochronology results correlate the site to chron C25r. The combination of the magnetic directions and select geochronology show a full polarity transition over the time between ~59 and 55.9 Ma.

6.5.1.2 Springsure

The sites range in age from 28 to 26 Ma at the Springsure volcano, covering a sufficient amount of time over which the field could be averaged. Periods of normal and reversed polarity appear to coincide with chrons C10n.1n, C9r and C9n (28.450 to 28.186 Ma, 28.186 to 27.826 Ma, and 27.826 to 26.714 Ma). The three oldest sites are normal polarity (chron C10n.1n), in contrast with the eight younger reversed polarity flows (chron C9r). A single basalt flow from the peak of the Springsure volcano is normally polarised, but it produced a pole with an excessive error radius.

6.5.1.3 Tweed

The lower section of the Beechmont basalt is normal polarity (one site), while the upper section is reverse polarity (one site). The change of polarity implies multiple flows comprising the Beechmont basalt (~24.3 Ma; *Cohen et al.*, 2007), but much of the 150 to 300 m-thick sequence of flows is inaccessible. The Binna Burra (three sites; 23.9 Ma; *Cohen et al.*, 2007) and Springbrook (four sites; <23.6 Ma; *Cohen et al.*, 2007) rhyolites are reverse polarity and correspond with chron C6Cr (24.044 to 23.375 Ma). The Springbrook rhyolite produced four successful poles, marking a change in composition. Lower layers are composed of an obsidian matrix, and rock magnetic studies indicate the presence of magnetite micro-phenocrysts grading up into feldspar- and quartz-rich layers. The intermediate basalt flows consist of two sites, although only one produced a usable pole, and it also falls within chron C6Cr.

6.5.1.4 Ebor

The bulk of the volcanic rocks from Ebor were erupted between 19 and 20 Ma. The MPTS after Kent and Cande (1995) shows this time period as entirely normal polarisation, however studies from Ebor (20-19.6) indicate reverse polarity. The ages are based on previous geochronological studies (*Ashley et al.*, 1995a). The upper two sites have normal polarity, and since the normal polarity central core of Ebor (*Ashley et al.*, 1995a) has been dated at 19.6 Ma (*Cohen et al.*, 2007), these flows may fall within chron C6n (19.722 to 18.748).

6.5.1.5 Warrumbungles

Magnetic intervals in the Warrumbungles volcano coincide with periods of normal and reverse polarity. Geochronology for sites W2, W3, W7, W10 and W11 are included in Crossingham (2017). Lower flows are normal polarity, coinciding with chron C5cn (17.1 to 15.97 Ma), and higher reverse polarity flows coincide with chron C5br (15.16-15.97 Ma). Intermediate reversals, such as sites W6 (16.8 (?) Ma) and 14 (16.1±0.1 (?) Ma), are located close to a polarity change boundary.

6.5.1.6 Canobolas and Undara

The timing of reversals and normal polarity cycles in the Canobolas volcano coincide with the polarity changes across its lifespan. Lower elevation flows are reversed polarity, coinciding with chron C5Ar (~12.5 Ma), and high elevation flows have normal polarity (chron C5n.2; ~10.4 Ma). Undara is entirely normal polarity (chron C1n) and is within error of the present-day field, as would be expected from 0.2 Ma volcanic rocks.

6.5.2 An updated Australian Cenozoic apparent polar wander path

Time averaged poles from volcanic centres that share a similar age range were used to construct an Australian Cenozoic APWP (Fig. 6.14a). The poles were determined for 55, 30, 24, 20, 14, and 0.5 Ma, and they are summarised in Table 6.3. Unfortunately, due to the small number of fair precision coherent sites ($\alpha 95 = <20^{\circ}$), the common means test cannot be used to determine if the site-mean population of poles 30 and 24 are distinct. As the sample mean and site-averaged mean are within error, and several sites include both normal and reverse polarity specimens from the same samples (*Schmidt and Williams.*, 2017), I chose to compare the sample mean directions in the common means test. The common means test shows that the null hypothesis can be discounted (chi squared = 0.04), so it is likely that the two poles are distinct. The 30 and 24 Ma poles indicate a period of longitudinal offset in the overall northward motion of Australia, which could imply plate rotation in the late Oligocene to early Miocene, with an angular distance between the poles of 7.79˚. The longitudinal offset and minor change in latitude between the 30 and 24 Ma poles corresponds with both the physical offset in offshore seamount chains and a period of slow plate velocity (*Knesel et al.*, 2008)

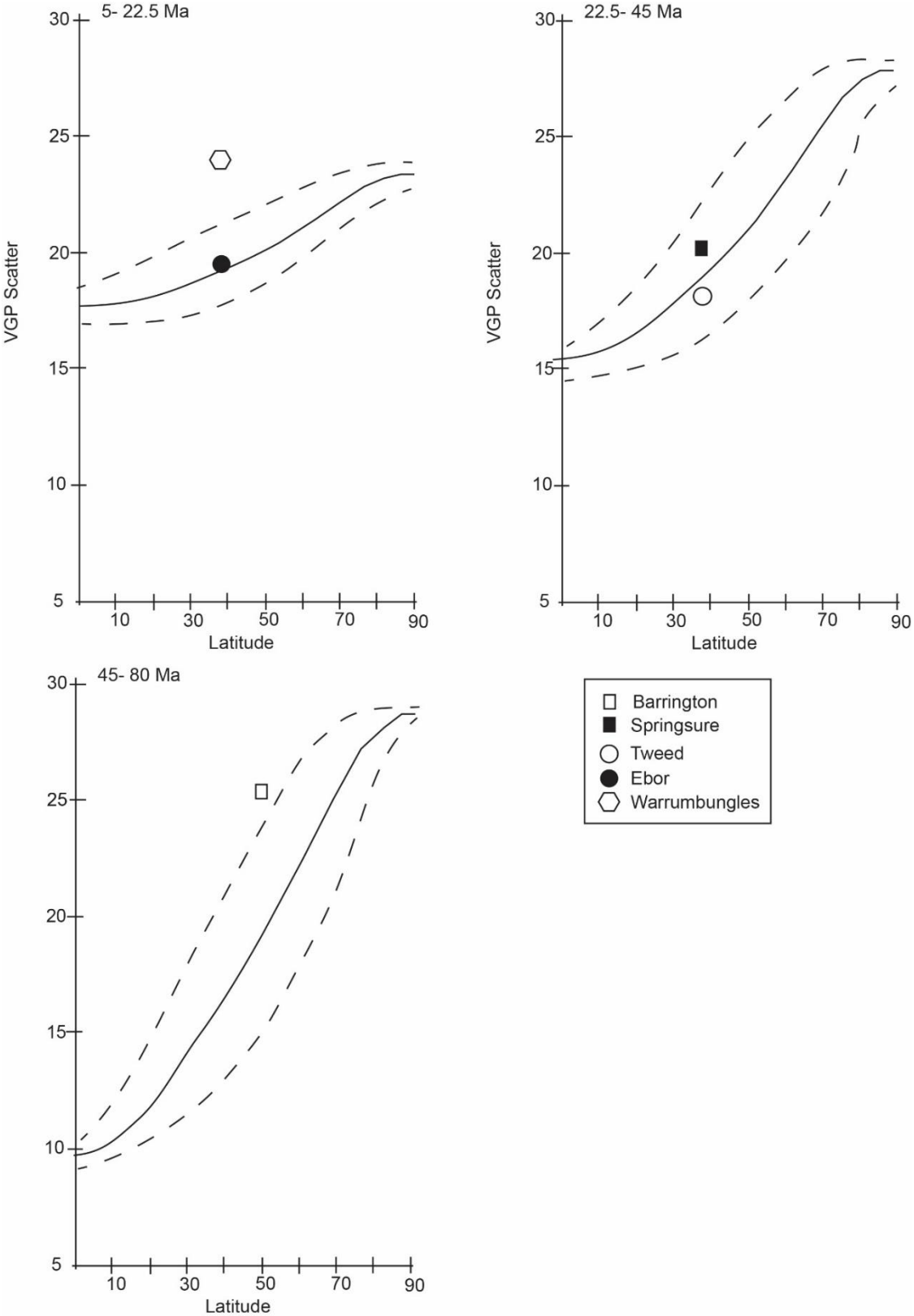

Figure 6.13: Dispersion estimates for poles calculated from east Australian Cenozoic magmas.

I compared the newly defined APWP with previous estimates of Australian plate motion (Fig. 6.14b). The results of this study compare favourably with the APWPs of Wellman and McElhinny (1975), Emblton and McElhinny (1982), and Musgrave (1989). Most significantly, the new APWP recreates an eastward divergence around the 25 Ma pole. While it was previously suggested that this divergence was an artefact due to incomplete time averaging of the magnetic field (*Idnurm,* 1985), the new results for 25 Ma are based on a record of nearly continuous volcanism over a period of a million years, sufficient to record at least one reversal. The inclinations of previous poles from Wellman and McElhinny (1975), Emblton and McElhinny (1982), and Musgrave (1989) are also comparable with the new results. The latitudes of these poles, and many others that utilise paleomagnetic results acquired from basalt, do not reproduce the results of the APWP of Idnurm (1985). For this latter study, the relationship between pole position and age relied on faunal assemblages, rather than radiometric dating. As such, the exact age of each pole was not fully understood, and the complex nature of remanence acquisition may have led to over-averaging of the magnetic field.

Paleomagnetic poles from the new APWP compare well with more modern paleomagnetic reconstructions (6.14b). The late Eocene pole (-65.5°N, 112.5°E; ~36.5 Ma) recalculated by Idnurm (1994) from sedimentary data in the Otway Basin is comparable with both the new 30 Ma pole and the poorly constrained 35 Ma pole. This late Eocene pole of Idnurm (1994) does, however, rely on biostratigraphic age estimates rather than radiometric dating. More recent work in the Hammersley Basin of Western Australia produced a pole at -78ºN 116 ºN for 24±3 Ma using "paleomagnetic dating," described below (*Schmidt and Williams,* 2017). The Hammersley Basin pole of Schmidt and Williams (2017) is similar in position, but not age, to the 19 Ma pole determined in the present study. However, the age of the Hammersley Basin pole is contingent upon prior APWPs that are reliant on few anchor poles constrained by K-Ar (*Musgrave,* 1989) or the adjusted African reference frame (*Torsvik et al.,* 2008), rather than the more recent global moving hotspot reference frame (GMHRF; *Doubrovine et al.,* 2012).

6.5.3 Plate velocities and the global moving hotspot reference frame

Australian Cenozoic plate velocities have been estimated previously from high-precision geochronology of age-progressive east Australian volcanoes (*Knesel et al.,* 2008; *Cohen et al.,* 2013). I compared these plate velocity estimates with the new independently-derived paleomagnetic estimates. Plate migration was modelled using GPLATES, and the VGPs were

used to create reconstruction poles. Using the reconstruction file, an arbitrary point from south-eastern Queensland at -27°N, 153°E was reconstructed back through time at 5 My increments (Fig. 6.14c). The plate velocity between 55 and 35 Ma was negligible, though motion between a poorly constrained 35 Ma pole (defined by the three mid-age range sites in the Peak Range province) and the 30 Ma pole was ~74 mm/yr. Motion from 30 to 23.5 Ma was ~26 mm/yr. In the period from 23 to 20 Ma, plate velocity increased to ~60 mm/yr. By 10 Ma, the reconstruction indicates that plate velocity was similar to the modern-day rate of ~60 to 70 mm/yr (*Tregoning,* 2002; *DeMets et al.,* 2010). The new APWP, as well as the APWP of Embleton and McElhinny (1982), are similar to the GMHRF of Doubrovine et al. (2012). The GMHRF was selected for comparison because it is the first multi-hemisphere, multi-plate GMHRF, and it agrees well with reconstructions of Torsvik et al. (2008). The positions of the 30, 23.5, 20, and 14 Ma poles are similar to those of the GMHRF. The 55 and 0.5 Ma poles deviate somewhat from the GMHRF pole locations, although the 0.5 Ma pole is dominated by the modern field.

6.5.4 Implications for "paleomagnetic dating"

Lateritic profiles are prevalent in Australia and have been previously targeted for paleomagnetic studies. Many of these profiles formed prior to ~20 Ma, during the Cenozoic deep weathering event (*Vasconcelos et al.,* 2008). Paleomagnetic "dating" has emerged as a tool to estimate the ages of these laterites. Paleomagnetic dating involves estimating ages of laterites by comparing their paleomagnetic orientations with the Australian APWP. Paleomagnetic "dates" are therefore critically dependent on an accurate and precise APWP. Unfortunately, previous paleomagnetic studies (e.g. *Schmidt and Ollier,* 1988; *Pillans et al.,* 1999) utilised the APWP of Idnurm (1985) as a means of dating lateritic profiles, and, in light of both my new results and the results of several previous studies (*Embleton and McElhinney,* 1982; *Trovisk et al.,* 2008; *Doubrovine et al.,* 2012), the APWP of Idnurm (1985) seems to be inaccurate. The deviation of the new APWP relative to more linear APWPs (such as *Idnurm,* 1985) suggests that some previous attempts at paleomagnetic dating overestimated the ages of Cenozoic lateritic profiles in Australia. Furthermore, laterites have long and complex histories of crystallisation and acquisition of magnetic minerals (*Riffel et al.,* 2016). The long duration over which these rocks are formed, upwards of millions of years, could produce over-averaged paleomagnetic poles.

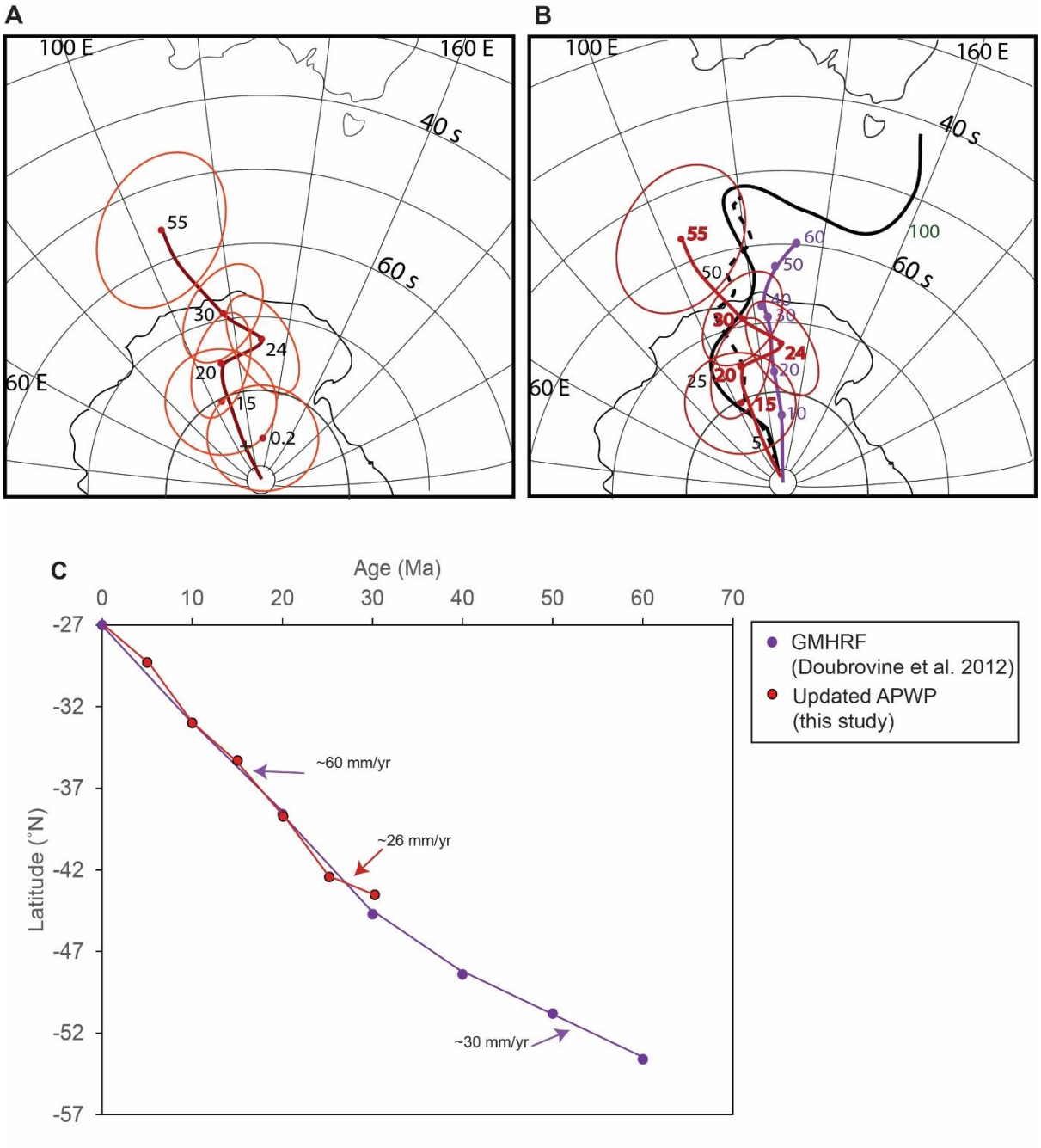

Figure 6.14: A) A new APWP for the Australian plate in the Cenozoic, using paleomagnetic data collected from a series over volcanic provinces. B) Comparison of the new APWP with Embleton 1981 (dashed line), Embleton and McElhinny (1982; Black) and the GMHRF (Doubrovine 2012). C) The relative latitude of a fixed point (-27˚N, 152˚E) when moved in the GMHRF (purple line) and new APWP (red line) reference frames. The GMHRF is taken every 10 Ma, while the new APWP is taken every 5 Ma.

6.5.5 Improving the paleopoles

As previous paleopoles from Wellman et al. (1969) and Wellman (1975) are within error of the data collected in this chapter, they were combined with their new counterparts to improve the paleopoles (Fig. 6.15). Common means tests show there is no statistical distinction (chi^2 = 0.7) between the 24 Ma pole produced in this study, and that produced by Wellman (1975); the same is true of the 19 and 30 Ma poles. The resulting paleopoles from the combined analysis are summarised in Table 6.3. By combining the datasets, I was able to improve the pole error (A95 ≤5), and dispersion estimates of the 30, 24, and 19 Ma poles are within error of expected dispersion. The 50 Ma pole still has dispersion well above the expected estimate, implying tectonic complications or, perhaps, over-averaging of the magnetic field. The difference in latitude between the 24 and 19 Ma poles is ~2˚, which agrees well with the observed latitudinal offset between the Tweed (24 Ma) and Ebor (19 Ma) provinces. As the provinces are believed to track the motion of the plate (e.g. *Knesel et al.,* 2008), this result gives legitimacy to the observed position of the average means about the pole. The divergence of the pole at 25 Ma away from the bracketing poles could mean either there is a significant non-dipole addition to the field, or the plate has experience rotation. As there was no error overlap between the mean of the 24 Ma pole and the poles on either side, the poles can be considered distinct (chi^2 = 0.04).

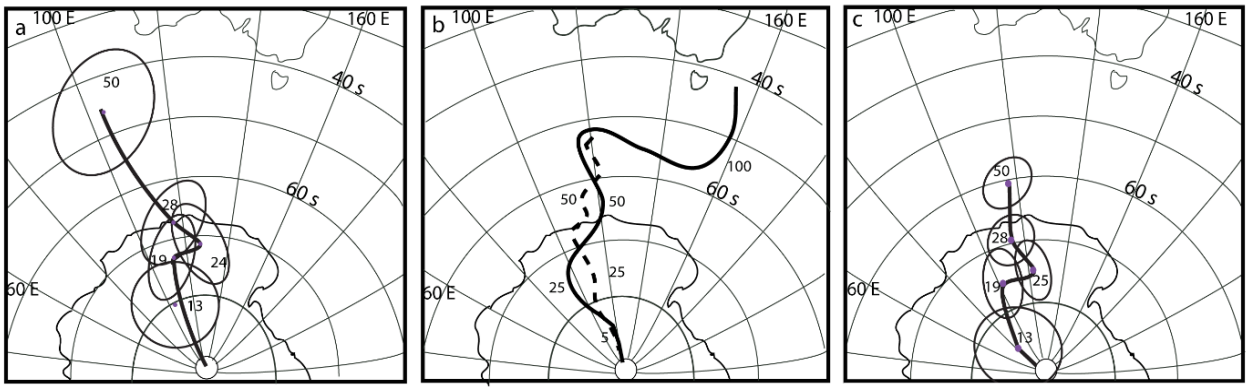

Figure 6.15: Improved paleopoles a) before and c) after the addition of data from Wellman et al. (1969) and Wellman (1975). Embleton and McElhinney (1982; figure 6.15b) included for comparison.

6.5.6 Cenozoic plate rotation

In both APWPs there is a divergence between 30 Ma and 23.4 Ma, overlapping with a period of slow plate velocity onshore (26-23 Ma) and offshore (~25-19 Ma), as well as a notable eastward divergence in the Tasmantid seamount chain (*Crossingham et al.,* 2017). This

coincidence implies that the divergence manifest in the hotspot track may be a result of plate rotation to the west, as hypothesised in detailed studies of $^{40}Ar/^{39}Ar$ geochronology from onshore volcanoes (*Knesel et al.*, 2008). However, a comparison between the 3 Ma pole from northern volcanic provinces with that of the Victorian Newer Volcanic province *(Opdyke and Musgrave*, 2004) suggests that there has been little rotation in the last 5 Ma. Given a lack of similar aged provinces dispersed along the eastern margin of Australia, the pole for the mid-Miocene was compared against the synthetic Australian reference pole after the GMHRF. The comparison indicates at least 10˚ clockwise rotation of the plate after approximately 30 Ma, but no rotation after 19 Ma, placing the rotation during the early-Miocene. Rotation was likely caused by initial collision between the Solomon Islands and OJP (*Knesel et al.*, 2008), or by the docking of Papua New Guinea and reversal of northward subduction. This rotation coincides with reduced spreading rates between Australia and Antarctica (*Cande and Stock*, 2004; *Cohen*, 2007). By taking three transects across the magnetic lineations it is possible to compare the half-spreading rate across the mid-ocean ridge. The rate from east to west decreases during the early Oligocene, meaning the eastern margin of Australia moved north at a faster rate than the western margin. In the late Oligocene to early Miocene (26 to 20 Ma), half-spreading rates dramatically reduce (*Cande and Stock*, 2004; *Cohen*, 2007), but not by the same rate (Fig. 6.16). The decrease in plate velocity is significantly higher in the east (10 km/My^2) than in the west (2 km/My^2), after which half-spreading rates become approximately the same (Fig. 6.16).

6.5.7 Comparison with the Indian APWP

Previous studies have rejected the APWPs from Australia on the basis that they do not agree with the Indian APWP (*Idnurm*, 1985). The APWP of the Indian plate was rotated into the Australian reference frame to assess the degree of similarity between the two APWPs (Fig. 6.17). Many of the Indian paleopoles are derived from lateritic profiles, but, as indicated previously, dating of lateritic profiles is complex and often inaccurate. The selected poles come from the Besse and Courtillet (2002) global APWP for the Indian continent, in which poles are averaged over a 10 Myr sliding window at 5 Myr intervals. This model was selected as it combines paleomagnetic pole considerations averaged in light of the global plate circuit. While a coarser average was proposed, the authors considered the 5 Myr window average more representative of the Indian plate circuit. As only a few direct rotations between Australia and India are recorded, the Indian APWP was first rotated to Africa using the rotation parameters

of Doubrovine et al. (2012), then through to Australia. The Indian and Australian APWPs are similar after 15 Ma, but vary significantly before this time.

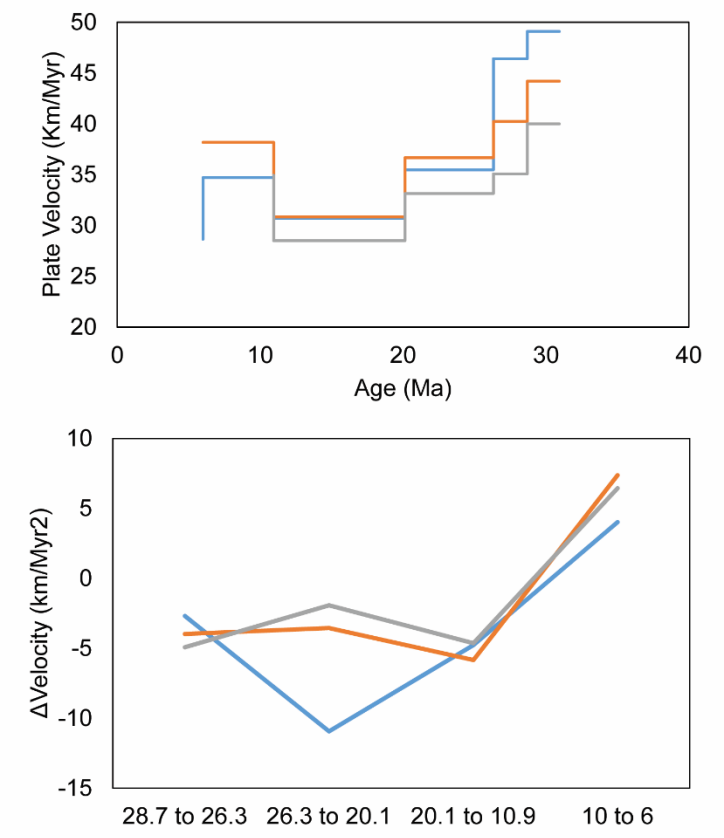

Figure 6.16: a) Half spreading rate on the Australian plate after Cande and Stock, (2004) and Cohen, (2007); b) relative rate of velocity change over the Cenozoic.

The variation is within error of each pole, however, and it has been noted previously that paleomagnetic data from the Indian continent consistently produce incorrect paleo-latitudes (*Dupont-Nivet*, 2010). Similar to the Australian plate, between the 30 and 25 Ma poles the Indian APWP indicates westerly plate offset when rotated to the Australian reference frame. As the rotation parameters are independent of the Australian APWP, it would imply that the eastward divergence is not an artefact of non-dipole additions to the 25 Ma paleopole. Indian plate speeds at this time were significantly slower than the Australian plate due to the collision with Asia, which accounts for the relatively small amount of motion between 25 and 15 Ma (*Klootwidk et al.*, 1992; *van Hinsbergen et al.*, 2012).

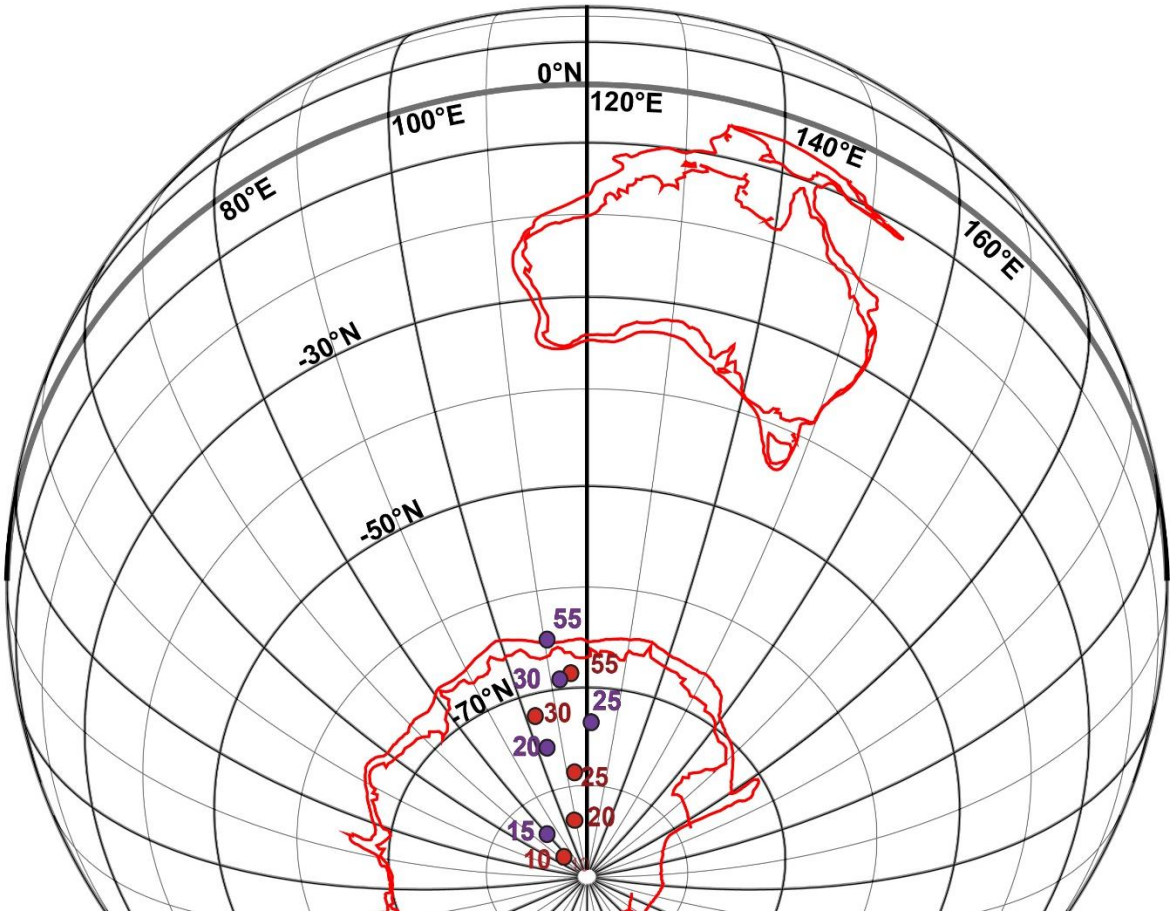

Figure 6.17: Comparison between the improved APWP (purple) and the Indian APWP (red; *Besse and Courtillot,* 2002). The Indian plate has been rotated to the Australian plate through the African plate circuit (*Doubrovine et al.,* 2012).

6.6 Conclusions

The Cenozoic Era is often mistakenly considered a period of relatively minor tectonic activity on the Australian continent, but, in fact, it was key time interval that included continental breakup, growth of oceanic crust, and changes in plate motion related to tectonic events in the SW Pacific (*Hall,* 2002; *Gaina and Müller,* 2007). The new Australian Cenozoic APWP indicates relatively fast plate motion from 20 Ma onward after a significant slow-down between 30 Ma and 23.5 Ma to 26 mm/yr, identical to the late Oligocene velocity determined by Knesel et al. (2008; 26 mm/yr) based on geochronology of age-progressive east Australian volcanoes. Furthermore, the new APWP matches the predictions of the GMHRF after 30 Ma, but, as with many previous paleomagnetic estimates, the new APWP and the GMHRF are mismatched prior to the 40 Ma pole. I attribute the discrepancy to uncertainties in the 55 Ma pole and slow plate velocity. The improved APWP also matches closely, or is within error, to the rotated Indian APWP after 30 Ma, and both APWPs show an apparent shift to the west at ~25 Ma. As the rotated Indian APWP does not rely on the Australian APWP, it is likely that the divergence of

the poles at 24 Ma is not related to non-dipole field inclusions. Rather, the Indian-Australian plate either shifted to the west or was rotated ~10° clockwise. This period of rotation is supported by an eastward offset in the Tasmantid hotspot chain (24 to 20 Ma), high volume and eruption rates at Tweed (24 to 23 Ma) and coincides with both a significant reduction in plate velocity (26 to 23 Ma; *Knesel et al.*, 2008) and a reduction in spreading rates between Australia and Antarctica that is greater in the east than the west.

Table 6.1: Site-mean flow directions for paleomagnetic samples collected from east Australian Cenozoic volcanoes.

Barrington										
Site	**Age (Ma)**	**Dec.**	**Inc.**	**a95 °**	**n**	**N**	**k**	**r**	**weighting in pole calculation**	**polarity**
Barrington										
BRT1	55.84	34	-51	9.7	6	6	5	5.1	1.5	N
BRT2	57.1	29.8	32.4	9.37	5	7	5	4.9	0.05	R
BRT3	56.55	340.9	-62.3	20.9	5	5	11	4.7	1	N
BRT5	58.5	17.4	32.3	19.4	4	6	9	4.7	0.01	R
BRT7	57.1	268.1	77	7	5	8	96	5.0	2	R
BRT9	52.7	201.4	71.4	12.09	6	6	26	5.8	2	R
BRT10	58.99	234.7	48.1	11.1	9	9	20	8.6	1.3	R
BRT4+6		194.6	-42.4	26.5	8	12	5	6.6	0.001	N
Peak Range										
Pr1	25	105	-13	17.2	4	6	45	3.9	0	N
Pr2	33.27	188.8	57	6.5	7	7	75	6.9	1	R
Pr6	31.63	263.5	83.6	5.2	5	5	150	5.0	0.5	R
Pr7	34.66	195.2	67.5	3.9	6	6	190	6.0	2	R
M	34.25	218.2	45.4	19.1	4	8	35	3.9	1	R
GM1	30.15	10.2	-39.8	10.6	17	27	11	15.9	0	N
Pr4		232	-66.3	8.8	5	6	76	4.9	0.01	N
Pr8		224.3	40	14.1	5	7	43	4.9	1.8	R
Pr9		236.4	58.7	14.2	4	5	32	3.9	0.6	R
Policeman's Knob										
PK	53.3	208	35.9	17.9	13	22	6	11.1	1.5	R
Springsure										
MC1	27.02	263.8	-19.4	23.8	4	8	41	3.9	0	N
MC2	27.4	185.7	56.0	15.0	5	7	182	5.0	0.8	R
MC4		196.6	54.8	8.9	4	5	41	3.9	1.8	R
MC5	27.92	140.0	72.5	40.1	3	5	-	-	0	R
MC6	27.89	162.9	68.5	7.4	4	6	156	3.9	1.8	R
MC7		205.5	20.1	7.8	6	7	70	5.9	1.8	R
MC8	28.41	028.7	-66.7	11.3	5	6	20	5.9	1	N
MC9	28.08	009.1	-59.1	5.7	4	4	79	4.0	2	N

MHV04	28.1	347.6	-57.0	9.8	4	4	68	4.0	1.5	N
MHV05	27.99	130.1	-66.7	61.1	7	7	-	-	0	N
MHV06	27.27	289.5	33.6	18.3	6	9	19	3.9	0	R
MHV07	27.84	050.1	83.2	24.5	4	9	-	-	0	R
MHV08		244.1	48.7	13.2	9	11	30	8.8	0.5	R
MHV09	28.445	205.0	69.0	12.7	4	5	23	4.9	1	R
MHV10	27.92	187.0	42.6	15.2	8	8	16	3.0	0.8	R
Tweed										
bb	24.1102	36.4	-54.6	6.55	11	11	45	10.8	2	N
l1	23	176.2	58.9	14.08	4	4	33	3.9	1.5	R
l2		154.3	42	20.9	3	3	24	2.9	0.01	R
l8		93.1	79.1	29.3	3	3	8	2.7		R
t2	23.5	191.4	62.5	17.2	4	4	22	3.9	2	R
t3		234.9	65.3	15.5	4	4	27	3.9	0.1	R
t5		204.1	74.2	8.93	6	6	48	5.9	1.2	R
t6		251.2	75.3	10.6	5	6	43	4.9	0.5	R
t1-3		175.8	51.1	12.1	10	10	15	9.5	2	R
tl6-7		168.4	53.4	8.81	12	12	23	11.6	1	R
Mitchell										
KF	24.2	358.8	-60.3	4.9	12	12	69	11.9	2.5	N
Ebor										
eb1	19.78	259	-9.9	4.6	5	5	268	5.0	0.03	N
eb2+19		175.4	55.9	16	5	5	21	4.8	2	R
eb3	19.78	217.8	49.2	11.6	5	5	36	4.9	0.5	R
eb5	20.39	196.7	53	4.9	5	5	196	5.0	3	R
eb6		184.4	76.8	6.9	5	5	99	5.0	1	R
eb8	20.1	198.9	77.2	10.9	4	5	54	4.0	0.8	R
eb11	20.23	242.3	54.6	14.9	4	5	29	3.9	0.3	R
eb14		187.3	52.9	10.1	8	8	31	7.8	2	R
eb18		193.3	50.9	6.9	6	7	94	5.9	2	R
eb20	19.8	189	79.1	3.8	9	9	141	9.0	1.5	R
Warrumbungles										
w1	15.95	334.8	-21.7	6.8	6	7	139	6.0	0.05	N
w4	15.9	0.8	-67.3	7.5	6	7	82	5.8	2	N
w6	16.14	195.5	-44.3	7.9	7	7	66	6.9	0.01	N
w7		342.6	-45.3	15.2	4	5	38	3.9	2	N
w10		197.5	79.9	21.5	4	5	19	3.8	0.5	R
w11	16.02	332.5	36.9	14.5	3	4	74	2.9	0.05	R
w13	16.31	37.1	-72.1	14.6	4	4	41	3.9	1	N
w14	16.25	170.9	-53.5	10.2	4	8	82	4.0	0.01	N
w15		21.8	-66.3	10.8	4	4	74	4.0	2.5	N
w2+3	15.85	346.9	-49.6	16	6	11	14	5.7	3	N

Canobolas										
ca3	11.55	201.9	41.1	12.3	6	6	26	5.8	2	R
ca4		234	55.8	5.4	5	5	103	5.0	1	R
ca5+8		247.5	51.3	15.8	5	5	16	4.8	0.5	R
ca6	11.26	14.2	-23.3	19.4	6	6	13	5.8	0.05	N
ca9		344.5	-53.2	11.7	7	8	11	5.8	3	N
ca1+ca2		216.4	46.6	14.7	7	8	16	6.8	2	R
McBride (Undara)										
KC1		347.1	-17.1	19	3	5	29	3.0	2	N
KC2		31.6	-22.3	13	3	3	61	3.0	0.1	N
KC3	0.41	333.4	-64.5	10.5	4	5	58	4.0	0.1	N
U1		10.4	-50.3	10.7	4	4	68	4.0	2	N
U2		16.1	-40.3	18.3	5	5	15	4.8	1	N
U3+ur1'	0.09	359.6	-55.5	22.6	10	12	4.9	8.6	2	N
UR2	0.257	356.8	-35.9	7.7	8	8	47	7.9	2	N
UR3	0.36	20.8	-16.7	20.9	5	6	7.8	4.8	0.5	N

Dec = declination, Inc= inclination, α95 = radius of the circular 95% confidence interval around the mean declination/ inclination by Fischer statistics, n = the number of samples used, N the number of samples available, k= kappa dispersion estimate, Polarity – either normal (N) or reverse (R).

Table 6.2: Calculated paleopoles collected from east Australian Cenozoic volcanoes.

Volcano	***age***	***D***	***I***	***α95***	***Lat***	***Long***	***A95 (Fisher on Fisher)***	***A95 (Fisher after Bingham)***	***dm***	***dp***	***A95 (weighted bingham)***	***dm***	***dp***	***Az***	***N***	***S***	***Q***
Undara	0.2	4.8	-37.8	12.9	-84.7	131.1	9.6								8	15.6	
Warrumbungles + Canobolas	10	7.9	-57.4	7.7	-80.1	108.4	10.2	9.9	7.6	12.8	8.8	7.2	8.5	104.6	17	24	5
Ebor	20	14	-58.9	8.4	-74.9	112.0	9.4	6.3	5.0	11.8	4.9	3.8	7.5	195.2	10	18.5	5
Tweed	23.5	8	-60.8	6.5	-73.0	128.0	9.5	7.8	5.5	9.3	5.1	3.7	7.5	150.8	13	18	5
Springsure	30	16	-58.2	6.5	-69.5	117.7	9.2	6.8	5.5	9.1	6.8	5.5	9.1	29.9	16	20.4	6
Barrington	55	38	-58.8	12.6	-56.9	95.2	14.7	11.3	8.6	10.9	11.3	8.6	10.9	206	11	25	5

D = declination, I= inclination, α95 = radius of the circular 95% confidence interval around the mean declination/ inclination by Fischer statistics, lat = latitude of the pole, long= longitude of the pole, A95 = radius of the circular 95% confidence interval around the mean pole by Fischer statistics, dm= error on the minor axis of the confidence ellipse, dp= error on the major axis of the confidence ellipse, Az = azimuth of the confidence ellipse, N the number of sites used, S = the calculated dispersion estimate of the pole, Q is the adherence to the quality-criteria.

Table 6.3: Improved paleopoles for Australia by combining the data from this study with data from Wellman and McElhinny (1969) and Wellman (1975).

Volcano	age	Paleolat	paleolong	A95 (Fisher on Fisher)	A95 (Fisher after Bingham)	dm	dp	Az	N	S
Warrumbungles + Canobolas	13.0	-82.0	90.0	9.2	7.3	6.5	7.3	110.1	34.0	25.0
Ebor +Nandewar	20.0	-75.5	105.0	5.6	3.6	3.0	5.5	172.0	66.0	20.2
Tweed	24.0	-73.5	122.8	5.4	3.5	2.7	4.8	163.6	53.0	19.3
Springsure + Central	30.0	-69.3	112.8	4.7	5.0	3.8	4.2	150.8	71.0	21.0
Barrington	55.0	-65.8	111.3	7.7	4.9	3.4	4.5	40.0	50.0	21.0

Chapter 7: Conclusions

7.1 $^{40}Ar/^{39}Ar$ dating, geochemistry and plate reconstructions

Animated plate reconstructions were utilised to examine the relationship between volcanism and plate motion in the SW Pacific. The compiled geochronology data illustrate spatial relationships between volcanic activity across east Australia. There was a decrease in volcanism in the north after ~20 Ma, while volcanism was continuous from ~60 Ma to ~10 Ma in the south. The distribution of volcanism, including multiple eruption events in "age-progressive" volcanism, is at odds with a simple plume model.

Several putative "plume-related" volcanic provinces in eastern Australia were active both before and after the main period of activity used to define their age progression. The Peak Range province, a central volcano, is a particularly good example of these protracted eruption histories. New geochronological data shows three distinct periods of activity. The oldest samples are far outside of the 34-6 Ma time frame for plume activity, and the youngest volcanism from the province (26 Ma) is over 3 My younger than the "final" phase of the volcano. While these older ages could reflect the main shield-phase overlying an older volcanic province, the geochemical source characteristics of the samples indicate generation from the same source as nearby central volcanoes (i.e. Springsure and Buckland). Either the plumes existed much earlier than assumed, or a plume was not responsible for volcanism. Peak Range is not an isolated example of a protracted history of volcanism: these anomalous phases of activity are also evident in surrounding volcanic provinces such as Nebo and the Hoy lava-field. These long periods of activity do not coincide with expected patterns of volcanism from single or even multiple plume sources. The widespread, almost continuous eruption of volcanic provinces across the east coast of Australia brings into question the traditional classification of "central volcanoes" and "lava-fields". If the central volcanoes are truly age-progressive, then why do they include activity beyond the scope of the "plume" source? Similarly, if lava-fields are not age-progressive and were sourced from a different mechanism and region of the mantle, why are some found both spatially and temporally associated with central volcanoes? Traditional classifications and the current geochronology data do not answer these questions.

The greatest problem with distinguishing between central volcanoes and lava-fields is their classification criteria. While the criteria have been generally strict since the introduction of these terms in the 1970s, a compilation of all available descriptions and mapping of volcanic provinces have shown that many fail to meet all of the criteria used in the classification. As

such, geometrical and superficial geochemical observations often fail to distinguish the two province types. This thesis is the first to examine both the geochemistry and high-precision geochronology of lava-fields in central Queensland and their associated central volcanoes, and one of the few to examine both the geochemistry and geochronology of any lava-fields. Major and trace elements for both central volcanoes and lava-fields indicate a common source with low (<5%) to very low (<1%) degrees of melting in the garnet stability field. REE and multi-element spidergrams all show an OIB-type pattern and, for samples with associated $^{40}Ar/^{39}Ar$, decreased melting over time. First order melt-generation models of the most primitive samples from each province show differences in the degree of melting of the same or similar source between province. Principal component analysis of a large geochemical data compilation that includes central volcanoes and lava-fields shows little variation between most lava-field and central volcanic provinces. As the major principal components seem to represent the crust (etc.) and mantle (Ni and HREE), compositional variations between provinces could be attributed to crustal contamination, rather than different source characteristics, as previously suggested (*Johnson et al.,* 1989; *O'Reilly and Zhang*, 1995; *Zhang et al.,* 2001). I tested this using a binary primitive mantle normalised trace element plot (Pb v. U), with primitive mantle, OIB, and crustal values plotted for comparison. These plots illustrate mixing between the OIB-type magmas and the upper or lower crust. Radiogenic isotope source component diagrams show a common source component. Both the "central volcanoes" and "lava-fields" fall along the EMI array, towards FOZO. Minor excursions toward EMII field in the McBride and Barrington provinces, which was previously described as subduction modified SCLM, reflect contamination by SCLM and assimilation of the crust. The modelling and data suggest, therefore, that the lava-fields and central volcanoes were sourced from the same region of the mantle. This is at odds with previous "plume-" and "rift-" related classifications, as there is no obvious geochemical distinctions between them that cannot be explained by crustal or lithospheric contamination.

7.2 Plate motion and volcanic province distribution

7.2.1 The updated APWP

Cenozoic paleomagnetic poles for the Australian continent were constructed using paleomagnetic data from east Australian Cenozoic volcanic provinces erupted at key time intervals. The poles represent the apparent polar wander of the Australian plate at 55, 35, 30, 23, 20, 10 and 0.2 Ma. The APWP shows roughly linear northward migration, with the

exception of a period of offset around the 23 Ma pole. The updated APWP is similar in both latitude and longitude as the models of Wellman (1969), Wellman et al. (1975) and Embleton and McElhinny (1982). Common means distribution indicates that there is no significant difference between the populations of the new data and the older data set (chi-squared = 0.05). The latitudes of the new APWP poles are at odds with the poles of Idnurm (1985). The new APWP places older poles at higher latitiudes than those defined by the Cenozoic sedimentary basins of Idnurm (1985). This disparity between poles is most likely related to the reliability of the dating systems. While the new APWP does not agree with the older Idnurm (1985) APWP, more recent work from the Hammersley weathering surface recreates a 24 ± 4 Ma pole that is similar in position to the 20 Ma pole defined in this study. More importantly, the new APWP is similar to the GMHRF (*Doubrovine et al.,* 2012) in terms of both latitude and longitude after 40 Ma and between the model's plate velocities is reasonably consistent.

7.2.2 Plate rotation, reduced velocity and patterns of volcanism

The common means distribution shows that the 30 and 23.5 Ma poles are distinct from each other. As the longitude of the 23.5 Ma pole is consistently offset from other poles, there may be a case for plate rotation during the formation of this pole. Calculation of the plate rotation at this point is approximately 10º clockwise relative to a synthetic pole from the GMHRF. The rotation calculated from the APWP is consistent with the 10º approximation of plate rotation defined by Knesel et al. (2008), which is needed to offset the Tasmantid and Lord Howe Seamount chains. The period of plate offset and rotation also corresponds with a period of plate velocity described by Knesel et al. (2008) and Cohen et al. (2013). The northward plate velocities defined by the Cenozoic APWP are consistent with those defined by $^{40}Ar/^{39}Ar$ geochronology both on- and off-shore (*Crossingham et al.,* 2017). Northward plate velocities were similar to modern rates (60-70 mm/yr) for the majority of the Cenozoic Era, though between the 30 and 23.5 Ma poles plate velocities reduced to 26 mm/yr. The periods of higher plate velocity appear to correspond with lower volume outputs and reduced eruption rates, as well as longer and more frequent hiatuses, in the central volcanos. Slower velocities are apparently correlated with the highest eruption rates and volumes. This correspondence may reflect different residence times above a hotspot, in which those that spend the most time over the hotspot have the shortest hiatuses and largest volumes.

7.2.3 Tectonics and volcanism in the SW Pacific during the Cenozoic

Animated tectonic reconstructions show the relative positioning of the Australian plate, the Cenozoic magmas, the opening of the Tasman and Coral Seas, the continental fragments of New Guinea and the Ontong Java Plateau during the Cenozoic. Opening of the Tasman and Coral Seas occurred during the Paleogene. Previous studies related the rifting of the Tasman and Coral Seas with the formation of some or all of the lava-fields. However, the animated reconstructions show that volcanism was often both too far away and much too young to be directly related to rift-driven upwelling. Furthermore, the generation of magmas was only on one side of the rift, despite the presence of the continental Lord Howe Rise to the east. Previous models fail to explain the restriction of volcanism to the west of the rift, which is at odds with modern rift environments, even with directly associated EDC (*King*, 2004). Significant westward diversion of the plate between 30 and 23 Ma seem to coincide with arrival of OJP at the Solomon Islands and the subsequent blocking of the subduction zone. While other work has suggested that this "soft-docking," which is characterised by a lack of deformation, was responsible for the change in motion, several other large-scale tectonics events were occurring during this time, including subduction cessation and slab detachment at the Loyalty Arc, as well as the collision of the New Guinea composite terranes with the Medial Mountains Subduction Zone. Unfortunately, even using animated reconstructions, it is not possible to distinguish the effects of one collision from the other. However, it is clear that tectonic reshuffling in the SW Pacific and the closure of the more northern subduction zones are intrinsically linked, not only to the motion of the plate, reflected by both Embleton and McElhinny (1982) and the updated APWP, but surficial patterns of volcanism on- and off-shore the eastern margin of Australia. Further research addressing the timing and nature of the accretion of the North New Guinea Terrains, through paleomagnetic analysis and high precision dating, would resolve uncertainties in the tectonic reconstructions in the SW Pacific.

As the work of Embleton and McElhinny (1982) more completely agrees with observations from independent systems, it is likely that paleomagnetic data from volcanic and lateritic rocks are a more suitable measure of the APWP than those from sedimentary basins.

7.3 Conclusions

The work in this thesis strives to answer the overarching question: how are relative plate motions and changes in mantle dynamics during the Cenozoic preserved in geological records

in eastern Australia? Results show that the motion of the Australia plate and changes in the mantle relate directly to the geological features of the Australian plate, in particular the distribution and geochemistry of volcanic provinces. Volumes and eruption rates in east Australia tend to decrease with time, and generally from north to south. Typically, it appears that Cenozoic plume magmatism, at least on the continent, was slowly waning. Furthermore, provinces believed to be unrelated to plume activity may not be as isolated as previously assumed. Geochemical trends in source composition and melt generation indicate melting below the garnet stability field in the asthenosphere from an EMI-type mantle. Radiogenic isotope mixing models between primitive samples and average crustal values imply that excursions toward EMII may result from mixing of magmas with the upper crust. Using the extensive database of geochemical data that is available, there also appears to be no time-space correlation between the isotopic Pb signature in volcanic provinces, as has been previously suggested (*Zhang and O'Reilly,* 1999), though interactions with the local SCLM may be responsible for the specific provinciality that is observed (*Zhang et al.,* 2001). I found that all provinces in eastern Australia likely originated from the same EMI-type source, accompanied by a DUPAL anomaly in the asthenosphere that was tapped by different mechanisms. In particular it seems likely that there was a combination of EDC and plume magmatism active on the continent during the Cenozoic. Furthermore, periods of changing plate velocity and plate rotation are recorded in these volcanic provinces, regardless of age or location. Most importantly, the morphological (including eruption rates, volumes, and geographic location), geochemical (including the degree of crustal assimilation; *Ewart*, 1982) and geochronological (eruption durations, age progressions and plate slowdowns; *Knesel et al.,* 2008) characteristics of many of the volcanoes can be explained by approximately 10º plate rotation between 30 and 24 Ma.

7.4 Future Work

Despite the best efforts of this thesis, there still remains avenues to extend and improve the reach of this study. Trace element and radiogenic isotope data from the majority of Cenozoic volcanic provinces, whether central volcano or lava-field, are often incomplete. Many previous studies only focused on specific applications of geochemistry and often omitted important trace elements or radiogenic isotopes. Because of the lack of incompatible trace element data from many provinces, particularly central volcanoes, they could not be included in PCA, contamination modelling or radiogenic isotope analysis. For a full understanding of the source

and variations between provinces, more detailed trace element and radiogenic isotope studies need to be conducted on both the central volcanoes and lava-fields, particularly from more mafic samples. Further work, including He and Cl isotope ratios, are required before the source and mechanism of magmatism, and whether it differs between lava-fields and central volcanoes, can be determined.

Resolution of plate slow down and possible rotation could be improved by the addition of more 30 to 20 Ma poles from either the north or south of the plate, though this would rely on far more extensive, accurate dating of lava-field provinces. As it stands, the precise dating of Cenozoic age mafic volcanism is under-developed and many of the paleopoles rely on the significantly less accurate K-Ar method of analysis.

References

Abbott, L.D., Silver, E.A., and Galewsky, J., (1994). Structural evolution of a modern arc-continent collision in Papua New Guinea. *Tectonics* 13, 1007-1034.

Abrajevitch, A., Van der Voo, R., and Rea, D. K. (2009). Variations in relative abundances of goethite and hematite in Bengal Fan sediments: Climatic vs. diagenetic signals. *Marine Geology*, 2673, 191-206.

Acton G. D. (1999). Apparent polar wander of India since the Cretaceous with implications for regional tectonics and true polar wander. Mem. Geol. Soc. India 44, 129-175.

Aitchison, J., Clarke, G.L., Meffre, S., and Cluzel, D., (1995). Eocene arc-continent collision in New Caledonia and implications for regional Southwest Pacific tectonic evolution. *Geology*, 23, pp. 161–164

Ashley, P. M., Duncan, R. A., and Feebrey, C. A., (1995). Ebor Volcano and crescent complex, northeastern New South Wales: age and geological development. *Australian Journal of Earth Sciences*, 425, 471-480.

Baldwin, S. L., Fitzgerald, P. G., and Webb, L. E., (2012), Tectonics of the New Guinea region. *Annual Review of Earth and Planetary Sciences* 40: 495–520 doi:10.1146/annurev-earth-040809-152540.

Besse, J., and Courtillot, V. (2002). Apparent and true polar wander and the geometry of the geomagnetic field over the last 200 Myr. *Journal of Geophysical Research: Solid Earth*, 107B11.

Blaney, L. (2007). Magnetite Fe3O4: Properties, Synthesis, and Applications. *Lehigh University* 15, 5.

Bourdon, B., Ribe, N. M., Stracke, A., Saal, A. E. and Turner, S. P. (2006). Insights into the dynamics of mantle plumes from uranium-series geochemistry. *Nature* 444, 713-717.

Butler, R. F., (2004). *Paleomagnetism: Magnetic domains to geologic terranes.* Electronic edition, 23.

Cande, S. C., and Mutter, J. C. (1982). A revised identification of the oldest sea-floor spreading anomalies between Australia and Antarctica. *Earth and Planetary Science Letters*, 582, 151-160.

Cande, S. C., and Stock, J. M. (2004). Pacific—Antarctic—Australia motion and the formation of the Macquarie Plate. *Geophysical Journal International*, *157*(1), 399-414.

Cisowski, S., (1981). Interacting vs. non-interacting single-domain behavior in natural and synthetic samples. *Physics of the Earth and Planetary Interiors.* 26, 56–62.

Class, C., and le Roex, A. P. (2008). Ce anomalies in Gough Island lavas—trace element characteristics of a recycled sediment component. *Earth and Planetary Science Letters*, 2653, 475-486. doi: 10.1016/j.epsl.2007.10.030

Cohen, B. E., (2007). *High resolution $^{40}Ar/^{39}Ar$ geochronology of intraplate volcanism in eastern Australia.* PhD thesis, University of Queensland

Cohen, B. E., Knesel, K. M., Vasconcelos, P. M., and Schellart, W. P., (2013). Tracking the Australian plate motion through the Cenozoic: Constraints from $^{40}Ar/^{39}Ar$ geochronology. Tectonics, 325, 1371-1383.

Cohen, B. E., Knesel, K. M., Vasconcelos, P. M., Thiede, D. S., and Hergt, J. M., (2008). $^{40}Ar/^{39}Ar$ constraints on the timing and origin of Miocene leucitite volcanism in southeastern Australia. Australian Journal of Earth Sciences, 553, 407-418.

Cohen, B. E., Mark, D. F., Fallon, S. J., and Stephenson, P. J., (2017). Holocene-Neogene volcanism in northeastern Australia: Chronology and eruption history. Quaternary Geochronology, 39, 79-91.

Cohen, B., Vasconcelos, P., and Knesel, K., (2007). $^{40}Ar/^{39}Ar$ constraints on the timing of Oligocene intraplate volcanism in southeast Queensland. Australian Journal of Earth Sciences 54, 105-125.

Condie, K. C. (1994). *Archean Crustal Evolution.* Elsevier Science and Technology Books.

Condie, K. C., (2001). *Mantle plumes and their record in Earth history.* Cambridge University Press, Cambridge, UK, 306 p.

Conrad, C. P., Bianco, T. A., Smith, E. I., and Wessel, P. (2011). Patterns of intraplate volcanism controlled by asthenospheric shear. *Nature Geoscience*, 45, 317-321. doi: 10.1038/ngeo1111

Conrad, C.P., Wu, B., Smith, E.I., Bianco, T.A. and Tibbetts, A. 2010, Shear-driven upwelling induced by lateral viscosity variations and asthenospheric shear: A mechanism for intraplate volcanism. *Physics of the Earth and Planetary Interiors*, 178, 162-175. doi: 10.1016/j.pepi.2009.10.001

Cook, C., Briggs, R., Smith, I., and Maas, R. (2005). Petrology and geochemistry of intraplate basalts in the South Auckland volcanic field, New Zealand: evidence for two coeval magma suites from distinct sources. *Journal of Petrology* 46: 473-503 doi: 10.1093/petrology/egh084

Cowley, S., Mann, P., Coffin, M. F., and Shipley, T. H., (2004), Oligocene to Recent tectonic history of the Central Solomon intra-arc basin as determined from marine seismic reflection data and compilation of onland geology. *Tectonophysics*, 3893, 267-307.

Creer, K. M. (1957). The remanent magnetization of unstable Keuper marls. *Philosophical Transactions of the Royal Society of London A: Mathematical, Physical and Engineering Sciences*, *250*(974), 130-143.

Crossingham, T. J. (2017). *Temporal and Petrogenetic Constrains on Age Progressive Volcanism in Eastern Australia*. University of Queensland PhD thesis

Crowhurst, P. V., Hill, K. C., Foster, D. A., and Bennett, A. P, (1996). Thermochronological and geochemical constraints on the tectonic evolution of northern Papua New Guinea. *Geological Society, London, Special Publications*, 1061, 525-537.

Davies, D. R., and Rawlinson, N., (2014). On the origin of recent intraplate volcanism in Australia. *Geology*, 4212, 1031-1034. doi: 10.1130/G36093.1

Davies, D. R., Rawlinson, N., Iaffaldano, G., and Campbell, I. H., (2015). Lithospheric controls on magma composition along Earth/'s longest continental hotspot track. *Nature*, 525(7570), 511-514. doi:10.1038/nature14903

Davies, H. L., (2012). The geology of New Guinea-the cordilleran margin of the Australian continent. *Episodes*, 351, 87-102.

Davies, H. L., Perembol, R. C. B., Winn, R. D., and KenGemar, P., (1997). Terranes of the New Guinea orogen. *Proceedings of the Geology, Exploration and Mining Conference, Madang, P.N.G.*, Oct. 10–12, pp. 61–66. Melbourne: Australasian Institute of Mining and Metallurgy

DeMets, C., Gordon, R. G., and Argus, D. F., (2010). Geologically current plate motions. *Geophysical Journal International*, 1811, 1-80.

Demidjuk, Z., Turner, S., Sandiford, M., Rhiannon, G., Foden, J., and Etheridge, M., (2007). U-series isotope and geodynamic constraints on mantle melting processes beneath the Newer Volcanic Province in South Australia. *Earth and Planetary Science Letters*, v. 261, p. 517–533, doi: 10.1016 /j .epsl.2007.07.006.

Doubrovine, P.V., Steinberger, B., and Torsvik, T.H., (2012). Absolute plate motions in a reference frame defined by moving hot spots in the Pacific, Atlantic, and Indian oceans. *Journal of Geophysical Research: Solid Earth* 117, B09101.

Duggan, M. B., (1989). Ebor. In Johnson, R. W., Knutson, J., and Taylor, S. R., eds., (1989) *Intraplate volcanism: in eastern Australia and New Zealand.* Cambridge University Press, 120-121.

Duncan, R.A., and McDougall, I. A., (1989). Volcanic Time-Space Relationships. In Johnson R.W., Knutson J., and Taylor S.R., eds. (1989). *Intraplate Volcanism in Eastern Australia and New Zealand*, pp. 43-54. Cambridge University Press.

Dunlop, D. J. (2007). Magnetization, Viscous Remanent (VRM). In *Encyclopedia of Geomagnetism and Paleomagnetism* (pp. 621-630). Springer Netherlands.

Dunlop, D. J., and Özdemir, Ö. (2001). *Rock magnetism: fundamentals and frontiers* (Vol. 3). Cambridge university press.

Dunlop, D. J., and Stirling, J. M. (1977). 'Hard'viscous remanent magnetization (VRM) in fine-grained hematite. *Geophysical Research Letters*, *4*(4), 163-166.

Dupont-Nivet, G., van Hinsbergen, D. J., and Torsvik, T. H. (2010). Persistently low Asian paleolatitudes: Implications for the India-Asia collision history. *Tectonics*, 295.

Eggins S. M., Woodhead J. D., Kinsley L. P. J., Mortimer G. E., Sylvester P., Mcculloch M. T., Hergt J. M. and Handler M. R. (1997). A simple method for the precise determination of ≥

40 trace elements in geological samples by ICPMS using enriched isotope internal standardisation. *Chemical Geology* 134, 311-326. doi: 10.1016/S0009-25419600100-3

Embleton, B., (1981). A review of the paleomagnetism of Australia and Antarctica.

Embleton, B. J. J., and McElhinny, M. W., (1982). Marine magnetic anomalies, palaeomagnetism and the drift history of Gondwanaland. *Earth and Planetary Science Letters* 58, 141-150.

Embleton, B. J. J., Schmidt, P. W., Hamilton, L. H., and Riley, G. H., (1985). Dating volcanism in the Sydney Basin: evidence from K–Ar ages and palaeomagnetism. Volcanism in eastern Australia, 1, 59-72.

Ewart, A. (1981). The mineralogy and chemistry of the anorogenic Tertiary silicic volcanics of S. E. Queensland and N. E. New South Wales, Australia. *Journal of Geophysical Research* 86, 10242 10256.

Ewart, A., (1982). Petrogenesis of the Tertiary anorogenic volcanic series of Southern Queensland, Australia, in the light of trace element geochemistry and O, Sr and Pb isotopes. *Journal of Petrology*, 233, 344-382.

Ewart, A. (1985). Aspects of the mineralogy and chemistry of the intermediate-silicic Cainozoic volcanic rocks of eastern Australia. Part 2: Mineralogy and petrogenesis. *Australian Journal of Earth Sciences* 32, 383-413.

Ewart, A. and Chappell, B. (1989). Trace element geochemistry. In: Johnson R. W., Knutson J. and Taylor S. R. eds. (1989) *Intraplate Volcanism: In Eastern Australia and New Zealand*, pp. 219 235. Cambridge University Press, Cambridge, UK.

Ewart, A., Chappell, B. W., and Le Maitre, R. W. (1985). Aspects of the mineralogy and chemistry of the intermediate-silicic Cainozoic volcanic rocks of eastern Australia. Part 1: Introduction and geochemistry. *Australian Journal of Earth Sciences,* 324, 359-382.

Ewart, A., Chappell, B., and Menzies, M. (1988). An Overview of The Geochemical And Isotopic Characteristics of the Eastern Australian Cainozoic Volcanic Provinces. *Journal of Petrology*, 225-273.

Ewart, A., Mateen, A., and Ross, J. (1976). Review of Mineralogy And Chemistry Of Tertiary central volcanic complexes in southeast Queensland and northeast New South Wales. In:

Johnson R. W. ed., *Volcanism in Australasia.* Pages: 421, Elsevier Scientific Publishing Company, Amsterdam.

Ewart, A., Oversby V. and Mateen, A. (1977). Petrology and isotope geochemistry of Tertiary lavas from the northern flank of the Tweed Volcano, southeastern Queensland. *Journal of Petrology* 18, 73 113.

Farrington, R.J., Stegman, D.R., Moresi, L.-N., Sandiford, M., and May, D.A., (2010). Interactions of 3D mantle flow and continental lithosphere near passive margins. *Tectonophysics* 483, 20-28.

Fishwick S., Heintz M., Kennett B. L. N., Reading A. M. and Yoshizawa K. (2008). Steps in lithospheric thickness within eastern Australia, evidence from surface wave tomography. *Tectonics* 27, TC4009. DOI: 10.1029/2007TC002116

Foulger, G. R., Pritchard, M. J., Julian, B. R., Evans, J. R., Allen, R. M., Nolet, G., ... and Ragnarsson, S. (2001). Seismic tomography shows that upwelling beneath Iceland is confined to the upper mantle. Geophysical Journal International, 146(2), 504-530.

Franke, D., (2013). Rifting, lithosphere breakup and volcanism: Comparison of magma-poor and volcanic rifted margins. *Marine and Petroleum Geology*, 43, 63-87.

Fuller, M., Cisowski, S., Hart, M., Haston, R., Schmidke, E., and Jarrard, R., (1988). NRM: IRMs demagnetization plots; an aid to the interpretation of natural remanent magnetization. *Geophysical Research Letters* 15, 518–521.

Gaina, C., and Müller, D., (2007). Cenozoic tectonic and depth/age evolution of the Indonesian gateway and associated back-arc basins. *Earth-Science Reviews*, 833, 177-203.

Gaina, C., Müller, D. R., Royer, J. Y., Stock, J., Hardebeck, J., and Symonds, P, (1998a). The Tasman Sea: a puzzle with 13 pieces. *Journal of Geophysical Research: Solid Earth,* 103B6, 12413-12433.

Gaina, C., Müller, R. D., Roest, W. R., and Symonds, P. (1998b). The opening of the Tasman Sea: a gravity anomaly animation. *Earth Interactions*, 24, 1-23. DOI: 10.1175/1087-35621998002<0001:TOOTTS>2.3.CO;2

Galloway, R. W., (1967). Pre-basalt, sub-basalt and post-basalt surfaces of the Hunter Valley. *New South Wales,* 293-314.

Garapić, G., Jackson, M. G., Hauri, E. H., Hart, S. R., Farley, K. A., Blusztajn, J. S., and Woodhead, J. D. (2015). A radiogenic isotopic He-Sr-Nd-Pb-Os study of lavas from the Pitcairn hotspot: Implications for the origin of EM-1 enriched mantle 1. *Lithos,* 228, 1-11. doi: 10.1016/j.lithos.2015.04.010

Gast, P. W., Tilton, G. R., and Hedge, C. (1964). Isotopic composition of lead and strontium from Ascension and Gough Islands. *Science,* 1453637, 1181-1185.

Geldmacher, J., Hoernle, K., Bogaard, P., Duggen, S., and Werner, R., (2005). New $^{40}Ar/^{39}Ar$ age and geochemical data from seamounts in the Canary and Madeira volcanic provinces: Support for the mantle plume hypothesis. *Earth and Planetary Science Letters,* 2371, 85-101.

Gladney, E.S., and Roelandts, I., (1988). 1987 Compilation of Elemental Concentration Data for USGS BIR-1, DNC-1, and W-2. *Geostandards Newsletter*, 12:63-118.

Grey, C. M., and McDougall I., (2009). K-Ar Geochronology Of Basalt Petrogenesis, Newer Volcanic Province, Victoria. *Australian Journal of Earth Sciences* 56, 245-258 doi: 10.1080/08120090802547066

Griffin, T. J., and McDougall, I. (1975). Geochronology of the Cainozoic McBride volcanic province, northern Queensland. *Journal of the Geological Society of Australia*, *22*(4), 387-396.

Hall, R., (2002). Cenozoic geological and plate tectonic evolution of SE Asia and the SW Pacific: computer-based reconstructions, model and animations. *Journal of Asian Earth Sciences*, 204, 353-431. doi: 10.1016/S1367-91200100069-4

Hamilton, W. B., (1979). Tectonics of the Indonesian region No. 1078. *US Govt. Print. Off.*.

Hammer, O., Harper, D. A. T. and Ryan, P. D. (2001). PAST: Paleontological Statistics Software Package for Education and Data Analysis. *Palaeontologia Electronica* 41, http://palaeo-electronica.org/2001_1/past/issue1_01.htm

Hasterok, D., and Gard, M., (2016). Utilizing thermal isostasy to estimate sub-lithospheric heat flow and anomalous crustal radioactivity. *Earth and Planetary Science Letters,* 450, 197-207.

Heider, F., and Dunlop, D. J. (1987) Two types of chemical remanent magnetization during oxidation of magnetite, *Phys. Earth Planet. Inter.*, 46, 24–45,.

Henley, K. J., and Webb, A. W., (1990). *Geological Survey of Victoria Unpublished Report 1990/27*. doi: 10.1016/j.epsl.2016.06.037

Hill, K., and Hall, R., (2003). Mesozoic-Cenozoic evolution of Australia's New Guinea margin in a west Pacific context. *Geological Society of America Special Papers*, 372, 265-290.

Hofmann A. W., Jochum K. P., Seufert M. and White W. M., (1986). Nb and Pb in oceanic basalts: new constraints on mantle evolution. *Earth and Planetary Science Letters* 79, 33-45.

Holm, R. J., (2013). Magmatic arcs of Papua New Guinea: insights into the late Cenozoic tectonic evolution of the northern Australian plate boundary. *Doctoral dissertation, James Cook University*.

Holm, R. J., Spandler, C., and Richards, S. W., (2013). Melanesian arc far-field response to collision of the Ontong Java Plateau: geochronology and petrogenesis of the Simuku Igneous Complex, New Britain, Papua New Guinea. *Tectonophysics*, 603, 189-212.

Holm, R.J., Rosenbaum, G., and Richards, S.W., (2016). Post 8 Ma reconstruction of Papua New Guinea and Solomon Islands: Microplate tectonics in a convergent plate boundary setting. *Earth-Science Reviews*, v. 156, p. 66-81.

Holt, S.J., Holford, S.P., and Foden, J., (2013). New insights into the magmatic plumbing system of the South Australian Quaternary Basalt province from 3D seismic and geochemical data. *Australian Journal of Earth Sciences*, v. 60, p. 797– 817, doi:10.1080/08120099.2013.865143.

Idnurm, M., (1985). Late Mesozoic and Cenozoic palaeomagnetism of Australia–I. A redetermined apparent polar wander path. *Geophysical Journal of the Royal Astronomical Society* 83, 399-418.

Idnurm M. (1986). Late Mesozoic and Cenozoic palaeomagnetism of Australia — III. Bias-corrected pole paths for Australia, Antarctica and India. *Geophysical Journal International* 86, 277-287.

Idnurm M. (1990). Comments on:‘A weighted least-squares fit of the Australian apparent polar wander path for the last 100 Myr’By RJ Musgrave. *Geophysical Journal International* 102, 191-193.

Idnurm, M. (1994). New Late Eocene pole for Australia, time-averaging of remanence directions, and palaeogeographic reference systems. *Geophysical Journal International*, 117(3), 827-833.

Jackson, M. G., Hart, S. R., Konter, J. G., Koppers, A. A., Staudigel, H., Kurz, M. D., and Sinton, J. M. (2010). Samoan hot spot track on a “hot spot highway”: Implications for mantle plumes and a deep Samoan mantle source. *Geochemistry, Geophysics, Geosystems,* 1112. doi: 10.1029/2010GC003232

Jackson, M. G., Hart, S. R., Konter, J. G., Kurz, M. D., Blusztajn, J., and Farley, K. A. (2014). Helium and lead isotopes reveal the geochemical geometry of the Samoan plume. *Nature,* 5147522, 355-358. doi: 10.1038/NATURE13794

Jackson, M. G., Hart, S. R., Koppers, A. A., Staudigel, H., Konter, J., Blusztajn, J., and Russell, J. A. (2007). The return of subducted continental crust in Samoan lavas. *Nature*, 4487154, 684-687. doi: 10.1038/nature06048

Jaques, A., and Robinson, G., (1977). The continent/island-arc collision in northern Papua New Guinea. *BMR Journal of Australian Geology and Geophysics*, 2, 289-303.

Jicha, B. R., Hart, G. L., Johnson, C. M., Hildreth, W., Beard, B. L., Shirey, S. B., and Valley, J. W. (2009). Isotopic and trace element constraints on the petrogenesis of lavas from the Mount Adams volcanic field, Washington. *Contributions to Mineralogy and Petrology*, 1572, 189-207 doi: doi:10.1007/s00410-008-0329-6

Johnson R. W. (1989). Volcano distribution and classification. In: Johnson R. W., Knutson J. And Taylor S. R. eds. *Intraplate Volcanism: In Eastern Australia and New Zealand*, pp. 7 11. Cambridge University Press, Cambridge, UK.

Johnson, H. P., Lowrie, W., and Kent, D. V. (1975). Stability of anhysteretic remanent magnetization in fine and coarse magnetite and maghemite particles. *Geophysical Journal International*, 411, 1-10.

Johnson, R. W., Knutson, J., and Taylor, S. R., eds., 1989, *Intraplate volcanism: in eastern Australia and New Zealand.* Cambridge University Press.

Joliffe, I. T. (2002). *Principal Component Analysis*, 2nd edn. Springer

Jones, C. H., (2002). User-driven Integrated Software Lives: "PaleoMag" Paleomagnetics Analysis on the Macintosh. *Computers and Geosciences,* 28 (10), 1145-1151.

Jones, I., and Verdel, C., (2015). Basalt distribution and volume estimates of Cenozoic volcanism in the Bowen Basin region of eastern Australia: Implications for a waning mantle plume. *Australian Journal of Earth Sciences* 62, 255-263. doi: 10.1080/08120099.2015.997796

Jones, I., Verdel, C., Crossingham, T., and Vasconcelos, P. (2017). Animated reconstructions of the Late Cretaceous to Cenozoic northward migration of Australia, and implications for the generation of east Australian mafic magmatism. *Geosphere,* GES01405-1. doi: 10.1130/GES01405.1

King, S. D., and Anderson, D. L. (1998). Edge driven convection. *Earth and Planetary Science Letters,* 160, 289-296.

King, SD. (2004). Understanding the edge-driven convection hypotheses. www.MantlePlums.org, last revision March, 2004

Kirschvink, J.L., (1980). The least-squares line and plane and the analysis of palaeomagnetic data. *Geophysical Journal International*, v. 62, p. 699-718.

Klootwijk, C. T., and Peirce, J. W. (1979). India's and Australia's pole path since the late Mesozoic and the India–Asia collision. *Nature, 282*(5739), 605-607.

Klootwijk C. T., Gee J. S., Peirce J. W., Smith G. M. and Mcfadden P. L. (1992). An early India-Asia contact: Paleomagnetic constraints from Ninetyeast Ridge, ODP Leg 121. *Geology* 20, 395-398.

Knesel, K. M., Cohen, B. E., Vasconcelos, P. M. and Thiede, D. S. (2008). Rapid change in drift of the Australian plate records collision with Ontong Java plateau. *Nature* 454, 754-757.

Korsch, R., Totterdell, J., Cathro, D. and Nicoll, M. (2009). Early Permian East Australian Rift System. *Australian Journal of Earth Sciences* 56, 381-400.

Kruiver, P. P., Dekkers, M. J., and Heslop, D. (2001). Quantification of magnetic coercivity components by the analysis of acquisition curves of isothermal remanent magnetisation. *Earth and Planetary Science Letters*, 1893, 269-276.

Kuiper, K. F., Deino, A., Hilgen, F. J., Krijgsman, W., Renne, P. R., and Wijbrans, J. R., (2008). Synchronizing rock clocks of Earth history. *Science*, 3205875, 500-504.

Kumar P., Yuan X., Kumar M. R., Kind R., Li X. and Chadha R. K. (2007). The rapid drift of the Indian tectonic plate. *Nature* 449, 894-897.

Le Bas, M. J., Le Maitre, R.W., Streckeisen, A. and Zanettin, B. (1986). A chemical classification of volcanic rocks based on the total alkali – silica diagram. *Journal of Petrology* 27, 745-750.

Le Pichon, X. and Heirtzler, J. R. (1968). Magnetic anomalies in the Indian Ocean and sea-floor spreading. *Journal of Geophysical Research* 73, 2101-2117.

Le Roex, A. P., Cliff, R. A., and Adair, B. J. I. (1990). Tristan da Cunha, South Atlantic: geochemistry and petrogenesis of a basanite-phonolite lava series. *Journal of Petrology*, 314, 779-812. doi: 10.1093/petrology/31.4.779

Lee, J-Y., Marti, K., Severinghaus, J. P., Kawamura, K., Yoo, H.-S., Lee, J. B., and Kim, J. S., (2006). A redetermination of the isotopic abundances of atmospheric Ar. *Geochimica et Cosmochimica Acta* 7017, 4507-4512

Li Q.-L., Li X.-H., Liu Y., Tang G.-Q., Yang J.-H. and Zhu W.-G. (2010). Precise U-Pb and Pb-Pb dating of Phanerozoic baddeleyite by SIMS with oxygen flooding technique. *Journal of Analytical Atomic Spectrometry* 25, 1107-1113.

Lister, G. S., and Etheridge, M. A. (1989). Detachment models for uplift and volcanism in the Eastern Highlands, and their application to the origin of passive margin mountains. In: Johnson R. W. eds Intraplate volcanism in eastern Australia and New Zealand. *Cambridge University Press, Cambridge*, 297-313.

Malitch, K. N., Badanina, I. Y., Belousova, E. A. and Tuganova, E. V. (2012). Results of U-Pb dating of zircon and baddeleyite from the Noril'sk-1 ultramafic-mafic intrusion Russia. *Russian Geology and Geophysics* 53, 123-130.

Mann, P., and Taira, A., (2004), Global tectonic significance of the Solomon Islands and Ontong Java Plateau convergent zone. *Tectonophysics*, 3893, 137-190.

Matchan, E., and Phillips, D., (2011). New $^{40}Ar/^{39}Ar$ ages for selected young < 1 Ma basalt flows of the Newer Volcanic Province, southeastern Australia. *Quaternary Geochronology,* 63, 356-368.

Mayer, B., Jung, S., Romer, R. L., Stracke, A., Haase, K. M., and Garbe-Schönberg, C. D. (2013). Petrogenesis of Tertiary hornblende-bearing lavas in the Rhön, Germany. *Journal of Petrology*, 54 10: 2095-2123.. doi: 10.1093/petrology/egt042

McBride, J. S., Lambert, D. D., Nicholls, I. A., and Price, R. C. (2001). Osmium isotopic evidence for crust–mantle interaction in the genesis of continental intraplate basalts from the Newer Volcanics Province, southeastern Australia. *Journal of Petrology,* 426, 1197-1218. Doi: 10.1093/petrology/42.6.1197

McDougall, I. and Harrison, T. M. (1999). Geochronology and Thermochronology by the $^{40}Ar/^{39}Ar$ Method. *Oxford University Press.*

McDougall, I., and Duncan, R. A., (1988). Age progressive volcanism in the Tasmantid Seamounts. *Earth and Planetary Science Letters*, 892, 207-220.

McDougall, I., and Harrison, T. M. (1999). *Geochronology and Thermochronology by the 40Ar/39Ar Method*. Oxford University Press on Demand.

McDougall, I., and Roksandic, Z., (1974). Total fusion $^{40}Ar/^{39}Ar$ ages using HIFAR reactor. *Journal of the Geological Society of Australia*, 211, 81-89.

McFadden, P. L., Merrill, R. T., McElhinny, M. W., and Lee, S. (1991). Reversals of the Earth's magnetic field and temporal variations of the dynamo families. *Journal of Geophysical Research: Solid Earth*, 96B3, 3923-3933.

Mckenzie, D. and Sclater, J. G. (1971). The Evolution of the Indian Ocean since the Late Cretaceous. *Geophysical Journal International* 24, 437-528.

Mckenzie, D. A., Nott, R. J., and Bolger, P. F. (1984). Radiometric age determinations. *Geological Survey of Victoria – Report*, 74.

Merrill, R. T. (1970). Low-temperature treatments of magnetite and magnetite-bearing rocks. *Journal of Geophysical Research*, *75*(17), 3343-3349.

Middlemost, E. A, (1981). The Canobolas complex, NSW, an alkaline shield volcano. *Journal of the Geological Society of Australia*, 281-2, 33-49.

Miková, J, and Denková, P. (2007). Modified chromatographic separation scheme for Sr and Nd isotope analysis in geological silicate samples. *Journal of Geoscience Prague* 524:221–226. DOI: 10.3190/jgeosci.015

Monroe, J. S. and Wicander, R. (2011). *The changing Earth: exploring geology and evolution*, Cengage Learning, Stamford CT, 736 p.

Montelli R., Nolet G., Dahlen F. A. And Masters G. (2006). A catalogue of deep mantle plumes: New results from finite-frequency tomography. *Geochemistry, Geophysics, Geosystems* 7, Q11007.

Mortimer, N., Gans, P. B., Palin, J. M., Meffre, S., Herzer, R. H., and Skinner, D. N. B., (2010). Location and migration of Miocene Quaternary volcanic arcs in the SW Pacific region. *Journal of Volcanology and Geothermal Research* 190, 1–10.

Mortimer, N., Herzer, R. H., Walker, N. W., Calvert, A. T., Seward, D., and Chaproniere, G. C. H., (2003). Cavalli Seamount, Northland Plateau, SW Pacific Ocean: a Miocene metamorphic core complex? *Journal of the Geological Society*, 1606, 971-983.

Müller, R. D., Royer, J.-Y., and Lawver, L. A., (1993). Revised plate motions relative to the hotspots from combined Atlantic and Indian Ocean hotspot tracks, *Geology*, 16, 275–278.

Mumme, W. G. (1963). Thermal and Alternating Magnetic Field Demagnetization Experiments on Cainozoic Basalts from Victoria, Australia. *Geophysical Journal of the Royal Astronomical Society* 7, 314-327.

Musgrave, R. J., (1989). A weighted least-squares fit of the Australian apparent polar wander path for the last 100 Myr. *Geophysical Journal International*, 962, 231-243.

Musgrave, R. J., (2013). Evidence for Late Eocene emplacement of the Malaita Terrane, Solomon Islands: Implications for an even larger Ontong Java Nui oceanic plateau. *Journal of Geophysical Research: Solid Earth*, 1186, 2670-2686.

Nishitani, T. and M. Kono, (1989). Effects of low-temperature oxidation on the remanence properties of titanomagnetites, *Journal of geomagnetism and geoelectricity*, 41, 19–38,

Niu, Y., Wilson, M., Humphreys, E. R., and O'Hara, M. J. (2011). The origin of intra-plate ocean island basalts OIB: the lid effect and its geodynamic implications. *Journal of Petrology*, 527-8, 1443-1468. Doi: 10.1093/petrology/egr030

Oberli F., Meier M., Berger A., Rosenberg C. L. and Gieré R. (2004). U-Th-Pb and 230Th/238U disequilibrium isotope systematics: Precise accessory mineral chronology and melt evolution tracing in the Alpine Bergell intrusion. *Geochimica et Cosmochimica Acta* 68, 2543-2560.

Ogg, J.G., (2012). *Geomagnetic polarity time scale.* In: Gradstein, F.M., Ogg, J.G., Schmitz, M.D., Ogg, G.D. (Eds.), *The Geologic Time Scale.* Elsevier, Oxford, UK, pp. 85–114.

O'Reilly, S. Y., and Zhang, M., (1995), Geochemical Characteristics Of Lava-Field Basalts From Eastern Australia And Inferred Sources: Connections With The Subcontinental Lithospheric Mantle? . *Contributions to Mineralogy and Petrology* 121 148-170

O'Reilly, S.Y. and Griffin,W. L. (1996). 4-D lithosphere mapping: methodology and examples. *Tectonophysics* 262, 3^18.

O'Neill, C., Müller, D., and Steinberger, B., (2005). On the uncertainties in hot spot reconstructions and the significance of moving hot spot reference frames. *Geochemistry, Geophysics, Geosystems* 6, Q04003.

Oostingh, K. F., Jourdan, F., Matchan, E. L., and Phillips, D. (2017). $^{40}Ar/^{39}Ar$ geochronology reveals rapid change from plume-assisted to stress-dependent volcanism in the Newer Volcanic Province, SE Australia. *Geochemistry, Geophysics, Geosystems.* Doi: 10.1002/2016GC006601

Opdyke, N. D., and Musgrave, R. (2004). Paleomagnetic results from the Newer Volcanics of Victoria: contribution to the time averaged field initiative. *Geochemistry, Geophysics, Geosystems*, 53.

O'Reilly, S. Y., and Griffin, W. L. (1988). Mantle metasomatism beneath western Victoria, Australia: I. Metasomatic processes in Cr-diopside lherzolites. *Geochimica et Cosmochimica Acta*, 522, 433-447.

Özdemir, Ö. and Dunlop, D. J. (1996). Thermoremanence and Néel temperature of goethite. *Geophysical Research Letters* 23, 921-924.

Özdemir, Ö., and, Dunlop, D. J., (1989). Chemico-viscous remanent magnetization in Fe3O4-γ Fe2O3 system. *Science*, 243, 1043–1047.

Ozima, M., Ozima, M., and Nagata, T. (1964). Low temperature treatment as an effective means of "magnetic cleaning" of natural remanent magnetization. *Journal of geomagnetism and geoelectricity*, *16*(1), 37-40.

Pain, C. F., (1983). Geomorphology of the Barrington Tops area, New South Wales. *Journal of the Geological Society of Australia*, 301-2, 187-194.

Paul, B., Hergt, J. M., and Woodhead, J. D. (2005). Mantle heterogeneity beneath the Cenozoic volcanic provinces of central Victoria inferred from trace-element and Sr, Nd, Pb and Hf isotope data. *Australian Journal of Earth Sciences*, 522, 243-260. DOI: 10.1080/08120090500139448

Petterson, M. G., Babbs, T., Neal, C. R., Mahoney, J. J., Saunders, A. D., Duncan, R. A., and Natogga, D., (1999). Geological–tectonic framework of Solomon Islands, SW Pacific: crustal accretion and growth within an intra-oceanic setting. *Tectonophysics*, 3011, 35-60.

Pigram, C. T., and Davies, H. L., (1987). Terranes and the accretion history of the New Guinea orogen. *BMR Journal of Australian Geology and Geophysics*, 10, 193-211.

Pillans, B., Tonui, E., and Idnurm, M., (1999). Paleomagnetic dating of weathered regolith at Northparkes mine, NSW. New Approaches to an Old Continent: Perth. *Cooperative Research Centre for Landscape Evolution and Mineral Exploration*, 237-242.

Rahman, A. U., (1971). Palaeomagnetic secular variation for recent normal and reversed epochs, from the Newer Volcanics of Victoria, Australia. *Geophysical Journal International*, *243*, 255-269.

Rawlinson, N., Davies, D. R., and Pilia, S. (2017). The mechanisms underpinning Cenozoic intraplate volcanism in eastern Australia: Insights from seismic tomography and geodynamic modeling. *Geophysical Research Letters*, *44*(19), 9681-9690.

Raymond L. S., Gallagher O. L., Zhang R. and Highet W. (2012). Surface Geology of Australia, 1:1 000 000 scale, 2012 edition. *Geoscience Australia*, Canberra ACT.

Raza, A., Hill, K. C., and Korsch, R. J. (2009). Mid-Cretaceous uplift and denudation of the Bowen and Surat Basins, eastern Australia: relationship to Tasman Sea rifting from apatite fission-track and vitrinite-reflectance data. *Australian Journal of Earth Sciences* 56, 501 531.

Renne, P. R., Swisher, C. C., Deino, A. L., Karner, D. B., Owens, T. L., and DePaolo, D. J., (1998). Intercalibration of standards, absolute ages and uncertainties in $^{40}Ar/^{39}Ar$ dating. *Chemical Geology*, 1451, 117-152.

Riffel, S. B., Vasconcelos, P. M., Carmo, I. O., and Farley, K. A. (2016). Goethite U–Th/He geochronology and precipitation mechanisms during weathering of basalts. *Chemical Geology*, 446, 18-32.

Rudnick R. L. and Fountain D. M. (1995). Nature and composition of the continental crust: a lower crustal perspective. *Reviews of Geophysics* 33, 267-309.

Salters, V. J., Mallick, S., Hart, S. R., Langmuir, C. E., and Stracke, A. (2011). Domains of depleted mantle: New evidence from hafnium and neodymium isotopes. *Geochemistry, Geophysics, Geosystems,* 128. DOI: 10.1029/2011GC003617

Sayers, J., Symonds, P. A., Direen, N. G., and Bernardel, G. (2001). Nature of the continent-ocean transition on the non-volcanic rifted margin of the central Great Australian Bight. *Geological Society, London, Special Publications,* 187(1), 51-76.

Schellart, W. P., Kennett, B. L. N., Spakman, W., and Amaru, M., (2009). Plate reconstructions and tomography reveal a fossil lower mantle slab below the Tasman Sea. *Earth and Planetary Science Letters* 278, 143-156.

Schellart, W. P., Lister, G. S., and Toy, V. G., (2006). Late cretaceous and Cenozoic reconstruction of the Southwest Pacific Region: Tectonics controlled by subduction and rollback processes. *Earth Science Reviews* 76, 191-233.

Schmidt, P. W., and Ollier, C. D. (1988). Palaeomagnetic dating of late Cretaceous to early Tertiary weathering in New England, NSW, Australia. *Earth-Science Reviews*, 255-6, 363-371.

Schmidt, P. W., and Williams, G. E. (2017). Paleomagnetic age of ferruginous weathering beneath the Hamersley Surface, Pilbara, Western Australia, and the Cenozoic apparent polar wander path. *Australian Journal of Earth Sciences, 64*(2), 239-249.

Serrano, L., Ferrari, L., Martínez, M.L., Petrone, C.M. and Jaramillo, C., (2011). An integrative geologic, geochronologic and geochemical study of Gorgona Island, Colombia: Implications for the formation of the Caribbean Large Igneous Province. *Earth and Planetary Science Letters,* 3093, pp.324-336. Doi: 10.1016/j.epsl.2011.07.011

Seton, M., Müller, R. D., Zahirovic, S., Gaina, C., Torsvik, T., Shephard, G., and Chandler, M., (2012). Global continental and ocean basin reconstructions since 200Ma. *Earth-Science Reviews,* 1133, 212-270.

Sharp, K. R., (2004). Cenozoic volcanism, tectonism and stream derangement in the Snowy Mountains and northern Monaro of New South Wales. *Australian Journal of Earth Sciences,* 511, 67-85.

Skae A. 1998. *The Petrology of the Buckland Volcanic Province, Central Queensland, Australia.* University of Oxford.

Spassov, S., Heller, F., Kretzschmar, R., Evans, M. E., Yue, L. P., and Nourgaliev, D. K. (2003). Detrital and pedogenic magnetic mineral phases in the loess/palaeosol sequence at Lingtai Central Chinese Loess Plateau. *Physics of the Earth and Planetary Interiors*, 1404, 255-275.

Späth, A., Le Roex, A. P., and Opiyo-Akech, N. (2001). Plume–lithosphere interaction and the origin of continental rift-related alkaline volcanism—the Chyulu Hills Volcanic Province, southern Kenya. *Journal of Petrology*, 424, 765-787.

Srinivasan, B. V., Duraiswami, R. And Murtugudde, R. (2010). Efficient kriging for real-time spatio-temporal interpolation. Proceedings of the 20th Conference on Probability and Statistics in the Atmospheric Sciences, pp. 228 235. *American Meteorological Society*, January 2010, Atlanta GA.

Stephenson, P. J., Griffin, T. J., and Sutherland, F. L., (1980). Cainozoic volcanism in northeastern Australia, The Geology and Geophysics of North-eastern Australia. RA Henderson, PJ Stephenson, 349–374, *Geological Society of Australia, Queensland Division, Brisbane.*

Sun, S. S. (1980). Lead isotopic study of young volcanic rocks from mid-ocean ridges, ocean islands and island arcs. *Philosophical Transactions of the Royal Society of London A: Mathematical, Physical and Engineering Sciences,* 2971431, 409-445. doi: 10.1098/rsta.1980.0224

Sun, S. S., and McDonough, W. S. (1989). Chemical and isotopic systematics of oceanic basalts: implications for mantle composition and processes. *Geological Society, London, Special Publications*, 421, 313-345.

Sutherland, F. L., (1981). Migration in relation to possible tectonic and regional controls on eastern Australian volcanism. *Journal of Vulcanology and Geothermal Research* 9, 181-215.

Sutherland, F. L., (2003). 'Boomerang' migratory intraplate Cenozoic volcanism, eastern Australian rift margins and the Indian-Pacific mantle boundary. In: Hillis R. R. and Mu¨ ller R. D. eds. Evolution and Dynamics of the Australian Plate, pp. 203–221. *Geological Society of Australia Special Publication 22 and Geological Society of America Special Paper* 372.

Sutherland, F. L., and Fanning, C. M., (2001). Gem-bearing basaltic volcanism, Barrington, New South Wales: Cenozoic evolution, based on basalt K–Ar ages and zircon fission track and U–Pb isotope dating*. *Australian Journal of Earth Sciences*, 482, 221-237.

Sutherland F., Hollis J. And Robertson A. (1989a). Bauhinia. In: Johnson R. W., Knutson J. And Taylor S. R. Eds. Intraplate Volcanism: In Eastern Australia and New Zealand, pp. 105 106. *Cambridge University Press, Cambridge*, UK.

Sutherland, F., Stephenson, P., Knutson, J., Hollis, J. and Robertson, A. (1989b). East Australia volcanic geology: Central Queensland. In: JOHNSON R. W., KNUTSON J. and TAYLOR S. R. eds. Intraplate Volcanism: In Eastern Australia and New Zealand, pp. 97 107. *Cambridge University Press, Cambridge*, UK.

Sutherland, F., Stubbs, D. and Green, D. (1977). K-Ar ages of Cainozoic volcanic suites, Bowen-St Lawrence Hinterland, north Queensland with some implications for petrologic models. *Journal of the Geological Society of Australia* 24, 447 460.

Sutherland, F. L., Graham I., Meffre S., Zwingmann H., and Pogson R., (2012) Passive-margin prolonged volcanism, East Australian Plate: outbursts, progressions, plate controls and suggested causes. *Australian Journal of Earth Sciences* 59, 983 1005.

Sutherland, F. L., Graham, I. T., Hollis, J. D., Meffre, S., Zwingmann, H., Jourdan, F., and Pogson, R. E., (2014). Multiple felsic events within post-10 Ma volcanism, Southeast Australia: inputs in appraising proposed magmatic models. *Australian journal of Earth Sciences* 61, 241-267.

Sutherland, F. L., Stubbs D. and Green D. C., (1977). K–Ar ages of Cainozoic volcanic suites, Bowen–St Lawrence Hinterland, north Queensland with some implications for petrologic models. *Journal of the Geological Society of Australia* 24, 447–460.

Sutherland, F.L., Hollis, J.D. and Robertson, A.D., (1989). Buckland and Mitchell. In Johnson, R. W., Knutson, J., and Taylor, S. R., eds., 1989, Intraplate volcanism: in eastern Australia and New Zealand. *Cambridge University Press*, 104-105.

Taylor, B., (2006). The single largest oceanic plateau: Ontong Java–Manihiki–Hikurangi. *Earth and Planetary Science Letters*, 2413, 372-380.

Torsvik, T.H., Müller, R.D., Van der Voo, R., Steinberger, B., and Gaina, C., (2008a). Global plate motion frames: toward a unified model. *Reviews of Geophysics* 46, RG3004.

Tregoning, P., (2002). Plate kinematics in the western Pacific derived from geodetic observations. *Journal of Geophysical Research: Solid Earth*, 107B1.

Turner, S. P., George, R. M. M., Evans, P. J., Hawkesworth, C. J., and Zellmer, G. F. (2000). Time-scales of magma formation, ascent and storage beneath subduction-zone volcanoes. *Philosophical Transactions of the Royal Society of London. Series A: Mathematical, Physical and Engineering Sciences*,3581770, 1443-1464.

Ubide, T., Galé, C., Larrea, P., Arranz, E., Lago, M., and Tierz, P. (2014). The relevance of crystal transfer to magma mixing: a case study in composite dykes from the Central Pyrenees. *Journal of Petrology*, 55 8: 1535-1559. DOI: 10.1093/petrology/egu033

van den Bogaard, P., (2013). The origin of the Canary Island Seamount Province-New ages of old seamounts. *Scientific reports*, 3.

Van der Voo, R. (1990). The reliability of paleomagnetic data. *Tectonophysics*, 184(1), 1-9.

Van Hinsbergen, D. J., Lippert, P. C., Dupont-Nivet, G., McQuarrie, N., Doubrovine, P. V., Spakman, W., and Torsvik, T. H. (2012). Greater India Basin hypothesis and a two-stage Cenozoic collision between India and Asia. *Proceedings of the National Academy of Sciences*, 10920, 7659-7664.

Van Otterloo, J., Raveggi, M., Cas, R. A. F., and Maas, R. (2014). Polymagmatic activity at the monogenetic Mt Gambier Volcanic Complex in the Newer Volcanics Province, SE

Australia: new insights into the occurrence of intraplate volcanic activity in Australia. *Journal of Petrology*, 557, 1317-1351. DOI: 10.1093/petrology/egu026

van Ufford, A. Q., and Cloos, M., (2005). Cenozoic tectonics of New Guinea. *AAPG bulletin*, 891, 119-140.

Vasconcelos, P. M., (1999). K– Ar and $^{40}Ar/^{39}Ar$ geochronology of weathering processes. *Annual Reviews of Earth and Planetary Science* 27, 183 – 229.

Vasconcelos, P. M., Onoe, A. T., Kawashita, K., Soares, A. J. and Teixaira, W., (2002). $^{40}Ar/^{39}Ar$ geochronology at the Instituto de Geocieˆncias, USP: instrumentation, analytical procedures, and calibration. *Annals of the Brazilian Academy of* Sciences 74, 297 – 342.

Vasconcelos, P., Knesel, K., Cohen, B., and Heim, J., (2008). Geochronology of the Australian Cenozoic: a history of tectonic and igneous activity, weathering, erosion, and sedimentation. Australian Journal of Earth Sciences 55, 865-914.

Vickery, Dawson, Sivell, Malloch and Dunlap (2007). *Quarterly Notes of the Geological Survey of New South Wales.* v123 p1-31.

Vogt, P. R. (1991). Bermuda and Appalachian-Labrador rises, Geology, 19, 41-44.

Waltenberg K. (2006). *$^{40}Ar/^{39}Ar$ geochronology of lava flows at Carnarvon Gorge, Buckland Volcano.* BSc Hons thesis. University of Queensland, Brisbane unpubl..

Webb, A. and McDougall, I. (1967). A comparison of mineral and whole rock potassium argon ages of Tertiary volcanics from central Queensland, Australia. *Earth and Planetary Science Letters* 3, 41 47.

Webb, A. W., Stevens, N. C. and McDougall, I. (1967). Isotopic age determinations on Tertiary volcanic rocks and intrusives of southeast Queensland. *Proceedings of the Royal Society of Queensland*, 79: 79–92.

Wellman, P. (1971). *The age and palaeomagnetism of the Australian Cenozoic volcanic rocks.* PhD thesis, Australian National University, Canberra ACT.

Wellman, P., McElhinny, M. W. and McDougall, I. (1969). On the Polar-Wander Path for Australia during the Cenozoic. *Geophysical Journal International* 18, 371-395.

Wellman, P., (1975). Palaeomagnetism of two mid-Tertiary basaltic volcanoes in Queensland, Australia. In *Proceedings of the Royal Society of Queensland* Vol. 86, pp. 147-153.

Wellman, P., and McDougall, I., (1974a). Cainozoic igneous activity in eastern Australia. *Tectonophysics*, 231, 49-65.

Wellman, P., and McDougall, I., (1974b). Potassium–argon ages on the Cainozoic volcanic rocks of New South Wales. Journal of the Geological Society of Australia 21, 247–272.

White R., and McKenzie, D., (1989). Magmatism at rift zones: the generation of volcanic continental margins and flood basalts. Journal of Geophysical Research: Solid Earth, 94B6, 7685-7729.

White, R.S., Spence, G.D., Fowler, S.R., McKenzie, D.P., Westbrook, G.K., and Bowen, A.N., (1987). Magmatism at rifted continental margins. Nature 330, 439-444.

Willbold, M., and Stracke, A. (2010). Formation of enriched mantle components by recycling of upper and lower continental crust. Chemical Geology, 2763, 188-197. DOI: 10.1016/j.chemgeo.2010.06.005

Wilson, J. T., (1963). A possible origin of the Hawaiian Islands. Canadian Journal of Physics, 416, 863-870.

Wilson, S.A., (1997a) Data compilation for USGS reference material BHVO-2, Hawaiian Basalt: *U.S. Geological Survey Open-File Report*

Wilson, S.A., (1997b) The collection, preparation, and testing of USGS reference material BCR-2, Columbia River, Basalt: *U.S. Geological Survey Open-File Report 98*

Winter, J. D. (2010). *Principles of igneous and metamorphic petrology Vol. 2.* Prentice Hall New York.

Wood, B. J. (2004). Melting of fertile peridotite with variable amounts of H2O. *The State of the Planet: Frontiers and Challenges in Geophysics*, 69-80.

Woodhead, J. D., and McCulloch, M. T. (1989). Ancient seafloor signals in Pitcairn Island lavas and evidence for large amplitude, small length-scale mantle heterogeneities. *Earth and Planetary Science Letters*, 943-4, 257-273. doi: 10.1016/0012-821X8990145-3

Workman, R. K., Hart, S. R., Jackson, M., Regelous, M., Farley, K. A., Blusztajn, J., and Staudigel, H. (2004). Recycled metasomatized lithosphere as the origin of the Enriched Mantle II EM2 end-member: Evidence from the Samoan Volcanic Chain. *Geochemistry, Geophysics, Geosystems*, 54. doi: 10.1029/2003GC000623

Wyatt, D. H., and Webb, A. W., (1970). K/Ar ages of some north Queensland basalts and an interpretation of Late Cainozoic history. *Journal of the Geological Society of Australia*, 17: 39–51.

Wyborn, D. and Owen, M. (1986). *Araluen New South Wales 1:100 000 Geological Map Commentary*. Bureau of Mineral Resources, Canberra.

Yan, C. Y., and Kroenke, L. W., (1993). A plate tectonic reconstruction of the Southwest Pacific, 0–100 Ma. In *Proceedings of the Ocean Drilling Program, Scientific Results* Vol. 130, pp. 697-709. Texas: College Station.

Yang, H-J, Frey, F, and Clague, D. (2003). Constraints on the source components of lavas forming the Hawaiian North Arch and Honolulu Volcanics. *Journal of Petrology* 44: 603-27 DOI: 10.1093/petrology/44.4.603

Zhang, M., and O'Reilly, S. Y. (1997). Multiple sources for basaltic rocks from Dubbo, eastern Australia: geochemical evidence for plume—lithospheric mantle interaction. *Chemical Geology*, 136(1), 33-54.

Zhang, M., O'Reilly, S. Y., and Chen, D. (1999). Location of Pacific and Indian mid-ocean ridge–type mantle in two time slices: Evidence from Pb, Sr, and Nd isotopes for Cenozoic Australian basalts. *Geology*, 27(1), 39-42.

Zhang, M., Stephenson, P. J., O'Reilly, S. Y., McCulloch, M. T., and Norman, M. (2001). Petrogenesis and geodynamic implications of late Cenozoic basalts in North Queensland, Australia: trace-element and Sr–Nd–Pb isotope evidence. *Journal of Petrology*, 424, 685-719.

Data repository references

Geochemistry

Demidjuk, Z., Turner, S., Sandiford, M., George, R., Foden, J., and Etheridge, M. (2007). U-series isotope and geodynamic constraints on mantle melting processes beneath the Newer

Volcanic Province in South Australia. *Earth and Planetary Science Letters,* 261(3), 517-533. doi: 10.1016/j.epsl.2007.07.006

McBride, J. S., Lambert, D. D., Nicholls, I. A., and Price, R. C. (2001). Osmium isotopic evidence for crust–mantle interaction in the genesis of continental intraplate basalts from the Newer Volcanics Province, southeastern Australia. *Journal of Petrology,* 42(6), 1197-1218. Doi: 10.1093/petrology/42.6.1197

O'Reilly S. Y., and Zhang Ming (1995). Geochemical Characteristics Of Lava-Field Basalts From Eastern Australia And Inferred Sources: Connections With The Subcontinental Lithospheric Mantle? . *Contributions to Mineralogy and Petrology* 121 148-170

Paul, B., Hergt, J. M., and Woodhead, J. D. (2005). Mantle heterogeneity beneath the Cenozoic volcanic provinces of central Victoria inferred from trace-element and Sr, Nd, Pb and Hf isotope data. *Australian Journal of Earth Sciences,* 52(2), 243-260. DOI: 10.1080/08120090500139448

Price, R.C., Gray, CM and Frey, FA. (1997) Strontium isotopic and trace element heterogeneity in the plains basalts of the Newer Volcanic Province, Victoria, Australia. *Geochimica et Cosmochimica Acta,* 61: 171–192.

Price, R. C., Nicholls, I. A., and Day, A. (2014). Lithospheric Influences On Magma Compositions Of Late Mesozoic And Cenozoic Intraplate Basalts (The Older Volcanics) Of Victoria, South-Eastern Australia. *Lithos,* 206, 179-200.

Van Otterloo, J., Raveggi, M., Cas, R. A. F., and Maas, R. (2014). Polymagmatic activity at the monogenetic Mt Gambier Volcanic Complex in the Newer Volcanics Province, SE Australia: new insights into the occurrence of intraplate volcanic activity in Australia. *Journal of Petrology,* 55(7), 1317-1351. DOI: 10.1093/petrology/egu026

Zhang, M., Stephenson, P. J., O'Reilly, S. Y., McCulloch, M. T., and Norman, M. (2001). Petrogenesis and geodynamic implications of late Cenozoic basalts in North Queensland, Australia: trace-element and Sr–Nd–Pb isotope evidence. *Journal of Petrology,* 42(4), 685-719.

Geochronology

Abele, C., and Page, R. W. (1974). Stratigraphic and isotopic ages of Tertiary basalts of Maude and Aireys Inlet, Victoria, Australia. *Proceedings of the Royal Society of Victoria,* 86, 143-150.

Ashley, P. M., Dawson, M., Sivell, W. J., Wilson, J. B., and Dunlap, W. J. (2003). New data on the geology and geochronology of the area south of Tooraweenah, New South Wales.

Ashley, P. M., Duncan, R. A., and Feebrey, C. A. (1995). Ebor Volcano and crescent complex, northeastern New South Wales: age and geological development. *Australian Journal of Earth Sciences*, 42(5), 471-480.

Rahman, A. U., and McDougall, I., (1972). Potassium-Argon Ages on The Newer Volcanics Of Victoria. *Proceedings of the Royal Society of Victoria,* 85 61-69

Baillie, P. W. (1986). A radiometric age for the Moriarty Basalt, north-western Tasmania. *Tasmania Department of Mines Unpublished Report, 38.*

Barron, B. J., Robertson, A. D., and Sutherland, F. L. (1996). Olivine 'leucitites', their xenolith and megacryst suites, Hoskings peaks, north Queensland. *Australian Journal of Earth Sciences*, 43(3), 231-244.

Bird, M. I., Chivas, A. R., and Mcdougall, I. (1990). An isotopic study of surficial alunite in Australia 2. Potassium-argon geochronology. Chemical Geology: *Isotope Geoscience section*, 80(2), 133-145.

Bishop, P., Young, R. W., and McDougall, I. (1985). Stream profile change and longterm landscape evolution: Early Miocene and modern rivers of the east Australian highland crest, central New South Wales, Australia. *The Journal of Geology*, 455-474.

Brown, A. V. (1977). Preliminary report on age determination of basalt samples from the Ringarooma 1:50 000 Sheet. *Tasmania Department of Mines Report* 1977/25, 1-2.

Brown, A. V. (1982). Whole rock K/Ar ages of basalts. In: McClenaghan M. P., et al. Geology of the Ringarooma- Boobyalla area. *Geological Survey of Tasmania Bulletin 61*, pp.178. Hobart.

Carr, P. F., and Facer, R. A. (1980). Radiometric ages of some igneous rocks from the Southern and Southwestern Coalfields of New South Wales.

Cayley, Webb, A. W. and Henley, K. J. (1995) *Geological Survey of Victoria Unpublished Report 1995/15*.

Cohen, B. E., Knesel, K. M., Vasconcelos, P. M., Thiede, D. S., and Hergt, J. M. (2008). $^{40}Ar/^{39}Ar$ constraints on the timing and origin of Miocene leucitite volcanism in southeastern Australia. *Australian Journal of Earth Sciences*, 55(3), 407-418.

Cohen B. E., Vasconcelos P. M., Knesel K. M. (2007). $^{40}Ar/^{39}Ar$ Constraints on the timing of Oligocene Intraplate Volcanism in Southeast Queensland. *Australian Journal of Earth Sciences*, 54, 105-125

Cohen, B. E., Knesel, K. M., Vasconcelos, P. M., and Schellart, W. P. (2013). Tracking the Australian plate motion through the Cenozoic: Constraints from $^{40}Ar/^{39}Ar$ geochronology. *Tectonics*, 32(5), 1371-1383.

Cooper, J. A., Richards, J. R., and Webb, A. W. (1963). Some potassium-argon ages in New England, New South Wales. *Journal of the Geological Society of Australia, 10*(2), 313-316.

Cornell, C. D., Cowan, W. C., Mosness, T. L., Rankin, J. G., and Walla, R. J., (1986). Appendix 10: Petrology and Geochronology of Tilana-1. In: *Tilana-1 Final Well Report,* pp.267-273. Sydney.

Coventry, R. J., Stephenson, P. J., and Webb, A. W. (1985). Chronology of landscape evolution and soil development in the upper Flinders River area, Queensland, based on isotopic dating of Cainozoic basalts. *Australian Journal of Earth Sciences*, 32(4), 433-447.

Cromer, W. C. (1980). A Late Eocene basalt date from northern Tasmania. *Search*, 11(9), 294-295.

Dulhunty, J. A. (1972). Potassium-argon dating and occurrence of Tertiary and Mesozoic basalts in the Binnaway District. *In Journal and Proceedings of the Royal Society of New South Wales*, 105, 71-76.

Dulhunty, J. A. (1973). Potassium-argon basalt ages and their significance in the Macquarie Valley. New South Wales. *Journal and Proceedings of the Royal Society of New South Wales*, 106, 104-110.

Dulhunty, J. A., and McDougall, I. (1966). Potassium–argon dating of basalts in the Coonabarabran–Gunnedah district. New South Wales. *Australian Journal of Science* 28(10), 393-394.

Dury, G.H., Langford-Smith, T., and McDougall, I., (1969). A minimum age for the duricrust. *Australian Journal of Science* 31, 362-363.

Edwards, J., Cayley, R. A., and Joyce, E. B. (2004). Geology and geomorphology of the Lady Julia Percy Island volcano, a late Miocene submarine and subaerial volcano off the coast of Victoria, Australia. *Proceedings of the Royal Society of Victoria*, 116(1), 15-35.

Embleton, B. J. J., Schmidt, P. W., Hamilton, L. H., and Riley, G. H. (1985). Dating volcanism in the Sydney Basin: evidence from K–Ar ages and palaeomagnetism. *Volcanism in eastern Australia*, 1, 59-72.

Evans (1976). *A study of the basic volcanic rocks of the Maleny-Mapleton area, southeast Queensland.* BSc. (Hons), University of Queensland, Brisbane.

Everard, J.L., Sutherland, F.L., and Forsyth, S. M., (2007). A Late Oligocene basalt from Keach Hill, near Campbell Town, and its stratigraphic significance. *Tasmanian Geological Survey Record* 2007/03.

Ewart, A., (1982). Petrogenesis of the Tertiary anorogenic volcanic series of Southern Queensland, Australia, in the light of trace element geochemistry and O, Sr and Pb isotopes. *Journal of Petrology,* 23(3), 344-382.

Ewart, A., Chappell, B. W., and Lemaitre, R. (1985). Aspects of the mineralogy and chemistry of the intermediate–silicic Cainozoic volcanic rocks of eastern Australia. *Part,* 1, 359-382.

Exon, N. F., Langford-Smith, T. and McDougall, I. (1970). The age and geomorphic correlations of deep-weathering profiles, silcrete, and basalt in the Roma-Amby region, Queensland. *Journal of the Geological Society of Australia* 17(1), 21-30.

Facer, R. A., and Carr, P. F. (1979). K-Ar dating of Permian and Tertiary igneous activity in the southeastern Sydney Basin, New South Wales. *Journal of the Geological Society of Australia,* 26(1-2), 73-79.

Galloway, R. W., and Webb, A. W. (1979). Ages of some volcanic rocks in the Hunter Valley, NSW. *Search,* 10, 87-88.

Gill, E. D. (1981). Potassium/argon age of basalt in floor of Hopkins River, Allansford, SW Victoria, Australia. *Victorian Naturalist,* 98, 188-190.

Gillen D., Honda M., Chivas A. R., Yatsevich I., Patterson D. B., Carr P. F. (2009). Cosmogenic ^{21}Ne Exposure Dating Of Young Basaltic Lava Flows From The Newer Volcanic Province, Western Victoria, Australia. *Quaternary Geochronology* 5 1-9

Gleadow A. J. W., and Ollier, C. D. (1987). The age of gabbro at The Crescent, New South Wales. *Australian Journal of Earth Sciences,* 34(2), 209-212.

Godthelp H., Archer, M., Cifelli, R., Hand, S. J., and Gilkeson, C. F. (1992). Earliest known Australian Tertiary mammal fauna. *Nature,* 356(6369), 514-516.

Green, D.C. (1975). *Isotope Geology Laboratory Report No 2, 1971-1974.* University of Queensland, Department of Geology and Mineralogy.

Green, D. C., and Stevens, N. C. (1975). Age and stratigraphy of Tertiary volcanic and sedimentary rocks of the Ipswich district, southeast Queensland. *Queensland Government Mining Journal*, 76(833), 148-150.

Green D. C. and Webb, A. W. (1974). Geochronology of the northern part of the Tasman Geosyncline. In: Denmead A. K., Tweedale G. W. and Wilson A. F. eds. *The Tasman Geosyncline - a symposium,* pp.275-291. Geological Society of Australia Incorporated, Queensland Division, Brisbane.

Grenfell (1984). *The Stratigraphy, Geochronology and Petrology of the Volcanic Rocks of the Main Range, southeastern Queensland.* UQ PhD thesis:

Grey, C. M. and McDougall, I. (2009) K-Ar Geochronology Of Basalt Petrogenesis, Newer Volcanic Province, Victoria. *Australian Journal of Earth Sciences* 56, 245-258

Griffin, T. J., and McDougall, I. (1975). Geochronology of the Cainozoic McBride volcanic province, northern Queensland. *Journal of the Geological Society of Australia*, 22(4), 387-396.

Harding, (1969), BMR report #117. In Bennett, R., Page, R. W., and Bladon, G. M. 1975. *Catalogue of isotopic age determinations on Australian rocks*, 1966-70. Australian Government Publishing Service.

Hare A. G., Cas, R. A. F., Musgrave, R., and Phillips, D. (2005). Magnetic and chemical stratigraphy for the Werribee Plains basaltic lava flow-field, Newer Volcanics Province, southeast Australia: implications for eruption frequency. *Australian Journal of Earth Sciences*, 52(1), 41-57.

Henley K. J. and Webb, A. W. (1990*). Geological Survey of Victoria Unpublished Report 1990/27*.

Jaques A. L., Webb, A. W., Fanning, C. M., Black, L. P., Pidgeon, R. T., Ferguson, J., and Gregory, G. P. (1984). The Age Of The Diamond-Bearing Pipes And Associated Leucite Lamproites Of The West Kimberley Region, Western-Australia. *BMR Journal Of Australian Geology and Geophysics*, 9(1), 1-7.

Knesel K. M., Cohen B. E., Vasconcelos P. M. and Thiede D. S. (2008). Rapid change in drift of the Australian plate records collision with Ontong Java plateau. *Nature* 454, 754-757.

Lafferty S., and Golding, S.D. (Eds.), (1985). *A memorial volume in honour of Ernest Albert Thompson. Isotope Geology Laboratory Report No. 3, 1975–1984*, Department of Geology and Mineralogy, University of Queensland, Brisbane, Queensland, Australia, 147pp.

Langford-Smith, T., Dury, G. H., and McDougall, I. (1966). Dating the duricrust in southern Queensland. *Australian Journal of Science*, 29(3), 79-80.

Mackness, B. S., Whitehead, P. W., and McNamara, G. C. (2000). New potassium–argon basalt date in relation to the Pliocene Bluff Downs Local Fauna, northern Australia. *Australian Journal of Earth Sciences*, 47(4), 807-811.

Macphail, M. K., and Hill, R. S. (1994). K-Ar dated palynofloras in Tasmania 1: Early Oligocene, Proteacidites tuberculatus Zone sediments, Wilmot Dam, northwestern Tasmania. *In Papers and Proceedings of the Royal Society of Tasmania* 128, 1-15.

Martin H.A. Worrall L. and Charlson J. (1987). The first occurrence of the Paleocene Lygistepollenites balmei zone in the eastern highlands region, New South Wales. *Australian Journal of Earth Sciences* 34, 359-365.

Matchan E., and Phillips, D. (2011). New 40 Ar/39 Ar ages for selected young (< 1 Ma) basalt flows of the Newer Volcanic Province, southeastern Australia. *Quaternary Geochronology*, 6(3), 356-368.

McDougall I., Allsopp H. L., and Chamalaun F. H. (1966). Isotopic Dating Of The Newer Volcanics Of Victoria, Australia And Geomagnetic Polarity Epochs. *Journal of Geophysical Research* 71 6107-6118

McDougall I., and Duncan, R. A. (1988). Age progressive volcanism in the Tasmantid Seamounts. *Earth and Planetary Science Letters*, 89(2), 207-220.

McDougall I., and Gill, E. D. (1975). Potassium-argon ages from the Quaternary succession in the Warrnambool-Port Fairy area, Victoria, Australia. *Proceedings of the Royal Society of Victoria*, 87(1/2), 175-178.

McDougall I., and Roksandic, Z. (1974). Total fusion $^{40}Ar/^{39}Ar$ ages using HIFAR reactor. *Journal of the Geological Society of Australia*, 21(1), 81-89.

McDougall I., and Slessar, G. C. (1972). Tertiary volcanism in the Cape Hillsborough area, north Queensland. *Journal of the Geological Society of Australia*, 18(4), 401-408.

McDougall I., and Wilkinson, J. F. G. (1967). Potassium-argon dates on some Cainozoic volcanic rocks from northeastern New South Wales. *Journal of the Geological Society of Australia*, 14(2), 225-233

McDougall I., Embleton, B. J. J., and Stone, D. B. (1981). Origin and evolution of Lord Howe Island, southwest Pacific Ocean. *Journal of the Geological Society of Australia*, 28(1-2), 155-176.

McKenzie, D. A., Nott, R. J., and Bolger, P. F. (1984). Radiometric age determinations. *Geological Survey of Victoria.*

McQueen, K. G., Gonzalez, O. R., Roach, I. C., Pillans, B. J., Dunlap, W. J., and Smith, M. L. (2007). Landscape and regolith features related to Miocene leucitite lava flows, El Capitan northeast of Cobar, New South Wales. *Australian Journal of Earth Sciences*, 54(1), 1-17.

Messenger (1986). *Geology and Geochemistry of the Central Glass House Mountains, Southeast Queensland* (UQ Honours thesis)

Nott J., Young, R., and McDougall, I. (1996). Wearing down, wearing back, and gorge extension in the long-term denudation of a highland mass: quantitative evidence from the Shoalhaven catchment, southeast Australia. *The Journal of Geology*, 224-232.

Ollier, C. D. (1985). Lava flows of Mount Rouse, western Victoria. *Proceedings of the Royal Society of Victoria*, 97(4), 167-174.

O'Reilly, S. Y., and Griffin, W. L. (1984). Sr isotopic heterogeneity in primitive basaltic rocks, southeastern Australia: correlation with mantle metasomatism. *Contributions to Mineralogy and Petrology*, 87(3), 220-230.

Owen, M. and Wyborn, D. (1979). *BMR Bulletin 204 Geology and geochemistry of the Tantangara and Brindabella 1:100 000 Sheet areas. p39*. and Jones 1987 K-Ar isotopic dates, New South Wales. Geological Survey of NSW Report 1987/237. p 79.

Pain, C. F. (1983). Geomorphology of the Barrington Tops area, New South Wales. *Journal of the Geological Society of Australia*, 30(1-2), 187-194.

Pickett, J., Hill, R. Macphail, M. and Holmes, W. (1990). A stratigraphic evaluation of Ettingshausen's New England Tertiary plant localities. *Australian Journal of Earth Sciences* 37, 293–303.

Robertson, A. D. (1993). Bundaberg volcanic province. *Queensland Geology*,5, 44-87.

Robertson, A. D., Sutherland, F. L., and Hollis, J. D. (1985). Upper mantle xenoliths and megacrysts and the origin of the Brigooda basalt and breccia, near Proston, Queensland. Department of Geology, University of Queensland, 11, 58-71.

Ross, J. A. (1977). *The Tertiary Focal Peak Shield Volcano, South-east Queensland - a Geological Study of its Eastern Flank.* PhD thesis University of Queensland.

Ruxton, B. P., and Taylor, G. (1982). The Cainozoic geology of the middle Shoalhaven plain. *Journal of the Geological Society of Australia*, 29(1-2), 239-246.

Sharp, K. R. (2004). Cenozoic volcanism, tectonism and stream derangement in the Snowy Mountains and northern Monaro of New South Wales. *Australian Journal of Earth Sciences*, 51(1), 67-85.

Singleton, O. P., McDougall, I., and Mallett, C. W. (1976). The Pliocene-Pleistocene boundary in Southeastern Australia. *Journal of the Geological Society of Australia*, 23(3), 299-311.

Spry, M. J., Gibson, D. L., and Eggleton, R. A. (1999). Tertiary evolution of the coastal lowlands and the Clyde River palaeovalley in southeast New South Wales. *Australian Journal of Earth Sciences*, 46(2), 173-180.

Stipp, J. and McDougall, I. (1968). Potassium–argon ages from the Nandewar volcano, near Narrabri. New South Wales. *Australian Journal of Science*, 31(2), 84-85.

Sutherland, F. L. (1976). Cainozoic volcanic rocks. In: Leaman D. E. ed. *Geological Survey Explanatory Report. Sheet 82 (8312S). Hobart.* Tasmania Department of Mines, pp.111. Hobart., also UQ Isotope Geology Laboratory Report #2 (1971-1974)

Sutherland, F. L. (1977). Cainozoic Basalts Of The Mt. Fox Area, North Queensland. *Records of the Australian Museum* 30 532-543

Sutherland, F. L. (1985). Regional controls in eastern Australian volcanism. *Volcanism in eastern Australia (with case histories from New South Wales),* 13-32.

Sutherland, F. L. (1989). Cainozoic volcanic rocks. In: Forsyth S. M. ed. *Geological Survey Explanatory Report. Sheet 61 (8313N). Interlaken. T*asmania Department of Mines, pp.56. Hobart.

Sutherland, F. L. (1991). Cainozoic volcanism, eastern Australia: a predictive model based on migration over multiple 'hotspot' magma sources (Vol. 18, pp. 15-43). *Geological Society of Australia Special Publication.*

Sutherland, F. L. (1998). Origin Of North Queensland Cenozoic Volcanism: Relationships To Long Lava Flow Basaltic Fields, Australia. *Journal of Geophysical Research* B103 27347-27358

Sutherland, F. L. (2003). 'Boomerang' migratory intraplate Cenozoic volcanism, eastern Australian rift margins and the Indian-Pacific mantle boundary. In: Hillis R. R. and Mu¨ ller R. D. eds. *Evolution and Dynamics of the Australian Plate,* pp. 203–221. Geological Society of Australia Special Publication 22 and Geological Society of America Special Paper 372.

Sutherland, F. L., and Fanning, C. M. (2001). Gem-bearing basaltic volcanism, Barrington, New South Wales: Cenozoic evolution, based on basalt K–Ar ages and zircon fission track and U–Pb isotope dating*. *Australian Journal of Earth Sciences*, 48(2), 221-237.

Sutherland, F. L., Green, D. C., and Wyatt, B. W. (1973). Age of the Great Lake basalts, Tasmania, in relation to Australian Cainozoic volcanism. *Journal of the Geological Society of Australia*, 20(1), 85-93.

Sutherland, F. L., Graham, I. T., Pogson, R. E., Schwarz, D., Webb, G. B., Coenraads, R. R., and Allen, T. C. (2002). The Tumbarumba basaltic gem field, New South Wales: in relation to sapphire-ruby deposits of eastern Australia. *Records of the Australian museum*, 54(2), 215-248.

Sutherland, F.L., Graham, I.T. and Zwingmann, H. (2004). Late Cenozoic basalts, Uplands Province, N.E. Victoria: in relation to the newer volcanics basalts of western Victoria. *Proceedings of the Royal Society of Victoria*, 116, 51-68.

Sutherland F. L., Graham I. T., Zwingmann H., Pogson R. E., Barron B. J. (2005). Belmore Volcanic Province, Northeastern New South Wales, And Some Implications For Plume Variations Along Cenozoic Migratory Trails. *Australian Journal of Earth Sciences* 52 897-919

Sutherland, F. L., Graham, I. T., Forsyth, S. M., Zwingmann, H., and Everard, J. L. (2006). The Tamar Trough revisited: correlations berween sedimentary beds, basalts, their ages and valley evolution, North Tasmania. In Papers and Proceedings of the Royal Society of Tasmania 140, 49).

Sutherland F. L. Hendry D. F. Barron B. J. Matthews W. L. and Hollis J. D. (1996). An unusual Tasmanian Tertiary basalt sequence, near Boat Harbour, northwest Tasmania. *Records of the Australian Museum* 48, 131-161.

Sutherland F. L., Hollis J. D., Birch W. D., Pogson R. E., Raynor L. R. (2004). Cumulate-Rich Xenolith Suite In Late Cenozoic Basaltic Eruptives, Hepburn Lagoon, Newlyn, In Relation To Western Victorian Lithosphere . *Australian Journal of Earth Sciences* 51 319-337. After Green P. F. 2001. Fission track dating of apatite and zircon from Victoria. *Geotrack International, Brunswick West, Vic., Australia. Report 797 (unpubl.).*

Sutherland F. L., Pogson R. E. and Hollis J. D. (1993). Growth of the central New England basaltic gemfields, New South Wales, based on zircon fission track dating. In: Flood P. G. and Aitchison J. C. eds. *New England Orogen: Eastern Australia*, pp. 483–491. Department of Geology and Geophysics University of New England, Armidale.

Sutherland, F. L., Robertson, A. D., Hendry, D. F., and Hollis, J. D. (1990). Xenolith studies from southern Queensland: the lithosphere below volcanic regions. The Eromanga-Brisbane Transect. *BMR Bulletin*, 232, 213-235.

Sutherland F. L., Stubbs D. and Green D. C. (1977). K–Ar ages of Cainozoic volcanic suites, Bowen–St Lawrence Hinterland, north Queensland (with some implications for petrologic models*). Journal of the Geological Society of Australia* 24, 447–460.

Sutherland, F. L., and Wellman, P. (1986). Potassium-argon ages of Tertiary volcanic rocks, Tasmania. In *Papers and Proceedings of the Royal Society of Tasmania*, 120, 77-86.

Sutherland, F. L., Graham I., Meffre S., Zwingmann H., and Pogson R., (2012). Passive-margin prolonged volcanism, East Australian Plate: outbursts, progressions, plate controls and suggested causes. *Australian Journal of Earth Sciences* 59, 983 1005.

Sutherland, F. L., Graham, I. T., Hollis, J. D., Meffre, S., Zwingmann, H., Jourdan, F., and Pogson, R. E., (2014), Multiple felsic events within post-10 Ma volcanism, Southeast Australia: inputs in appraising proposed magmatic models. *Australian journal of Earth Sciences* 61, 241-267.

Tedford R. H., Banks M. R., Kemp N. R., McDougall I. and Sutherland F. L. (1975). Recognition of the oldest known fossil marsupials from Australia. *Nature* 255, 141–142.

Tickell (1991) *"Radiometric dating of the Tower Hill volcano and Colca Quarry"*. Geological Survey of Victoria, Unpublished Report 1991/38.

van der Beek, P., Pulford, A., and Braun, J. (2001). Cenozoic landscape development in the Blue Mountains (SE Australia): lithological and tectonic controls on rifted margin morphology. *The Journal of Geology*, 109(1), 35-56.

Vickery, Dawson, Sivell, Malloch, Dunlap (2007*). Quarterly Notes of the Geological Survey of New South Wales.* v123 p1-31.

Wallace D.A. and Ollier C.D. (1990). The Cainozoic lava flows of Barfold Gorge. *Victorian Naturalist,* 103(6), 175-177.

Webb, A. W., and McDougall, I. (1967). A comparison of mineral and whole rock potassium-argon ages of Tertiary volcanics from central Queensland, Australia. *Earth and Planetary Science Letters,* 3, 41-47.

Webb, A. W., Stevens, N. C. and McDougall, I. (1967). Isotopic age determinations on Tertiary volcanic rocks and intrusives of southeast Queensland. *Proceedings of the Royal Society of Queensland,* 79: 79–92.

Webb, A. W., Osborne, C. R., Taylor, D. H., and Cayley, R. A. (1998). K–Ar geochronology of Newer Volcanics on the Ballarat 1: 250 000 map sheet. *Geological Survey of Victoria Report, 10.*

Wellman, P. (1973). Early Miocene potassium–argon age for the Fitzroy lamproites of Western Australia. *Journal of the Geological Society of Australia* 19, 471–474.

Wellman, P. (1974). Potassium-Argon Ages Of The Cainozoic Volcanic Rocks Of Eastern Victoria, Australia . *J. Geol. Soc. Australia* 21 359-376

Wellman, P. (1978). K/Ar ages on the Cainozoic volcanic rocks from the Bundaberg, Rockhampton and Clermont areas of eastern Queensland. *Proceedings of the Royal Society of Queensland*, 89: 59–64.

Wellman, P., Cundari, A. and McDougall, I. (1970). Potassium–argon ages for leucite-bearing rocks from New South Wales, Australia. Journal and Proceedings of the Royal Society of New South Wales 103, 103–107.

Wellman P. and McDougall I. (1974b). Potassium–argon ages on the Cainozoic volcanic rocks of New South Wales. *Journal of the Geological Society of Australia* 21, 247–272.

Wellman P., McElhinny M. W. and McDougall I. (1969). On the polarwander path for Australia during the Cenozoic. *Geophysical Journal of the Royal Astronomical Society* 18, 371–395.

Wheeler and Kjellgren 1986, Yolla-1 Final Well Report (Amoco Australia Petroleum Company (unpubl.)

Whitehead P. W., Stephenson P. J., McDougall I., Hopkins M. S., Graham A. W., Collerson K. D. and Johnson D. P. (2007). Temporal development of the Atherton Basalt Province, north Queensland. *Australian Journal of Earth Sciences* 54, 691–709.

Wyatt, D. H. and Webb, A. W. (1970). K/Ar ages of some north Queensland basalts and an interpretation of Late Cainozoic history. *Journal of the Geological Society of Australia*, 17: 39–51.

Wyborn D. and Owen M. (1986). Araluen New South Wales 1:100 000 Geological Map Commentary. *Bureau of Mineral Resources,* Canberra.

Young, R. W. (1981). Denudational history of the south-central uplands of New South Wales. *The Australian Geographer*, 15(2), 77-88.

Young, R. W., and Bishop, P. (1980). Potassium-argon ages on Cainozoic volcanic-rocks in the Crookwell-Goulburn area, New-South-Wales. *Search*, 11(10), 340-341.

Young, R. W., and McDougall, I. (1982). Basalts and silcretes on the coast near Ulladulla, southern New South Wales. *Journal of the Geological Society of Australia*, 29(3-4), 425-430.

Appendix A: Sample locality

Sample	Location	UTM	Latitude	Longitude	Elev. (m)
CA3	Canobolas	55H	688796	6308909	1178
CA3	Canobolas	55H	688796	6308909	1178
CA6	Canobolas	55H	686456	6309225	1108
W11	Mt Exmouth, Warrumbungles	55J	685517	6534155	1096
W11	Mt Exmouth, Warrumbungles	55J	685517	6534155	1096
W14	Mt Exmouth, Warrumbungles	55J	686474	6533970	932
BB1	Beechmont basalt, Tweed	56J	523502	6896038	419
BRT1	Barrington Tops	56J	354223	6465157	1503
BRT10	Barrington Tops	56J	365636	6469984	1157
BRT2	Barrington Tops	56J	358379	6468134	1448
BRT3	Barrington Tops	56J	359711	6468369	1427
BRT5	Barrington Tops	56J	364828	6469998	1224
BRT7	Barrington Tops	56J	355580	6467098	1454
BRT9	Barrington Tops	56J	363961	6470127	1297
EB1	Ebor	56J	443404	6626996	1549
EB11	Ebor	56J	443354	6626919	1573
EB13	Ebor	56J	439464	6639810	1322
EB14	Ebor	56J	442074	6641622	1261
EB14	Ebor	56J	442074	6641622	1261
EB20	Ebor	56J	458532	6638753	1085
EB3	Ebor	56J	443411	6627037	1501
EB5	Ebor	56J	443406	6626838	1478
EB8	Ebor	56J	443172	6626681	1459
W1	Siding Spring road, Warrumbungles	56J	697143	6538241	1107
W3	Siding Spring road, Warrumbungles	56J	697995	6538517	1058
W4	Siding Spring road, Warrumbungles	56J	697701	6538472	1024
W4	Siding Spring road, Warrumbungles	56J	697701	6538472	1024
W6	Siding Spring road, Warrumbungles	56J	696908	6537382	920
IJS06	Springsure	55J	7333575	605515	569
IJS07	Springsure, Dawson Developmental Rd	55J	7330443	593105	497
IJS08	Springsure	55J	7330790	594271	316
IJS11	Springsure	55J	7360256	614585	245
IJLF01	Dawson Highway, Callide	56J	7307147	260778	313
TRLF01	Dawson Highway	56J	7272654	705695	388
TRLF04	Dawson Highway	56J	7276452	721654	28
TRLF05	Dawson Highway	56J	7271963	707174	373
CVLF01	Dawson Highway	56J	7321276	622152	442
PR01	Peak Range	55K	7527724	578419	369
PR02	Peak Range	55K	7506560	585055	369
PR04	Peak Range	55K	7493793	572522	286
PR05	Peak Range	55K	7492249	605872	413

PR07	Peak Range	55K	7487547	598782	391
PR08	Peak Range	55K	7486564	592705	351
PR09	Peak Range	55K	7480302	581260	287
Sample	**Location**	**Coord. System**	**Easting**	**Northing**	**Elev. (m)**
GM1	Near Gemini Mountains, Peak Range	GAD94	-22.46605	147.8741	363
GM2	Near Gemini Mountains, Peak Range	GAD94	-22.4657	147.87428	413
GM3	Near Gemini Mountains, Peak Range	GAD94	-22.46579	147.87468	421
KC3	Kalkarney Crator, McBride	GAD94	-18.21809	144.66824	846
KF1	Kilmorey Falls, Mitchell	GAD94	-26.08417	148.16182	553
M01	Moranbah road cutting, Peak Range	GAD94	-22.0555	148.12627	208
MC1	Mount Catherine, Springsure	GAD94	-24.40891	148.16695	588
MC2	Mount Catherine, Springsure	GAD94	-24.4087	148.16695	594
MC5	Mount Catherine, Springsure	GAD94	-24.41037	148.16545	512
MC6	Mount Catherine, Springsure	GAD94	-24.41069	148.16533	488
MC8	Mount Catherine, Springsure	GAD94	-24.41476	148.16779	423
MC9	Mount Catherine, Springsure	GAD94	-24.40305	148.15608	425
MHV04	Springsure	GAD94	-24.10975	148.03081	425
MHV05	Springsure	GAD94	-24.10135	148.04739	419
MHV06	Springsure	GAD94	-24.13557	147.91646	324
MHV07	Springsure	GAD94	-24.11604	148.07285	372
MHV09	Springsure	GAD94	-23.99122	147.92859	322
MHV10	Springsure	GAD94	-24.0578	147.93517	310
PK01	Policeman's Knob, Hoy	GAD94	-23.41987	147.66992	272
UR1	Kalkarney Crator, McBride	GAD94	-18.15344	144.70584	792
UR2	Road cutting, McBride	GAD94	-18.68849	144.71429	522
UR3	Road cutting, McBride	GAD94	-18.72643	144.32063	488
CIB	Bauhinia Downs	GAD94	-24.58054	149.26264	-
CIS	Springsure	GAD94	-24.09573	148.17414	-
CIK	West of Rolleston	GAD94	-23.93930	148.70663	-

Appendix B: $^{40}Ar/^{39}$ Ar Numerical data

Samples are arranged by laboratory number and presented in order of analysis date. Run 129 was analysed from the 25/12/2014 to 20/2/2017. The irradiation factors (J) are as follows:

Samples 8413 – 8429 J= 0.0021 ± 0.000005

Samples 8433 – 8436 J= 0.002088 ± 0.000005

Samples 9123 – 9126 J= 0.003694 ± 0.000005

Samples 9243 – 9260 J= 0.0037 ± 0.000006

Samples 9264 – 9282 J= 0.003699 ± 0.000004

The J-factor error was not included in the tabulated error in the ages presented in Appendix 2 but is used in the calculation of all plateau, isochron and ideogram ages reported in the text. Not including laser ramp-up, laser heating time was ~47 seconds. The mass spectrometer gain was calculated from analysis of air pipette (1.72×10^{-13} moles ^{40}Ar) on a faraday detector (~4 mV) fitted with a 10^{11} Ohm resistor, with a sensitivity of $\sim 4 \times 10^{-14}$ moles/mV. Abbreviations used in the data table are: W-R, whole rock; Plag., plagioclase; % Rad., % radiogenic argon; Discr., discrimination; P, parabolic fit; L, linear fit.

Irradiation correction factors for the CLICIT facility, TRIGA reactor, Oregon State University, USA are: $(2.64 \pm 0.02) \times 10^{-4}$ for ($^{36}Ar/^{37}Ar$) Ca, $(7.04 \pm 0.06) \times 10^{-4}$ for ($^{39}Ar/^{37}Ar$) Ca, and $(8 \pm 3) \times 10^{-4}$ for ($^{40}Ar/^{39}$ Ar) K.

Table A1: $^{40}Ar/^{39}Ar$ run numerical data summary.

Sample-Material	Run Date	Run Hour	Run ID	40Ar/39Ar	Er (1σ)	38Ar/39Ar	Er (1σ)	37Ar/39Ar	Er (1σ)	36Ar/39Ar	Er (1σ)	% Rad.	Er (1σ)	Age	Age Er	Moles 40Ar	Moles 39Ar	Discrim.	Er (1σ)	Laser (W)	Fit Type
CIS-W.R																					
	10/09/2014	14.10	8412-01A	11.71	0.07	0.017	0.0007	0.48	0.019	0.014	0.0005	63.9	1.2	28.15	0.58	1.36E-14	1.16E-15	**0.9996**	**0.0019**	0.1	PPLLLL
		15.10	8412-01B	10.91	0.08	0.014	0.0007	0.92	0.027	0.009	0.0005	77	1.4	31.54	0.6	1.20E-14	1.10E-15			0.2	PPLLLL
		16.03	8412-01C	9.684	0.08	0.012	0.0009	1.32	0.033	0.006	0.0005	82.3	1.6	29.98	0.61	8.21E-15	8.48E-16			0.3	PPLLLL
		16.88	8412-01D	9.037	0.06	0.012	0.0008	1.01	0.03	0.006	0.0004	82.2	1.4	27.95	0.51	9.60E-15	1.06E-15			0.4	PPLLLL
		17.88	8412-01E	8.182	0.07	0.012	0.0008	0.95	0.023	0.002	0.0004	92.2	1.3	28.38	0.45	1.05E-14	1.28E-15			0.49	PPLLLL
		18.74	8412-01F	7.995	0.06	0.013	0.0008	1.02	0.022	0.002	0.0003	95.1	1.4	28.58	0.45	9.60E-15	1.20E-15			0.59	PPLLLL
		19.63	8412-01G	7.844	0.03	0.013	0.0003	1.01	0.013	0.002	0.0001	94.27	0.47	27.82	0.17	3.61E-14	4.60E-15			0.79	PPLLLL
		20.54	8412-01H	7.685	0.04	0.013	0.0004	1.69	0.019	0.001	0.0002	95.93	0.68	27.75	0.22	2.36E-14	3.07E-15			0.99	PPLLLL
		21.44	8412-01I	7.716	0.05	0.013	0.0005	3.48	0.041	0.002	0.0003	97	1.1	28.19	0.36	1.49E-14	1.94E-15			1.48	PPLLLL
		22.29	8412-01J	7.7	0.07	0.012	0.0012	5.43	0.083	0.002	0.0005	99.5	2.2	28.9	0.67	6.09E-15	7.91E-16			1.98	PPLLLL
		23.10	8412-01K	7.798	0.06	0.012	0.0006	6.76	0.06	0.003	0.0003	95.9	1.4	28.24	0.44	1.10E-14	1.40E-15			3.45	PPLLLL
	10/10/2014	2.73	8412-02A	8.053	0.05	0.014	0.0006	0.42	0.013	0.006	0.0003	77.3	1.1	23.43	0.37	1.44E-14	1.79E-15			0.1	PPLLLL
		3.74	8412-02B	9.026	0.07	0.014	0.0006	0.91	0.028	0.002	0.0004	94.4	1.4	32	0.51	1.09E-14	1.21E-15			0.2	PPLLLL
		4.62	8412-02C	8.547	0.06	0.011	0.0007	1.19	0.036	0.002	0.0004	93.6	1.6	30.09	0.52	9.34E-15	1.09E-15			0.3	PPLLLL
		5.52	8412-02D	8.246	0.06	0.012	0.0006	1.01	0.026	0.001	0.0003	95.7	1.2	29.66	0.42	1.19E-14	1.44E-15			0.4	PPLLLL
		6.46	8412-02E	7.97	0.05	0.012	0.0005	0.91	0.017	3E-04	0.0004	99.7	1.5	29.87	0.47	1.52E-14	1.91E-15			0.49	LPLLPL
		7.30	8412-02F	7.725	0.05	0.012	0.0005	0.83	0.02	0.001	0.0003	96.9	1.1	28.16	0.35	1.27E-14	1.64E-15			0.59	PPLLLL
		8.24	8412-02G	7.675	0.03	0.013	0.0003	0.96	0.017	0.001	0.0002	96.27	0.62	27.79	0.21	2.88E-14	3.75E-15			0.79	PPLLLL
		9.05	8412-02H	7.839	0.03	0.013	0.0002	1.05	0.0082	0.002	0.0001	95.25	0.5	28.08	0.18	7.45E-14	9.51E-15			0.99	PPLLPL
		9.88	8412-02I	7.64	0.03	0.013	0.0002	1.59	0.01	0.001	0.0001	96.99	0.45	27.89	0.17	6.67E-14	8.72E-15			1.48	PPLLPL
		10.78	8412-02J	7.788	0.05	0.012	0.0006	2.53	0.037	0.002	0.0003	93.9	1.2	27.55	0.39	1.17E-14	1.51E-15			1.98	PPLLLL
		11.67	8412-02K	7.706	0.04	0.012	0.0003	4.61	0.04	0.002	0.0003	97.2	1.4	28.25	0.42	2.01E-14	2.61E-15			3.45	PPLLPL

IJSO8B-W.R																					
	10/10/2014	15.21	8413-01A	14.04	0.66	0.024	0.0066	4.79	0.33	0.011	0.0044	78.8	9.4	41.6	5.3	1.33E-15	9.47E-17	**0.9996**	**0.0019**	0.1	PPLLLL
		15.98	8413-01B	8.94	0.11	0.009	0.0014	2.72	0.074	8E-04	0.0008	99.6	2.7	33.48	0.96	4.55E-15	5.09E-16			0.2	PPLLLL
		16.79	8413-01C	8.541	0.09	0.012	0.0009	2.44	0.05	0.003	0.0005	92.8	2	29.83	0.69	6.51E-15	7.62E-16			0.3	PPLLLL
		17.54	8413-01D	7.898	0.06	0.011	0.0006	1.79	0.031	1E-04	0.0003	101.4	1.3	30.12	0.41	1.05E-14	1.33E-15			0.4	PPLLLL
		18.39	8413-01E	7.513	0.06	0.012	0.0007	1.42	0.03	4E-04	0.0003	99.7	1.3	28.18	0.42	9.88E-15	1.32E-15			0.49	PPLLLL
		19.24	8413-01F	7.582	0.05	0.013	0.0009	1.13	0.031	-0	0.0004	102.5	1.6	29.24	0.48	6.98E-15	9.20E-16			0.59	PLLLLL
		19.99	8413-01G	7.442	0.07	0.011	0.0011	1.50	0.041	-0	0.0005	102.8	2.1	28.77	0.63	5.97E-15	8.03E-16			0.79	PPLLLL
		20.80	8413-01H	7.687	0.06	0.011	0.0008	2.81	0.049	1E-03	0.0005	99	2	28.67	0.6	6.08E-15	7.91E-16			0.99	PLLLLL
		21.57	8413-01I	7.63	0.06	0.009	0.0007	6.58	0.091	0.002	0.0004	99.5	1.8	28.65	0.54	8.09E-15	1.06E-15			1.48	PPLLLL
		22.38	8413-01J	7.431	0.10	0.011	0.0015	8.80	0.15	0.003	0.0009	98.9	3.7	27.8	1.1	3.20E-15	4.30E-16			1.98	PPLLLL
		23.11	8413-01K	7.802	0.09	0.016	0.0013	18.34	0.25	0.007	0.0008	92.6	3.7	27.5	1.1	3.82E-15	4.90E-16			3.45	PPLLLL
	10/11/2014	2.56	8413-02A	10.34	0.30	0.011	0.0042	5.75	0.24	0.012	0.0029	71	8.3	27.7	3.3	1.55E-15	1.50E-16			0.1	PPLLLL
		3.33	8413-02B	8.73	0.11	0.01	0.0012	2.64	0.059	0.002	0.0008	96.3	2.7	31.63	0.95	4.45E-15	5.10E-16			0.2	PPLLLL
		4.12	8413-02C	7.894	0.07	0.009	0.0008	2.18	0.037	1E-03	0.0004	98.5	1.7	29.25	0.53	8.17E-15	1.04E-15			0.3	PPLLLL
		5.01	8413-02D	7.554	0.05	0.012	0.0006	1.49	0.026	5E-04	0.0003	99.8	1.3	28.35	0.38	1.01E-14	1.34E-15			0.4	PPLLLL
		5.84	8413-02E	7.624	0.05	0.012	0.0008	0.93	0.028	0.001	0.0005	95.3	2.2	27.33	0.63	8.98E-15	1.18E-15			0.49	PPLLPL
		6.74	8413-02F	7.586	0.07	0.012	0.0009	0.76	0.025	0.001	0.0005	96.6	1.9	27.56	0.58	6.57E-15	8.66E-16			0.59	PPLLLL
		7.58	8413-02G	7.631	0.06	0.013	0.0008	1.90	0.042	0.001	0.0005	96.2	1.9	27.64	0.56	7.18E-15	9.41E-16			0.79	PPLLLL
		8.36	8413-02H	7.545	0.05	0.013	0.0010	3.24	0.055	0.002	0.0005	95.4	2.1	27.11	0.59	6.00E-15	7.95E-16			0.99	PLLLLL
		9.23	8413-02I	7.479	0.07	0.013	0.0007	6.12	0.097	0.003	0.0004	95.8	1.8	27.05	0.53	7.23E-15	9.66E-16			1.48	PPLLLL
		10.02	8413-02J	7.565	0.06	0.012	0.0013	10.58	0.12	0.004	0.0008	94.9	3.4	27.2	0.98	4.00E-15	5.28E-16			1.98	PLLLLL
		10.77	8413-02K	7.527	0.10	0.014	0.0018	16.46	0.25	0.005	0.0012	98.9	4.9	28.3	1.4	2.98E-15	3.96E-16			3.46	PPLLLL
CVLF01-W.R																					
	10/11/2014	14.24	8415-01A	23.81	0.38	0.023	0.0024	1.89	0.074	0.066	0.0023	18.3	2.7	16.5	2.5	7.67E-15	3.22E-16	**0.9996**	**0.0019**	0.1	PPLLLL
		15.23	8415-01B	9.952	0.09	0.012	0.0008	1.52	0.037	0.011	0.0006	69.1	1.7	25.9	0.67	8.46E-15	8.50E-16			0.2	PPLLLL
		16.04	8415-01C	8.276	0.05	0.012	0.0005	1.07	0.018	0.004	0.0003	88.04	0.99	27.41	0.33	1.63E-14	1.96E-15			0.3	PPLLLL

		16.88	8415-01D	7.959	0.04	0.013	0.0004	0.78	0.014	0.002	0.0002	94.22	0.65	28.2	0.23	2.23E-14	2.80E-15	**0.998**	**0.0019**	0.4	PPLLLL
		17.81	8415-01E	7.664	0.04	0.012	0.0004	0.92	0.016	0.001	0.0003	96	1.3	27.67	0.39	1.81E-14	2.36E-15			0.49	PPLLPL
		18.75	8415-01F	7.771	0.06	0.013	0.0007	1.03	0.029	0.002	0.0003	93.5	1.3	27.33	0.42	1.13E-14	1.45E-15			0.59	PPLLLL
		19.59	8415-01G	7.868	0.05	0.012	0.0005	0.96	0.02	0.002	0.0005	94.6	1.7	28.01	0.53	1.41E-14	1.80E-15			0.79	LPLLPL
		20.46	8415-01H	7.94	0.06	0.015	0.0007	2.30	0.04	0.004	0.0003	88.5	1.3	26.48	0.43	1.10E-14	1.39E-15			0.99	LPLLLL
		21.28	8415-01I	8.075	0.07	0.014	0.0007	7.11	0.075	0.006	0.0004	85.2	1.8	26	0.57	8.99E-15	1.11E-15			1.48	PPLLLL
		22.18	8415-01J	7.978	0.07	0.013	0.0010	6.68	0.089	0.003	0.0006	93.7	2.3	28.21	0.71	6.31E-15	7.90E-16			1.98	PPLLLL
		22.98	8415-01K	7.87	0.06	0.013	0.0005	7.98	0.09	0.004	0.0003	91.9	1.5	27.33	0.48	1.20E-14	1.52E-15			3.45	PPLLLL
	10/12/2014	2.55	8415-02A	21.47	0.32	0.024	0.0019	1.95	0.075	0.053	0.0019	26.4	2.5	21.3	2.1	7.74E-15	3.60E-16	**0.998**	**0.0019**	0.1	PPLLLL
		3.54	8415-02B	10.27	0.09	0.016	0.0010	1.67	0.032	0.011	0.0006	69.5	1.6	26.86	0.66	9.76E-15	9.50E-16			0.2	PPLLLL
		4.46	8415-02C	8.265	0.05	0.012	0.0005	1.14	0.021	0.004	0.0002	87.86	0.91	27.32	0.31	1.72E-14	2.08E-15			0.3	PPLLLL
		5.32	8415-02D	7.716	0.04	0.011	0.0004	0.91	0.016	0.002	0.0002	94.14	0.69	27.33	0.23	2.26E-14	2.93E-15			0.4	PPLLLL
		6.18	8415-02E	7.628	0.04	0.012	0.0004	0.93	0.017	8E-04	0.0002	98.01	0.71	28.12	0.23	2.22E-14	2.91E-15			0.49	PPLLLL
		7.03	8415-02F	7.676	0.05	0.011	0.0005	1.14	0.018	9E-04	0.0003	97.8	1.1	28.24	0.35	1.35E-14	1.75E-15			0.59	PPLLLL
		7.96	8415-02G	7.76	0.04	0.012	0.0003	0.96	0.018	8E-04	0.0002	97.83	0.88	28.55	0.28	1.83E-14	2.36E-15			0.79	PPLLLL
		8.85	8415-02H	7.675	0.04	0.011	0.0007	1.81	0.033	0.001	0.0003	96.9	1.1	27.98	0.34	1.38E-14	1.79E-15			0.99	PPLLLL
		9.71	8415-02I	7.815	0.06	0.015	0.0008	5.89	0.071	0.002	0.0004	97.5	1.5	28.76	0.47	1.08E-14	1.38E-15			1.48	PPLLLL
		10.56	8415-02J	7.926	0.06	0.015	0.0008	7.66	0.087	0.004	0.0004	92.1	1.7	27.59	0.52	8.71E-15	1.10E-15			1.98	PPLLLL
		11.38	8415-02K	7.826	0.04	0.012	0.0005	8.00	0.065	0.003	0.0003	95.6	1.4	28.27	0.42	1.57E-14	2.01E-15			3.45	PPLLLL
IJS11B-W.R																					
	10/12/2014	15.07	8416-01A	11.85	0.08	0.017	0.0004	0.35	0.0091	0.015	0.0003	63.26	0.84	28.18	0.43	3.46E-14	2.92E-15	**0.998**	**0.0019**	0.1	PPLLLL
		16.01	8416-01B	8.721	0.04	0.013	0.0004	0.76	0.012	0.002	0.0002	95.36	0.57	31.25	0.22	2.73E-14	3.12E-15			0.2	PPLLLL
		16.90	8416-01C	8.117	0.03	0.013	0.0003	1.27	0.013	0.001	0.0002	95.95	0.71	29.29	0.23	3.42E-14	4.21E-15			0.3	PPLLPL
		17.80	8416-01D	8.049	0.03	0.013	0.0003	0.99	0.016	0.001	0.0002	96.59	0.79	29.23	0.26	2.99E-14	3.72E-15			0.4	PPLLPL
		18.68	8416-01E	7.925	0.04	0.013	0.0004	0.79	0.014	0.002	0.0003	94	1	28	0.32	2.63E-14	3.32E-15			0.49	PPLLPL
		19.55	8416-01F	7.613	0.04	0.014	0.0004	0.77	0.016	6E-04	0.0002	98.37	0.99	28.16	0.3	2.27E-14	2.99E-15			0.59	PPLLPL
		20.41	8416-01G	7.519	0.03	0.013	0.0004	1.16	0.016	8E-04	0.0003	98	1.1	27.71	0.32	2.43E-14	3.23E-15			0.79	PPLLPL

		21.23	8416-01H	7.505	0.04	0.013	0.0005	1.85	0.032	0.002	0.0002	92.98	0.94	26.28	0.3	1.44E-14	1.92E-15			0.99	LPLLLL
		22.08	8416-01I	7.768	0.05	0.015	0.0005	4.78	0.05	0.003	0.0003	92.9	1.1	27.22	0.35	1.61E-14	2.07E-15			1.48	PPLLLL
		22.92	8416-01J	7.675	0.04	0.016	0.0006	4.39	0.045	0.003	0.0003	92.2	1.3	26.7	0.38	1.29E-14	1.68E-15			1.98	PPLLLL
		23.86	8416-01K	7.744	0.03	0.015	0.0002	5.58	0.039	0.003	0.0001	94.62	0.71	27.65	0.22	4.73E-14	6.10E-15			3.45	PPLLLL
	10/13/2014	3.48	8416-02A	12.77	0.13	0.016	0.0007	0.28	0.016	0.017	0.0005	59.6	1.2	28.61	0.65	1.77E-14	1.38E-15	**0.998**	**0.0019**	0.09	PPLLLL
		4.44	8416-02B	8.817	0.05	0.015	0.0005	0.53	0.013	0.002	0.0002	92.55	0.81	30.66	0.31	2.03E-14	2.30E-15			0.2	PPLLLL
		5.34	8416-02C	8.358	0.04	0.013	0.0003	1.01	0.017	0.001	0.0001	95.61	0.57	30.04	0.21	2.93E-14	3.50E-15			0.3	PPLLLL
		6.18	8416-02D	8.193	0.04	0.012	0.0003	1.04	0.014	0.001	0.0001	97	0.56	29.88	0.2	2.77E-14	3.38E-15			0.39	PPLLLL
		7.03	8416-02E	7.981	0.04	0.012	0.0003	0.74	0.015	8E-04	0.0002	97.82	0.64	29.35	0.23	2.06E-14	2.58E-15			0.49	PPLLLL
		7.87	8416-02F	7.807	0.05	0.013	0.0005	0.71	0.018	0.001	0.0002	95.67	0.83	28.09	0.29	1.81E-14	2.32E-15			0.59	PPLLLL
		8.70	8416-02G	7.637	0.04	0.013	0.0004	0.95	0.017	9E-04	0.0002	97.34	0.72	27.96	0.24	2.02E-14	2.64E-15			0.79	PPLLLL
		9.57	8416-02H	7.605	0.04	0.012	0.0004	1.38	0.022	0.001	0.0002	97.02	0.8	27.76	0.25	1.77E-14	2.33E-15			0.99	PPLLLL
		10.41	8416-02I	7.767	0.04	0.014	0.0005	3.98	0.038	0.002	0.0002	94.38	0.95	27.63	0.3	1.67E-14	2.15E-15			1.48	PPLLLL
		11.31	8416-02J	7.819	0.05	0.013	0.0006	4.60	0.044	0.002	0.0003	95.5	1.1	28.15	0.35	1.44E-14	1.84E-15			1.98	PPLLLL
		12.23	8416-02K	7.929	0.03	0.016	0.0003	5.02	0.037	0.003	0.0001	93.81	0.71	28.06	0.23	3.72E-14	4.69E-15			3.45	PPLLLL
CIK-W.R																					
	10/13/2014	15.97	8418-01A	17.66	0.44	0.024	0.0023	0.67	0.059	0.034	0.0019	42.2	3.2	28	2.2	5.83E-15	3.30E-16	**0.998**	**0.0019**	0.14	PPLLLL
		16.76	8418-01B	9.82	0.20	0.019	0.0022	1.14	0.066	0.007	0.0012	80.7	3.8	29.8	1.5	3.69E-15	3.75E-16			0.2	PPLLLL
		17.51	8418-01C	8.48	0.06	0.016	0.0007	0.64	0.019	0.002	0.0003	95.2	1.3	30.33	0.44	1.14E-14	1.35E-15			0.3	PPLLLL
		18.42	8418-01D	7.823	0.03	0.013	0.0003	0.37	0.01	4E-04	0.0002	98.71	0.8	29.02	0.26	2.84E-14	3.63E-15			0.4	PPLLPL
		19.26	8418-01E	7.801	0.04	0.013	0.0005	0.42	0.014	8E-04	0.0003	97.2	1.2	28.52	0.38	1.88E-14	2.41E-15			0.49	PPLLPL
		20.11	8418-01F	7.664	0.05	0.012	0.0005	0.38	0.01	7E-04	0.0002	97.82	0.87	28.18	0.29	1.68E-14	2.20E-15			0.59	PPLLLL
		20.95	8418-01G	7.69	0.05	0.013	0.0005	0.58	0.015	9E-04	0.0002	97.25	0.89	28.12	0.29	1.73E-14	2.26E-15			0.79	PPLLLL
		21.88	8418-01H	7.643	0.05	0.012	0.0005	1.38	0.025	5E-04	0.0002	99.35	1	28.56	0.32	1.50E-14	1.96E-15			0.99	PPLLLL
		22.75	8418-01I	7.557	0.04	0.013	0.0005	2.29	0.034	0.001	0.0002	97.78	0.94	27.82	0.3	1.41E-14	1.87E-15			1.48	LPLLLL
		23.58	8418-01J	7.704	0.04	0.012	0.0004	2.46	0.034	8E-04	0.0002	99.45	0.93	28.84	0.3	1.56E-14	2.02E-15			1.98	LPLLLL
	10/14/2014	0.40	8418-01K	7.573	0.03	0.013	0.0002	3.44	0.022	0.001	0.0001	99.28	0.64	28.33	0.2	5.21E-14	6.88E-15			3.45	PPLLPL

	10/14/2014	3.97	8418-02A	13.02	0.24	0.02	0.0010	0.71	0.03	0.022	0.0007	50.6	2.2	24.8	1.1	1.26E-14	9.68E-16	**0.998**	**0.0019**	0.1	PPLLLL
		5.04	8418-02B	9.71	0.14	0.021	0.0028	1.12	0.068	0.008	0.0012	76.9	3.8	28.1	1.4	3.78E-15	3.90E-16			0.2	PPLLLL
		5.89	8418-02C	8.098	0.04	-0	0.0003	0.79	0.015	8E-04	0.0002	97.63	0.79	29.72	0.26	1.74E-14	2.14E-15			0.3	PPLLLL
		6.65	8418-02D	7.711	0.04	2E-04	0.0002	0.67	0.013	7E-04	0.0002	97.88	0.66	28.38	0.22	2.20E-14	2.86E-15			0.4	PPLLLL
		7.40	8418-02E	7.75	0.05	4E-04	0.0003	0.32	0.013	1E-03	0.0002	96.53	0.84	28.13	0.29	1.69E-14	2.18E-15			0.49	PPLLLL
		8.17	8418-02F	7.786	0.05	1E-04	0.0003	0.43	0.017	1E-03	0.0003	96.6	1.1	28.28	0.34	1.29E-14	1.66E-15			0.59	PPLLLL
		8.88	8418-02G	7.585	0.04	5E-05	0.0003	0.70	0.016	1E-03	0.0002	96.8	0.94	27.62	0.29	1.49E-14	1.97E-15			0.79	PPLLLL
		9.66	8418-02H	7.629	0.05	2E-04	0.0003	1.53	0.03	0.001	0.0003	96.2	1.2	27.62	0.36	1.24E-14	1.62E-15			0.99	PPLLLL
		10.41	8418-02I	7.572	0.05	7E-04	0.0002	2.87	0.035	0.001	0.0002	97.83	0.93	27.9	0.3	1.70E-14	2.24E-15			1.48	PPLLLL
		11.18	8418-02J	7.582	0.05	3E-04	0.0003	2.86	0.035	0.002	0.0002	96.42	0.99	27.54	0.31	1.51E-14	1.99E-15			1.98	PPLLLL
		11.95	8418-02K	7.701	0.03	4E-04	0.0001	3.98	0.031	0.002	0.0001	97.43	0.59	28.28	0.19	4.52E-14	5.86E-15			3.45	PPLLLL
TRLF04-W.R																					
	10/14/2014	15.47	8419-01A	27.19	0.33	0.031	0.0015	1.95	0.054	0.072	0.0016	21	1.5	21.6	1.7	1.32E-14	4.84E-16	**0.998**	**0.0019**	0.16	PPLLLL
		16.45	8419-01B	10.73	0.08	0.014	0.0008	0.91	0.026	0.009	0.0005	75.4	1.4	30.41	0.61	1.16E-14	1.08E-15	**0.9996**	**0.0018**	0.2	PPLLLL
		17.36	8419-01C	8.934	0.05	0.012	0.0004	0.63	0.013	0.004	0.0002	86.27	0.69	28.97	0.28	2.32E-14	2.59E-15			0.3	PPLLLL
		18.31	8419-01D	8.335	0.03	0.013	0.0002	0.63	0.011	0.002	0.0002	92.56	0.57	29	0.2	2.70E-14	3.24E-15			0.4	PPLLLL
		19.24	8419-01E	7.874	0.04	0.012	0.0004	0.87	0.015	0.001	0.0002	95.72	0.78	28.35	0.26	2.01E-14	2.56E-15			0.49	PPLLLL
		20.10	8419-01F	7.715	0.04	0.012	0.0005	1.02	0.018	8E-04	0.0002	97.88	0.95	28.4	0.3	1.57E-14	2.03E-15			0.59	PPLLLL
		20.98	8419-01G	7.615	0.04	0.013	0.0003	0.93	0.016	0.001	0.0002	96.44	0.68	27.62	0.22	2.26E-14	2.97E-15			0.79	PPLLLL
		21.83	8419-01H	7.491	0.04	0.012	0.0004	2.01	0.027	1E-03	0.0002	98.13	0.98	27.67	0.31	1.53E-14	2.04E-15			0.99	PPLLLL
		22.69	8419-01I	7.615	0.06	0.013	0.0006	7.36	0.078	0.002	0.0004	100.4	1.6	28.88	0.5	1.09E-14	1.43E-15			1.48	PPLLLL
		23.57	8419-01J	7.538	0.06	0.013	0.0006	6.35	0.071	0.002	0.0005	97.3	2.1	27.71	0.63	7.21E-15	9.56E-16			1.98	PPLLLL
	10/15/2014	0.39	8419-01K	7.6	0.04	0.013	0.0004	8.32	0.074	0.003	0.0002	97.2	1.1	27.92	0.33	2.37E-14	3.12E-15			3.45	PPLLLL
	10/15/2014	4.10	8419-02A	35.25	0.43	0.034	0.0012	1.63	0.034	0.095	0.0015	19.68	0.95	26.1	1.5	3.66E-14	1.04E-15	**0.9996**	**0.0018**	0.13	PPLLLL
		5.03	8419-02B	11.65	0.12	0.012	0.0011	0.80	0.043	0.013	0.0007	67.6	1.9	29.62	0.87	7.20E-15	6.18E-16			0.2	PPLLLL
		5.92	8419-02C	10.64	0.07	0.014	0.0006	0.67	0.02	0.011	0.0004	70.3	1.1	28.15	0.47	1.54E-14	1.45E-15			0.3	PPLLLL

		6.88	8419-02D	8.099	0.04	0.011	0.0004	0.66	0.012	0.002	0.0002	94.07	0.75	28.64	0.25	2.07E-14	2.56E-15			0.4	PPLLLL
		7.80	8419-02E	8.024	0.06	0.01	0.0006	1.00	0.019	0.002	0.0003	93.2	1.1	28.12	0.36	1.38E-14	1.72E-15			0.49	PPLLLL
		8.68	8419-02F	7.97	0.05	0.01	0.0006	0.96	0.022	0.002	0.0003	95.1	1.1	28.5	0.35	1.40E-14	1.75E-15			0.59	PPLLLL
		9.65	8419-02G	7.746	0.04	0.012	0.0003	1.06	0.017	0.002	0.0001	94.56	0.6	27.56	0.21	2.51E-14	3.23E-15			0.79	PPLLLL
		10.57	8419-02H	7.674	0.06	0.012	0.0008	4.29	0.077	0.002	0.0004	97.7	1.6	28.26	0.5	8.26E-15	1.08E-15			0.99	PPLLLL
		11.38	8419-02I	7.581	0.06	0.011	0.0007	6.67	0.082	0.003	0.0003	96.8	1.5	27.7	0.47	1.03E-14	1.35E-15			1.48	PPLLLL
		12.21	8419-02J	7.662	0.06	0.013	0.0011	7.58	0.083	0.003	0.0005	96.3	2.1	27.87	0.61	7.63E-15	9.96E-16			1.98	PPLLLL
		13.03	8419-02K	7.617	0.06	0.015	0.0007	9.49	0.097	0.004	0.0003	95.1	1.7	27.42	0.51	1.06E-14	1.39E-15			3.45	PPLLLL
TRLF01-W.R																					
	12/23/2014	14.13	8421-01A	13.14	0.08	0.016	0.0007	0.71	0.042	0.013	0.0004	70.03	0.9	34.55	0.49	2.07E-14	1.58E-15	**0.9996**	**0.0018**	0.1	PPLLLL
		14.97	8421-01B	8.858	0.05	0.014	0.0005	1.94	0.048	0.003	0.0004	91.6	1.3	30.51	0.44	2.05E-14	2.31E-15			0.2	PPLLPL
		15.83	8421-01C	7.759	0.05	0.013	0.0006	4.63	0.11	0.003	0.0003	91.6	1.4	26.8	0.42	9.68E-15	1.25E-15			0.3	PPLLLL
		16.70	8421-01D	7.416	0.07	0.016	0.0011	5.92	0.2	0.003	0.0005	92.9	2.3	26.01	0.67	4.60E-15	6.20E-16			0.4	PPLLLL
		17.50	8421-01E	6.779	0.08	0.014	0.0015	6.38	0.26	0.002	0.0021	97.8	9.3	25.1	2.4	1.91E-15	2.81E-16			0.49	PLLLPL
		18.28	8421-01F	6.99	0.23	0.021	0.0043	16.02	0.9	0.01	0.0047	77	20	20.4	5.4	7.36E-16	1.05E-16			0.59	PPLLPL
		19.03	8421-01G	7.4	0.14	0.021	0.0028	30.65	0.83	0.014	0.0017	76.8	7.6	21.9	2.2	1.41E-15	1.91E-16			0.79	PPLLLL
		19.77	8421-01H	7.29	0.31	0.021	0.0067	35.30	2	0.019	0.0045	60	19	16.9	5.3	5.55E-16	7.62E-17			0.99	PPLLLL
		20.59	8421-01I	7.29	0.26	0.025	0.0049	47.10	1.9	0.023	0.0036	54	15	15.5	4.3	6.42E-16	8.81E-17			1.48	PPLLLL
		21.35	8421-01J	7.17	0.50	0.021	0.0110	69.90	4.7	0.036	0.0077	24	32	6.9	9.1	2.96E-16	4.12E-17			1.98	PPLLLL
		22.19	8421-01K	8.15	0.83	0.022	0.0160	98.60	9.7	0.03	0.0110	82	41	27	14	2.30E-16	2.82E-17			2.96	PPLLLL
	12/24/2014	1.71	8421-02A	16.63	0.13	0.019	0.0008	0.63	0.065	0.024	0.0007	58	1.2	36.16	0.8	1.66E-14	9.97E-16	**0.9996**	**0.0018**	0.1	PPLLLL
		2.63	8421-02B	9.724	0.05	0.015	0.0004	1.06	0.044	0.003	0.0002	90.41	0.58	33.03	0.27	2.69E-14	2.76E-15			0.2	PPLLLL
		3.43	8421-02C	8.144	0.04	0.014	0.0004	3.28	0.067	0.002	0.0003	96.1	1.2	29.48	0.37	1.73E-14	2.13E-15			0.3	PPLLPL
		4.34	8421-02D	7.562	0.05	0.016	0.0007	5.33	0.11	0.004	0.0005	87.9	2.1	25.1	0.62	8.28E-15	1.10E-15			0.4	PPLLPL
		5.14	8421-02E	7.206	0.07	0.018	0.0011	7.22	0.22	0.004	0.0005	89.9	2.4	24.5	0.67	4.20E-15	5.83E-16			0.49	PPLLLL
		5.92	8421-02F	6.418	0.08	0.019	0.0016	6.46	0.29	0.005	0.0018	84.3	8.3	20.5	2	2.13E-15	3.32E-16			0.59	PLLLPL
		6.67	8421-02G	6.89	0.16	0.022	0.0032	17.49	0.72	0.016	0.0020	49.4	9	13	2.4	1.10E-15	1.59E-16			0.79	PPLLLL

		7.46	8421-02H	7.88	0.20	0.022	0.0040	27.00	1	0.012	0.0038	79	15	23.9	4.5	1.02E-15	1.29E-16			0.99	PPLLPL
		8.23	8421-02I	7.41	0.15	0.021	0.0025	36.28	0.86	0.016	0.0015	72.3	7	20.7	2	1.61E-15	2.18E-16			1.48	PPLLLL
		9.07	8421-02J	7.11	0.41	0.027	0.0074	38.00	2.3	0.006	0.0051	115	22	31.6	6.2	4.11E-16	5.78E-17			1.98	PPLLLL
		9.84	8421-02K	7.21	0.24	0.028	0.0044	62.60	2.2	0.023	0.0033	70	15	19.9	4.3	7.34E-16	1.02E-16			2.96	PPLLLL
CIB-W.R																					
	12/24/2014	13.38	8422-01A	421	12.00	0.27	0.0097	4.13	0.28	1.401	0.0400	0.61	0.67	10	16	8.75E-14	2.08E-16	**0.9996**	**0.0018**	0.1	PPLLLL
		14.18	8422-01B	26.58	0.10	0.026	0.0006	1.48	0.057	0.063	0.0008	29.9	0.83	29.89	1	4.50E-14	1.69E-15			0.2	PLLLLL
		15.06	8422-01C	12.53	0.05	0.015	0.0004	1.24	0.038	0.018	0.0003	58.3	0.62	27.49	0.35	3.93E-14	3.13E-15			0.3	PPLLLL
		16.04	8422-01D	10.82	0.05	0.014	0.0004	1.31	0.045	0.012	0.0003	68	0.85	27.69	0.38	2.08E-14	1.92E-15			0.39	PPLLLL
		17.00	8422-01E	11.31	0.08	0.015	0.0006	2.42	0.081	0.015	0.0005	62.2	1.4	26.51	0.63	1.17E-14	1.04E-15			0.49	LPLLLL
		17.85	8422-01F	10.42	0.07	0.016	0.0009	2.46	0.1	0.013	0.0006	63.9	1.8	25.09	0.73	6.83E-15	6.55E-16			0.59	PLLLLL
		18.57	8422-01G	10.07	0.07	0.014	0.0007	2.55	0.086	0.011	0.0004	69.6	1.3	26.39	0.52	1.07E-14	1.06E-15			0.79	PPLLLL
		19.36	8422-01H	9.902	0.07	0.016	0.0010	4.66	0.14	0.01	0.0007	73.7	2	27.53	0.77	6.26E-15	6.32E-16			0.99	PLLLLL
		20.16	8422-01I	9.34	0.12	0.015	0.0013	7.88	0.2	0.01	0.0007	73.6	2.4	26.01	0.89	4.82E-15	5.16E-16			1.48	PPLLLL
		20.92	8422-01J	9.4	0.11	0.016	0.0013	10.63	0.27	0.012	0.0009	70.3	3.1	25	1.1	4.20E-15	4.46E-16			1.98	PPLLLL
		21.71	8422-01K	9.882	0.08	0.015	0.0007	21.24	0.3	0.016	0.0005	67.6	2.3	25.49	0.9	8.74E-15	8.84E-16			2.96	PPLLLL
	12/25/2014	1.19	8422-02A	307.5	6.70	0.21	0.0072	6.10	0.31	1.004	0.0230	2.64	0.72	31	12	6.82E-14	2.22E-16	**0.9994**	**0.0018**	0.1	PPLLLL
		2.01	8422-02B	32.72	0.18	0.03	0.0005	1.78	0.049	0.086	0.0009	22.13	0.73	27.3	1.2	6.66E-14	2.03E-15			0.2	PPLLLL
		2.88	8422-02C	10.96	0.04	0.016	0.0002	1.23	0.018	0.013	0.0002	65.19	0.52	26.9	0.27	6.77E-14	6.17E-15			0.3	PPLLLL
		3.69	8422-02D	9.791	0.04	0.015	0.0002	1.18	0.025	0.009	0.0002	72.51	0.52	26.72	0.24	5.56E-14	5.67E-15			0.39	PPLLLL
		4.62	8422-02E	9.787	0.04	0.014	0.0003	1.80	0.04	0.01	0.0002	71.38	0.76	26.31	0.32	2.70E-14	2.76E-15			0.49	PPLLLL
		5.59	8422-02F	10.34	0.06	0.013	0.0005	2.83	0.078	0.012	0.0004	68.4	1.1	26.65	0.45	1.56E-14	1.51E-15			0.59	PPLLLL
		6.60	8422-02G	9.583	0.05	0.014	0.0004	2.74	0.059	0.009	0.0003	75.02	0.97	27.08	0.38	1.95E-14	2.03E-15			0.79	PPLLLL
		7.48	8422-02H	9.46	0.06	0.012	0.0005	4.17	0.088	0.009	0.0004	74.7	1.3	26.66	0.49	1.40E-14	1.48E-15			0.99	PPLLLL
		8.37	8422-02I	9.154	0.07	0.015	0.0007	5.76	0.13	0.009	0.0004	76	1.4	26.28	0.52	9.37E-15	1.02E-15			1.48	PPLLLL
		9.20	8422-02J	9.182	0.06	0.013	0.0007	7.10	0.17	0.006	0.0005	85.6	1.7	29.66	0.62	7.11E-15	7.75E-16			1.98	PLLLLL
		9.98	8422-02K	9.37	0.08	0.013	0.0007	12.79	0.25	0.01	0.0004	78.9	1.8	28.04	0.67	9.37E-15	1.00E-15			2.96	PPLLLL

PR01a-W.R																					
	12/25/2014	13.67	8423-01A	9.65	0.17	0.022	0.0018	1.22	0.16	0.013	0.0011	60.6	3.4	22	1.3	3.09E-15	3.20E-16	**0.9994**	**0.0018**	0.1	PPLLLL
		14.38	8423-01B	7.957	0.05	0.016	0.0007	0.64	0.044	0.002	0.0003	92.2	1.1	27.6	0.36	1.10E-14	1.39E-15			0.2	PPLLLL
		15.15	8423-01C	7.508	0.06	0.016	0.0007	0.82	0.053	0.001	0.0003	95.6	1.2	27	0.37	9.13E-15	1.22E-15			0.3	PPLLLL
		15.88	8423-01D	7.393	0.05	0.013	0.0006	0.69	0.05	8E-04	0.0003	97.3	1.3	27.07	0.36	9.59E-15	1.30E-15			0.4	PPLLLL
		16.63	8423-01E	7.234	0.05	0.013	0.0006	0.48	0.046	-0	0.0002	101.05	0.98	27.49	0.32	1.07E-14	1.48E-15			0.49	LPLLLL
		17.40	8423-01F	7.288	0.06	0.013	0.0007	0.89	0.071	5E-04	0.0003	98.8	1.5	27.09	0.43	6.65E-15	9.13E-16			0.59	PPLLLL
		18.07	8423-01G	7.077	0.03	0.013	0.0002	1.24	0.02	7E-04	0.0001	98.21	0.31	26.16	0.12	5.51E-14	7.79E-15			0.79	PPLLLL
		19.01	8423-01H	7.112	0.04	0.014	0.0004	2.11	0.052	0.001	0.0001	97.2	0.67	26.04	0.21	2.03E-14	2.85E-15			0.99	PPLLLL
		19.87	8423-01I	7.019	0.04	0.012	0.0006	3.17	0.079	0.002	0.0002	96.24	0.97	25.46	0.29	1.22E-14	1.74E-15			1.48	LPLLLL
		20.73	8423-01J	7.183	0.05	0.014	0.0005	4.73	0.12	0.002	0.0003	94.8	1.4	25.69	0.39	8.66E-15	1.21E-15			1.98	PPLLLL
		21.53	8423-01K	7.297	0.04	0.015	0.0005	5.78	0.1	0.003	0.0005	92.8	2	25.58	0.55	1.07E-14	1.47E-15			2.96	PPLLPL
	12/26/2014	1.06	8423-02A	12.46	0.15	0.02	0.0014	0.65	0.11	0.019	0.0009	55.5	2.2	26	1.1	5.53E-15	4.44E-16	**0.9994**	**0.0018**	0.1	PPLLLL
		1.74	8423-02B	9.637	0.06	0.017	0.0005	0.83	0.038	0.008	0.0003	77.1	0.91	27.95	0.37	1.63E-14	1.69E-15			0.2	PPLLLL
		2.55	8423-02C	8.317	0.04	0.016	0.0005	0.68	0.03	0.004	0.0002	86.14	0.86	26.95	0.29	1.62E-14	1.95E-15			0.3	PPLLLL
		3.31	8423-02D	7.885	0.05	0.015	0.0007	0.65	0.042	0.002	0.0003	91.5	0.99	27.14	0.33	1.36E-14	1.72E-15			0.4	LPLLLL
		4.10	8423-02E	7.539	0.05	0.013	0.0005	0.71	0.039	0.001	0.0002	95.11	0.77	26.97	0.27	1.47E-14	1.95E-15			0.49	LPLLLL
		4.82	8423-02F	7.463	0.04	0.012	0.0005	0.87	0.053	0.002	0.0003	94	1.1	26.4	0.32	1.02E-14	1.37E-15			0.59	PPLLLL
		5.59	8423-02G	7.44	0.03	0.013	0.0002	1.17	0.015	0.002	0.0001	92.81	0.45	25.99	0.15	8.87E-14	1.19E-14			0.79	PPLLPL
		6.47	8423-02H	7.543	0.04	0.013	0.0004	2.04	0.061	0.003	0.0002	91.41	0.93	25.97	0.29	1.54E-14	2.04E-15			0.99	PPLLLL
		7.33	8423-02I	7.548	0.05	0.014	0.0005	3.31	0.071	0.003	0.0002	90.5	1.1	25.74	0.32	1.32E-14	1.75E-15			1.48	PPLLLL
		8.19	8423-02J	7.575	0.03	0.013	0.0003	3.66	0.078	0.003	0.0002	90.75	0.91	25.92	0.28	1.74E-14	2.30E-15			1.98	LPLLLL
		9.01	8423-02K	7.709	0.04	0.013	0.0004	6.28	0.069	0.005	0.0002	87.23	0.88	25.41	0.28	2.44E-14	3.16E-15			2.96	PPLLLL
IJS07b-W.R																					
	12/26/2014	12.88	8424-01A	8.888	0.05	0.015	0.0005	0.62	0.037	0.003	0.0002	89.08	0.81	29.76	0.31	1.57E-14	1.77E-15	**0.9994**	**0.0018**	0.1	PPLLLL
		13.65	8424-01B	8.775	0.04	0.012	0.0003	0.81	0.041	4E-04	0.0003	99.41	0.92	32.76	0.32	2.17E-14	2.47E-15			0.2	PPLLPL
		14.48	8424-01C	8.504	0.06	0.013	0.0006	1.16	0.059	0.002	0.0002	95.43	0.91	30.51	0.34	1.21E-14	1.42E-15			0.3	LPLLLL

		15.28	8424-01D	8.176	0.06	0.013	0.0006	1.53	0.067	0.002	0.0006	94.5	2.2	29.06	0.69	9.75E-15	1.19E-15			0.4	PPLLPL
		16.04	8424-01E	8.031	0.05	0.014	0.0006	2.12	0.094	0.001	0.0003	98.1	1.3	29.64	0.42	8.41E-15	1.05E-15			0.49	PLLLLL
		16.81	8424-01F	7.733	0.04	0.013	0.0003	1.76	0.046	0.002	0.0002	94.96	0.65	27.64	0.23	2.02E-14	2.61E-15			0.59	PPLLLL
		17.66	8424-01G	7.545	0.03	0.014	0.0004	2.28	0.044	0.002	0.0002	95.23	0.87	27.06	0.26	2.63E-14	3.48E-15			0.79	PPLLPL
		18.57	8424-01H	6.921	0.05	0.016	0.0009	3.68	0.13	0.002	0.0004	94.4	1.9	24.64	0.49	5.69E-15	8.23E-16			0.99	PLLLLL
		19.31	8424-01I	6.722	0.08	0.015	0.0011	4.59	0.18	0.002	0.0007	97.2	3.1	24.67	0.81	3.37E-15	5.01E-16			1.48	PPLLLL
		20.10	8424-01J	7.09	0.14	0.018	0.0023	5.64	0.32	0.003	0.0013	94.6	5.8	25.3	1.6	1.58E-15	2.23E-16			1.98	PPLLLL
		20.82	8424-01K	7.414	0.09	0.013	0.0014	6.09	0.2	0.002	0.0008	98.9	3.2	27.69	0.93	3.18E-15	4.28E-16			2.96	PPLLLL
	12/27/2014	0.31	8424-02A	8.916	0.05	0.014	0.0004	0.94	0.039	0.003	0.0002	89.9	0.74	30.13	0.29	1.85E-14	2.07E-15	**0.9994**	**0.0018**	0.1	PPLLLL
		1.09	8424-02B	8.947	0.05	0.013	0.0003	0.85	0.032	9E-04	0.0001	97.76	0.51	32.85	0.24	2.43E-14	2.72E-15			0.2	PPLLLL
		1.96	8424-02C	8.481	0.06	0.012	0.0005	1.24	0.057	0.002	0.0002	95.66	0.81	30.5	0.31	1.38E-14	1.63E-15			0.3	PPLLLL
		2.82	8424-02D	8.237	0.05	0.013	0.0006	1.92	0.078	0.002	0.0005	95.6	1.9	29.63	0.61	1.05E-14	1.27E-15			0.4	LPLLPL
		3.64	8424-02E	8.018	0.08	0.014	0.0007	2.20	0.099	0.003	0.0004	92.8	1.6	28.01	0.52	6.85E-15	8.55E-16			0.49	PPLLLL
		4.39	8424-02F	7.947	0.04	0.015	0.0003	1.88	0.055	0.002	0.0001	96.03	0.59	28.72	0.22	2.33E-14	2.94E-15			0.59	PPLLLL
		5.15	8424-02G	7.568	0.03	0.014	0.0003	2.50	0.031	0.002	0.0002	94.01	0.89	26.8	0.27	3.10E-14	4.09E-15			0.79	PPLLPL
		5.99	8424-02H	6.583	0.06	0.015	0.0009	4.24	0.13	0.003	0.0004	91.7	2	22.8	0.53	4.95E-15	7.52E-16			0.99	PPLLLL
		6.76	8424-02I	6.91	0.10	0.015	0.0018	4.52	0.22	0.004	0.0009	88.8	3.8	23.2	1	2.20E-15	3.19E-16			1.48	PPLLLL
		7.45	8424-02J	7.35	0.16	0.012	0.0023	5.51	0.32	4E-04	0.0015	104.3	6.2	28.9	1.8	1.58E-15	2.14E-16			1.97	PPLLLL
		8.15	8424-02K	7.6	0.16	0.019	0.0019	6.37	0.27	0.007	0.0012	78	5	22.4	1.5	2.01E-15	2.64E-16			2.95	PPLLLL
PR05-W.R																					
	12/27/2014	11.59	8425-01A	37.31	0.86	0.034	0.0030	4.05	0.34	0.098	0.0036	22.8	2.3	32.1	3.4	6.90E-15	1.85E-16	**0.9994**	**0.0018**	0.1	PPLLLL
		12.35	8425-01B	14.63	0.17	0.014	0.0011	2.33	0.14	0.016	0.0009	69.4	1.8	38.1	1	7.76E-15	5.30E-16			0.2	PPLLLL
		13.03	8425-01C	10.86	0.06	0.013	0.0006	2.61	0.075	0.006	0.0003	84.48	1	34.49	0.44	1.71E-14	1.57E-15			0.3	PPLLLL
		13.91	8425-01D	8.935	0.05	0.011	0.0005	2.24	0.068	0.002	0.0002	95.44	0.79	32.07	0.3	1.39E-14	1.56E-15			0.4	PPLLLL
		14.74	8425-01E	8.852	0.07	0.012	0.0007	1.84	0.098	0.002	0.0004	96.1	1.3	31.99	0.47	8.84E-15	9.98E-16			0.49	PPLLLL
		15.45	8425-01F	8.866	0.07	0.012	0.0009	1.91	0.1	0.002	0.0005	94	1.8	31.33	0.63	5.70E-15	6.43E-16			0.59	PLLLLL
		16.12	8425-01G	9.06	0.13	0.011	0.0013	3.64	0.23	0.003	0.0008	93.7	2.7	32	1	3.46E-15	3.82E-16			0.79	PPLLLL

		16.82	8425-01H	8.9	0.19	0.015	0.0021	5.71	0.34	0.003	0.0023	94.3	7.7	31.6	2.6	2.12E-15	2.38E-16			0.99	PPLLPL
		17.54	8425-01I	8.887	0.10	0.012	0.0013	7.52	0.32	0.006	0.0009	87.5	3	29.4	1	3.64E-15	4.10E-16			1.48	PLLLLL
		18.30	8425-01J	9.53	0.22	0.011	0.0022	10.31	0.49	0.005	0.0030	93.3	9.3	33.6	3.4	1.76E-15	1.84E-16			1.98	PPLLPL
		19.04	8425-01K	9.165	0.10	0.016	0.0012	12.60	0.3	0.007	0.0006	89.2	2.3	30.96	0.86	4.81E-15	5.25E-16			2.96	PPLLLL
	12/27/2014	22.53	8425-02A	31.57	0.51	0.028	0.0018	4.85	0.22	0.083	0.0024	22.9	1.9	27.3	2.5	9.78E-15	3.10E-16	**0.9966**	**0.0026**	0.1	PPLLLL
		23.31	8425-02B	15.02	0.15	0.012	0.0010	3.66	0.13	0.016	0.0008	70.8	1.6	39.94	0.97	1.02E-14	6.82E-16			0.2	PPLLLL
		0.04	8425-02C	12.5	0.07	0.013	0.0004	2.69	0.054	0.012	0.0003	73.77	0.8	34.67	0.45	2.17E-14	1.74E-15			0.3	PPLLLL
		1.07	8425-02D	9.021	0.04	0.012	0.0004	2.11	0.051	0.002	0.0001	94.43	0.53	32.03	0.23	2.55E-14	2.83E-15			0.39	PPLLLL
		1.92	8425-02E	8.713	0.05	0.011	0.0005	1.83	0.061	0.002	0.0002	95.72	0.67	31.36	0.27	1.84E-14	2.11E-15			0.49	PPLLLL
		2.81	8425-02F	8.842	0.06	0.012	0.0006	1.54	0.064	0.002	0.0002	94.98	0.9	31.57	0.35	1.22E-14	1.38E-15			0.6	PPLLLL
		3.64	8425-02G	8.893	0.06	0.011	0.0007	2.01	0.096	0.003	0.0004	92.5	1.4	30.92	0.47	8.17E-15	9.18E-16			0.79	PLLLLL
		4.39	8425-02H	8.8	0.13	0.013	0.0018	5.41	0.22	0.005	0.0009	88.8	3.3	29.5	1.1	2.70E-15	3.07E-16			0.99	PPLLLL
		5.05	8425-02I	8.669	0.08	0.012	0.0008	6.28	0.19	0.004	0.0004	93.4	1.6	30.54	0.58	6.80E-15	7.84E-16			1.48	PPLLLL
		5.82	8425-02J	8.631	0.07	0.012	0.0013	8.04	0.24	0.003	0.0012	95.9	4.4	31.3	1.4	4.43E-15	5.13E-16			1.98	PLLLPL
		6.62	8425-02K	8.471	0.07	0.013	0.0007	8.63	0.18	0.004	0.0004	95.4	1.7	30.53	0.58	7.29E-15	8.61E-16			2.96	PPLLLL
PR04-W.R																					
	12/28/2014	10.18	8426-01A	72.9	3.50	0.057	0.0070	5.15	0.65	0.221	0.0120	10.2	2.6	28.1	7.7	6.78E-15	9.29E-17	**0.9966**	**0.0026**	0.1	PPLLLL
		10.95	8426-01B	27.33	0.37	0.022	0.0015	3.75	0.15	0.049	0.0014	47.4	1.4	48.6	1.7	1.23E-14	4.51E-16			0.2	PPLLLL
		11.75	8426-01C	24.73	0.18	0.02	0.0008	2.82	0.093	0.041	0.0008	51.53	0.91	47.7	1.1	2.73E-14	1.10E-15			0.3	PPLLLL
		12.65	8426-01D	15.85	0.09	0.014	0.0004	2.05	0.066	0.012	0.0003	79.12	0.59	46.97	0.47	2.83E-14	1.79E-15			0.4	PPLLLL
		13.69	8426-01E	13.83	0.11	0.013	0.0006	2.94	0.099	0.004	0.0003	91.94	0.81	47.62	0.52	1.55E-14	1.12E-15			0.49	PPLLLL
		14.55	8426-01F	14.12	0.13	0.013	0.0009	3.70	0.14	0.006	0.0006	89.9	1.2	47.57	0.76	9.82E-15	6.95E-16			0.59	PPLLLL
		15.31	8426-01G	13.34	0.13	0.013	0.0009	2.79	0.14	0.004	0.0005	93	1.1	46.49	0.7	1.00E-14	7.53E-16			0.79	PPLLLL
		16.05	8426-01H	12.98	0.20	0.014	0.0017	5.64	0.28	0.003	0.0010	95.5	2.3	46.5	1.3	4.56E-15	3.51E-16			0.99	PPLLLL
		16.77	8426-01I	13.3	0.10	0.017	0.0010	11.81	0.23	0.007	0.0007	90.8	1.8	45.51	0.93	7.25E-15	5.45E-16			1.48	PLLLLL
		17.53	8426-01J	13.39	0.20	0.014	0.0016	15.11	0.51	0.008	0.0019	90.1	4.3	45.6	2.3	4.05E-15	3.02E-16			1.97	PPLLPL
		18.30	8426-01K	12.95	0.12	0.012	0.0008	15.11	0.27	0.008	0.0005	89.7	1.5	43.93	0.81	1.06E-14	8.17E-16			2.96	PPLLLL

	12/28/2014	21.76	8426-02A	104.3	4.80	0.071	0.0072	3.33	0.69	0.286	0.0150	18.2	2.2	70.7	9.5	1.05E-14	1.01E-16	**0.9966**	**0.0026**	0.1	PPLLLL
		22.50	8426-02B	37.52	0.45	0.029	0.0014	3.56	0.17	0.084	0.0018	33.6	1.2	47.2	2.1	2.02E-14	5.38E-16			0.2	PPLLLL
		23.37	8426-02C	29.9	0.17	0.022	0.0006	3.08	0.091	0.059	0.0008	41.75	0.7	46.8	1.1	4.94E-14	1.65E-15			0.3	PPLLLL
	12/29/2014	0.25	8426-02D	15.75	0.07	0.014	0.0004	1.74	0.037	0.011	0.0003	80.34	0.5	47.36	0.41	4.42E-14	2.80E-15			0.4	PPLLLL
		1.21	8426-02E	13.88	0.09	0.012	0.0006	2.70	0.084	0.004	0.0004	92.83	0.84	48.24	0.53	2.00E-14	1.44E-15			0.49	PPLLLL
		2.07	8426-02F	13.64	0.11	0.013	0.0007	3.22	0.12	0.005	0.0004	91.9	1	46.99	0.63	1.19E-14	8.76E-16			0.59	PPLLLL
		2.82	8426-02G	13.43	0.12	0.012	0.0007	3.38	0.13	0.003	0.0005	94.7	1.1	47.62	0.66	1.13E-14	8.42E-16			0.79	PPLLLL
		3.56	8426-02H	13.56	0.23	0.02	0.0018	10.29	0.45	0.008	0.0013	87.4	3	44.7	1.6	3.73E-15	2.75E-16			0.99	PPLLLL
		4.29	8426-02I	13.77	0.14	0.013	0.0009	9.96	0.23	0.007	0.0006	90.8	1.4	47.09	0.85	9.36E-15	6.80E-16			1.48	PPLLLL
		5.04	8426-02J	12.99	0.13	0.014	0.0010	14.05	0.33	0.007	0.0007	91.1	1.9	44.74	0.99	7.30E-15	5.62E-16			1.98	PPLLLL
		5.81	8426-02K	13.41	0.13	0.012	0.0008	15.68	0.28	0.007	0.0005	92.7	1.5	46.98	0.88	1.14E-14	8.52E-16			2.96	PPLLLL
PR02-W.R																					
	12/29/2014	9.34	8427-01A	44.7	2.80	0.035	0.0081	0.59	0.8	0.104	0.0092	30.8	4.4	51.5	8	2.78E-15	6.22E-17	**0.9966**	**0.0026**	0.1	PPLLLL
		10.02	8427-01B	14.02	0.27	0.029	0.0027	2.20	0.21	0.013	0.0015	72.6	3.2	38.2	1.8	3.65E-15	2.60E-16			0.2	PPLLLL
		10.69	8427-01C	12.19	0.11	0.017	0.0010	0.98	0.074	0.008	0.0005	80.4	1.3	36.77	0.64	9.46E-15	7.76E-16			0.3	PPLLLL
		11.41	8427-01D	10.08	0.08	0.016	0.0006	1.12	0.063	0.004	0.0003	89.75	0.94	33.97	0.43	1.37E-14	1.36E-15			0.39	PPLLLL
		12.19	8427-01E	9.444	0.06	0.015	0.0008	1.52	0.071	0.001	0.0003	97	1.1	34.41	0.41	9.68E-15	1.02E-15			0.49	PLLLLL
		12.90	8427-01F	8.995	0.09	0.014	0.0007	0.90	0.064	1E-03	0.0003	97.5	1.2	32.96	0.48	8.60E-15	9.56E-16			0.59	PPLLLL
		13.56	8427-01G	8.779	0.07	0.013	0.0007	1.43	0.068	0.002	0.0003	95.6	1.1	31.56	0.41	9.41E-15	1.07E-15			0.79	PPLLLL
		14.22	8427-01H	9.43	0.16	0.016	0.0023	5.54	0.23	0.003	0.0012	95.5	3.9	33.9	1.5	2.38E-15	2.53E-16			0.99	PPLLLL
		14.91	8427-01I	9.228	0.09	0.015	0.0012	9.52	0.24	0.005	0.0006	90.5	2.3	31.57	0.82	5.20E-15	5.63E-16			1.48	PPLLLL
		15.73	8427-01J	9.053	0.09	0.016	0.0010	8.10	0.25	0.004	0.0005	92.6	1.9	31.66	0.7	4.77E-15	5.27E-16			1.97	PPLLLL
		16.47	8427-01K	9.275	0.10	0.016	0.0009	8.49	0.22	0.005	0.0005	90.6	1.9	31.73	0.73	5.85E-15	6.31E-16			2.96	PPLLLL
	12/29/2014	19.87	8427-02A	21.21	0.65	0.037	0.0037	1.09	0.38	0.04	0.0030	44.6	3.9	35.5	3.3	2.85E-15	1.34E-16	**0.9966**	**0.0026**	0.1	PPLLLL
		20.57	8427-02B	11.6	0.14	0.026	0.0012	1.30	0.1	0.009	0.0006	77	1.5	33.57	0.77	7.86E-15	6.77E-16			0.2	PPLLLL
		21.28	8427-02C	9.928	0.06	0.019	0.0007	1.02	0.054	0.003	0.0002	90.68	0.71	33.81	0.32	1.96E-14	1.97E-15			0.3	PPLLLL

		22.09	8427-02D	9.215	0.05	0.015	0.0005	1.09	0.043	0.001	0.0002	96.62	0.55	33.44	0.24	2.38E-14	2.58E-15			0.4	PPLLLL
		22.90	8427-02E	9.052	0.05	0.014	0.0005	0.96	0.055	6E-04	0.0002	98.98	0.81	33.65	0.32	1.69E-14	1.87E-15			0.49	PPLLLL
		23.68	8427-02F	8.947	0.05	0.013	0.0006	0.77	0.036	3E-04	0.0002	99.53	0.76	33.44	0.29	1.55E-14	1.73E-15			0.59	PPLLLL
	12/30/2014	0.43	8427-02G	9.072	0.08	0.012	0.0007	1.64	0.077	0.001	0.0003	96.9	1.2	33.05	0.46	9.87E-15	1.09E-15			0.79	PPLLLL
		1.16	8427-02H	9.19	0.12	0.013	0.0013	5.01	0.25	0.003	0.0009	95.4	2.9	33	1.1	3.82E-15	4.16E-16			0.99	PPLLLL
		1.93	8427-02I	9.125	0.08	0.011	0.0008	8.52	0.16	0.005	0.0004	92.4	1.6	31.86	0.58	8.44E-15	9.25E-16			1.48	PPLLLL
		2.74	8427-02J	9.017	0.09	0.011	0.0008	6.90	0.16	0.004	0.0004	93.8	1.6	31.91	0.59	7.38E-15	8.19E-16			1.98	PPLLLL
		3.54	8427-02K	8.991	0.07	0.014	0.0007	7.38	0.17	0.003	0.0004	98	1.5	33.22	0.54	9.79E-15	1.09E-15			2.96	PPLLLL
TRLF05-W.R																					
	12/30/2014	6.99	8428-01A	28.13	0.24	0.026	0.0011	1.49	0.085	0.058	0.0012	39.1	1.2	41.2	1.5	2.29E-14	8.16E-16	**0.9966**	**0.0026**	0.1	PPLLLL
		7.91	8428-01B	15.33	0.10	0.018	0.0006	3.03	0.082	0.021	0.0004	60.72	0.73	35	0.56	2.84E-14	1.85E-15			0.2	PPLLLL
		8.85	8428-01C	9.378	0.07	0.014	0.0006	4.28	0.11	0.006	0.0007	83.1	2.3	29.37	0.82	1.21E-14	1.29E-15			0.3	PPLLPL
		9.68	8428-01D	7.954	0.07	0.015	0.0010	4.94	0.19	0.006	0.0013	82.3	5.1	24.7	1.5	4.57E-15	5.74E-16			0.39	PLLLPL
		10.51	8428-01E	7.61	0.12	0.015	0.0018	4.91	0.3	0.003	0.0011	94.6	4.5	27.1	1.3	2.13E-15	2.80E-16			0.49	PPLLLL
		11.21	8428-01F	8.4	0.21	0.023	0.0035	6.77	0.42	0.006	0.0019	83.6	6.7	26.5	2.2	1.37E-15	1.63E-16			0.59	PPLLLL
		11.90	8428-01G	9.75	0.28	0.037	0.0044	22.80	1.1	0.017	0.0028	64.6	8.8	24.1	3.3	1.22E-15	1.25E-16			0.79	PPLLLL
		12.70	8428-01H	8.9	0.45	0.016	0.0071	24.30	1.7	0.009	0.0055	90	19	30.5	6.4	5.55E-16	6.24E-17			0.99	PPLLLL
		13.47	8428-01I	9.25	0.44	0.023	0.0066	47.60	2.6	0.037	0.0095	20	30	7	11	6.02E-16	6.51E-17			1.48	PPLLPL
		14.24	8428-01J	9.18	0.47	0.026	0.0069	45.40	2.7	0.017	0.0057	84	19	29.8	6.8	5.68E-16	6.18E-17			1.98	PPLLLL
		15.07	8428-01K	9.08	0.34	0.026	0.0048	28.00	1.4	0.013	0.0037	80	13	27.7	4.4	8.78E-16	9.67E-17			2.96	PPLLLL
	12/30/2014	18.54	8428-02A	36.43	0.31	0.031	0.0013	1.13	0.077	0.085	0.0014	30.52	0.97	41.7	1.8	3.30E-14	9.07E-16	**0.9975**	**0.0028**	0.1	PPLLLL
		19.41	8428-02B	16.89	0.09	0.018	0.0005	2.24	0.065	0.024	0.0004	58.34	0.76	37.01	0.64	3.27E-14	1.93E-15			0.2	PPLLLL
		20.38	8428-02C	11.04	0.08	0.016	0.0007	4.14	0.12	0.012	0.0004	71.2	1.2	29.61	0.57	1.43E-14	1.30E-15			0.3	LPLLLL
		21.36	8428-02D	8.489	0.09	0.013	0.0011	5.31	0.18	0.005	0.0007	85.7	2.6	27.47	0.87	4.96E-15	5.84E-16			0.4	PPLLLL
		22.13	8428-02E	7.4	0.15	0.017	0.0021	5.74	0.33	0.004	0.0023	89.1	9.2	24.9	2.6	1.86E-15	2.52E-16			0.49	PPLLPL
		22.80	8428-02F	7.84	0.29	0.026	0.0041	9.27	0.81	0.014	0.0028	55	11	16.2	3.2	1.04E-15	1.32E-16			0.59	PPLLLL
		23.50	8428-02G	9.85	0.40	0.027	0.0057	32.50	1.6	0.027	0.0041	43	12	16.4	4.8	9.18E-16	9.32E-17			0.79	PPLLLL

	12/31/2014	0.28	8428-02H	9.67	0.65	0.021	0.0110	50.10	3.8	0.029	0.0064	50	19	18.8	7.4	5.04E-16	5.22E-17			0.99	PPLLLL
		1.05	8428-02I	9.74	0.66	0.026	0.0093	67.90	4.7	0.038	0.0073	37	22	14.4	8.5	4.87E-16	5.00E-17			1.48	PPLLLL
		1.84	8428-02J	8.33	0.58	0.024	0.0095	47.10	3.6	0.027	0.0070	47	25	15.2	8.1	3.96E-16	4.75E-17			1.98	PPLLLL
		2.54	8428-02K	9.17	0.76	0.023	0.0110	44.20	4.1	0.015	0.0080	88	26	31.1	9.5	3.84E-16	4.19E-17			2.96	PPLLLL
AA2-W.R																					
	12/31/2014	5.90	8429-01A	94.1	1.60	0.074	0.0030	4.20	0.27	0.294	0.0059	7	1.1	25	5.3	2.61E-14	2.78E-16	**0.9975**	**0.0028**	0.1	PPLLLL
		6.81	8429-01B	22.73	0.20	0.021	0.0008	1.19	0.077	0.048	0.0010	37.6	1.2	32.1	1.2	2.35E-14	1.03E-15			0.2	PPLLLL
		7.64	8429-01C	11.61	0.05	0.014	0.0004	0.56	0.025	0.012	0.0002	70.57	0.51	30.78	0.33	5.11E-14	4.40E-15			0.3	PPLLLL
		8.47	8429-01D	8.654	0.04	0.012	0.0003	0.81	0.029	0.003	0.0002	90.94	0.73	29.59	0.28	3.00E-14	3.46E-15			0.4	PPLLPL
		9.35	8429-01E	8.484	0.06	0.013	0.0005	0.88	0.043	0.002	0.0002	92.07	0.8	29.37	0.31	1.49E-14	1.76E-15			0.49	PPLLLL
		10.07	8429-01F	8.217	0.05	0.012	0.0004	0.91	0.046	0.002	0.0002	94.54	0.76	29.21	0.28	1.48E-14	1.81E-15			0.59	PPLLLL
		10.85	8429-01G	8.247	0.05	0.013	0.0006	2.01	0.08	0.003	0.0003	91.5	1.1	28.41	0.38	1.26E-14	1.53E-15			0.79	PPLLLL
		11.67	8429-01H	8.093	0.07	0.013	0.0006	4.65	0.12	0.003	0.0003	93.7	1.3	28.6	0.44	9.10E-15	1.12E-15			0.99	PPLLLL
		12.53	8429-01I	7.979	0.05	0.012	0.0005	7.28	0.12	0.003	0.0002	94.9	1.2	28.61	0.39	1.37E-14	1.72E-15			1.48	PPLLLL
		13.44	8429-01J	7.969	0.06	0.016	0.0010	7.07	0.18	0.003	0.0010	94.8	4	28.5	1.2	5.08E-15	6.38E-16			1.98	PLLLPL
		14.22	8429-01K	7.773	0.07	0.011	0.0009	7.70	0.2	0.003	0.0005	96.7	2	28.39	0.6	6.46E-15	8.31E-16			2.96	PPLLLL
	12/31/2014	17.64	8429-02A	124.6	2.50	0.094	0.0044	1.98	0.28	0.397	0.0091	5	1.1	23.6	7.1	2.62E-14	2.10E-16	**0.9975**	**0.0028**	0.1	PPLLLL
		18.57	8429-02B	25.91	0.21	0.035	0.0008	1.02	0.074	0.056	0.0009	36.07	0.96	35.1	1.2	2.43E-14	9.39E-16			0.2	PPLLLL
		19.45	8429-02C	11.95	0.05	0.016	0.0003	0.53	0.021	0.013	0.0002	68.54	0.56	30.77	0.36	4.78E-14	4.00E-15			0.3	PPLLLL
		20.34	8429-02D	9.08	0.04	0.013	0.0002	0.58	0.021	0.004	0.0001	88.71	0.35	30.27	0.18	5.78E-14	6.37E-15			0.4	PPLLLL
		21.22	8429-02E	8.44	0.05	0.013	0.0003	0.77	0.033	0.002	0.0001	94.43	0.54	29.96	0.22	2.61E-14	3.09E-15			0.49	PPLLLL
		22.03	8429-02F	8.259	0.04	0.012	0.0003	0.78	0.039	0.002	0.0001	94.91	0.59	29.47	0.23	2.16E-14	2.62E-15			0.59	PPLLLL
		22.81	8429-02G	8.084	0.04	0.013	0.0003	1.46	0.043	0.002	0.0003	95.8	1	29.13	0.33	2.20E-14	2.72E-15			0.79	PPLLPL
		23.72	8429-02H	7.935	0.06	0.013	0.0006	3.46	0.1	0.002	0.0003	96.2	1.1	28.75	0.37	1.06E-14	1.34E-15			0.99	PPLLLL
	1/01/2015	0.52	8429-02I	7.97	0.05	0.013	0.0005	5.41	0.097	0.002	0.0002	98.2	1.1	29.5	0.35	1.62E-14	2.04E-15			1.48	PPLLLL
		1.38	8429-02J	7.775	0.07	0.012	0.0008	5.73	0.15	0.001	0.0005	101.5	2	29.75	0.58	6.13E-15	7.88E-16			1.98	PLLLLL
		2.14	8429-02K	7.729	0.06	0.013	0.0008	7.12	0.14	0.003	0.0003	96.3	1.4	28.12	0.45	8.98E-15	1.16E-15			2.95	PPLLLL

GA1550 MD2 – Biotite																				
	1/01/2015	5.75	8430-01A	31.9	0.49	0.023	0.0019	0.17	0.15	0.025	0.0013	76.2	1.3	89.9	2	1.03E-14	3.22E-16	**0.9975**	**0.0028**	0.2	PPLLLL
		6.41	8430-01B	27.61	0.24	0.017	0.0008	0.09	0.046	0.002	0.0003	97.47	0.43	99.17	0.91	3.07E-14	1.11E-15			0.3	PPLLLL
		7.25	8430-01C	27.84	0.20	0.015	0.0007	0.04	0.049	0.001	0.0003	98.81	0.42	101.34	0.78	2.90E-14	1.04E-15			0.35	PPLLLL
		8.02	8430-01D	27.27	0.25	0.017	0.0006	0.00	0.047	-0	0.0003	100.35	0.45	100.81	0.94	2.89E-14	1.06E-15			0.4	PPLLLL
		8.78	8430-01E	27.62	0.18	0.016	0.0006	0.05	0.04	8E-04	0.0003	99.14	0.37	100.85	0.71	3.62E-14	1.31E-15			0.44	PPLLLL
		9.51	8430-01F	27.35	0.19	0.016	0.0007	0.01	0.032	1E-04	0.0002	99.88	0.28	100.62	0.7	4.57E-14	1.67E-15			0.49	PPLLLL
		10.24	8430-01G	27.25	0.15	0.016	0.0005	0.04	0.023	6E-04	0.0002	99.31	0.23	99.72	0.57	6.53E-14	2.40E-15			0.59	PPLLLL
		10.98	8430-01H	27.2	0.14	0.015	0.0004	0.02	0.018	5E-04	0.0001	99.49	0.29	99.73	0.53	8.06E-14	2.96E-15			0.79	PPLLLL
		11.71	8430-01I	27.3	0.19	0.017	0.0006	0.03	0.036	3E-04	0.0003	99.69	0.32	100.27	0.72	3.90E-14	1.43E-15			0.99	PPLLLL
		12.41	8430-01J	26.55	0.66	0.013	0.0026	0.25	0.26	-0	0.0018	101.9	2	99.7	3	4.93E-15	1.86E-16			2.47	PPLLLL
	1/01/2015	15.83	8430-02A	42.05	0.41	0.024	0.0012	-0.04	0.084	0.05	0.0012	64.75	0.84	100.3	1.8	2.31E-14	5.48E-16	**0.9975**	**0.0028**	0.2	PPLLLL
		16.72	8430-02B	28.65	0.19	0.016	0.0007	0.00	0.035	0.006	0.0003	94.2	0.39	99.45	0.76	3.72E-14	1.30E-15	**0.9986**	**0.003**	0.3	PPLLLL
		17.53	8430-02C	27.43	0.17	0.017	0.0007	-0.10	0.048	0.003	0.0004	96.98	0.51	98.05	0.74	2.52E-14	9.19E-16			0.35	PLLLLL
		18.26	8430-02D	27.7	0.26	0.018	0.0008	-0.05	0.045	0.002	0.0004	97.32	0.5	99.3	1	2.63E-14	9.51E-16			0.4	PPLLLL
		18.97	8430-02E	27.21	0.23	0.014	0.0010	-0.10	0.056	-0	0.0004	100.32	0.5	100.56	0.92	2.28E-14	8.36E-16			0.44	PPLLLL
		19.72	8430-02F	27.69	0.39	0.014	0.0015	0.29	0.12	0.003	0.0009	96.4	1	98.4	1.6	9.80E-15	3.54E-16			0.49	PPLLLL
		20.41	8430-02G	28.51	0.56	0.017	0.0022	-0.16	0.18	0.001	0.0013	98.5	1.4	103.4	2.4	7.51E-15	2.63E-16			0.59	PPLLLL
		21.09	8430-02H	26.84	0.29	0.017	0.0010	0.02	0.084	0.002	0.0006	97.78	0.81	96.8	1.2	1.52E-14	5.66E-16			0.79	PPLLLL
		21.78	8430-02I	28.47	0.51	0.013	0.0022	-0.38	0.18	3E-04	0.0012	99.6	1.3	104.3	2.2	7.61E-15	2.67E-16			0.99	PPLLLL
		22.46	8430-02J	26.33	0.21	0.014	0.0008	-0.02	0.053	0.001	0.0004	98.3	0.53	95.47	0.86	2.39E-14	9.09E-16			2.48	PPLLLL
PR07-W.R																				
	1/02/2015	1.91	8433-01A	15.98	0.51	0.014	0.0035	2.82	0.39	0.039	0.0029	29.1	4.9	17.5	3	2.27E-15	1.42E-16	**0.9986**	**0.003**	0.1	PPLLLL
		2.59	8433-01B	12.44	0.22	0.018	0.0017	2.65	0.23	0.013	0.0011	69.7	2.5	32.4	1.3	3.95E-15	3.18E-16			0.2	PPLLLL
		3.24	8433-01C	11.73	0.08	0.014	0.0007	1.47	0.062	0.008	0.0003	80.77	0.84	35.38	0.46	1.61E-14	1.37E-15			0.3	PPLLLL
		4.12	8433-01D	10.15	0.06	0.014	0.0004	1.39	0.053	0.004	0.0002	90.5	0.59	34.31	0.31	2.26E-14	2.23E-15			0.4	PPLLLL

		4.97	8433-01E	9.737	0.08	0.012	0.0006	1.49	0.066	0.002	0.0003	96.37	0.9	35.04	0.41	1.26E-14	1.29E-15			0.49	PPLLLL
		5.79	8433-01F	9.606	0.08	0.014	0.0008	1.63	0.081	0.002	0.0003	94.8	1.1	34.02	0.47	9.09E-15	9.46E-16			0.59	PPLLLL
		6.46	8433-01G	9.547	0.07	0.011	0.0005	1.47	0.091	0.001	0.0005	97.1	1.5	34.62	0.56	1.01E-14	1.06E-15			0.79	PPLLPL
		7.19	8433-01H	9.25	0.16	0.012	0.0018	5.33	0.31	0.006	0.0013	84.3	4.2	29.2	1.5	2.56E-15	2.77E-16			0.99	PPLLLL
		7.94	8433-01I	9.5	0.13	0.015	0.0016	12.63	0.37	0.008	0.0011	84	3.5	30.1	1.3	3.10E-15	3.26E-16			1.48	PPLLLL
		8.70	8433-01J	9.58	0.11	0.01	0.0013	12.03	0.3	0.007	0.0008	87.1	2.6	31.4	1	4.41E-15	4.60E-16			1.98	PPLLLL
		9.50	8433-01K	10.19	0.08	0.013	0.0008	13.15	0.24	0.008	0.0005	87.8	1.7	33.67	0.7	9.29E-15	9.12E-16			2.96	PPLLLL
	1/02/2015	13.05	8433-02A	80.3	2.70	0.066	0.0053	2.81	0.45	0.255	0.0099	5.6	1.9	17	6.6	1.07E-14	1.33E-16	**0.9986**	**0.003**	0.1	PPLLLL
		13.83	8433-02B	11.19	0.17	0.011	0.0016	2.50	0.19	0.017	0.0015	56.5	4	23.7	1.7	4.24E-15	3.79E-16			0.2	PPLLPL
		14.52	8433-02C	10.54	0.08	0.011	0.0005	1.62	0.065	0.004	0.0003	90.08	0.87	35.44	0.42	1.37E-14	1.30E-15			0.3	PPLLLL
		15.23	8433-02D	10.11	0.05	0.012	0.0004	1.82	0.053	0.003	0.0001	93.66	0.5	35.36	0.25	3.04E-14	3.00E-15			0.4	PPLLLL
		16.10	8433-02E	9.459	0.06	0.012	0.0005	2.32	0.069	0.001	0.0003	97.18	0.87	34.35	0.37	1.53E-14	1.61E-15			0.49	LPLLLL
		16.90	8433-02F	9.609	0.08	0.01	0.0007	2.36	0.083	0.002	0.0003	94.5	1.1	33.95	0.46	9.40E-15	9.78E-16			0.59	PPLLLL
		17.68	8433-02G	9.476	0.09	0.012	0.0009	2.04	0.11	0.002	0.0004	96.9	1.4	34.32	0.54	7.33E-15	7.73E-16			0.79	PPLLLL
		18.33	8433-02H	9.93	0.25	0.011	0.0030	12.76	0.73	0.005	0.0022	95.1	6.7	35.5	2.6	1.76E-15	1.77E-16			0.99	PPLLLL
		19.09	8433-02I	10.45	0.16	0.015	0.0017	21.05	0.49	0.009	0.0010	89.6	3.3	35.4	1.4	3.82E-15	3.66E-16			1.48	PPLLLL
		19.89	8433-02J	10.76	0.14	0.016	0.0012	17.19	0.41	0.01	0.0008	85.2	2.5	34.6	1.1	4.90E-15	4.55E-16			1.98	PPLLLL
		20.64	8433-02K	10.74	0.08	0.013	0.0006	16.86	0.25	0.011	0.0009	82	2.8	33.3	1.2	1.09E-14	1.02E-15			2.96	LPLLPL
PR08b-W.R																					
	1/03/2015	0.14	8434-01A	18.98	0.18	0.021	0.0012	1.74	0.13	0.046	0.0012	27.8	1.9	19.8	1.5	1.09E-14	5.72E-16	**0.9986**	**0.003**	0.1	PPLLLL
		0.99	8434-01B	17.27	0.11	0.015	0.0006	1.16	0.061	0.02	0.0005	66.01	0.82	42.47	0.68	2.70E-14	1.56E-15			0.2	PPLLLL
		1.82	8434-01C	15.94	0.07	0.013	0.0004	1.01	0.036	0.013	0.0003	75.78	0.56	44.97	0.46	4.18E-14	2.62E-15			0.3	PPLLLL
		2.70	8434-01D	13.79	0.09	0.013	0.0006	1.09	0.044	0.005	0.0003	90.56	0.7	46.47	0.48	2.31E-14	1.67E-15			0.4	PPLLLL
		3.47	8434-01E	13.61	0.10	0.013	0.0006	0.89	0.054	0.006	0.0004	88.19	0.84	44.67	0.53	1.75E-14	1.29E-15			0.49	PPLLLL
		4.21	8434-01F	13.08	0.09	0.012	0.0006	0.65	0.056	0.003	0.0003	92.9	0.7	45.22	0.45	1.84E-14	1.40E-15			0.59	PPLLLL
		4.96	8434-01G	12.36	0.06	0.01	0.0003	0.93	0.028	0.001	0.0002	96.97	0.44	44.6	0.28	3.86E-14	3.12E-15			0.79	PPLLLL
		5.80	8434-01H	12.47	0.12	0.013	0.0008	3.60	0.12	0.003	0.0004	94.3	1	43.87	0.62	1.12E-14	8.99E-16			0.99	PPLLLL

		6.55	8434-01I	12.61	0.11	0.014	0.0008	5.54	0.15	0.004	0.0004	93.7	1	44.13	0.61	1.20E-14	9.49E-16			1.48	PPLLLL
		7.34	8434-01J	12.29	0.15	0.018	0.0011	5.61	0.25	0.004	0.0007	94.5	1.7	43.38	0.92	6.36E-15	5.17E-16			1.98	PPLLLL
		8.09	8434-01K	13.13	0.12	0.016	0.0007	5.64	0.16	0.006	0.0005	90.6	1.2	44.43	0.69	1.23E-14	9.35E-16			2.96	PPLLLL
	1/03/2015	11.58	8434-02A	16.43	0.14	0.019	0.0007	1.34	0.081	0.035	0.0007	37.2	1.1	22.88	0.89	1.78E-14	1.08E-15	**0.9986**	**0.003**	0.1	PPLLLL
		12.44	8434-02B	15.88	0.08	0.014	0.0004	1.01	0.04	0.013	0.0003	76.47	0.54	45.2	0.47	4.11E-14	2.59E-15			0.2	PPLLLL
		13.27	8434-02C	14.18	0.06	0.013	0.0003	0.98	0.034	0.007	0.0002	85.7	0.38	45.23	0.32	5.37E-14	3.79E-15			0.3	PPLLLL
		14.22	8434-02D	12.91	0.07	0.013	0.0006	0.84	0.035	0.002	0.0002	94.82	0.58	45.55	0.35	3.03E-14	2.34E-15			0.4	PPLLLL
		15.07	8434-02E	12.56	0.07	0.012	0.0005	0.72	0.044	0.002	0.0003	95.06	0.79	44.42	0.44	2.60E-14	2.07E-15			0.49	PPLLPL
		15.84	8434-02F	12.48	0.07	0.011	0.0004	0.65	0.031	0.001	0.0002	97.14	0.49	45.12	0.32	3.14E-14	2.51E-15			0.59	PPLLLL
		16.63	8434-02G	12.25	0.06	0.012	0.0003	0.91	0.038	9E-04	0.0001	98.36	0.32	44.85	0.24	4.95E-14	4.05E-15			0.79	PPLLLL
		17.43	8434-02H	12.17	0.10	0.012	0.0006	2.55	0.11	0.002	0.0003	97.38	0.93	44.19	0.53	1.27E-14	1.04E-15			0.99	PPLLLL
		18.23	8434-02I	12.39	0.08	0.012	0.0008	3.86	0.13	0.002	0.0004	96.8	1.1	44.72	0.55	1.03E-14	8.34E-16			1.48	PLLLLL
		18.96	8434-02J	12.44	0.08	0.012	0.0008	4.55	0.14	0.004	0.0004	93.3	1.1	43.32	0.53	1.11E-14	8.95E-16			1.98	PLLLLL
		19.80	8434-02K	12.42	0.11	0.013	0.0009	4.73	0.15	0.003	0.0004	95.5	1.1	44.27	0.6	1.15E-14	9.29E-16			2.96	PPLLLL
PR09b-W.R																					
	1/03/2015	23.38	8436-01A	182	7.50	0.132	0.0087	2.38	0.59	0.557	0.0240	8.8	1.2	59	11	1.84E-14	1.01E-16	**0.9984**	**0.003**	0.1	PPLLLL
	1/04/2015	0.22	8436-01B	37.8	0.54	0.032	0.0015	2.54	0.2	0.081	0.0020	36.3	1.3	51.1	2.3	1.66E-14	4.38E-16			0.2	PPLLLL
		1.01	8436-01C	24.52	0.15	0.02	0.0007	2.21	0.07	0.039	0.0006	53.03	0.7	48.4	0.94	3.42E-14	1.39E-15			0.3	PPLLLL
		1.90	8436-01D	17.03	0.09	0.014	0.0003	1.25	0.031	0.017	0.0003	70.72	0.51	44.84	0.5	6.64E-14	3.90E-15			0.4	PPLLLL
		2.81	8436-01E	13.01	0.07	0.013	0.0005	1.22	0.041	0.004	0.0002	92.15	0.6	44.64	0.36	2.70E-14	2.07E-15			0.49	PPLLLL
		3.71	8436-01F	13.13	0.12	0.012	0.0007	1.31	0.073	0.004	0.0004	91.65	0.98	44.81	0.59	1.52E-14	1.16E-15			0.59	PPLLLL
		4.43	8436-01G	12.72	0.10	0.011	0.0007	2.52	0.099	0.002	0.0004	96.7	0.93	45.83	0.55	1.54E-14	1.21E-15			0.79	PPLLLL
		5.30	8436-01H	11.72	0.13	0.013	0.0012	3.80	0.24	-0	0.0007	104.8	2	45.79	0.96	6.04E-15	5.15E-16			0.99	PPLLLL
		6.04	8436-01I	11.61	0.10	0.009	0.0009	4.82	0.2	-0	0.0005	104.9	1.5	45.46	0.67	8.52E-15	7.34E-16			1.48	PPLLLL
		6.77	8436-01J	11.37	0.14	0.01	0.0010	6.33	0.23	-0	0.0007	106	1.9	45.06	0.91	6.25E-15	5.50E-16			1.98	PPLLLL
		7.51	8436-01K	12.07	0.09	0.013	0.0007	8.00	0.18	0.001	0.0004	101.5	1.1	45.83	0.59	1.25E-14	1.04E-15			2.96	PPLLLL

	1/04/2015	11.04	8436-02A	227.9	7.70	0.158	0.0074	3.36	0.59	0.7	0.0250	8.44	0.94	71	12	3.11E-14	1.36E-16	**0.9984**	**0.003**	0.1	PPLLLL
		11.88	8436-02B	61.47	0.80	0.043	0.0020	2.53	0.2	0.158	0.0031	23.8	1.2	54.4	3.5	2.53E-14	4.12E-16			0.2	PPLLLL
		12.81	8436-02C	26.22	0.19	0.02	0.0008	2.07	0.089	0.043	0.0007	51.2	0.83	49.9	1.1	3.12E-14	1.19E-15			0.3	PPLLLL
		13.70	8436-02D	22.19	0.10	0.018	0.0004	1.87	0.052	0.033	0.0004	56.42	0.55	46.63	0.73	6.69E-14	3.02E-15			0.39	PPLLLL
		14.60	8436-02E	14.92	0.06	0.014	0.0002	1.23	0.026	0.01	0.0001	81.43	0.33	45.22	0.33	1.04E-13	7.00E-15			0.49	PPLLLL
		15.50	8436-02F	13.58	0.07	0.012	0.0003	1.33	0.045	0.005	0.0002	88.97	0.46	44.99	0.34	3.68E-14	2.71E-15			0.59	PPLLLL
		16.34	8436-02G	13.17	0.06	0.012	0.0004	1.35	0.051	0.004	0.0002	92.59	0.43	45.39	0.31	3.41E-14	2.59E-15			0.79	PPLLLL
		17.23	8436-02H	12.88	0.08	0.013	0.0006	2.89	0.073	0.003	0.0002	94.39	0.6	45.31	0.4	2.36E-14	1.83E-15			0.99	PPLLLL
		18.10	8436-02I	12.31	0.10	0.012	0.0007	3.82	0.12	0.002	0.0004	97.2	1	44.65	0.56	1.26E-14	1.02E-15			1.48	PPLLLL
		18.90	8436-02J	12.31	0.08	0.011	0.0006	3.45	0.12	0.002	0.0003	96.11	0.78	44.11	0.46	1.42E-14	1.15E-15			1.98	LPLLLL
		19.75	8436-02K	12.5	0.10	0.011	0.0010	6.09	0.21	0.004	0.0005	95	1.3	44.34	0.68	8.39E-15	6.71E-16			2.96	PLLLLL
W4-W.R																					
	11/13/2016	12.25	9123-01A	46.41	0.13	0.043	0.0004	0.05	0.0095	0.149	0.0007	3.96	0.37	12.2	1.4	6.83E-13	1.47E-14	**1.00289**	**0.0007**	0.1	PPLLLL
		13.20	9123-01B	5.268	0.01	0.014	0.0001	0.02	0.0018	0.008	0.0001	52.16	0.42	18.22	0.16	4.44E-13	8.42E-14			0.2	PPLLLL
		14.20	9123-01C	2.6	0.00	0.011	0.0001	0.02	0.0012	1E-04	0.0000	98.6	0.21	17.001	0.044	3.62E-13	1.39E-13			0.25	PPLLLL
		15.18	9123-01D	2.511	0.00	0.011	0.0001	0.02	0.00072	3E-05	0.0000	99.73	0.13	16.604	0.028	5.51E-13	2.19E-13			0.3	PPLLLL
		16.19	9123-01E	2.455	0.00	0.011	0.0000	0.02	0.00063	3E-05	0.0000	99.69	0.16	16.229	0.029	6.10E-13	2.48E-13			0.35	PPLLLL
		17.22	9123-01F	2.447	0.00	0.011	0.0001	0.02	0.00072	3E-05	0.0000	99.75	0.15	16.19	0.031	5.32E-13	2.17E-13			0.4	PPLLLL
		18.20	9123-01G	2.431	0.00	0.012	0.0000	0.02	0.00077	#####	0.0000	100.04	0.14	16.131	0.029	4.99E-13	2.05E-13			0.5	PPLLLL
		19.17	9123-01H	2.419	0.00	0.012	0.0001	0.03	0.00095	5E-05	0.0000	99.5	0.17	15.965	0.033	3.81E-13	1.58E-13			0.7	PPLLLL
		20.13	9123-01I	2.421	0.00	0.012	0.0001	0.04	0.0028	5E-05	0.0000	99.49	0.44	15.979	0.075	1.51E-13	6.23E-14			1	LPLLLL
		21.28	9123-01J	2.464	0.01	0.012	0.0001	0.04	0.0038	7E-05	0.0001	99.32	0.69	16.23	0.11	9.53E-14	3.87E-14			1.5	PPLLLL
		22.32	9123-01K	2.478	0.01	0.012	0.0001	0.03	0.003	1E-04	0.0000	98.89	0.55	16.253	0.091	1.16E-13	4.69E-14			2	PPLLLL
		23.37	9123-01L	2.499	0.01	0.012	0.0001	0.02	0.004	2E-04	0.0001	97.08	0.66	16.09	0.11	9.61E-14	3.85E-14			3.5	PPLLLL
	11/14/2016	4.62	9123-02A	19.63	0.03	0.025	0.0002	0.02	0.003	0.058	0.0003	11.74	0.4	15.3	0.62	8.19E-13	4.17E-14	**1.00289**	**0.0007**	0.1	PPLLLL
		5.60	9123-02B	2.549	0.00	0.011	0.0000	0.02	0.00055	2E-04	0.0000	98.1	0.14	16.582	0.027	9.61E-13	3.77E-13			0.2	PPLLLL
		6.79	9123-02C	2.458	0.00	0.011	0.0000	0.02	0.00058	3E-05	0.0000	99.71	0.15	16.254	0.027	7.33E-13	2.98E-13			0.25	PPLLLL

		7.79	9123-02D	2.44	0.00	0.011	0.0001	0.01	0.00071	2E-05	0.0000	99.83	0.16	16.158	0.032	4.63E-13	1.90E-13			0.3	PPLLLL
		8.85	9123-02E	2.427	0.00	0.012	0.0001	0.02	0.0013	7E-05	0.0000	99.21	0.27	15.973	0.049	2.44E-13	1.01E-13			0.35	PPLLLL
		9.92	9123-02F	2.424	0.01	0.011	0.0001	0.02	0.0023	1E-04	0.0000	98.62	0.54	15.854	0.09	1.28E-13	5.27E-14			0.4	PPLLLL
		10.98	9123-02G	2.423	0.00	0.012	0.0001	0.05	0.003	1E-04	0.0000	98.63	0.6	15.85	0.098	1.01E-13	4.18E-14			0.5	PPLLLL
		12.02	9123-02H	2.456	0.01	0.012	0.0002	0.06	0.0044	2E-04	0.0001	97.44	0.97	15.88	0.16	6.95E-14	2.83E-14			0.7	PPLLLL
		13.06	9123-02I	2.483	0.02	0.011	0.0002	0.01	0.0065	3E-04	0.0001	96.6	1.5	15.91	0.24	4.35E-14	1.75E-14			1	PPLLLL
		14.18	9123-02J	2.507	0.01	0.011	0.0001	0.02	0.0025	2E-04	0.0000	97.75	0.53	16.253	0.09	1.17E-13	4.67E-14			2	PPLLLL
		15.20	9123-02K	2.556	0.01	0.012	0.0002	0.02	0.0049	5E-04	0.0001	94.4	1.1	16	0.19	5.54E-14	2.17E-14			3.5	PPLLLL
W11-W.R																					
	11/14/2016	20.36	9124-01A	98.1	1.30	0.077	0.0016	1.47	0.07	0.314	0.0047	4.52	0.79	29.3	5.5	2.26E-13	2.31E-15	**1.00424**	**0.0009**	0.1	PPLLLL
		21.42	9124-01B	5.277	0.02	0.014	0.0001	0.64	0.0093	0.009	0.0001	51.59	0.78	18.06	0.28	1.44E-13	2.73E-14			0.2	PPLLLL
		22.54	9124-01C	2.947	0.04	0.012	0.0002	0.60	0.0099	0.002	0.0000	82.2	1.1	16.08	0.24	1.69E-13	5.75E-14			0.25	LPLLLL
		23.63	9124-01D	3.256	0.01	0.012	0.0001	0.56	0.0035	0.003	0.0000	75.08	0.45	16.22	0.1	2.76E-13	8.47E-14			0.3	PPLLLL
	11/15/2016	0.59	9124-01E	3.148	0.01	0.012	0.0001	0.56	0.0036	0.003	0.0000	77.22	0.36	16.129	0.078	3.43E-13	1.09E-13			0.35	PPLLLL
		1.61	9124-01F	2.674	0.01	0.012	0.0001	0.50	0.0032	1E-03	0.0000	90.45	0.36	16.047	0.065	2.98E-13	1.11E-13			0.4	PPLLLL
		2.58	9124-01G	2.554	0.01	0.012	0.0001	0.56	0.0044	6E-04	0.0000	94.62	0.34	16.035	0.058	3.41E-13	1.33E-13			0.5	PPLLLL
		3.55	9124-01H	2.55	0.01	0.012	0.0001	0.78	0.0064	6E-04	0.0000	95.09	0.42	16.093	0.072	2.94E-13	1.15E-13			0.7	PPLLLL
		4.62	9124-01I	2.538	0.01	0.012	0.0001	1.71	0.012	9E-04	0.0000	94.82	0.92	15.98	0.14	1.21E-13	4.75E-14			1	PPLLLL
		5.64	9124-01J	2.522	0.02	0.012	0.0002	1.92	0.02	0.001	0.0001	92.3	1.7	15.46	0.25	5.62E-14	2.23E-14			1.5	PPLLLL
		6.73	9124-01K	2.544	0.02	0.013	0.0002	5.90	0.038	0.002	0.0001	92.6	2.2	15.69	0.36	6.46E-14	2.54E-14			2	PPLLLL
		7.69	9124-01L	2.621	0.01	0.013	0.0001	7.54	0.032	0.003	0.0001	90.6	2.3	15.84	0.39	1.43E-13	5.47E-14			3.5	PPLLLL
	11/15/2016	12.87	9124-02A	61.41	0.51	0.055	0.0010	2.24	0.063	0.197	0.0022	4.53	0.76	18.5	3.4	1.74E-13	2.84E-15	**1.00424**	**0.0009**	0.1	PPLLLL
		13.94	9124-02B	4.291	0.01	0.013	0.0002	0.66	0.011	0.006	0.0001	62.84	0.83	17.89	0.24	1.04E-13	2.42E-14			0.2	PPLLLL
		15.00	9124-02C	2.868	0.06	0.012	0.0002	0.68	0.015	0.001	0.0001	88	2.3	16.75	0.42	1.34E-13	4.67E-14			0.25	PPLLLL
		15.98	9124-02D	2.679	0.04	0.011	0.0002	0.61	0.011	0.001	0.0000	87.1	1.3	15.49	0.23	2.05E-13	7.64E-14			0.3	LPLLLL
		16.97	9124-02E	2.704	0.01	0.012	0.0001	0.59	0.004	0.001	0.0000	89.18	0.4	15.997	0.075	2.73E-13	1.01E-13			0.35	PPLLLL
		18.02	9124-02F	2.504	0.02	0.012	0.0001	0.54	0.0046	5E-04	0.0000	95.66	0.97	15.9	0.14	2.52E-13	1.01E-13			0.4	PPLLLL

		19.08	9124-02G	2.479	0.03	0.012	0.0001	0.61	0.007	4E-04	0.0000	97.5	1.2	16.04	0.18	2.45E-13	9.88E-14			0.5	PPLLLL
		20.09	9124-02H	2.499	0.01	0.012	0.0001	0.75	0.0062	5E-04	0.0000	96.64	0.42	16.027	0.07	2.08E-13	8.34E-14			0.7	PPLLLL
		21.13	9124-02I	2.53	0.01	0.013	0.0001	3.96	0.027	0.002	0.0001	92.6	1.4	15.59	0.24	8.93E-14	3.53E-14			1	PPLLLL
		22.15	9124-02J	3.001	0.05	0.013	0.0004	3.01	0.088	0.001	0.0002	95.5	2.7	19.03	0.55	3.01E-14	1.00E-14			1.5	PLLLLL
		23.16	9124-02K	2.541	0.02	0.012	0.0002	3.98	0.037	0.002	0.0002	89.1	2.4	15.06	0.4	3.15E-14	1.24E-14			2	PPLLLL
	11/16/2016	0.22	9124-02L	2.98	0.02	0.014	0.0002	7.47	0.039	0.004	0.0002	75.8	2.5	15.07	0.49	4.13E-14	1.38E-14			3.5	PPLLLL
W3-W.R																					
	12/21/2016	20.68	9244-01A	42.25	0.43	0.039	0.0015	2.05	0.38	0.13	0.0021	8.4	1.3	23.7	3.7	6.41E-14	1.52E-15	**1.00723**	**0.0009**	0.1	PPLLLL
		21.78	9244-01B	4.461	0.02	0.013	0.0002	0.63	0.057	0.006	0.0002	58.2	1.2	17.26	0.36	4.79E-14	1.07E-14			0.2	PPLLLL
		22.87	9244-01C	2.707	0.01	0.012	0.0002	0.48	0.03	0.001	0.0001	89.8	1.1	16.15	0.19	4.70E-14	1.74E-14			0.25	PPLLLL
		23.87	9244-01D	2.633	0.01	0.012	0.0001	0.39	0.029	8E-04	0.0001	92.19	0.72	16.13	0.13	6.60E-14	2.51E-14			0.3	PPLLLL
	12/22/2016	0.98	9244-01E	2.572	0.01	0.012	0.0001	0.49	0.017	6E-04	0.0000	94.25	0.52	16.107	0.089	9.67E-14	3.76E-14			0.35	PPLLLL
		2.07	9244-01F	2.478	0.01	0.012	0.0001	0.42	0.011	3E-04	0.0000	97.34	0.42	16.028	0.071	1.39E-13	5.61E-14			0.4	PPLLLL
		3.17	9244-01G	2.444	0.01	0.012	0.0001	0.38	0.012	3E-04	0.0000	97.38	0.34	15.815	0.059	1.88E-13	7.69E-14			0.5	PPLLLL
		4.24	9244-01H	2.427	0.00	0.012	0.0001	0.39	0.0062	3E-04	0.0000	97.99	0.26	15.804	0.046	2.99E-13	1.23E-13			0.7	PPLLLL
		5.25	9244-01I	2.417	0.01	0.012	0.0001	1.20	0.013	7E-04	0.0000	95.71	0.62	15.38	0.1	1.20E-13	4.96E-14			1	PPLLLL
		6.22	9244-01J	2.482	0.01	0.013	0.0001	2.74	0.031	0.001	0.0000	94.4	1	15.6	0.17	1.00E-13	4.04E-14			1.5	PPLLLL
		7.27	9244-01K	2.53	0.01	0.013	0.0002	1.75	0.032	9E-04	0.0001	94.2	1.1	15.86	0.19	4.99E-14	1.97E-14			2	PPLLLL
		8.30	9244-01L	2.572	0.01	0.013	0.0001	1.86	0.032	0.001	0.0001	89.8	0.91	15.37	0.16	7.19E-14	2.80E-14			3.5	PPLLLL
	12/22/2016	13.49	9244-02A	34.11	0.36	0.035	0.0015	0.96	0.52	0.107	0.0018	6.5	1.3	14.8	3.1	4.31E-14	1.26E-15	**1.00723**	**0.0009**	0.1	PPLLLL
		14.55	9244-02B	4.256	0.02	0.013	0.0002	0.51	0.065	0.006	0.0002	60.5	1.3	17.09	0.37	4.19E-14	9.84E-15			0.2	PPLLLL
		15.57	9244-02C	2.652	0.01	0.012	0.0001	0.52	0.012	7E-04	0.0000	93.99	0.56	16.56	0.1	9.95E-14	3.75E-14			0.3	PPLLLL
		16.61	9244-02D	2.505	0.01	0.012	0.0001	0.46	0.014	6E-04	0.0000	94.4	0.56	15.716	0.092	1.04E-13	4.17E-14			0.35	PPLLLL
		17.66	9244-02E	2.466	0.01	0.012	0.0001	0.47	0.014	3E-04	0.0000	97.62	0.49	15.999	0.079	1.26E-13	5.12E-14			0.4	PPLLLL
		18.64	9244-02F	2.441	0.01	0.012	0.0001	0.41	0.0083	3E-04	0.0000	97.71	0.31	15.851	0.057	2.18E-13	8.92E-14			0.5	PPLLLL
		19.63	9244-02G	2.426	0.01	0.012	0.0001	0.37	0.0073	3E-04	0.0000	97.8	0.35	15.764	0.062	2.06E-13	8.50E-14			0.6	PPLLLL
		20.63	9244-02H	2.431	0.01	0.012	0.0001	0.33	0.012	3E-04	0.0000	97.58	0.41	15.761	0.068	1.43E-13	5.86E-14			0.7	PPLLLL

		21.68	9244-02I	2.416	0.01	0.012	0.0001	1.89	0.027	1E-03	0.0001	93.98	0.92	15.11	0.15	7.93E-14	3.28E-14			1	PPLLLL
		22.75	9244-02J	2.457	0.01	0.013	0.0002	3.24	0.043	0.001	0.0001	92.9	1.5	15.2	0.24	5.25E-14	2.14E-14			1.5	PPLLLL
		23.73	9244-02K	2.482	0.01	0.013	0.0002	2.19	0.047	0.001	0.0001	92.3	1.3	15.25	0.22	4.02E-14	1.62E-14			2	PPLLLL
	12/23/2016	0.80	9244-02L	2.591	0.01	0.013	0.0001	1.92	0.032	0.001	0.0000	90.94	0.79	15.68	0.14	8.85E-14	3.42E-14			3.5	LPLLLL
EB14-Plagi.																					
	01/20/2017	22.60	9126-01A	90	24.00	-0.05	0.0430	11.00	18	0.168	0.0620	45	15	250	100	2.54E-15	2.84E-17	**1.008**	**0.0009**	0.1	PPLLLL
		23.70	9126-01B	12	1.00	0.01	0.0096	5.10	5	0.009	0.0120	80	31	63	24	1.29E-15	1.08E-16			0.2	PPLLLL
	01/21/2017	0.81	9126-01C	5.55	0.12	0.017	0.0019	11.16	0.78	0.011	0.0021	55	12	20.4	4.4	3.80E-15	6.85E-16			0.3	PPLLLL
		1.90	9126-01D	3.679	0.08	0.011	0.0015	12.48	0.67	0.007	0.0016	70	13	17.2	3.3	3.03E-15	8.23E-16			0.35	PPLLLL
		2.98	9126-01E	3.224	0.07	0.013	0.0014	12.64	0.59	0.009	0.0013	47	13	10.1	2.9	3.14E-15	9.74E-16			0.4	PPLLLL
		4.14	9126-01F	3.036	0.03	0.012	0.0008	13.06	0.39	0.005	0.0007	81.2	7.8	16.5	1.6	5.94E-15	1.96E-15			0.5	PLLLLL
		5.21	9126-01G	2.935	0.03	0.013	0.0006	12.89	0.33	0.005	0.0006	86.6	6.8	17	1.3	6.53E-15	2.22E-15			0.6	PPLLLL
		6.32	9126-01H	2.917	0.04	0.011	0.0009	12.41	0.44	0.004	0.0007	89.1	8.1	17.4	1.6	4.89E-15	1.68E-15			0.7	PPLLLL
		7.42	9126-01I	3.028	0.03	0.013	0.0007	12.46	0.53	0.003	0.0006	103.6	7.1	21	1.4	6.73E-15	2.22E-15			1	PPLLLL
		8.45	9126-01J	2.94	0.03	0.012	0.0007	12.65	0.44	0.005	0.0007	80.7	7.6	15.9	1.5	6.05E-15	2.06E-15			1.5	PPLLLL
		9.56	9126-01K	3.035	0.05	0.013	0.0010	11.40	0.58	0.003	0.0009	100.9	9.6	20.4	1.9	3.60E-15	1.19E-15			2	PPLLLL
		10.66	9126-01L	3	0.01	0.012	0.0002	14.53	0.094	0.004	0.0001	92.7	3.8	18.63	0.76	5.84E-14	1.95E-14			3.5	PPLLLL
	01/21/2017	15.88	9126-02A	-300	1000.00	-0.5	1.7000	#####	670	-0.26	0.9400	81	46	-3000	28000	8.94E-16	-2.77E-18	**1.008**	**0.0009**	0.1	PPLLLL
		16.96	9126-02B	7.13	0.83	0.039	0.0160	17.40	5	0.036	0.0120	-32	52	-15	25	7.22E-16	1.01E-16			0.2	PPLLLL
		18.05	9126-02C	4.74	0.10	0.011	0.0020	10.35	0.78	0.006	0.0017	76	11	24.1	3.6	3.60E-15	7.60E-16			0.3	PPLLLL
		19.22	9126-02D	3.266	0.04	0.012	0.0009	10.77	0.42	0.002	0.0007	109	7.5	23.7	1.6	6.01E-15	1.84E-15			0.4	PLLLLL
		20.29	9126-02E	3.071	0.03	0.011	0.0007	9.98	0.31	0.001	0.0006	115.1	7	23.6	1.4	6.75E-15	2.20E-15			0.5	PPLLLL
		21.35	9126-02F	3.01	0.03	0.01	0.0008	10.06	0.36	0.004	0.0006	90	6.8	18.1	1.4	6.64E-15	2.20E-15			0.6	PPLLLL
		22.39	9126-02G	2.905	0.04	0.011	0.0009	9.63	0.35	0.003	0.0007	94.1	7.4	18.2	1.4	5.70E-15	1.96E-15			0.7	PPLLLL
		23.43	9126-02H	2.945	0.03	0.012	0.0005	9.73	0.3	0.003	0.0005	91.5	5.5	18	1.1	9.91E-15	3.37E-15			1	PPLLLL
	01/22/2017	0.51	9126-02I	2.976	0.02	0.012	0.0006	10.42	0.26	0.003	0.0005	94.3	5.6	18.7	1.1	9.02E-15	3.03E-15			1.5	PPLLLL
		1.56	9126-02J	3.033	0.04	0.011	0.0010	10.88	0.49	0.003	0.0008	99.3	8.9	20.1	1.8	4.80E-15	1.58E-15			2	PPLLLL

		2.68	9126-02K	3.023	0.01	0.012	0.0003	13.02	0.13	0.004	0.0002	97.1	3.6	19.63	0.73	3.06E-14	1.01E-14			3	PPLLLL
		3.73	9126-02L	2.832	0.06	0.011	0.0015	11.62	0.59	0.004	0.0013	92	14	17.5	2.7	3.05E-15	1.08E-15			3.5	PPLLLL
W1-W.R																					
	01/22/2017	8.89	9243-01A	14.71	0.10	0.02	0.0006	2.17	0.21	0.035	0.0008	29.9	1.6	29.2	1.6	3.58E-14	2.44E-15	**1.008**	**0.0009**	0.1	PPLLLL
		9.95	9243-01B	3.545	0.01	0.012	0.0002	0.70	0.031	0.002	0.0001	84.96	0.92	20	0.22	5.80E-14	1.64E-14			0.2	PPLLLL
		11.00	9243-01C	2.559	0.01	0.011	0.0001	0.43	0.011	4E-04	0.0000	97.02	0.39	16.495	0.067	1.66E-13	6.49E-14			0.3	PPLLLL
		12.12	9243-01D	2.515	0.01	0.011	0.0001	0.48	0.013	3E-04	0.0000	97.52	0.37	16.294	0.062	1.71E-13	6.78E-14			0.35	PPLLLL
		13.14	9243-01E	2.461	0.01	0.011	0.0001	0.44	0.011	3E-04	0.0000	97.77	0.34	15.987	0.058	1.96E-13	7.97E-14			0.4	PPLLLL
		14.16	9243-01F	2.453	0.00	0.012	0.0001	0.41	0.0091	2E-04	0.0000	98.56	0.25	16.065	0.048	2.71E-13	1.11E-13			0.5	PPLLLL
		15.19	9243-01G	2.436	0.01	0.012	0.0001	0.33	0.0088	2E-04	0.0000	98.34	0.31	15.917	0.058	2.22E-13	9.12E-14			0.6	PPLLLL
		16.22	9243-01H	2.42	0.01	0.012	0.0001	0.37	0.011	3E-04	0.0000	97.46	0.4	15.671	0.067	1.46E-13	6.05E-14			0.7	PPLLLL
		17.30	9243-01I	2.445	0.01	0.012	0.0001	0.85	0.027	6E-04	0.0000	95.54	0.51	15.529	0.084	1.16E-13	4.73E-14			1	PPLLLL
		18.31	9243-01J	2.562	0.01	0.013	0.0003	2.03	0.07	0.002	0.0001	81.7	1.7	13.93	0.29	2.81E-14	1.09E-14			1.5	PPLLLL
		19.42	9243-01K	2.654	0.01	0.013	0.0003	3.53	0.087	0.003	0.0002	79.4	2.1	14.04	0.37	2.62E-14	9.86E-15			2	PPLLLL
		20.45	9243-01L	2.749	0.01	0.014	0.0002	4.98	0.072	0.003	0.0001	80.6	1.6	14.77	0.3	6.50E-14	2.37E-14			3.5	PPLLLL
	01/23/2017	1.80	9243-02A	16.05	0.11	0.02	0.0007	1.63	0.22	0.041	0.0009	24.2	1.6	25.8	1.8	3.97E-14	2.47E-15	**1.008**	**0.0009**	0.1	PPLLLL
		2.82	9243-02B	3.226	0.01	0.012	0.0002	0.51	0.035	0.002	0.0001	84.9	1.2	18.19	0.25	4.58E-14	1.42E-14			0.2	PPLLLL
		3.83	9243-02C	2.566	0.01	0.011	0.0001	0.37	0.016	4E-04	0.0000	96.7	0.47	16.484	0.08	1.14E-13	4.45E-14			0.3	PPLLLL
		4.91	9243-02D	2.54	0.01	0.011	0.0001	0.40	0.017	3E-04	0.0000	98.03	0.48	16.543	0.081	1.13E-13	4.46E-14			0.35	PPLLLL
		5.90	9243-02E	2.501	0.01	0.012	0.0001	0.44	0.011	2E-04	0.0000	98.64	0.4	16.389	0.069	1.34E-13	5.37E-14			0.4	PPLLLL
		6.96	9243-02F	2.462	0.00	0.011	0.0001	0.37	0.01	2E-04	0.0000	98.48	0.29	16.111	0.053	2.01E-13	8.16E-14			0.5	PPLLLL
		7.95	9243-02G	2.434	0.01	0.011	0.0001	0.32	0.0093	2E-04	0.0000	99.1	0.29	16.025	0.051	1.90E-13	7.81E-14			0.6	PPLLLL
		8.92	9243-02H	2.428	0.01	0.012	0.0001	0.28	0.014	2E-04	0.0000	98.35	0.39	15.867	0.064	1.29E-13	5.31E-14			0.7	PPLLLL
		10.03	9243-02I	2.471	0.01	0.012	0.0001	1.00	0.023	7E-04	0.0000	94.26	0.54	15.489	0.092	1.36E-13	5.50E-14			1	PPLLLL
		11.12	9243-02J	2.732	0.01	0.013	0.0001	4.35	0.041	0.003	0.0001	83.6	1.4	15.22	0.25	8.59E-14	3.14E-14			2	PPLLLL
		12.17	9243-02K	6.756	0.04	0.016	0.0006	0.72	0.2	0.014	0.0006	38.4	2.6	17.2	1.2	1.98E-14	2.93E-15			3.5	PPLLLL
W4-W.R																					

	01/23/2017	17.64	9246-01A	69.58	0.96	0.061	0.0019	0.93	0.66	0.219	0.0039	6.3	1.1	29.2	5.5	6.37E-14	9.16E-16	**1.008**	**0.0009**	0.1	PPLLLL
		18.73	9246-01B	3.417	0.01	0.012	0.0002	-0.05	0.049	0.002	0.0001	80.7	1.2	18.3	0.27	3.70E-14	1.08E-14			0.2	PPLLLL
		19.78	9246-01C	2.489	0.01	0.012	0.0001	0.06	0.016	4E-05	0.0000	99.69	0.49	16.482	0.081	9.10E-14	3.66E-14			0.3	PPLLLL
		20.78	9246-01D	2.446	0.01	0.012	0.0001	0.08	0.017	1E-04	0.0000	98.83	0.54	16.059	0.089	8.13E-14	3.32E-14			0.35	PPLLLL
		21.84	9246-01E	2.431	0.01	0.012	0.0001	0.05	0.017	1E-04	0.0000	98.72	0.48	15.941	0.079	8.81E-14	3.62E-14			0.4	PPLLLL
		22.85	9246-01F	2.405	0.01	0.012	0.0001	0.07	0.01	1E-04	0.0000	98.7	0.39	15.771	0.065	1.28E-13	5.33E-14			0.5	PPLLLL
		23.90	9246-01G	2.422	0.01	0.012	0.0001	0.06	0.012	9E-05	0.0000	99.02	0.39	15.934	0.064	1.18E-13	4.89E-14			0.6	PPLLLL
	01/24/2017	0.94	9246-01H	2.416	0.01	0.012	0.0001	0.06	0.017	9E-05	0.0000	99.11	0.52	15.907	0.083	8.48E-14	3.51E-14			0.7	PPLLLL
		2.02	9246-01I	2.42	0.01	0.012	0.0001	0.04	0.01	1E-04	0.0000	98.68	0.4	15.865	0.066	1.28E-13	5.30E-14			1	PPLLLL
		3.08	9246-01J	2.423	0.00	0.012	0.0001	0.06	0.005	1E-04	0.0000	98.88	0.23	15.916	0.039	2.59E-13	1.07E-13			1.5	PPLLLL
		4.14	9246-01K	2.424	0.00	0.012	0.0001	0.08	0.0063	9E-05	0.0000	99.08	0.24	15.954	0.041	2.55E-13	1.05E-13			2	PPLLLL
		5.24	9246-01L	2.433	0.00	0.012	0.0001	0.08	0.0065	1E-04	0.0000	98.53	0.28	15.927	0.05	2.03E-13	8.33E-14			3.5	PPLLLL
	01/24/2017	10.44	9246-02A	43.25	0.91	0.04	0.0031	1.50	1.3	0.146	0.0050	-0.3	2.9	-1	8.4	1.86E-14	4.31E-16	**1.008**	**0.0009**	0.1	PPLLLL
		11.47	9246-02B	2.782	0.01	0.012	0.0003	0.17	0.068	0.001	0.0002	89.2	1.9	16.49	0.36	2.28E-14	8.21E-15			0.2	PPLLLL
		12.52	9246-02C	2.406	0.01	0.012	0.0001	0.21	0.021	2E-04	0.0000	97.69	0.67	15.62	0.11	6.36E-14	2.64E-14			0.3	PPLLLL
		13.60	9246-02D	2.431	0.01	0.012	0.0001	0.16	0.027	5E-04	0.0001	94.94	0.85	15.34	0.14	4.97E-14	2.04E-14			0.35	PPLLLL
		14.71	9246-02E	2.406	0.01	0.012	0.0002	0.20	0.03	2E-04	0.0001	98.32	0.83	15.72	0.13	4.76E-14	1.98E-14			0.4	PPLLLL
		15.75	9246-02F	2.415	0.01	0.012	0.0002	0.27	0.033	4E-04	0.0001	95.96	0.96	15.4	0.16	4.49E-14	1.86E-14			0.5	PPLLLL
		16.77	9246-02G	2.42	0.01	0.012	0.0002	0.20	0.051	5E-05	0.0001	100	1.4	16.09	0.23	2.82E-14	1.16E-14			0.6	PPLLLL
		17.87	9246-02H	2.406	0.01	0.012	0.0001	0.18	0.035	4E-04	0.0001	95.2	1	15.23	0.16	4.20E-14	1.74E-14			0.8	PPLLLL
		18.99	9246-02I	2.429	0.01	0.012	0.0001	0.24	0.0099	2E-04	0.0000	98.37	0.33	15.88	0.058	1.71E-13	7.03E-14			1.2	PPLLLL
		20.05	9246-02J	2.414	0.01	0.012	0.0001	0.26	0.013	3E-04	0.0000	97.27	0.55	15.604	0.09	9.66E-14	4.00E-14			1.7	PPLLLL
		21.07	9246-02K	2.451	0.01	0.011	0.0002	0.22	0.051	3E-04	0.0001	96.7	1.6	15.75	0.25	2.78E-14	1.13E-14			2.2	PPLLLL
		22.22	9246-02L	2.431	0.01	0.012	0.0001	0.30	0.015	2E-04	0.0000	98.53	0.53	15.918	0.088	8.93E-14	3.67E-14			3.5	PPLLLL
		23.24	9246-02M	2.446	0.01	0.012	0.0001	0.18	0.034	3E-04	0.0001	96.6	1.1	15.7	0.17	4.19E-14	1.71E-14			4	PPLLLL
W6-W.R																					
	01/25/2017	4.44	9247-01A	9.819	0.08	0.018	0.0009	1.49	0.32	0.023	0.0008	30.5	2.4	19.9	1.6	1.91E-14	1.94E-15	**1.008**	**0.0009**	0.1	PPLLLL

		5.47	9247-01B	2.547	0.00	0.012	0.0001	0.08	0.0078	3E-04	0.0000	97.06	0.3	16.42	0.057	1.81E-13	7.11E-14			0.2	PPLLLL
		6.49	9247-01C	2.464	0.00	0.011	0.0000	0.04	0.0018	6E-05	0.0000	99.43	0.12	16.276	0.024	8.35E-13	3.39E-13			0.3	PPLLLL
		7.51	9247-01D	2.444	0.00	0.012	0.0000	0.04	0.0027	5E-05	0.0000	99.45	0.12	16.146	0.026	5.35E-13	2.19E-13			0.35	PPLLLL
		8.52	9247-01E	2.434	0.00	0.012	0.0001	0.03	0.0036	7E-05	0.0000	99.25	0.17	16.051	0.034	3.85E-13	1.58E-13			0.4	PPLLLL
		9.50	9247-01F	2.428	0.00	0.012	0.0001	0.04	0.0036	5E-05	0.0000	99.5	0.18	16.047	0.035	3.93E-13	1.62E-13			0.5	PPLLLL
		10.48	9247-01G	2.416	0.00	0.012	0.0001	0.09	0.0046	7E-05	0.0000	99.37	0.17	15.953	0.032	4.18E-13	1.73E-13			0.6	PPLLLL
		11.51	9247-01H	2.427	0.01	0.012	0.0001	0.26	0.019	1E-04	0.0000	99.24	0.56	16.005	0.091	8.85E-14	3.65E-14			0.7	LPLLLL
		12.54	9247-01I	2.402	0.00	0.012	0.0001	1.04	0.032	4E-04	0.0000	98.89	0.57	15.794	0.092	9.86E-14	4.10E-14			1	PPLLLL
		13.70	9247-01J	2.398	0.01	0.012	0.0001	0.70	0.028	3E-04	0.0000	98.63	0.61	15.718	0.097	8.20E-14	3.42E-14			1.5	PPLLLL
		14.73	9247-01K	2.422	0.01	0.012	0.0001	0.40	0.034	3E-05	0.0001	100.9	1	16.24	0.17	4.34E-14	1.79E-14			2	PPLLLL
		15.78	9247-01L	2.463	0.01	0.012	0.0001	0.35	0.015	2E-04	0.0000	98.45	0.49	16.114	0.081	9.81E-14	3.98E-14			4	PPLLLL
	01/25/2017	21.10	9247-02A	12.37	0.11	0.015	0.0009	0.24	0.33	0.031	0.0010	26.2	2.5	21.5	2	2.19E-14	1.77E-15	**1.008**	**0.0009**	0.1	PPLLLL
		22.25	9247-02B	2.947	0.01	0.012	0.0001	0.03	0.017	0.001	0.0001	85.7	0.62	16.78	0.12	9.21E-14	3.12E-14			0.2	PPLLLL
		23.33	9247-02C	2.476	0.00	0.011	0.0001	0.02	0.0054	9E-05	0.0000	98.91	0.18	16.267	0.04	2.76E-13	1.11E-13			0.3	PPLLLL
	01/26/2017	0.38	9247-02D	2.467	0.00	0.011	0.0001	0.03	0.0035	9E-05	0.0000	98.98	0.17	16.221	0.035	3.53E-13	1.43E-13			0.35	PPLLLL
		1.40	9247-02E	2.461	0.00	0.012	0.0001	0.02	0.0032	8E-05	0.0000	99.11	0.15	16.199	0.03	4.27E-13	1.74E-13			0.4	PPLLLL
		2.41	9247-02F	2.432	0.00	0.011	0.0001	0.02	0.0022	5E-05	0.0000	99.47	0.13	16.069	0.028	6.25E-13	2.57E-13			0.5	PPLLLL
		3.41	9247-02G	2.427	0.00	0.011	0.0001	0.02	0.0024	7E-05	0.0000	99.18	0.13	15.993	0.026	5.96E-13	2.45E-13			0.6	PPLLLL
		4.40	9247-02H	2.42	0.00	0.012	0.0000	0.02	0.0032	6E-05	0.0000	99.33	0.16	15.971	0.033	4.25E-13	1.76E-13			0.7	PPLLLL
		5.43	9247-02I	2.424	0.00	0.012	0.0001	0.06	0.0027	9E-05	0.0000	99.1	0.16	15.961	0.031	5.27E-13	2.17E-13			1	PPLLLL
		6.42	9247-02J	2.429	0.00	0.012	0.0001	0.06	0.0054	1E-04	0.0000	98.56	0.26	15.904	0.045	2.52E-13	1.04E-13			1.5	PPLLLL
		7.50	9247-02K	2.441	0.01	0.012	0.0002	0.02	0.035	3E-04	0.0001	96.84	0.86	15.7	0.14	4.51E-14	1.85E-14			2	PPLLLL
		8.66	9247-02L	2.473	0.01	0.012	0.0001	0.02	0.017	2E-04	0.0000	97.77	0.56	16.062	0.094	7.71E-14	3.12E-14			4	PPLLLL
W11-W.R																					
	01/26/2017	14.02	9249-01A	-28	47.00	0.7	1.1000	#####	490	0.37	0.6500	410	300	-1400	4600	1.52E-16	-5.48E-18	**1.008**	**0.0009**	0.1	PPLLLL
		15.08	9249-01B	8.52	0.72	-0	0.0100	12.80	4.4	0.041	0.0100	-33	36	-19	21	1.14E-15	1.34E-16			0.3	PPLLLL
		16.16	9249-01C	3.008	0.08	0.008	0.0016	14.98	0.74	0.006	0.0018	82	19	16.5	3.8	2.23E-15	7.43E-16			0.4	PPLLLL

		17.22	9249-01D	2.598	0.05	0.009	0.0009	15.57	0.55	0.005	0.0010	92	13	16	2.2	3.70E-15	1.43E-15			0.5	PPLLLL
		18.41	9249-01E	2.431	0.04	0.009	0.0010	14.00	0.47	0.005	0.0010	81	14	13.2	2.3	3.27E-15	1.34E-15			0.6	PPLLLL
		19.50	9249-01F	2.533	0.09	8E-04	0.0024	10.20	1.1	0.003	0.0022	101	27	17.2	4.6	1.51E-15	5.97E-16			0.7	PPLLLL
		20.65	9249-01G	2.71	0.15	0.012	0.0037	10.70	1.6	-0.01	0.0034	219	40	39.6	7	9.45E-16	3.48E-16			1	PPLLLL
		21.79	9249-01H	2.94	0.16	9E-04	0.0037	11.50	1.7	0	0.0035	129	37	25.4	7.2	1.08E-15	3.68E-16			1.5	PPLLLL
		22.96	9249-01I	2.52	0.12	0.004	0.0029	13.80	1.4	-0.01	0.0030	223	38	37.5	6.2	1.13E-15	4.47E-16			2	PPLLLL
	01/27/2017	0.00	9249-01J	2.418	0.01	0.012	0.0001	16.81	0.12	0.005	0.0001	96.3	5.3	15.65	0.86	7.41E-14	3.06E-14			3	PPLLLL
		1.01	9249-01K	2.384	0.02	0.012	0.0003	14.11	0.2	0.004	0.0003	92.2	5.8	14.76	0.92	1.18E-14	4.96E-15			4	PPLLLL
	01/27/2017	6.31	9249-02A	143	38.00	0.136	0.0550	-18.00	21	0.55	0.1500	-16.1	8.9	-160	100	4.16E-15	2.91E-17	**1.008**	**0.0009**	0.1	PPLLLL
		7.51	9249-02B	6.888	0.05	0.015	0.0005	11.22	0.29	0.019	0.0007	29.2	3.1	13.5	1.4	2.34E-14	3.39E-15			0.3	PPLLLL
		8.61	9249-02C	3.209	0.02	0.012	0.0005	10.91	0.23	0.007	0.0003	60.7	4.2	13.05	0.9	1.33E-14	4.13E-15			0.4	PPLLLL
		9.66	9249-02D	2.697	0.03	0.011	0.0007	7.89	0.38	0.004	0.0005	75.5	5.9	13.6	1.1	7.05E-15	2.61E-15			0.5	PPLLLL
		10.73	9249-02E	2.862	0.04	0.014	0.0010	9.62	0.47	0.006	0.0008	66	9.1	12.6	1.7	4.38E-15	1.53E-15			0.6	PPLLLL
		11.88	9249-02F	2.836	0.02	0.013	0.0005	8.67	0.27	0.005	0.0004	72.5	4.5	13.74	0.86	1.16E-14	4.09E-15			1	PPLLLL
		12.98	9249-02G	2.479	0.01	0.012	0.0002	13.99	0.13	0.004	0.0001	93.3	4.4	15.51	0.73	4.54E-14	1.83E-14			2	PPLLLL
		14.04	9249-02H	2.456	0.01	0.012	0.0002	14.13	0.13	0.005	0.0002	89.1	4.8	14.69	0.78	2.42E-14	9.86E-15			2.5	PPLLLL
		15.06	9249-02I	2.354	0.04	0.012	0.0010	11.81	0.48	0.006	0.0009	63	12	9.9	1.9	3.31E-15	1.40E-15			3	PPLLLL
		16.22	9249-02J	2.395	0.02	0.011	0.0006	13.62	0.37	0.005	0.0005	81.9	7.6	13.2	1.2	7.51E-15	3.14E-15			4	PPLLLL
W14-W.R																					
	01/27/2017	21.59	9250-01A	6.265	0.03	0.013	0.0005	0.22	0.16	0.01	0.0005	52.4	2.3	21.76	0.97	2.13E-14	3.40E-15	**1.008**	**0.0009**	0.1	PPLLLL
		22.61	9250-01B	2.577	0.01	0.012	0.0001	0.02	0.0077	3E-04	0.0000	96.42	0.27	16.506	0.053	2.13E-13	8.28E-14			0.2	PPLLLL
		23.61	9250-01C	2.502	0.00	0.012	0.0000	0.03	0.0024	9E-05	0.0000	98.96	0.1	16.444	0.024	6.45E-13	2.58E-13			0.3	PPLLLL
	01/28/2017	0.61	9250-01D	2.502	0.00	0.012	0.0001	0.03	0.0041	1E-04	0.0000	98.81	0.18	16.422	0.035	3.74E-13	1.50E-13			0.4	PPLLLL
		1.60	9250-01E	2.485	0.01	0.012	0.0001	0.04	0.0071	8E-05	0.0000	99.12	0.26	16.364	0.049	2.25E-13	9.06E-14			0.5	PPLLLL
		2.63	9250-01F	2.502	0.01	0.012	0.0001	0.10	0.0074	2E-04	0.0000	97.97	0.26	16.288	0.05	2.24E-13	8.97E-14			0.6	PPLLLL
		3.65	9250-01G	2.538	0.01	0.012	0.0001	0.27	0.0089	4E-04	0.0000	96.4	0.27	16.258	0.054	2.20E-13	8.66E-14			0.7	PPLLLL
		4.63	9250-01H	2.59	0.01	0.012	0.0001	0.54	0.01	7E-04	0.0000	93.89	0.35	16.16	0.065	2.13E-13	8.23E-14			1	PPLLLL

		5.72	9250-01I	2.616	0.01	0.012	0.0001	0.38	0.015	6E-04	0.0000	94.38	0.52	16.403	0.094	1.06E-13	4.07E-14			1.5	PPLLLL
		6.88	9250-01J	2.764	0.01	0.012	0.0001	0.25	0.026	0.001	0.0001	89.49	0.79	16.43	0.14	6.64E-14	2.40E-14			2	PPLLLL
		7.94	9250-01K	2.884	0.01	0.012	0.0002	0.18	0.031	0.001	0.0001	87.5	0.9	16.77	0.17	5.24E-14	1.82E-14			3	PPLLLL
		9.02	9250-01L	2.862	0.02	0.012	0.0003	0.23	0.083	0.001	0.0002	89.4	2.3	17	0.44	1.95E-14	6.80E-15			4	PPLLLL
	01/28/2017	14.23	9250-02A	4.572	0.03	0.012	0.0005	0.20	0.18	0.006	0.0004	63.1	3	19.14	0.9	1.41E-14	3.08E-15	**1.008**	**0.0009**	0.1	PPLLLL
		15.25	9250-02B	2.548	0.01	0.012	0.0001	0.03	0.0072	3E-04	0.0000	97.02	0.26	16.423	0.052	2.08E-13	8.14E-14			0.2	PPLLLL
		16.29	9250-02C	2.488	0.01	0.012	0.0001	0.03	0.0046	1E-04	0.0000	98.45	0.21	16.271	0.042	2.84E-13	1.14E-13			0.25	PPLLLL
		17.34	9250-02D	2.481	0.00	0.012	0.0001	0.03	0.0046	2E-04	0.0000	98.26	0.22	16.197	0.038	3.41E-13	1.37E-13			0.3	PPLLLL
		18.34	9250-02E	2.499	0.00	0.012	0.0001	0.03	0.0039	9E-05	0.0000	99.03	0.18	16.437	0.038	3.65E-13	1.46E-13			0.4	PPLLLL
		19.35	9250-02F	2.469	0.00	0.012	0.0001	0.04	0.0058	2E-04	0.0000	97.8	0.2	16.042	0.038	2.62E-13	1.06E-13			0.5	PPLLLL
		20.38	9250-02G	2.473	0.01	0.012	0.0001	0.07	0.0059	1E-04	0.0000	98.58	0.23	16.195	0.046	2.49E-13	1.01E-13			0.6	PPLLLL
		21.49	9250-02H	2.467	0.00	0.012	0.0001	0.15	0.0052	2E-04	0.0000	98.53	0.2	16.151	0.039	2.95E-13	1.20E-13			0.7	PPLLLL
		22.61	9250-02I	2.49	0.00	0.012	0.0000	0.33	0.0061	2E-04	0.0000	98.42	0.23	16.282	0.042	3.74E-13	1.50E-13			1	PPLLLL
		23.66	9250-02J	2.512	0.01	0.012	0.0001	0.32	0.0088	3E-04	0.0000	97.23	0.29	16.23	0.054	2.17E-13	8.64E-14			2.5	PPLLLL
		0.65	9250-02K	2.52	0.01	0.011	0.0001	0.33	0.021	4E-04	0.0001	96	0.68	16.08	0.11	7.23E-14	2.87E-14			4	PPLLLL
EB1-W.R																					
	01/29/2017	6.00	9252-01A	164.1	4.50	0.12	0.0052	-8.20	1.7	0.524	0.0150	4.3	1.1	46	12	6.15E-14	3.75E-16	**1.008**	**0.0009**	0.1	PPLLLL
		7.02	9252-01B	17.78	0.09	0.027	0.0004	0.44	0.12	0.053	0.0007	11.5	1.1	13.6	1.3	9.69E-14	5.45E-15			0.2	PPLLLL
		8.03	9252-01C	9.186	0.04	0.015	0.0003	0.87	0.094	0.019	0.0003	40.4	1.1	24.64	0.66	6.60E-14	7.19E-15			0.3	PPLLLL
		9.01	9252-01D	7.077	0.02	0.014	0.0002	0.70	0.048	0.012	0.0002	49.56	0.75	23.27	0.37	8.80E-14	1.24E-14			0.4	PPLLLL
		10.01	9252-01E	5.069	0.01	0.012	0.0001	0.63	0.036	0.006	0.0001	63.98	0.53	21.52	0.19	1.18E-13	2.33E-14			0.5	PPLLLL
		11.05	9252-01F	3.822	0.01	0.012	0.0001	0.51	0.019	0.002	0.0000	83.5	0.42	21.18	0.11	1.68E-13	4.41E-14			0.6	PPLLLL
		12.04	9252-01G	3.485	0.01	0.012	0.0001	0.55	0.017	0.001	0.0000	90.11	0.42	20.85	0.1	1.46E-13	4.18E-14			0.7	PPLLLL
		13.02	9252-01H	3.384	0.01	0.012	0.0001	0.57	0.0092	0.001	0.0000	90.9	0.26	20.417	0.066	4.89E-13	1.45E-13			1	PPLLLL
		13.97	9252-01I	3.197	0.01	0.012	0.0001	0.78	0.01	8E-04	0.0000	93.98	0.31	19.949	0.071	2.95E-13	9.22E-14			1.5	PPLLLL
		15.00	9252-01J	3.283	0.01	0.012	0.0001	1.07	0.013	0.001	0.0000	91.07	0.4	19.859	0.092	2.29E-13	6.97E-14			2	PPLLLL
		16.01	9252-01K	3.396	0.01	0.012	0.0001	1.76	0.016	0.002	0.0000	87.5	0.48	19.74	0.11	3.45E-13	1.02E-13			3	PPLLLL

		17.00	9252-01L	3.505	0.01	0.012	0.0001	1.23	0.037	0.002	0.0001	85.14	0.79	19.82	0.19	8.87E-14	2.53E-14			4	PPLLLL
	01/29/2017	22.29	9252-02A	34.19	0.28	0.032	0.0009	1.35	0.25	0.105	0.0014	8.6	1	19.4	2.5	7.68E-14	2.25E-15	**1.008**	**0.0009**	0.1	LPLLLL
		23.34	9252-02B	9.927	0.03	0.017	0.0002	0.95	0.037	0.023	0.0002	32.04	0.59	21.12	0.42	1.81E-13	1.82E-14			0.35	PPLLLL
	01/30/2017	0.33	9252-02C	5.262	0.01	0.013	0.0001	0.56	0.02	0.007	0.0001	62.93	0.45	21.98	0.17	1.91E-13	3.63E-14			0.5	PPLLLL
		1.39	9252-02D	3.473	0.01	0.012	0.0001	0.44	0.012	0.001	0.0000	90.17	0.29	20.786	0.074	2.64E-13	7.61E-14			0.6	PPLLLL
		2.42	9252-02E	3.254	0.01	0.012	0.0001	0.43	0.01	7E-04	0.0000	94.52	0.26	20.418	0.063	3.09E-13	9.50E-14			0.7	PPLLLL
		3.40	9252-02F	3.133	0.01	0.012	0.0001	0.41	0.008	6E-04	0.0000	95.54	0.27	19.867	0.058	3.20E-13	1.02E-13			0.85	PPLLLL
		4.42	9252-02G	3.126	0.01	0.012	0.0001	0.64	0.016	6E-04	0.0000	95.52	0.34	19.823	0.078	1.99E-13	6.38E-14			1	PPLLLL
		5.44	9252-02H	3.34	0.01	0.013	0.0001	1.92	0.016	0.002	0.0000	88.82	0.52	19.71	0.12	2.18E-13	6.52E-14			1.5	PPLLLL
		6.46	9252-02I	3.394	0.01	0.013	0.0002	1.04	0.04	0.002	0.0001	86.63	0.74	19.53	0.17	7.33E-14	2.16E-14			2	PPLLLL
		7.54	9252-02J	3.416	0.01	0.012	0.0001	1.28	0.037	0.002	0.0001	87.45	0.57	19.84	0.13	1.25E-13	3.65E-14			2.5	PPLLLL
		8.63	9252-02K	3.372	0.01	0.012	0.0001	1.45	0.031	0.002	0.0001	88.92	0.63	19.92	0.15	1.04E-13	3.08E-14			3	PPLLLL
		9.59	9252-02L	3.491	0.01	0.012	0.0002	1.04	0.051	0.002	0.0001	84.89	0.79	19.68	0.19	6.83E-14	1.96E-14			4	PPLLLL
EB5-W.R																					
	01/30/2017	14.90	9253-01A	19.05	0.28	0.029	0.0016	1.41	0.61	0.061	0.0019	5.4	2.8	6.9	3.6	1.85E-14	9.69E-16	**1.008**	**0.0009**	0.1	PPLLLL
		15.96	9253-01B	8.484	0.02	0.017	0.0001	0.49	0.019	0.02	0.0001	30.96	0.52	17.45	0.33	2.68E-13	3.16E-14			0.3	PPLLLL
		16.95	9253-01C	3.396	0.01	0.012	0.0001	0.42	0.012	6E-04	0.0000	96.01	0.28	21.632	0.074	2.53E-13	7.44E-14			0.4	PPLLLL
		18.01	9253-01D	3.223	0.01	0.012	0.0001	0.46	0.0095	3E-04	0.0000	98.12	0.22	20.991	0.056	3.58E-13	1.11E-13			0.5	PPLLLL
		19.13	9253-01E	3.127	0.01	0.012	0.0001	0.50	0.0088	3E-04	0.0000	98.62	0.21	20.466	0.053	4.05E-13	1.29E-13			0.6	PPLLLL
		20.12	9253-01F	3.102	0.01	0.012	0.0001	0.43	0.0084	3E-04	0.0000	98.58	0.24	20.298	0.055	3.18E-13	1.02E-13			0.7	PPLLLL
		21.13	9253-01G	3.073	0.01	0.012	0.0001	0.26	0.0063	4E-04	0.0000	97.23	0.18	19.836	0.044	4.57E-13	1.49E-13			1	PPLLLL
		22.12	9253-01H	3.265	0.01	0.013	0.0001	0.26	0.011	0.001	0.0000	90.93	0.36	19.708	0.083	1.76E-13	5.39E-14			1.5	PPLLLL
		23.14	9253-01I	3.55	0.01	0.013	0.0002	0.35	0.046	0.002	0.0001	79.8	1.1	18.81	0.26	4.78E-14	1.35E-14			2	PPLLLL
	01/31/2017	0.20	9253-01J	3.877	0.02	0.013	0.0004	0.69	0.12	0.003	0.0003	77.7	2.3	19.99	0.58	1.92E-14	4.96E-15			2.5	PPLLLL
		1.29	9253-01K	3.809	0.06	0.015	0.0012	0.91	0.43	0.007	0.0009	43.2	7.6	11	1.9	5.33E-15	1.40E-15			3	PPLLLL
		2.44	9253-01L	3.413	0.06	0.015	0.0013	0.80	0.52	0.006	0.0012	47	10	10.6	2.4	4.21E-15	1.23E-15			4	PPLLLL

	01/31/2017	7.88	9253-02A	20.69	0.15	0.028	0.0009	1.01	0.34	0.064	0.0010	8	1.3	11	1.8	4.12E-14	1.99E-15	**1.008**	**0.0009**	0.1	PPLLLL
		9.04	9253-02B	11.31	0.04	0.02	0.0003	0.54	0.063	0.029	0.0003	23.02	0.9	17.3	0.71	1.15E-13	1.01E-14			0.2	PPLLLL
		10.07	9253-02C	3.721	0.01	0.012	0.0001	0.38	0.025	0.002	0.0001	86.12	0.45	21.27	0.12	1.10E-13	2.95E-14			0.3	PPLLLL
		11.16	9253-02D	3.302	0.01	0.011	0.0001	0.47	0.012	5E-04	0.0000	96.95	0.27	21.242	0.071	2.35E-13	7.12E-14			0.4	PPLLLL
		12.21	9253-02E	3.149	0.01	0.012	0.0001	0.53	0.0072	3E-04	0.0000	98.65	0.23	20.621	0.054	3.55E-13	1.13E-13			0.5	PPLLLL
		13.23	9253-02F	3.113	0.01	0.012	0.0001	0.46	0.01	3E-04	0.0000	98.66	0.26	20.384	0.061	3.20E-13	1.03E-13			0.6	PPLLLL
		14.19	9253-02G	3.113	0.01	0.012	0.0001	0.27	0.011	4E-04	0.0000	97	0.28	20.046	0.064	2.03E-13	6.51E-14			0.7	PPLLLL
		15.27	9253-02H	3.267	0.01	0.012	0.0001	0.24	0.015	1E-03	0.0000	91.49	0.43	19.843	0.095	1.43E-13	4.37E-14			0.8	PPLLLL
		16.27	9253-02I	4.018	0.01	0.013	0.0001	0.30	0.013	0.004	0.0001	73.57	0.42	19.62	0.12	2.05E-13	5.11E-14			1.5	PPLLLL
		17.34	9253-02J	4.476	0.03	0.015	0.0006	1.38	0.18	0.006	0.0004	65	2.8	19.33	0.84	1.69E-14	3.77E-15			2.5	PPLLLL
		18.35	9253-02K	4.174	0.08	0.014	0.0017	3.43	0.81	0.004	0.0015	76	11	21	3	3.62E-15	8.67E-16			4	PPLLLL
EB8-W.R																					
	01/31/2017	23.62	9254-01A	7.68	0.16	0.015	0.0023	2.49	0.91	0.019	0.0021	30	8.2	15.3	4.2	5.64E-15	7.33E-16	**1.008**	**0.0009**	0.1	PPLLLL
	2/01/2017	0.70	9254-01B	2.41	0.01	0.015	0.0003	0.23	0.067	0.001	0.0001	83.8	1.9	13.43	0.3	2.28E-14	9.48E-15			0.2	PPLLLL
		1.84	9254-01C	3.503	0.01	0.012	0.0001	0.19	0.025	4E-04	0.0001	97.11	0.51	22.56	0.12	9.02E-14	2.58E-14			0.3	PPLLLL
		2.90	9254-01D	3.316	0.01	0.011	0.0001	0.10	0.012	2E-04	0.0000	98.13	0.3	21.589	0.073	1.97E-13	5.95E-14			0.4	PPLLLL
		3.92	9254-01E	3.088	0.01	0.011	0.0001	0.11	0.0057	1E-04	0.0000	99.16	0.18	20.319	0.044	3.66E-13	1.19E-13			0.5	PPLLLL
		4.94	9254-01F	3.046	0.01	0.012	0.0001	0.09	0.0046	1E-04	0.0000	99.29	0.17	20.071	0.044	4.08E-13	1.34E-13			0.6	PPLLLL
		5.94	9254-01G	3.034	0.01	0.011	0.0001	0.09	0.0073	1E-04	0.0000	98.87	0.2	19.906	0.048	2.86E-13	9.43E-14			0.7	PPLLLL
		7.02	9254-01H	2.983	0.01	0.012	0.0001	0.19	0.011	2E-04	0.0000	98.41	0.31	19.491	0.066	1.75E-13	5.87E-14			1	PPLLLL
		8.09	9254-01I	3.06	0.01	0.012	0.0002	0.59	0.074	1E-04	0.0001	100.3	1.3	20.37	0.27	3.04E-14	9.92E-15			1.5	PPLLLL
		9.13	9254-01J	3.017	0.02	0.012	0.0004	0.59	0.11	7E-04	0.0002	94.1	2.3	18.86	0.46	1.87E-14	6.21E-15			2	PPLLLL
		10.15	9254-01K	3.048	0.01	0.012	0.0002	0.84	0.041	2E-04	0.0001	100.53	0.76	20.35	0.16	5.33E-14	1.75E-14			3	PPLLLL
		11.11	9254-01L	4.154	0.03	0.012	0.0005	1.10	0.15	0.004	0.0003	73.2	2.4	20.2	0.68	1.78E-14	4.28E-15			4	PPLLLL
	2/01/2017	16.23	9254-02A	5.584	0.04	0.015	0.0006	0.42	0.18	0.009	0.0005	52.4	2.8	19.4	1	1.73E-14	3.10E-15	**1.008**	**0.0009**	0.1	PPLLLL
		17.31	9254-02B	3.25	0.01	0.012	0.0001	0.08	0.0046	2E-04	0.0000	98.15	0.17	21.161	0.048	4.18E-13	1.29E-13			0.3	PPLLLL
		18.27	9254-02C	3.041	0.00	0.012	0.0001	0.06	0.0036	1E-04	0.0000	99.2	0.12	20.024	0.032	5.02E-13	1.65E-13			0.4	PPLLLL

		19.32	9254-02D	3.014	0.01	0.012	0.0001	0.05	0.006	1E-04	0.0000	99.19	0.22	19.839	0.047	2.76E-13	9.16E-14			0.45	PPLLLL
		20.43	9254-02E	3.029	0.01	0.012	0.0001	0.05	0.011	2E-04	0.0000	97.95	0.32	19.693	0.07	1.80E-13	5.93E-14			0.5	PPLLLL
		21.55	9254-02F	3.018	0.01	0.012	0.0001	0.03	0.015	2E-04	0.0000	98.53	0.35	19.737	0.079	1.21E-13	4.02E-14			0.55	PPLLLL
		22.64	9254-02G	3.015	0.01	0.012	0.0001	0.06	0.018	2E-04	0.0000	97.79	0.47	19.568	0.097	9.00E-14	2.99E-14			0.6	PPLLLL
		23.68	9254-02H	3.032	0.01	0.012	0.0001	0.21	0.02	3E-04	0.0000	97.66	0.54	19.66	0.11	8.12E-14	2.68E-14			0.7	PPLLLL
	2/02/2017	0.74	9254-02I	3.101	0.01	0.012	0.0002	0.60	0.054	8E-04	0.0001	93.5	1.1	19.26	0.24	3.30E-14	1.06E-14			1	PPLLLL
		1.77	9254-02J	3.11	0.01	0.012	0.0003	0.28	0.063	5E-04	0.0001	96.1	1.4	19.85	0.29	2.85E-14	9.17E-15			1.5	PPLLLL
		2.91	9254-02K	3.058	0.01	0.012	0.0002	0.40	0.045	4E-04	0.0001	96.7	1	19.63	0.21	3.96E-14	1.30E-14			2.5	PPLLLL
		3.92	9254-02L	3.083	0.02	0.012	0.0004	0.57	0.1	7E-04	0.0002	94.9	2.1	19.44	0.44	1.92E-14	6.23E-15			4	PPLLLL
EB11-W.R																					
	2/02/2017	9.07	9255-01A	140	27.00	0.082	0.0390	15.00	16	0.473	0.0950	0.1	7.9	1	75	5.40E-15	3.85E-17	**1.008**	**0.0009**	0.1	PPLLLL
		10.17	9255-01B	30.54	0.21	0.036	0.0009	0.90	0.29	0.099	0.0013	3.4	1.2	6.9	2.5	6.35E-14	2.08E-15			0.2	PPLLLL
		11.20	9255-01C	8.306	0.04	0.021	0.0004	0.57	0.12	0.024	0.0004	13.8	1.4	7.66	0.81	4.68E-14	5.63E-15			0.3	PPLLLL
		12.19	9255-01D	5.231	0.03	0.016	0.0005	0.65	0.16	0.009	0.0004	48.7	2.2	16.92	0.76	2.01E-14	3.84E-15			0.35	PPLLLL
		13.19	9255-01E	5.06	0.03	0.014	0.0003	0.41	0.12	0.006	0.0003	64.6	1.8	21.7	0.59	2.56E-14	5.06E-15			0.4	PPLLLL
		14.25	9255-01F	4.654	0.02	0.013	0.0003	0.42	0.076	0.004	0.0002	73	1.2	22.53	0.39	4.08E-14	8.77E-15			0.45	PPLLLL
		15.33	9255-01G	4.383	0.02	0.011	0.0003	0.35	0.089	0.003	0.0002	77.5	1.3	22.54	0.4	3.20E-14	7.29E-15			0.5	PPLLLL
		16.42	9255-01H	4.369	0.02	0.012	0.0002	0.37	0.048	0.003	0.0001	77.29	0.88	22.4	0.26	5.71E-14	1.31E-14			0.6	LPLLLL
		17.42	9255-01I	3.813	0.01	0.011	0.0001	0.37	0.03	0.002	0.0001	84.97	0.66	21.5	0.17	7.58E-14	1.99E-14			0.7	PPLLLL
		18.51	9255-01J	3.191	0.01	0.011	0.0000	0.30	0.0088	4E-04	0.0000	96.77	0.22	20.493	0.051	3.45E-13	1.08E-13			1	PPLLLL
	2/03/2017	7.35	9255-01K	3.202	0.01	0.012	0.0001	1.09	0.011	8E-04	0.0000	95.48	0.3	20.306	0.07	5.00E-13	1.56E-13			2	PPLLLL
		8.34	9255-01L	3.219	0.01	0.012	0.0001	0.66	0.015	8E-04	0.0000	94.14	0.33	20.117	0.078	2.14E-13	6.66E-14			3	PPLLLL
		9.36	9255-01M	4.421	0.01	0.012	0.0002	0.58	0.036	0.005	0.0001	69.36	0.72	20.36	0.22	8.89E-14	2.01E-14			4	PPLLLL
	2/03/2017	14.73	9255-02A	45.72	0.40	0.049	0.0015	1.32	0.43	0.148	0.0019	3.87	0.97	11.8	3.1	6.55E-14	1.43E-15	**1.008**	**0.0009**	0.1	LPLLLL
		15.77	9255-02B	6.644	0.02	0.017	0.0002	0.43	0.045	0.012	0.0002	44.47	0.74	19.62	0.34	9.77E-14	1.47E-14			0.3	PPLLLL
		16.75	9255-02C	4.699	0.02	0.012	0.0002	0.50	0.045	0.004	0.0001	74.67	0.9	23.27	0.29	6.85E-14	1.46E-14			0.4	PPLLLL
		17.78	9255-02D	3.698	0.01	0.011	0.0001	0.34	0.03	0.002	0.0001	87.97	0.7	21.59	0.17	8.63E-14	2.33E-14			0.5	PPLLLL

		18.82	9255-02E	3.241	0.01	0.011	0.0001	0.33	0.016	5E-04	0.0000	96.16	0.37	20.686	0.085	1.41E-13	4.36E-14			0.6	PPLLLL
		19.87	9255-02F	3.121	0.01	0.012	0.0001	0.34	0.013	3E-04	0.0000	97.53	0.37	20.205	0.074	1.59E-13	5.11E-14			0.7	PPLLLL
		20.92	9255-02G	3.123	0.01	0.012	0.0001	0.40	0.014	3E-04	0.0000	98.46	0.31	20.408	0.067	1.76E-13	5.64E-14			0.85	PPLLLL
		21.92	9255-02H	3.137	0.01	0.012	0.0001	0.65	0.028	5E-04	0.0001	97.19	0.71	20.24	0.15	7.19E-14	2.29E-14			1	LPLLLL
		22.97	9255-02I	3.335	0.01	0.012	0.0001	1.33	0.017	0.001	0.0000	90.64	0.41	20.079	0.096	3.03E-13	9.09E-14			1.5	PPLLLL
	2/04/2017	0.03	9255-02J	3.315	0.01	0.012	0.0001	0.76	0.032	0.001	0.0000	91.78	0.52	20.2	0.12	1.07E-13	3.22E-14			2	PPLLLL
		1.07	9255-02K	3.336	0.01	0.012	0.0001	1.13	0.039	0.001	0.0001	93.25	0.65	20.66	0.15	8.68E-14	2.60E-14			3	PPLLLL
		2.09	9255-02L	3.964	0.01	0.012	0.0002	1.44	0.047	0.003	0.0001	78.97	0.87	20.79	0.23	5.79E-14	1.46E-14			4	PPLLLL
EB13-W.R																					
	2/04/2017	7.37	9256-01A	26.69	0.17	0.031	0.0007	1.74	0.26	0.082	0.0011	8.5	1.2	15	2.1	7.25E-14	2.72E-15	**1.008**	**0.0009**	0.1	PPLLLL
		8.38	9256-01B	7.01	0.03	0.016	0.0003	1.55	0.085	0.015	0.0003	39.4	1.2	18.34	0.58	5.16E-14	7.36E-15			0.2	PPLLLL
		9.43	9256-01C	5.276	0.02	0.013	0.0002	1.35	0.052	0.007	0.0002	65.18	0.91	22.83	0.33	6.85E-14	1.30E-14			0.3	PPLLLL
		10.41	9256-01D	4.674	0.01	0.012	0.0002	1.61	0.038	0.005	0.0001	68.92	0.71	21.4	0.23	9.84E-14	2.11E-14			0.4	PPLLLL
		11.45	9256-01E	3.664	0.01	0.012	0.0001	1.31	0.03	0.002	0.0000	84.12	0.51	20.47	0.13	1.44E-13	3.92E-14			0.5	PPLLLL
		12.55	9256-01F	3.495	0.01	0.012	0.0001	1.36	0.032	0.002	0.0000	86.81	0.51	20.15	0.12	1.35E-13	3.85E-14			0.6	PPLLLL
		13.51	9256-01G	3.513	0.01	0.012	0.0001	1.26	0.034	0.002	0.0001	85.97	0.59	20.06	0.14	1.00E-13	2.85E-14			0.7	PPLLLL
		14.55	9256-01H	3.549	0.01	0.013	0.0002	1.89	0.059	0.003	0.0001	82.73	0.88	19.52	0.21	6.39E-14	1.80E-14			1	PPLLLL
		15.57	9256-01I	4.46	0.01	0.013	0.0002	3.40	0.06	0.006	0.0001	66	1	19.59	0.31	8.62E-14	1.93E-14			1.5	PPLLLL
		16.59	9256-01J	4.649	0.01	0.014	0.0002	2.87	0.067	0.006	0.0001	65.13	0.9	20.14	0.29	8.73E-14	1.88E-14			2	PPLLLL
		17.55	9256-01K	4.882	0.01	0.013	0.0001	2.87	0.053	0.007	0.0001	64.11	0.82	20.81	0.27	1.07E-13	2.19E-14			3	PPLLLL
		18.63	9256-01L	4.546	0.01	0.013	0.0001	3.45	0.027	0.006	0.0001	67.17	0.72	20.31	0.23	1.84E-13	4.05E-14			4	PPLLLL
	2/04/2017	23.96	9256-02A	29.58	0.26	0.033	0.0012	1.44	0.46	0.092	0.0016	7.1	1.5	13.9	3	4.50E-14	1.52E-15	**1.008**	**0.0009**	0.1	PPLLLL
	2/05/2017	0.99	9256-02B	7.41	0.03	0.016	0.0004	1.19	0.13	0.016	0.0004	35.2	1.6	17.32	0.78	4.04E-14	5.45E-15			0.2	PPLLLL
		2.00	9256-02C	4.586	0.02	0.012	0.0002	0.85	0.054	0.003	0.0001	79.48	0.92	24.18	0.28	5.25E-14	1.15E-14			0.3	PPLLLL
		3.06	9256-02D	4.733	0.02	0.011	0.0002	1.24	0.054	0.005	0.0001	68.32	0.88	21.47	0.28	6.22E-14	1.31E-14			0.4	PPLLLL
		4.12	9256-02E	3.538	0.01	0.012	0.0001	1.25	0.044	0.001	0.0001	90.16	0.58	21.18	0.14	1.07E-13	3.03E-14			0.5	PPLLLL
		5.14	9256-02F	3.302	0.01	0.011	0.0001	1.24	0.033	0.001	0.0000	93.37	0.55	20.48	0.12	1.17E-13	3.53E-14			0.6	PPLLLL

		6.20	9256-02G	3.247	0.01	0.012	0.0001	1.20	0.043	1E-03	0.0001	93.9	0.62	20.25	0.14	9.22E-14	2.84E-14			0.7	PPLLLL
		7.27	9256-02H	3.195	0.01	0.011	0.0002	1.87	0.055	0.001	0.0001	94.28	0.84	20.02	0.18	6.40E-14	2.00E-14			1	PPLLLL
		8.33	9256-02I	3.726	0.01	0.013	0.0002	4.03	0.071	0.003	0.0001	84.2	1.2	20.86	0.3	7.60E-14	2.04E-14			1.5	PPLLLL
		9.33	9256-02J	3.714	0.01	0.013	0.0002	3.57	0.07	0.003	0.0001	85	1.2	21	0.3	5.60E-14	1.51E-14			2	PPLLLL
		14.85	9256-02K	3.858	0.01	0.013	0.0001	3.92	0.03	0.004	0.0001	79.99	0.91	20.53	0.23	1.62E-13	4.21E-14			3	PPLLLL
		15.81	9256-02L	4.011	0.01	0.013	0.0002	3.43	0.048	0.004	0.0001	75.8	1	20.21	0.28	1.02E-13	2.55E-14			4	PPLLLL
EB14-W.R																					
	2/05/2017	21.11	9257-01A	64.07	0.70	0.052	0.0017	2.29	0.7	0.201	0.0030	6.8	1.1	28.7	4.7	6.81E-14	1.06E-15	**1.008**	**0.0009**	0.1	LPLLLL
		8.38	9257-01B	4.648	0.02	0.012	0.0002	0.57	0.079	0.004	0.0002	77.6	1.1	23.92	0.34	5.03E-14	1.08E-14			0.2	PPLLLL
		9.41	9257-01C	3.809	0.01	0.012	0.0001	0.57	0.02	0.002	0.0000	83.27	0.41	21.05	0.11	1.89E-13	4.97E-14			0.3	PPLLLL
		10.47	9257-01D	3.288	0.01	0.012	0.0001	0.51	0.014	9E-04	0.0000	92.96	0.29	20.293	0.07	2.91E-13	8.85E-14			0.4	PPLLLL
		11.54	9257-01E	3.24	0.10	0.01	0.0022	-2.80	1.3	-0.01	0.0021	144	21	30.8	4.4	1.95E-15	6.01E-16			0.5	PPLLLL
		12.62	9257-01F	3.207	0.06	0.01	0.0013	-0.67	0.75	-0.01	0.0013	169	12	35.9	2.6	3.22E-15	1.01E-15			0.6	PPLLLL
		13.63	9257-01G	3.132	0.04	0.012	0.0010	0.58	0.5	-0	0.0008	131.7	7.7	27.3	1.6	5.08E-15	1.62E-15			0.7	PPLLLL
		14.67	9257-01H	3.094	0.02	0.011	0.0003	0.49	0.14	-0	0.0002	109	2	22.37	0.42	1.83E-14	5.92E-15			1	PPLLLL
		15.76	9257-01I	11.6	7.80	-0.2	0.1600	-78.00	75	-0.26	0.1800	720	330	470	280	1.44E-16	1.24E-17			1.5	PPLLLL
		16.80	9257-01J	3.081	0.01	0.012	0.0001	0.95	0.032	5E-04	0.0000	97.07	0.42	19.86	0.089	1.42E-13	4.61E-14			2	PPLLLL
		17.91	9257-01K	3.111	0.01	0.012	0.0002	0.52	0.082	2E-04	0.0001	99.5	1.3	20.54	0.28	3.12E-14	1.00E-14			3	PPLLLL
		19.02	9257-01L	3.142	0.01	0.012	0.0001	0.90	0.047	7E-04	0.0001	95.72	0.84	19.97	0.18	5.36E-14	1.70E-14			4	PPLLLL
	2/07/2017	0.20	9257-02A	55.17	0.64	0.047	0.0019	2.79	0.63	0.167	0.0030	10.2	1.4	37.2	5.1	5.69E-14	1.03E-15	**1.008**	**0.0009**	0.1	PPLLLL
		1.21	9257-02B	5.607	0.02	0.014	0.0003	0.85	0.068	0.008	0.0002	58.7	1.2	21.85	0.46	4.88E-14	8.70E-15			0.2	PPLLLL
		2.20	9257-02C	3.708	0.01	0.012	0.0001	0.76	0.03	0.002	0.0001	84.86	0.52	20.89	0.13	1.36E-13	3.66E-14			0.3	PPLLLL
		3.26	9257-02D	3.368	0.01	0.012	0.0001	0.62	0.019	0.001	0.0000	90.78	0.43	20.3	0.1	1.21E-13	3.58E-14			0.35	PPLLLL
		4.35	9257-02E	3.128	0.01	0.012	0.0001	0.56	0.014	6E-04	0.0000	95.42	0.4	19.819	0.089	1.30E-13	4.15E-14			0.4	PPLLLL
		5.48	9257-02F	3.047	0.01	0.011	0.0001	0.50	0.015	3E-04	0.0000	97.98	0.44	19.82	0.091	1.17E-13	3.85E-14			0.45	PPLLLL
		6.60	9257-02G	3.04	0.01	0.012	0.0001	0.43	0.019	4E-04	0.0000	97.37	0.48	19.65	0.1	1.06E-13	3.50E-14			0.5	PPLLLL
		7.66	9257-02H	3.049	0.01	0.012	0.0001	0.43	0.012	3E-04	0.0000	97.79	0.31	19.796	0.069	1.77E-13	5.80E-14			0.7	PPLLLL

		8.68	9257-02I	3.082	0.01	0.013	0.0002	2.55	0.052	0.001	0.0001	92.4	0.91	18.94	0.19	8.51E-14	2.76E-14			1	PPLLLL
		9.73	9257-02J	3.256	0.01	0.013	0.0001	3.65	0.055	0.002	0.0001	90.63	0.98	19.63	0.22	9.59E-14	2.95E-14			2	PPLLLL
		10.83	9257-02K	3.297	0.01	0.012	0.0002	2.83	0.073	0.002	0.0001	89.2	1.5	19.56	0.33	3.36E-14	1.02E-14			3	PPLLLL
		11.84	9257-02L	3.328	0.02	0.012	0.0003	1.74	0.1	0.002	0.0002	86.5	2	19.14	0.46	2.12E-14	6.36E-15			4	PPLLLL
EB20-W.R																					
	2/07/2017	19.55	9258-01A	10.8	0.08	0.021	0.0009	0.80	0.36	0.025	0.0009	32.2	2.6	23.1	1.9	1.92E-14	1.78E-15	**1.008**	**0.0009**	0.1	PPLLLL
		20.63	9258-01B	3.599	0.01	0.012	0.0001	0.04	0.028	8E-04	0.0001	93.75	0.5	22.38	0.12	9.86E-14	2.74E-14			0.2	PPLLLL
		21.70	9258-01C	3.183	0.01	0.011	0.0001	0.04	0.0091	1E-04	0.0000	98.89	0.21	20.887	0.054	2.52E-13	7.92E-14			0.3	PPLLLL
		22.74	9258-01D	3.046	0.00	0.011	0.0001	0.03	0.0054	8E-05	0.0000	99.27	0.17	20.066	0.039	4.37E-13	1.43E-13			0.4	PPLLLL
		23.77	9258-01E	3.01	0.01	0.012	0.0001	0.03	0.0055	8E-05	0.0000	99.28	0.16	19.832	0.043	3.69E-13	1.23E-13			0.5	PPLLLL
	2/08/2017	0.88	9258-01F	3.023	0.01	0.012	0.0001	0.04	0.0099	8E-05	0.0000	99.36	0.27	19.934	0.061	2.19E-13	7.24E-14			0.6	PPLLLL
		1.94	9258-01G	3.042	0.01	0.012	0.0001	0.19	0.015	9E-05	0.0000	99.56	0.34	20.103	0.07	1.62E-13	5.32E-14			0.7	PPLLLL
		2.97	9258-01H	3.153	0.01	0.012	0.0001	3.94	0.045	0.002	0.0001	92	1.1	19.31	0.23	1.12E-13	3.54E-14			1	PPLLLL
		4.01	9258-01I	3.39	0.01	0.012	0.0002	7.06	0.094	0.003	0.0001	86.7	1.8	19.62	0.41	6.63E-14	1.95E-14			1.5	PPLLLL
		5.00	9258-01J	3.63	0.01	0.012	0.0002	1.79	0.053	0.003	0.0001	81.29	0.79	19.61	0.2	7.91E-14	2.18E-14			2	PPLLLL
		6.00	9258-01K	4.004	0.01	0.013	0.0002	0.90	0.033	0.003	0.0001	75.93	0.69	20.19	0.19	7.87E-14	1.97E-14			3	PPLLLL
		7.13	9258-01L	3.618	0.02	0.013	0.0003	0.42	0.15	0.002	0.0003	87.6	2.3	21.04	0.56	1.72E-14	4.76E-15			4	PPLLLL
	2/08/2017	12.58	9258-02A	3.804	0.01	0.012	0.0002	-0.06	0.054	0.002	0.0001	81.02	0.85	20.45	0.22	5.46E-14	1.43E-14	**1.008**	**0.0009**	0.2	PPLLLL
		13.69	9258-02B	3.318	0.01	0.012	0.0001	0.05	0.02	3E-04	0.0000	97.36	0.39	21.428	0.088	1.41E-13	4.26E-14			0.3	PPLLLL
		14.77	9258-02C	3.14	0.01	0.011	0.0001	0.03	0.0095	2E-04	0.0000	98.2	0.25	20.46	0.062	2.24E-13	7.14E-14			0.37	PPLLLL
		15.86	9258-02D	3.058	0.01	0.011	0.0001	0.00	0.0072	1E-04	0.0000	98.74	0.19	20.035	0.047	2.88E-13	9.44E-14			0.44	PPLLLL
		16.96	9258-02E	3.017	0.01	0.012	0.0001	0.01	0.0076	9E-05	0.0000	99.17	0.21	19.855	0.048	3.00E-13	9.96E-14			0.5	PPLLLL
		17.98	9258-02F	3.015	0.01	0.012	0.0001	0.01	0.0068	1E-04	0.0000	99.01	0.18	19.812	0.046	3.35E-13	1.11E-13			0.6	PPLLLL
		19.04	9258-02G	3.016	0.01	0.012	0.0001	0.00	0.0088	1E-04	0.0000	98.73	0.2	19.764	0.047	2.77E-13	9.19E-14			0.7	PPLLLL
		20.17	9258-02H	3.022	0.01	0.012	0.0001	0.26	0.011	2E-04	0.0000	98.4	0.24	19.736	0.055	3.27E-13	1.08E-13			1	PPLLLL
		21.24	9258-02I	3.068	0.01	0.012	0.0001	0.62	0.02	5E-04	0.0000	96.29	0.32	19.618	0.07	1.93E-13	6.30E-14			2	PPLLLL
		22.28	9258-02J	3.095	0.01	0.012	0.0001	0.21	0.015	4E-04	0.0000	96.85	0.31	19.897	0.069	1.74E-13	5.62E-14			4	PPLLLL

BB1-W.R																					
	2/09/2017	3.51	9259-01A	5.36	0.03	0.021	0.0005	0.65	0.16	0.012	0.0004	31.6	2.1	11.27	0.74	2.36E-14	4.40E-15	**1.008**	**0.0009**	0.1	PPLLLL
		4.51	9259-01B	4.381	0.01	0.014	0.0002	0.48	0.033	0.002	0.0001	90.15	0.52	26.18	0.16	9.98E-14	2.28E-14			0.2	PPLLLL
		5.61	9259-01C	4.486	0.01	0.011	0.0001	0.52	0.018	7E-04	0.0000	96.52	0.3	28.68	0.1	1.90E-13	4.24E-14			0.3	PPLLLL
		6.70	9259-01D	4.016	0.01	0.011	0.0001	0.53	0.014	2E-04	0.0000	99.27	0.23	26.418	0.071	2.89E-13	7.20E-14			0.4	PPLLLL
		7.81	9259-01E	3.819	0.01	0.011	0.0001	0.44	0.011	2E-04	0.0000	99.19	0.19	25.108	0.062	3.81E-13	9.99E-14			0.5	PPLLLL
		8.85	9259-01F	3.733	0.01	0.012	0.0001	0.31	0.012	2E-04	0.0000	99.15	0.19	24.538	0.064	3.80E-13	1.02E-13			0.6	PPLLLL
		9.82	9259-01G	3.723	0.01	0.012	0.0001	0.26	0.0089	2E-04	0.0000	99.06	0.18	24.448	0.058	3.30E-13	8.86E-14			0.7	PPLLLL
		10.90	9259-01H	3.72	0.01	0.012	0.0001	0.56	0.012	3E-04	0.0000	98.7	0.23	24.347	0.063	3.50E-13	9.42E-14			1	PPLLLL
		12.00	9259-01I	3.719	0.01	0.012	0.0001	1.17	0.016	5E-04	0.0000	98.3	0.31	24.254	0.084	4.11E-13	1.11E-13			2	PPLLLL
		12.97	9259-01J	3.723	0.01	0.012	0.0001	0.67	0.017	4E-04	0.0000	97.88	0.32	24.166	0.083	2.01E-13	5.40E-14			3	PPLLLL
		14.08	9259-01K	3.735	0.01	0.012	0.0001	0.76	0.017	4E-04	0.0000	98.06	0.29	24.289	0.082	2.34E-13	6.28E-14			4	PPLLLL
KF1-W.R																					
	2/09/2017	19.36	9260-01A	4.635	0.02	0.014	0.0003	0.38	0.12	0.004	0.0002	72.7	1.4	22.35	0.43	3.50E-14	7.56E-15	**1.008**	**0.0009**	0.1	PPLLLL
		20.43	9260-01B	4.129	0.01	0.013	0.0002	0.53	0.039	9E-04	0.0001	94.57	0.58	25.88	0.17	8.69E-14	2.10E-14			0.2	PPLLLL
		21.55	9260-01C	4.052	0.01	0.013	0.0002	0.85	0.05	9E-04	0.0001	94.95	0.67	25.51	0.19	6.92E-14	1.71E-14			0.3	PPLLLL
		22.62	9260-01D	4.223	0.02	0.014	0.0002	1.27	0.07	0.002	0.0001	89.26	0.86	25.01	0.24	5.29E-14	1.25E-14			0.4	PPLLLL
		23.65	9260-01E	3.899	0.02	0.014	0.0003	2.28	0.093	0.002	0.0002	90.5	1.4	23.44	0.36	3.39E-14	8.68E-15			0.5	PPLLLL
	2/10/2017	0.70	9260-01F	3.733	0.02	0.015	0.0005	3.40	0.18	0.002	0.0003	87.6	2.6	21.74	0.64	1.65E-14	4.43E-15			0.6	PPLLLL
		1.73	9260-01G	4.595	0.02	0.015	0.0003	2.38	0.088	0.004	0.0002	77.7	1.1	23.72	0.34	4.72E-14	1.03E-14			0.7	PPLLLL
		2.77	9260-01H	4.286	0.01	0.015	0.0002	4.53	0.054	0.004	0.0001	82.24	0.94	23.45	0.27	1.29E-13	3.02E-14			1	PPLLLL
		3.80	9260-01I	4.182	0.03	0.013	0.0006	10.31	0.35	0.004	0.0004	87.9	3.6	24.55	0.99	1.47E-14	3.53E-15			2	PPLLLL
		4.87	9260-01J	3.973	0.04	0.015	0.0008	12.38	0.43	0.007	0.0006	74.7	5	19.9	1.3	8.35E-15	2.10E-15			3	PPLLLL
		6.00	9260-01K	4.023	0.07	0.013	0.0015	12.01	0.86	0.009	0.0011	56.8	8.9	15.3	2.4	4.50E-15	1.12E-15			4	PPLLLL
Eb3-W.R																					
	2/10/2017	11.14	9264-01A	6.409	0.03	0.016	0.0003	1.17	0.082	0.012	0.0002	47.4	1	20.17	0.46	6.34E-14	9.90E-15	**1.008**	**0.0009**	0.2	PPLLLL
		12.22	9264-01B	3.273	0.01	0.011	0.0001	0.62	0.016	5E-04	0.0000	97.03	0.28	21.072	0.07	2.46E-13	7.52E-14			0.3	PPLLLL
		13.28	9264-01C	3.135	0.01	0.011	0.0001	0.49	0.0086	3E-04	0.0000	98.76	0.2	20.545	0.051	3.96E-13	1.26E-13			0.37	PPLLLL

		14.27	9264-01D	3.071	0.01	0.011	0.0001	0.31	0.013	2E-04	0.0000	98.46	0.23	20.062	0.053	2.87E-13	9.34E-14			0.44	PPLLLL
		15.32	9264-01E	3.044	0.01	0.012	0.0001	0.25	0.012	3E-04	0.0000	97.99	0.3	19.791	0.069	1.97E-13	6.48E-14			0.5	PPLLLL
		16.43	9264-01F	3.046	0.01	0.012	0.0001	0.30	0.02	3E-04	0.0000	98.01	0.36	19.813	0.078	1.31E-13	4.31E-14			0.6	PPLLLL
		17.54	9264-01G	3.008	0.01	0.012	0.0001	0.36	0.042	5E-04	0.0001	96.45	0.65	19.25	0.13	6.73E-14	2.24E-14			0.7	LPLLLL
		18.66	9264-01H	2.801	0.01	0.014	0.0002	4.21	0.07	0.002	0.0001	91.6	1.5	17.08	0.28	5.32E-14	1.90E-14			1	PPLLLL
		19.76	9264-01I	2.968	0.02	0.015	0.0004	7.63	0.18	0.004	0.0002	80.8	3.1	16.02	0.61	1.86E-14	6.28E-15			2	PPLLLL
		20.76	9264-01J	3.193	0.03	0.016	0.0007	13.44	0.57	0.007	0.0006	63.3	6.4	13.6	1.4	8.51E-15	2.67E-15			3	PLLLLL
		21.83	9264-01K	5.61	0.21	0.011	0.0038	4.50	2	0.011	0.0031	50	17	18.8	6.5	2.16E-15	3.85E-16			4	PPLLLL
BRT2-W.R																					
	2/11/2017	3.32	9265-01A	15.86	0.15	0.021	0.0010	5.25	0.53	0.037	0.0013	33.8	2.4	35.5	2.5	2.22E-14	1.40E-15	**1.008**	**0.0009**	0.15	PPLLLL
		4.35	9265-01B	11.91	0.04	0.015	0.0002	2.45	0.073	0.009	0.0002	79.81	0.47	62.43	0.41	1.35E-13	1.14E-14			0.3	PPLLLL
		5.43	9265-01C	9.88	0.02	0.012	0.0001	0.82	0.022	0.002	0.0000	94.9	0.19	61.53	0.16	3.86E-13	3.91E-14			0.4	PPLLLL
		6.44	9265-01D	9.2	0.02	0.012	0.0001	0.44	0.018	7E-04	0.0000	98.01	0.17	59.2	0.14	4.16E-13	4.53E-14			0.5	PPLLLL
		7.50	9265-01E	8.98	0.02	0.012	0.0001	0.53	0.022	7E-04	0.0000	98.03	0.2	57.83	0.16	3.07E-13	3.42E-14			0.6	PPLLLL
		8.54	9265-01F	8.892	0.02	0.014	0.0002	0.66	0.045	0.001	0.0001	96.35	0.34	56.31	0.23	1.48E-13	1.67E-14			0.7	PPLLLL
		9.62	9265-01G	9.044	0.02	0.019	0.0002	1.66	0.039	0.002	0.0001	95.95	0.38	57.06	0.25	1.67E-13	1.85E-14			1	PPLLLL
		10.68	9265-01H	8.878	0.02	0.023	0.0001	7.02	0.049	0.003	0.0000	95.93	0.61	56.23	0.37	8.81E-13	9.93E-14			2	PPLLLL
		11.65	9265-01I	9.177	0.03	0.028	0.0004	11.07	0.16	0.006	0.0002	89.7	1.1	54.53	0.7	8.97E-14	9.77E-15			3	PPLLLL
		12.66	9265-01J	8.939	0.03	0.028	0.0004	12.85	0.13	0.005	0.0002	92.8	1.2	54.98	0.74	9.67E-14	1.08E-14			4	PPLLLL
BRT5-W.R																					
	2/11/2017	17.88	9267-01A	11.73	0.07	0.02	0.0005	1.73	0.16	0.012	0.0004	70.1	1	54.08	0.82	4.75E-14	4.05E-15	**1.008**	**0.0009**	0.2	PPLLLL
		18.88	9267-01B	10.32	0.05	0.018	0.0004	1.40	0.15	0.004	0.0003	89.36	0.91	60.57	0.67	4.78E-14	4.63E-15			0.3	PPLLLL
		19.96	9267-01C	10.63	0.05	0.016	0.0003	1.24	0.1	0.005	0.0002	86.19	0.7	60.18	0.53	7.41E-14	6.97E-15			0.4	PPLLLL
		20.97	9267-01D	10.36	0.03	0.013	0.0002	1.21	0.061	0.005	0.0001	87.85	0.45	59.8	0.34	1.21E-13	1.17E-14			0.5	PPLLLL
		22.05	9267-01E	9.658	0.03	0.012	0.0002	1.02	0.052	0.002	0.0001	95.01	0.4	60.26	0.3	1.22E-13	1.27E-14			0.6	PPLLLL
		23.15	9267-01F	9.305	0.03	0.012	0.0002	0.85	0.07	0.001	0.0001	96.07	0.47	58.72	0.32	1.03E-13	1.11E-14			0.7	PPLLLL
	2/12/2017	0.23	9267-01G	9.187	0.02	0.012	0.0001	2.30	0.026	0.001	0.0000	97.88	0.25	59.12	0.16	5.24E-13	5.71E-14			1	PPLLLL
		1.25	9267-01H	9.085	0.02	0.013	0.0001	4.55	0.042	0.002	0.0001	97.83	0.43	58.53	0.27	3.23E-13	3.56E-14			1.5	PPLLLL

		2.26	9267-01I	9.085	0.03	0.013	0.0002	5.21	0.11	0.002	0.0001	97.31	0.68	58.25	0.43	1.09E-13	1.20E-14			2	PPLLLL
		3.31	9267-01J	8.999	0.03	0.013	0.0002	6.59	0.073	0.002	0.0001	97.62	0.64	57.94	0.39	1.78E-13	1.97E-14			3	PPLLLL
		4.29	9267-01K	9.039	0.03	0.013	0.0003	5.99	0.17	0.003	0.0002	96.46	0.83	57.5	0.51	6.47E-14	7.16E-15			4	LPLLLL
BRT7-W.R																					
	2/12/2017	9.67	9268-01A	21.84	0.08	0.028	0.0003	2.32	0.094	0.046	0.0004	37.36	0.59	53.73	0.93	2.21E-13	1.01E-14	**1.008**	**0.0009**	0.2	PPLLLL
		10.66	9268-01B	12.62	0.04	0.025	0.0002	0.81	0.052	0.011	0.0001	74.87	0.35	62	0.36	2.11E-13	1.67E-14			0.3	PPLLLL
		11.61	9268-01C	11.7	0.03	0.024	0.0002	1.01	0.074	0.01	0.0002	74.81	0.53	57.52	0.43	1.45E-13	1.24E-14			0.4	PPLLLL
		12.59	9268-01D	11.21	0.04	0.021	0.0003	1.18	0.072	0.008	0.0002	78.71	0.51	57.96	0.42	1.39E-13	1.24E-14			0.5	PPLLLL
		13.62	9268-01E	12.13	0.05	0.023	0.0003	1.56	0.13	0.011	0.0003	74.09	0.74	59.05	0.62	8.29E-14	6.84E-15			0.6	PPLLLL
		14.70	9268-01F	12.36	0.07	0.025	0.0005	1.69	0.18	0.012	0.0004	71.07	0.97	57.74	0.83	6.08E-14	4.92E-15			0.7	PPLLLL
		15.69	9268-01G	13.32	0.04	0.026	0.0003	6.10	0.11	0.016	0.0002	66.87	0.62	58.71	0.57	1.45E-13	1.09E-14			1	PPLLLL
		16.87	9268-01H	18.25	0.08	0.03	0.0004	15.01	0.19	0.035	0.0003	49.69	0.81	60.1	1	1.87E-13	1.02E-14			1.5	PPLLLL
		17.90	9268-01I	15.29	0.11	0.031	0.0008	13.88	0.32	0.025	0.0007	58	1.5	58.8	1.6	4.79E-14	3.13E-15			2	PPLLLL
		18.92	9268-01J	14.42	0.04	0.032	0.0003	25.02	0.2	0.026	0.0002	60.5	1.4	58.3	1.3	2.86E-13	1.99E-14			3	PPLLLL
		19.90	9268-01K	12.48	0.07	0.029	0.0006	21.20	0.35	0.02	0.0004	64.5	1.6	53.7	1.4	5.49E-14	4.40E-15			4	PPLLLL
BRT9-W.R																					
	02/13/2017	1.23	9270-01A	10.86	0.09	0.018	0.0008	6.11	0.47	0.023	0.0009	40.8	2.5	29.4	1.8	2.05E-14	1.89E-15	**1.008**	**0.0009**	0.2	PPLLLL
		2.31	9270-01B	11.28	0.05	0.013	0.0004	2.18	0.2	0.004	0.0003	89.71	0.85	66.4	0.67	5.29E-14	4.69E-15			0.3	PPLLLL
		3.36	9270-01C	10.49	0.03	0.012	0.0002	0.84	0.061	7E-04	0.0001	98.7	0.3	67.85	0.28	1.63E-13	1.55E-14			0.4	PPLLLL
		4.38	9270-01D	9.498	0.02	0.012	0.0001	0.68	0.036	5E-04	0.0001	99.1	0.24	61.77	0.19	2.44E-13	2.57E-14			0.5	PPLLLL
		5.48	9270-01E	9.14	0.02	0.013	0.0002	0.80	0.04	5E-04	0.0001	99.11	0.3	59.49	0.21	2.20E-13	2.40E-14			0.6	PPLLLL
		6.57	9270-01F	8.955	0.03	0.015	0.0002	0.98	0.056	5E-04	0.0001	99.23	0.39	58.38	0.28	1.41E-13	1.58E-14			0.7	PPLLLL
		7.58	9270-01G	8.632	0.02	0.024	0.0002	4.10	0.065	0.002	0.0001	98.15	0.5	55.82	0.31	1.72E-13	1.99E-14			1	PPLLLL
		8.60	9270-01H	8.754	0.02	0.027	0.0002	13.37	0.12	0.006	0.0001	92.4	1.2	53.67	0.71	1.69E-13	1.94E-14			1.5	PPLLLL
		9.56	9270-01I	9.364	0.03	0.03	0.0003	28.68	0.19	0.012	0.0002	84.1	2.4	52.9	1.5	9.13E-14	9.75E-15			2	PPLLLL
		10.50	9270-01J	11.85	0.05	0.031	0.0008	49.40	0.81	0.024	0.0006	71.6	3.5	57.7	2.8	3.29E-14	2.77E-15			3	PLLLLL
		11.56	9270-01K	13.9	1.10	-0.01	0.0110	#####	12	0.014	0.0120	136	27	132	28	1.79E-15	1.29E-16			4	PPLLLL
BRT10-W.R																					

	02/13/2017	16.93	9271-01A	61.47	0.22	0.064	0.0010	5.14	0.23	0.181	0.0014	12.86	0.65	52.2	2.9	2.34E-13	3.81E-15	**1.008**	**0.0009**	0.2	PLLLLL
		17.97	9271-01B	27.44	0.11	0.028	0.0003	1.74	0.093	0.059	0.0005	36.85	0.52	66.3	1	2.32E-13	8.45E-15			0.3	PPLLLL
		19.01	9271-01C	13.14	0.03	0.015	0.0002	1.00	0.038	0.012	0.0001	72.87	0.35	62.82	0.33	2.92E-13	2.22E-14			0.4	PPLLLL
		20.03	9271-01D	11.02	0.02	0.014	0.0001	0.81	0.021	0.006	0.0001	83.73	0.19	60.59	0.18	5.54E-13	5.02E-14			0.5	PPLLLL
		21.07	9271-01E	10.29	0.02	0.012	0.0001	0.83	0.022	0.004	0.0001	88.13	0.23	59.56	0.2	3.62E-13	3.51E-14			0.6	PPLLLL
		22.06	9271-01F	9.465	0.02	0.012	0.0001	0.76	0.027	0.002	0.0001	95.03	0.25	59.07	0.2	2.70E-13	2.85E-14			0.7	PPLLLL
		23.10	9271-01G	9.174	0.02	0.012	0.0001	2.56	0.03	0.002	0.0000	96.41	0.28	58.17	0.2	3.93E-13	4.29E-14			1	PPLLLL
	02/14/2017	0.09	9271-01H	9.091	0.03	0.013	0.0002	4.37	0.11	0.003	0.0001	95.06	0.58	56.93	0.37	1.27E-13	1.40E-14			1.5	PPLLLL
		1.13	9271-01I	9.07	0.03	0.012	0.0001	8.89	0.11	0.003	0.0001	96.67	0.82	57.93	0.51	1.75E-13	1.93E-14			2	PPLLLL
		2.14	9271-01J	8.995	0.03	0.014	0.0002	21.84	0.22	0.007	0.0002	96.1	1.9	57.7	1.2	1.06E-13	1.18E-14			3	PPLLLL
		3.14	9271-01K	8.836	0.05	0.013	0.0005	35.46	0.41	0.01	0.0004	95.6	3.3	56.9	2	3.82E-14	4.33E-15			4	PPLLLL
CA3-W.R																					
	02/14/2017	8.38	9273-01A	6.4	1.80	0.023	0.0410	9.00	23	0.106	0.0410	-390	190	-173	90	2.10E-16	3.30E-17	**1.008**	**0.0009**	0.1	PPLLLL
		9.48	9273-01B	2.52	0.13	0.016	0.0038	-2.10	1.8	0.011	0.0033	-36	41	-6	6.8	9.73E-16	3.86E-16			0.2	PPLLLL
		10.57	9273-01C	1.947	0.02	0.011	0.0006	-0.22	0.24	8E-05	0.0004	97.9	6	12.67	0.77	6.08E-15	3.12E-15			0.3	PPLLLL
		11.67	9273-01D	1.782	0.01	0.012	0.0002	-0.19	0.083	2E-05	0.0001	98.8	2.1	11.7	0.25	1.65E-14	9.25E-15			0.4	PPLLLL
		12.75	9273-01E	1.736	0.01	0.012	0.0002	-0.11	0.057	3E-04	0.0001	94.5	1.9	10.91	0.22	2.24E-14	1.29E-14			0.5	PPLLLL
		13.80	9273-01F	1.769	0.01	0.011	0.0002	-0.21	0.052	4E-04	0.0001	92.5	1.6	10.88	0.19	2.43E-14	1.37E-14			0.6	PPLLLL
		14.94	9273-01G	1.724	0.01	0.012	0.0002	-0.13	0.055	2E-04	0.0001	96.6	1.6	11.08	0.18	2.31E-14	1.34E-14			0.7	PPLLLL
		16.08	9273-01H	1.747	0.01	0.012	0.0002	0.00	0.037	2E-04	0.0001	96.9	1	11.26	0.12	3.66E-14	2.10E-14			1	PPLLLL
		17.17	9273-01I	1.744	0.00	0.012	0.0001	0.02	0.0049	7E-05	0.0000	98.85	0.18	11.46	0.024	2.84E-13	1.63E-13			2	PPLLLL
		18.19	9273-01J	1.737	0.00	0.012	0.0001	0.00	0.0058	7E-05	0.0000	98.72	0.27	11.403	0.033	2.38E-13	1.37E-13			3	PPLLLL
		19.20	9273-01K	0.6	2.00	-0.06	0.0650	-47.00	38	0.047	0.0580	-2700	9000	-110	130	1.33E-17	2.14E-17			4	PPLLLL
CA6-W.R																					
	02/15/2017	1.50	9274-01A	2.726	0.07	0.012	0.0020	-1.62	0.84	7E-04	0.0014	87	16	15.8	2.8	2.40E-15	8.81E-16	**1.008**	**0.0009**	0.1	PPLLLL
		2.56	9274-01B	2.068	0.01	0.012	0.0002	0.03	0.057	6E-04	0.0001	91.2	1.4	12.54	0.19	2.72E-14	1.32E-14			0.2	PPLLLL
		3.61	9274-01C	1.908	0.01	0.011	0.0001	0.08	0.022	2E-04	0.0000	97.38	0.69	12.35	0.088	6.89E-14	3.61E-14			0.3	PPLLLL
		4.65	9274-01D	1.831	0.00	0.012	0.0001	0.01	0.009	1E-04	0.0000	98.02	0.32	11.934	0.044	1.58E-13	8.63E-14			0.4	PPLLLL

		5.68	9274-01E	1.806	0.00	0.012	0.0001	0.02	0.0061	6E-05	0.0000	99.11	0.25	11.901	0.034	2.13E-13	1.18E-13			0.5	PPLLLL
		6.79	9274-01F	1.783	0.00	0.012	0.0001	0.01	0.0075	5E-05	0.0000	99.16	0.26	11.753	0.034	2.13E-13	1.19E-13			0.6	PPLLLL
		7.88	9274-01G	1.788	0.00	0.012	0.0001	0.02	0.0072	5E-05	0.0000	99.32	0.25	11.804	0.034	1.80E-13	1.01E-13			0.7	PPLLLL
		8.93	9274-01H	1.778	0.00	0.012	0.0001	0.10	0.0057	7E-05	0.0000	99.29	0.24	11.736	0.03	2.51E-13	1.41E-13			1	PPLLLL
		9.96	9274-01I	1.779	0.00	0.012	0.0001	0.38	0.014	2E-04	0.0000	98.67	0.37	11.673	0.046	1.64E-13	9.20E-14			2	PPLLLL
		11.02	9274-01J	1.828	0.00	0.012	0.0001	0.11	0.017	2E-04	0.0000	97.48	0.58	11.851	0.071	8.66E-14	4.73E-14			3	PPLLLL
		12.10	9274-01K	1.804	0.00	0.012	0.0001	0.15	0.014	1E-04	0.0000	98.19	0.43	11.78	0.054	1.10E-13	6.11E-14			4	PPLLLL
CA3-W.R																					
	02/15/2017	17.34	9275-01A	3.645	0.04	0.015	0.0008	-0.01	0.35	0.01	0.0006	21.1	5.4	5.1	1.3	8.61E-15	2.36E-15	**1.008**	**0.0009**	0.1	PPLLLL
		18.48	9275-01B	1.995	0.01	0.012	0.0001	0.13	0.037	4E-04	0.0001	94.19	0.99	12.49	0.13	4.18E-14	2.10E-14			0.2	PPLLLL
		19.56	9275-01C	1.901	0.00	0.011	0.0001	0.02	0.011	1E-04	0.0000	98.31	0.32	12.42	0.042	1.58E-13	8.33E-14			0.3	PPLLLL
		20.61	9275-01D	1.762	0.00	0.011	0.0001	0.01	0.0041	8E-05	0.0000	98.73	0.2	11.568	0.025	3.16E-13	1.79E-13			0.4	PPLLLL
		21.63	9275-01E	1.74	0.00	0.012	0.0001	0.01	0.0036	7E-05	0.0000	98.9	0.17	11.443	0.024	3.96E-13	2.27E-13			0.5	PPLLLL
		22.66	9275-01F	1.736	0.00	0.012	0.0001	0.01	0.0041	5E-05	0.0000	99.14	0.18	11.44	0.024	3.18E-13	1.84E-13			0.6	PPLLLL
		23.72	9275-01G	1.727	0.00	0.012	0.0001	0.02	0.0076	9E-05	0.0000	98.49	0.29	11.309	0.033	2.05E-13	1.19E-13			0.7	PPLLLL
		0.77	9275-01H	1.735	0.00	0.012	0.0001	0.05	0.0078	1E-04	0.0000	98.5	0.28	11.361	0.036	1.94E-13	1.12E-13			1	PPLLLL
		1.77	9275-01I	1.779	0.00	0.012	0.0001	0.04	0.02	2E-04	0.0000	96.21	0.63	11.377	0.073	7.40E-14	4.16E-14			2	PPLLLL
		2.85	9275-01J	1.804	0.01	0.012	0.0001	0.00	0.033	3E-04	0.0001	95.5	1	11.45	0.13	4.12E-14	2.29E-14			3	PPLLLL
	02/16/2017	3.89	9275-01K	1.836	0.02	0.012	0.0005	-0.15	0.18	-0	0.0003	100	5.6	12.21	0.68	7.70E-15	4.20E-15			4	PPLLLL
KC3-W.R																					
	02/16/2017	9.17	9276-01A	3.702	0.02	0.019	0.0004	0.55	0.13	0.012	0.0003	3.9	2.3	0.96	0.58	2.07E-14	5.59E-15	**1.008**	**0.0009**	0.1	PPLLLL
		10.21	9276-01B	0.321	0.00	0.013	0.0001	0.28	0.022	0.001	0.0000	-2.8	4	-0.061	0.086	1.11E-14	3.45E-14			0.2	PPLLLL
		11.28	9276-01C	0.143	0.00	0.012	0.0001	0.35	0.019	3E-04	0.0000	49.3	7	0.466	0.066	6.60E-15	4.63E-14			0.3	PPLLLL
		12.34	9276-01D	0.245	0.00	0.012	0.0001	0.94	0.034	9E-04	0.0001	22.1	7.8	0.36	0.13	6.38E-15	2.60E-14			0.4	PPLLLL
		13.45	9276-01E	0.393	0.00	0.014	0.0002	0.73	0.053	0.001	0.0001	19	6.3	0.5	0.16	6.84E-15	1.74E-14			0.5	PPLLLL
		14.54	9276-01F	0.621	0.00	0.014	0.0002	0.73	0.058	0.002	0.0001	13.6	5.1	0.56	0.21	8.88E-15	1.43E-14			0.6	PPLLLL
		15.59	9276-01G	1.149	0.00	0.015	0.0002	1.09	0.048	0.004	0.0001	2.6	2.7	0.2	0.21	2.49E-14	2.17E-14			0.7	PPLLLL
		16.60	9276-01H	1.492	0.00	0.016	0.0001	2.67	0.043	0.005	0.0001	4.7	2.2	0.47	0.22	4.77E-14	3.20E-14			1	PPLLLL

		17.67	9276-01I	1.6	0.00	0.016	0.0002	3.71	0.052	0.006	0.0001	2	2.6	0.21	0.28	3.94E-14	2.46E-14			2	PPLLLL
		18.72	9276-01J	1.705	0.01	0.016	0.0002	8.34	0.094	0.008	0.0002	2	4.6	0.22	0.53	2.40E-14	1.40E-14			3	PPLLLL
		19.76	9276-01K	1.923	0.02	0.019	0.0006	26.60	0.6	0.014	0.0005	-18	14	-2.4	1.8	5.34E-15	2.78E-15			4	PPLLLL
URC1-W.R																					
	02/17/2017	0.95	9277-01A	2.313	0.04	0.018	0.0011	0.77	0.58	0.006	0.0008	19	11	3	1.7	3.29E-15	1.42E-15	**1.008**	**0.0009**	0.1	PPLLLL
		1.98	9277-01B	0.307	0.00	0.017	0.0002	0.95	0.064	0.001	0.0001	7	11	0.15	0.22	4.10E-15	1.34E-14			0.2	PPLLLL
		3.01	9277-01C	0.108	0.00	0.014	0.0001	0.88	0.029	7E-04	0.0000	-19	15	-0.14	0.11	3.25E-15	3.00E-14			0.3	PPLLLL
		4.07	9277-01D	0.085	0.00	0.014	0.0001	0.77	0.031	4E-04	0.0000	14	19	0.08	0.11	2.42E-15	2.85E-14			0.4	PPLLLL
		5.18	9277-01E	0.097	0.00	0.015	0.0001	0.74	0.035	4E-04	0.0001	30	18	0.19	0.12	2.20E-15	2.28E-14			0.5	PPLLLL
		6.20	9277-01F	0.099	0.00	0.014	0.0001	0.90	0.041	6E-04	0.0001	-9	21	-0.06	0.14	2.08E-15	2.09E-14			0.6	PPLLLL
		7.27	9277-01G	0.115	0.00	0.013	0.0002	0.95	0.044	5E-04	0.0001	37	19	0.28	0.14	2.33E-15	2.04E-14			0.7	PPLLLL
		8.32	9277-01H	0.129	0.00	0.013	0.0001	1.83	0.026	8E-04	0.0000	14	13	0.12	0.11	7.85E-15	6.09E-14			1	PPLLLL
		9.35	9277-01I	0.168	0.00	0.013	0.0001	3.30	0.052	0.002	0.0001	-28	19	-0.31	0.21	3.80E-15	2.26E-14			2	PPLLLL
		10.39	9277-01J	0.191	0.00	0.013	0.0002	4.25	0.065	0.002	0.0001	16	21	0.21	0.27	4.12E-15	2.16E-14			3	PPLLLL
		11.40	9277-01K	0.239	0.00	0.013	0.0002	7.31	0.13	0.003	0.0001	15	29	0.25	0.46	2.80E-15	1.17E-14			4	PPLLLL
BRT1-W.R																					
	02/17/2017	16.62	9278-01A	18.69	0.07	0.02	0.0004	2.41	0.12	0.04	0.0005	36.96	0.78	45.6	1	1.33E-13	7.14E-15	**1.008**	**0.0009**	0.2	PPLLLL
		17.71	9278-01B	12.44	0.03	0.015	0.0002	1.32	0.054	0.014	0.0002	67.92	0.46	55.58	0.41	1.96E-13	1.58E-14			0.3	PPLLLL
		18.73	9278-01C	9.865	0.03	0.012	0.0002	0.68	0.042	0.003	0.0001	91.36	0.32	59.19	0.25	1.73E-13	1.75E-14			0.4	PPLLLL
		19.80	9278-01D	9.643	0.03	0.012	0.0002	0.69	0.048	0.003	0.0001	91.5	0.37	57.97	0.27	1.51E-13	1.57E-14			0.5	PPLLLL
		20.81	9278-01E	10.21	0.03	0.012	0.0002	0.73	0.049	0.005	0.0001	85.36	0.45	57.27	0.33	1.51E-13	1.48E-14			0.6	PPLLLL
		21.84	9278-01F	10.05	0.03	0.013	0.0002	0.90	0.068	0.005	0.0001	87.3	0.42	57.67	0.31	1.18E-13	1.17E-14			0.7	PPLLLL
		22.87	9278-01G	9.474	0.03	0.018	0.0002	2.28	0.068	0.004	0.0001	89.46	0.46	55.77	0.31	1.60E-13	1.69E-14			1	PPLLLL
		23.93	9278-01H	9.15	0.02	0.025	0.0002	15.15	0.12	0.007	0.0001	89.6	1.3	54.47	0.77	3.32E-13	3.62E-14			1.5	PPLLLL
	02/18/2017	0.93	9278-01I	9.4	0.04	0.022	0.0004	12.60	0.29	0.008	0.0003	86	1.4	53.6	0.9	5.20E-14	5.53E-15			2	PPLLLL
		1.94	9278-01J	9.663	0.03	0.019	0.0002	11.06	0.12	0.007	0.0001	85.65	0.96	54.81	0.64	1.38E-13	1.42E-14			3	PPLLLL
		3.02	9278-01K	9.42	0.13	0.017	0.0016	4.10	1	2E-04	0.0013	102.6	4.4	63.5	2.8	9.30E-15	9.88E-16			4	PPLLLL
URC2-W.R																					

	02/18/2017	8.49	9279-01A	14.89	0.33	0.025	0.0026	9.20	1.7	0.057	0.0030	-8.6	5.9	-8.6	5.9	8.26E-15	5.55E-16	**1.008**	**0.0009**	0.1	PPLLLL
		9.62	9279-01B	0.496	0.01	0.014	0.0004	1.05	0.21	0.006	0.0004	-232	23	-7.67	0.73	2.08E-15	4.20E-15			0.2	PPLLLL
		10.76	9279-01C	0.1	0.00	0.012	0.0002	0.67	0.055	6E-04	0.0001	-31	25	-0.21	0.17	1.73E-15	1.72E-14			0.3	PPLLLL
		11.87	9279-01D	0.075	0.00	0.011	0.0001	0.61	0.024	3E-04	0.0000	47	16	0.234	0.079	2.92E-15	3.88E-14			0.4	PPLLLL
		12.88	9279-01E	0.072	0.00	0.011	0.0001	0.50	0.024	3E-04	0.0000	22	16	0.107	0.076	2.82E-15	3.92E-14			0.5	PPLLLL
		14.02	9279-01F	0.074	0.00	0.012	0.0001	0.63	0.037	3E-04	0.0000	27	20	0.132	0.099	2.09E-15	2.81E-14			0.6	PPLLLL
		15.06	9279-01G	0.079	0.00	0.012	0.0002	0.67	0.07	4E-04	0.0001	20	36	0.1	0.19	1.21E-15	1.53E-14			0.7	PPLLLL
		16.21	9279-01H	0.086	0.00	0.012	0.0001	1.36	0.036	6E-04	0.0001	10	23	0.06	0.13	2.18E-15	2.52E-14			1	PPLLLL
		17.33	9279-01I	0.096	0.00	0.012	0.0002	5.03	0.066	0.002	0.0001	-57	46	-0.37	0.29	2.11E-15	2.20E-14			2	PPLLLL
		18.40	9279-01J	0.162	0.01	0.013	0.0003	13.55	0.22	0.004	0.0002	-21	73	-0.22	0.79	1.26E-15	7.75E-15			3	PPLLLL
		19.51	9279-01K	0.24	0.02	0.012	0.0008	21.08	0.52	0.009	0.0007	-310	120	-5	1.9	5.12E-16	2.13E-15			4	PPLLLL
URC3-W.R																					
	02/19/2017	0.86	9280-01A	30.52	0.13	0.033	0.0004	1.19	0.13	0.102	0.0007	0.59	0.64	1.2	1.5	2.05E-13	6.71E-15	**1.008**	**0.0009**	0.1	PPLLLL
		1.87	9280-01B	10.68	0.02	0.019	0.0002	0.32	0.026	0.036	0.0002	0.22	0.48	0.16	0.42	3.92E-13	3.67E-14			0.2	PPLLLL
		2.86	9280-01C	8.437	0.01	0.017	0.0001	0.57	0.018	0.028	0.0002	0.94	0.54	0.53	0.36	4.55E-13	5.39E-14			0.3	PPLLLL
		3.90	9280-01D	9.748	0.02	0.018	0.0001	1.08	0.034	0.032	0.0002	2.28	0.54	1.48	0.41	3.38E-13	3.47E-14			0.4	PPLLLL
		4.92	9280-01E	8.588	0.03	0.017	0.0002	0.71	0.052	0.028	0.0002	2.45	0.65	1.4	0.42	1.62E-13	1.89E-14			0.5	PPLLLL
		5.96	9280-01F	6.697	0.02	0.016	0.0002	0.57	0.079	0.021	0.0002	6.7	0.93	2.99	0.44	8.66E-14	1.29E-14			0.6	PPLLLL
		7.00	9280-01G	3.258	0.01	0.014	0.0002	0.91	0.066	0.01	0.0002	7.5	1.5	1.63	0.33	4.41E-14	1.35E-14			0.7	PPLLLL
		8.04	9280-01H	0.688	0.00	0.013	0.0001	1.65	0.038	0.002	0.0001	10.7	3	0.49	0.14	2.58E-14	3.75E-14			1	PPLLLL
		9.09	9280-01I	0.374	0.00	0.012	0.0001	2.45	0.028	0.002	0.0000	8.9	5.7	0.22	0.14	2.24E-14	5.98E-14			2	PPLLLL
		10.08	9280-01J	2.881	0.01	0.015	0.0003	7.61	0.1	0.012	0.0002	-0.4	2.8	-0.08	0.55	4.14E-14	1.44E-14			3	PPLLLL
		11.10	9280-01K	1.252	0.02	0.014	0.0006	11.97	0.35	0.007	0.0005	2	14	0.2	1.2	3.19E-15	2.55E-15			4	PPLLLL
BRT3-W.R																					
	02/19/2017	16.49	9281-01A	57.48	0.50	0.051	0.0011	3.81	0.51	0.16	0.0020	17.26	0.82	65.2	3.3	1.16E-13	2.03E-15	**1.008**	**0.0009**	0.2	PPLLLL
		17.56	9281-01B	31.65	0.10	0.052	0.0005	1.92	0.15	0.079	0.0006	25.91	0.5	54	1.2	2.10E-13	6.65E-15			0.3	PPLLLL
		18.61	9281-01C	22.86	0.09	0.035	0.0005	1.53	0.16	0.046	0.0005	40.08	0.65	60.2	1	1.48E-13	6.50E-15			0.4	PPLLLL
		19.70	9281-01D	19.61	0.06	0.025	0.0003	1.66	0.11	0.036	0.0003	46.34	0.51	59.71	0.72	1.92E-13	9.77E-15			0.5	PPLLLL

		20.75	9281-01E	15.49	0.04	0.019	0.0002	1.46	0.063	0.023	0.0002	56.98	0.37	58.03	0.44	2.42E-13	1.56E-14			0.6	PPLLLL
		21.74	9281-01F	13.09	0.04	0.016	0.0002	1.50	0.053	0.014	0.0002	68.66	0.41	59.04	0.4	2.49E-13	1.90E-14			0.7	PPLLLL
		22.76	9281-01G	10.44	0.02	0.014	0.0002	1.61	0.04	0.006	0.0001	83.14	0.3	57.07	0.23	2.86E-13	2.74E-14			1	PPLLLL
		23.82	9281-01H	9.778	0.03	0.017	0.0002	6.82	0.1	0.006	0.0001	87	0.68	56.15	0.46	1.82E-13	1.86E-14			1.5	PPLLLL
	02/20/2017	0.89	9281-01I	10.18	0.05	0.017	0.0003	8.26	0.17	0.008	0.0003	83.53	1	56.16	0.7	7.38E-14	7.25E-15			2	PPLLLL
		1.90	9281-01J	10.44	0.02	0.017	0.0001	8.93	0.056	0.009	0.0001	81.96	0.67	56.54	0.47	6.74E-13	6.45E-14			3	PPLLLL
		2.85	9281-01K	10.48	0.03	0.017	0.0002	11.71	0.1	0.01	0.0001	79.52	0.94	55.22	0.66	1.71E-13	1.63E-14			4	PPLLLL
GA1550 MD2-W.R																					
	02/20/2017	8.27	9282-01A	28.26	0.22	0.024	0.0008	0.48	0.48	0.047	0.0010	50.9	1.1	93.5	2.1	5.37E-14	1.90E-15	**1.008**	**0.0009**	0.2	PPLLLL
		9.32	9282-01B	16.13	0.05	0.016	0.0002	-0.02	0.078	0.003	0.0001	94.37	0.25	98.81	0.37	2.25E-13	1.39E-14			0.3	PPLLLL
		10.37	9282-01C	15.66	0.04	0.015	0.0002	0.12	0.058	0.001	0.0001	97.82	0.25	99.46	0.34	2.40E-13	1.53E-14			0.35	PPLLLL
		11.57	9282-01D	15.5	0.03	0.015	0.0002	0.00	0.049	7E-04	0.0001	98.58	0.19	99.2	0.25	3.20E-13	2.07E-14			0.4	PPLLLL
		12.60	9282-01E	15.45	0.03	0.015	0.0002	-0.02	0.045	5E-04	0.0001	98.99	0.15	99.26	0.24	3.47E-13	2.24E-14			0.45	PPLLLL
		13.72	9282-01F	15.32	0.03	0.015	0.0002	0.02	0.033	4E-04	0.0000	99.24	0.14	98.67	0.23	4.25E-13	2.78E-14			0.5	PPLLLL
		14.74	9282-01G	15.43	0.03	0.015	0.0001	0.05	0.016	3E-04	0.0000	99.41	0.12	99.55	0.19	9.09E-13	5.89E-14			0.6	PPLLLL
		15.70	9282-01H	15.47	0.04	0.015	0.0001	0.03	0.005	3E-04	0.0000	99.51	0.26	99.91	0.25	2.75E-12	1.78E-13			0.8	PPLLLL
		16.76	9282-01I	15.45	0.04	0.016	0.0002	0.10	0.051	5E-04	0.0001	99.11	0.19	99.39	0.32	3.01E-13	1.95E-14			1	PPLLLL
		17.76	9282-01J	15.38	0.15	0.016	0.0009	1.23	0.5	7E-04	0.0007	99.3	1.5	99.2	1.7	2.66E-14	1.73E-15			2.5	PPLLLL
	02/20/2017	23.09	9282-02A	36.85	0.17	0.03	0.0008	0.34	0.24	0.073	0.0010	40.57	0.78	97.1	1.9	1.23E-13	3.34E-15	**1.008**	**0.0009**	0.2	PLLLLL
	02/21/2017	0.16	9282-02B	19.62	0.05	0.019	0.0002	0.10	0.049	0.014	0.0002	78.77	0.32	100.3	0.48	2.95E-13	1.50E-14			0.3	PPLLLL
		1.16	9282-02C	16.27	0.06	0.016	0.0002	0.08	0.046	0.003	0.0001	93.79	0.25	99.06	0.43	2.64E-13	1.62E-14			0.35	PPLLLL
		2.23	9282-02D	15.84	0.04	0.016	0.0002	0.00	0.031	0.001	0.0001	97.52	0.14	100.24	0.25	4.37E-13	2.76E-14			0.4	PPLLLL
		3.28	9282-02E	15.71	0.04	0.016	0.0001	0.05	0.025	0.001	0.0001	97.69	0.17	99.58	0.28	5.18E-13	3.30E-14			0.45	PPLLLL
		4.29	9282-02F	15.5	0.03	0.016	0.0001	0.01	0.024	7E-04	0.0000	98.61	0.13	99.21	0.19	5.62E-13	3.63E-14			0.5	PPLLLL
		5.39	9282-02G	15.53	0.02	0.016	0.0001	0.05	0.0098	6E-04	0.0000	98.866	0.09	99.65	0.15	1.09E-12	7.01E-14			0.6	PPLLLL
		6.39	9282-02H	15.48	0.04	0.016	0.0001	0.02	0.0054	6E-04	0.0000	98.93	0.16	99.39	0.25	2.50E-12	1.62E-13			0.8	PPLLLL

		7.39	9282-02I	15.43	0.04	0.015	0.0001	0.03	0.0058	5E-04	0.0000	99.04	0.23	99.19	0.27	2.33E-12	1.51E-13			1	PPLLLL
		8.43	9282-02J	15.44	0.03	0.015	0.0001	0.04	0.023	6E-04	0.0001	98.9	0.14	99.13	0.2	5.39E-13	3.49E-14			2.5	PPLLLL
PK01-W.R.	20/02/2016	5.98	8760-01A	10.97	0.07	0.016	0.0006	0.41	0.1163695	0.016	0.0007	56.676	1.83	42.13	1.39	5.79E-14	5.28E-15	**0.9983**	**0.0017**	0.06	PPLLLL
		6.70	8760-01B	8.134	0.04	0.013	0.0003	0.21	0.0627021	0.005	0.0003	83.597	1.07	46.03	0.62	9.40E-14	1.16E-14			0.1	PPLLLL
		7.41	8760-01C	9.032	0.02	0.013	0.0001	0.15	0.0170596	0.002	0.0001	94.633	0.25	57.67	0.21	3.71E-13	4.11E-14			0.2	PPLLLL
		8.06	8760-01D	9.891	0.02	0.013	0.0001	0.21	0.0178641	9E-04	0.0001	97.375	0.21	64.85	0.20	5.02E-13	5.08E-14			0.3	PPLLLL
		8.70	8760-01E	10.11	0.02	0.012	0.0001	0.20	0.0204066	0.001	0.0001	96.647	0.22	65.76	0.21	4.66E-13	4.61E-14			0.4	PPLLLL
		9.40	8760-01F	10.21	0.03	0.012	0.0001	0.22	0.0199965	0.001	0.0001	96.745	0.27	66.48	0.25	3.78E-13	3.70E-14			0.5	PPLLLL
		10.07	8760-01G	10.29	0.03	0.012	0.0001	0.25	0.0260727	0.001	0.0001	96.973	0.23	67.14	0.23	4.47E-13	4.35E-14			0.7	PPLLLL
		10.74	8760-01H	10.04	0.03	0.012	0.0002	0.35	0.028893	7E-04	0.0001	98.075	0.28	66.25	0.26	3.51E-13	3.50E-14			1	PPLLLL
		11.42	8760-01I	10.02	0.04	0.014	0.0002	0.90	0.0644128	0.002	0.0002	96.064	0.53	64.83	0.41	1.92E-13	1.92E-14			1.5	PPLLLL
		12.13	8760-01J	10.11	0.04	0.013	0.0003	0.85	0.1072285	0.002	0.0002	95.595	0.75	65.12	0.56	1.23E-13	1.21E-14			2	PPLLLL
		12.83	8760-01K	10.22	0.03	0.014	0.0001	1.56	0.1372811	0.002	0.0001	94.074	0.4	64.78	0.33	3.12E-13	3.05E-14			3.5	PPLLLL
	20/02/2016	16.33	8760-02A	26.09	0.44	0.024	0.0027	0.03	0.6564458	0.085	0.0034	2.88	3.55	5.15	6.44	2.81E-14	1.08E-15			0.06	PPLLLL
		17.08	8760-02B	9.611	0.06	0.015	0.0007	0.12	0.1733783	0.016	0.0008	50.44	2.57	32.93	1.69	3.88E-14	4.04E-15			0.1	PPLLLL
		17.79	8760-02C	7.755	0.03	0.013	0.0002	0.20	0.0363426	0.005	0.0001	79.68	0.59	41.87	0.35	1.53E-13	1.98E-14			0.2	PPLLLL
		18.46	8760-02D	9.129	0.02	0.013	0.0002	0.13	0.0208081	0.002	0.0001	93.40	0.29	57.52	0.23	3.13E-13	3.43E-14			0.3	PPLLLL
		19.13	8760-02E	9.895	0.02	0.012	0.0001	0.15	0.0172958	0.001	0.0001	96.87	0.23	64.55	0.21	4.67E-13	4.72E-14			0.4	PPLLLL
		19.79	8760-02F	10.15	0.02	0.012	0.0001	0.17	0.0176316	9E-04	0.0001	97.44	0.21	66.53	0.20	4.67E-13	4.60E-14			0.5	PPLLLL
		20.45	8760-02G	10.27	0.03	0.012	0.0001	0.19	0.0143133	9E-04	0.0001	97.56	0.19	67.41	0.21	6.43E-13	6.26E-14			0.7	PPLLLL
		21.11	8760-02H	10.08	0.03	0.012	0.0001	0.27	0.0166407	6E-04	0.0000	98.55	0.16	66.83	0.20	7.70E-13	7.64E-14			1	PPLLLL
		21.78	8760-02I	9.953	0.03	0.013	0.0002	0.63	0.0405239	0.001	0.0001	97.39	0.22	65.28	0.22	5.01E-13	5.03E-14			1.5	PPLLLL
		22.45	8760-02J	10.03	0.04	0.014	0.0002	1.24	0.0721316	0.002	0.0002	96.22	0.49	65.04	0.39	2.18E-13	2.17E-14			2	PPLLLL
		23.17	8760-02K	10.11	0.03	0.014	0.0001	0.96	0.0693363	0.002	0.0001	95.77	0.25	65.24	0.24	4.63E-13	4.58E-14			3.5	PPLLLL
MHV09-W.R.	21/02/2016	2.64	8761-01A	104.1	3.15	0.059	0.0078	3.28	2.157226	0.283	0.0130	19.12	2.82	131.78	19.53	3.84E-14	3.69E-16	**0.9983**	**0.0017**	0.06	PPLLLL

		3.38	8761-01B	15.5	0.13	0.022	0.0013	0.61	0.2917144	0.05	0.0013	3.27	2.47	3.47	2.72	4.09E-14	2.64E-15			0.1	PPLLLL
		4.13	8761-01C	10.66	0.05	0.018	0.0004	0.58	0.0817434	0.021	0.0004	41.59	1.12	30.16	0.88	1.11E-13	1.04E-14			0.2	PPLLLL
		4.91	8761-01D	5.01	0.02	0.012	0.0002	0.19	0.0277786	0.002	0.0001	88.20	0.71	30.04	0.26	1.39E-13	2.77E-14			0.3	PPLLLL
		5.61	8761-01E	4.504	0.01	0.011	0.0001	0.20	0.0146175	6E-04	0.0000	96.28	0.34	29.48	0.13	2.88E-13	6.40E-14			0.4	PPLLLL
		6.33	8761-01F	4.374	0.01	0.011	0.0001	0.16	0.010933	4E-04	0.0000	97.23	0.23	28.92	0.10	4.72E-13	1.08E-13			0.5	PPLLLL
		6.99	8761-01G	4.255	0.01	0.011	0.0001	0.13	0.0111478	3E-04	0.0000	98.07	0.14	28.38	0.07	1.01E-12	2.38E-13			0.7	PPLLLL
		7.68	8761-01H	4.202	0.01	0.012	0.0000	0.04	0.0093473	3E-04	0.0000	98.17	0.17	28.06	0.07	1.29E-12	3.07E-13			1	PPLPP
		8.35	8761-01I	4.363	0.01	0.014	0.0001	0.26	0.0244729	0.001	0.0000	91.89	0.24	27.28	0.10	9.47E-13	2.17E-13			1.5	PPLLP
		9.11	8761-01J	4.555	0.01	0.014	0.0002	0.37	0.0318013	0.002	0.0001	85.92	0.62	26.64	0.21	1.56E-13	3.42E-14			2	PPLLLL
		9.82	8761-01K	4.712	0.02	0.015	0.0002	0.33	0.0397541	0.003	0.0001	83.86	0.69	26.89	0.24	1.63E-13	3.46E-14			3.5	PPLLLL
	21/02/2016	14.01	8761-02A	20.27	0.08	0.025	0.0006	0.30	0.0926313	0.055	0.0007	19.56	0.97	26.97	1.55	1.44E-13	7.11E-15			0.1	PPLLLL
		14.85	8761-02B	6.879	0.02	0.013	0.0002	0.20	0.0286732	0.008	0.0002	66.20	0.69	30.96	0.36	1.93E-13	2.81E-14			0.2	PPLLLL
		15.65	8761-02C	4.516	0.01	0.011	0.0001	0.18	0.0173328	7E-04	0.0000	95.92	0.27	29.45	0.11	3.97E-13	8.79E-14			0.3	PPLLLL
		16.31	8761-02D	4.323	0.01	0.011	0.0001	0.20	0.0158839	4E-04	0.0000	97.38	0.29	28.63	0.10	6.21E-13	1.44E-13			0.4	PPLLP
		16.99	8761-02E	4.241	0.01	0.011	0.0001	0.18	0.0132846	2E-04	0.0000	98.64	0.26	28.45	0.09	6.96E-13	1.64E-13			0.5	PPLLP
		17.65	8761-02F	4.261	0.01	0.012	0.0001	0.17	0.0108321	3E-04	0.0000	98.04	0.19	28.41	0.08	5.50E-13	1.29E-13			0.6	PLLLL
		18.33	8761-02G	4.244	0.01	0.012	0.0001	0.21	0.017643	5E-04	0.0001	96.73	0.49	27.92	0.15	3.37E-13	7.95E-14			0.7	PLLLP
		18.99	8761-02H	4.172	0.01	0.013	0.0002	0.21	0.0220075	7E-04	0.0001	95.49	0.55	27.10	0.17	1.64E-13	3.94E-14			0.8	PPLLLL
		19.67	8761-02I	4.303	0.01	0.015	0.0002	0.34	0.0287986	0.002	0.0001	86.59	0.79	25.36	0.24	1.22E-13	2.83E-14			1	PPLLLL
		20.39	8761-02J	4.676	0.02	0.019	0.0002	0.83	0.0572003	0.004	0.0001	75.83	0.93	24.16	0.31	1.18E-13	2.53E-14			1.5	PPLLLL
		21.10	8761-02K	5.021	0.02	0.019	0.0002	0.80	0.0707318	0.005	0.0001	69.93	0.73	23.92	0.27	1.54E-13	3.06E-14			3.5	PPLLLL
MC1-W.R.	22/02/2016	0.77	8739-01A	8.11	0.04	0.016	0.0004	0.62	0.0817712	0.014	0.0005	49.56	1.74	27.32	0.98	6.20E-14	7.64E-15	**0.9983**	**0.0017**	0.1	PPLLLL
		1.53	8739-01B	4.478	0.01	0.012	0.0001	0.34	0.0292448	0.001	0.0001	91.04	0.58	27.70	0.19	1.59E-13	3.54E-14			0.2	PPLLLL
		2.27	8739-01C	4.293	0.01	0.011	0.0001	0.30	0.0263849	8E-04	0.0001	94.69	0.48	27.62	0.15	2.11E-13	4.91E-14			0.3	PPLLLL
		3.02	8739-01D	4.22	0.01	0.012	0.0001	0.16	0.0359281	8E-04	0.0001	94.94	0.43	27.22	0.14	2.16E-13	5.11E-14			0.4	PPLPL
		3.72	8739-01E	4.192	0.01	0.012	0.0001	0.18	0.021923	8E-04	0.0001	94.72	0.43	26.98	0.14	2.38E-13	5.67E-14			0.5	PPLLLL

		4.46	8739-01F	4.221	0.01	0.012	0.0001	0.19	0.0202864	9E-04	0.0001	94.03	0.49	26.97	0.16	2.15E-13	5.10E-14			0.6	PPLLLL
		5.18	8739-01G	4.298	0.01	0.012	0.0001	0.18	0.0255745	0.001	0.0001	92.26	0.8	26.94	0.24	1.75E-13	4.07E-14			0.7	PPLLP
		5.92	8739-01H	4.403	0.01	0.012	0.0001	0.33	0.0301752	0.002	0.0002	88.45	1.16	26.47	0.35	1.71E-13	3.87E-14			0.9	PPLLP
		6.64	8739-01I	4.577	0.01	0.013	0.0002	0.65	0.0544763	0.003	0.0001	81.77	0.72	25.45	0.24	1.26E-13	2.74E-14			1.2	PPLLLL
		7.34	8739-01J	4.616	0.02	0.012	0.0002	0.80	0.0596902	0.003	0.0002	81.88	1.13	25.71	0.37	8.68E-14	1.88E-14			1.5	PPLLLL
		8.04	8739-01K	4.608	0.01	0.013	0.0001	1.06	0.1157337	0.003	0.0001	81.73	0.45	25.62	0.17	3.58E-13	7.78E-14			3.5	PPLLLL
MC2-W.R.	8/03/2016	12.68	8740-02A	12.06	0.07	0.019	0.0012	0.17	0.3970059	0.025	0.0014	37.62	3.4	30.81	2.79	3.15E-14	2.61E-15			0.06	PLLLLL
		13.51	8740-02B	4.947	0.03	0.014	0.0004	0.52	0.129197	0.004	0.0003	77.90	2.02	26.19	0.69	3.83E-14	7.74E-15			0.12	PPLLLL
		14.30	8740-02C	4.438	0.02	0.012	0.0003	0.47	0.0740139	7E-04	0.0002	96.14	1.33	28.98	0.41	6.00E-14	1.35E-14			0.17	PPLLLL
		15.07	8740-02D	4.36	0.01	0.012	0.0002	0.67	0.036679	7E-04	0.0001	96.08	0.78	28.46	0.24	1.15E-13	2.63E-14			0.23	PPLLLL
		15.88	8740-02E	4.238	0.01	0.011	0.0001	1.02	0.0416859	4E-04	0.0001	98.74	0.66	28.44	0.20	1.53E-13	3.60E-14			0.3	PPLLLL
		16.67	8740-02F	4.214	0.01	0.012	0.0001	1.06	0.0346136	7E-04	0.0001	96.97	0.63	27.77	0.19	1.37E-13	3.24E-14			0.35	PPLLLL
		17.45	8740-02G	4.125	0.01	0.012	0.0001	1.00	0.0374721	4E-04	0.0001	98.63	0.68	27.66	0.20	1.33E-13	3.21E-14			0.4	PPLLLL
		18.31	8740-02H	4.128	0.01	0.012	0.0002	0.91	0.0350068	2E-04	0.0001	100.52	0.73	28.20	0.21	1.19E-13	2.87E-14			0.45	PPLLLL
		19.09	8740-02I	4.13	0.01	0.012	0.0002	1.04	0.0429218	6E-04	0.0001	97.36	0.81	27.33	0.24	1.04E-13	2.53E-14			0.5	PPLLLL
		19.90	8740-02J	4.132	0.01	0.012	0.0002	1.02	0.0478257	6E-04	0.0001	97.84	0.91	27.48	0.26	8.70E-14	2.11E-14			0.55	PPLLLL
		20.66	8740-02K	4.126	0.01	0.012	0.0002	1.37	0.0649179	3E-04	0.0002	100.51	1.27	28.19	0.36	7.15E-14	1.73E-14			0.6	PPLLLL
		21.49	8740-02L	4.201	0.02	0.012	0.0003	1.83	0.083393	7E-04	0.0002	98.45	1.72	28.13	0.49	5.47E-14	1.30E-14			0.65	PPLLLL
		22.32	8740-02M	4.218	0.02	0.012	0.0003	2.20	0.0807427	5E-04	0.0002	100.31	1.81	28.77	0.52	4.54E-14	1.08E-14			0.7	PPLLLL
		23.10	8740-02N	4.268	0.02	0.013	0.0004	2.87	0.0800506	0.001	0.0002	96.94	1.69	28.15	0.49	5.01E-14	1.17E-14			0.8	PPLLLL
		23.93	8740-02O	4.445	0.02	0.015	0.0004	5.01	0.1026471	0.003	0.0003	90.29	2.09	27.36	0.64	4.12E-14	9.28E-15			0.9	PPLLLL
	9/03/2016	0.73	8740-02P	4.396	0.02	0.013	0.0004	7.72	0.1569274	0.003	0.0003	92.97	2.55	27.91	0.77	4.81E-14	1.09E-14			1.2	PPLLLL
		1.56	8740-02Q	4.436	0.03	0.013	0.0005	10.45	0.1806333	0.004	0.0004	92.28	3.21	28.01	0.98	3.53E-14	7.96E-15			1.5	PPLLLL
		2.38	8740-02R	4.462	0.01	0.013	0.0001	8.37	0.0938948	0.004	0.0001	86.72	1.65	26.45	0.51	1.14E-13	2.55E-14			3	PPLLLL
MC5-W.R.	9/03/2016	5.96	8742-01A	82.7	0.99	0.073	0.0021	1.57	0.7902339	0.278	0.0043	-0.33	1.01	-1.88	6.91	1.20E-13	1.45E-15	**0.9983**	**0.0017**	0.06	PPLLLL
		6.81	8742-01B	25.4	0.18	0.033	0.0013	3.78	0.4045785	0.081	0.0015	6.37	1.62	11.07	3.02	6.95E-14	2.74E-15			0.1	PPLLLL

	7.65	8742-01C	8.401	0.04	0.015	0.0004	1.40	0.1098841	0.015	0.0003	48.03	1.11	27.44	0.68	8.98E-14	1.07E-14			0.17	PPLLLL
	8.36	8742-01D	6.01	0.02	0.013	0.0002	1.12	0.0662172	0.006	0.0002	69.36	0.8	28.34	0.36	1.24E-13	2.07E-14			0.23	PPLLLL
	9.09	8742-01E	5.34	0.01	0.012	0.0001	1.53	0.0319429	0.004	0.0001	79.24	0.59	28.77	0.24	1.78E-13	3.33E-14			0.3	PPLLLL
	10.08	8742-01F	4.797	0.01	0.012	0.0002	1.36	0.0333402	0.002	0.0001	87.52	0.62	28.54	0.22	1.63E-13	3.39E-14			0.35	PPLLLL
	10.91	8742-01G	4.417	0.01	0.011	0.0001	1.53	0.0332828	0.001	0.0001	94.05	0.68	28.25	0.22	1.50E-13	3.39E-14			0.4	PPLLLL
	11.71	8742-01H	4.397	0.01	0.012	0.0002	1.70	0.0371358	0.002	0.0001	92.44	0.75	27.64	0.23	1.29E-13	2.93E-14			0.45	PPLLLL
	12.52	8742-01I	4.413	0.01	0.012	0.0002	2.00	0.0410262	0.001	0.0001	93.94	0.85	28.20	0.26	1.09E-13	2.47E-14			0.5	PPLLLL
	13.36	8742-01J	4.348	0.01	0.012	0.0001	1.67	0.0354896	0.001	0.0001	93.62	0.71	27.68	0.22	1.37E-13	3.15E-14			0.6	PPLLLL
	14.20	8742-01K	4.24	0.01	0.012	0.0002	1.87	0.0391947	9E-04	0.0001	96.86	0.76	27.93	0.23	1.33E-13	3.14E-14			0.7	PPLLLL
	15.03	8742-01L	4.259	0.01	0.012	0.0001	3.96	0.0526951	0.002	0.0001	95.35	0.95	27.66	0.28	1.46E-13	3.42E-14			1	PPLLLL
	15.94	8742-01M	4.288	0.02	0.012	0.0002	5.27	0.0782766	0.002	0.0001	94.98	1.42	27.76	0.42	8.65E-14	2.02E-14			1.5	PPLLLL
	16.72	8742-01N	4.326	0.01	0.012	0.0001	8.44	0.0579424	0.003	0.0001	93.22	1.59	27.55	0.47	1.79E-13	4.15E-14			3.5	PPLLLL
9/03/2016	20.40	8742-02A	228.8	12.37	0.172	0.0158	4.37	5.855728	0.709	0.0433	7.65	2.66	116.29	40.75	4.54E-14	1.98E-16			0.06	PPLLLL
	21.21	8742-02B	84.15	1.89	0.065	0.0053	4.13	1.68602	0.282	0.0089	0.19	2.24	1.07	13.49	5.04E-14	5.98E-16			0.1	PPLLLL
	21.95	8742-02C	32.66	0.28	0.039	0.0015	2.81	0.4896383	0.102	0.0018	7.17	1.51	16.00	3.65	6.46E-14	1.98E-15			0.17	PPLLLL
	22.76	8742-02D	18.72	0.13	0.024	0.0009	2.05	0.3421353	0.056	0.0010	11.44	1.48	14.62	2.04	6.05E-14	3.23E-15			0.23	PPLLLL
	23.53	8742-02E	9.031	0.04	0.015	0.0004	1.84	0.1377074	0.017	0.0004	46.50	1.42	28.56	0.91	6.49E-14	7.19E-15			0.3	PPLLLL
10/03/2016	0.22	8742-02F	5.869	0.03	0.012	0.0004	1.29	0.1085483	0.007	0.0003	68.50	1.68	27.33	0.68	5.71E-14	9.73E-15			0.35	PPLLLL
	0.93	8742-02G	5.236	0.02	0.013	0.0003	1.06	0.0713647	0.004	0.0002	81.35	1.24	28.95	0.45	8.00E-14	1.53E-14			0.4	PPLLLL
	1.64	8742-02H	5.472	0.02	0.012	0.0002	1.09	0.0474843	0.005	0.0001	74.52	0.84	27.72	0.34	1.16E-13	2.13E-14			0.45	PPLLLL
	2.36	8742-02I	5.201	0.02	0.012	0.0002	0.91	0.039816	0.004	0.0001	78.55	0.77	27.77	0.29	1.31E-13	2.52E-14			0.5	PPLLLL
	3.07	8742-02J	5.006	0.01	0.012	0.0001	1.42	0.0198378	0.003	0.0001	82.88	0.46	28.21	0.18	2.26E-13	4.51E-14			0.6	PPLLLL
	4.05	8742-02K	4.553	0.01	0.011	0.0001	1.40	0.0243232	0.002	0.0001	90.55	0.48	28.03	0.17	2.82E-13	6.20E-14			0.7	PPLLLL
	4.89	8742-02L	4.348	0.01	0.012	0.0001	1.76	0.0258522	0.001	0.0000	94.06	0.43	27.81	0.15	3.56E-13	8.19E-14			1	PPLLLL
	5.67	8742-02M	4.333	0.01	0.012	0.0001	4.09	0.0477408	0.002	0.0001	92.75	0.83	27.38	0.25	2.27E-13	5.25E-14			1.5	PPLLLL
	6.48	8742-02N	4.496	0.01	0.013	0.0001	13.56	0.1049272	0.005	0.0001	89.79	2.33	27.68	0.72	2.42E-13	5.38E-14			3.5	PPLLLL

MC6-W.R.	10/03/2016	10.30	8743-01A	63.28	0.52	0.054	0.0014	3.49	0.3467326	0.219	0.0025	-2.74	0.82	-11.93	4.71	1.57E-13	2.49E-15	**0.9983**	**0.0017**	0.06	PPLLLL
		11.17	8743-01B	31.73	0.21	0.03	0.0011	3.11	0.326565	0.102	0.0014	4.69	1.17	10.18	2.91	9.78E-14	3.08E-15			0.1	PPLLLL
		12.00	8743-01C	9.876	0.04	0.015	0.0005	1.87	0.130407	0.02	0.0004	39.52	1.34	26.56	0.96	7.36E-14	7.45E-15			0.17	PPLLLL
		12.77	8743-01D	5.535	0.03	0.013	0.0004	1.28	0.1141192	0.006	0.0003	72.08	1.88	27.13	0.72	4.38E-14	7.91E-15			0.23	PPLLLL
		13.51	8743-01E	5.137	0.02	0.011	0.0003	1.20	0.1045789	0.004	0.0002	79.07	1.46	27.61	0.52	5.56E-14	1.08E-14			0.3	PPLLLL
		14.25	8743-01F	5.637	0.02	0.013	0.0004	1.35	0.0953124	0.006	0.0003	70.46	1.49	27.01	0.58	5.58E-14	9.90E-15			0.35	PPLLLL
		14.94	8743-01G	5.462	0.02	0.012	0.0003	1.45	0.0836779	0.005	0.0002	73.96	1.15	27.47	0.44	7.96E-14	1.46E-14			0.4	PPLLLL
		15.67	8743-01H	4.756	0.02	0.012	0.0002	1.43	0.0513333	0.003	0.0001	85.45	0.99	27.63	0.33	9.84E-14	2.07E-14			0.45	PPLLLL
		16.39	8743-01I	4.425	0.01	0.011	0.0002	2.41	0.0439914	0.002	0.0001	92.00	0.91	27.70	0.28	1.11E-13	2.52E-14			0.5	PPLLLL
		17.46	8743-01J	4.293	0.01	0.012	0.0001	1.73	0.0322629	0.001	0.0001	95.91	0.62	28.00	0.19	1.59E-13	3.69E-14			0.6	PPLLLL
		18.24	8743-01K	4.237	0.01	0.012	0.0001	1.63	0.0286705	6E-04	0.0001	98.60	0.59	28.40	0.18	1.76E-13	4.17E-14			0.7	PPLLLL
		19.06	8743-01L	4.35	0.01	0.012	0.0001	1.17	0.018312	0.001	0.00004	93.65	0.35	27.70	0.12	3.57E-13	8.20E-14			1	PPLLLL
		20.03	8743-01M	4.412	0.01	0.012	0.0001	2.46	0.039368	0.002	0.0001	91.33	0.6	27.42	0.19	2.21E-13	5.00E-14			1.5	PPLLLL
		20.89	8743-01N	4.25	0.01	0.012	0.0001	3.36	0.0338861	0.001	0.0000	95.74	0.68	27.70	0.21	3.61E-13	8.49E-14			3.5	PPLLLL
	11/03/2016	1.15	8743-02A	131.5	3.43	0.095	0.0059	5.54	1.973821	0.471	0.0155	-6.57	2.18	-60.35	21.51	6.67E-14	5.07E-16			0.06	PPLLLL
		1.99	8743-02B	52.64	0.68	0.042	0.0023	-0.84	0.7659001	0.181	0.0040	-3.05	1.86	-11.01	7.20	6.12E-14	1.16E-15			0.1	PPLLLL
		2.78	8743-02C	24.14	0.13	0.027	0.0008	2.05	0.2741011	0.074	0.0010	9.24	1.12	15.23	2.11	1.10E-13	4.54E-15			0.2	PPLLLL
		3.65	8743-02D	14.32	0.07	0.019	0.0004	1.67	0.1366935	0.037	0.0005	24.57	1.06	23.96	1.16	1.16E-13	8.13E-15			0.3	PPLLLL
		4.47	8743-02E	9.859	0.04	0.015	0.0005	1.64	0.1184384	0.021	0.0004	37.22	1.36	24.98	0.97	7.32E-14	7.42E-15			0.35	PPLLLL
		5.21	8743-02F	6.334	0.03	0.012	0.0003	1.17	0.1065098	0.008	0.0003	65.12	1.56	28.04	0.69	6.02E-14	9.50E-15			0.4	PPLLLL
		5.94	8743-02G	5.374	0.03	0.012	0.0003	1.23	0.0774175	0.005	0.0002	72.65	1.36	26.55	0.51	6.43E-14	1.20E-14			0.45	PPLLLL
		6.64	8743-02H	4.741	0.01	0.012	0.0001	1.77	0.0359135	0.003	0.0001	86.17	0.59	27.78	0.21	1.71E-13	3.60E-14			0.5	PPLLLL
		7.53	8743-02I	4.638	0.01	0.012	0.0002	2.11	0.0286469	0.002	0.0001	88.92	0.68	28.05	0.23	1.74E-13	3.75E-14			0.6	PPLLLL
		8.30	8743-02J	4.522	0.01	0.012	0.0001	2.10	0.0378921	0.002	0.0001	89.22	0.68	27.45	0.22	1.64E-13	3.62E-14			0.7	PPLLLL
		9.08	8743-02K	4.513	0.01	0.012	0.0001	1.61	0.025304	0.002	0.0001	90.76	0.44	27.85	0.16	3.21E-13	7.11E-14			0.9	PPLLLL
		9.91	8743-02L	4.37	0.01	0.012	0.0001	1.30	0.0158714	0.001	0.00003	93.39	0.34	27.75	0.12	4.95E-13	1.13E-13			1	PPLLLL
		10.70	8743-02M	4.428	0.01	0.013	0.0001	2.22	0.0207481	0.002	0.00005	92.46	0.49	27.85	0.17	3.23E-13	7.29E-14			1.5	PPLLLL

		11.46	8743-02N	4.339	0.01	0.012	0.0001	6.23	0.0430856	0.003	0.00004	93.24	1.12	27.60	0.34	4.21E-13	9.71E-14			3.5	PPLLLL
MC8-W.R.	11/03/2016	15.17	8745-01A	9.66	0.03	0.018	0.0003	0.31	0.0666304	0.026	0.0003	20.23	0.94	13.33	0.73	1.56E-13	1.61E-14	**0.9983**	**0.0017**	0.06	PPLLLL
		15.98	8745-01B	8.079	0.02	0.016	0.0002	0.40	0.0286613	0.016	0.0002	41.47	0.59	22.80	0.42	2.37E-13	2.93E-14			0.1	PPLLLL
		16.75	8745-01C	6.926	0.02	0.015	0.0001	1.27	0.025158	0.009	0.0001	62.36	0.42	29.35	0.26	3.57E-13	5.16E-14			0.17	PPLLLL
		17.82	8745-01D	5.849	0.01	0.013	0.0001	1.94	0.0534083	0.005	0.0001	74.62	0.55	29.67	0.25	2.86E-13	4.89E-14			0.23	PPLLLL
		18.83	8745-01E	4.997	0.01	0.012	0.0001	2.47	0.0378782	0.003	0.0001	85.53	0.69	29.07	0.25	2.16E-13	4.32E-14			0.3	PPLLLL
		19.66	8745-01F	4.562	0.01	0.012	0.0002	2.87	0.0548076	0.002	0.0001	91.17	0.81	28.31	0.26	1.28E-13	2.80E-14			0.35	PPLLLL
		20.50	8745-01G	4.328	0.02	0.012	0.0002	3.40	0.0672942	0.002	0.0001	94.71	1.02	27.91	0.31	8.72E-14	2.01E-14			0.4	PPLLLL
		21.38	8745-01H	4.228	0.02	0.011	0.0002	4.59	0.0728232	0.002	0.0002	97.35	1.87	28.04	0.54	5.66E-14	1.34E-14			0.45	PPLLLL
		22.31	8745-01I	4.157	0.02	0.011	0.0003	5.16	0.1094546	8E-04	0.0003	103.64	2.31	29.36	0.66	3.71E-14	8.92E-15			0.5	PPLLLL
		23.10	8745-01J	4.166	0.02	0.011	0.0004	5.54	0.1575346	0.001	0.0003	102.90	2.44	29.22	0.69	3.34E-14	8.02E-15			0.6	PPLLLL
		23.97	8745-01K	6.248	0.13	0.018	0.0005	9.17	0.1481376	0.009	0.0004	68.94	3.29	29.43	1.28	4.79E-14	7.67E-15			0.7	LPLLLL
	12/03/2016	0.77	8745-01L	4.176	0.02	0.013	0.0005	10.88	0.187198	0.004	0.0004	91.10	3.39	26.05	0.97	3.86E-14	9.24E-15			1	PPLLLL
		1.61	8745-01M	4.248	0.02	0.012	0.0006	18.81	0.2697546	0.005	0.0005	98.02	5.02	28.65	1.46	2.60E-14	6.12E-15			1.5	PPLLLL
		2.46	8745-01N	4.253	0.02	0.012	0.0004	24.34	0.2279596	0.008	0.0003	90.60	4.88	26.63	1.43	4.02E-14	9.46E-15			3.5	PPLLLL
	12/03/2016	6.09	8745-02A	9.201	0.04	0.018	0.0004	0.33	0.0956044	0.025	0.0004	19.09	1.41	11.99	0.96	1.03E-13	1.12E-14			0.06	PPLLLL
		6.92	8745-02B	8.008	0.02	0.016	0.0002	0.31	0.041975	0.017	0.0002	38.21	0.58	20.83	0.41	2.27E-13	2.83E-14			0.1	PPLLLL
		7.74	8745-02C	7.129	0.02	0.015	0.0001	1.18	0.0220288	0.011	0.0001	57.19	0.4	27.72	0.27	3.75E-13	5.26E-14			0.17	PPLLLL
		8.75	8745-02D	6.158	0.02	0.014	0.0001	1.76	0.0294691	0.006	0.0001	71.46	0.42	29.91	0.22	4.00E-13	6.50E-14			0.25	PPLLLL
		9.68	8745-02E	5.497	0.01	0.013	0.0002	2.35	0.0272062	0.005	0.0001	77.91	0.56	29.13	0.23	2.61E-13	4.75E-14			0.3	PPLLLL
		10.54	8745-02F	4.875	0.01	0.013	0.0001	2.66	0.0400324	0.003	0.0001	87.76	0.6	29.10	0.21	2.69E-13	5.52E-14			0.4	PPLLLL
		11.38	8745-02G	4.515	0.01	0.012	0.0001	2.79	0.0424107	0.002	0.0001	92.08	0.68	28.29	0.22	1.85E-13	4.10E-14			0.5	PPLLLL
		12.16	8745-02H	4.261	0.01	0.012	0.0001	2.96	0.0488357	0.002	0.0001	93.95	0.76	27.25	0.23	1.56E-13	3.66E-14			0.7	PPLLLL
		12.97	8745-02I	4.178	0.02	0.013	0.0002	6.01	0.0824356	0.002	0.0002	94.07	1.55	26.81	0.45	8.76E-14	2.10E-14			1	PPLLLL
		13.75	8745-02J	4.208	0.02	0.014	0.0005	16.79	0.2273429	0.006	0.0004	86.66	3.97	25.08	1.15	3.62E-14	8.61E-15			1.5	PPLLLL
		14.54	8745-02K	4.183	0.02	0.014	0.0004	28.93	0.2426613	0.009	0.0003	86.53	5.73	25.11	1.66	3.86E-14	9.23E-15			3.5	PPLLLL

MC9-W.R.	12/03/2016	18.18	8746-01A	5.613	0.02	0.015	0.0003	0.46	0.0904168	0.015	0.0003	22.11	1.57	8.48	0.64	7.39E-14	1.32E-14	**0.9983**	**0.0017**	0.06	PPLLLL
		18.99	8746-01B	5.715	0.01	0.014	0.0002	0.28	0.0318301	0.01	0.0001	46.44	0.72	18.08	0.33	2.07E-13	3.62E-14			0.1	PPLLLL
		19.80	8746-01C	5.701	0.02	0.014	0.0001	0.40	0.017969	0.008	0.0001	60.73	0.38	23.55	0.21	3.54E-13	6.21E-14			0.17	PPLLLL
		20.56	8746-01D	5.566	0.01	0.014	0.0001	0.63	0.0205228	0.005	0.0001	71.85	0.42	27.18	0.20	3.32E-13	5.97E-14			0.23	PPLLLL
		21.35	8746-01E	5.431	0.01	0.014	0.0001	0.91	0.0264069	0.004	0.0001	77.72	0.5	28.68	0.21	2.77E-13	5.10E-14			0.3	PPLLLL
		22.23	8746-01F	5.165	0.01	0.013	0.0001	1.68	0.0350216	0.004	0.0001	80.97	0.62	28.44	0.24	1.93E-13	3.73E-14			0.35	PPLLLL
		23.31	8746-01G	5.001	0.02	0.013	0.0002	1.94	0.0518751	0.003	0.0001	86.43	0.77	29.39	0.28	1.30E-13	2.60E-14			0.4	PPLLLL
	13/03/2016	0.08	8746-01H	5.819	0.05	0.014	0.0003	3.24	0.0719849	0.004	0.0002	82.52	1.45	32.65	0.53	1.06E-13	1.82E-14			0.45	LPLLLL
		0.84	8746-01I	4.811	0.02	0.012	0.0004	3.69	0.0765038	0.003	0.0002	86.63	1.6	28.38	0.53	6.78E-14	1.41E-14			0.5	PPLLLL
		1.69	8746-01J	4.621	0.02	0.013	0.0003	4.10	0.0881008	0.003	0.0002	87.76	1.54	27.63	0.49	7.32E-14	1.58E-14			0.6	PPLLLL
		2.43	8746-01K	4.569	0.02	0.013	0.0004	4.65	0.0846979	0.003	0.0002	89.31	1.79	27.81	0.56	6.68E-14	1.46E-14			0.7	PPLLLL
		3.24	8746-01L	4.344	0.01	0.014	0.0002	6.19	0.1057992	0.003	0.0001	91.19	1.28	27.03	0.38	1.48E-13	3.42E-14			1	PPLPL
		4.11	8746-01M	4.496	0.01	0.014	0.0001	9.15	0.1085068	0.004	0.0001	86.92	1.66	26.72	0.52	1.80E-13	4.01E-14			1.5	PPLPLL
		4.95	8746-01N	4.427	0.01	0.013	0.0002	18.18	0.1300381	0.007	0.0001	85.05	3.21	25.92	0.98	1.38E-13	3.13E-14			3.5	LPLLL
	13/03/2016	8.71	8746-02A	5.822	0.02	0.014	0.0003	0.30	0.0654233	0.015	0.0003	21.78	1.75	8.66	0.73	7.35E-14	1.26E-14			0.06	PPLLLL
		9.52	8746-02B	5.951	0.02	0.015	0.0002	0.32	0.0345528	0.012	0.0002	41.99	0.78	17.03	0.37	1.56E-13	2.62E-14			0.1	PPLLLL
		10.30	8746-02C	5.699	0.01	0.014	0.0001	0.42	0.0134762	0.008	0.0001	59.90	0.45	23.23	0.23	3.84E-13	6.74E-14			0.2	PPLLLL
		11.05	8746-02D	5.575	0.01	0.014	0.0001	0.90	0.0153999	0.006	0.0001	69.04	0.35	26.17	0.18	3.89E-13	6.97E-14			0.3	PPLLLL
		12.09	8746-02E	5.496	0.01	0.014	0.0001	1.29	0.0223726	0.005	0.0001	73.63	0.46	27.51	0.21	2.75E-13	5.00E-14			0.4	PPLLLL
		13.01	8746-02F	5.242	0.01	0.014	0.0001	1.80	0.0268321	0.004	0.0001	78.19	0.53	27.88	0.22	2.19E-13	4.18E-14			0.5	LPLLL
		13.88	8746-02G	5.011	0.01	0.013	0.0002	2.32	0.0627092	0.004	0.0002	80.36	1.13	27.40	0.40	1.75E-13	3.49E-14			0.7	PPLPP
		14.87	8746-02H	4.625	0.01	0.013	0.0002	4.84	0.0851557	0.004	0.0001	85.19	0.99	26.86	0.32	1.85E-13	4.00E-14			1	PPLPL
		15.77	8746-02I	4.465	0.01	0.014	0.0001	8.73	0.0948336	0.004	0.0002	88.44	1.83	26.99	0.56	2.43E-13	5.44E-14			1.5	PPLPP
		16.70	8746-02J	4.416	0.01	0.014	0.0002	16.08	0.0953774	0.006	0.0002	86.14	2.94	26.14	0.89	1.04E-13	2.35E-14			3.5	LLLLL
MHV04-W.R.	13/03/2016	20.44	8748-01A	175.6	28.28	0.111	0.0477	2.51	14.61049	0.453	0.0866	23.04	8	258.15	92.44	1.14E-14	6.51E-17	**0.9983**	**0.0017**	0.06	PPLLLL

		21.19	8748-01B	18.4	0.33	0.032	0.0038	0.83	1.241035	0.043	0.0041	31.00	6.58	38.66	8.17	1.53E-14	8.30E-16			0.1	PPLLLL
		21.93	8748-01C	11.21	0.10	0.019	0.0011	1.82	0.3563827	0.018	0.0012	53.53	3.15	40.65	2.40	3.10E-14	2.77E-15			0.17	PPLLLL
		22.67	8748-01D	6.075	0.03	0.013	0.0005	1.40	0.1482377	0.003	0.0005	89.42	2.39	36.84	0.98	4.04E-14	6.65E-15			0.25	PPLLLL
		23.39	8748-01E	4.789	0.03	0.012	0.0004	1.28	0.1049663	2E-04	0.0003	100.76	1.79	32.76	0.60	4.88E-14	1.02E-14			0.3	PPLLLL
	14/03/2016	0.11	8748-01F	4.507	0.01	0.011	0.0001	1.12	0.0595586	3E-04	0.0001	99.64	0.62	30.50	0.20	1.55E-13	3.43E-14			0.4	PPLLLL
		0.97	8748-01G	4.375	0.01	0.011	0.0001	1.48	0.022619	5E-04	0.0001	99.35	0.49	29.54	0.16	2.43E-13	5.55E-14			0.5	PPLLLL
		1.79	8748-01H	4.278	0.01	0.011	0.0001	1.40	0.0219767	3E-04	0.0001	100.59	0.45	29.25	0.14	2.63E-13	6.14E-14			0.6	PPLLLL
		2.66	8748-01I	4.223	0.01	0.012	0.0001	1.46	0.0205954	7E-05	0.0001	102.18	0.51	29.33	0.16	2.38E-13	5.64E-14			0.7	PPLLLL
		3.42	8748-01J	4.17	0.01	0.012	0.0001	1.42	0.0151583	4E-04	0.0000	99.91	0.42	28.32	0.13	3.87E-13	9.28E-14			1	PPLLLL
		4.23	8748-01K	4.243	0.01	0.012	0.0001	2.15	0.0279417	9E-04	0.0001	97.36	0.59	28.10	0.18	2.28E-13	5.37E-14			1.5	PPLLLL
		5.05	8748-01L	4.466	0.01	0.012	0.0001	5.40	0.0378834	0.003	0.0001	86.28	1	26.29	0.32	2.88E-13	6.45E-14			3.5	PPLLLL
	14/03/2016	8.84	8748-02A	16.62	0.07	0.021	0.0007	0.84	0.2558441	0.049	0.0009	11.88	1.64	13.48	1.98	6.99E-14	4.21E-15			0.06	PLLLLL
		9.65	8748-02B	15.52	0.06	0.02	0.0005	0.48	0.1415429	0.04	0.0006	24.13	1.23	25.47	1.42	1.26E-13	8.12E-15			0.1	PPLLLL
		10.46	8748-02C	5.129	0.02	0.012	0.0002	0.91	0.0377022	0.004	0.0001	79.50	0.67	27.72	0.26	1.79E-13	3.48E-14			0.2	PPLLLL
		11.24	8748-02D	4.378	0.01	0.011	0.0001	0.86	0.018455	6E-04	0.00003	97.47	0.3	29.00	0.11	3.32E-13	7.59E-14			0.3	PPLLLL
		12.09	8748-02E	4.315	0.01	0.011	0.0001	0.89	0.0137812	4E-04	0.00003	98.81	0.28	28.97	0.10	4.82E-13	1.12E-13			0.4	PPLLLL
		12.89	8748-02F	4.254	0.01	0.011	0.0001	0.77	0.0135838	4E-04	0.00003	98.54	0.27	28.49	0.10	4.82E-13	1.13E-13			0.5	PPLLLL
		13.67	8748-02G	4.211	0.01	0.012	0.0001	0.73	0.0132622	5E-04	0.00003	98.03	0.3	28.05	0.11	3.89E-13	9.25E-14			0.6	PPLLLL
		14.45	8748-02H	4.197	0.01	0.012	0.0001	0.92	0.018828	4E-04	0.00004	98.62	0.35	28.13	0.12	2.91E-13	6.94E-14			0.7	PPLLLL
		15.32	8748-02I	4.232	0.01	0.012	0.0001	1.41	0.0249704	0.001	0.0001	95.42	0.49	27.46	0.15	2.37E-13	5.60E-14			0.9	PPLLLL
		16.09	8748-02J	4.324	0.02	0.013	0.0002	2.73	0.0553098	0.002	0.0001	91.81	1.08	27.02	0.33	9.58E-14	2.21E-14			1	PPLLLL
		16.94	8748-02K	4.717	0.01	0.013	0.0002	4.28	0.0720183	0.004	0.0001	83.00	1.18	26.68	0.39	1.13E-13	2.40E-14			1.5	PPLLLL
		17.82	8748-02L	4.847	0.01	0.013	0.0001	2.87	0.0439769	0.004	0.0001	82.07	0.75	27.08	0.26	1.97E-13	4.06E-14			3.5	PPLLLL
MHV05-W.R.	14/03/2016	21.59	8749-01A	53.86	0.82	0.051	0.0029	1.43	1.005975	0.182	0.0048	-0.60	2.23	-2.21	8.63	5.46E-14	1.01E-15	**0.9983**	**0.0017**	0.06	PPLLLL
		22.39	8749-01B	39.78	0.36	0.04	0.0014	1.39	0.6082611	0.127	0.0021	4.68	1.37	12.72	4.10	8.96E-14	2.25E-15			0.1	PPLLLL
		23.20	8749-01C	15.73	0.10	0.02	0.0011	1.17	0.3881059	0.043	0.0012	18.61	2.21	19.94	2.44	5.55E-14	3.53E-15			0.15	PPLLLL

	15/03/2016	0.03	8749-01D	8.51	0.04	0.019	0.0007	2.75	0.2929228	0.021	0.0006	30.47	2.28	17.70	1.35	5.07E-14	5.95E-15			0.2	PPLLLL
		0.73	8749-01E	7.064	0.02	0.014	0.0002	1.31	0.0558882	0.01	0.0001	57.45	0.6	27.59	0.35	1.62E-13	2.29E-14			0.3	PPLLLL
		1.50	8749-01F	5.287	0.01	0.012	0.0001	1.09	0.0180281	0.004	0.0001	78.12	0.35	28.07	0.17	4.30E-13	8.14E-14			0.4	PPLLLL
		2.34	8749-01G	4.288	0.01	0.012	0.0001	0.95	0.0149319	8E-04	0.00003	96.41	0.26	28.09	0.10	5.59E-13	1.30E-13			0.5	PPLLLL
		3.14	8749-01H	4.24	0.01	0.012	0.0001	0.78	0.0133994	6E-04	0.00003	97.06	0.25	27.97	0.10	4.47E-13	1.05E-13			0.6	PPLLLL
		3.91	8749-01I	4.205	0.01	0.012	0.0001	0.78	0.0176181	5E-04	0.00004	98.16	0.32	28.05	0.11	3.36E-13	7.99E-14			0.7	PPLLLL
		4.74	8749-01J	4.206	0.01	0.013	0.0001	1.28	0.0192729	7E-04	0.00005	97.47	0.42	27.87	0.13	2.88E-13	6.86E-14			1	PPLLLL
		5.52	8749-01K	4.202	0.01	0.013	0.0001	2.01	0.0353974	9E-04	0.0001	97.40	0.57	27.84	0.17	2.93E-13	6.96E-14			1.5	PPLLLL
		6.33	8749-01L	4.212	0.01	0.013	0.0001	1.92	0.0184597	1E-03	0.0000	96.49	0.4	27.65	0.13	6.16E-13	1.46E-13			3.5	PPLLLL
	15/03/2016	9.97	8749-02A	46.68	0.53	0.041	0.0022	1.48	0.7158272	0.167	0.0033	-6.41	1.73	-20.61	6.07	6.59E-14	1.41E-15			0.06	PPLLLL
		10.82	8749-02B	17.92	0.08	0.022	0.0004	1.73	0.0945361	0.05	0.0005	17.06	0.75	20.84	1.17	1.74E-13	9.72E-15			0.2	PPLLLL
		11.62	8749-02C	6.214	0.02	0.013	0.0002	1.18	0.062909	0.007	0.0002	66.73	0.86	28.19	0.39	1.36E-13	2.18E-14			0.3	PPLLLL
		12.36	8749-02D	5.345	0.01	0.012	0.0001	1.07	0.016432	0.004	0.0001	78.59	0.37	28.55	0.17	4.25E-13	7.95E-14			0.4	PPLLLL
		13.28	8749-02E	4.306	0.01	0.012	0.0001	0.94	0.0093936	8E-04	0.00003	96.25	0.26	28.16	0.10	7.41E-13	1.72E-13			0.5	PPLLLL
		14.13	8749-02F	4.206	0.01	0.012	0.0001	0.78	0.0130257	5E-04	0.00002	97.68	0.23	27.92	0.09	5.89E-13	1.40E-13			0.6	PPLLLL
		14.88	8749-02G	4.198	0.01	0.012	0.0001	0.69	0.0118753	5E-04	0.00003	97.75	0.25	27.89	0.09	5.49E-13	1.31E-13			0.7	PPLLLL
		15.68	8749-02H	4.202	0.01	0.013	0.0001	1.32	0.0252278	6E-04	0.00004	97.88	0.41	27.96	0.13	2.70E-13	6.42E-14			1	PPLLLL
		16.49	8749-02I	4.193	0.01	0.013	0.0001	2.08	0.0171568	0.001	0.00003	96.68	0.42	27.58	0.14	5.64E-13	1.35E-13			2	PPLLLL
		17.27	8749-02J	4.307	0.01	0.013	0.0001	1.98	0.0229761	0.001	0.00004	95.75	0.47	28.05	0.15	3.32E-13	7.71E-14			3.5	PPLLLL
MHV06-W.R.	15/03/2016	20.94	8750-01A	13.95	0.05	0.02	0.0003	0.60	0.0734223	0.039	0.0004	16.42	0.81	15.62	0.96	1.81E-13	1.30E-14	**0.9983**	**0.0017**	0.06	PPLLLL
		21.79	8750-01B	7.483	0.02	0.016	0.0002	0.24	0.0316165	0.015	0.0001	41.97	0.58	21.38	0.38	2.68E-13	3.58E-14			0.1	PPLLLL
		22.61	8750-01C	5.655	0.01	0.014	0.0001	0.37	0.0195255	0.006	0.0001	69.89	0.49	26.86	0.23	2.87E-13	5.08E-14			0.15	PPLLLL
		23.38	8750-01D	5.193	0.01	0.013	0.0001	0.59	0.0228833	0.003	0.0001	83.02	0.44	29.28	0.18	2.89E-13	5.57E-14			0.2	PPLLLL
	16/03/2016	0.23	8750-01E	6.932	0.03	0.014	0.0001	1.33	0.0188954	0.006	0.0001	74.16	0.62	34.89	0.32	4.25E-13	6.14E-14			0.3	PPLLLL
		1.27	8750-01F	4.935	0.01	0.013	0.0001	1.79	0.0218137	0.004	0.0001	76.99	0.56	25.86	0.21	2.91E-13	5.89E-14			0.4	PPLLLL
		2.14	8750-01G	4.541	0.01	0.013	0.0001	2.15	0.0351594	0.003	0.0001	83.27	0.69	25.74	0.23	2.39E-13	5.26E-14			0.5	PPLLLL

		2.99	8750-01H	4.472	0.01	0.013	0.0002	3.38	0.0696769	0.003	0.0002	83.94	1.52	25.57	0.47	1.29E-13	2.88E-14			0.6	PLLPP
		3.82	8750-01I	4.399	0.01	0.014	0.0002	4.89	0.1345837	0.004	0.0003	79.82	2.42	23.96	0.73	7.63E-14	1.73E-14			0.7	PLLPP
		4.65	8750-01J	4.402	0.01	0.014	0.0002	5.48	0.0534122	0.004	0.0001	83.89	1.23	25.20	0.38	1.59E-13	3.61E-14			1	PPLLLL
		5.49	8750-01K	4.395	0.01	0.014	0.0002	9.52	0.0653852	0.004	0.0001	89.04	1.78	26.77	0.54	1.80E-13	4.10E-14			1.5	LPLLL
		6.33	8750-01L	4.277	0.01	0.013	0.0002	21.28	0.150215	0.007	0.0002	89.42	3.95	26.38	1.16	9.59E-14	2.24E-14			3.5	PPLLL
	16/03/2016	10.16	8750-02A	9.963	0.04	0.017	0.0003	0.64	0.0860062	0.027	0.0003	20.27	1.01	13.78	0.79	1.39E-13	1.39E-14			0.06	PPLLLL
		11.01	8750-02B	5.711	0.01	0.015	0.0001	0.34	0.0225413	0.007	0.0001	63.78	0.42	24.77	0.22	3.22E-13	5.64E-14			0.15	PPLLLL
		11.77	8750-02C	4.934	0.01	0.014	0.0001	0.52	0.0309978	0.003	0.0001	82.93	0.51	27.81	0.19	2.08E-13	4.22E-14			0.2	PPLLLL
		12.58	8750-02D	4.886	0.01	0.013	0.0001	1.37	0.0333017	0.003	0.0001	85.54	0.52	28.41	0.19	2.11E-13	4.31E-14			0.3	PPLLLL
		13.71	8750-02E	4.868	0.01	0.013	0.0002	1.83	0.0756429	0.003	0.0002	84.70	1.51	28.04	0.51	1.33E-13	2.73E-14			0.35	PPLPP
		14.56	8750-02F	4.596	0.02	0.013	0.0002	2.57	0.0487913	0.003	0.0001	87.18	1.04	27.27	0.34	1.15E-13	2.51E-14			0.4	PPLLLL
		15.38	8750-02G	4.462	0.01	0.012	0.0002	3.01	0.0524132	0.002	0.0001	92.40	1.06	28.06	0.33	1.26E-13	2.82E-14			0.5	LPLLL
		16.20	8750-02H	4.361	0.02	0.013	0.0002	4.10	0.0651694	0.002	0.0002	91.59	1.35	27.21	0.41	1.03E-13	2.35E-14			0.7	PPLLLL
		17.03	8750-02I	4.376	0.02	0.013	0.0003	5.18	0.0926511	0.003	0.0002	90.64	1.58	27.05	0.47	7.63E-14	1.74E-14			0.9	PPLLLL
		17.79	8750-02J	4.426	0.02	0.013	0.0003	5.60	0.1036486	0.003	0.0002	90.44	1.74	27.30	0.53	6.70E-14	1.51E-14			1	PPLLLL
		18.57	8750-02K	4.361	0.01	0.013	0.0002	9.07	0.0987512	0.004	0.0002	88.79	1.94	26.48	0.58	9.36E-14	2.15E-14			1.5	LPLLL
		19.41	8750-02L	4.438	0.02	0.013	0.0002	13.88	0.2065281	0.005	0.0002	92.47	2.76	28.14	0.84	8.06E-14	1.82E-14			3.5	PPLLLL
MHV07-W.R.	16/03/2016	23.17	8751-01A	133.3	99.84	-0.243	0.2814	78.61	90.67296	-0.34	0.3226	180.48	45.6	1218.90	##########	2.08E-15	1.56E-17	**0.9983**	**0.0017**	0.06	PPLLLL
		23.92	8751-01B	18.37	0.45	0.037	0.0067	9.70	2.502875	0.052	0.0059	18.82	9.52	23.67	11.93	1.14E-14	6.20E-16			0.1	PPLLLL
	17/03/2016	0.64	8751-01C	12.46	0.10	0.017	0.0012	0.45	0.3737088	0.023	0.0012	45.60	2.85	38.51	2.42	3.81E-14	3.05E-15			0.17	PPLLLL
		1.36	8751-01D	7.068	0.04	0.014	0.0007	0.76	0.2231904	0.012	0.0006	52.12	2.71	25.05	1.31	4.01E-14	5.67E-15			0.23	PPLLLL
		2.08	8751-01E	4.855	0.02	0.012	0.0003	0.69	0.1079275	0.003	0.0003	81.77	1.71	26.98	0.57	5.93E-14	1.22E-14			0.3	PPLLLL
		2.77	8751-01F	4.197	0.01	0.012	0.0001	0.68	0.0334813	0.001	0.0001	94.09	0.66	26.84	0.20	1.44E-13	3.43E-14			0.4	PPLLLL
		3.50	8751-01G	4.121	0.01	0.011	0.0001	0.94	0.0207769	8E-04	0.00005	96.17	0.4	26.94	0.12	2.67E-13	6.47E-14			0.5	PPLLLL
		4.48	8751-01H	4.157	0.01	0.012	0.0001	0.94	0.0150786	5E-04	0.00003	97.93	0.31	27.67	0.11	3.77E-13	9.07E-14			0.6	PPLLLL
		5.31	8751-01I	4.136	0.01	0.011	0.0001	0.80	0.0300619	3E-04	0.0001	99.06	0.46	27.84	0.14	4.43E-13	1.07E-13			0.7	PPLPP

		6.10	8751-01J	4.182	0.01	0.011	0.0001	0.64	0.009531	4E-04	0.00004	98.38	0.27	27.96	0.10	9.55E-13	2.28E-13			1	PPLLP
		6.94	8751-01K	4.75	0.01	0.012	0.0000	0.69	0.008 2031	0.002	0.00004	85.90	0.19	27.73	0.10	1.33E-12	2.79E-13			1.5	PPLLLL
		7.76	8751-01L	8.581	0.02	0.015	0.0001	2.30	0.056 2459	0.016	0.00006	45.74	0.48	26.72	0.38	4.54E-13	5.29E-14			3.5	PPLPL
	17/03/2016	11.53	8751-02A	11.78	0.08	0.02	0.0008	-0.55	0.302 8759	0.026	0.00107	32.87	2.82	26.31	2.28	4.37E-14	3.71E-15			0.06	PPLLLL
		12.31	8751-02B	5.877	0.03	0.013	0.0005	-0.20	0.158 6526	0.008	0.00044	57.89	2.21	23.14	0.89	4.55E-14	7.75E-15			0.1	PPLLLL
		13.07	8751-02C	4.14	0.01	0.012	0.0001	0.57	0.039 5707	0.001	0.00006	90.26	0.58	25.41	0.18	1.66E-13	4.00E-14			0.2	PPLLLL
		13.78	8751-02D	4.121	0.01	0.011	0.0001	0.70	0.021 3853	7E-04	0.00004	96.22	0.34	26.95	0.11	3.37E-13	8.19E-14			0.3	PPLLLL
		14.59	8751-02E	4.196	0.01	0.012	0.0001	0.71	0.010 9698	5E-04	0.00003	97.70	0.26	27.86	0.10	4.89E-13	1.16E-13			0.4	PPLLLL
		15.35	8751-02F	4.181	0.01	0.012	0.0001	0.55	0.014 8148	4E-04	0.00003	98.04	0.26	27.85	0.09	5.15E-13	1.23E-13			0.5	PPLLLL
		16.13	8751-02G	4.175	0.01	0.011	0.0001	0.39	0.012 7582	4E-04	0.00003	98.09	0.23	27.82	0.09	4.11E-13	9.85E-14			0.6	PPLLLL
		16.96	8751-02H	4.217	0.01	0.012	0.0001	0.48	0.016 7645	6E-04	0.00004	96.84	0.32	27.75	0.11	3.10E-13	7.34E-14			0.7	PPLLLL
		17.83	8751-02I	4.407	0.01	0.012	0.0001	0.42	0.021 783	0.001	0.00006	91.74	0.4	27.47	0.14	2.61E-13	5.92E-14			0.85	PPLLLL
		18.61	8751-02J	4.874	0.01	0.012	0.0002	0.60	0.036 6445	0.003	0.00006	82.08	0.6	27.19	0.22	1.68E-13	3.45E-14			1	PPLLLL
		19.42	8751-02K	7.544	0.02	0.014	0.0002	1.75	0.059 7681	0.013	0.00015	50.13	0.68	25.74	0.41	2.01E-13	2.66E-14			1.2	PPLLLL
		20.34	8751-02L	9.727	0.03	0.016	0.0002	1.63	0.061 6289	0.02	0.00015	40.03	0.64	26.49	0.52	3.15E-13	3.24E-14			3.5	PPLLLL
MHV10-W.R.	18/03/2016	0.20	8752-01A	80.58	2.00	0.113	0.0075	51.78	2.037 837	0.334	0.00977	-18.64	2.41	-109.94	15.63	7.46E-14	9.26E-16	**0.9983**	**0.0017**	0.06	LPLLLL
		1.30	8752-01B	30.48	0.52	0.036	0.0037	26.61	1.408 018	0.135	0.00488	-25.74	4.37	-55.57	9.80	2.71E-14	8.88E-16			0.1	PPLLLL
		2.10	8752-01C	15.24	0.18	0.027	0.0019	13.58	0.699 6202	0.054	0.00211	1.09	4.04	1.15	4.32	2.54E-14	1.67E-15			0.15	PPLLLL
		2.88	8752-01D	18.94	0.14	0.026	0.0013	8.63	0.440 7705	0.062	0.00137	5.69	2.17	7.41	2.95	5.10E-14	2.69E-15			0.2	PPLLLL
		3.67	8752-01E	12.89	0.07	0.018	0.0006	3.96	0.187 4528	0.031	0.00064	29.67	1.43	26.05	1.33	7.80E-14	6.06E-15			0.3	PPLLLL
		4.50	8752-01F	5.231	0.02	0.012	0.0003	2.28	0.102 8142	0.004	0.00026	79.59	1.65	28.32	0.59	6.18E-14	1.18E-14			0.4	PPLLLL
		5.25	8752-01G	5.109	0.02	0.012	0.0002	1.13	0.037 784	0.003	0.00013	81.49	0.74	28.30	0.28	1.46E-13	2.86E-14			0.5	PPLLLL
		6.05	8752-01H	4.563	0.01	0.012	0.0001	0.75	0.019 1532	0.002	0.00013	89.83	0.43	27.86	0.15	2.87E-13	6.29E-14			0.6	PPLLLL
		6.81	8752-01I	4.322	0.01	0.012	0.0001	0.73	0.016 4423	7E-04	0.00004	96.27	0.35	28.27	0.13	3.54E-13	8.20E-14			0.7	PPLLLL
		7.61	8752-01J	4.299	0.01	0.012	0.0001	0.69	0.018 1131	8E-04	0.00003	95.68	0.23	27.95	0.09	6.53E-13	1.52E-13			1	PPLLLL
		8.63	8752-01K	4.395	0.01	0.013	0.0001	1.57	0.021 7053	0.001	0.00004	93.45	0.38	27.93	0.13	4.79E-13	1.09E-13			1.5	PPLLLL

		9.46	8752-01L	4.252	0.01	0.013	0.0001	2.75	0.0213663	0.001	0.00004	97.08	0.56	28.09	0.17	4.82E-13	1.13E-13			3.5	PPLLLL
	18/03/2016	13.21	8752-02A	59.89	0.52	0.057	0.0018	2.96	0.4534414	0.205	0.0027	-1.77	1.06	-7.28	5.22	1.32E-13	2.20E-15			0.06	LPLLLL
		14.04	8752-02B	23.54	0.17	0.03	0.0012	3.72	0.4121739	0.077	0.0014	3.40	1.7	5.48	2.94	7.29E-14	3.10E-15			0.1	PPLLLL
		14.84	8752-02C	8.1	0.04	0.015	0.0004	1.49	0.1297755	0.015	0.0004	44.33	1.44	24.44	0.83	7.59E-14	9.37E-15			0.2	PPLLLL
		15.67	8752-02D	4.822	0.01	0.012	0.0001	0.98	0.0139455	0.003	0.00004	85.54	0.33	28.03	0.14	4.19E-13	8.69E-14			0.4	PPLLLL
		16.58	8752-02E	4.256	0.01	0.012	0.0001	0.98	0.0192318	8E-04	0.00004	95.94	0.37	27.75	0.13	3.78E-13	8.88E-14			0.5	PPLLLL
		17.38	8752-02F	4.304	0.01	0.012	0.0001	1.11	0.0190056	0.001	0.00005	94.97	0.4	27.79	0.13	2.56E-13	5.96E-14			0.6	PPLLLL
		18.24	8752-02G	4.376	0.01	0.012	0.0001	1.38	0.0252274	0.001	0.0001	94.36	0.55	28.08	0.18	2.11E-13	4.82E-14			0.7	PPLLLL
		19.17	8752-02H	4.402	0.01	0.012	0.0001	1.72	0.0294841	0.001	0.0001	94.55	0.62	28.30	0.19	1.79E-13	4.08E-14			0.85	PPLLLL
		19.94	8752-02I	4.365	0.02	0.013	0.0003	3.76	0.0860851	0.002	0.0002	91.54	1.51	27.22	0.46	7.14E-14	1.64E-14			1	PPLLLL
		20.77	8752-02J	4.314	0.01	0.015	0.0002	5.33	0.0665113	0.002	0.0002	95.73	1.47	28.15	0.44	9.52E-14	2.21E-14			1.5	PPLLLL
		21.66	8752-02K	4.269	0.01	0.014	0.0001	6.69	0.0557268	0.002	0.0001	96.27	1.28	28.04	0.38	2.19E-13	5.12E-14			3.5	PPLLLL
MO1-W.R.	19/03/2016	1.41	8753-01A	49.09	0.23	0.042	0.0007	0.90	0.1517066	0.155	0.0013	6.11	0.7	20.42	3.18	3.42E-13	6.96E-15	**0.9983**	**0.0017**	0.06	PPLLLL
		2.20	8753-01B	28.6	0.12	0.027	0.0005	0.87	0.1053428	0.075	0.0006	22.35	0.6	43.27	1.59	2.87E-13	1.00E-14			0.1	PPLLLL
		3.01	8753-01C	17.49	0.06	0.02	0.0004	1.39	0.0889664	0.036	0.0003	39.69	0.55	46.95	0.86	2.17E-13	1.24E-14			0.15	PPLLLL
		3.83	8753-01D	12.48	0.05	0.017	0.0004	1.47	0.0981634	0.021	0.0003	50.76	0.84	42.91	0.80	1.40E-13	1.12E-14			0.2	PPLLLL
		4.63	8753-01E	12.15	0.05	0.016	0.0004	3.01	0.1237748	0.022	0.0005	47.66	1.18	39.30	1.04	1.00E-13	8.24E-15			0.3	PPLLLL
		5.41	8753-01F	8.397	0.03	0.015	0.0003	5.90	0.1141251	0.012	0.0004	62.31	1.37	35.61	0.81	8.57E-14	1.02E-14			0.4	PPLLLL
		6.52	8753-01G	7.341	0.04	0.015	0.0006	11.02	0.2251261	0.009	0.0006	74.44	2.66	37.31	1.34	4.52E-14	6.16E-15			0.5	PPLLLL
		7.36	8753-01H	6.724	0.05	0.017	0.0008	15.60	0.3726986	0.01	0.0009	72.74	4.22	33.54	1.94	2.62E-14	3.90E-15			0.6	PPLLLL
		8.17	8753-01I	6.694	0.05	0.016	0.0011	20.29	0.4425445	0.01	0.0010	78.70	4.91	36.21	2.26	1.99E-14	2.98E-15			0.7	PPLLLL
		9.00	8753-01J	7.049	0.03	0.016	0.0005	13.17	0.1840308	0.01	0.0005	70.12	2.44	33.83	1.18	6.20E-14	8.79E-15			1	PPLLLL
		9.91	8753-01K	7.051	0.03	0.015	0.0004	18.64	0.1960397	0.012	0.0003	69.87	2.43	33.85	1.18	6.96E-14	9.86E-15			1.5	PPLLLL
		10.79	8753-01L	6.609	0.03	0.015	0.0004	28.27	0.2153673	0.014	0.0004	68.82	3.62	31.48	1.65	6.85E-14	1.04E-14			3.5	PPLLLL
	19/03/2016	14.59	8753-02A	60.1	0.28	0.049	0.0007	0.36	0.1347428	0.19	0.0015	5.74	0.61	23.48	3.63	4.60E-13	7.65E-15			0.06	PPLLLL

		15.39	8753-02B	38.57	0.15	0.034	0.0005	0.63	0.0813208	0.11	0.0008	14.74	0.49	38.54	2.03	5.32E-13	1.38E-14			0.1	PPLLLL
		16.17	8753-02C	26.12	0.08	0.024	0.0003	0.93	0.067041	0.067	0.0005	23.82	0.54	42.13	1.37	4.54E-13	1.74E-14			0.15	PPLLLL
		16.92	8753-02D	18.7	0.06	0.02	0.0003	1.10	0.071134	0.042	0.0005	33.75	0.72	42.73	1.11	2.97E-13	1.59E-14			0.2	PPLLLL
		17.71	8753-02E	16.21	0.05	0.019	0.0003	1.71	0.084 2359	0.034	0.0003	37.85	0.64	41.57	0.88	2.60E-13	1.60E-14			0.3	PPLLLL
		18.54	8753-02F	10.72	0.03	0.015	0.0002	3.14	0.098776	0.017	0.0003	55.07	0.75	40.05	0.62	1.85E-13	1.72E-14			0.4	PPLLLL
		19.64	8753-02G	8.923	0.04	0.015	0.0003	5.41	0.129356	0.013	0.0003	61.25	1.09	37.17	0.70	9.79E-14	1.10E-14			0.5	LPLLL
		20.51	8753-02H	7.67	0.03	0.016	0.0003	7.44	0.212 9405	0.01	0.0003	68.43	1.43	35.76	0.77	8.77E-14	1.14E-14			0.7	LPLPL
		21.34	8753-02I	7.234	0.02	0.015	0.0003	6.75	0.097 8543	0.009	0.0002	69.97	1.21	34.48	0.62	1.32E-13	1.82E-14			1	LPLLLL
		22.31	8753-02J	7.474	0.02	0.016	0.0003	10.16	0.101 0655	0.011	0.0002	67.27	1.26	34.33	0.66	1.78E-13	2.38E-14			1.5	PLLLL
		23.21	8753-02K	7.295	0.02	0.015	0.0003	22.23	0.145 3673	0.015	0.0002	63.12	2.43	31.73	1.23	1.44E-13	1.98E-14			3.5	PLLLL
GM1-W.R.	20/03/2016	2.88	8754-01A	90.89	0.24	0.068	0.0004	0.22	0.034 5591	0.297	0.0009	2.51	0.24	15.54	4.38	2.81E-12	3.09E-14	**0.9983**	**0.0017**	0.1	PPLLLL
		3.63	8754-01B	13	0.03	0.017	0.0001	0.06	0.006 2724	0.028	0.0001	35.83	0.22	31.60	0.48	2.19E-12	1.69E-13			0.2	PPLLLL
		4.42	8754-01C	5.727	0.01	0.012	0.0001	0.04	0.004 1744	0.004	0.00003	80.32	0.16	31.22	0.12	1.57E-12	2.74E-13			0.3	PPLLLL
		5.17	8754-01D	4.91	0.01	0.012	0.0001	0.03	0.004 9919	0.001	0.00002	91.74	0.15	30.57	0.09	1.17E-12	2.37E-13			0.4	PPLLL
		5.95	8754-01E	4.825	0.01	0.012	0.0001	0.06	0.007 4482	0.001	0.00003	92.06	0.2	30.15	0.10	7.29E-13	1.51E-13			0.5	PPLLLL
		6.75	8754-01F	4.99	0.01	0.012	0.0001	0.04	0.010 8411	0.002	0.00004	88.69	0.26	30.05	0.12	4.69E-13	9.40E-14			0.6	PPLLLL
		7.54	8754-01G	5.327	0.01	0.012	0.0001	0.16	0.022 04	0.003	0.0001	83.36	0.32	30.15	0.16	3.72E-13	6.98E-14			0.7	PPLPL
		8.33	8754-01H	6.017	0.01	0.013	0.0001	0.02	0.013 1317	0.005	0.0001	74.48	0.31	30.42	0.18	4.36E-13	7.25E-14			0.9	PPLLL
		9.11	8754-01I	6.927	0.02	0.013	0.0001	0.33	0.047 6123	0.009	0.0001	63.38	0.55	29.81	0.31	2.30E-13	3.33E-14			1	PPLPL
		9.91	8754-01J	7.848	0.02	0.014	0.0001	0.07	0.015 0923	0.011	0.0001	56.98	0.42	30.36	0.31	3.94E-13	5.02E-14			1.5	PPLLLL
		10.68	8754-01K	8.591	0.02	0.014	0.0001	0.12	0.016 623	0.014	0.0001	52.12	0.32	30.40	0.31	6.11E-13	7.11E-14			3.5	PPLLLL
	20/03/2016	14.31	8754-02A	36.16	0.14	0.034	0.0005	0.06	0.102 2411	0.114	0.0008	5.82	0.6	14.35	2.17	3.70E-13	1.02E-14			0.06	PPLLLL
		15.08	8754-02B	13.82	0.03	0.018	0.0002	-0.01	0.028 1297	0.032	0.0002	30.55	0.45	28.68	0.64	5.16E-13	3.73E-14			0.12	PPLLLL
		15.87	8754-02C	7.019	0.01	0.013	0.0001	0.02	0.005 7951	0.008	0.0001	65.50	0.22	31.20	0.20	1.16E-12	1.65E-13			0.2	PPLLLL
		16.66	8754-02D	5.895	0.01	0.012	0.0000	0.02	0.003 1241	0.005	0.00002	77.11	0.14	30.85	0.13	1.91E-12	3.24E-13			0.3	PPLLLL
		17.42	8754-02E	6.313	0.01	0.013	0.0001	0.02	0.007 1499	0.006	0.00005	70.47	0.24	30.20	0.17	8.98E-13	1.42E-13			0.35	PPLLLL

		18.16	8754-02F	5.926	0.01	0.013	0.0001	0.01	0.0043691	0.005	0.00004	73.96	0.21	29.76	0.15	1.39E-12	2.34E-13			0.4	PPLLLL
		18.94	8754-02G	6.474	0.01	0.013	0.0001	0.01	0.0048072	0.007	0.00004	67.20	0.22	29.54	0.18	1.26E-12	1.94E-13			0.5	PPLLLL
		19.68	8754-02H	8.878	0.03	0.015	0.0001	-0.04	0.0143204	0.015	0.0001	49.41	0.33	29.78	0.33	6.11E-13	6.88E-14			0.7	PPLLLL
		20.42	8754-02I	10.27	0.02	0.016	0.0001	0.02	0.0098004	0.02	0.0001	42.46	0.25	29.60	0.37	1.19E-12	1.16E-13			1	PPLLLL
		21.18	8754-02J	11.78	0.03	0.017	0.0001	0.00	0.0076324	0.025	0.0001	37.71	0.27	30.16	0.45	1.38E-12	1.17E-13			1.5	PPLLLL
		21.93	8754-02K	29.68	0.07	0.028	0.0002	0.01	0.0170263	0.084	0.0003	15.84	0.26	31.90	1.31	1.83E-12	6.17E-14			3.5	PPLLLL
GM2-W.R.	21/03/2016	1.55	8755-01A	288.9	1.91	0.193	0.0017	0.27	0.1561558	0.981	0.0068	-1.41	0.28	-28.14	14.97	1.78E-12	6.16E-15	**0.9983**	**0.0017**	0.06	PPLLLL
		2.36	8755-01B	174.9	0.51	0.121	0.0006	-0.01	0.0368373	0.584	0.0019	0.32	0.22	3.80	8.55	5.10E-12	2.91E-14			0.12	PPLLLL
		3.10	8755-01C	56.1	0.13	0.045	0.0002	0.04	0.0109142	0.176	0.0004	6.09	0.17	23.24	2.55	5.07E-12	9.04E-14			0.2	PPLLLL
		3.81	8755-01D	22.21	0.04	0.022	0.0001	0.04	0.0058184	0.06	0.0001	19.56	0.15	29.50	0.90	4.18E-12	1.88E-13			0.3	PPLLLL
		4.55	8755-01E	18.73	0.04	0.02	0.0001	0.05	0.0078434	0.048	0.0002	23.92	0.23	30.42	0.77	2.76E-12	1.47E-13			0.35	PPLLLL
		5.34	8755-01F	17.46	0.04	0.02	0.0001	0.01	0.0079847	0.044	0.0001	24.74	0.24	29.33	0.71	2.24E-12	1.28E-13			0.4	PPLLLL
		6.07	8755-01G	16.83	0.04	0.02	0.0001	0.01	0.0081287	0.042	0.0001	25.80	0.24	29.49	0.68	2.15E-12	1.28E-13			0.5	PPLLLL
		6.81	8755-01H	17.2	0.04	0.02	0.0001	0.01	0.0083909	0.043	0.0001	25.61	0.22	29.91	0.69	2.25E-12	1.31E-13			0.7	PPLLLL
		7.59	8755-01I	14.03	0.03	0.018	0.0001	0.01	0.0072648	0.032	0.0001	31.46	0.2	29.97	0.53	2.32E-12	1.66E-13			1	PPLLLL
		8.38	8755-01J	16.25	0.04	0.019	0.0001	0.03	0.0122185	0.04	0.0002	26.90	0.27	29.68	0.66	1.62E-12	9.96E-14			1.5	PPLLLL
		9.14	8755-01K	57.58	0.12	0.046	0.0001	0.03	0.004648	0.178	0.0003	7.69	0.12	30.07	2.54	1.41E-11	2.45E-13			3.5	PPLLLL
	21/03/2016	12.72	8755-02A	166.5	1.41	0.11	0.0019	1.08	0.3811646	0.549	0.0054	1.57	0.54	17.84	9.72	5.32E-13	3.19E-15			0.06	PPLLLL
		13.47	8755-02B	89.14	6.66	0.054	0.0154	2.40	5.503799	0.331	0.030	-10.82	5.71	-67.39	36.86	1.81E-14	2.03E-16			0.12	PPLLLL
		14.21	8755-02C	49.61	0.38	0.044	0.0012	0.95	0.3004147	0.172	0.0019	-3.08	0.89	-10.48	3.86	1.61E-13	3.25E-15			0.2	PPLLLL
		15.02	8755-02D	46.12	0.17	0.041	0.0004	0.42	0.0913978	0.151	0.0009	2.37	0.52	7.47	2.68	5.40E-13	1.17E-14			0.3	PPLLLL
		15.77	8755-02E	37.84	0.15	0.036	0.0005	0.19	0.0921226	0.119	0.0008	6.46	0.52	16.65	2.14	4.59E-13	1.21E-14			0.35	PPLLLL
		16.55	8755-02F	24.76	0.07	0.026	0.0003	0.13	0.0554845	0.071	0.0004	14.89	0.47	25.07	1.28	4.57E-13	1.84E-14			0.4	PPLLLL
		17.33	8755-02G	14.45	0.04	0.018	0.0002	0.05	0.0220727	0.034	0.0002	29.83	0.4	29.27	0.65	6.41E-13	4.43E-14			0.5	PPLLLL
		18.09	8755-02H	9.704	0.02	0.015	0.0001	0.06	0.010881	0.017	0.0001	48.47	0.27	31.92	0.34	1.09E-12	1.12E-13			0.7	PPLLLL
		18.88	8755-02I	7.012	0.01	0.013	0.0001	0.04	0.0051351	0.008	0.00004	66.58	0.19	31.68	0.19	1.53E-12	2.18E-13			1	PPLLLL

		19.65	8755-02J	5.876	0.01	0.012	0.0000	0.03	0.0036126	0.005	0.00002	77.09	0.13	30.75	0.13	1.99E-12	3.39E-13			2	PPLLLL
		20.44	8755-02K	8.919	0.02	0.015	0.0001	0.02	0.0094114	0.015	0.0001	49.59	0.24	30.02	0.30	9.73E-13	1.09E-13			2.5	PPLLLL
		21.17	8755-02L	21.44	0.06	0.022	0.0002	0.01	0.0166693	0.056	0.0002	21.38	0.27	31.12	0.91	1.38E-12	6.45E-14			3	PPLLLL
		21.92	8755-02M	16.62	0.07	0.02	0.0005	-0.55	0.1587775	0.041	0.0007	25.58	1.19	28.86	1.47	1.18E-13	7.08E-15			3.5	PLLLLL
GM3-W.R.	22/03/2016	1.62	8756-01A	147.5	0.76	0.106	0.0011	0.33	0.1570146	0.508	0.0033	-2.72	0.44	-27.67	8.45	1.01E-12	6.85E-15	**0.9983**	**0.0017**	0.06	PPLLLL
		2.40	8756-01B	99.5	0.29	0.074	0.0004	0.16	0.0385197	0.327	0.0012	1.97	0.28	13.39	4.91	2.90E-12	2.91E-14			0.12	PPLLLL
		3.16	8756-01C	14.87	0.04	0.018	0.0001	0.04	0.0125177	0.035	0.0002	29.51	0.33	29.79	0.63	1.17E-12	7.85E-14			0.2	PPLLLL
		3.90	8756-01D	6.124	0.01	0.012	0.0001	0.01	0.0069944	0.004	0.0000	78.81	0.18	32.74	0.14	1.07E-12	1.74E-13			0.3	PPLLLL
		4.66	8756-01E	5.483	0.01	0.012	0.0001	0.04	0.0087984	0.003	0.0000	86.33	0.22	32.12	0.13	7.00E-13	1.28E-13			0.35	PPLLLL
		5.43	8756-01F	5.275	0.01	0.012	0.0001	0.04	0.0116617	0.002	0.0000	87.97	0.25	31.49	0.13	5.52E-13	1.05E-13			0.4	PPLLLL
		6.18	8756-01G	5.56	0.01	0.012	0.0001	0.05	0.0101717	0.003	0.0000	81.90	0.27	30.91	0.15	6.41E-13	1.15E-13			0.5	PPLLLL
		6.94	8756-01H	5.111	0.01	0.012	0.0001	0.01	0.0105853	0.002	0.0000	87.97	0.23	30.52	0.12	5.67E-13	1.11E-13			0.7	PPLLLL
		7.73	8756-01I	5.63	0.02	0.012	0.0001	0.04	0.0133782	0.004	0.0001	78.89	0.49	30.15	0.22	4.74E-13	8.42E-14			1	PPLLP
		8.50	8756-01J	6.593	0.02	0.013	0.0001	0.04	0.0096973	0.007	0.0001	66.74	0.28	29.88	0.20	7.05E-13	1.07E-13			1.5	PPLLL
		9.26	8756-01K	6.853	0.02	0.013	0.0001	0.10	0.0243754	0.008	0.0001	64.42	0.37	29.97	0.24	4.03E-13	5.88E-14			2	PPLPL
		10.05	8756-01L	9.342	0.02	0.015	0.0001	0.15	0.0344459	0.017	0.0002	46.20	0.49	29.31	0.42	4.03E-13	4.32E-14			2.5	PPLPL
		10.81	8756-01M	8.92	0.02	0.014	0.0001	0.07	0.0286978	0.015	0.0002	49.74	0.52	30.12	0.41	3.66E-13	4.10E-14			3.5	PPLLLL
	22/03/2016	14.44	8756-02A	217.6	0.89	0.152	0.0011	0.08	0.0875547	0.741	0.0033	-1.71	0.25	-25.69	11.10	2.93E-12	1.35E-14			0.06	PPLLLL
		15.21	8756-02B	67.7	0.17	0.053	0.0003	0.05	0.0237905	0.215	0.0007	5.08	0.27	23.40	3.24	2.97E-12	4.38E-14			0.12	PPLLLL
		15.96	8756-02C	8.764	0.02	0.014	0.0001	0.05	0.0086487	0.013	0.0001	55.49	0.24	32.99	0.28	1.10E-12	1.26E-13			0.2	PPLLLL
		16.70	8756-02D	5.943	0.01	0.012	0.0001	0.01	0.0055068	0.004	0.00003	81.53	0.18	32.87	0.13	1.28E-12	2.15E-13			0.3	PPLLLL
		17.47	8756-02E	5.483	0.01	0.012	0.0001	0.03	0.0084987	0.003	0.00004	86.00	0.24	31.99	0.13	6.74E-13	1.23E-13			0.35	PPLLLL
		18.25	8756-02F	5.276	0.01	0.012	0.0001	0.03	0.0118617	0.002	0.00004	89.00	0.26	31.86	0.13	4.85E-13	9.19E-14			0.4	PPLLLL
		19.01	8756-02G	5.255	0.01	0.012	0.0001	0.03	0.0117425	0.002	0.00004	87.32	0.26	31.14	0.13	4.68E-13	8.91E-14			0.5	PPLLLL
		19.81	8756-02H	5.631	0.01	0.012	0.0001	0.02	0.0135133	0.004	0.00005	80.65	0.28	30.82	0.15	4.74E-13	8.42E-14			0.7	PPLLLL
		20.58	8756-02I	6.461	0.01	0.013	0.0001	0.03	0.0111615	0.007	0.0001	69.35	0.28	30.42	0.19	6.32E-13	9.78E-14			1	PPLLLL

		21.38	8756-02J	6.609	0.01	0.013	0.0001	0.02	0.0085131	0.007	0.00005	67.82	0.22	30.43	0.18	8.14E-13	1.23E-13			1.5	PPLLLL
		22.17	8756-02K	8.708	0.02	0.014	0.0001	-0.01	0.0150581	0.014	0.0001	51.76	0.37	30.60	0.33	6.59E-13	7.57E-14			2	PPLLLL
		22.92	8756-02L	10.58	0.02	0.015	0.0001	0.00	0.0164288	0.02	0.0002	43.74	0.57	31.39	0.52	6.76E-13	6.39E-14			2.5	PPLLP
		23.67	8756-02M	13.33	0.06	0.017	0.0004	0.38	0.1196735	0.029	0.0004	34.63	0.91	31.33	0.94	1.27E-13	9.54E-15			3.5	PPLLLL
GA1550-Biotite	23/03/2016	3.33	8757-01A	21.53	0.10	0.021	0.0006	-0.05	0.1315293	0.03	0.0006	58.06	0.82	83.61	1.31	1.57E-13	7.31E-15	**0.9983**	**0.0017**	0.2	PPLLLL
		4.19	8757-01B	15.36	0.05	0.015	0.0002	-0.01	0.041218	0.002	0.0001	95.50	0.27	97.70	0.39	3.67E-13	2.39E-14			0.3	PPLLLL
		4.87	8757-01C	15.21	0.04	0.016	0.0002	0.07	0.0591153	0.001	0.0001	97.94	0.28	99.22	0.38	3.17E-13	2.08E-14			0.35	PPLLLL
		5.56	8757-01D	15.19	0.04	0.016	0.0002	-0.05	0.0348239	0.001	0.0001	97.92	0.23	99.07	0.33	4.25E-13	2.80E-14			0.4	PPLLLL
		6.23	8757-01E	15.19	0.04	0.015	0.0002	0.04	0.0296768	8E-04	0.0001	98.44	0.19	99.58	0.33	5.10E-13	3.36E-14			0.45	PPLLLL
		6.89	8757-01F	15.03	0.04	0.016	0.0001	0.01	0.0248673	5E-04	0.0001	98.96	0.16	99.08	0.27	6.47E-13	4.30E-14			0.5	PPLLLL
		7.58	8757-01G	14.98	0.04	0.015	0.0001	-0.02	0.0151644	3E-04	0.00005	99.42	0.13	99.16	0.28	1.13E-12	7.55E-14			0.6	PPLLLL
		8.28	8757-01H	14.96	0.03	0.015	0.0001	0.00	0.0054617	1E-04	0.00002	99.73	0.08	99.37	0.21	2.80E-12	1.87E-13			0.8	PPLLLL
		8.96	8757-01I	15.01	0.04	0.015	0.0001	0.00	0.0097739	2E-04	0.00002	99.68	0.09	99.64	0.24	1.83E-12	1.22E-13			1	PPLLLL
		9.68	8757-01J	15.05	0.04	0.016	0.0001	0.04	0.0145188	4E-04	0.00004	99.15	0.12	99.39	0.27	1.17E-12	7.74E-14			2.5	PPLLLL
	23/03/2016	13.30	8757-02A	28.42	0.12	0.023	0.0005	0.08	0.1233104	0.046	0.0005	52.13	0.46	98.67	1.19	3.23E-13	1.13E-14			0.2	PPLLLL
		14.11	8757-02B	15.5	0.04	0.015	0.0002	0.02	0.0390965	0.002	0.0001	96.87	0.19	99.99	0.33	5.06E-13	3.26E-14			0.3	PPLLLL
		14.80	8757-02C	15.11	0.04	0.016	0.0002	0.05	0.0455595	9E-04	0.0001	98.23	0.22	98.83	0.32	4.73E-13	3.13E-14			0.35	PPLLLL
		15.48	8757-02D	15.18	0.04	0.016	0.0002	0.05	0.0379905	5E-04	0.0001	98.99	0.19	100.02	0.33	5.38E-13	3.55E-14			0.4	PPLLLL
		16.16	8757-02E	15.04	0.05	0.016	0.0002	-0.08	0.0418355	6E-04	0.0001	98.68	0.22	98.83	0.36	5.05E-13	3.36E-14			0.45	PPLLLL
		16.87	8757-02F	15.09	0.04	0.016	0.0002	0.02	0.0377316	6E-04	0.0001	98.83	0.18	99.31	0.29	5.50E-13	3.64E-14			0.5	PPLLLL
		17.55	8757-02G	14.94	0.04	0.016	0.0001	0.02	0.0198886	4E-04	0.00004	99.25	0.13	98.75	0.25	8.95E-13	5.99E-14			0.6	PPLLLL
		18.26	8757-02H	14.95	0.04	0.015	0.0001	-0.01	0.0148225	3E-04	0.00004	99.46	0.12	99.03	0.26	1.42E-12	9.47E-14			0.8	PPLLLL
		18.94	8757-02I	15.03	0.04	0.015	0.0001	0.09	0.0319408	3E-04	0.0001	99.39	0.19	99.48	0.30	6.67E-13	4.44E-14			1	PPLLLL
		19.60	8757-02J	15.16	0.04	0.016	0.0003	0.00	0.0656604	5E-04	0.0001	99.02	0.26	99.94	0.36	3.51E-13	2.31E-14			2.5	PPLLLL

Appendix C: Accuracy and precision data from geochemical analysis

11.1 Major element precision calculations from repeat analysis

Springsure and Bauhinia 1	Row Labels	SiO2	TiO2	Al2O3	Fe2O3	MnO	MgO	CaO	Na2O	K2O	P2O5
	CVLF01	46.73	1.87	14.98	11.96	0.21	8.45	9.02	2.44	1.54	0.47
	CVLF01_D	45.77	1.85	14.80	11.68	0.20	8.34	8.89	2.33	1.54	0.44
	Average	46.25	1.86	14.89	11.82	0.21	8.40	8.96	2.38	1.54	0.46
	stdev	0.68	0.01	0.13	0.19	0.01	0.08	0.10	0.08	0.01	0.02
	%RSD	1.47	0.63	0.88	1.63	3.03	0.99	1.09	3.32	0.39	4.46
	IJS07B	50.39	2.48	15.03	10.31	0.15	5.37	7.70	3.88	1.55	0.65
	IJS07B_D	48.91	2.43	14.93	10.04	0.14	5.25	7.61	3.38	1.59	0.63
	Average	49.65	2.46	14.98	10.18	0.15	5.31	7.65	3.63	1.57	0.64
	stdev	34.60	1.31	10.01	6.14	2.04	3.10	4.68	0.39	0.82	2.69
	%RSD	70.73	53.67	67.04	61.20	1428.04	59.09	61.45	11.69	51.67	429.20
	IJS11®	47.55	3.09	14.91	13.88	0.23	5.03	7.92	3.55	1.67	1.39
	IJS11®_D	45.50	3.00	14.68	13.36	0.22	4.87	7.69	3.31	1.73	1.30
	Average	46.52	3.04	14.79	13.62	0.22	4.95	7.80	3.43	1.70	1.35
	stdev	1.45	0.07	0.16	0.37	0.01	0.12	0.16	0.17	0.04	0.06
	%RSD	25.73	1.70	8.42	7.58	0.12	2.77	4.38	1.85	0.97	0.73
Peak Range	Row Labels	SiO2	TiO2	Al2O3	Fe2O3	MnO	MgO	CaO	Na2O	K2O	P2O5
	IJM_04	72.93	1.61	23.62	0.62	0.00	0.18	0.10	0.14	0.43	0.04
	IJM_04-d	72.91	1.65	24.31	0.63	0.00	0.18	0.11	0.11	0.44	0.03
	Average	72.92	1.63	23.97	0.62	0.00	0.18	0.10	0.13	0.44	0.03
	stdev	0.02	0.03	0.49	0.01	0.00	0.00	0.00	0.02	0.01	0.00
	%RSD	0.02	1.79	2.05	1.74	2.49	1.36	2.32	14.98	1.87	5.43

	IJM_06	87.35	0.75	10.71	0.31	0.00	0.08	0.07	0.18	0.18	<DL
	IJM_06-d	87.67	0.76	10.79	0.31	0.00	0.08	0.07	0.17	0.23	<DL
	Average	87.51	0.75	10.75	0.31	0.00	0.08	0.07	0.18	0.21	<DL
	stdev	0.22	0.01	0.06	0.00	0.00	0.00	0.00	0.01	0.04	
	%RSD	0.26	0.82	0.52	0.88	2.18	2.00	0.28	4.13	18.73	
	IJM_07R	81.45	0.96	16.27	0.27	0.00	0.11	0.06	0.11	0.34	0.03
	IJM_07R-d	81.66	0.96	16.44	0.27	0.00	0.11	0.06	0.17	0.34	0.03
	Average	81.55	0.96	16.36	0.27	0.00	0.11	0.06	0.14	0.34	0.03
	stdev	0.15	0.00	0.12	0.00	0.00	0.00	0.00	0.04	0.00	0.00
	%RSD	0.18	0.05	0.72	0.09	1.61	0.53	0.75	27.51	0.32	4.37
Barrington, Undara and Mount Catherine	sample	SiO2	TiO2	Al2O3	Fe2O3	MnO	MgO	CaO	Na2O	K2O	P2O5
	BRT5	44.89	2.27	15.08	11.54	0.18	8.59	10.40	2.71	1.08	0.73
	BRT5D	44.89	2.29	15.09	11.56	0.17	8.59	10.32	2.68	1.06	0.74
	Average	44.89	2.28	15.08	11.55	0.18	8.59	10.36	2.69	1.07	0.74
	stdev	0.00	0.01	0.01	0.01	0.00	0.00	0.06	0.02	0.02	0.00
	%RSD	0.00	0.43	0.04	0.09	0.96	0.00	0.59	0.71	1.46	0.59
	MC2	50.14	2.39	15.07	12.00	0.15	5.54	7.67	3.02	1.21	0.43
	MC2D	50.56	2.35	14.90	11.79	0.15	5.45	7.77	3.06	1.18	0.44
	Average	50.35	2.37	14.98	11.90	0.15	5.49	7.72	3.04	1.20	0.44
	stdev	0.29	0.03	0.12	0.14	0.00	0.06	0.08	0.02	0.02	0.01
	%RSD	0.58	1.16	0.79	1.21	1.60	1.12	0.99	0.78	1.59	1.94
	UPW4	49.18	1.72	15.54	11.44	0.16	8.91	7.83	3.44	1.64	0.48

	UPW4D	49.42	1.68	15.50	11.20	0.15	8.69	7.83	3.42	1.62	0.49
	Average	49.30	1.70	15.52	11.32	0.15	8.80	7.83	3.43	1.63	0.48
	stdev	0.17	0.03	0.03	0.16	0.00	0.15	0.00	0.02	0.02	0.01
	%RSD	0.34	1.77	0.20	1.46	2.33	1.75	0.00	0.45	1.18	1.32
Mitchell, Monto and Bauhinia	names	SiO2	TiO2	Al2O3	Fe2O3	MnO	MgO	CaO	Na2O	K2O	P2O5
	BHVO-2	50.24	2.61	13.65	11.77	0.16	6.84	10.91	2.41	0.48	0.31
	BHVO-2D	49.33	2.73	13.59	12.25	0.17	7.28	11.38	2.12	0.53	0.32
	Average	49.78	2.67	13.62	12.01	0.17	7.06	11.15	2.27	0.51	0.31
	stdev	0.64	0.09	0.04	0.34	0.01	0.31	0.33	0.20	0.04	0.01
	%RSD	1.29	3.30	0.27	2.87	4.57	4.44	2.94	8.93	6.92	2.73
	name	SiO2	TiO2	Al2O3	Fe2O3	MnO	MgO	CaO	Na2O	K2O	P2O5
	BC21	44.52	2.63	13.06	13.08	0.22	8.93	8.98	4.00	1.95	0.63
	BC-21d	44.87	2.64	12.76	13.27	0.22	8.84	9.12	3.94	1.92	0.63
	Average	44.69	2.64	12.91	13.18	0.22	8.89	9.05	3.97	1.94	0.63
	stdev	0.25	0.01	0.21	0.13	0.00	0.07	0.10	0.04	0.02	0.00
	%RSD	0.55	0.23	1.64	1.01	1.54	0.77	1.08	0.97	1.15	0.77

11.2 Major element accuracy calculations from repeat analysis

Peak Range run													
AGV-2	**Certified value**	**Experimental values**	**Accuracy (%)**		**BCR-2**	**Certified value**	**Experimental values**	**Accuracy (%)**		**JP-1**	**Certified value**	**Experimental values**	**Accuracy (%)**
Al	17	17	101		**SiO2**	13	13	98		**SiO2**	1	1	104
Ca	5	5	101		**TiO2**	7	7	100		**TiO2**	1	1	102
Fe	7	7	101		**Al2O3**	14	14	101		**Al2O3**	8	9	105
K	2	3	117		**Fe2O3**	2	2	94		**Fe2O3**	0	0	
Mg	2	2	95		**MnO**	4	3	97		**MnO**	44	43	97
Mn	0	0	99		**MgO**	0	0	102		**MgO**	0	0	101
Na	4	4	100		**CaO**	3	3	102		**CaO**	0	0	129
P	0	0	104		**Na2O**	0	0	93		**Na2O**	0	<DL	
Si	59	58	98		**K2O**	54	52	97		**K2O**	42	44	103
Ti	1	1	98		**P2O5**	2	2	100		**P2O5**	0	0	
Springsure and Bauhinia 1													
CERTIFIED VALUES													
BHV02	**Certified value**	**Experimental values**	**Accuracy (%)**		**JB2**	**Certified value**	**Experimental values**	**Accuracy (%)**					
SiO2	50	48	96		**SiO2**	53	53	100					
TiO2	3	3	100		**TiO2**	1	1	99					
Al2O3	14	13	98		**Al2O3**	15	15	100					
Fe2O3	12	12	98		**Fe2O3**	14	14	101					
MnO	0	0	103		**MnO**	0	0	122					
MgO	7	7	95		**MgO**	5	5	102					
CaO	11	12	103		**CaO**	10	10	100					
Na2O	2	2	87		**Na2O**	2	1	72					
K2O	1	1	103		**K2O**	0	0	102					
P2O5	0	0	97		**P2O5**	0	0	93					

Total	100	98				101	100	
Barrington, Undara and Mount Catherine								
AGV-2	**Certified value**	**Experimental values**	**Accuracy (%)**					
Al2O3	17	17	99					
CaO	5	5	99					
Fe2O3	7	7	101					
K2O	2	3	111					
MgO	2	2	101					
MnO	0	0	102					
Na2O	4	4	101					
P2O5	0	0	100					
SiO2	59	59	100					
TiO2	1	1	96					
Total	98	98						
Mitchell, Monto and Bauhinia								
AGV-2	**Certified values**	**Experimental values**	**Accuracy (%)**		**BCR-1**	**Certified values**	**Experimental values**	**Accuracy (%)**
Al2O3	17	17	99		Al2O3	13	13	100
CaO	5	5	102		CaO	7	7	96
Fe2O3	7	7	104		Fe2O3	14	13	96
K2O	2	3	118		K2O	2	2	94
MgO	2	2	100		MgO	4	4	101
MnO	0	0	103		MnO	0	0	95
Na2O	4	4	97		Na2O	3	3	97
P2O5	0	1	119		P2O5	0	0	107

SiO2	59	59	100		SiO2	54	54	101
TiO2	1	1	101		TiO2	2	2	96
Total	98	99			Total	100	99	

11.3 Trace element precision calculations from repeat analysis

Springsure and Bauhinia 1																																				
Sample	**Sc**	**V**	**Cr**	**Co**	**Ni**	**Cu**	**Zn**	**Ga**	**Ge**	**Rb**	**Sr**	**Y**	**Zr**	**Nb**	**Sn**	**Cs**	**Ba**	**La**	**Ce**	**Pr**	**Nd**	**Sm**	**Eu**	**Tb**	**Gd**	**Dy**	**Ho**	**Er**	**Tm**	**Yb**	**Lu**	**Hf**	**Ta**	**Tl**	**Pb**	**Th**	**U**
TRLF01	21	196	311	47	190	65	118	20	8	14	393	19	133	20	1.2	0.2	146	11	24	3.0	14	4.0	1.4	0.7	4.5	4.0	0.7	2.0	0.2	1.5	0.2	3.0	1.4	0.0	3.6	1.2	0.4
TRLF01_D	20	196	313	46	186	63	116	20	8	14	401	19	132	21	1.2	0.2	147	11	23	3.0	14	4.0	1.4	0.7	4.6	4.0	0.7	2.0	0.2	1.5	0.2	3.0	1.5	0.0	3.6	1.2	0.4
average	20	196	312	46	188	64	117	20	8	14	397	19	133	21	1.2	0.2	146	11	23	3.0	14	4.0	1.4	0.7	4.6	4.0	0.7	2.0	0.2	1.5	0.2	3.0	1.4	0.0	3.6	1.2	0.4
stdev	0.2	0.2	1.1	0.5	2.3	0.8	1.4	0.2	0.1	0.0	5.7	0.2	0.9	0.6	0.0	0.0	0.2	0.1	1.1	0.0	0.0	0.0	0.0	0.0	0.0	0.0	0.0	0.0	0.0	0.0	0.0	0.0	0.0	0.0	0.0	0.0	0.0
%RSD	**1.1**	**0.1**	**0.4**	**1.0**	**1.2**	**1.2**	**1.2**	**1.2**	**1.8**	**0.3**	**1.4**	**0.8**	**0.7**	**3.0**	**0.4**	**0.7**	**0.2**	**0.5**	**4.6**	**0.0**	**0.1**	**0.3**	**0.3**	**0.1**	**0.2**	**0.0**	**0.3**	**0.1**	**0.2**	**0.3**	**0.2**	**0.1**	**1.4**	**7.0**	**0.1**	**0.4**	**0.3**
IJS11	19	208	82	43	63	56	166	25	10	30	671	40	343	43	2.0	0.3	360	35	79	9.9	46	10.3	3.4	1.3	9.8	7.6	1.3	3.6	0.4	2.8	0.4	6.5	3.0	0.1	9.1	2.9	0.9
IJS11_D	19	209	81	43	63	57	168	25	10	30	721	40	343	44	2.0	0.3	362	35	79	9.9	45	10.3	3.4	1.3	9.8	7.6	1.3	3.6	0.4	2.8	0.4	6.5	3.0	0.1	9.1	2.9	0.9
average	19	209	82	43	63	57	167	25	10	30	696	40	343	44	2.0	0.3	361	35	79	9.9	45	10.3	3.4	1.3	9.8	7.6	1.3	3.6	0.4	2.8	0.4	6.5	3.0	0.1	9.1	2.9	0.9
stdev	0.1	0.5	1.1	0.1	0.3	0.3	1.0	0.0	0.1	0.1	35.9	0.1	0.1	0.6	0.0	0.0	1.4	0.0	0.1	0.0	0.0	0.0	0.0	0.0	0.0	0.0	0.0	0.0	0.0	0.0	0.0	0.0	0.0	0.0	0.0	0.0	0.0
%RSD	**0.5**	**0.2**	**1.3**	**0.2**	**0.4**	**0.6**	**0.6**	**0.1**	**0.8**	**0.3**	**5.2**	**0.2**	**0.0**	**1.4**	**0.3**	**0.1**	**0.4**	**0.1**	**0.2**	**0.0**	**0.1**	**0.2**	**0.3**	**0.2**	**0.3**	**0.3**	**0.0**	**0.4**	**0.2**	**0.2**	**0.6**	**0.2**	**0.3**	**1.3**	**0.3**	**0.0**	**0.1**
CIS	17	205	138	39	87	40	159	23	8	28	889	26	322	52	2.1	0.3	360	34	74	8.7	38	8.3	2.6	1.0	7.4	5.5	0.9	2.4	0.3	1.7	0.2	6.5	3.5	0.1	8.2	3.6	1.0
CIS_D	17	203	137	39	87	40	159	23	8	28	915	26	321	52	2.1	0.3	345	34	73	8.7	38	8.3	2.6	1.0	7.5	5.5	0.9	2.4	0.3	1.7	0.2	6.5	3.5	0.1	8.2	3.6	1.0
average	17	204	138	39	87	40	159	23	8	28	902	26	322	52	2.1	0.3	352	34	74	8.7	38	8.3	2.6	1.0	7.5	5.5	0.9	2.4	0.3	1.7	0.2	6.5	3.5	0.1	8.2	3.6	1.0
stdev	0.1	1.0	1.1	0.2	0.3	0.3	0.0	0.0	0.2	0.1	18.7	0.0	0.4	0.4	0.0	0.0	10.8	0.0	0.1	0.0	0.0	0.0	0.0	0.0	0.0	0.0	0.0	0.0	0.0	0.0	0.0	0.0	0.0	0.0	0.0	0.0	0.0
%RSD	**0.4**	**0.5**	**0.8**	**0.6**	**0.4**	**0.8**	**0.0**	**0.1**	**1.8**	**0.4**	**2.1**	**0.1**	**0.1**	**0.7**	**0.0**	**0.2**	**3.1**	**0.1**	**0.1**	**0.1**	**0.0**	**0.1**	**0.0**	**0.3**	**0.2**	**0.3**	**0.0**	**0.2**	**0.7**	**0.3**	**0.3**	**0.3**	**0.1**	**0.5**	**0.2**	**0.1**	**0.1**
Peak Range																																					
Sample	**Sc**	**V**	**Cr**	**Co**	**Ni**	**Cu**	**Zn**	**Ga**	**Ge**	**Rb**	**Sr**	**Y**	**Zr**	**Nb**	**Sn**	**Cs**	**Ba**	**La**	**Ce**	**Pr**	**Nd**	**Sm**	**Eu**	**Tb**	**Gd**	**Dy**	**Ho**	**Er**	**Tm**	**Yb**	**Lu**	**Hf**	**Ta**	**Tl**	**Pb**	**Th**	**U**

AGV-2	15	110	14	14	20	45	109	20	2	59	636	17	227	11	1.5	1.1	1094	36	62	7.7	28	5.4	1.5	4.7	0.6	3.3	0.6	1.8	0.2	1.6	0.3	5.4	1.0	0.3	11.4	5.8	1.8
AGV-2D	14	109	14	14	20	45	108	20	2	59	628	17	225	11	1.4	1.0	1080	36	62	7.5	28	5.3	1.4	4.6	0.6	3.3	0.6	1.8	0.2	1.6	0.2	5.4	1.0	0.3	11.5	5.8	1.8
average	14	110	14	14	20	45	108	20	2	59	632	17	226	11	1.4	1.1	1087	36	62	7.6	28	5.3	1.5	4.6	0.6	3.3	0.6	1.8	0.2	1.6	0.2	5.4	1.0	0.3	11.4	5.8	1.8
stdev	0.6	0.8	0.1	0.1	0.1	0.2	0.9	0.4	0.1	0.6	5.5	0.1	1.1	0.0	0.0	0.0	10	0	0	0.1	0	0.1	0.0	0.0	0.0	0.0	0.0	0.0	0.0	0.0	0.0	0.0	0.0	0.0	0.0	0.0	0.0
%RSD	**3.9**	**0.7**	**0.6**	**0.4**	**0.5**	**0.4**	**0.8**	**1.9**	**4.9**	**0.9**	**0.9**	**0.5**	**0.5**	**0.4**	**1.5**	**2.3**	**1**	**0**	**0**	**1.2**	**0**	**1.5**	**1.9**	**0.6**	**0.6**	**0.0**	**0.8**	**0.1**	**0.4**	**0.2**	**1.0**	**0.5**	**0.4**	**0.9**	**0.2**	**0.1**	**0.0**
BHVO-2	33	308	289	41	117	119	97	20	4	8	384	23	169	0.1	0.1	0.1	127	14	34	4.9	23	5.8	2.0	6.2	0.9	5.1	0.9	2.5	0.3	1.9	0.3	4.6	16.2	0.0	1.7	1.1	0.4
BHVO-2D	33	306	287	41	115	118	96	21	4	8	392	23	166	0.1	0.1	0.1	128	15	34	5.0	23	5.9	2.0	5.8	0.9	5.1	0.9	2.5	0.3	2.0	0.3	4.6	19.9	0.0	1.7	1.1	0.4
average	33	307	288	41	116	119	96	20	4	8	388	23	168	0.1	0.1	0.1	127	15	34	5.0	23	5.8	2.0	6.0	0.9	5.1	0.9	2.5	0.3	2.0	0.3	4.6	18.1	0.0	1.7	1.1	0.4
stdev	0.2	1.2	1.5	0.6	0.9	0.8	0.5	0.6	0.0	0.1	5.3	0.3	1.9	0.0	0.0	0.0	1	0	0	0.1	0	0.0	0.0	0.3	0.0	0.0	0.0	0.0	0.0	0.0	0.0	0.0	2.6	0.0	0.0	0.0	0.0
%RSD	**0.7**	**0.4**	**0.5**	**1.5**	**0.8**	**0.7**	**0.5**	**2.9**	**1.3**	**1.2**	**1.4**	**1.2**	**1.1**	**1.3**	**1.8**	**2.5**	**1**	**0**	**1**	**1.5**	**1**	**0.5**	**0.2**	**4.6**	**0.1**	**0.8**	**0.2**	**0.5**	**0.2**	**1.2**	**1.2**	**0.1**	**14.6**	**5.4**	**0.1**	**0.1**	**1.0**
PRO-9b	19	132	152	36	209	85	100	14	1	13	695	14	99	16	1.1	0.6	203	11	22	2.8	12	3.0	1.1	3.4	0.5	3.0	0.6	1.6	0.2	1.4	0.2	2.4	2.3	0.0	1.8	1.6	0.4
PRO-9b-d	19	132	152	36	209	85	101	14	1	13	697	14	99	16	1.2	0.6	205	11	22	2.8	12	3.0	1.1	3.4	0.5	3.0	0.6	1.6	0.2	1.3	0.2	2.5	2.3	0.0	1.8	1.6	0.4
average	19	132	152	36	209	85	101	14	1	13	696	14	99	16	1.2	0.6	204	11	22	2.8	12	3.0	1.1	3.4	0.5	3.0	0.6	1.6	0.2	1.3	0.2	2.5	2.3	0.0	1.8	1.6	0.4
stdev	0.3	0.5	0.0	0.0	0.3	0.1	0.5	0.0	0.0	0.0	1.6	0.0	0.3	0.1	0.0	0.0	1.6	0.0	0.0	0.0	0.1	0.0	0.0	0.0	0.0	0.0	0.0	0.0	0.0	0.0	0.0	0.0	0.0	0.0	0.0	0.0	0.0
%RSD	**1.5**	**0.4**	**0.0**	**0.0**	**0.2**	**0.1**	**0.5**	**0.0**	**0.4**	**0.2**	**0.2**	**0.3**	**0.3**	**0.4**	**0.7**	**0.3**	**0.8**	**0.4**	**0.2**	**0.3**	**0.6**	**0.6**	**0.2**	**0.1**	**0.7**	**0.3**	**0.8**	**0.3**	**0.7**	**0.8**	**0.0**	**1.6**	**0.8**	**4.6**	**1.1**	**0.3**	**2.0**
Mitchell, Monto and Bauhinia																																					
Sample	**Sc**	**V**	**Cr**	**Co**	**Ni**	**Cu**	**Zn**	**Ga**	**Ge**	**Rb**	**Sr**	**Y**	**Zr**	**Nb**	**Sn**	**Cs**	**Ba**	**La**	**Ce**	**Pr**	**Nd**	**Sm**	**Eu**	**Tb**	**Gd**	**Dy**	**Ho**	**Er**	**Tm**	**Yb**	**Lu**	**Hf**	**Ta**	**Tl**	**Pb**	**Th**	**U**
195R	1	20	149	3	10	5	16	6	1	82	24	13	43	5	1.3	1.4	225	10	21	2.5	9	2.0	0.4	2.0	0.3	2.1	0.5	1.4	0.2	1.3	0.2	1.6	0.7	0.5	12.4	7.1	1.7
195Rd	1	20	150	3	10	5	16	6	1	81	24	12	43	5	1.3	1.4	227	10	21	2.5	9	2.1	0.4	2.0	0.3	2.1	0.5	1.4	0.2	1.3	0.2	1.6	0.7	0.5	12.4	7.1	1.7
average	1	20	150	3	10	5	16	6	1	81	24	12	43	5	1.3	1.4	226	10	21	2.5	9	2.1	0.4	2.0	0.3	2.1	0.5	1.4	0.2	1.3	0.2	1.6	0.7	0.5	12.4	7.1	1.7
stdev	0.0	0.2	1.1	0.0	0.1	0.0	0.1	0.1	0.1	0.7	0.1	0.1	0.3	0.0	0.0	0.0	1.6	0.0	0.0	0.0	0.0	0.0	0.0	0.0	0.0	0.0	0.0	0.0	0.0	0.0	0.0	0.0	0.0	0.0	0.1	0.0	0.0
%RSD	**0.2**	**1.1**	**0.7**	**0.2**	**0.7**	**0.7**	**0.6**	**1.7**	**10.2**	**0.8**	**0.5**	**0.9**	**0.6**	**0.3**	**0.2**	**0.1**	**0.7**	**0.1**	**0.2**	**0.9**	**0.3**	**0.9**	**0.5**	**1.2**	**1.0**	**0.3**	**1.0**	**0.2**	**0.7**	**0.3**	**1.2**	**0.2**	**0.2**	**0.3**	**0.4**	**0.7**	**0.6**
BCR 2-5	2	413	15	35	12	17	124	21	2	20	325	30	170	11	1.7	0.3	616	22	43	5.9	24	5.7	1.7	6.0	0.9	5.5	1.2	3.3	0.5	2.9	0.5	4.7	1.2	0.3	7.9	4.6	1.6
BCR 2-5_d	2	413	15	35	12	17	126	21	2	20	324	30	170	12	1.8	0.3	625	22	44	5.9	24	5.8	1.7	6.2	1.0	5.5	1.2	3.4	0.5	2.9	0.4	4.9	1.2	0.3	8.1	4.8	1.7
average	2	413	15	35	12	17	125	21	2	20	324	30	170	12	1.7	0.3	620	22	43	5.9	24	5.7	1.7	6.1	1.0	5.5	1.2	3.4	0.5	2.9	0.4	4.8	1.2	0.3	8.0	4.7	1.7
stdev	0.1	0.2	0.1	0.0	0.0	0.0	0.9	0.1	0.1	0.0	1.0	0.1	0.1	0.0	0.0	0.0	6.5	0.1	0.7	0.0	0.0	0.0	0.0	0.1	0.0	0.0	0.0	0.0	0.0	0.0	0.0	0.1	0.0	0.0	0.2	0.1	0.0

%RSD	**3.6**	**0.0**	**0.4**	**0.1**	**0.1**	**0.2**	**0.7**	**0.3**	**3.5**	**0.0**	**0.3**	**0.2**	**0.1**	**0.2**	**0.6**	**1.2**	**1.0**	**0.6**	**1.6**	**0.0**	**0.1**	**0.4**	**0.4**	**1.8**	**1.4**	**0.7**	**0.1**	**1.2**	**1.1**	**0.7**	**0.5**	**2.1**	**1.2**	**1.9**	**1.9**	**2.9**	**1.4**
BHVO-2	1	317	293	43	113	127	100	21	3	9	386	23	169	18	1.8	0.1	129	15	35	4.9	22	5.6	2.0	6.0	0.9	4.9	1.0	2.5	0.3	1.9	0.3	4.5	1.8	0.0	1.5	1.3	0.4
BHVO-2_d	1	320	295	43	116	128	101	21	3	10	389	24	169	18	1.9	0.2	133	15	35	5.0	22	5.7	2.0	6.1	0.9	4.9	1.0	2.6	0.3	1.9	0.3	4.5	1.8	0.0	1.7	1.4	0.5
average	1	319	294	43	114	128	100	21	3	9	387	24	169	18	1.8	0.1	131	15	35	4.9	22	5.7	2.0	6.1	0.9	4.9	1.0	2.6	0.3	1.9	0.3	4.5	1.8	0.0	1.6	1.4	0.5
stdev	0.1	1.9	1.5	0.1	1.7	0.9	0.5	0.3	0.1	1.0	2.4	0.4	0.2	0.2	0.0	0.0	2.3	0.1	0.1	0.1	0.2	0.1	0.0	0.1	0.0	0.0	0.0	0.1	0.0	0.0	0.0	0.0	0.0	0.0	0.2	0.1	0.0
%RSD	**7.8**	**0.6**	**0.5**	**0.2**	**1.5**	**0.7**	**0.5**	**1.3**	**3.7**	**11.0**	**0.6**	**1.6**	**0.1**	**1.2**	**2.3**	**35.0**	**1.8**	**0.8**	**0.3**	**1.4**	**0.9**	**1.6**	**0.4**	**0.9**	**0.4**	**0.1**	**0.3**	**2.5**	**0.9**	**0.2**	**0.4**	**0.2**	**1.4**	**22.8**	**10.5**	**7.2**	**5.1**
Barrington, Undara and Mount Catherine																																					
Sample	**Sc**	**V**	**Cr**	**Co**	**Ni**	**Cu**	**Zn**	**Ga**	**Ge**	**Rb**	**Sr**	**Y**	**Zr**	**Nb**	**Sn**	**Cs**	**Ba**	**La**	**Ce**	**Pr**	**Nd**	**Sm**	**Eu**	**Tb**	**Gd**	**Dy**	**Ho**	**Er**	**Tm**	**Yb**	**Lu**	**Hf**	**Ta**	**Tl**	**Pb**	**Th**	**U**
UBA3	100	167	256	45	176	48	102	19	3	30	657	27	203	41	1.5		377	32	55	7.4	24	6.5	2.1	5.2	0.9	5.0	0.9	2.5	0.3	2.1	0.3	3.8	2.9	0.1	3.4	4.7	1.2
UBA3D	107	174	242	47	181	50	105	21	3	32	693	28	212	43	1.5		391	33	57	7.6	24	6.7	2.2	5.4	0.9	5.1	1.0	2.6	0.4	2.1	0.3	3.9	2.9	0.1	3.5	4.7	1.2
average	103	171	249	46	179	49	104	20	3	31	675	28	208	42	1.5		384	32	56	7.5	24	6.6	2.2	5.3	0.9	5.1	1.0	2.6	0.4	2.1	0.3	3.9	2.9	0.1	3.4	4.7	1.2
stdev	5.0	5.1	10.3	1.2	4.1	0.9	2.4	0.8	0.1	1.2	25.6	0.9	5.7	0.9	0.0		9.6	0.8	1.2	0.2	0.4	0.1	0.0	0.1	0.0	0.1	0.0	0.0	0.0	0.0	0.0	0.1	0.0	0.0	0.0	0.0	0.0
%RSD	**4.9**	**3.0**	**4.1**	**2.5**	**2.3**	**1.9**	**2.3**	**4.0**	**3.4**	**4.0**	**3.8**	**3.3**	**2.8**	**2.2**	**2.9**		**2.5**	**2.3**	**2.1**	**2.2**	**1.8**	**1.4**	**1.6**	**2.1**	**1.1**	**1.3**	**1.9**	**1.3**	**2.2**	**1.4**	**4.2**	**1.4**	**1.2**	**2.4**	**0.5**	**0.3**	**0.6**
MC1	66	176	270	38	155	26	129	21	2	19	602	30	258	30	2.0		360	27	54	8.2	28	8.3	2.8	6.5	1.1	6.0	1.1	2.8	0.4	2.0	0.3	5.0	2.2	0.0	2.3	2.6	0.8
MC1D	60	163	243	34	140	24	118	19	2	18	564	28	238	28	1.8		343	25	50	7.7	26	7.8	2.6	6.0	1.0	5.6	1.0	2.6	0.3	1.9	0.3	4.7	2.2	0.0	2.2	2.4	0.8
average	63	169	256	36	148	25	124	20	2	18	583	29	248	29	1.9		352	26	52	8.0	27	8.1	2.7	6.3	1.1	5.8	1.0	2.7	0.3	2.0	0.3	4.8	2.2	0.0	2.3	2.5	0.8
stdev	4.3	9.7	18.8	2.2	10.2	1.8	7.9	1.4	0.1	0.8	27.5	1.8	13.8	0.9	0.1		12.2	1.3	2.7	0.4	1.4	0.4	0.1	0.4	0.1	0.3	0.0	0.2	0.0	0.1	0.0	0.2	0.1	0.0	0.0	0.1	0.0
%RSD	**6.7**	**5.7**	**7.4**	**6.2**	**6.9**	**7.3**	**6.4**	**6.9**	**3.9**	**4.5**	**4.7**	**6.1**	**5.6**	**3.0**	**4.6**		**3.5**	**4.9**	**5.2**	**5.0**	**5.2**	**4.6**	**4.6**	**5.6**	**7.2**	**5.1**	**3.9**	**6.4**	**3.5**	**4.2**	**3.8**	**4.5**	**2.7**	**9.4**	**1.9**	**4.3**	**5.1**

11.4 Trace element accuracy calculations from repeat analysis

Springsure and Bauhinia 1							
AGV-2				**BCR-2**			
Element	**Certified analysis**	**Experimental results**	**Accuracy (%)**	**Element**	**Certified analysis**	**Experimental results**	**Accuracy (%)**
Ba	1140	1161	102	**Ba**	681	672	99
Be	2		0	**Ce**	53	47	89
Ce	68	66	97	**Co**	36	34	95
Co	16	15	93	**Cr**	20	16	77
Cr	17	19	112	**Cs**	1	1	87

Cu	53	52	97	**Cu**	19	23	123
Dy	4	3	92	**Dy**	6	6	91
Gd	20	4	22	**Er**	4	3	93
La	38	36	95	**Eu**	2	2	87
Nb	15	15	98	**Ga**	22	22	98
Nd	30	29	98	**Gd**	7	6	91
Ni	19	17	90	**Hf**	5	5	96
Pb	13	12	94	**Ho**	1	1	85
Pb	13	13	103	**La**	25	22	88
Pb	13	13	99	**Lu**	1	0	86
Pr	8	7	89	**Nb**	13	13	104
Rb	69	66	96	**Nd**	29	26	91
Sc	13	11	82	**Ni**	12	11	89
Sr	658	772	117	**Pb**	11	10	89
Th	6	5	90	**Pb**	11	11	98
U	2	2	89	**Pb**	11	10	95
V	120	133	110	**Pr**	7	6	84
Y	20	18	90	**Rb**	47	43	92
Yb	2	2	98	**Sc**	34	26	76
Zn	86	85	99	**Sm**	7	6	92
Zr	230	254	110	**Sn**	2	2	93
				Sr	338	366	108
				Ta	1	1	116
				Tb	1	1	85
				Th	6	4	75
				Tl	0	0	114
				Tm	1	0	81
				U	2	1	87
				V	424	465	110
				Y	36	31	88
				Yb	3	3	91
				Zn	134	125	93
				Zr	185	204	110

Peak Range				**BCR-2**							
W-2				**Element**	**Certified analysis**	**Experimental results**	**Accuracy (%)**	**JP-1**			
Element	**Certified analysis**	**Experimental results**	**Accuracy (%)**	**7Be**	2077	1808	87	**Element**	**Certified analysis**	**Experimental results**	**Accuracy (%)**
Sc	36000	36708	102	**45Sc**	34661	34798	100	**45Sc**	7240	7144	99
V	260000	257174	99	**51V**	416000	398072	96	**51V**	27600	23661	86
Cr	92000	79557	86	**52Cr**	18000	13218	73	**52Cr**	2807000	2521779	90
Co	43000	40505	94	**59Co**	37000	34153	92	**59Co**	116000	104295	90
Ni	70000	63240	90	**60Ni**	11000	15499	141	**60Ni**	2460000	2043788	83
Cu	110000	97828	89	**63Cu**	19000	16516	87	**63Cu**	6720	4436	66
Zn	77000	78254	102	**66Zn**	127000	121064	95	**66Zn**	41800	46771	112

Ga	17000	15855	93	**71Ga**	22178	21076	95	**71Ga**	700	430	61
As	1200	1422	118	**72Ge**	1312	2264	173	**72Ge**	490	793	162
Rb	21000	17940	85	**75As**	913	1670	183	**85Rb**	800	354	44
Sr	190000	192323	101	**85Rb**	48000	41672	87	**86Sr**	3320	748	23
Y	23000	19021	83	**86Sr**	346000	332222	96	**89Y**	1540	108	7
Zr	100000	90098	90	**89Y**	35637	31028	87	**90Zr**	5920	5231	88
Nb	7900	7151	91	**90Zr**	188000	185125	98	**93Nb**	1480	48	3
Cd	77	103	133	**93Nb**	12674	11721	92	**111Cd**	11	22	202
Sb	790	8855	1121	**111Cd**	230	228	99	**118Sn**	50	239	478
Cs	990	821	83	**118Sn**	2269	2146	95	**121Sb**	34	39905	117366
Ba	172000	164032	95	**121Sb**	310	8667	2799	**133Cs**	150	39	26
La	10000	10096	101	**133Cs**	1110	1068	96	**135Ba**	19500	9614	49
Ce	23000	20892	91	**135Ba**	683000	656981	96	**La_139**	84	37	44
Nd	13000	12222	94	**140Ce**	53363	47729	89	**140Ce**	190	94	49
Sm	3300	3226	98	**Lu_175**	510	497	97	**Pr_141**	20	10	51
Eu	1000	1076	108	**178Hf**	4939	5202	105	**Nd_143**	72	39	54
Tb	630	3808	604	**181Ta**	802	1883	235	**Sm_149**	19	10	51
Dy	3600	3765	105	**184W**	508	549	108	**Eu_153**	4	4	105
Ho	760	759	100	**205Tl**	260	20093	7731	**Gd_160**	15	11	73
Er	2500	2257	90	**205Tl**	260	263	101	**Tb_159**	3	4	137
Tm	380	313	82	**206Pb**	11000	9988	91	**Dy_161**	22	19	84
Yb	2100	2057	98	**207Pb**	11000	9988	91	**Ho_165**	18	6	33
Lu	330	304	92		11000	9988	91	**Er_167**	16	42	265
Hf	2600	2593	100	**232Th**	5687	5641	99	**Tm_169**	35	5	14
Ta	500	1102	220	**238U**	1689	1586	94	**Yb_172**	22	21	96
W	300	372	124					**Lu_175**	4	7	168
Pb	9300	6875	74					**178Hf**	200	118	59
Pb	9300	7649	82					**181Ta**	20	16	80
Pb	9300	7361	79					**184W**	850	977	115
Th	2400	2056	86					**205Tl**	3	17092	569717
U	530	471	89					**205Tl**	3	4	129
								206Pb	120	139	116
								207Pb	120	170	142
								209Bi		10	
								232Th	190	17	9
								238U	36	24	68
Mitchell, Monto and Bauhinia											
BHV02				**BIR**							
Element	**Certified analysis**	**Experimental results**	**Accuracy (%)**	**Element**	**Certified analysis**	**Experimental results**	**Accuracy (%)**	**W-2**			
7Li	5	7	138	**7Li**	3	6	189	**Element**	**Certified analysis**	**Experimental results**	**Accuracy (%)**
45Sc	32	34	105	**9Be**	0	0	167	**45Sc**	36	37	104

51V	317	320	101	**45Sc**	43	43	100	**51V**	268	273	102
52Cr	280	295	105	**51V**	319	318	100	**52Cr**	93	93	100
59Co	45	43	95	**52Cr**	391	383	98	**59Co**	45	43	95
60Ni	119	116	97	**59Co**	52	49	94	**60Ni**	72	70	97
63Cu	127	128	101	**60Ni**	166	162	97	**65Cu**	105	107	102
66Zn	103	75	73	**65Cu**	119	119	100	**66Zn**	77	78	102
71Ga	22	21	97	**66Zn**	72	52	73	**71Ga**	18	17	94
85Rb	10	10	102	**71Ga**	15	14	89	**72Ge**	2	3	171
86Sr	389	389	100	**85Rb**	0	0	132	**85Rb**	21	19	92
89Y	26	24	92	**86Sr**	109	105	96	**86Sr**	196	199	102
90Zr	172	169	98	**89Y**	16	14	90	**89Y**	22	20	91
93Nb	18	18	100	**90Zr**	14	14	102	**90Zr**	92	88	96
137Ba	130	133	102	**93Nb**	1	1	90	**93Nb**	8	7	91
139La	15	15	100	**111Cd**	0	0	105	**111Cd**	0	0	322
140Ce	38	35	93	**120Sn**	1	1	156	**120Sn**	2	2	102
143Nd	25	22	89	**121Sb**	0	1	135	**121Sb**	1	1	118
147Sm	6	6	93	**133Cs**	0	0	210	**133Cs**	1	1	83
160Gd	6	6	97	**137Ba**	7	7	93	**137Ba**	172	170	99
159Tb	1	1	103	**139La**	1	1	96	**139La**	11	10	94
165Ho	1	1	96	**140Ce**	2	2	92	**140Ce**	23	21	92
172Yb	2	2	94	**141Pr**	0	0	91	**141Pr**	3	3	93
175Lu	0	0	99	**146Nd**	2	2	88	**146Nd**	13	12	90
178Hf	4	4	109	**147Sm**	1	1	94	**147Sm**	3	3	93
181Ta	1	2	132	**153Eu**	1	0	93	**153Eu**	1	1	97
232Th	1	1	119	**159Tb**	0	2	499	**159Tb**	1	4	599
				160Gd	2	0	19	**160Gd**	4	1	16
				161Dy	3	2	96	**161Dy**	4	4	95
				165Ho	1	1	102	**165Ho**	1	1	101
				167Er	2	2	103	**167Er**	3	2	90
				169Tm	0	0	102	**169Tm**	0	0	101
				172Yb	2	2	97	**172Yb**	2	2	94
				175Lu	0	0	98	**175Lu**	0	0	94
				178Hf	1	1	96	**178Hf**	3	3	97
				181Ta	0	0	235	**181Ta**	1	1	158
				184W	0	0	46	**184W**	0	0	106
				205Tl	0	0	96	**205Tl**	0	0	75
				206Pb	3	3	87	**206Pb**	8	7	91
				207Pb	3	3	94	**207Pb**	8	8	101
				208Pb	3	3	94	**208Pb**	8	8	99
				232Th	0	0	108	**232Th**	2	2	95
				238U	0	0	253	**238U**	1	1	102
								209Bi	0	0	135
								232Th	2	2	95
								238U	1	1	102
Barrington, Undara and Mount Catherine											

W-2a			**Accuracy (%)**	**BCR-2**			
Element	**Certified analysis**	**Experimental results**	96	**Element**	**Certified analysis**	**Experimental results**	**Accuracy (%)**
7Li	9	9	99	**7Li**	9	8	82
8B	12	12	133	**9Be**	2	1	34
9Be	36	48	102	**45Sc**	35	113	327
45Sc	6354	6477	104	**47Ti**	13500	10358	77
51V	268	279	107	**51V**	416	325	78
52Cr	93	100	98	**52Cr**	18	13	70
59Co	45	44	100	**59Co**	37	28	76
60Ni	72	72	102	**60Ni**	11	11	96
65Cu	105	107	102	**65Cu**	19	14	71
66Zn	77	78	95	**66Zn**	127	104	82
71Ga	17	16	123	**71Ga**	22	16	74
75As	1	1	106	**72Ge**	1	2	123
85Rb	21	22	101	**75As**	1	1	147
86Sr	196	197	101	**85Rb**	48	47	98
89Y	23	23	104	**86Sr**	346	265	77
90Zr	100	104	84	**89Y**	36	36	100
93Nb	8	7	101	**90Zr**	188	168	89
96Mo	0	0	148	**93Nb**	13	10	77
111Cd	0	0	163	**96Mo**	252	173	69
114Cd	0	0	92	**120Sn**	2	2	75
121Sb	1	1	124	**137Ba**	683	676	99
137Ba	172	214	118	**139La**	25	24	95
139La	10	12	105	**140Ce**	53	46	86
140Ce	23	24	95	**141Pr**	7	7	97
146Nd	13	12	96	**146Nd**	29	22	77
147Sm	3	3	107	**147Sm**	7	6	97
153Eu	1	1	116	**153Eu**	2	2	95
159Tb	1	1	102	**160Gd**	7	5	78
161Dy	4	4	121	**159Tb**	1	1	97
165Ho	1	1	87	**161Dy**	6	6	94
167Er	3	2	104	**165Ho**	1	1	96
169Tm	0	0	117	**167Er**	4	4	99
172Yb	2	2	113	**169Tm**	1	1	101
175Lu	0	0	94	**172Yb**	3	3	97
178Hf	3	2	119	**175Lu**	1	0	98
181Ta	1	1	105	**178Hf**	5	4	76
206Pb	8	8	101	**181Ta**	1	1	95
207Pb	8	8	103	**184W**	1	1	105
208Pb	8	8	122	**205Tl**	0	0	104
232Th	2	3	123	**206Pb**	11	8	77

238U	1	1		**207Pb**	11	8	73
				208Pb	11	8	75
				232Th	6	6	101
				238U	2	2	99

11.5 Isotope element precision calculations from repeat analysis

Springsure and Bauhinia 1			
	Average	Stdev	RSD%
Pb			
207/206	0.914607	4.53E-05	0.004954
208/206	2.167023	0.000152	0.007011
Nd	0.511967	6.01E-06	0.001173
Sr	0.710246	1.24E-05	0.001744
Hf	0.282144	1.37E-05	0.004865
Peak Range			
	Average	Stdev	RSD%
Pb			
207/206	0.914607	4.53E-05	0.004954
208/206	2.167023	0.000152	0.007011
Nd	0.511967	6.01E-06	0.001173
Sr	0.710246	1.24E-05	0.001744
Hf	0.282144	1.37E-05	0.004865
Mitchell, Monto and Bauhinia			
	Average	Stdev	RSD%
Pb			
207/206	0.914603	3.23E-05	0.003536
208/206	2.16764	0.000145	0.006672
Nd	0.511966	2.04E-06	0.000399
Hf	0.282145	5.83E-06	0.002067
Barrington, Undara and Mount Catherine			
	Average	Stdev	RSD%

Pb			
207/206	0.914617	1.16E-05	0.001271
208/206	2.16822	3.94E-05	0.001817
Nd	0.511965	3.67E-06	0.000717
Sr	0.710249	1.47E-05	0.002064

11.6 Isotope element accuracy calculations from repeat analysis

Springsure and Bauhinia 1			
	Certified	Experimental	Accuracy
Pb			
207/206	0.91640	0.91461	99.80
208/206	2.16810	2.16702	99.95
Nd	-	0.51197	
Sr	0.71034	0.71025	99.99
Hf	-	0.28214	
Peak Range			
	Certified	Experimental	Accuracy
Pb			
207/206	0.91640	0.91461	99.80
208/206	2.16810	2.16702	99.95
Nd	-	0.51197	
Sr	0.71034	0.71025	99.99
Hf	-	0.28214	
Mitchell, Monto and Bauhinia			
	Certified	Experimental	Accuracy
Pb			
207/206	0.91640	0.91460	99.80

208/206	2.16810	2.16764	99.98
Nd	-	0.51197	
Sr	0.71034	0.71025	99.99
Hf	-	0.28215	

Appendix D – Paleomagnetic Zerdfeld results

12.1 Barrington

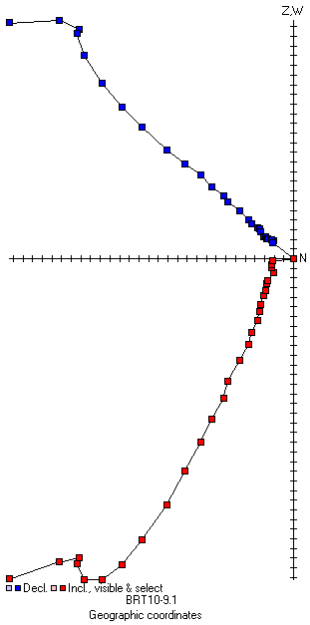

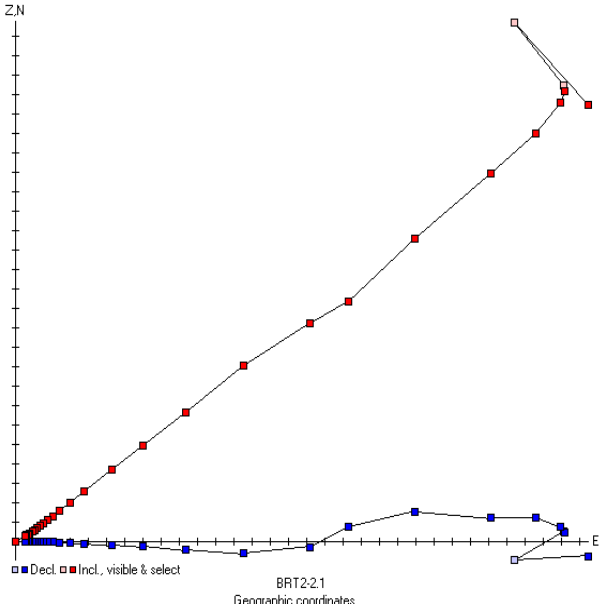

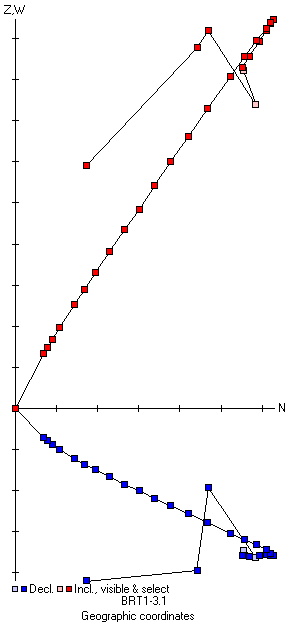

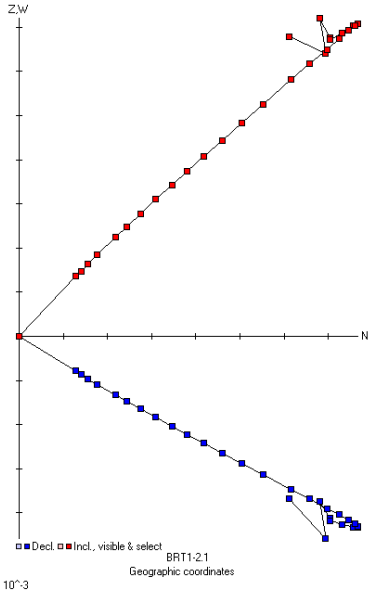

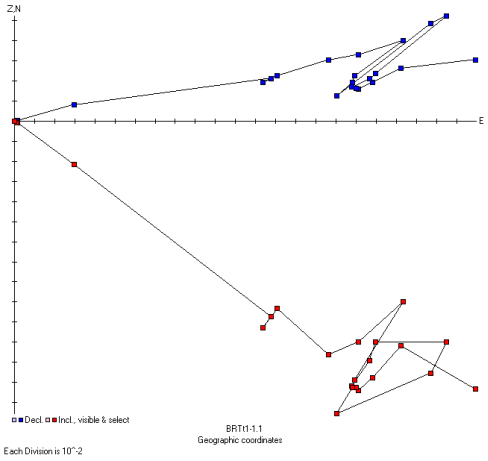

BRT1-1.1
Geographic coordinates

Each Division is 10^-2

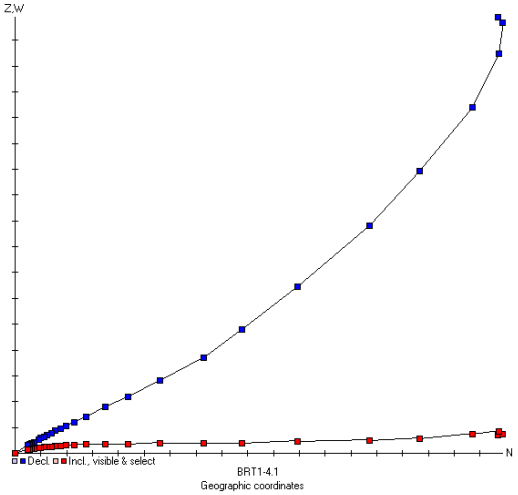

BRT1-4.1
Geographic coordinates

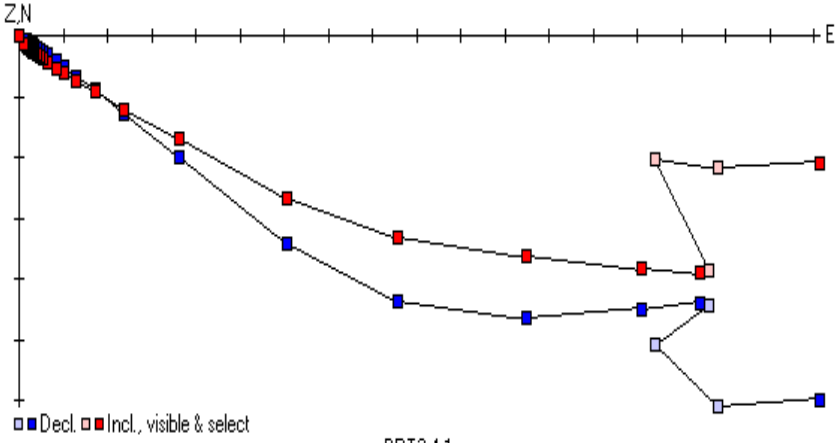

BRT2-4.1
Geographic coordinates

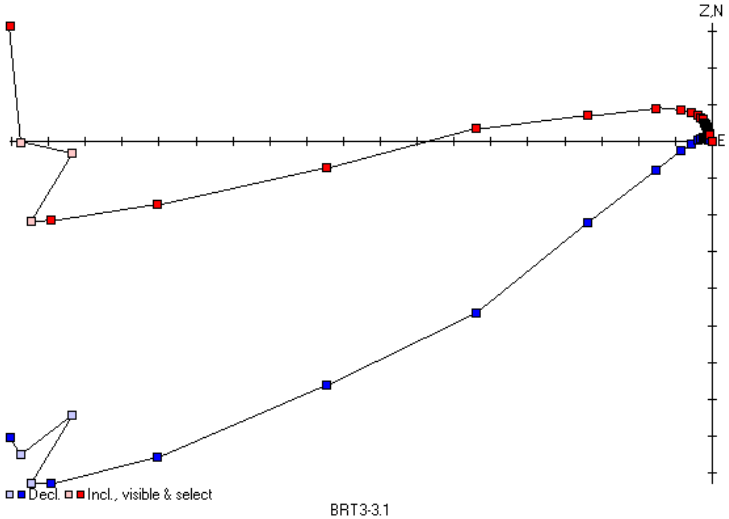

BRT3-3.1
Geographic coordinates

Each Division is 10^-2

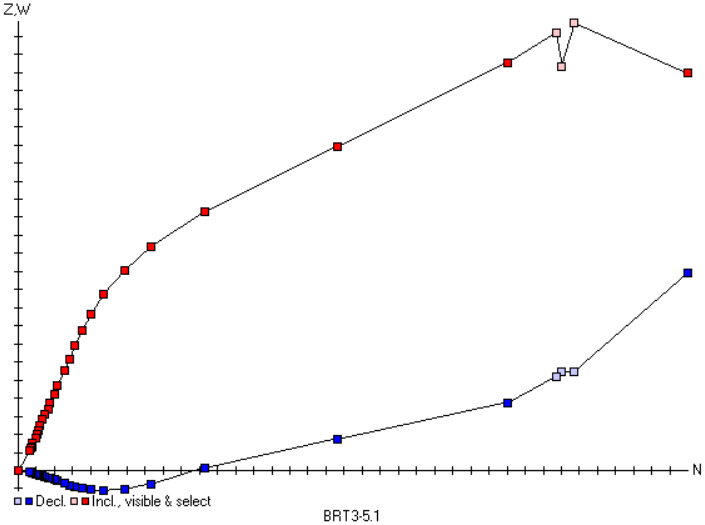

BRT3-5.1
Geographic coordinates

Each Division is 10^-3

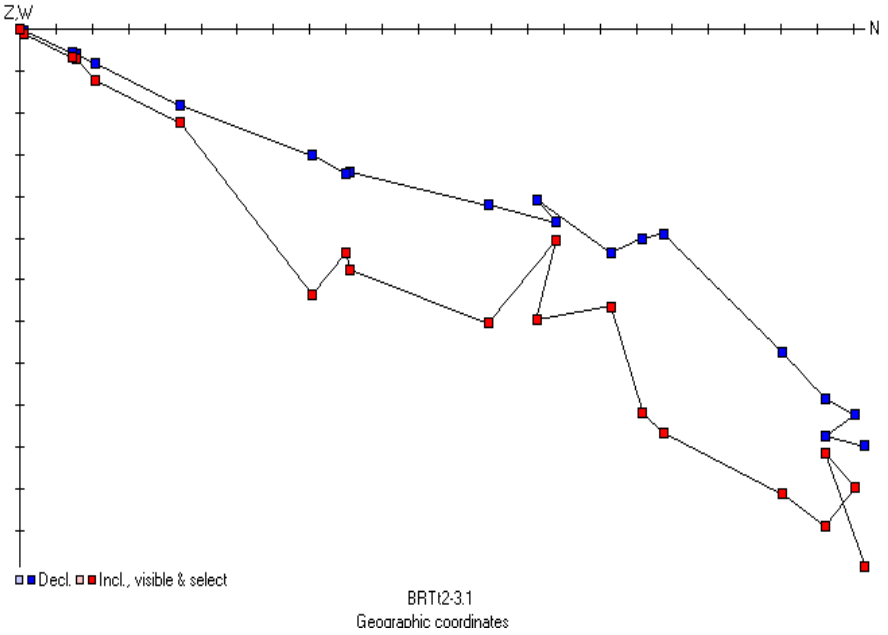

BRTt2-3.1
Geographic coordinates

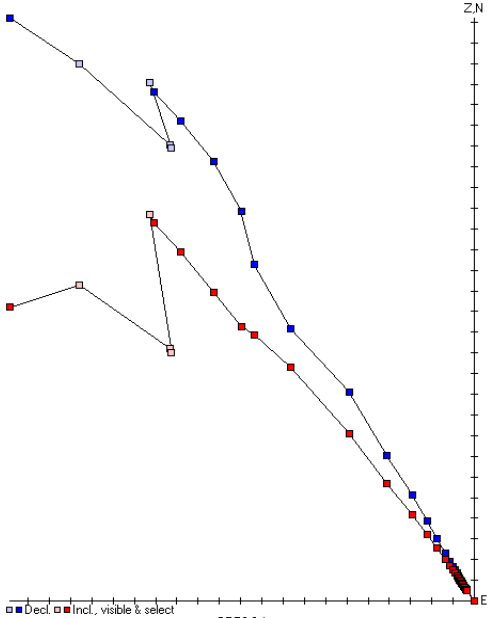

BRT3-2.1
Geographic coordinates

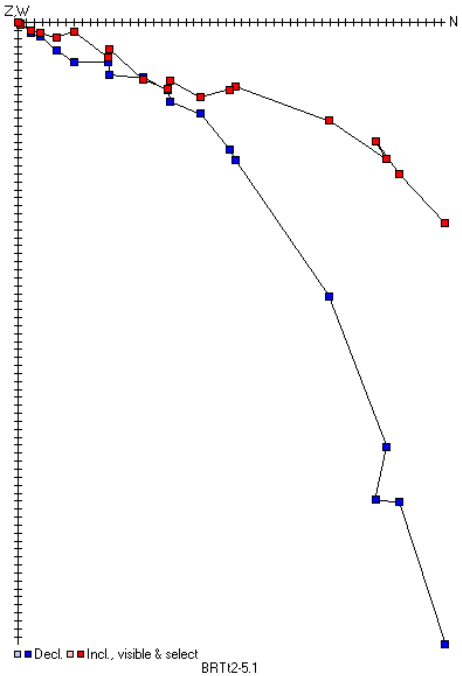

BRTt2-5.1
Geographic coordinates

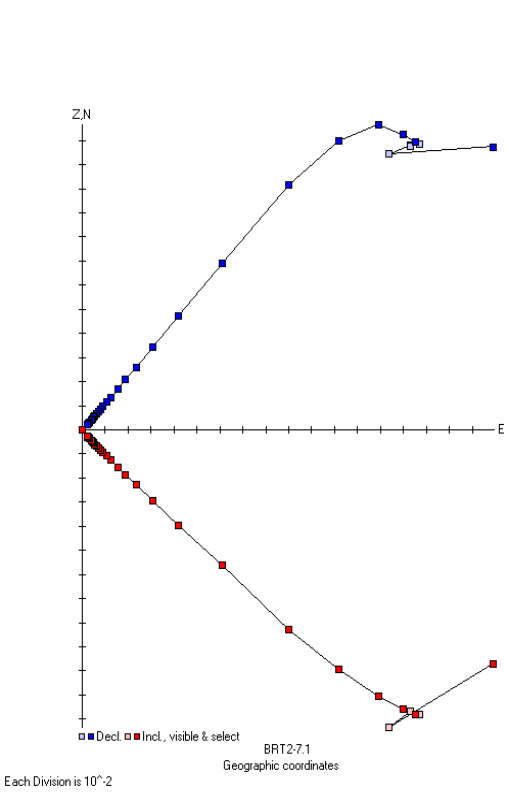
Z,N
E
Decl. Incl., visible & select
BRT2-7.1
Geographic coordinates
Each Division is 10^-2

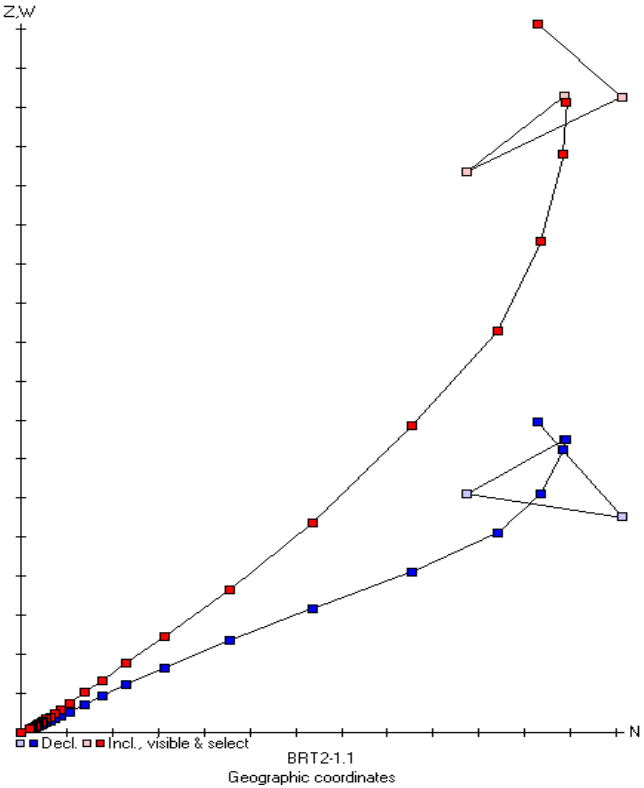
Z,W
N
Decl. Incl., visible & select
BRT2-1.1
Geographic coordinates

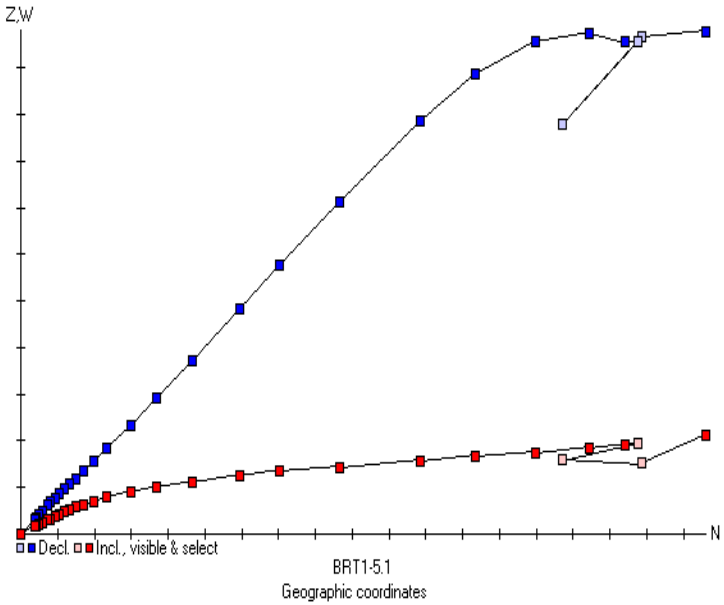
Z,W
N
Decl. Incl., visible & select
BRT1-5.1
Geographic coordinates

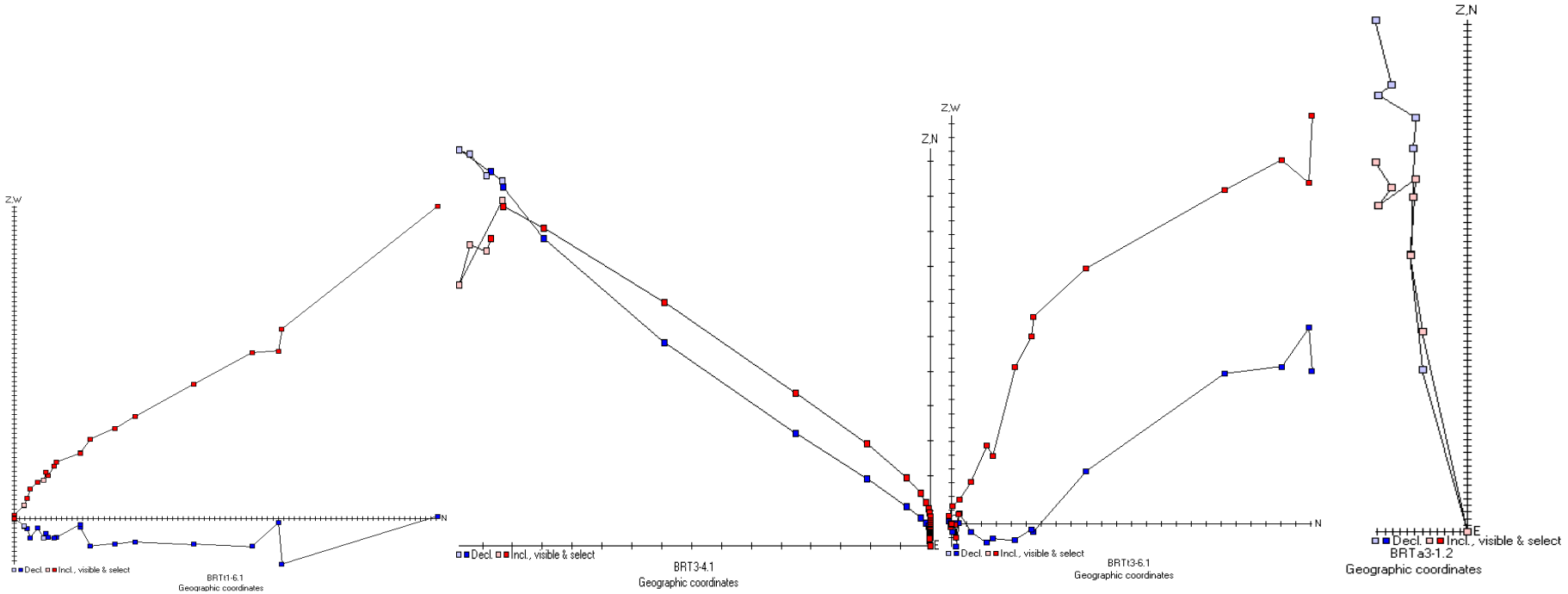
Z,W
N
Decl. Incl., visible & select
BRT1-6.1
Geographic coordinates
Z,N
Z,W
N
Decl. Incl., visible & select
BRT3-4.1
Geographic coordinates
Z,W
N
Decl. Incl., visible & select
BRT3-6.1
Geographic coordinates
Z,N
E
Decl. Incl., visible & select
BRTa3-1.2
Geographic coordinates

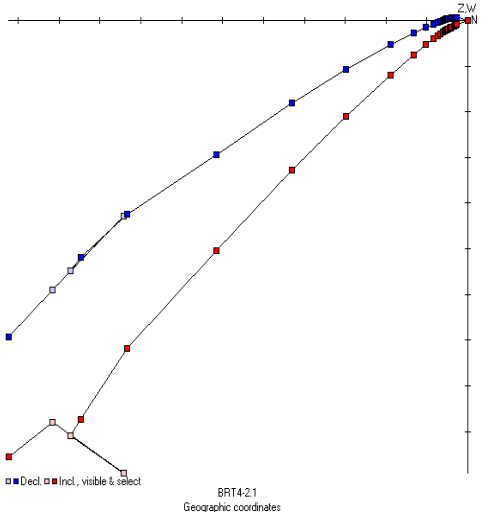
Z,W
N
Decl. Incl., visible & select
BRT4-2.1
Geographic coordinates

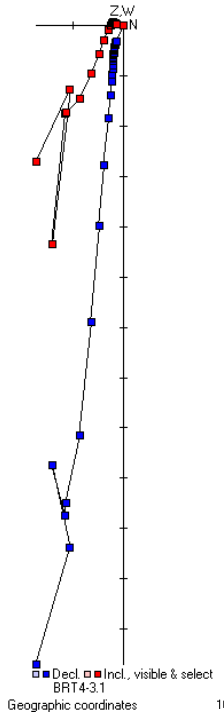
Z,W
N
Decl. Incl., visible & select
BRT4-3.1
Geographic coordinates

10^-3

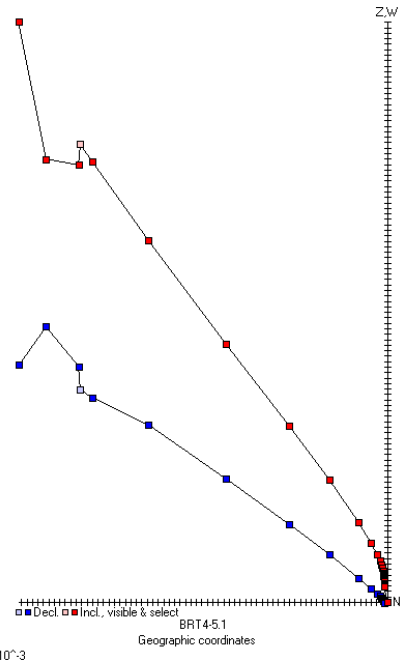
Z,W
N
Decl. Incl., visible & select
BRT4-5.1
Geographic coordinates

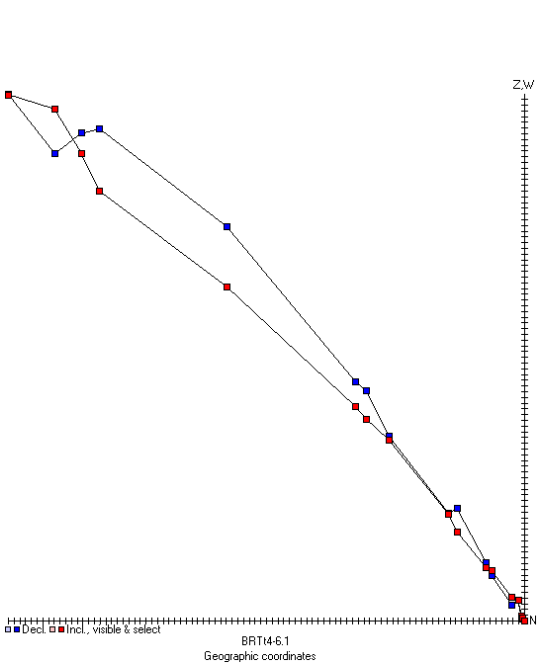
Z,W
N
Decl. Incl., visible & select
BRT4-6.1
Geographic coordinates

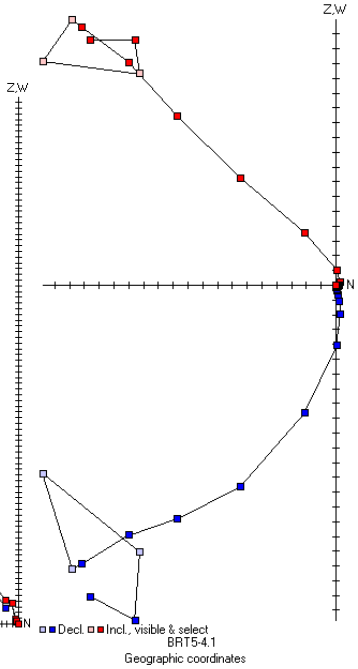
Z,W
N
Decl. Incl., visible & select
BRT5-4.1
Geographic coordinates

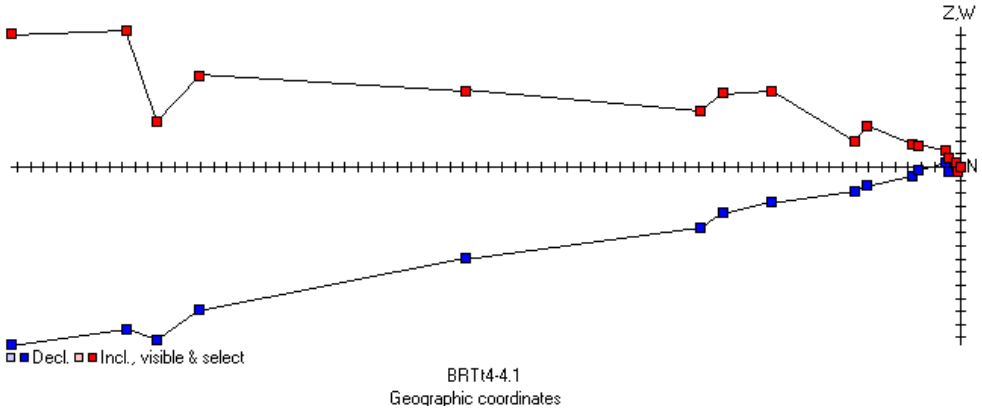

BRTt4-4.1
Geographic coordinates

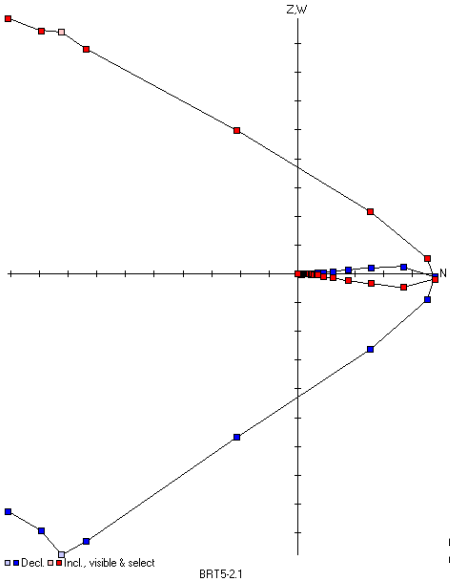

BRT5-2.1

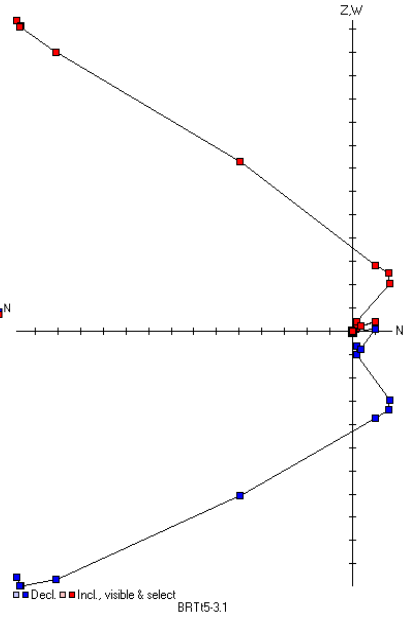

BRTt5-3.1

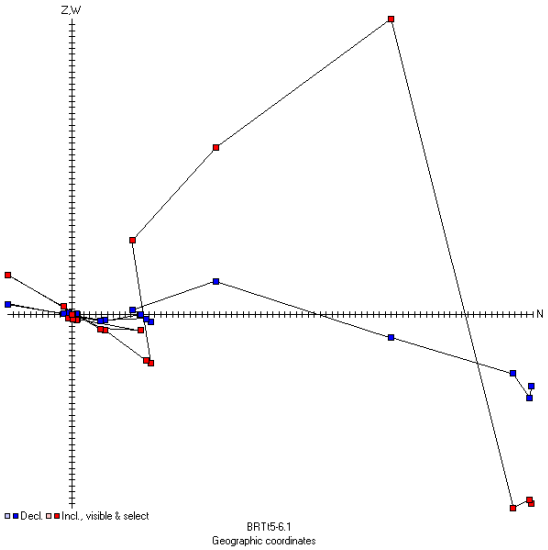

BRTt5-6.1
Geographic coordinates

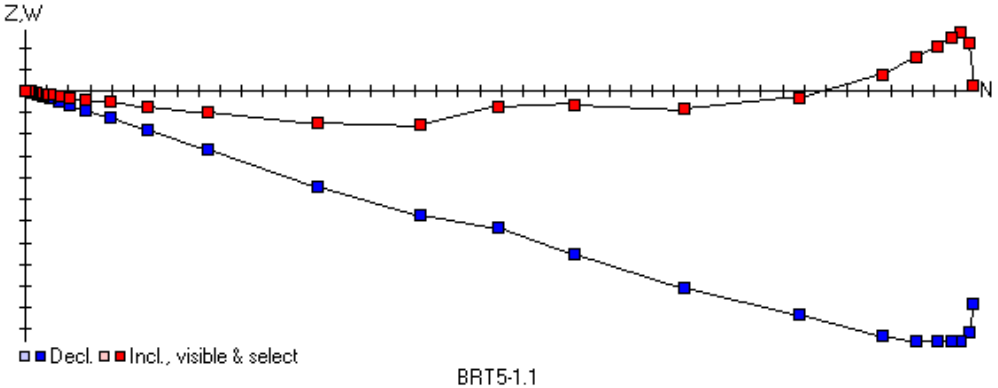

BRT5-1.1
Geographic coordinates

Each Division is 10^-2

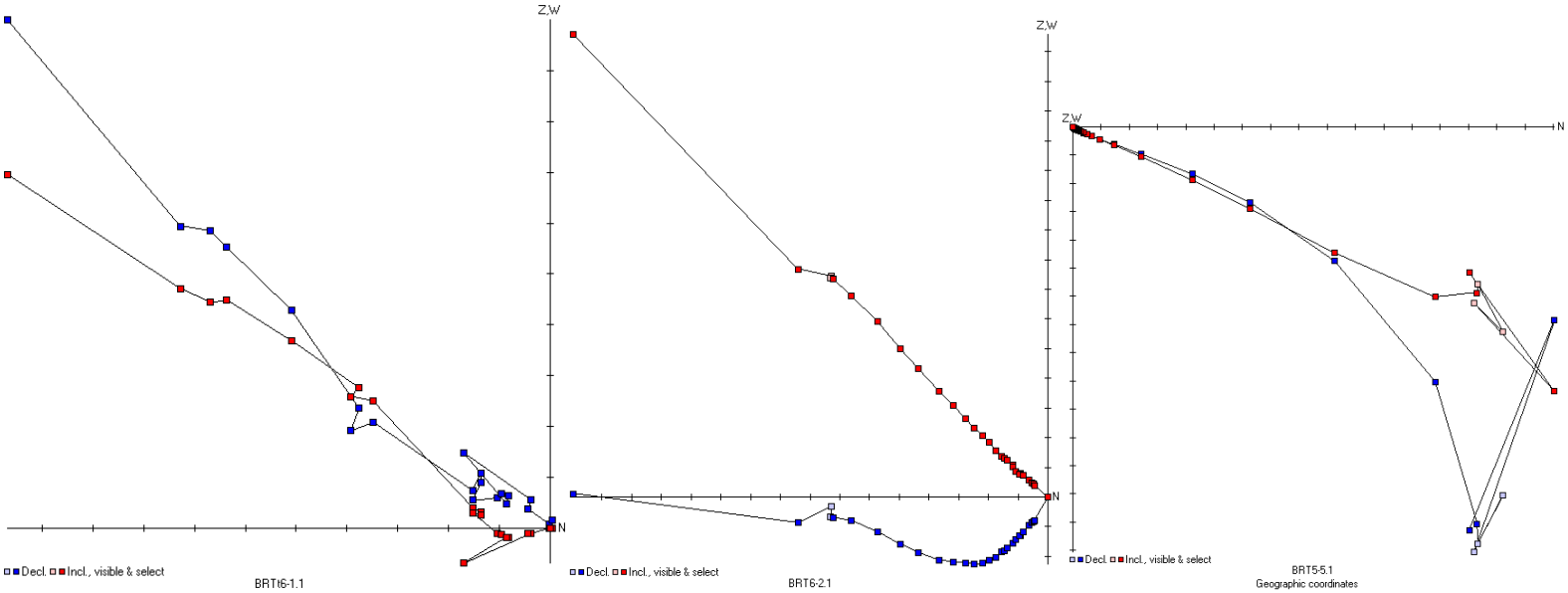
Z,W
N
Decl. Incl., visible & select
BRT6-1.1
Z,W
N
Decl. Incl., visible & select
BRT6-2.1
Z,W
N
Decl. Incl., visible & select
BRT5-5.1
Geographic coordinates

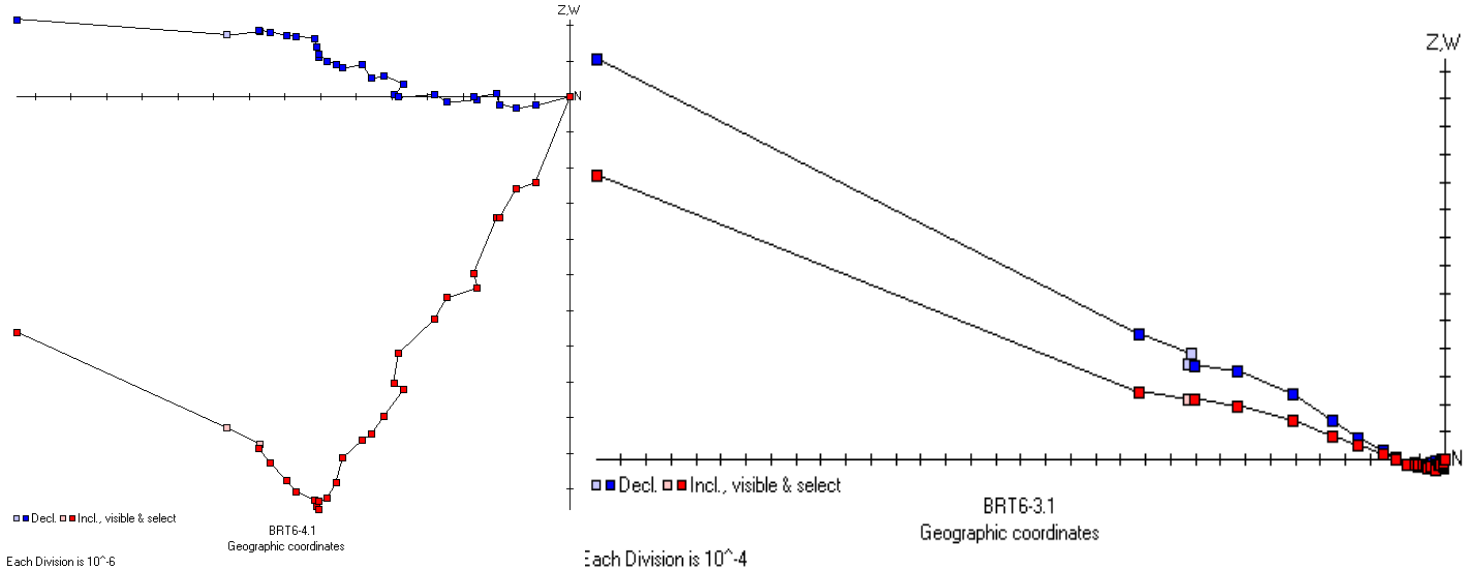
Z,W
N
Decl. Incl., visible & select
BRT6-4.1
Geographic coordinates
Each Division is 10^-6
Z,W
N
Decl. Incl., visible & select
BRT6-3.1
Geographic coordinates
Each Division is 10^-4

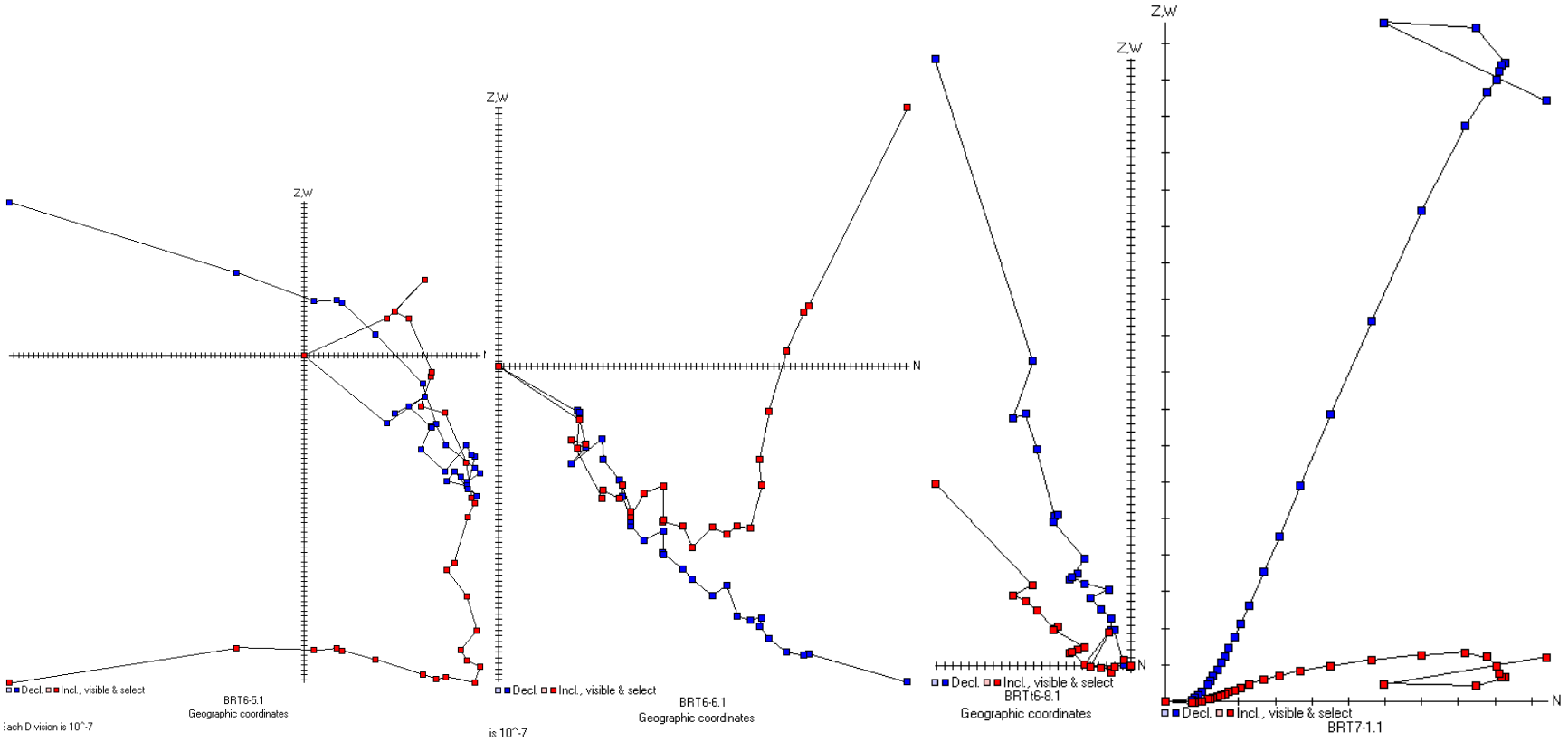
Z,W
N
Decl. Incl., visible & select
BRT6-5.1
Geographic coordinates
ach Division is 10^-7
Z,W
N
Decl. Incl., visible & select
BRT6-6.1
Geographic coordinates
is 10^-7
Z,W
N
Decl. Incl., visible & select
BRTt6-8.1
Geographic coordinates
Z,W
N
Decl. Incl., visible & select
BRT7-1.1

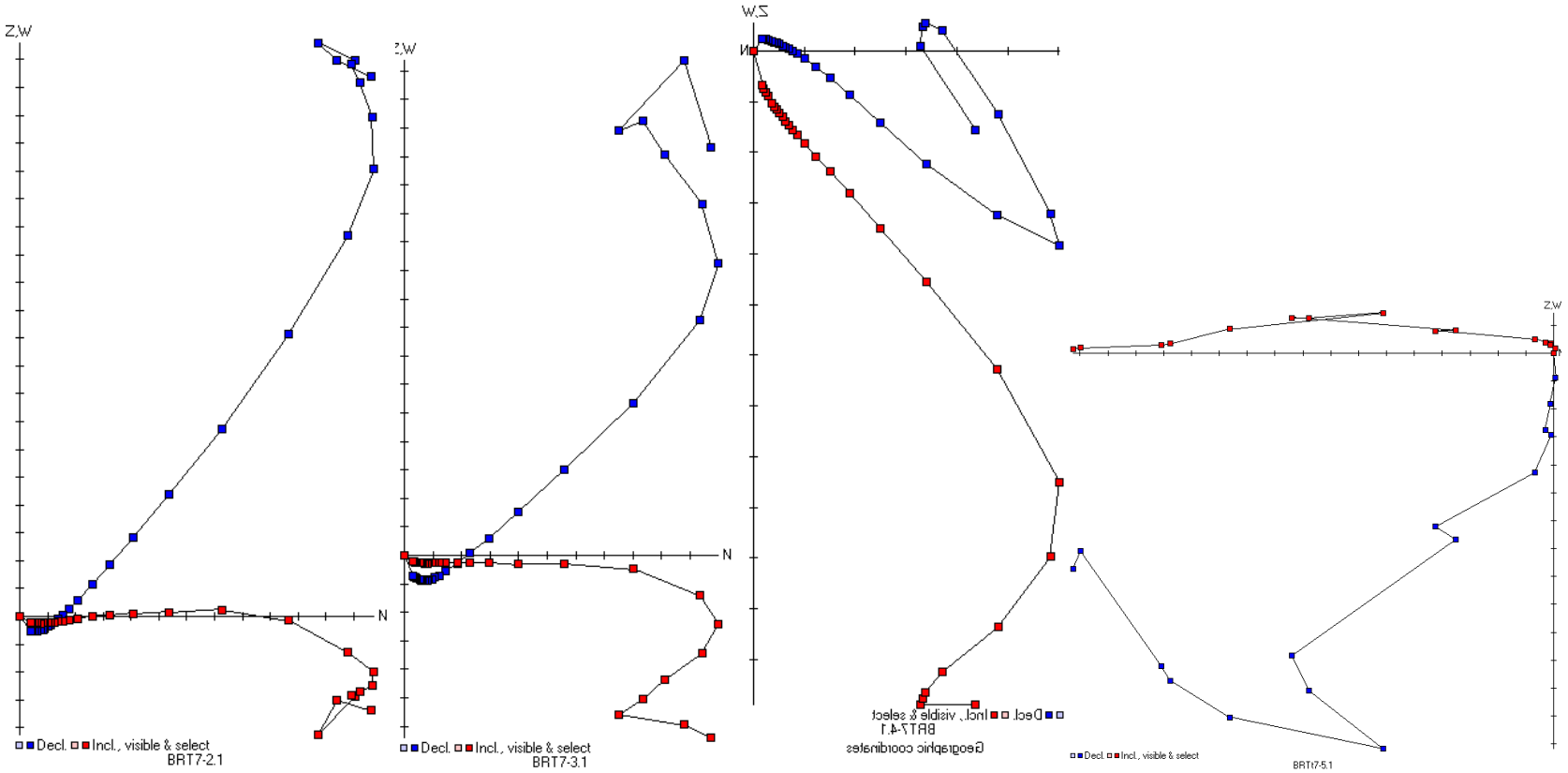
W,Z
N
Decl. Incl., visible & select
BRT7-2.1
W,Z
N
Decl. Incl., visible & select
BRT7-3.1
Z,W
N
Decl. Incl., visible & select
BRT7-4.1
Geographic coordinates
W,Z
Decl. Incl., visible & select
BRT7-5.1

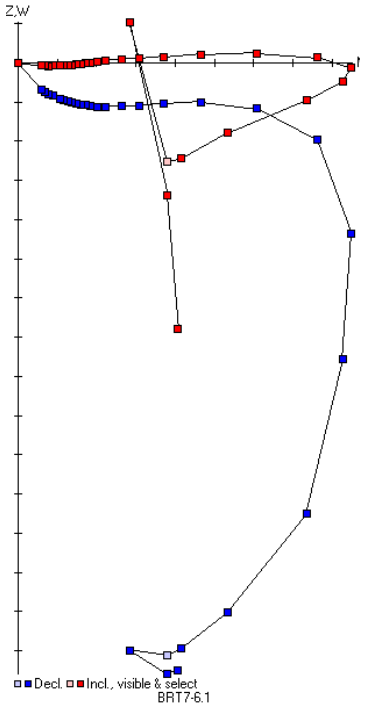
Z,W
Decl. Incl., visible & select
BRT7-6.1

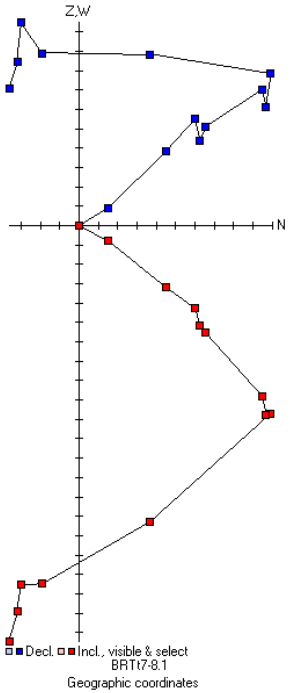
Z,W
N
Decl. Incl., visible & select
BRTt7-8.1
Geographic coordinates

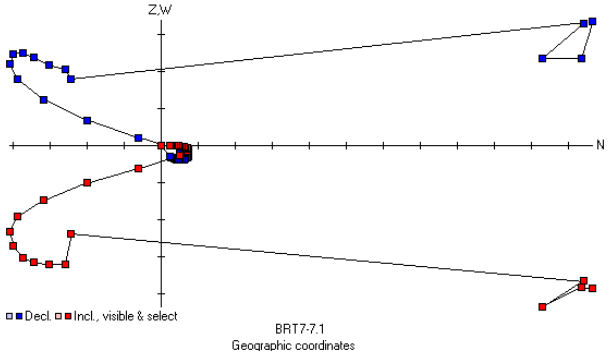
Z,W
N
Decl. Incl., visible & select
BRT7-7.1
Geographic coordinates

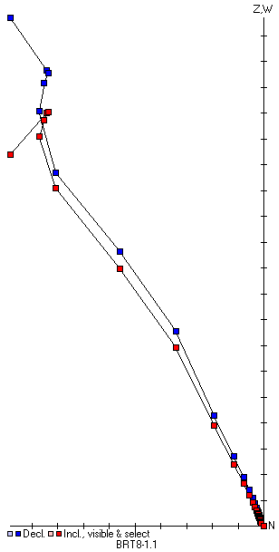
Z,W
N
Decl. Incl., visible & select
BRT8-1.1

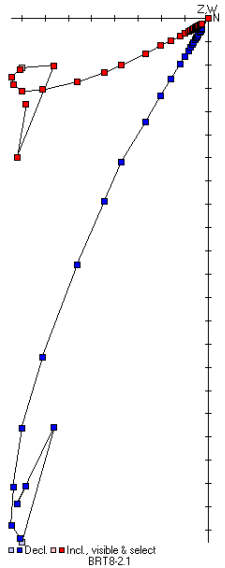
Z,W
N
Decl. Incl., visible & select
BRT8-2.1

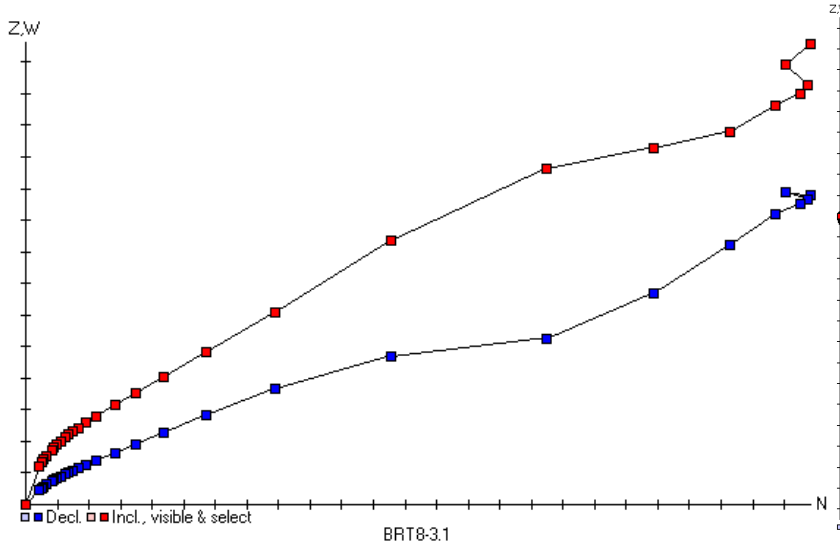

BRT8-3.1

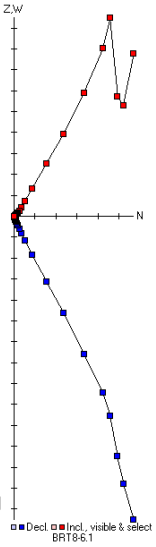

BRT8-6.1

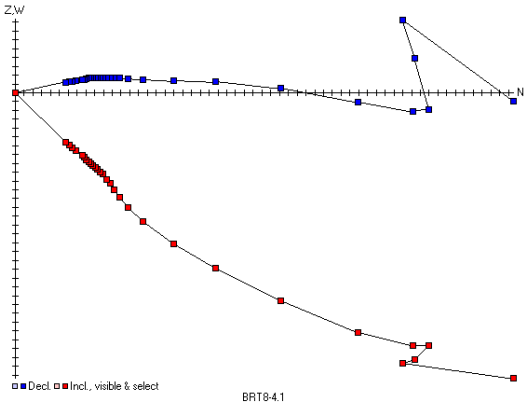

BRT8-4.1

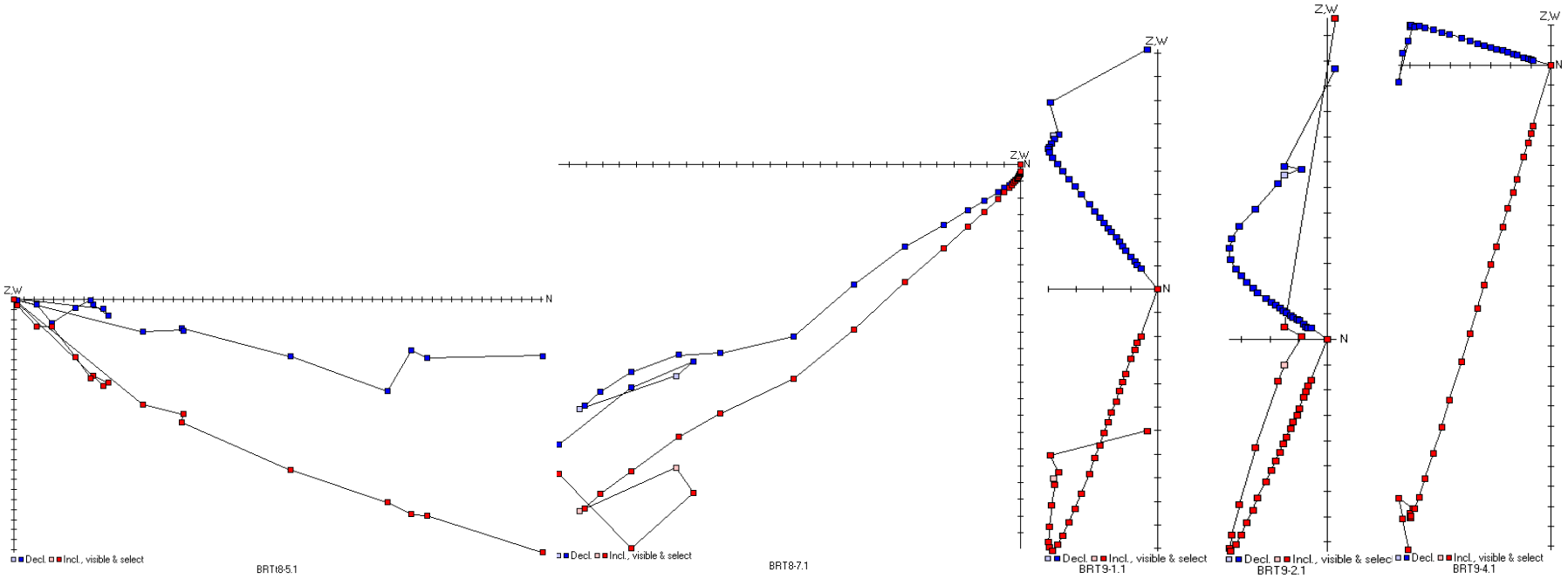
Z,W
N
Decl. Incl., visible & select
BRT8-5.1
Z,W
N
Decl. Incl., visible & select
BRT8-7.1
Z,W
N
Decl. Incl., visible & select
BRT9-1.1
Z,W
N
Decl. Incl., visible & selec
BRT9-2.1
Z,W
N
Decl. Incl., visible & select
BRT9-4.1

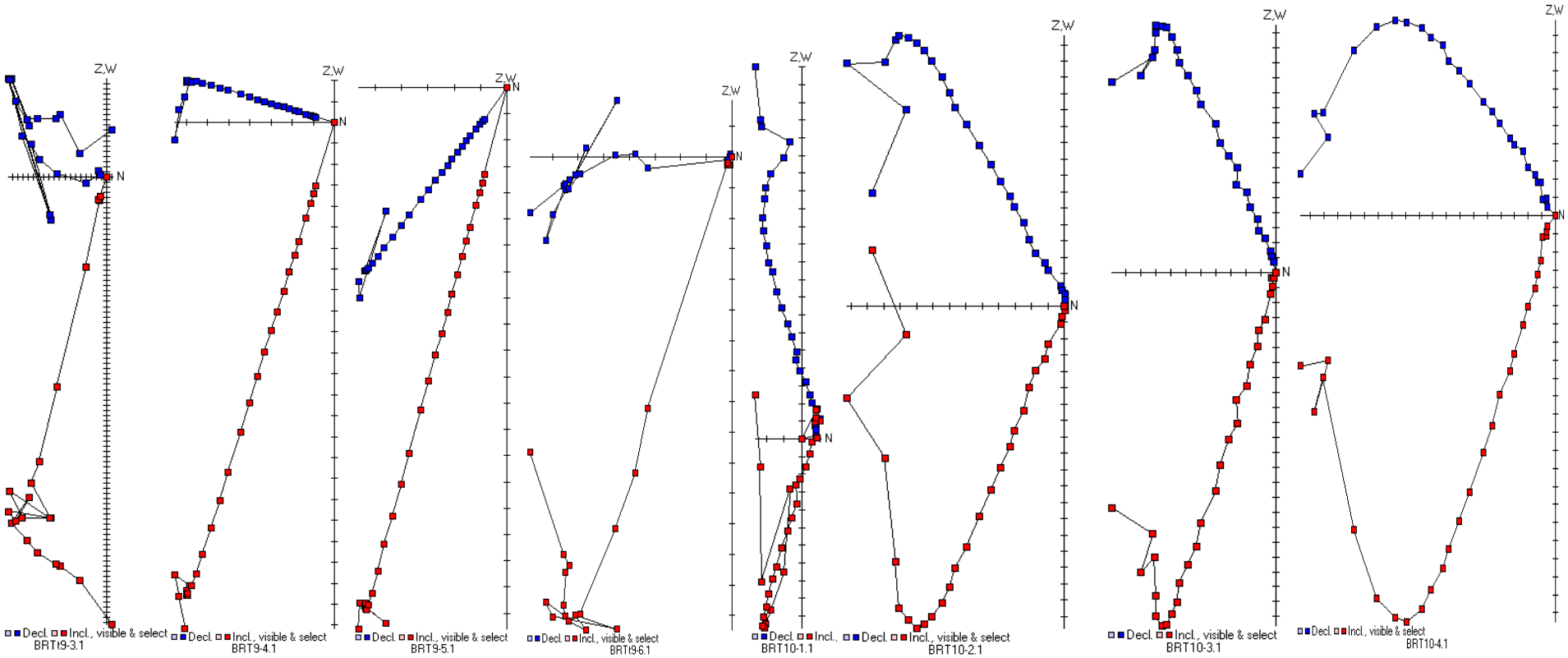
Z,W
N
Decl. Incl., visible & select
BRT9-3.1
BRT9-4.1
BRT9-5.1
BRT9-6.1
BRT10-1.1
BRT10-2.1
BRT10-3.1
BRT10-4.1

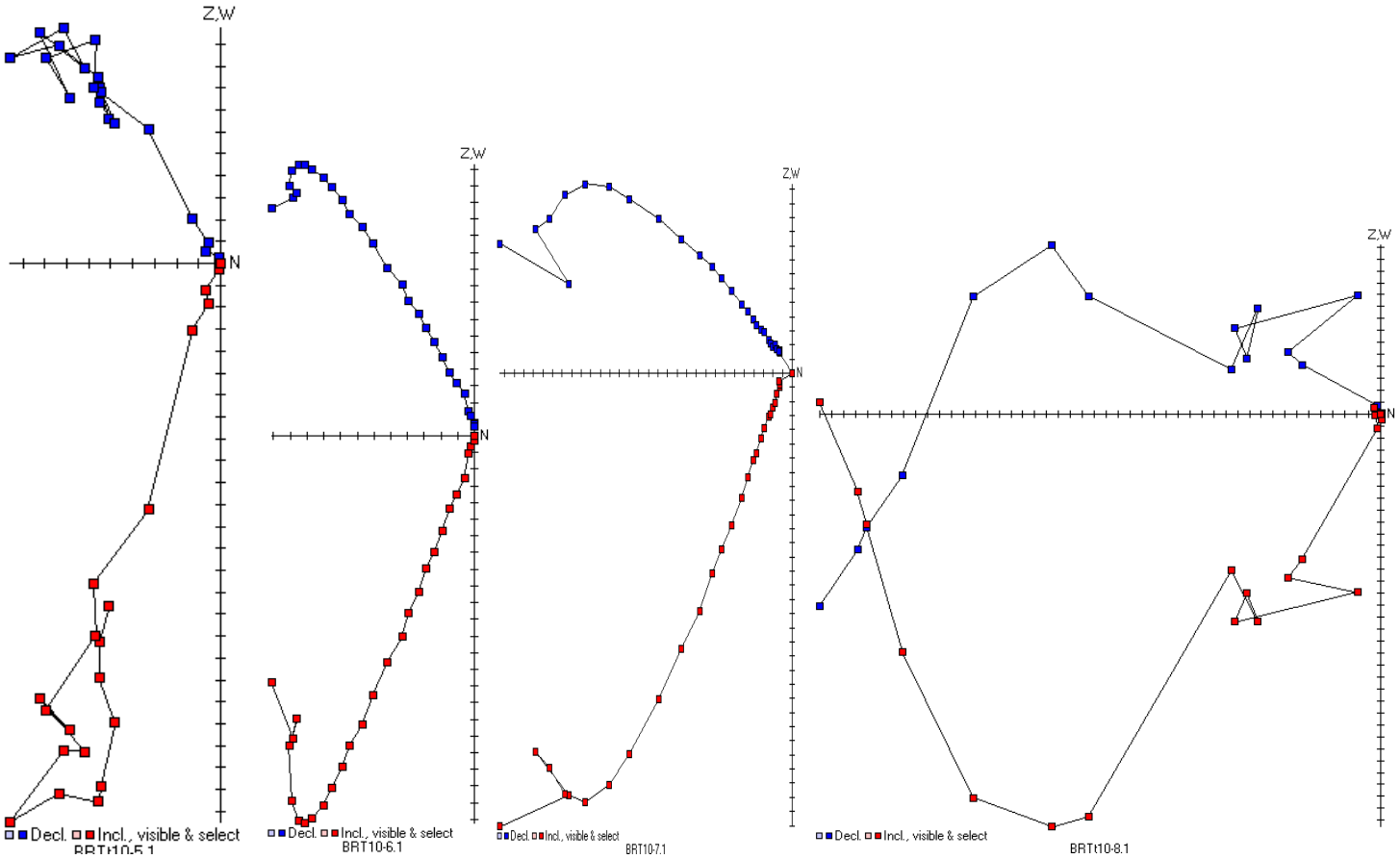
Z,W
N
Decl.
Incl., visible & select
BRT10-5.1
Z,W
N
Decl.
Incl., visible & select
BRT10-6.1
Z,W
N
Decl.
Incl., visible & select
BRT10-7.1
Z,W
N
Decl.
Incl., visible & select
BRT10-8.1

12.2 Ebor

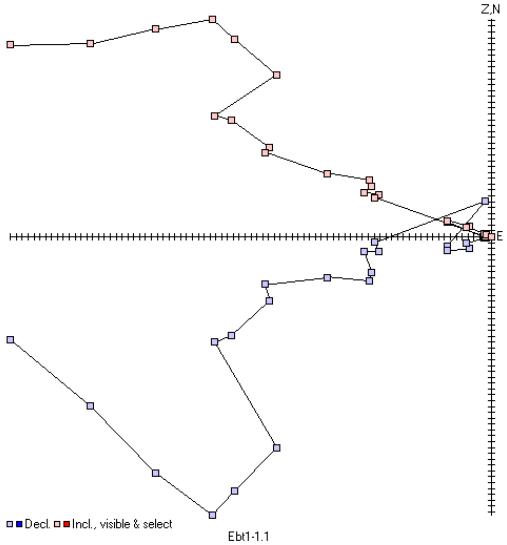

Ebt1-1.1

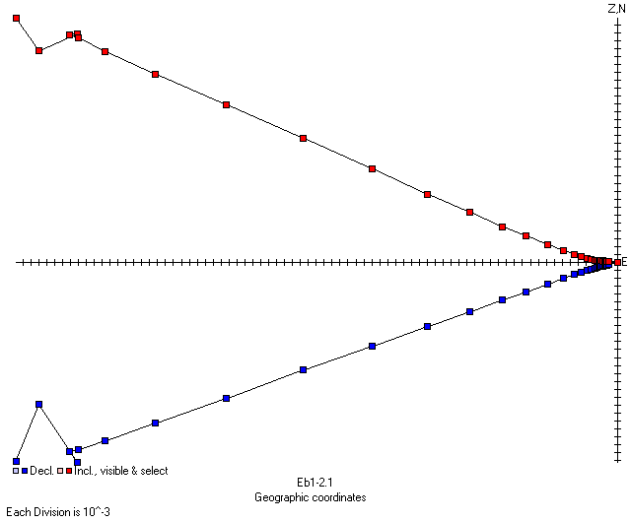

Eb1-2.1
Geographic coordinates
Each Division is 10^-3

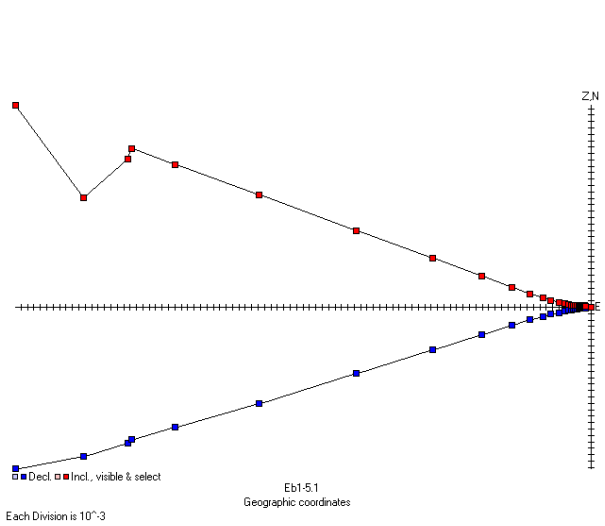

Eb1-5.1
Geographic coordinates
Each Division is 10^-3

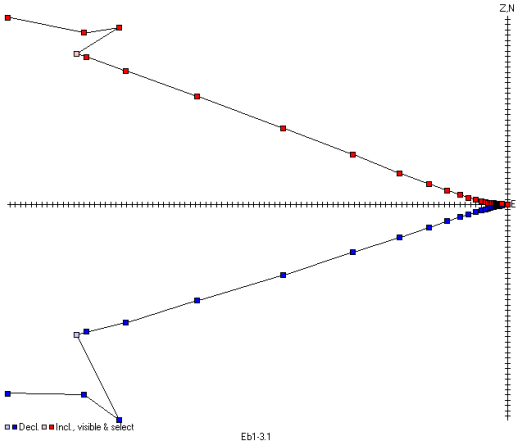

Eb1-3.1
Geographic coordinates
Each Division is 10^-3

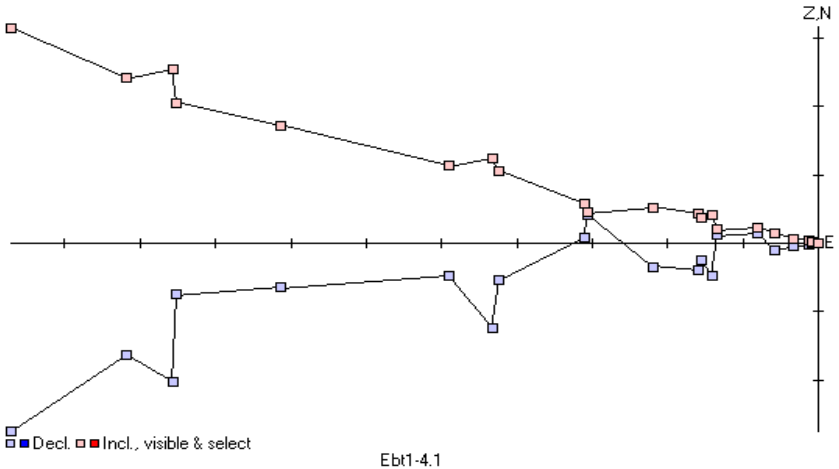

Ebt1-4.1
Geographic coordinates
Each Division is 10^-2

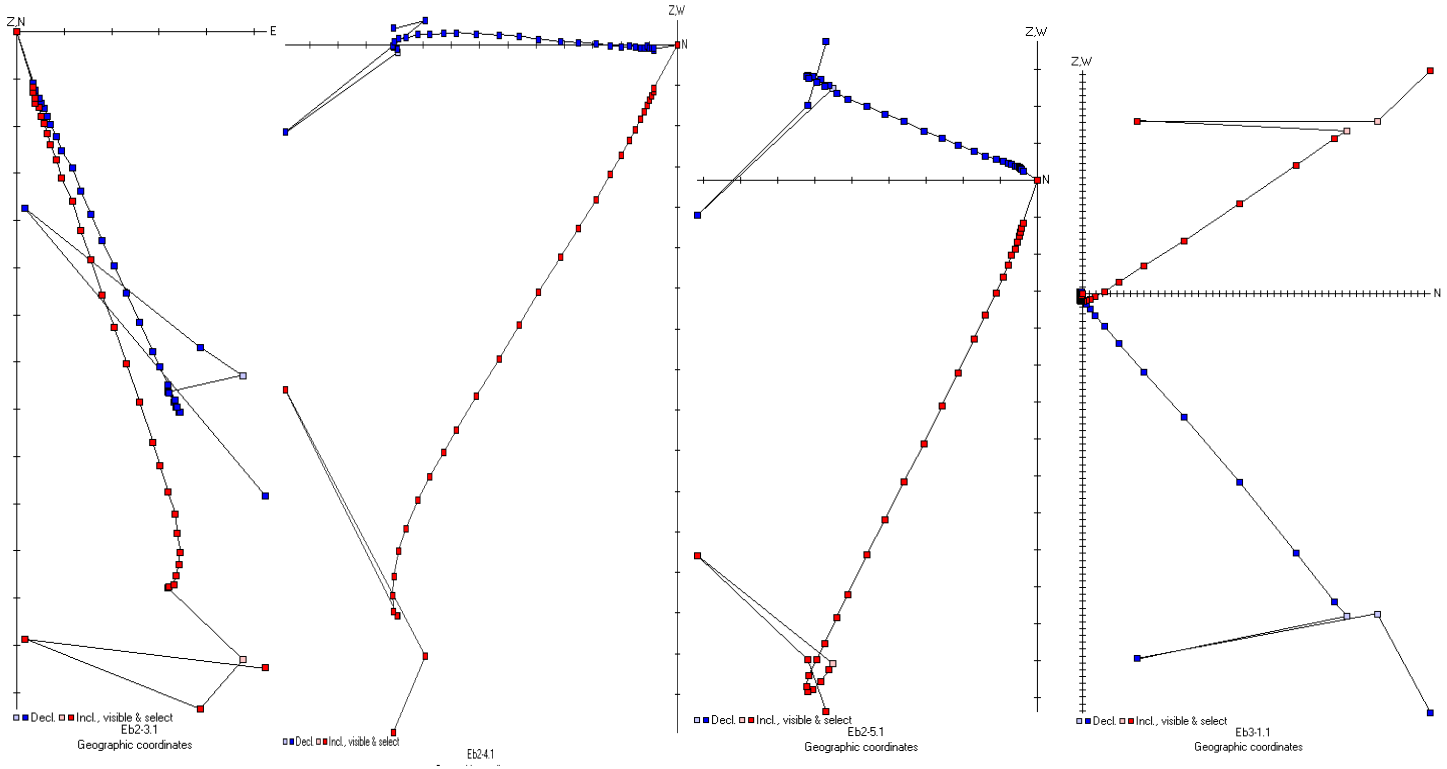
Z,N
E
Decl. Incl., visible & select
Eb2-3.1
Geographic coordinates
Z,W
N
Decl. Incl., visible & select
Eb2-4.1
Z,W
N
Decl. Incl., visible & select
Eb2-5.1
Geographic coordinates
Z,W
N
Decl. Incl., visible & select
Eb3-1.1
Geographic coordinates

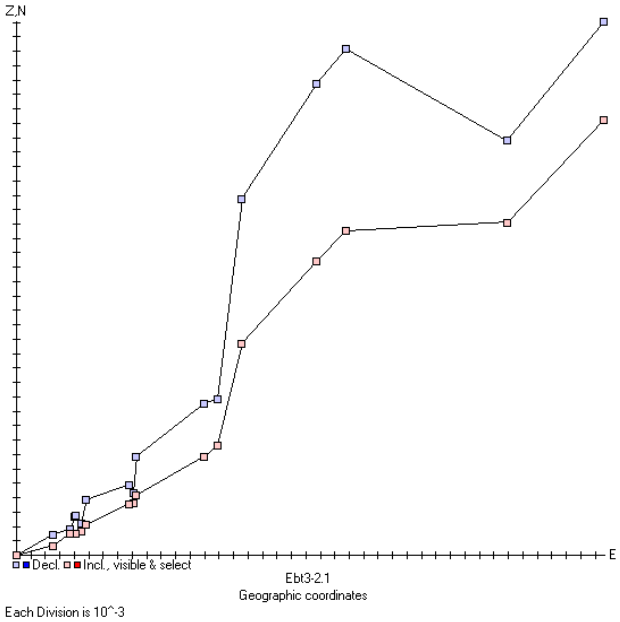

Ebt3-2.1
Geographic coordinates
Each Division is 10^-3

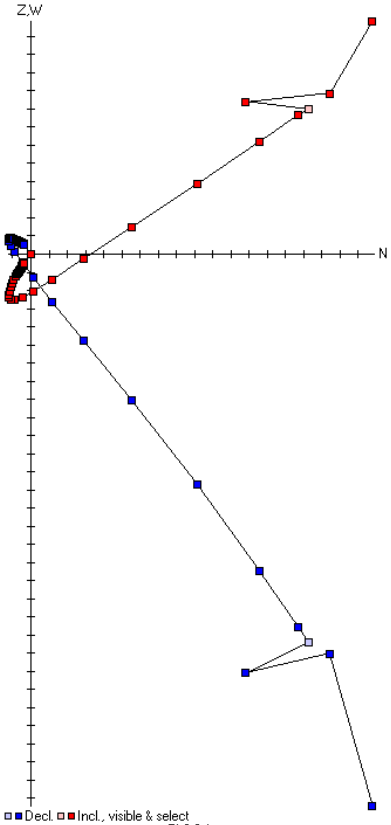

Eb3-3.1
Geographic coordinates

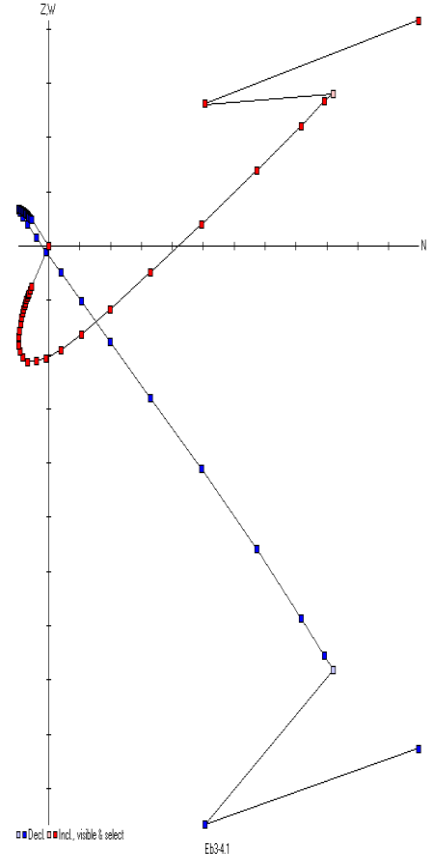

Eb3-4.1
Geographic coordinates
Each Division is 10^-3

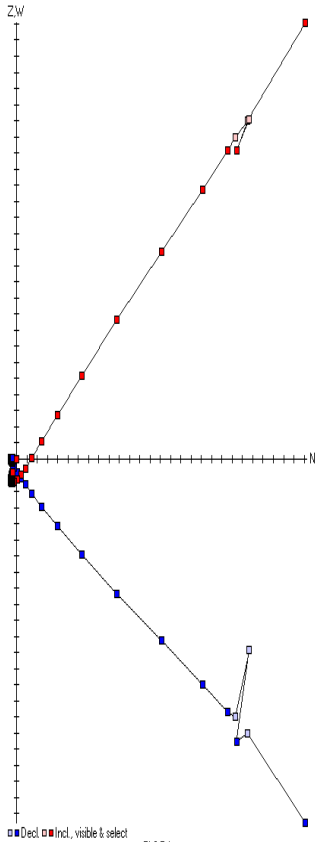

Eb3-5.1
Geographic coordinates

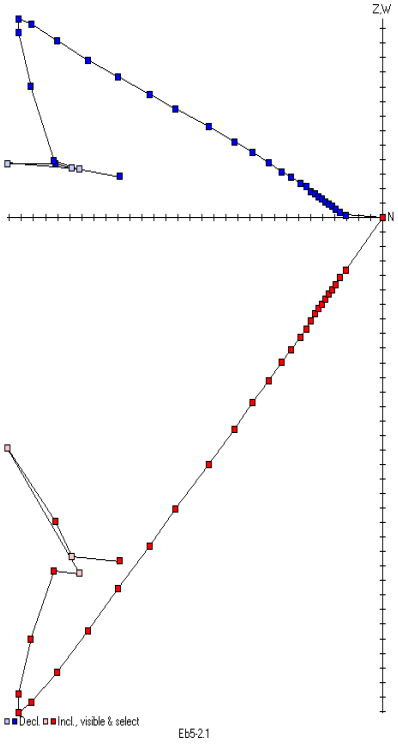
Z,W
N
Decl. Incl., visible & select
Eb5-2.1

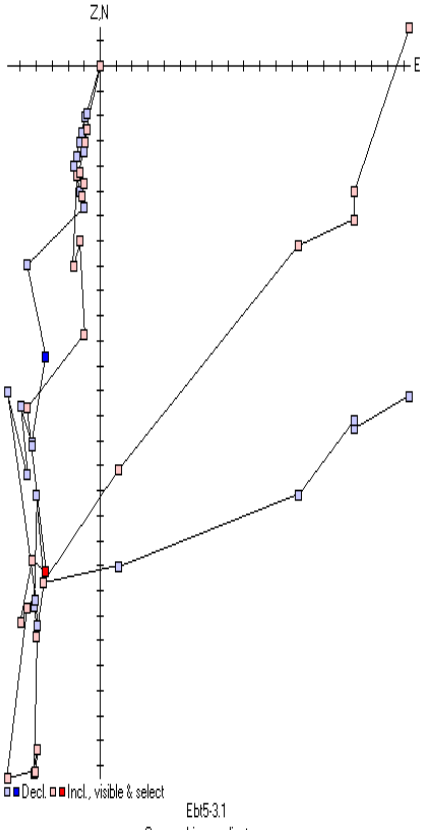
Z,N
E
Decl. Incl., visible & select
Eb5-3.1

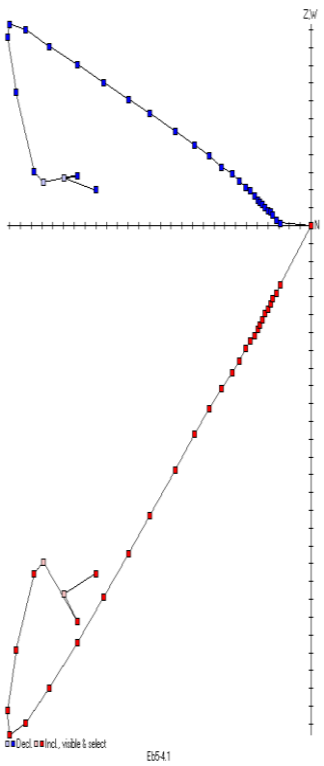
Z,W
N
Decl. Incl., visible & select
Eb5-4.1

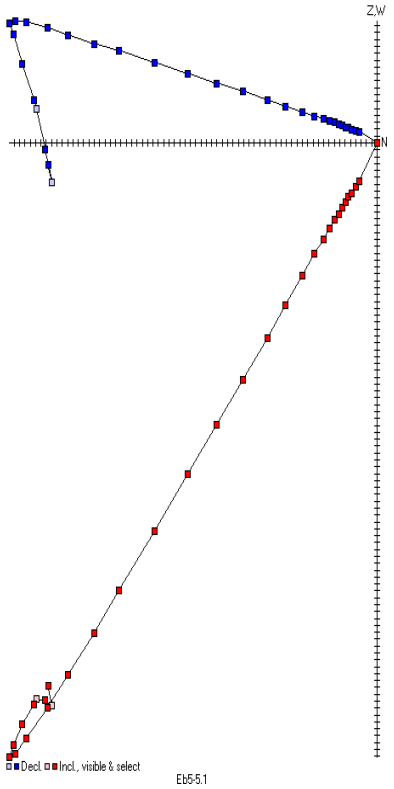
Z,W
N
Decl. Incl., visible & select
Eb5-5.1

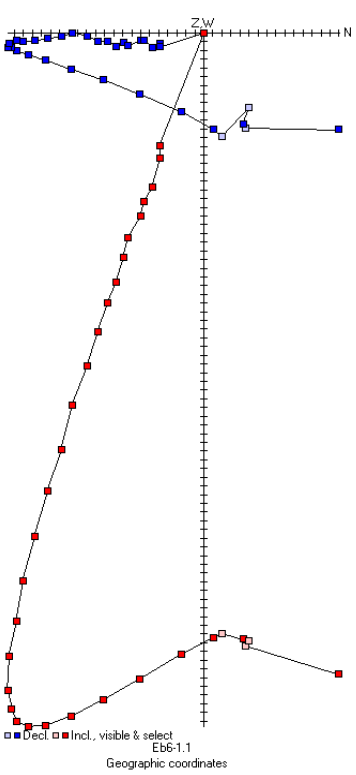
Z,W
N
Decl. Incl., visible & select
Eb6-1.1
Geographic coordinates

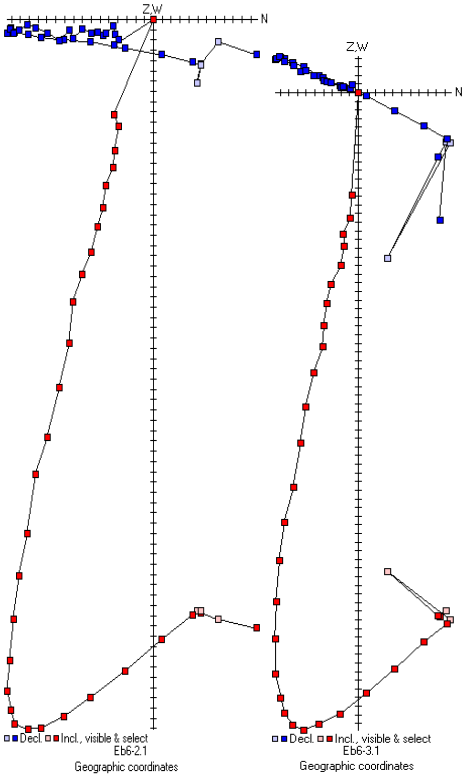
Z,W
N
Decl. Incl., visible & select
Eb6-2.1
Geographic coordinates

Z,W
N
Decl. Incl., visible & select
Eb6-3.1
Geographic coordinates

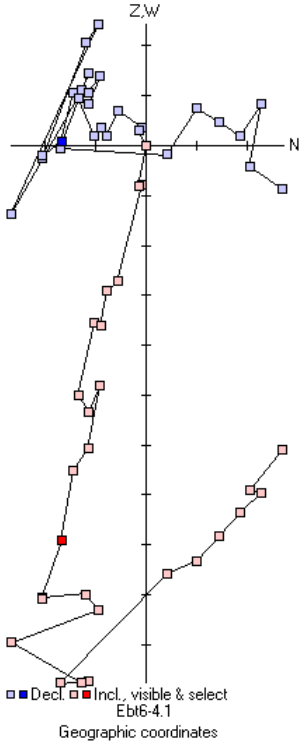
Z,W
N
Decl. Incl., visible & select
Ebt6-4.1
Geographic coordinates

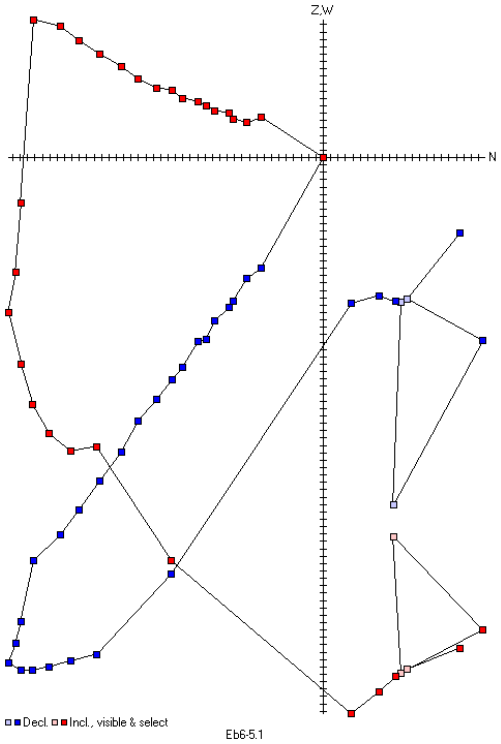
Z,W
N
Decl. Incl., visible & select
Eb6-5.1

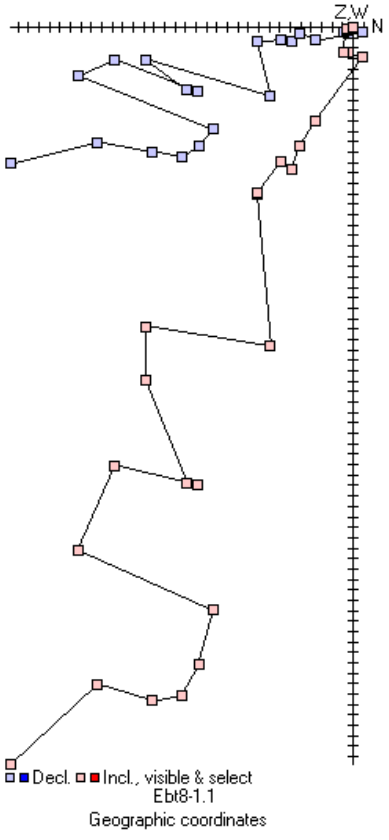
Z,W
N
Decl. Incl., visible & select
Ebt8-1.1
Geographic coordinates

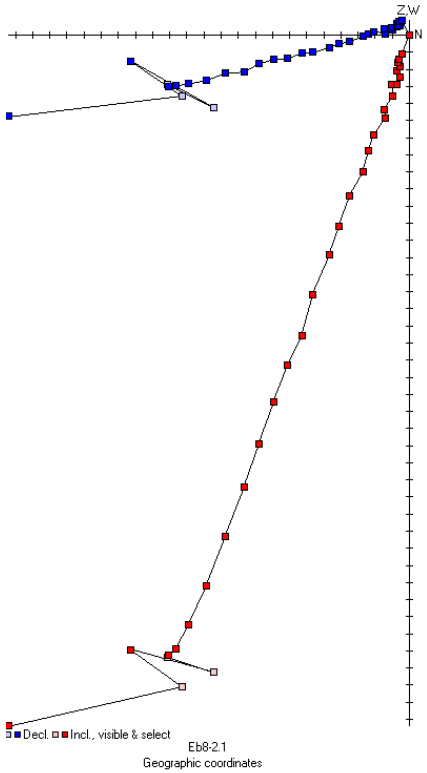
Z,W
N
Decl. Incl., visible & select
Eb8-2.1
Geographic coordinates

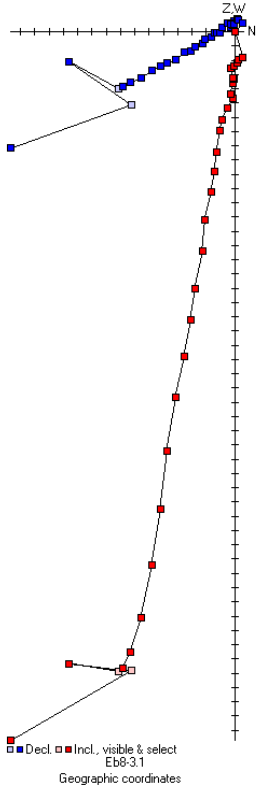
Z,W
N
Decl. Incl., visible & select
Eb8-3.1
Geographic coordinates

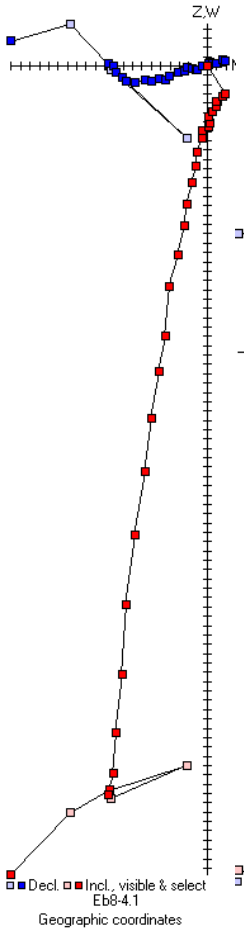
Z,W
N
Decl. Incl., visible & select
Eb8-4.1
Geographic coordinates

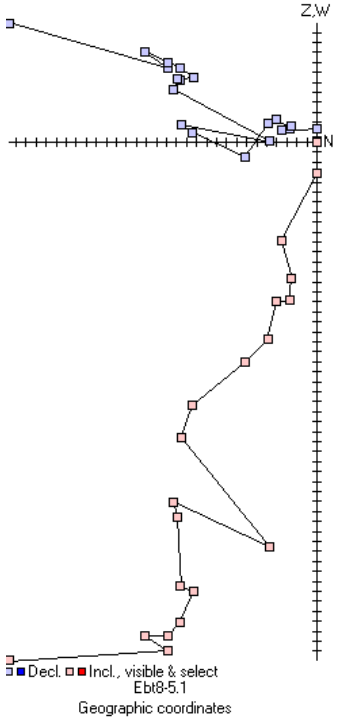
Z,W
N
Decl. Incl., visible & select
Ebt8-5.1
Geographic coordinates

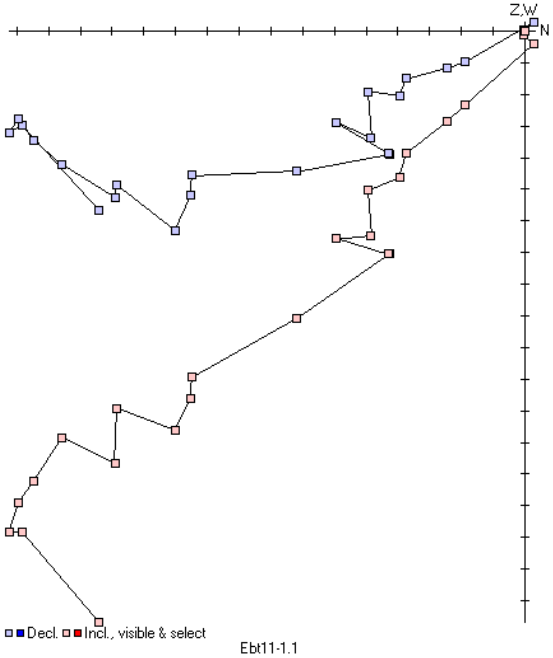
Z,W
N
Decl. Incl., visible & select
Ebt11-1.1

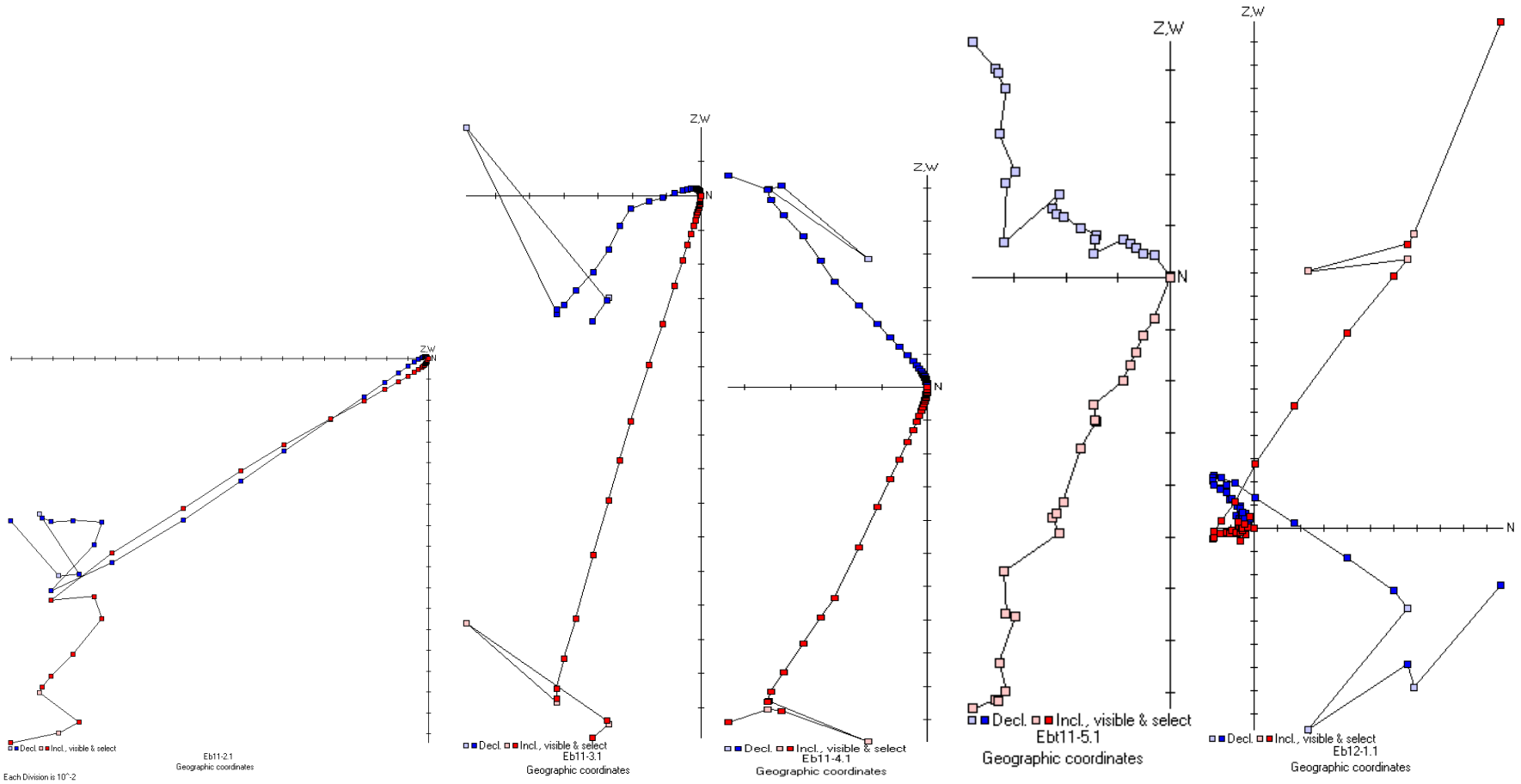
Z,W
N
Decl. Incl., visible & select
Eb11-2.1
Geographic coordinates
Each Division is 10^-2
Z,W
N
Decl. Incl., visible & select
Eb11-3.1
Geographic coordinates
Z,W
N
Decl. Incl., visible & select
Eb11-4.1
Geographic coordinates
Z,W
N
Decl. Incl., visible & select
Ebt11-5.1
Geographic coordinates
Z,W
N
Decl. Incl., visible & select
Eb12-1.1
Geographic coordinates

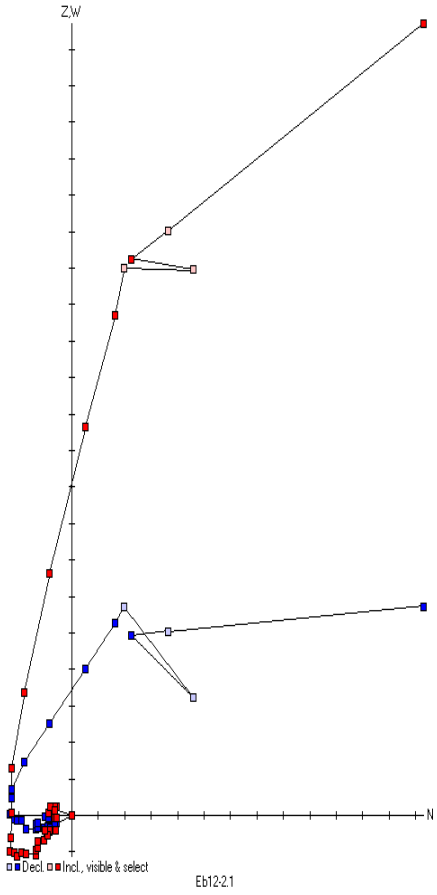

Eb12-2.1

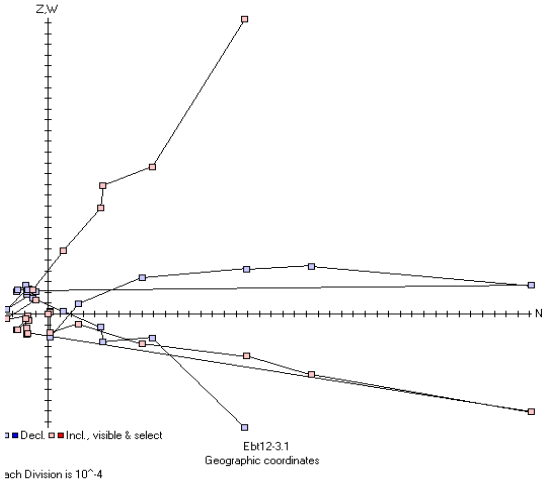

ach Division is 10^-4

Ebt12-3.1
Geographic coordinates

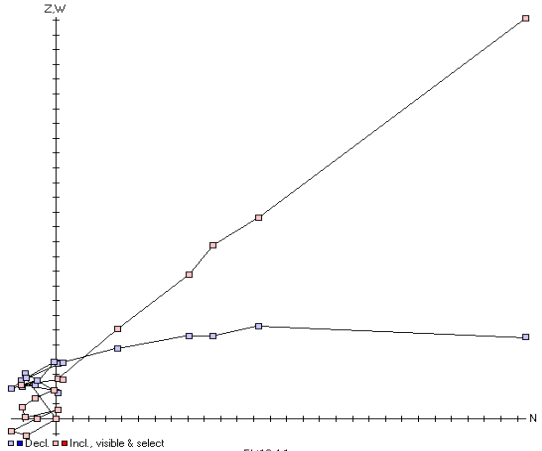

Each Division is 10^-4

Ebt12-4.1
Geographic coordinates

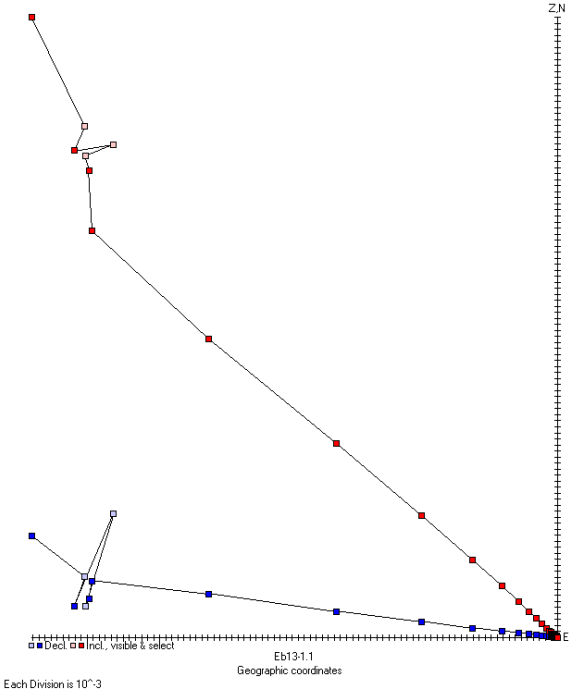

Eb13-1.1
Geographic coordinates
Each Division is 10^-3

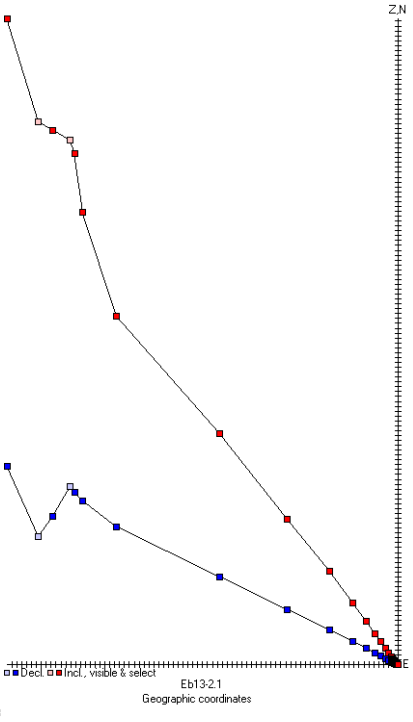

Eb13-2.1
Geographic coordinates
Each Division is 10^-3

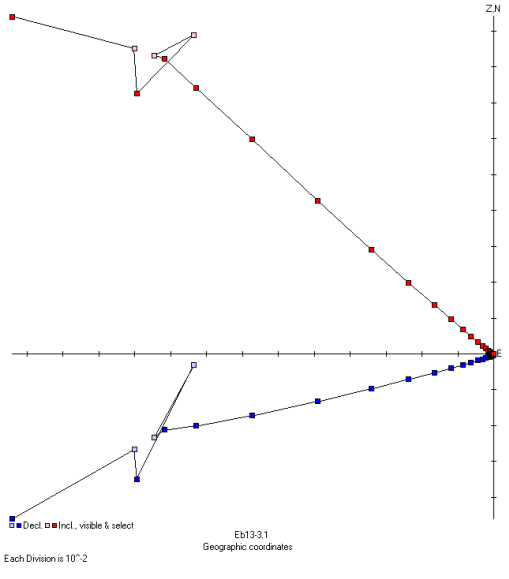

Eb13-3.1
Geographic coordinates
Each Division is 10^-2

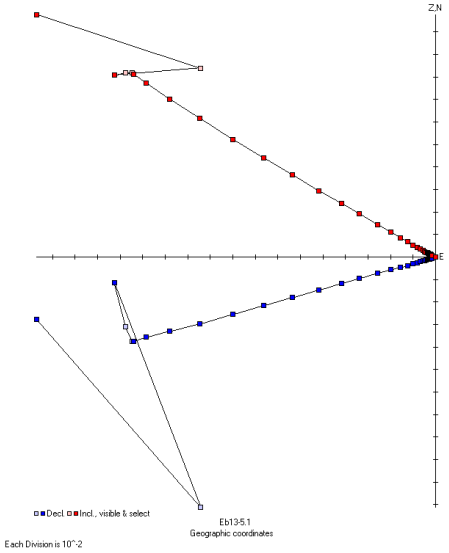
Z,N
N
Decl. Incl., visible & select
Eb13-5.1
Geographic coordinates
Each Division is 10^-2

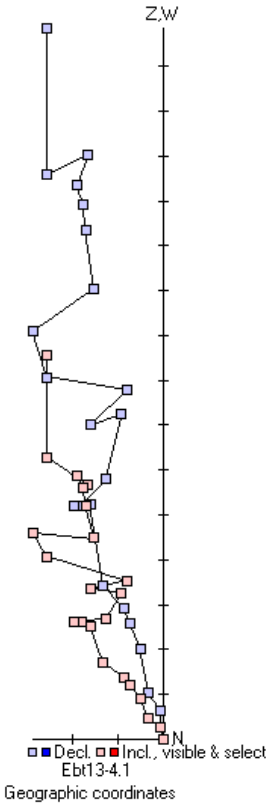
Z,W
N
Decl. Incl., visible & select
Ebt13-4.1
Geographic coordinates

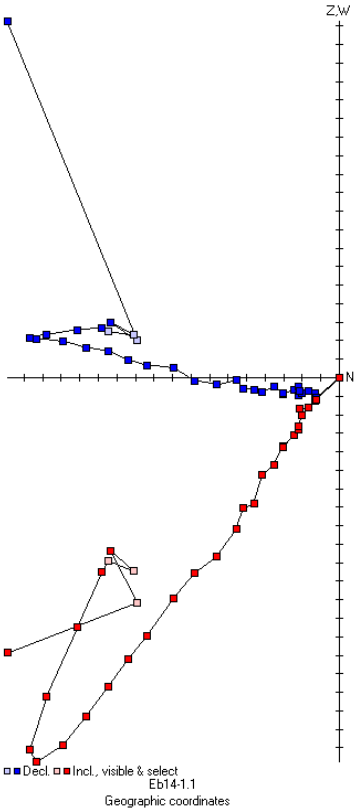
Z,W
N
Decl. Incl., visible & select
Eb14-1.1
Geographic coordinates

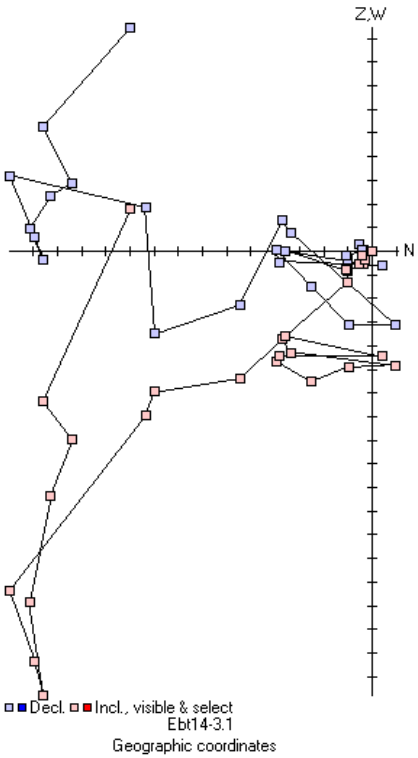
Z,W
N
Decl. Incl., visible & select
Ebt14-3.1
Geographic coordinates

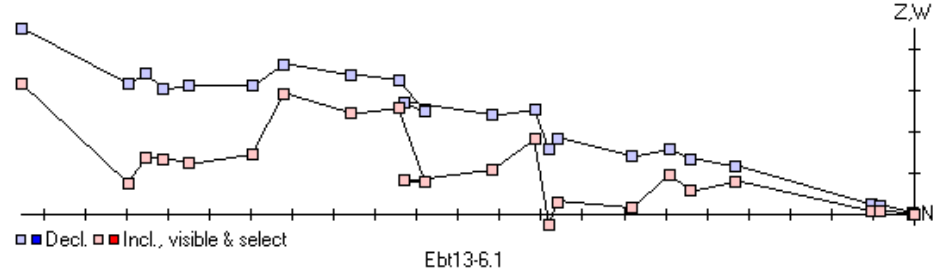

Ebt13-6.1
Geographic coordinates

Each Division is 10^-2

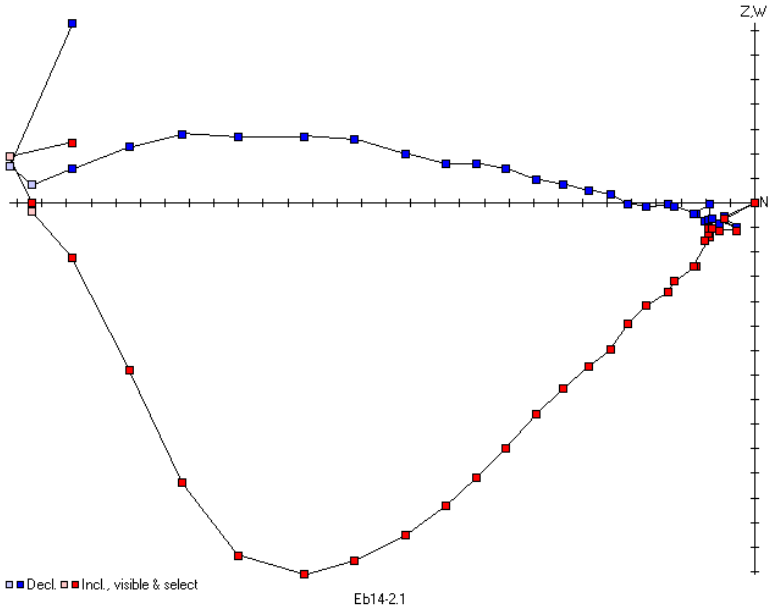

Eb14-2.1
Geographic coordinates

Each Division is 10^-4

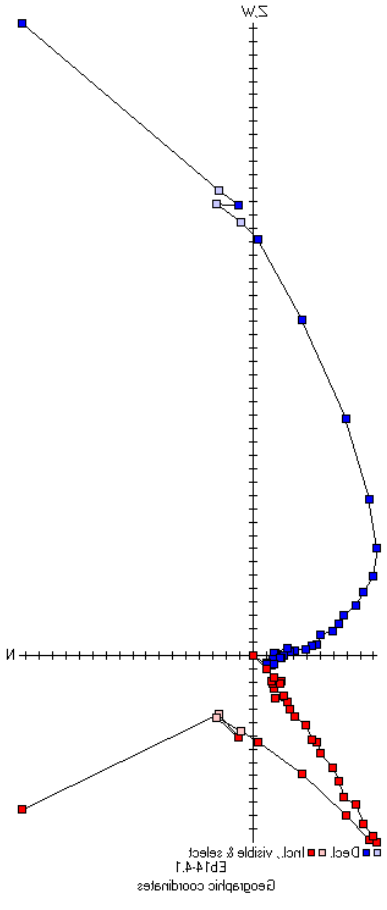
Z,W
N
Decl. Incl., visible & select
Eb14-4.1
Geographic coordinates

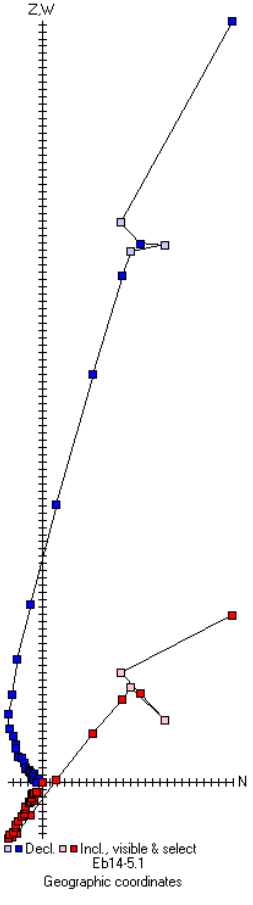
W,Z
N
Decl. Incl., visible & select
Eb14-5.1
Geographic coordinates

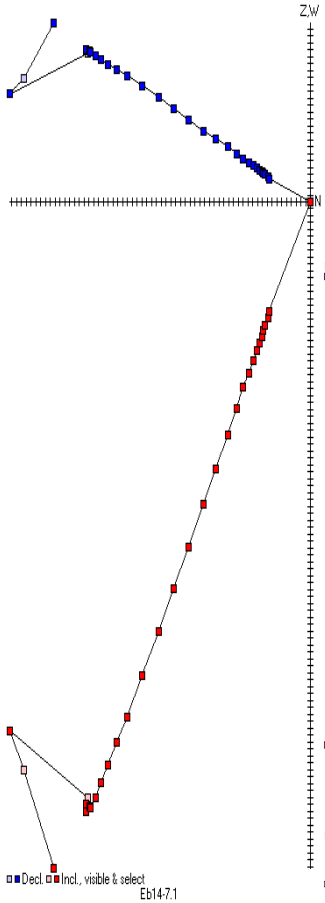
W,Z
N
Decl. Incl., visible & select
Eb14-7.1

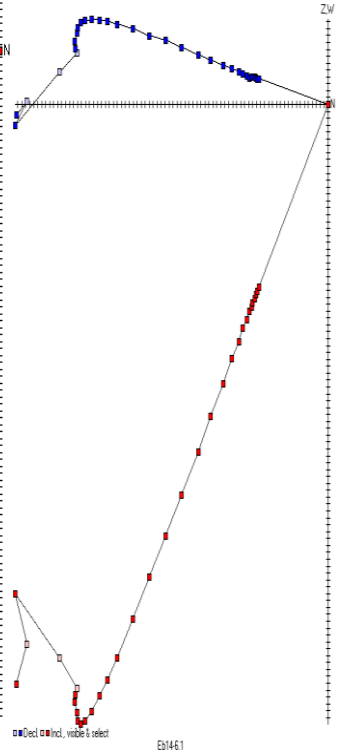
W,Z
N
Decl. Incl., visible & select
Eb14-6.1

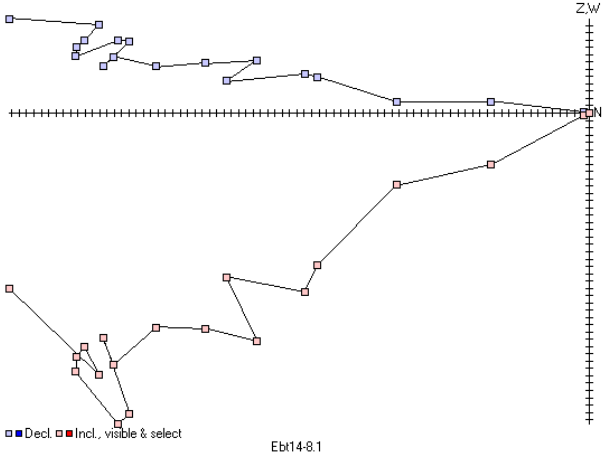
W,Z
N
Decl. Incl., visible & select
Ebt14-8.1

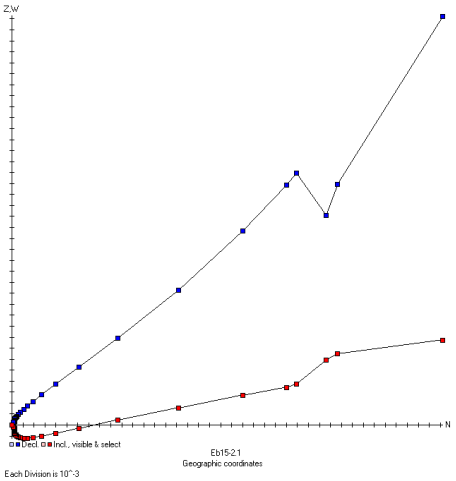
Z,W
N
Decl. Incl., visible & select
Eb15-2.1
Geographic coordinates
Each Division is 10^-3

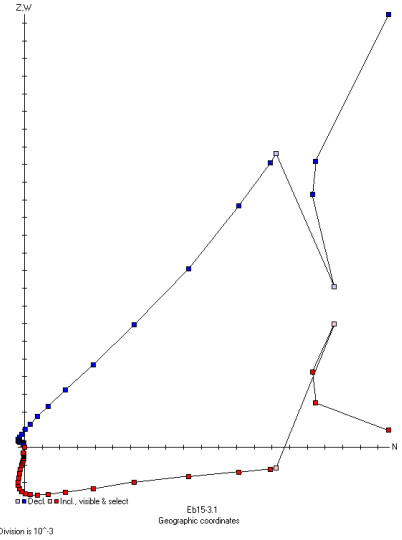
Z,W
N
Decl. Incl., visible & select
Eb15-3.1
Geographic coordinates
Each Division is 10^-3

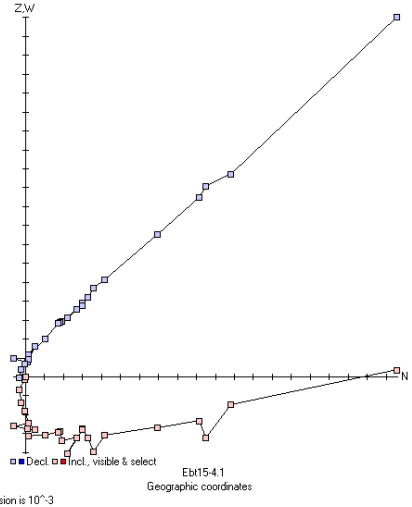
Z,W
N
Decl. Incl., visible & select
Eb15-4.1
Geographic coordinates
Each Division is 10^-3

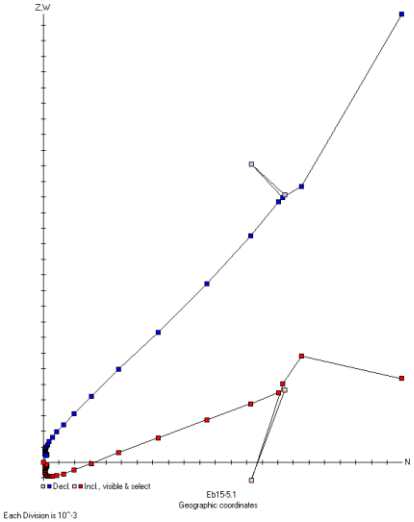
Z,W
N
Decl. Incl., visible & select
Eb15-5.1
Geographic coordinates
Each Division is 10^-3

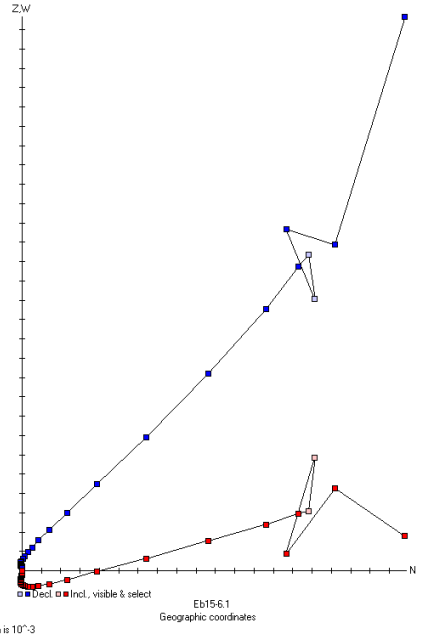
Z,W
N
Decl. Incl., visible & select
Eb15-6.1
Geographic coordinates
Each Division is 10^-3

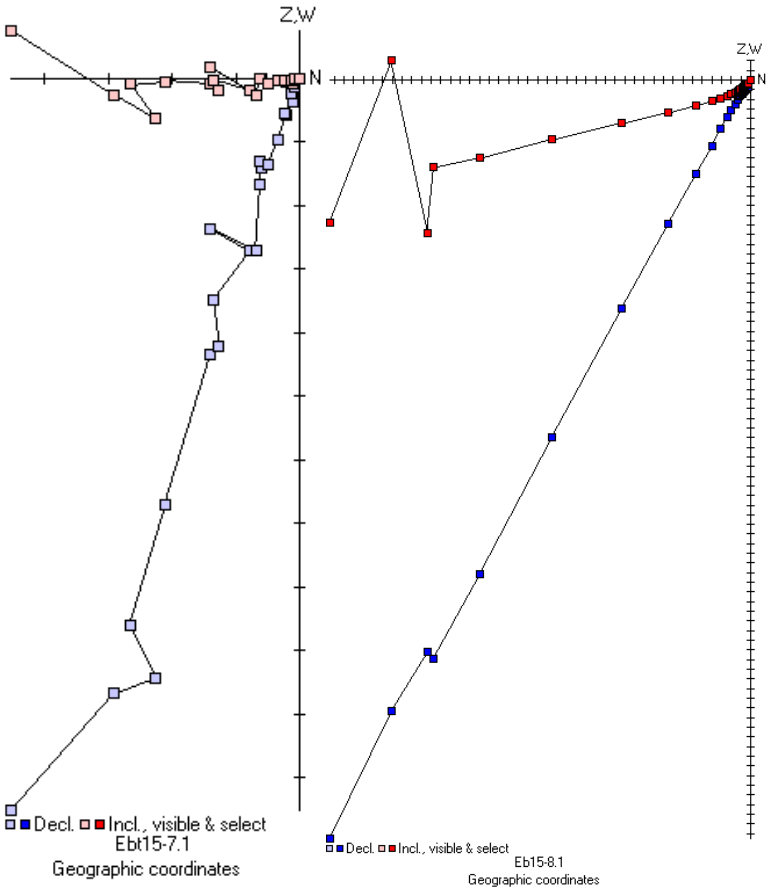
Z,W
N
Decl. Incl., visible & select
Ebt15-7.1
Geographic coordinates

Z,W
N
Decl. Incl., visible & select
Eb15-8.1
Geographic coordinates

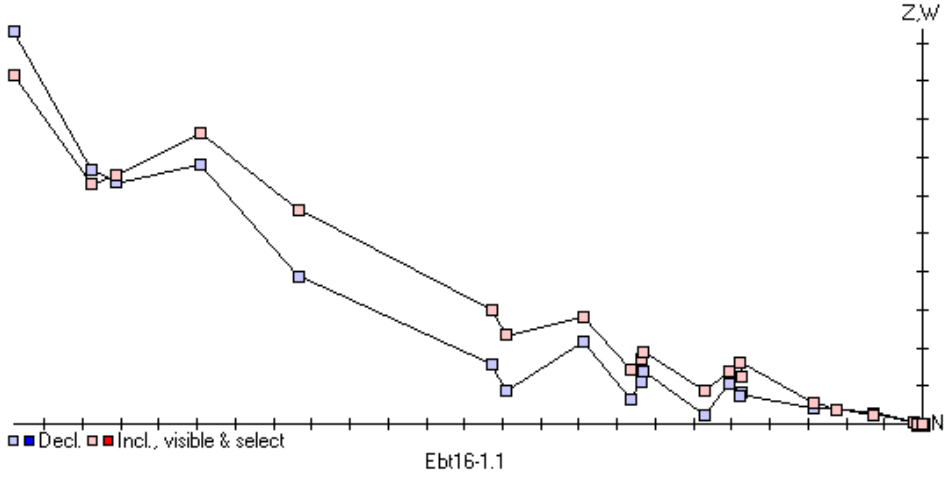
Z,W
N
Decl. Incl., visible & select
Ebt16-1.1

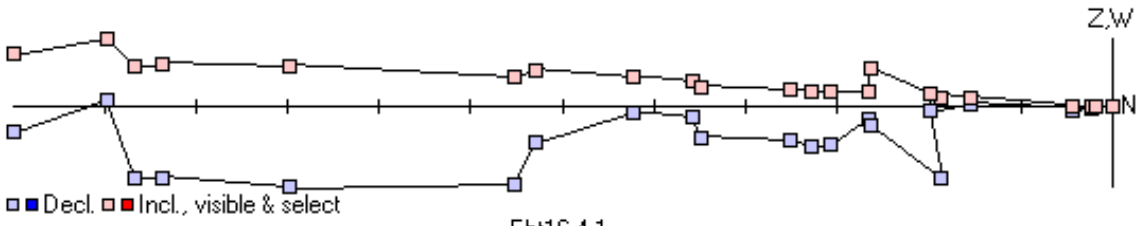

Ebt16-4.1
Geographic coordinates

Each Division is 10^-2

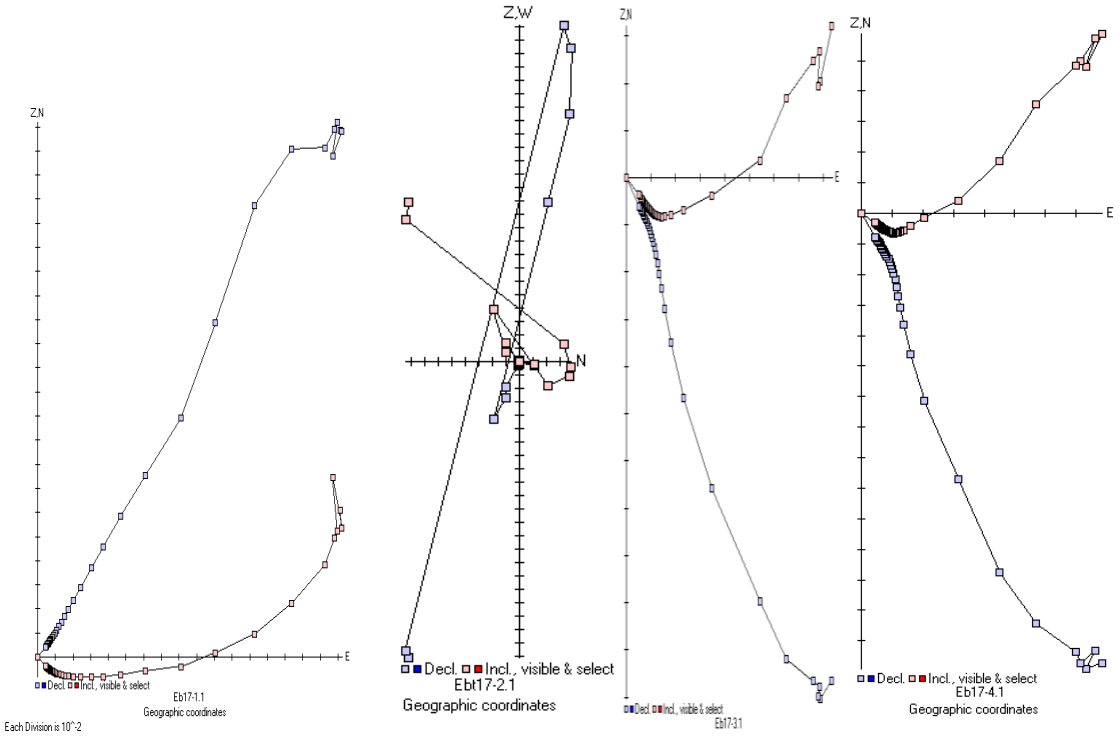
Z,N
E
Decl. Incl., visible & select
Eb17-1.1
Geographic coordinates
Each Division is 10^-2
Z,W
N
Decl. Incl., visible & select
Ebt17-2.1
Geographic coordinates
Z,N
E
Ebt17-3.1
Z,N
E
Decl. Incl., visible & select
Eb17-4.1
Geographic coordinates

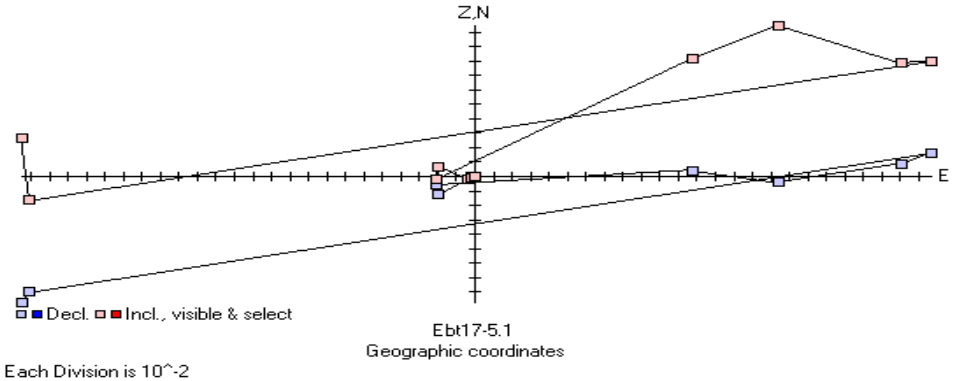
Z,N
E
Decl. Incl., visible & select
Ebt17-5.1
Geographic coordinates
Each Division is 10^-2

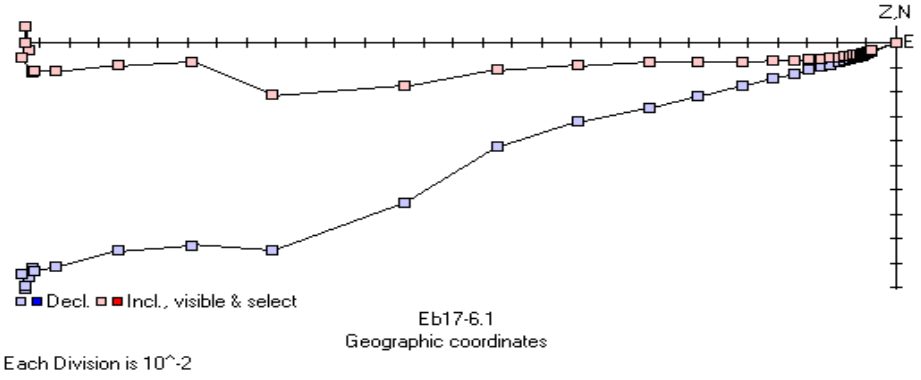
Z,N
E
Decl. Incl., visible & select
Eb17-6.1
Geographic coordinates
Each Division is 10^-2

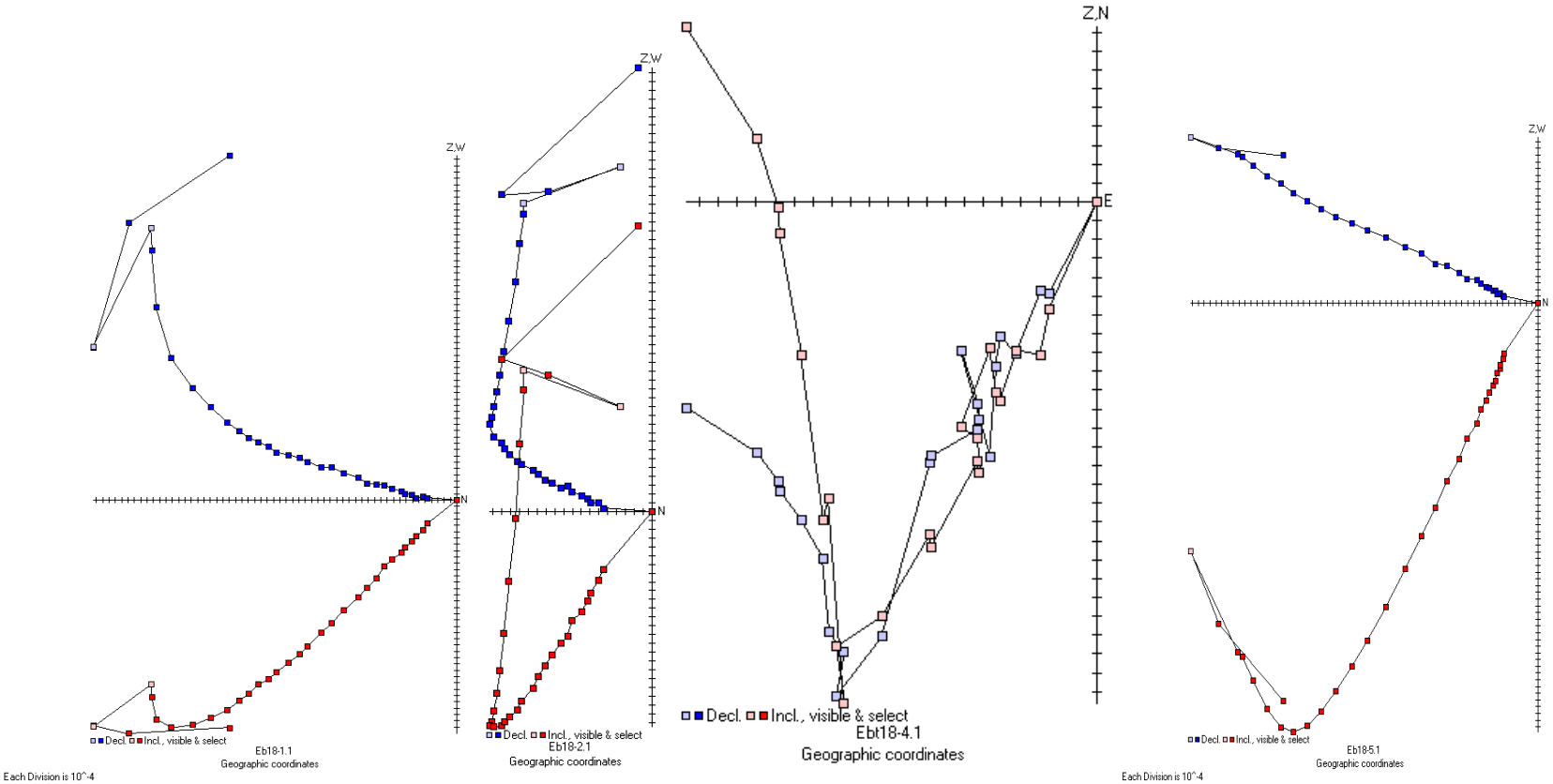
Z,W
N
Decl. Incl., visible & select
Eb18-1.1
Geographic coordinates
Each Division is 10^-4
Z,W
N
Decl. Incl., visible & select
Eb18-2.1
Geographic coordinates
Z,N
E
Decl. Incl., visible & select
Ebt18-4.1
Geographic coordinates
Z,W
N
Decl. Incl., visible & select
Eb18-5.1
Geographic coordinates
Each Division is 10^-4

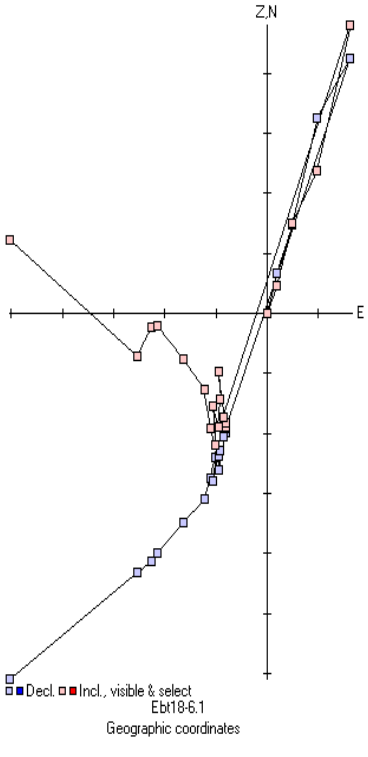
Z,N
E
Decl. Incl., visible & select
Ebt18-6.1
Geographic coordinates

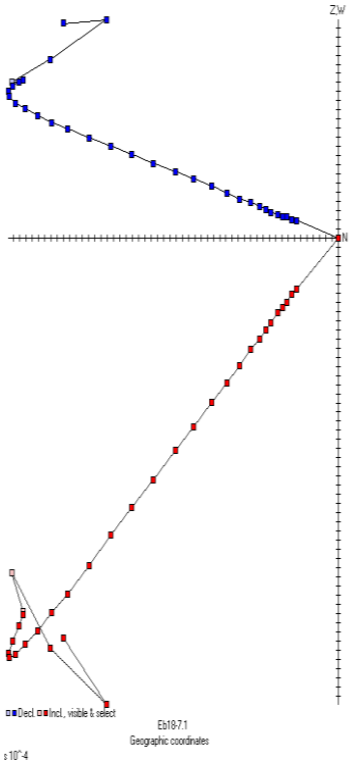
Z,W
N
Decl. Incl., visible & select
Ebt18-7.1
Geographic coordinates
s 10^-4

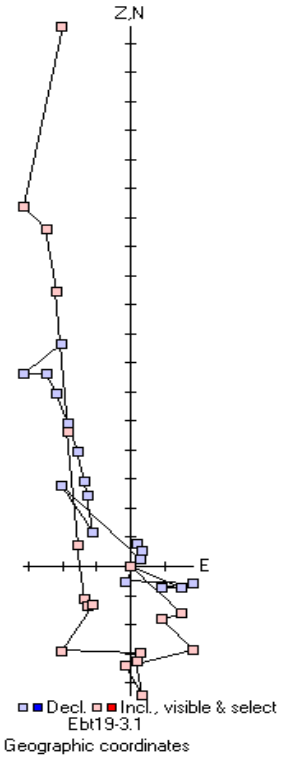
Z,N
E
N
Decl. Incl., visible & select
Ebt19-3.1
Geographic coordinates

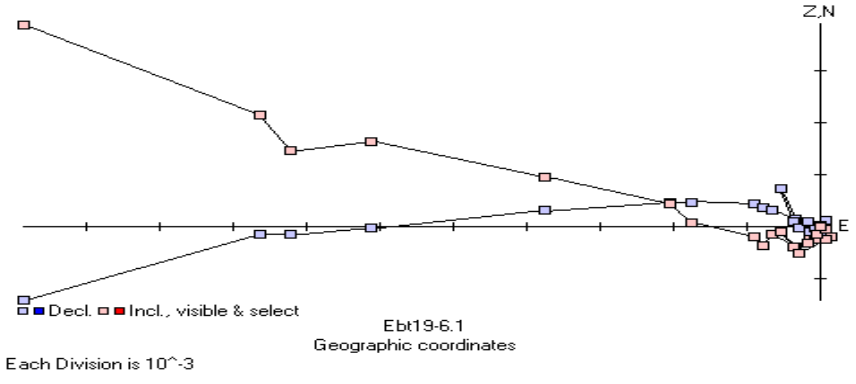
Z,N
E
Decl. Incl., visible & select
Ebt19-6.1
Geographic coordinates
Each Division is 10^-3

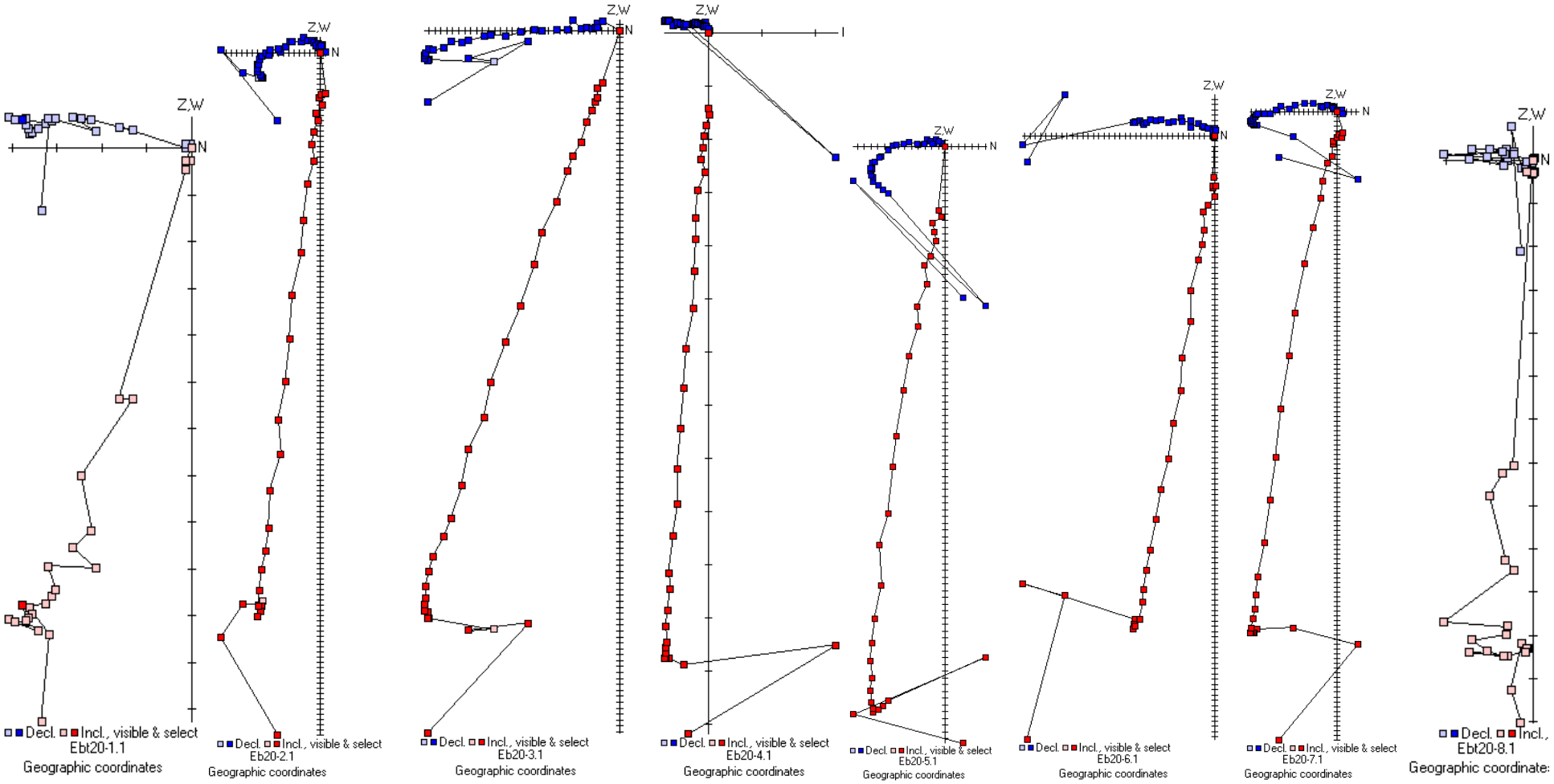
Z,W
N
Decl.
Incl., visible & select
Ebt20-1.1
Geographic coordinates
Eb20-2.1
Eb20-3.1
Eb20-4.1
Eb20-5.1
Eb20-6.1
Eb20-7.1
Ebt20-8.1

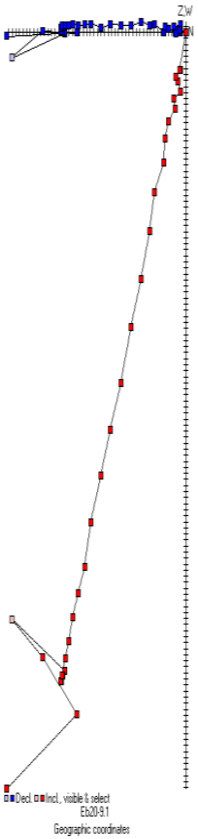
Z,W
Decl. Incl., visible & select
Eb20-9.1
Geographic coordinates

12.3 Canobolas

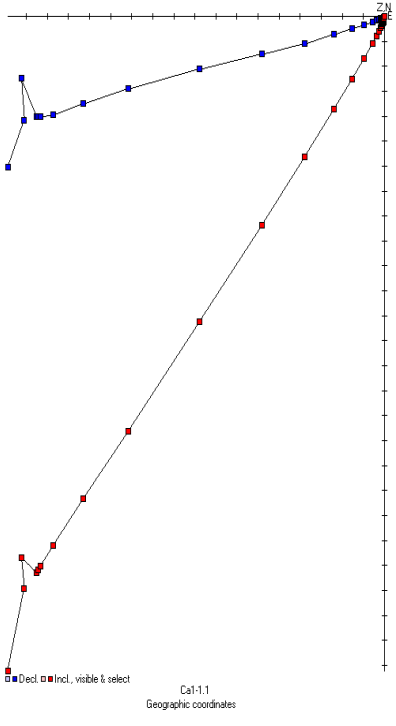

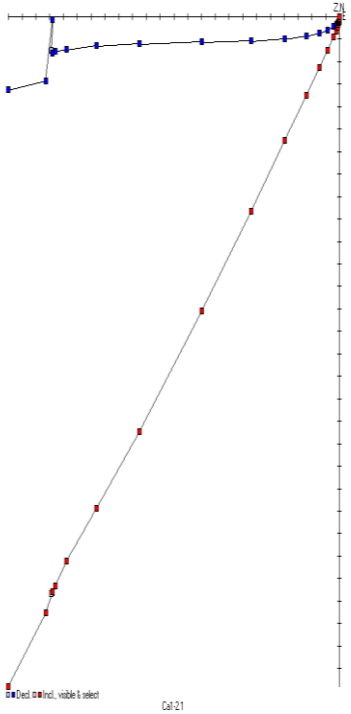

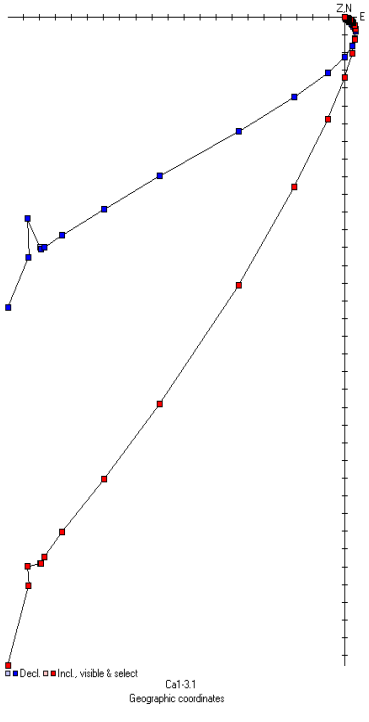

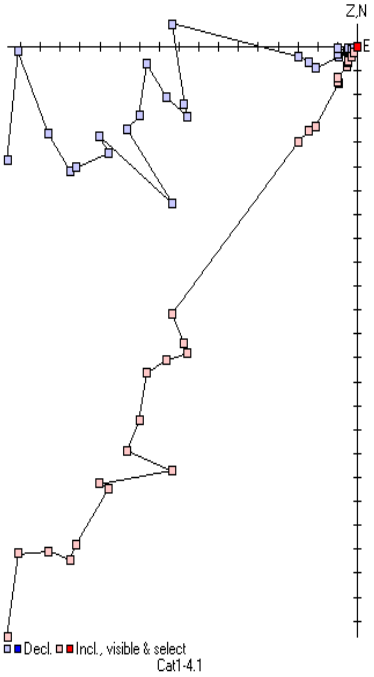

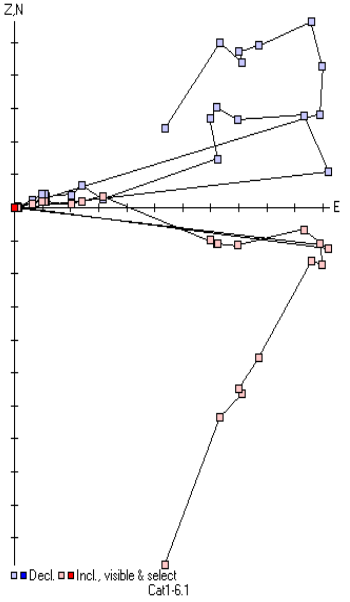

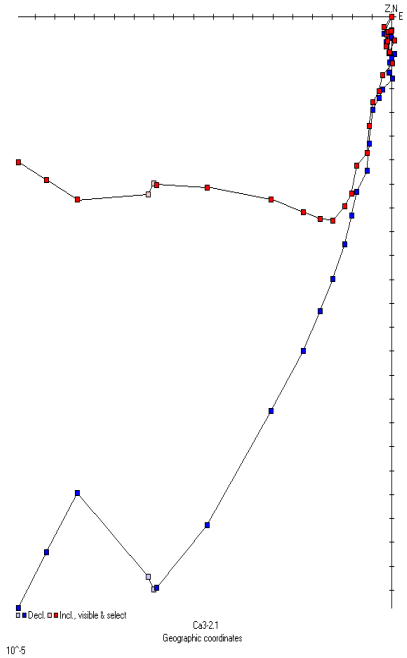
Z,N
E
Decl. Incl., visible & select
Ca3-2.1
Geographic coordinates
10^-5

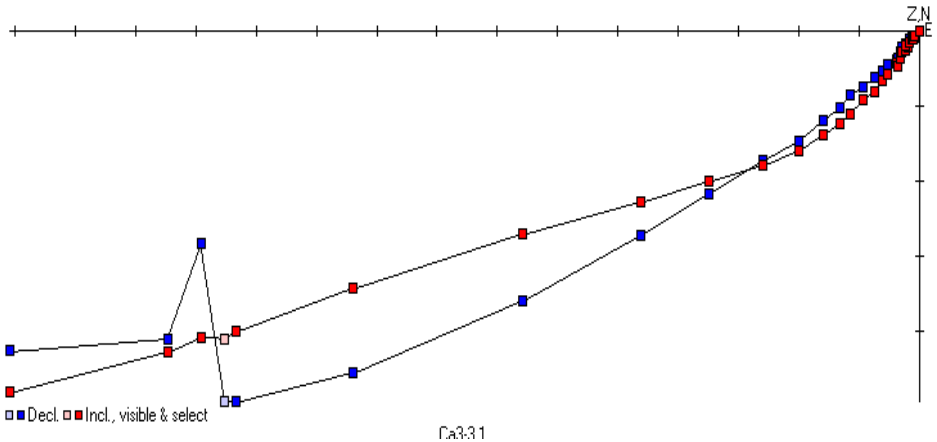
Z,N
E
Decl. Incl., visible & select
Ca3-3.1

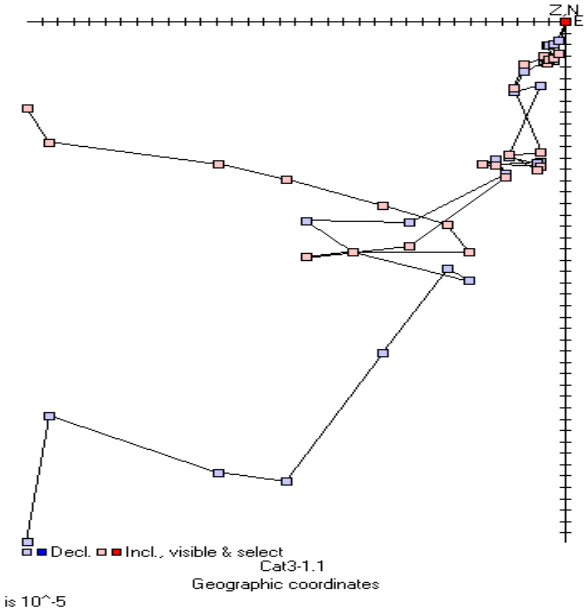
Z,N
E
Decl. Incl., visible & select
Cat3-1.1
Geographic coordinates
is 10^-5

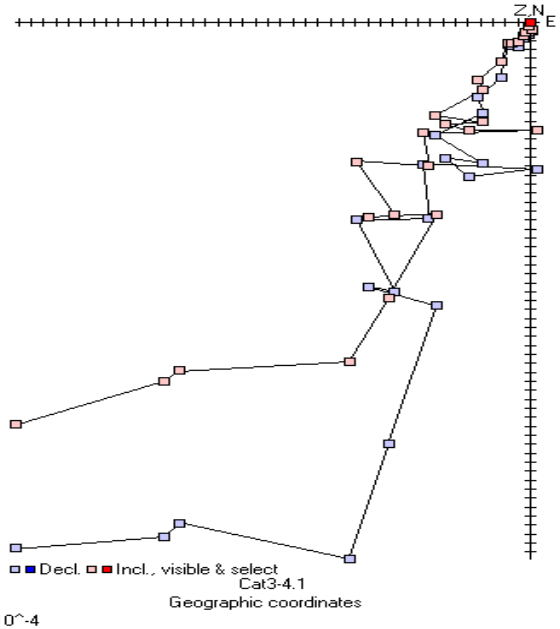

is 10^-4

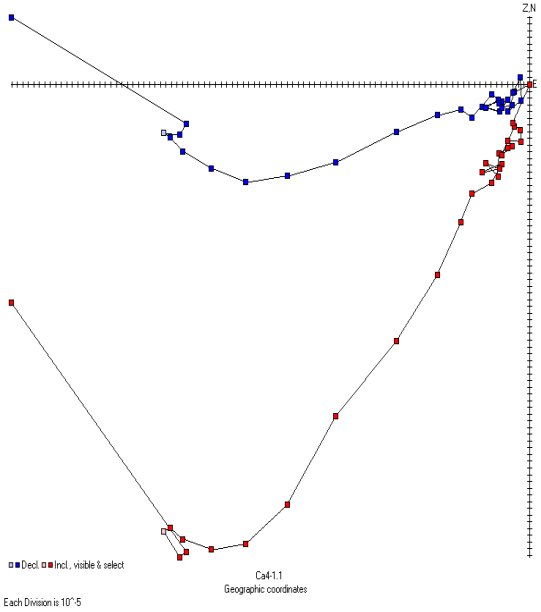

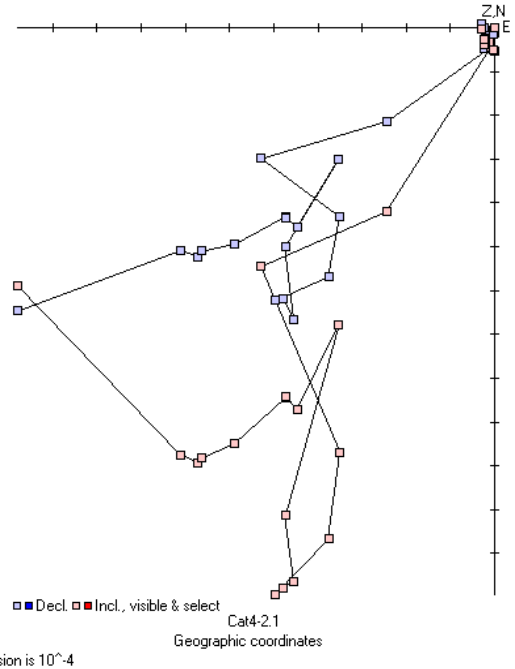

Each Division is 10^-4

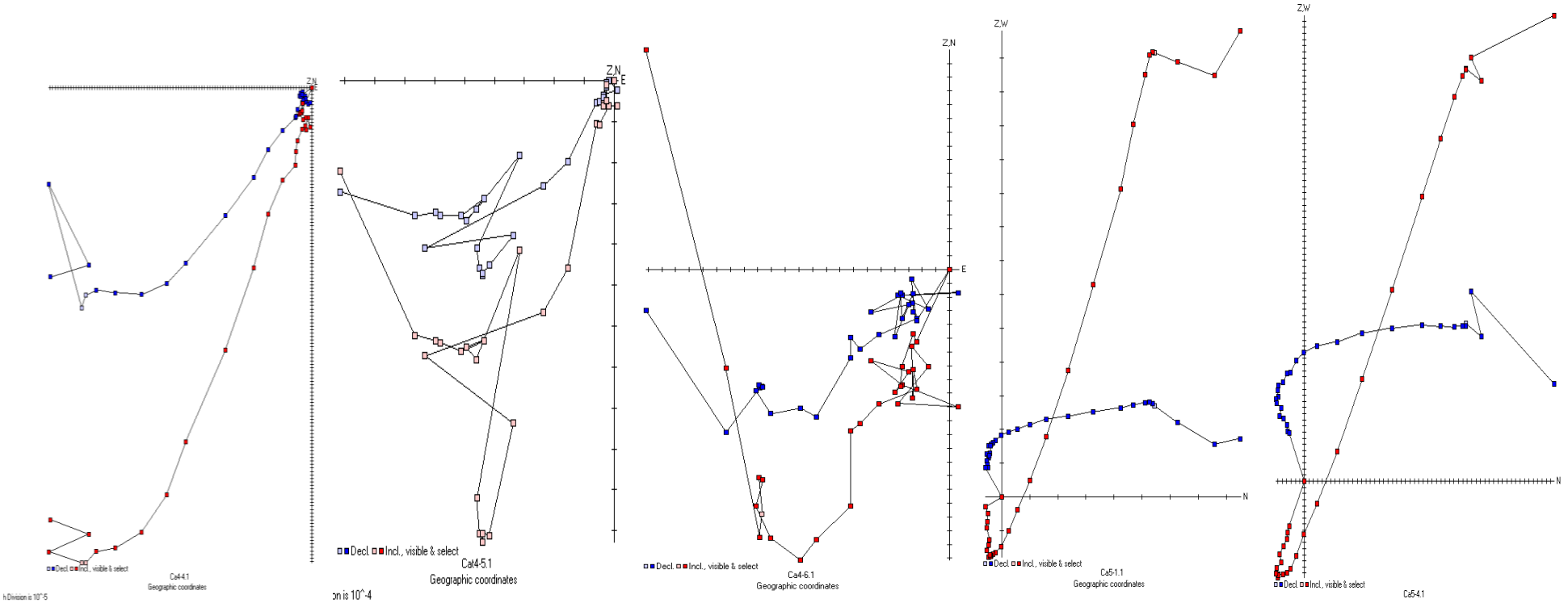
Z,N
E
Decl. Incl., visible & select
Ca4-4.1
Geographic coordinates
Z,N
E
Decl. Incl., visible & select
Cat4-5.1
Geographic coordinates
Z,N
E
Decl. Incl., visible & select
Ca4-6.1
Geographic coordinates
Z,W
N
Decl. Incl., visible & select
Ca5-1.1
Geographic coordinates
Z,W
N
Decl. Incl., visible & select
Ca5-4.1

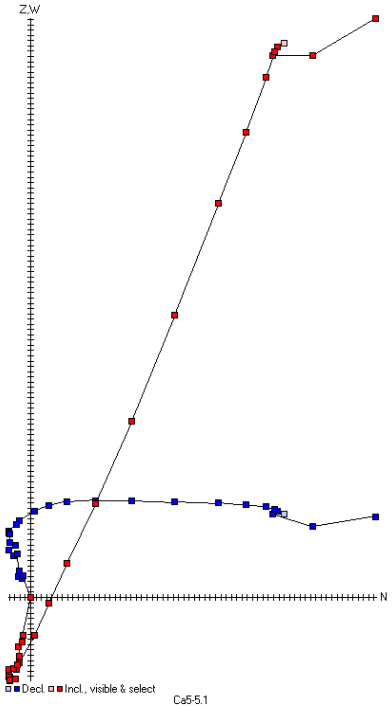
Z,W
N
Decl.
Incl., visible & select
Ca5-5.1

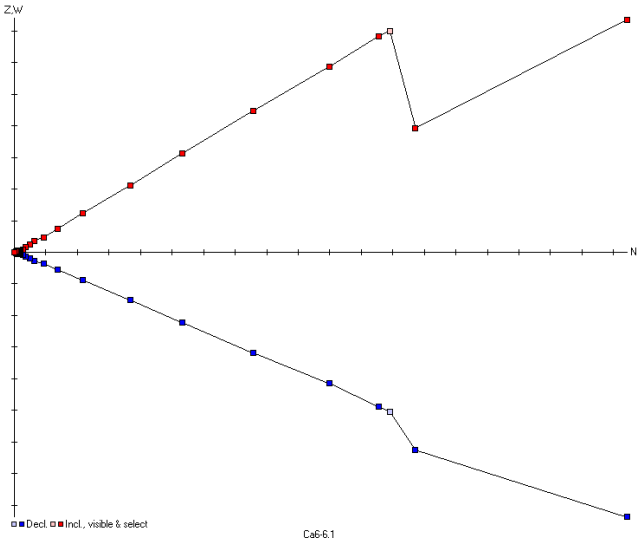
Z,W
N
Decl.
Incl., visible & select
Ca6-6.1

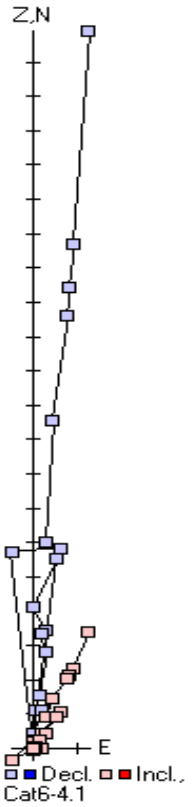
Z,N
E
Decl.
Incl.,
Cat6-4.1

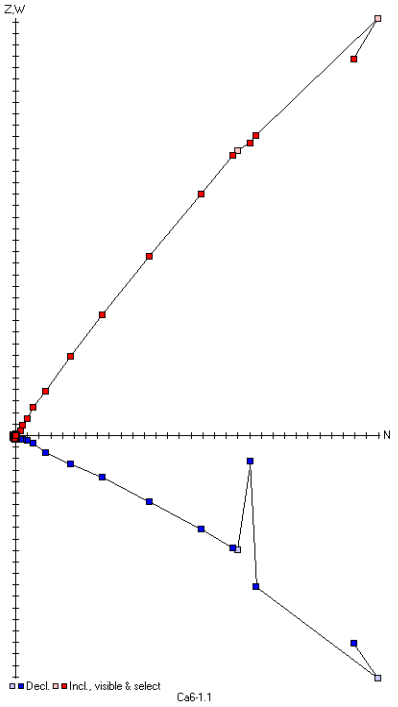
Z,W
N
Decl.
Incl., visible & select
Ca6-1.1

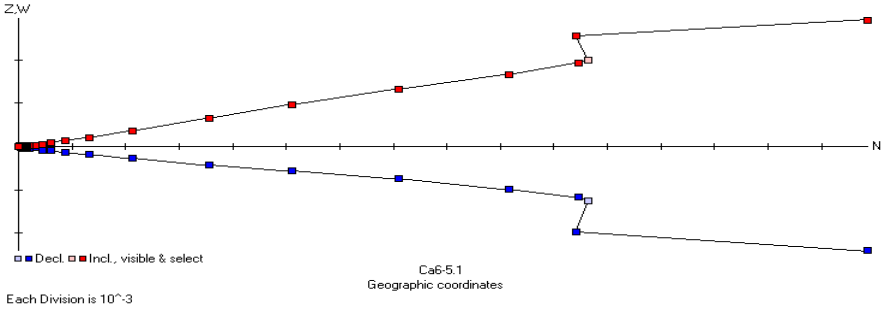
Z,W
N
Decl. Incl., visible & select
Each Division is 10^-3
Ca6-5.1
Geographic coordinates

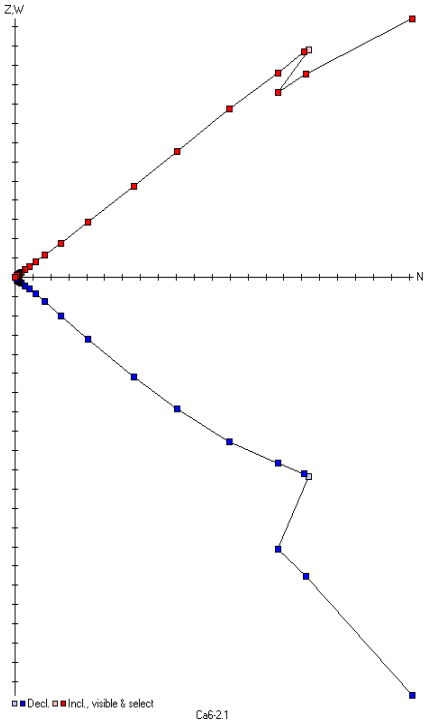
Z,W
N
Decl. Incl., visible & select
Ca6-2.1

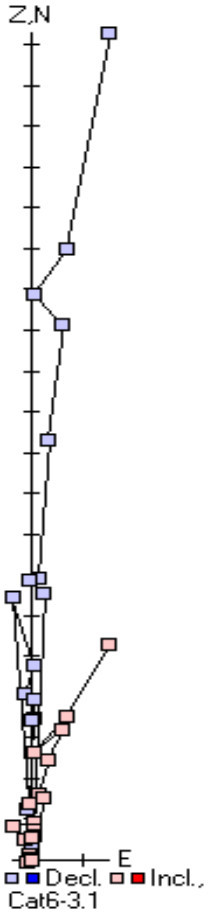
Z,N
E
Decl. Incl.,
Cat6-3.1

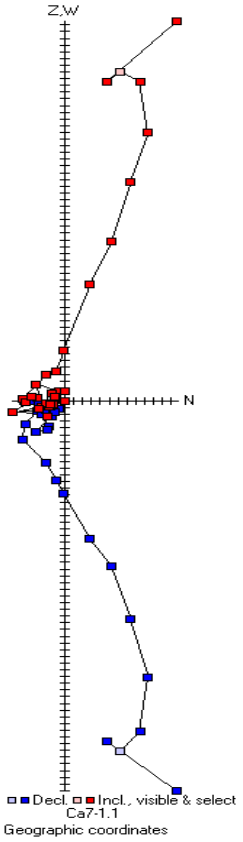
Z,W
N
Decl. Incl., visible & select
Ca7-1.1
Geographic coordinates

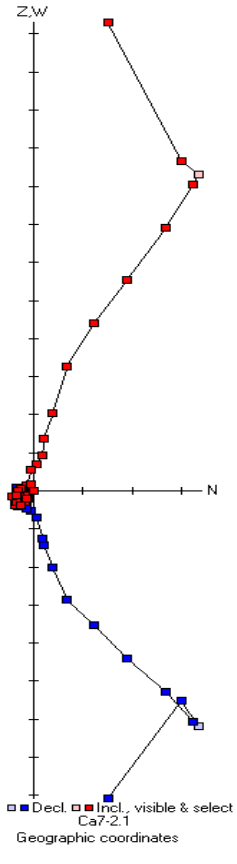
Z,W
N
Decl. Incl., visible & select
Ca7-2.1
Geographic coordinates

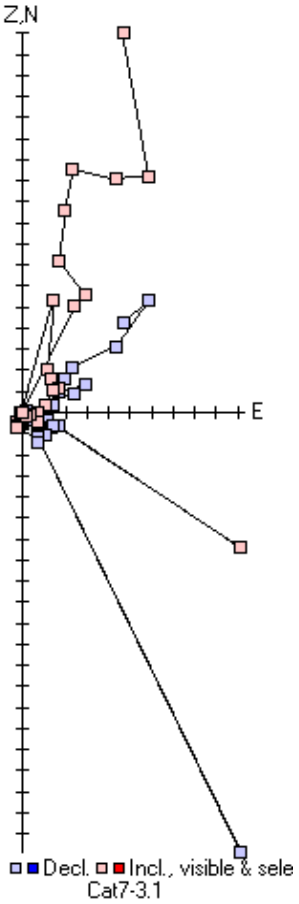
Z,N
E
Decl. Incl., visible & sele
Cat7-3.1

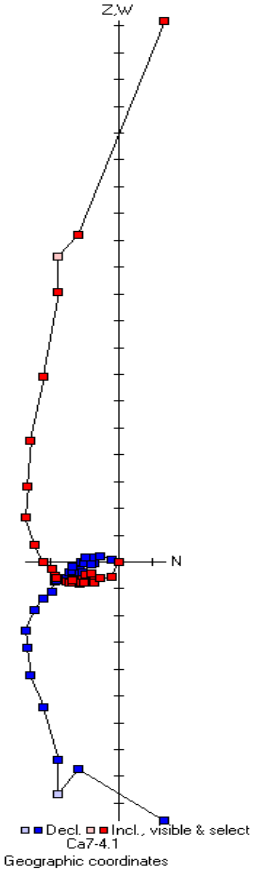
Z,W
N
Decl. Incl., visible & select
Ca7-4.1
Geographic coordinates

s 10^-5

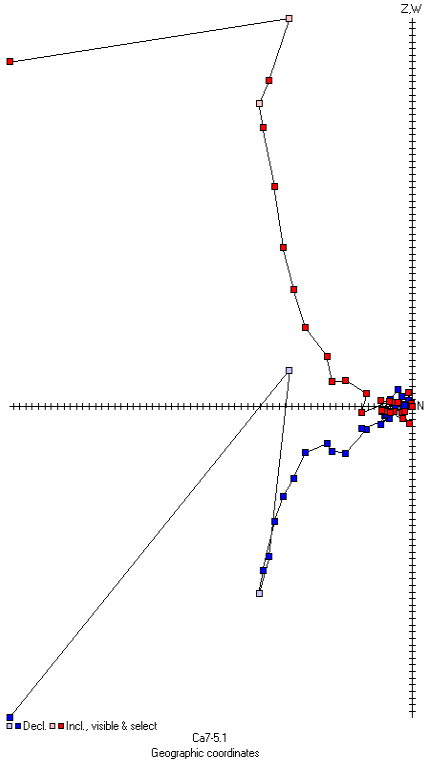
Z,W
N
Decl. Incl., visible & select
Ca7-5.1
Geographic coordinates

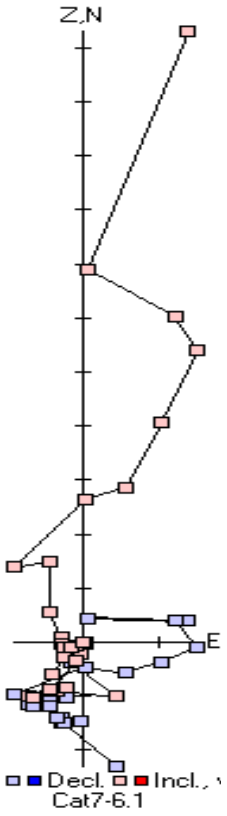
Z,N
E
Decl. Incl.,
Cat7-6.1

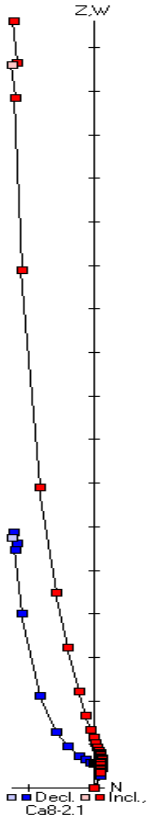
Z,W
N
Decl. Incl.,
Ca8-2.1

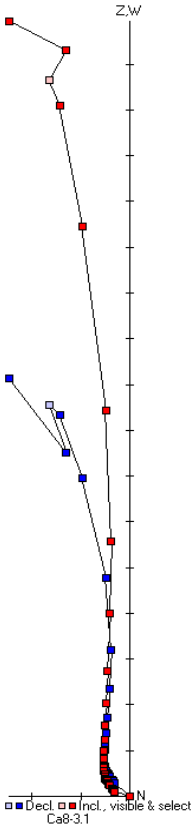

Ca8-3.1

Each Division is 10^-4

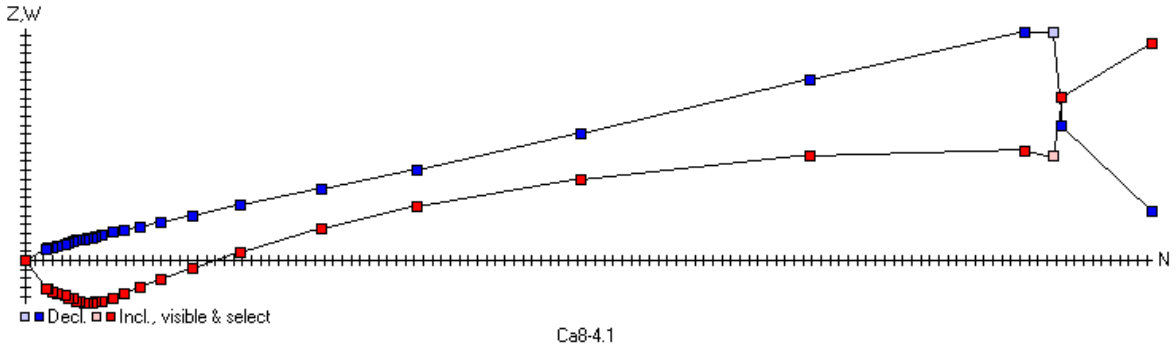

Ca8-4.1
Geographic coordinates

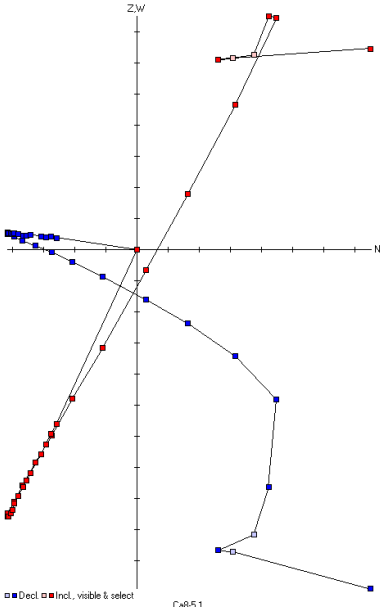

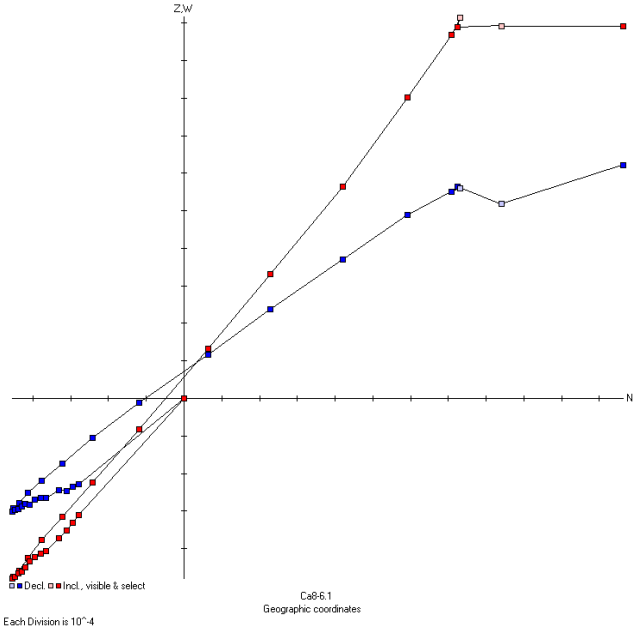

Ca8-6.1
Geographic coordinates
Each Division is 10^-4

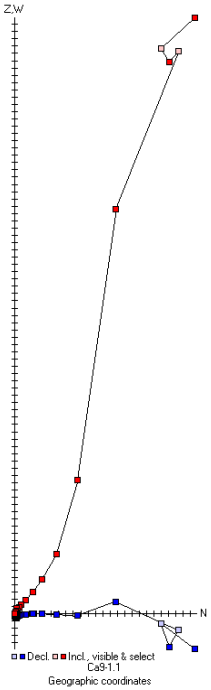

Ca9-1.1
Geographic coordinates

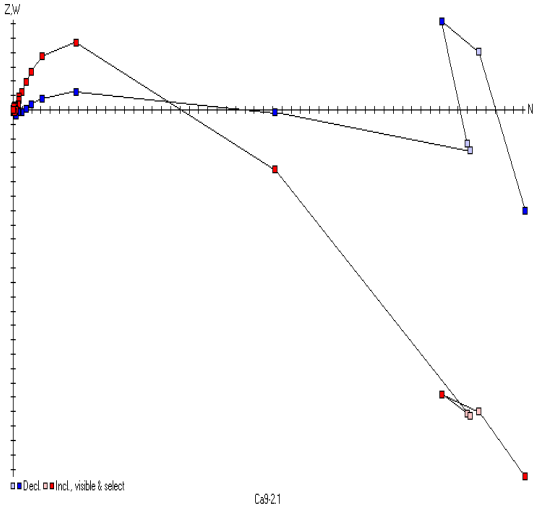

Ca9-2.1
Geographic coordinates
Each Division is 10^-5

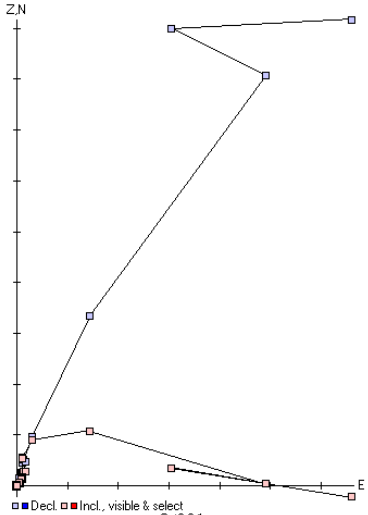

Cat9-3.1
Geographic coordinates
: 10^-4

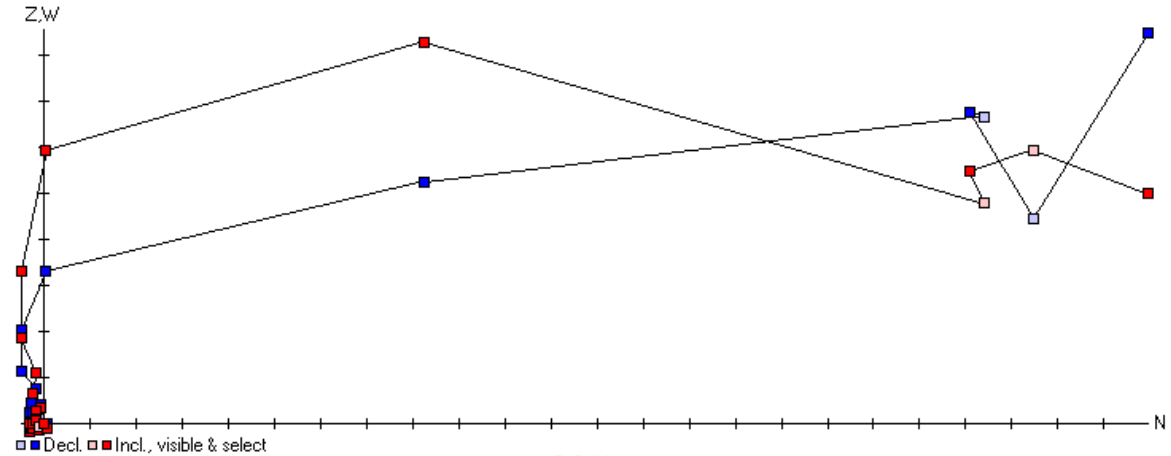

Ca9-4.1
Geographic coordinates

Each Division is 10^-5

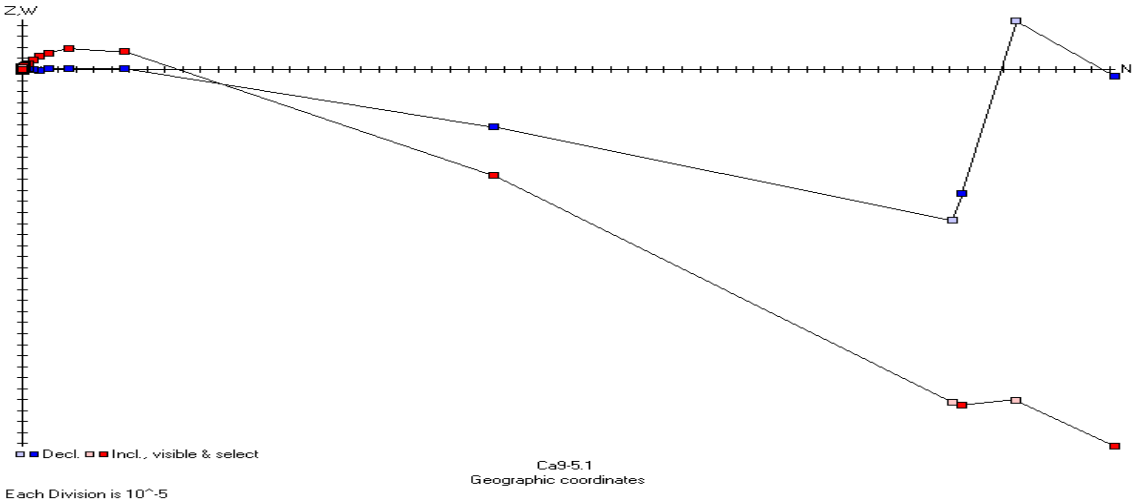

Ca9-5.1
Geographic coordinates

Each Division is 10^-5

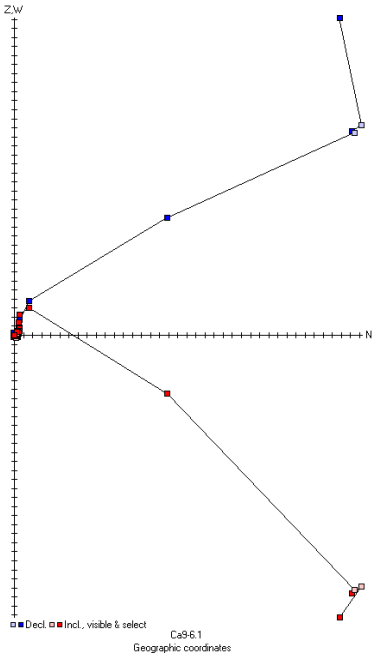

Ca9-6.1
Geographic coordinates

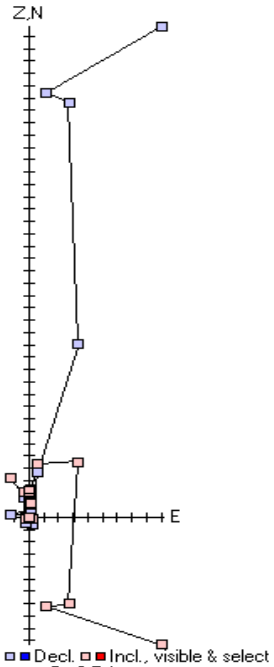

Cat9-7.1

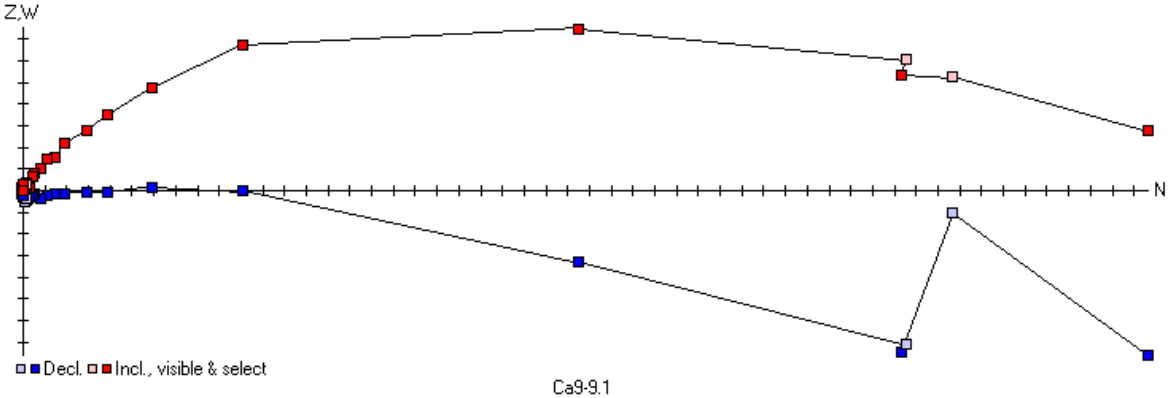

Ca9-9.1
Geographic coordinates

Each Division is 10^-5

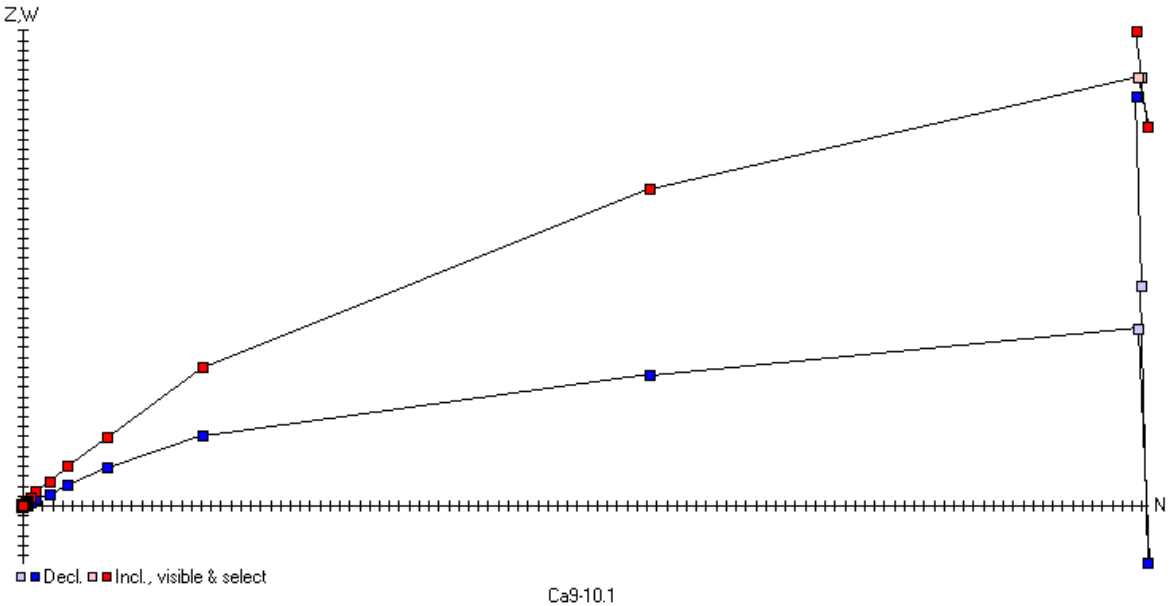

Ca9-10.1
Geographic coordinates

Each Division is 10^-5

12.4 Springsure

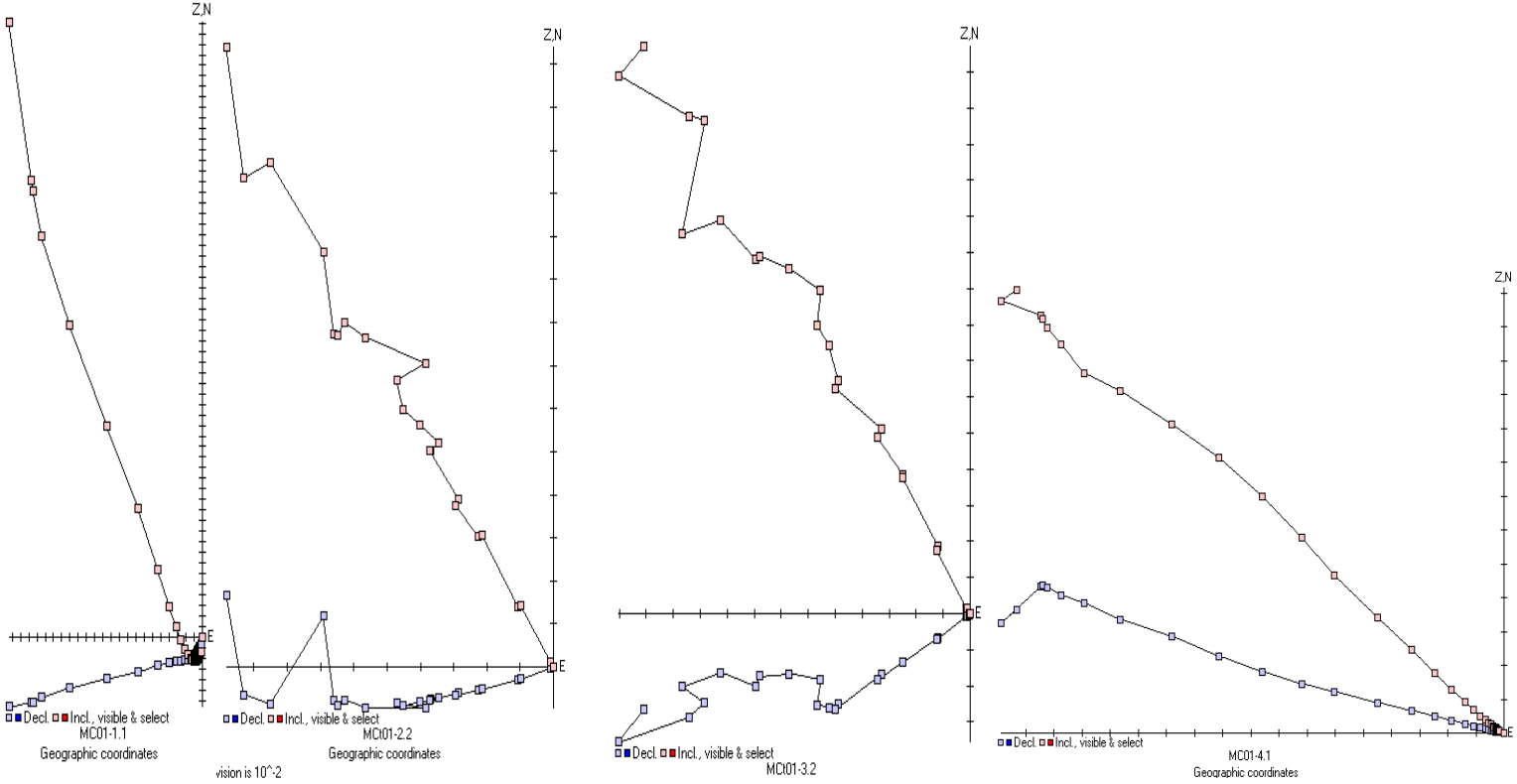

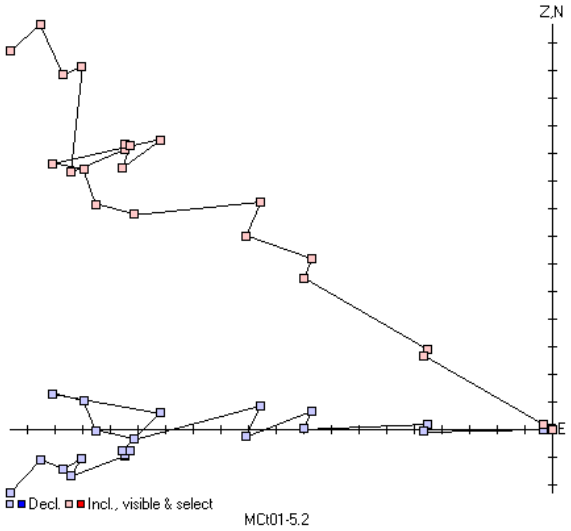

MCt01-5.2

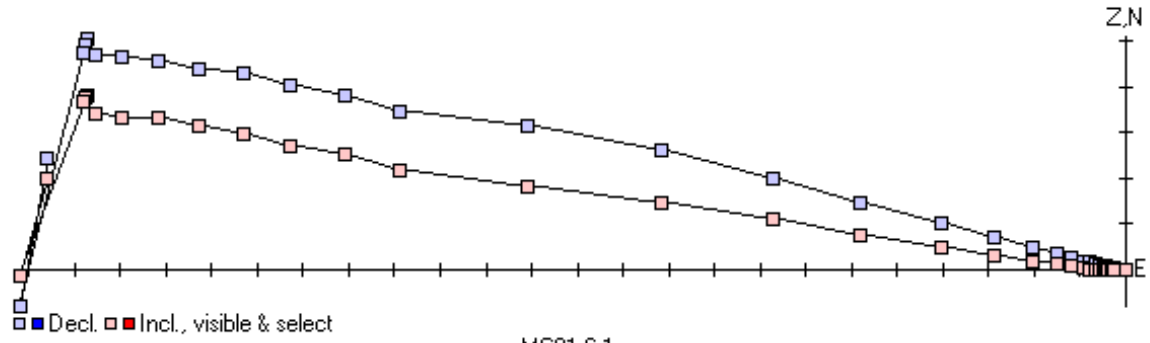

MC01-6.1
Geographic coordinates

Each Division is 10^-2

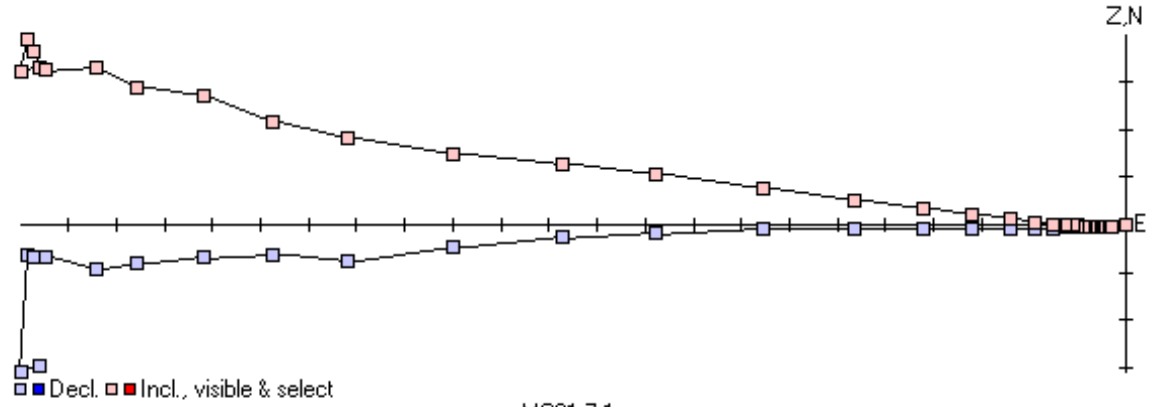

MC01-7.1
Geographic coordinates

Each Division is 10^-2

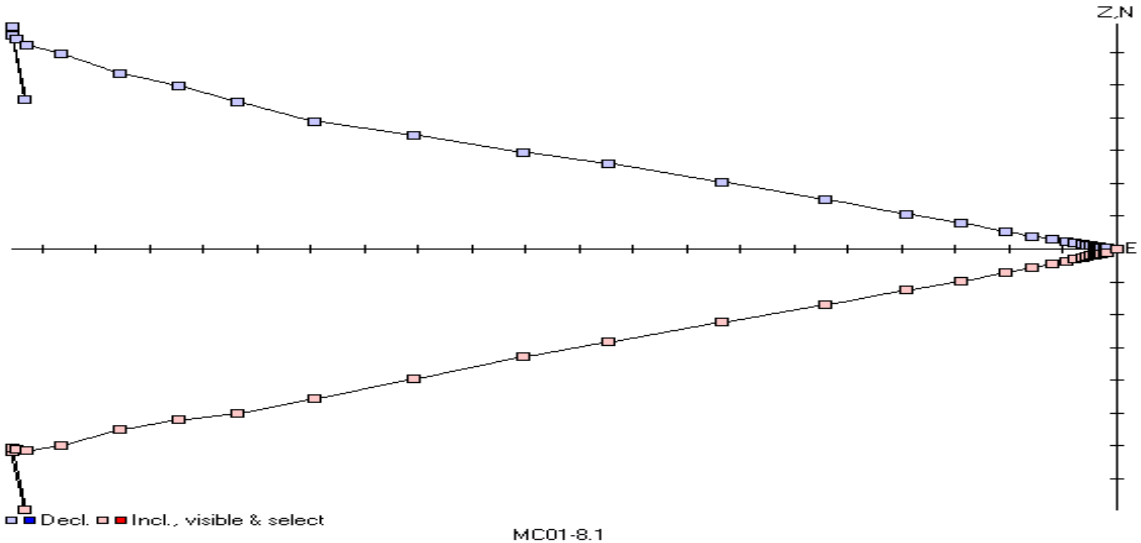

MC01-8.1

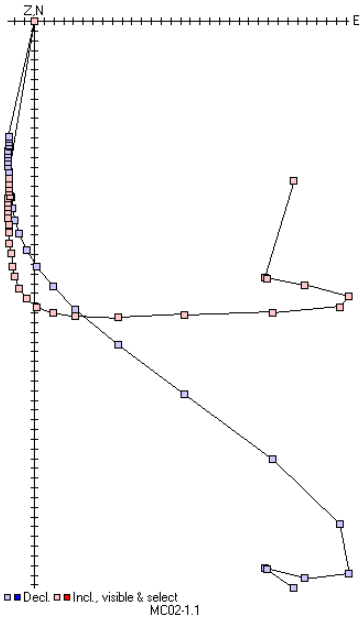

MC02-1.1

Geographic coordinates

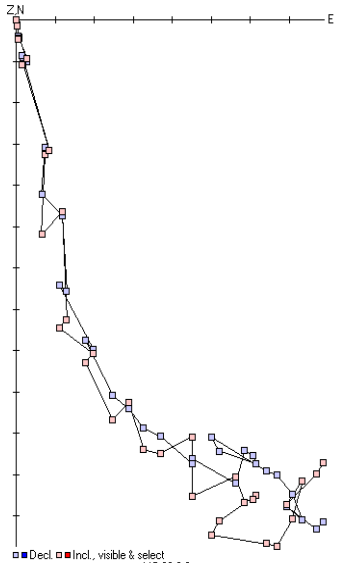

MC02-2.2

Geographic coordinates

Each Division is 10^-3

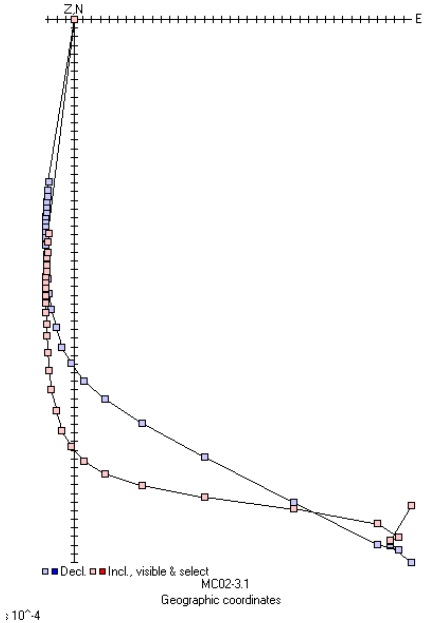

; 10^-4

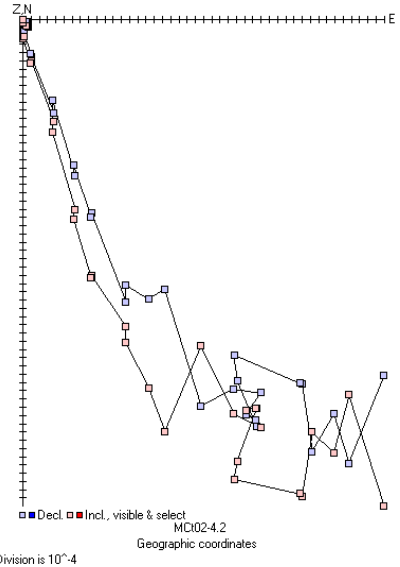

Each Division is 10^-4

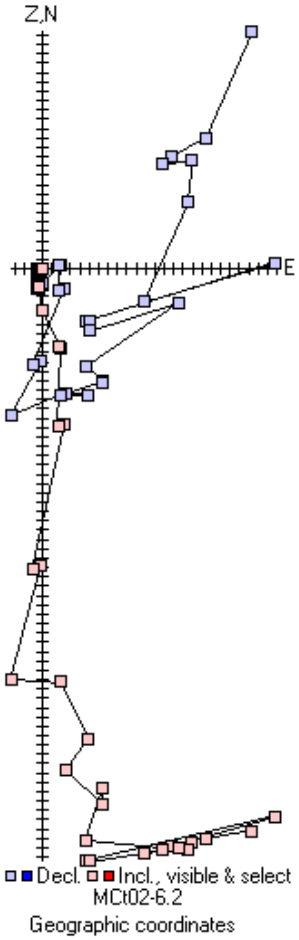

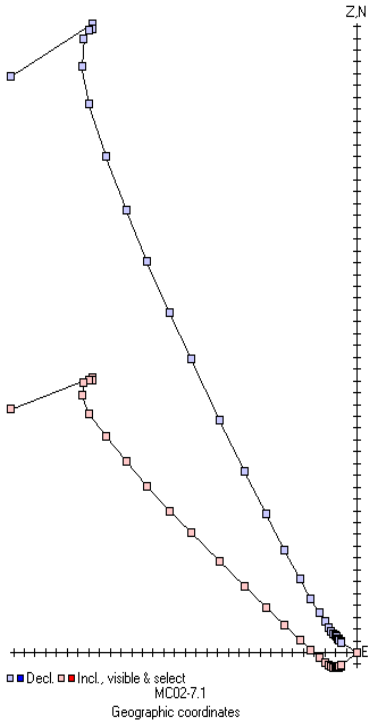

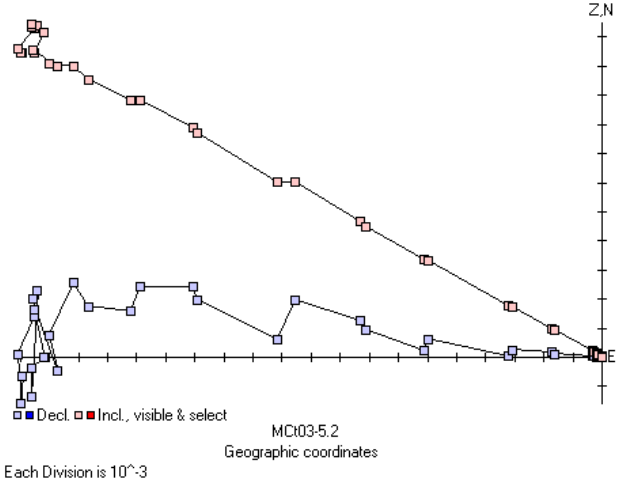
Z,N
E
Decl. Incl., visible & select
MCt03-5.2
Geographic coordinates
Each Division is 10^-3

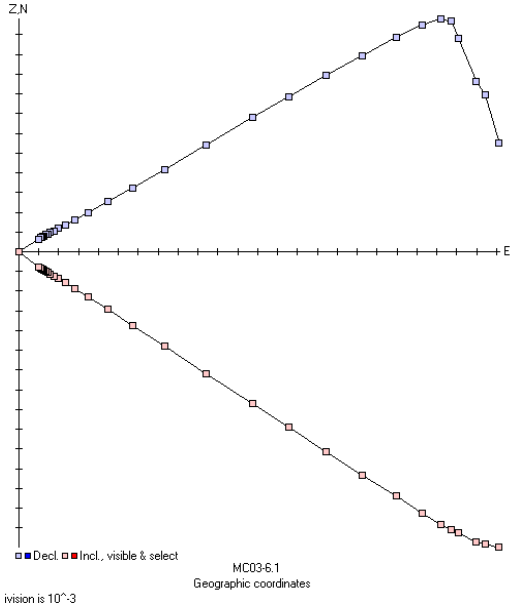
Z,N
E
Decl. Incl., visible & select
MC03-6.1
Geographic coordinates
ivision is 10^-3

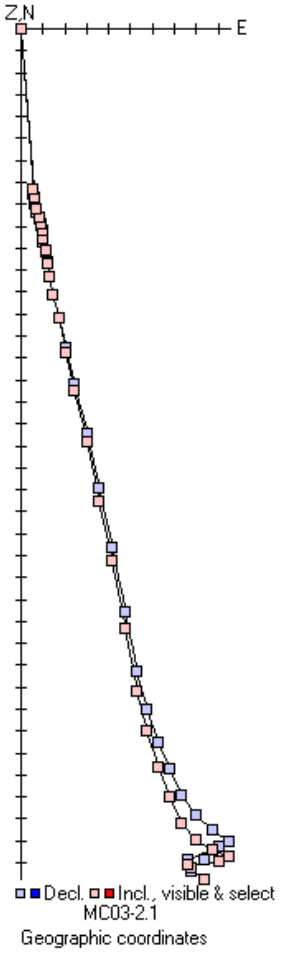
Z,N
E
Decl. Incl., visible & select
MC03-2.1
Geographic coordinates

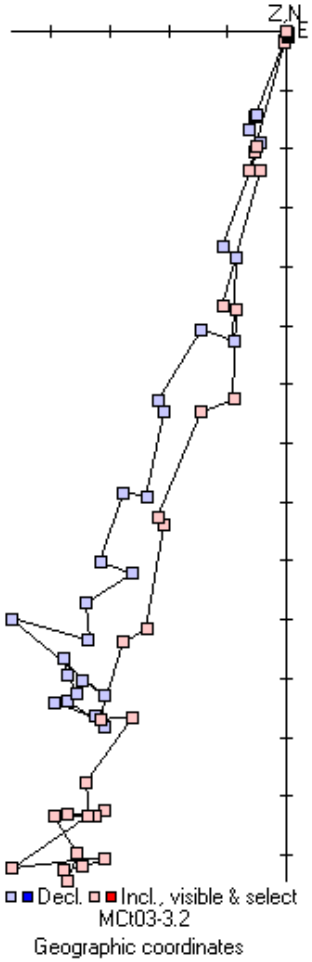
Z,N
E
Decl. Incl., visible & select
MCt03-3.2
Geographic coordinates

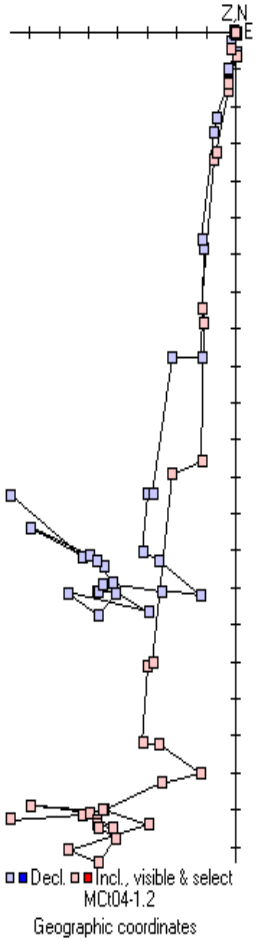

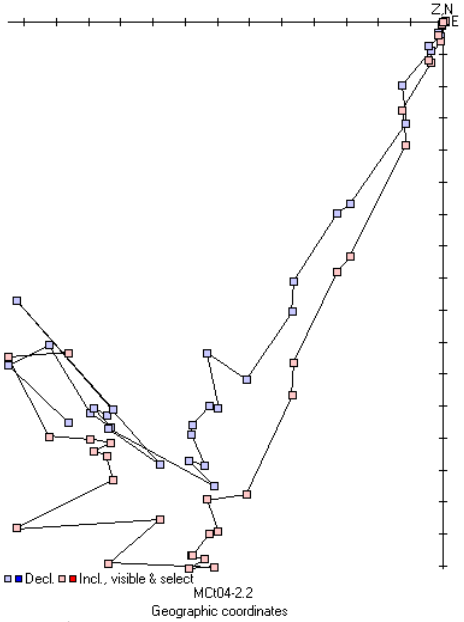

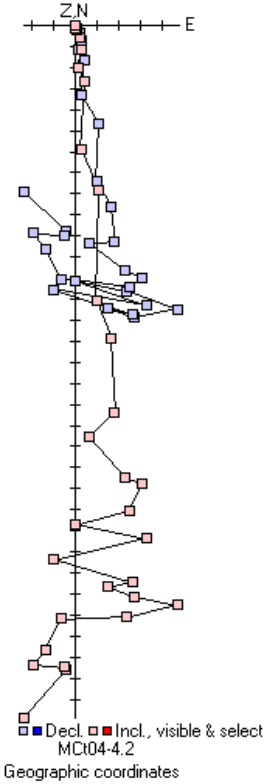

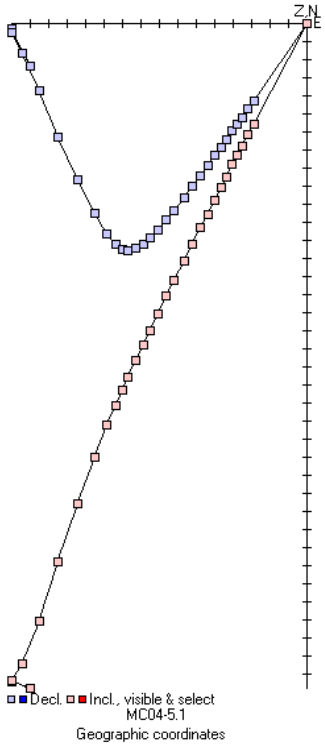

10^-4

Each Division is 10^-4

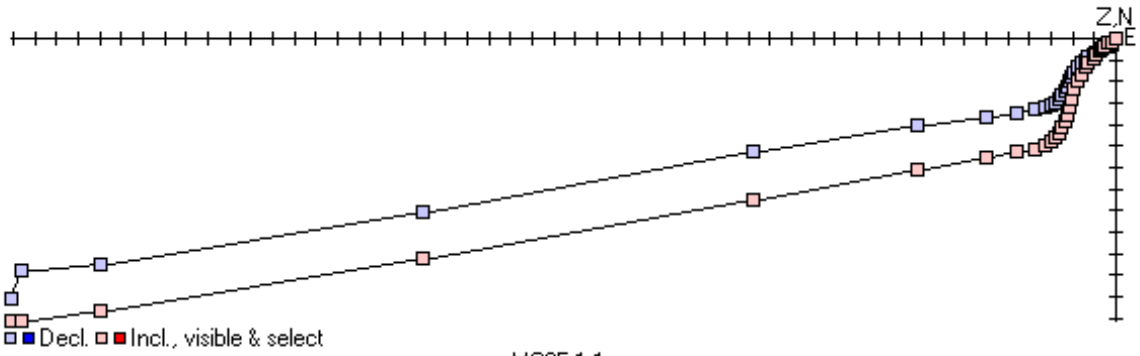

MC05-1.1
Geographic coordinates

Each Division is 10^-3

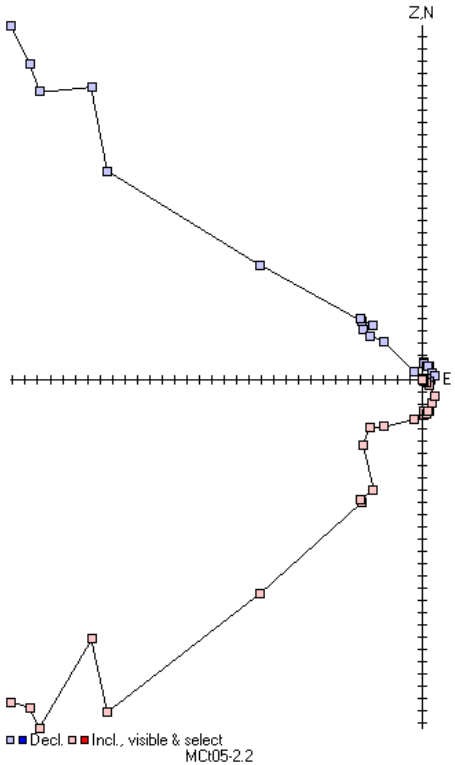

MCt05-2.2
Geographic coordinates

vision is 10^-3

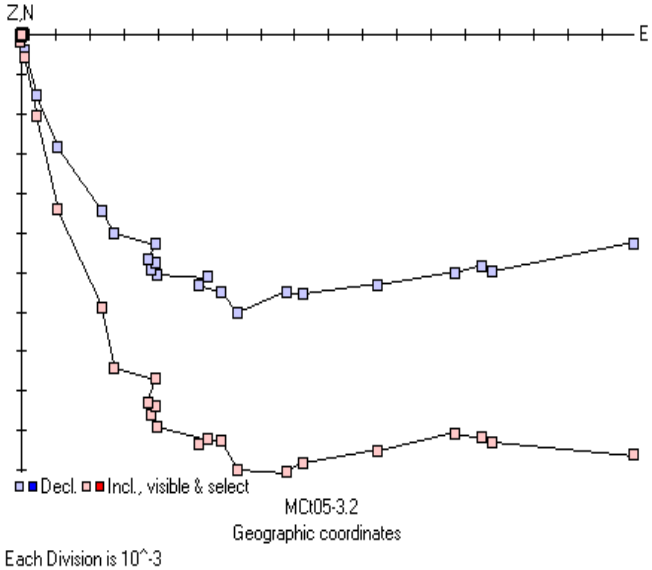
Z,N
E
Decl.
Incl., visible & select
MCt05-3.2
Geographic coordinates
Each Division is 10^-3

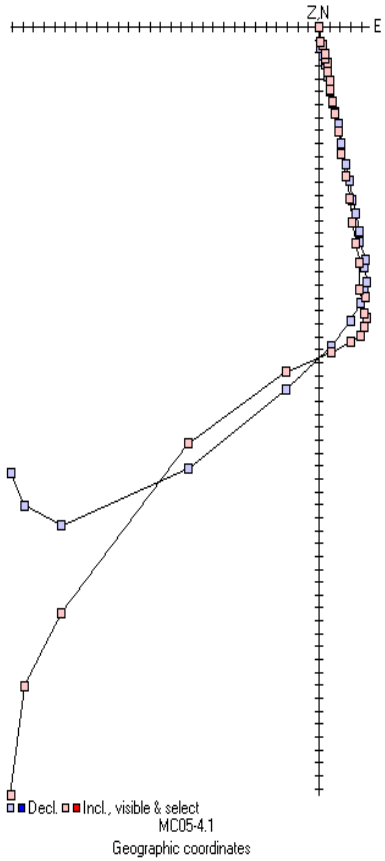
Z,N
E
Decl.
Incl., visible & select
MC05-4.1
Geographic coordinates

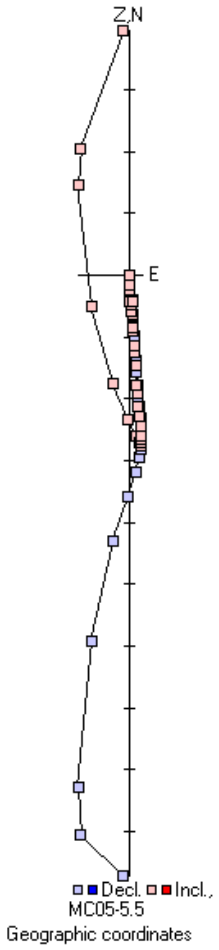
Z,N
E
Decl.
Incl.,
MC05-5.5
Geographic coordinates

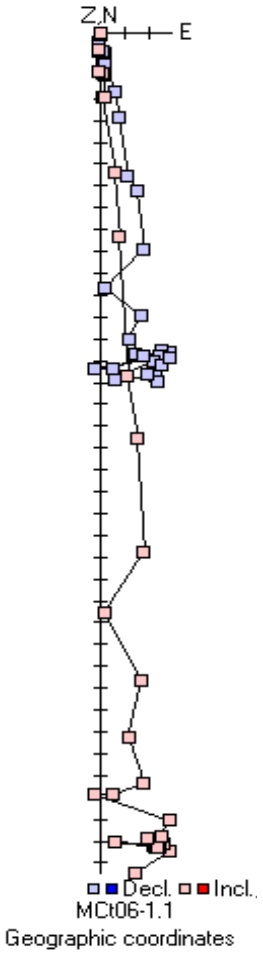
Z,N
E
Decl.
Incl.,
MCt06-1.1
Geographic coordinates

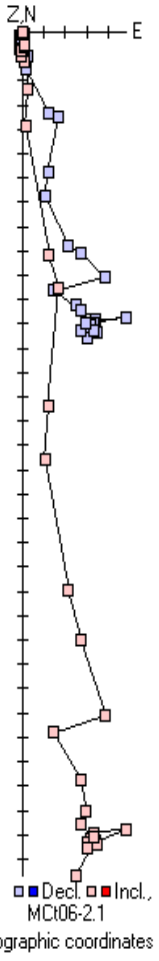
Z,N
E
Decl.
Incl.,
MCt06-2.1
Geographic coordinates

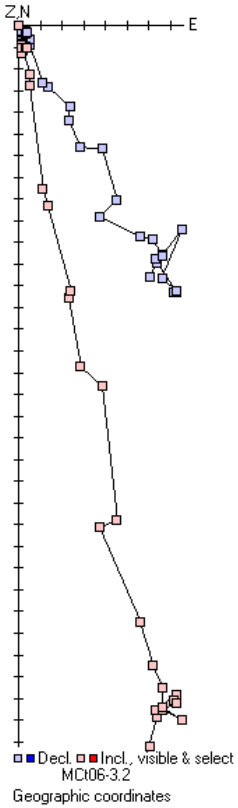

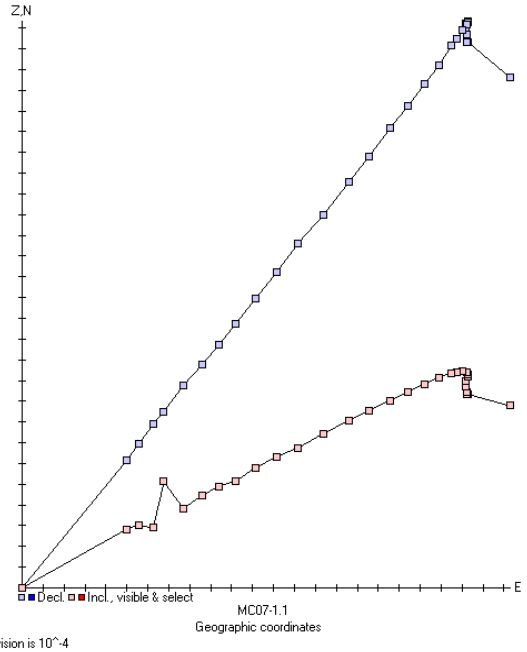

Each Division is 10^-4

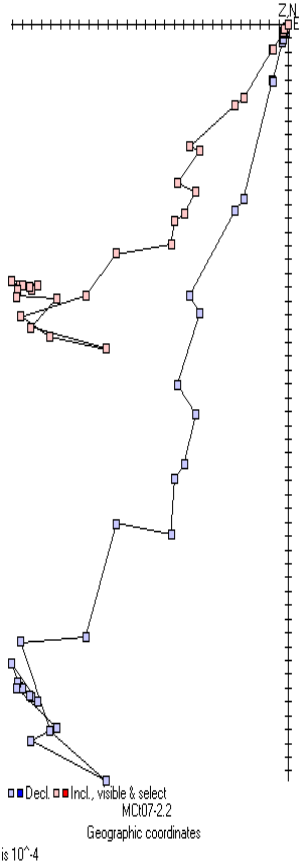

is 10^-4

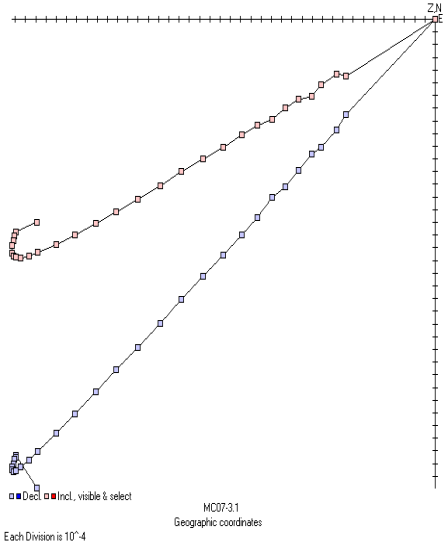

Each Division is 10^-4

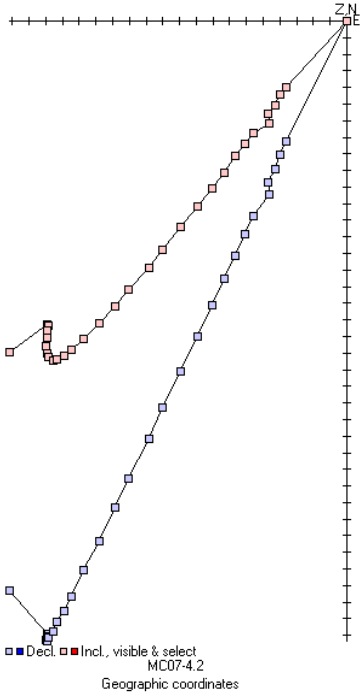
Z,N
E
Decl. Incl., visible & select
MC07-4.2
Geographic coordinates

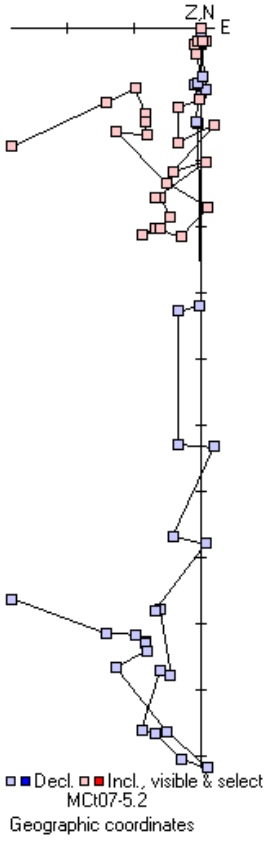
Z,N
E
Decl. Incl., visible & select
MCt07-5.2
Geographic coordinates

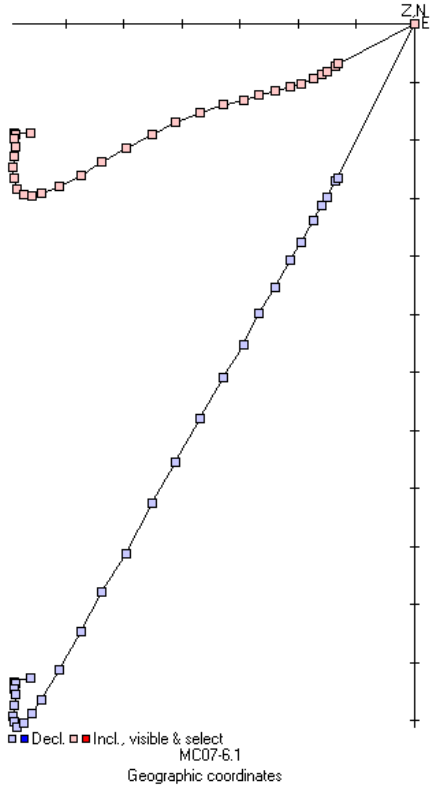
Z,N
E
Decl. Incl., visible & select
MC07-6.1
Geographic coordinates

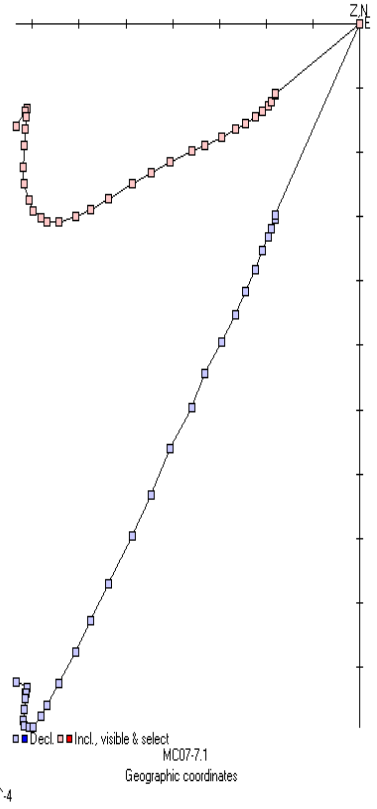
Z,N
E
Decl. Incl., visible & select
MC07-7.1
Geographic coordinates
s 10^-4

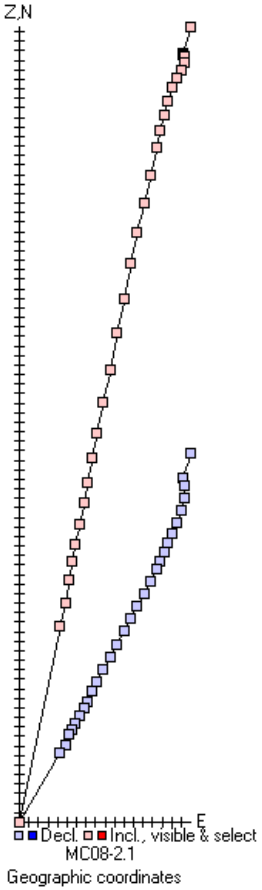
Z,N
E
Decl. Incl., visible & select
MC08-2.1
Geographic coordinates

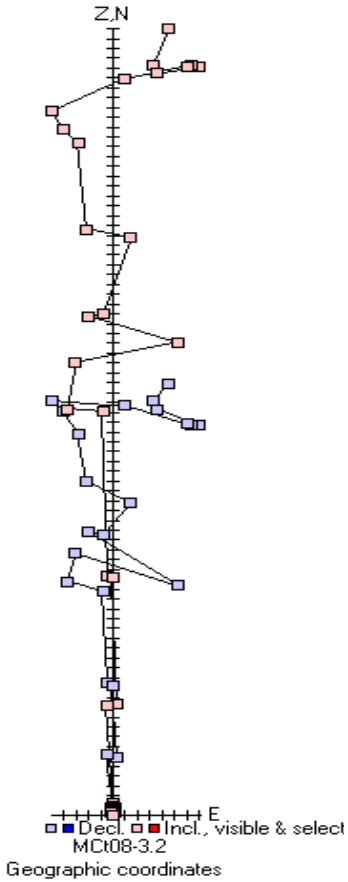
Z,N
E
Decl.
Incl., visible & select
MCt08-3.2
Geographic coordinates

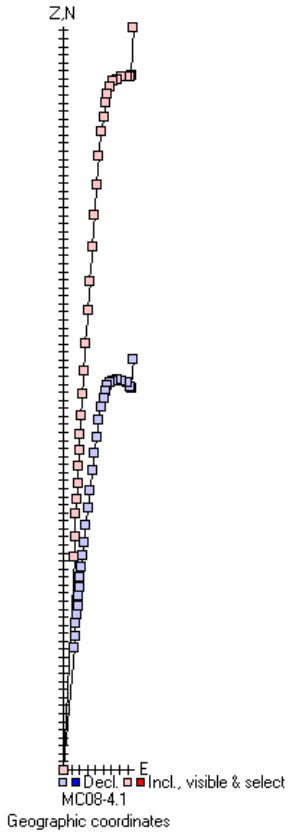
Z,N
E
Decl.
Incl., visible & select
MC08-4.1
Geographic coordinates

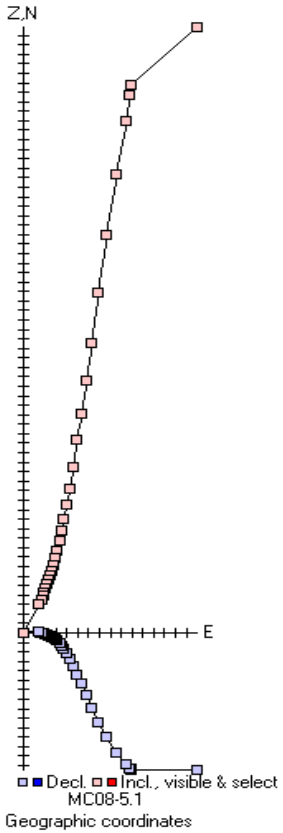
Z,N
E
Decl.
Incl., visible & select
MC08-5.1
Geographic coordinates

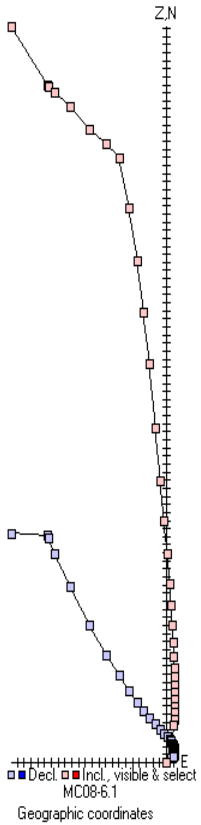
Z,N
E
Decl.
Incl., visible & select
MC08-6.1
Geographic coordinates

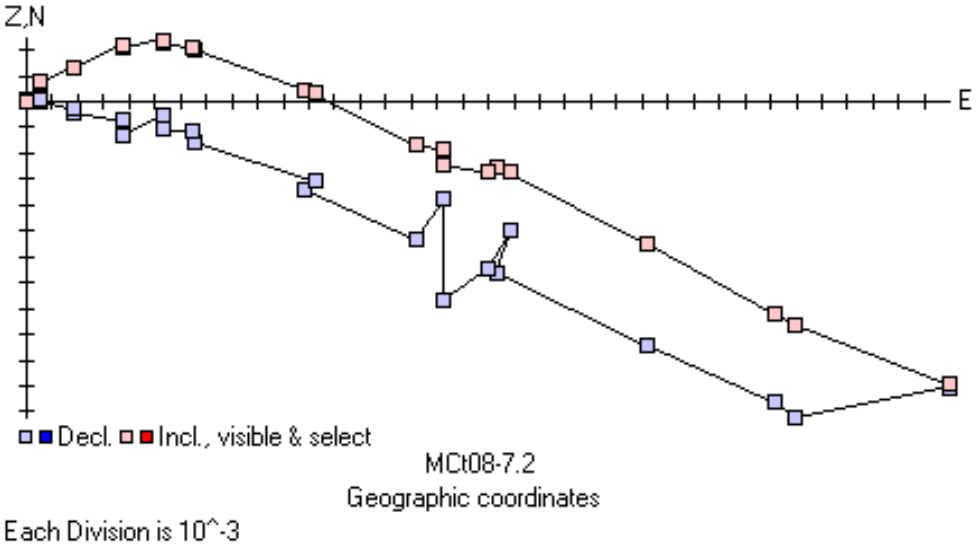

MCt08-7.2
Geographic coordinates

Each Division is 10^-3

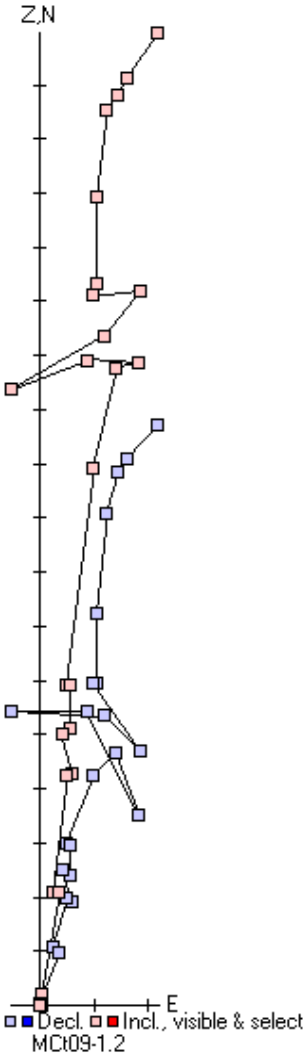

MCt09-1.2
Geographic coordinates

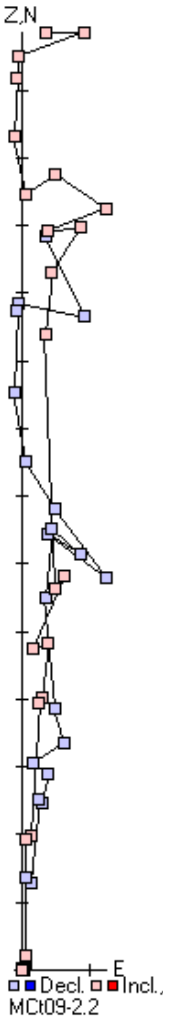

MCt09-2.2
Geographic coordinates

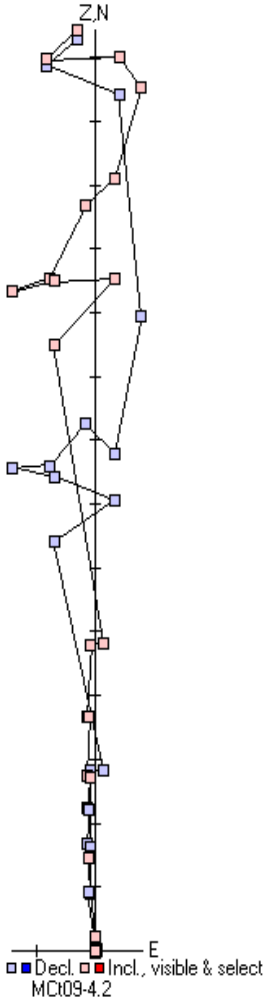

MCt09-4.2
Geographic coordinates

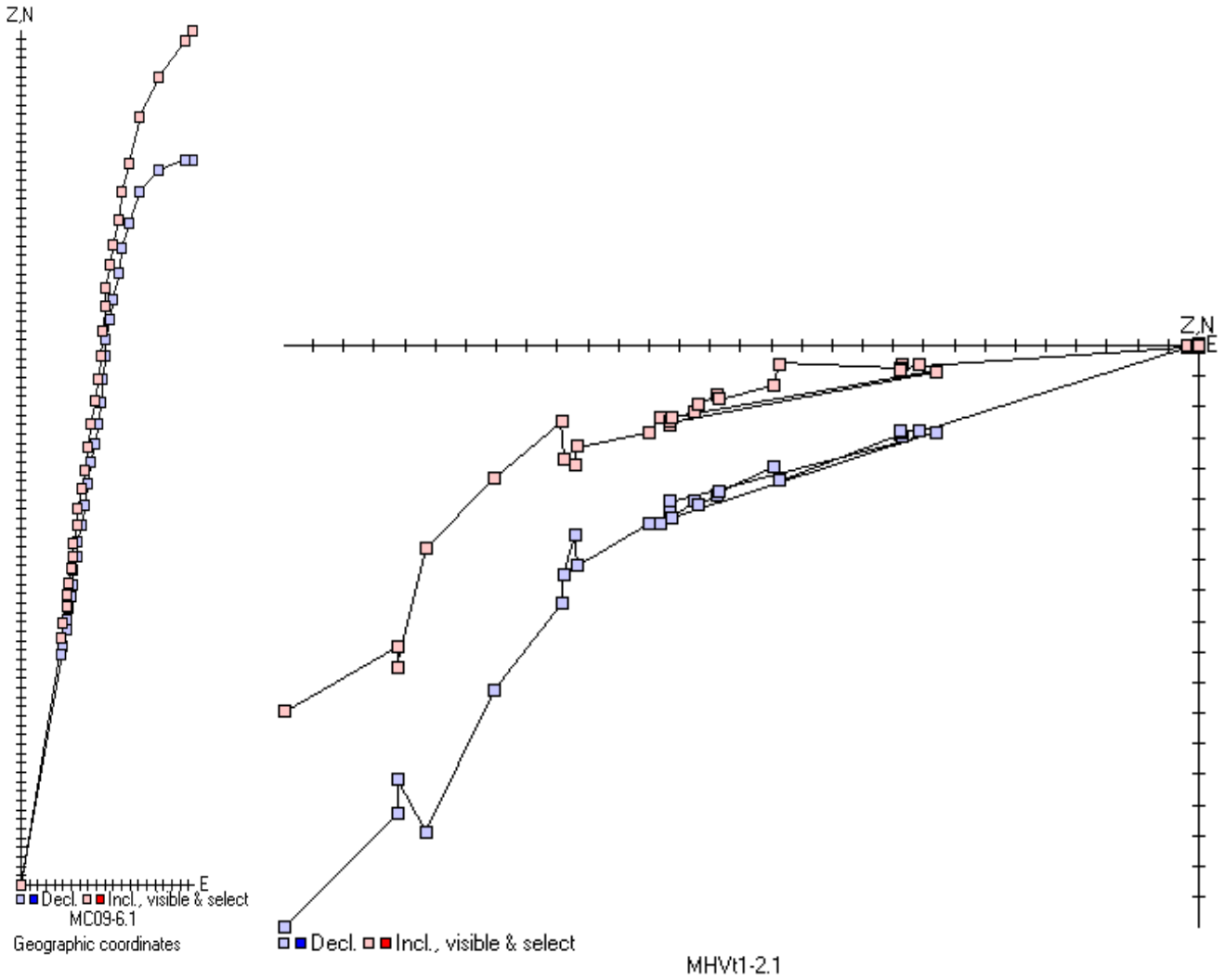
Z,N
E
Decl. Incl., visible & select
MC09-6.1
Geographic coordinates
Z,N
E
Decl. Incl., visible & select
MHVt1-2.1

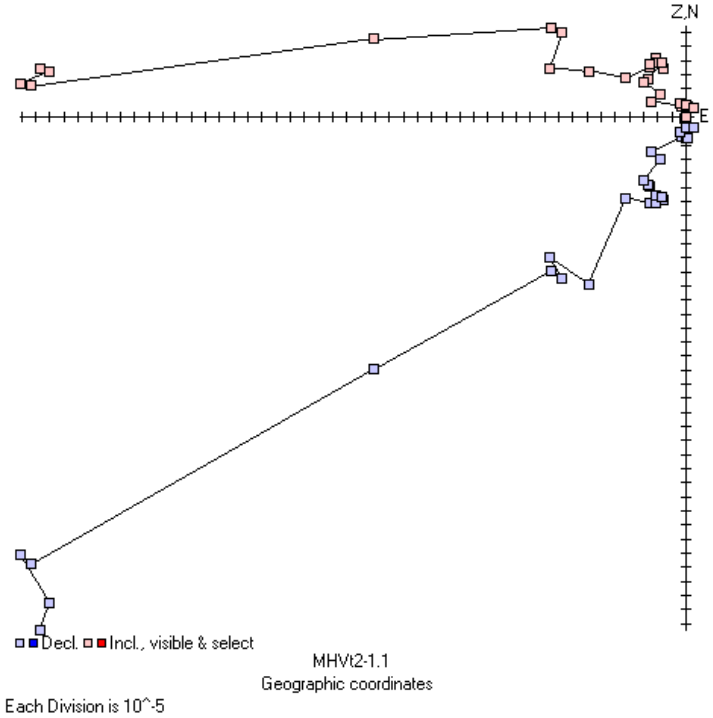

MHVt2-1.1
Geographic coordinates

Each Division is 10^-5

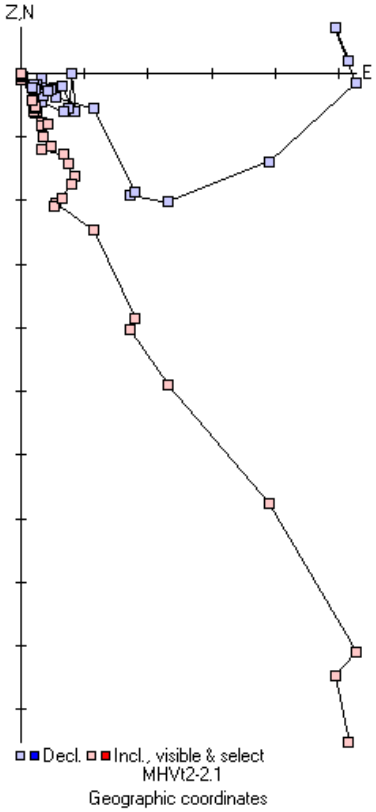

MHVt2-2.1
Geographic coordinates

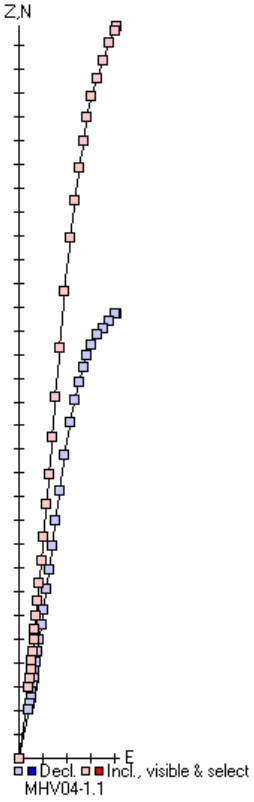

MHV04-1.1
Geographic coordinates

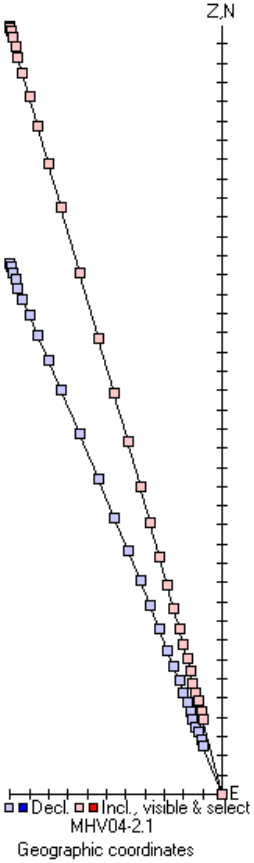

MHV04-2.1
Geographic coordinates

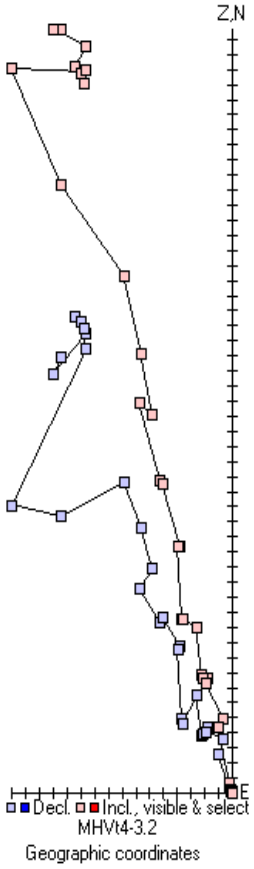

MHVt4-3.2

Geographic coordinates

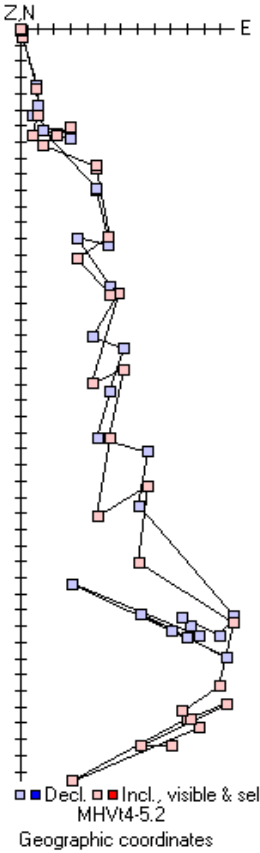

MHVt4-5.2

Geographic coordinates

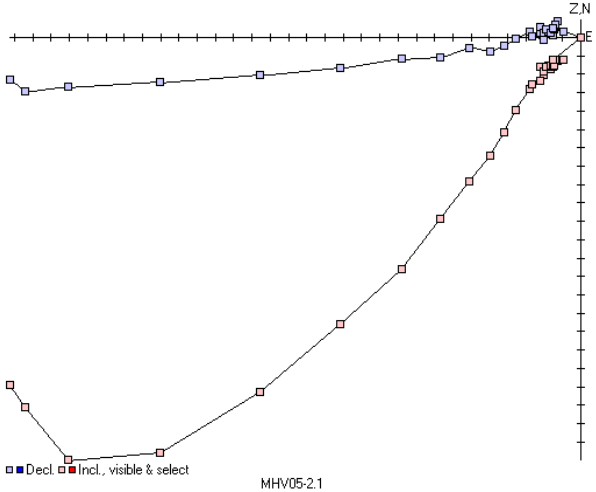

MHV05-2.1

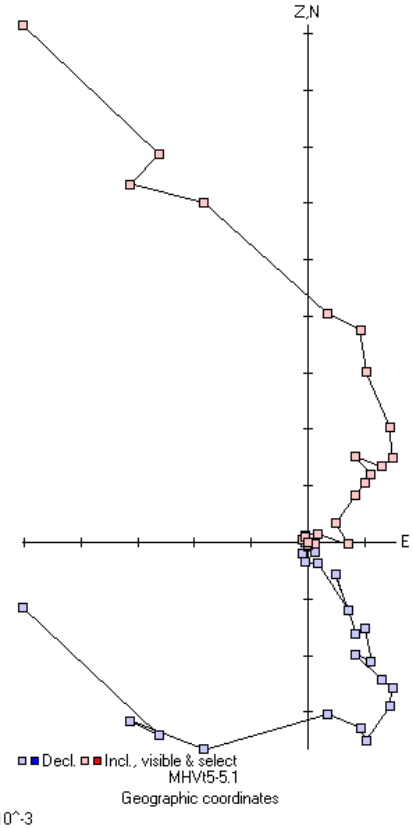

MHVt5-5.1

Geographic coordinates

10^-3

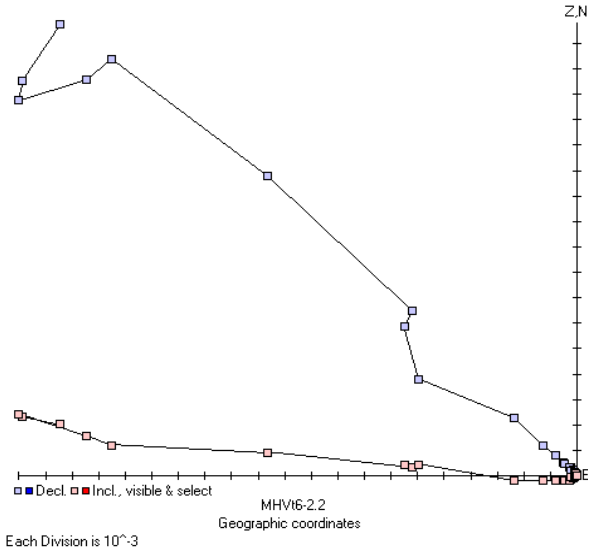

MHVt6-2.2
Geographic coordinates
Each Division is 10^-3

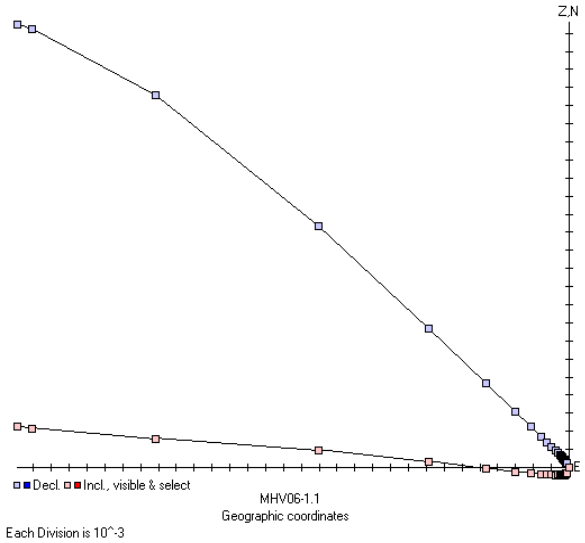

MHV06-1.1
Geographic coordinates
Each Division is 10^-3

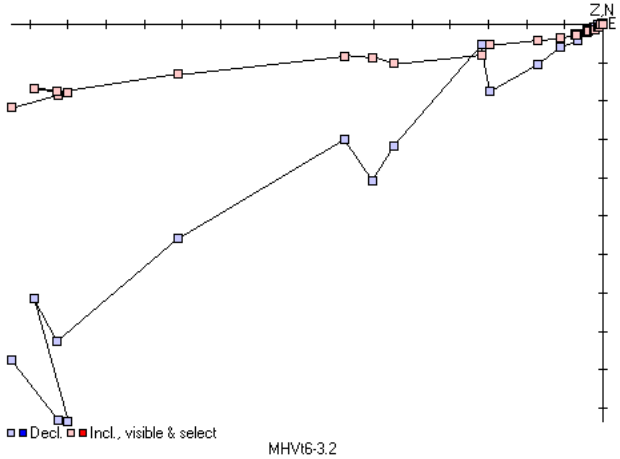

MHVt6-3.2

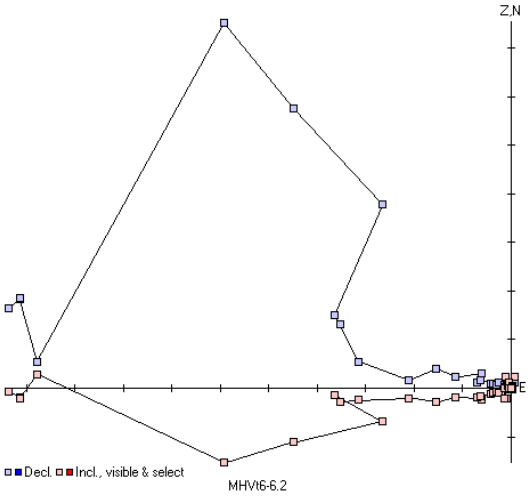

MHVt6-6.2

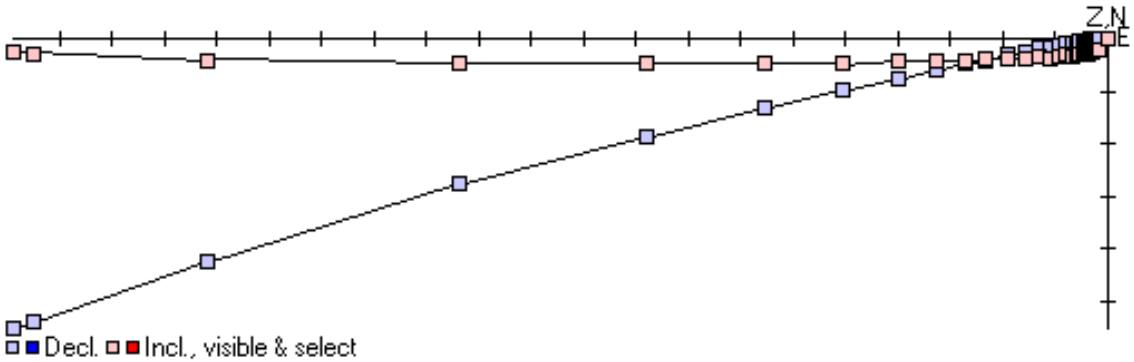

MHV06-4.1

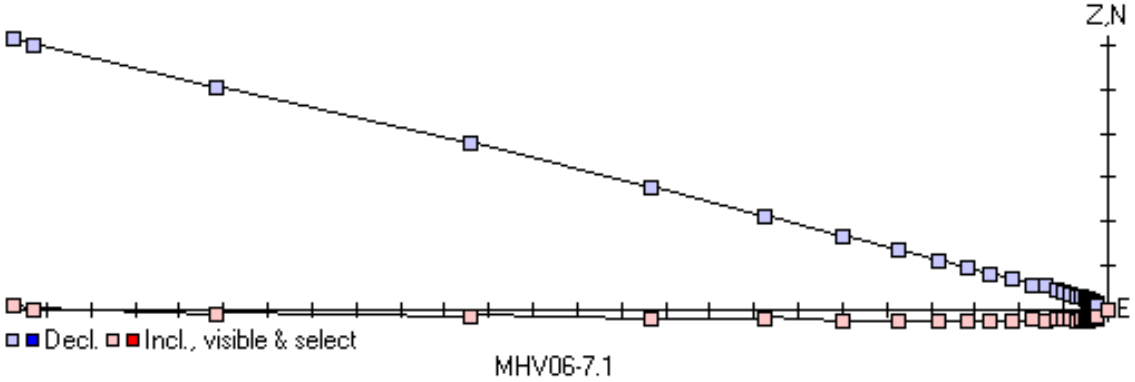
Z,N
E
Decl. Incl., visible & select
MHV06-7.1

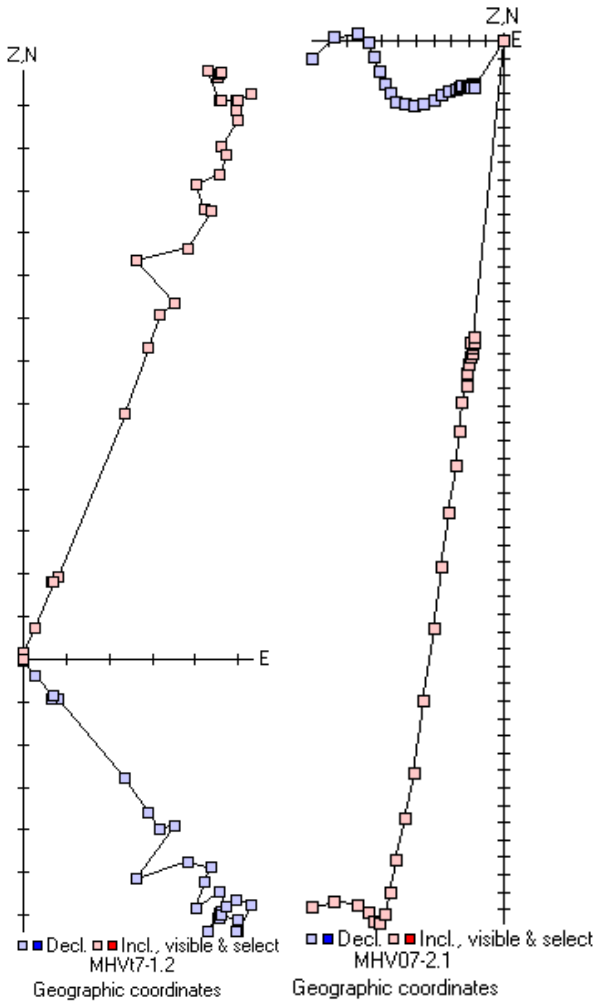
Z,N
E
Decl. Incl., visible & select
MHVt7-1.2
Geographic coordinates
Z,N
E
Decl. Incl., visible & select
MHV07-2.1
Geographic coordinates

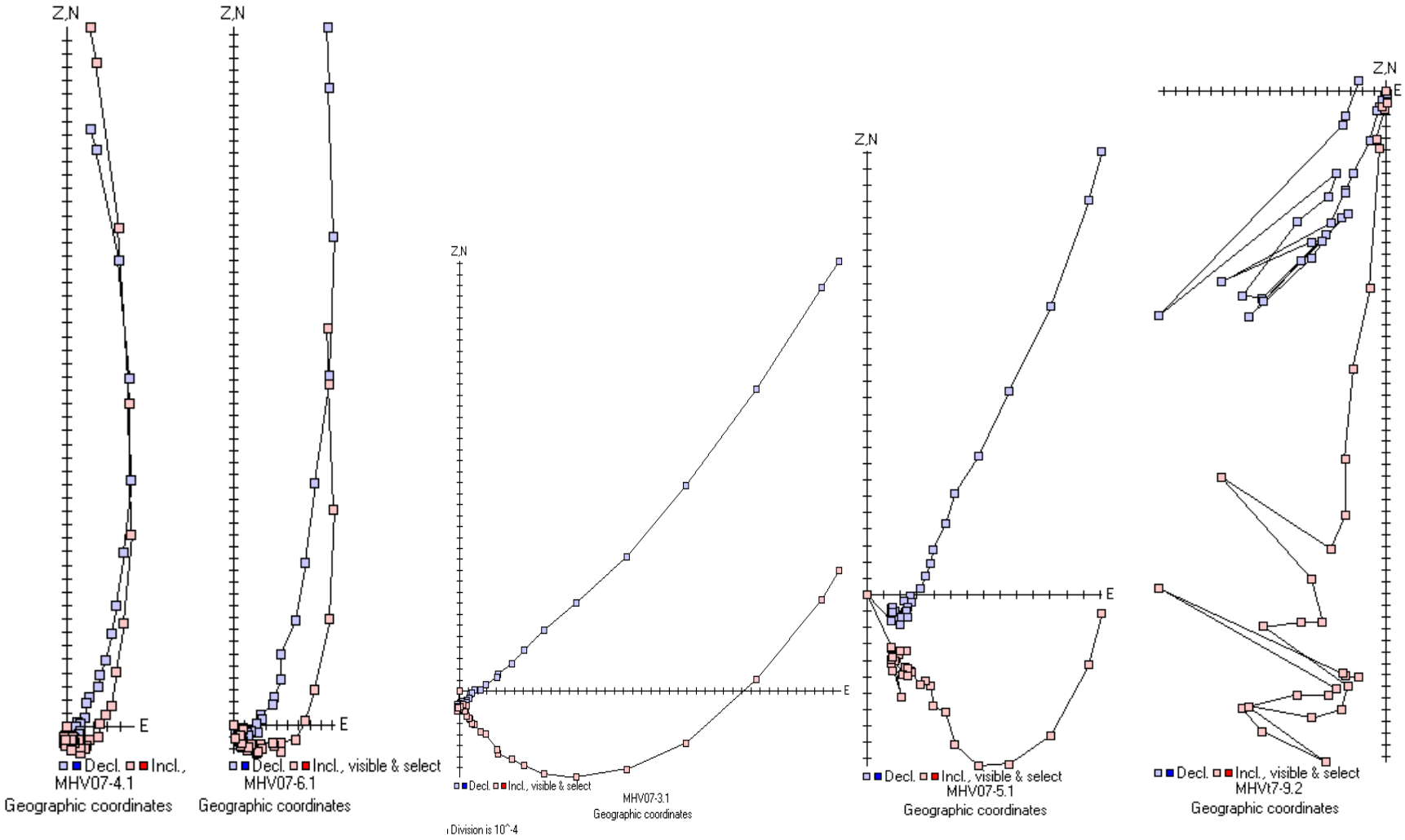
Z,N
E
Decl.
Incl.,
MHV07-4.1
Geographic coordinates
Z,N
E
Decl.
Incl., visible & select
MHV07-6.1
Geographic coordinates
Z,N
E
Decl.
Incl., visible & select
MHV07-3.1
Geographic coordinates
Division is 10^-4
Z,N
E
Decl.
Incl., visible & select
MHV07-5.1
Geographic coordinates
Z,N
E
Decl.
Incl., visible & select
MHVt7-9.2
Geographic coordinates

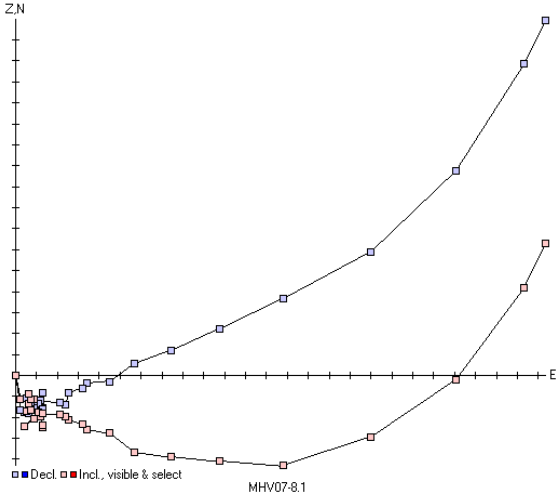
Z,N
E
Decl.
Incl., visible & select
MHV07-8.1

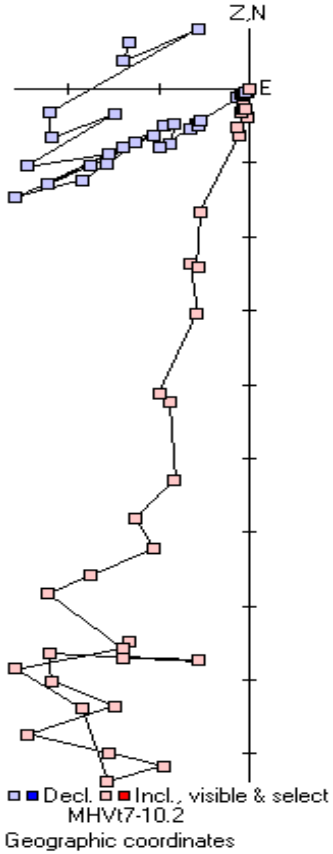
Z,N
E
Decl.
Incl., visible & select
MHVt7-10.2
Geographic coordinates

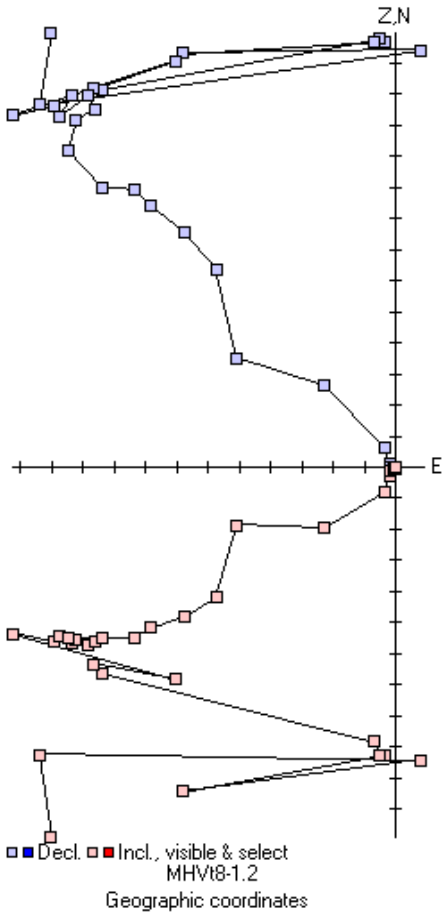
Z,N
E
Decl.
Incl., visible & select
MHVt8-1.2
Geographic coordinates

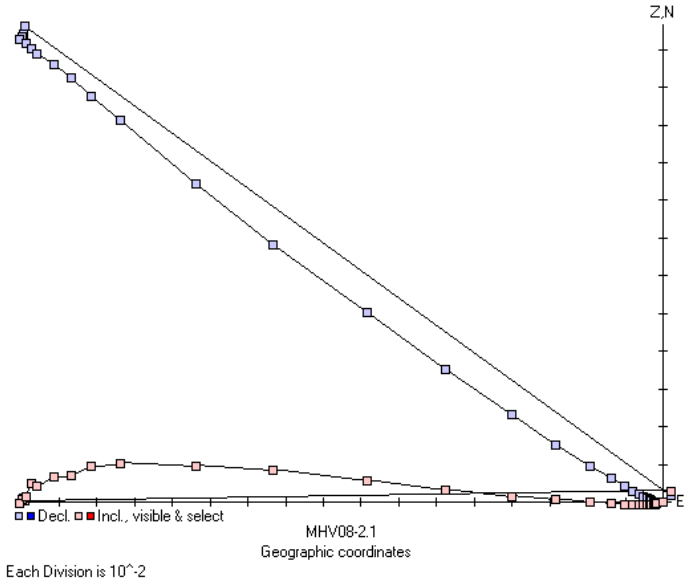

MHV08-2.1
Geographic coordinates

Each Division is 10^-2

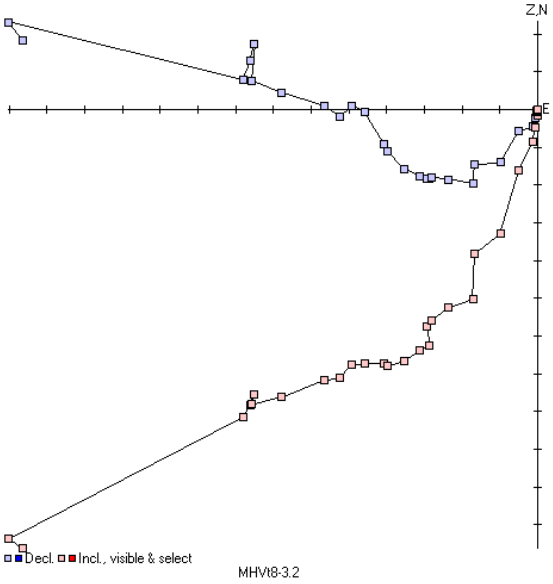

MHVt8-3.2

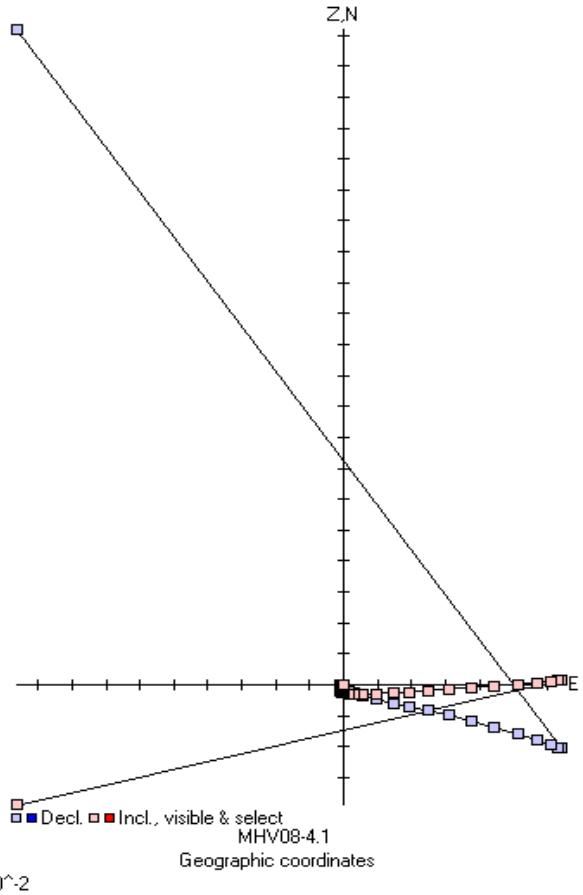

MHV08-4.1
Geographic coordinates

; 10^-2

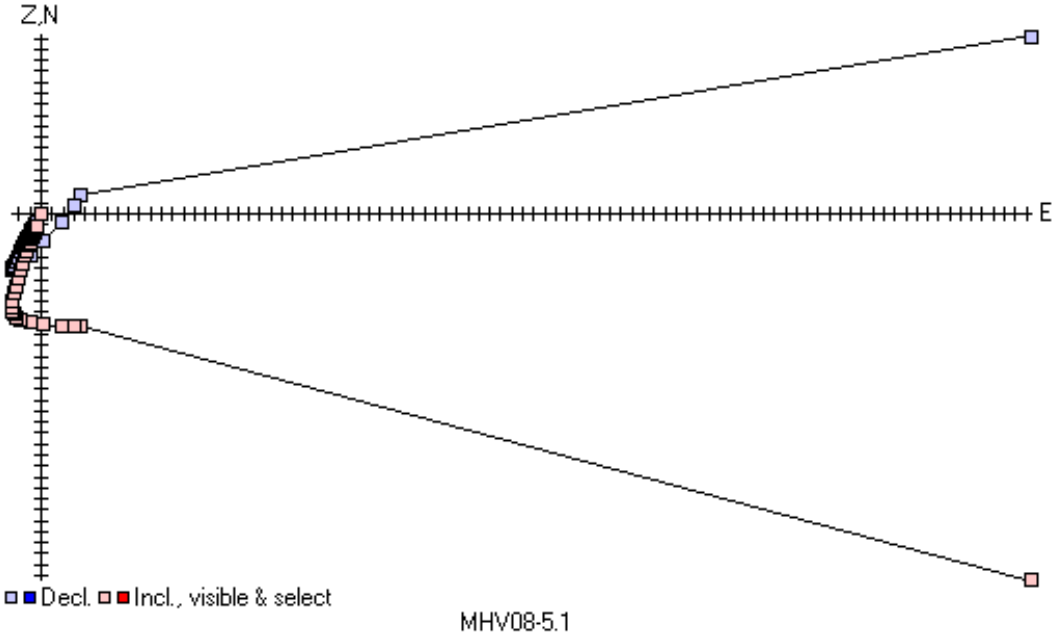

MHV08-5.1

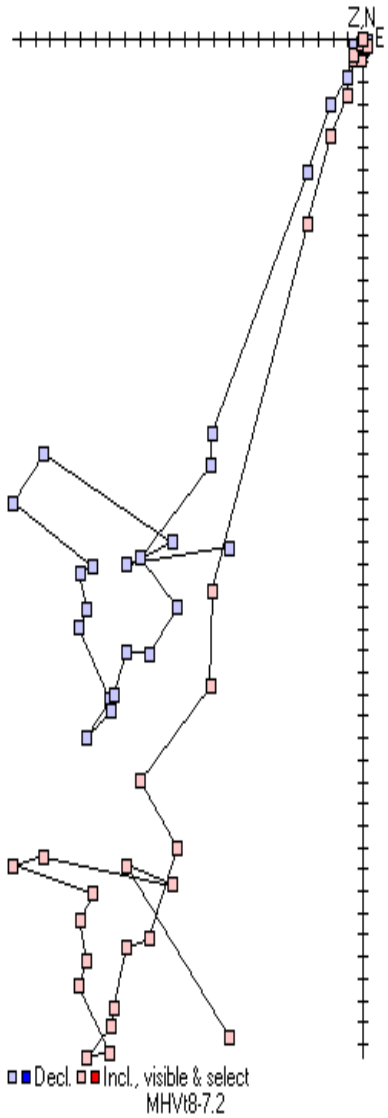

MHVt8-7.2

Geographic coordinates

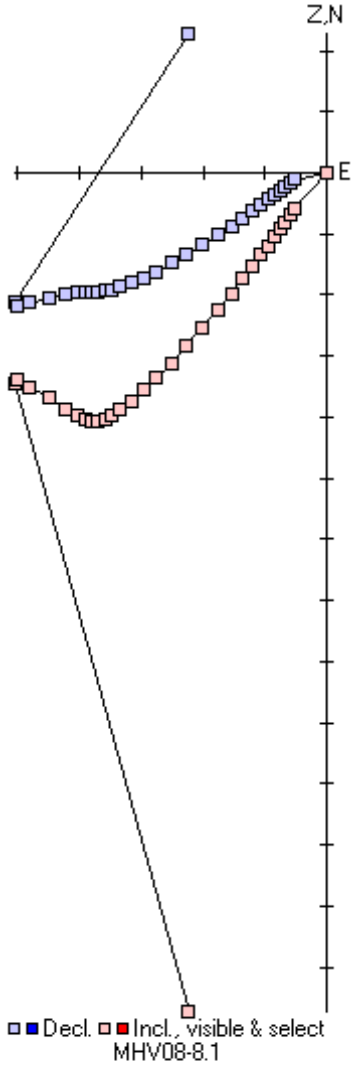

MHV08-8.1

Geographic coordinates

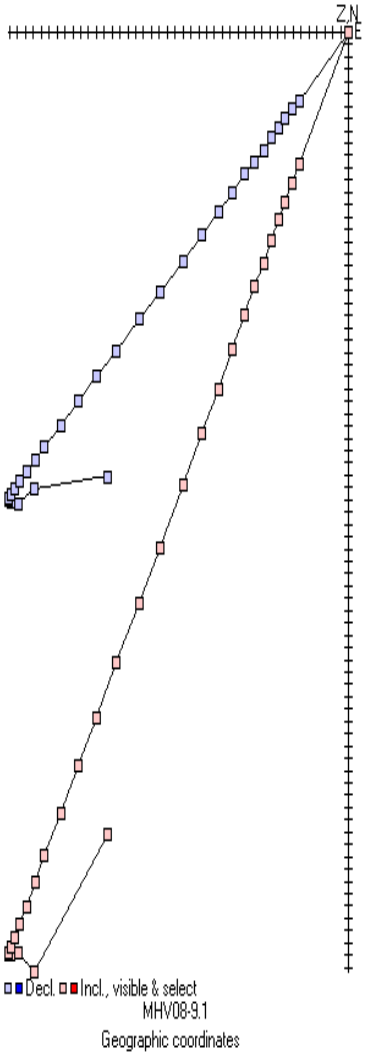

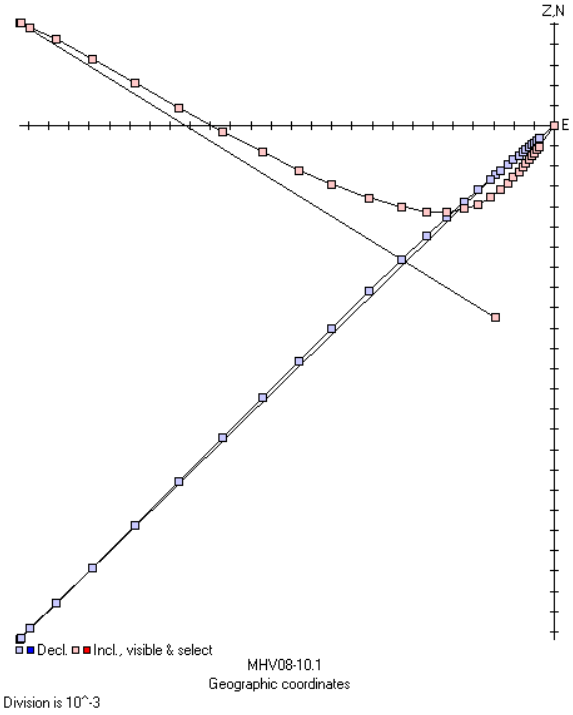

Division is 10^-3

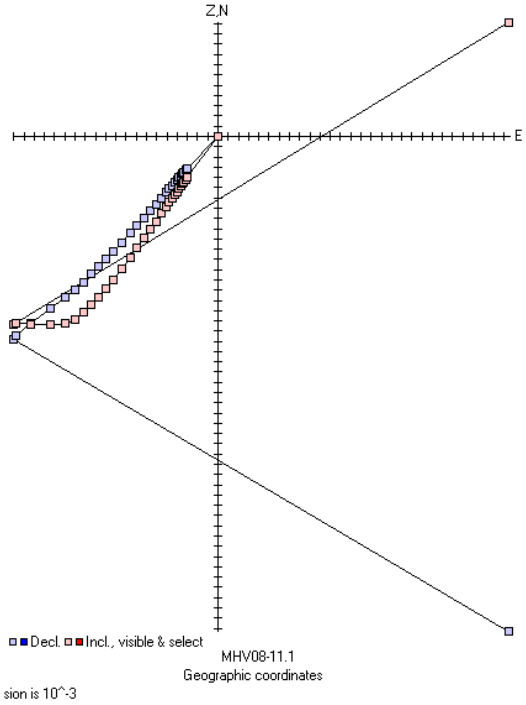

sion is 10^-3

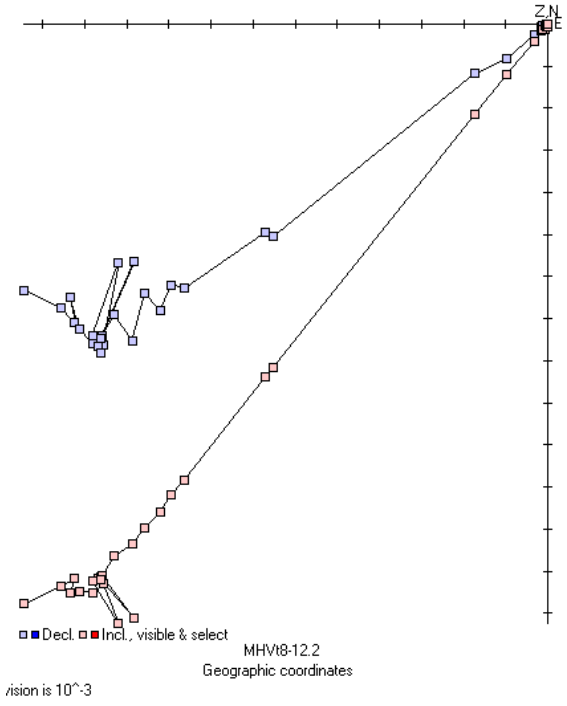
Z,N
E
Decl. Incl., visible & select
MHVt8-12.2
Geographic coordinates
vision is 10^-3

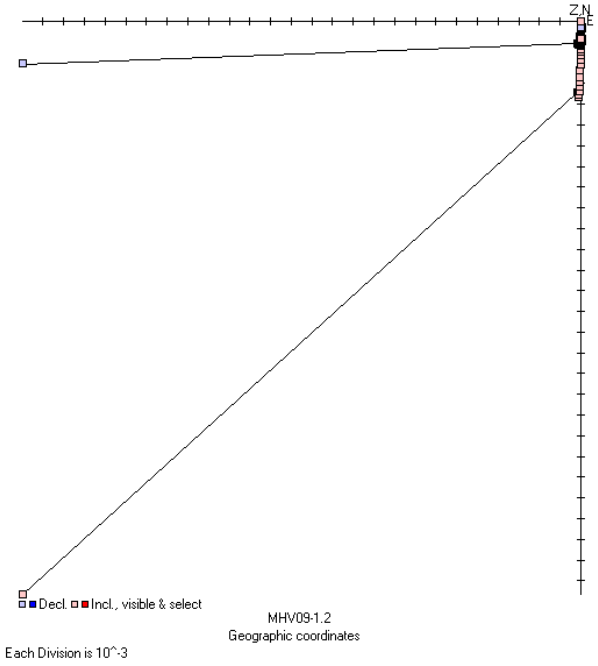
Z,N
E
Decl. Incl., visible & select
MHV09-1.2
Geographic coordinates
Each Division is 10^-3

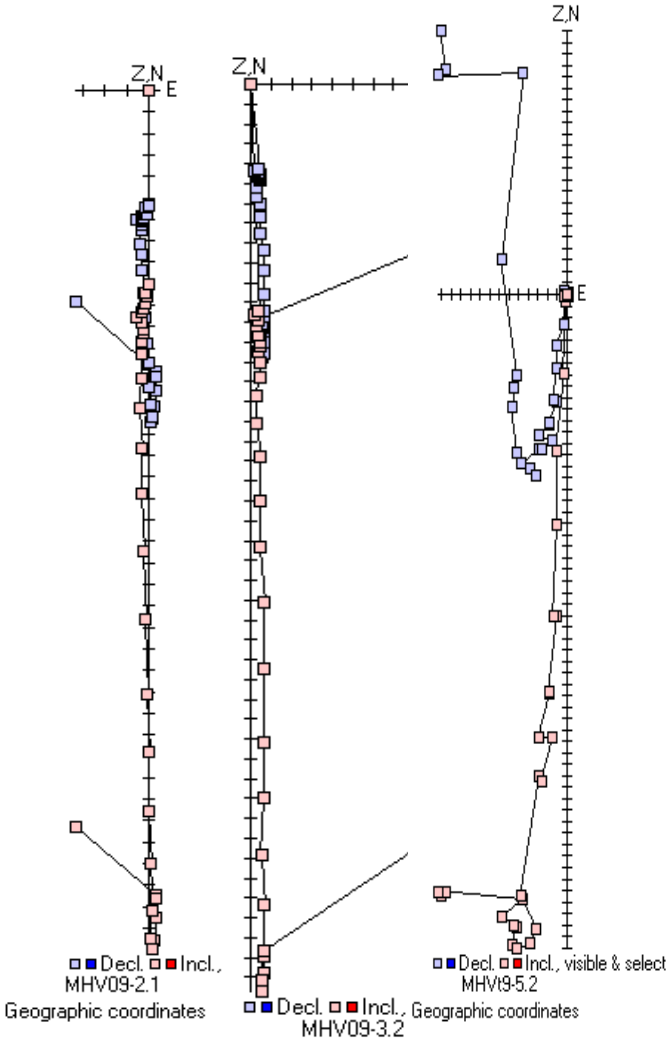
Z,N
E
Decl. Incl.,
MHV09-2.1
Geographic coordinates
Z,N
Decl. Incl., Geographic coordinates
MHV09-3.2
Z,N
E
Decl. Incl., visible & select
MHVt9-5.2

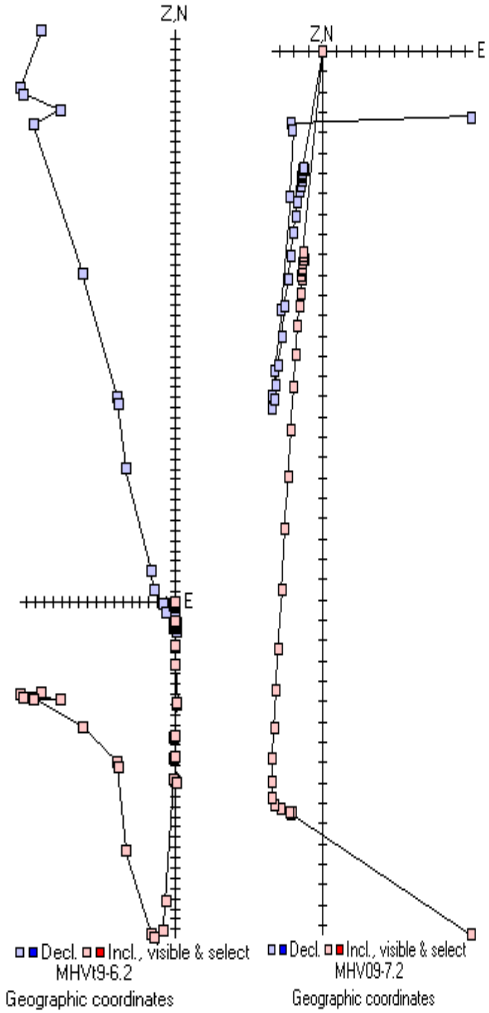
Z,N
E
Decl. Incl., visible & select
MHVt9-6.2
Geographic coordinates

Z,N
E
Decl. Incl., visible & select
MHV09-7.2
Geographic coordinates

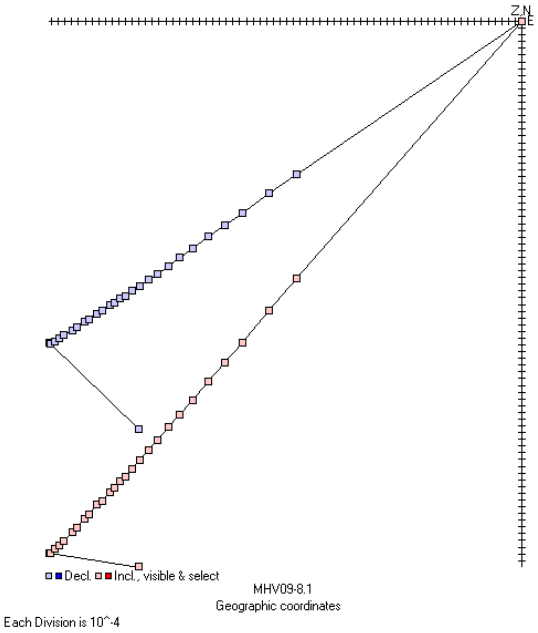
Z,N
E
Decl. Incl., visible & select
MHV09-8.1
Geographic coordinates
Each Division is 10^-4

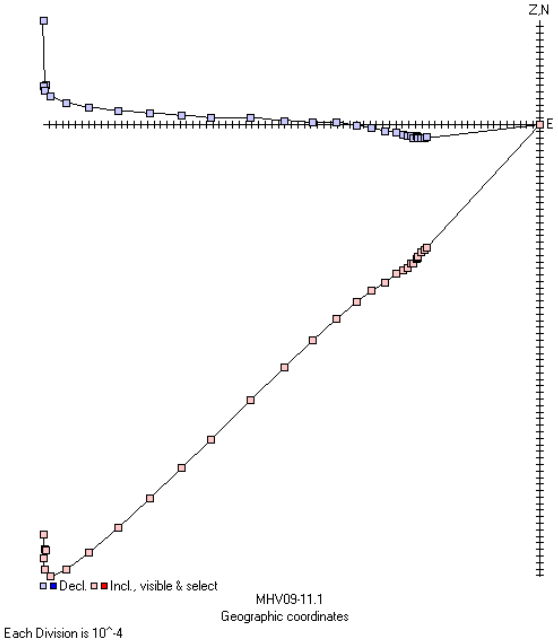
Z,N
E
Decl. Incl., visible & select
MHV09-11.1
Geographic coordinates
Each Division is 10^-4

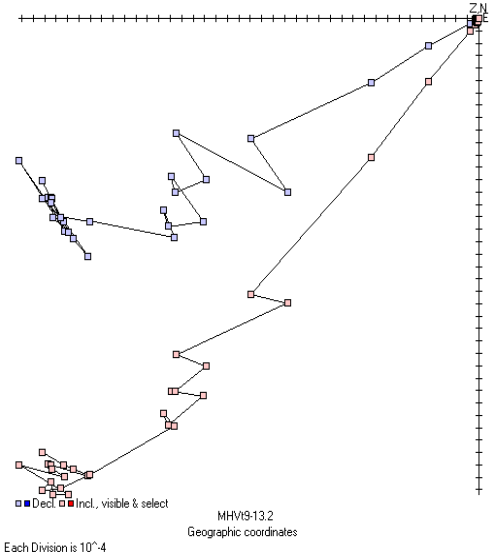
Z,N
E
Decl.
Incl., visible & select
MHVt9-13.2
Geographic coordinates
Each Division is 10^-4

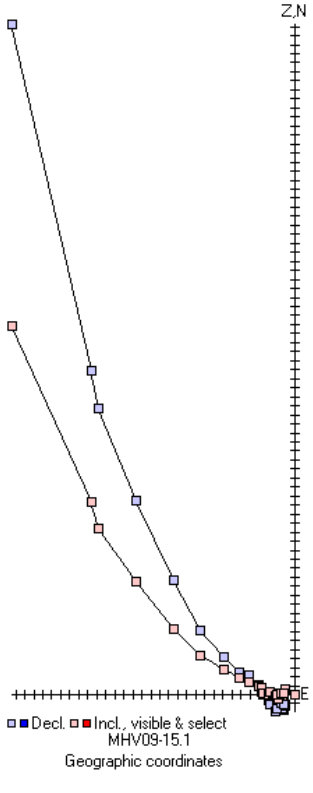
Z,N
E
Decl.
Incl., visible & select
MHV09-15.1
Geographic coordinates

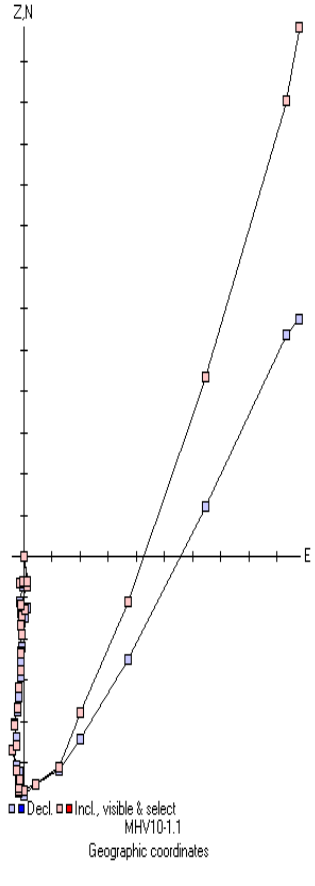
Z,N
E
Decl.
Incl., visible & select
MHV10-1.1
Geographic coordinates

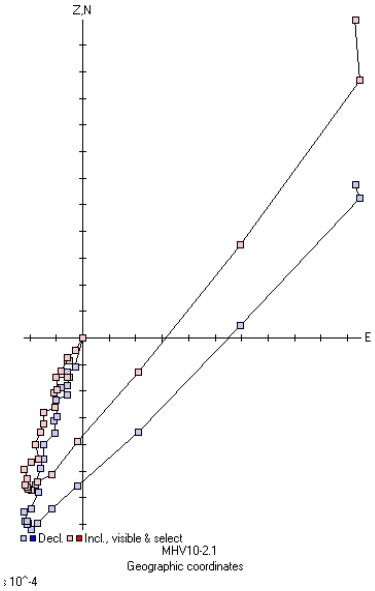
Z,N
E
Decl.
Incl., visible & select
MHV10-2.1
Geographic coordinates
10^-4

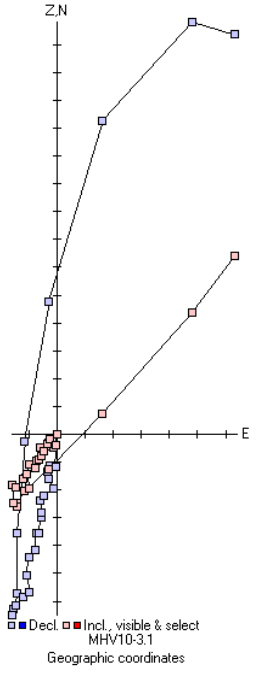
Z,N
E
Decl.
Incl., visible & select
MHV10-3.1
Geographic coordinates

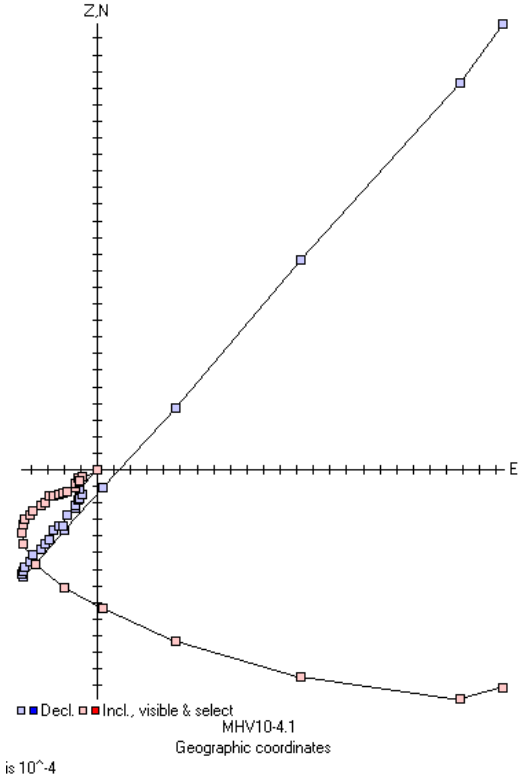

is 10^-4

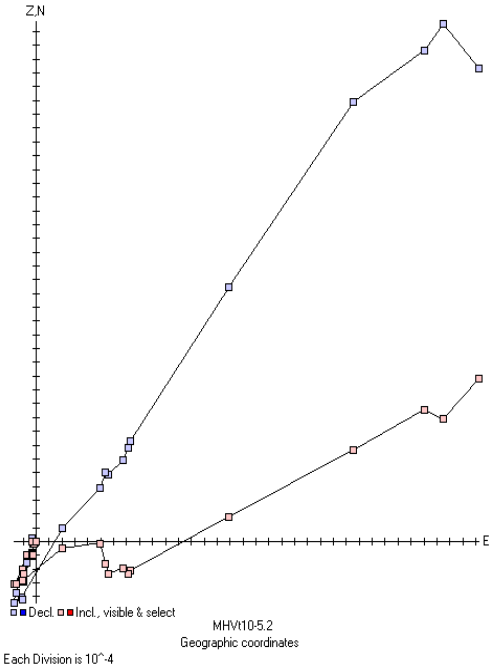

Each Division is 10^-4

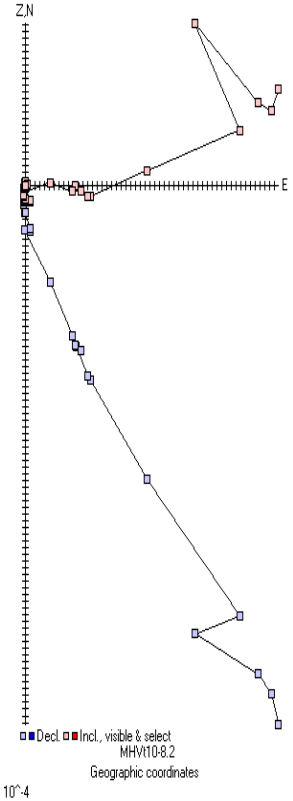

10^-4

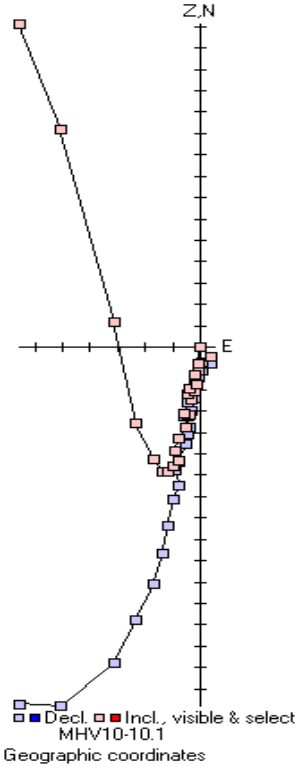

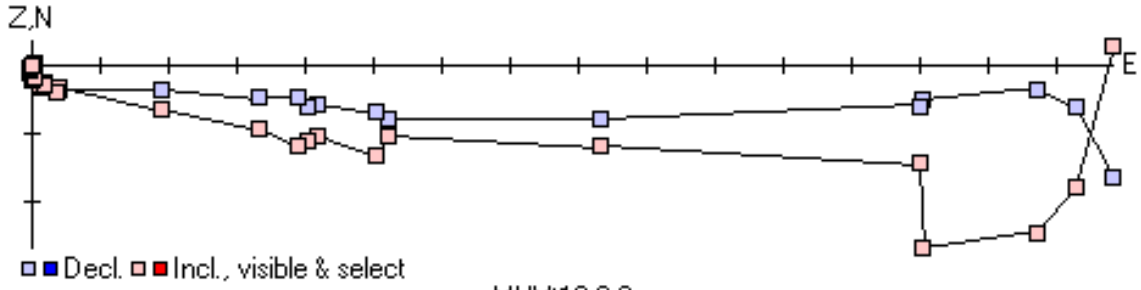

MHVt10-6.2

Geographic coordinates

Each Division is 10^-3

12.5 Peak Range

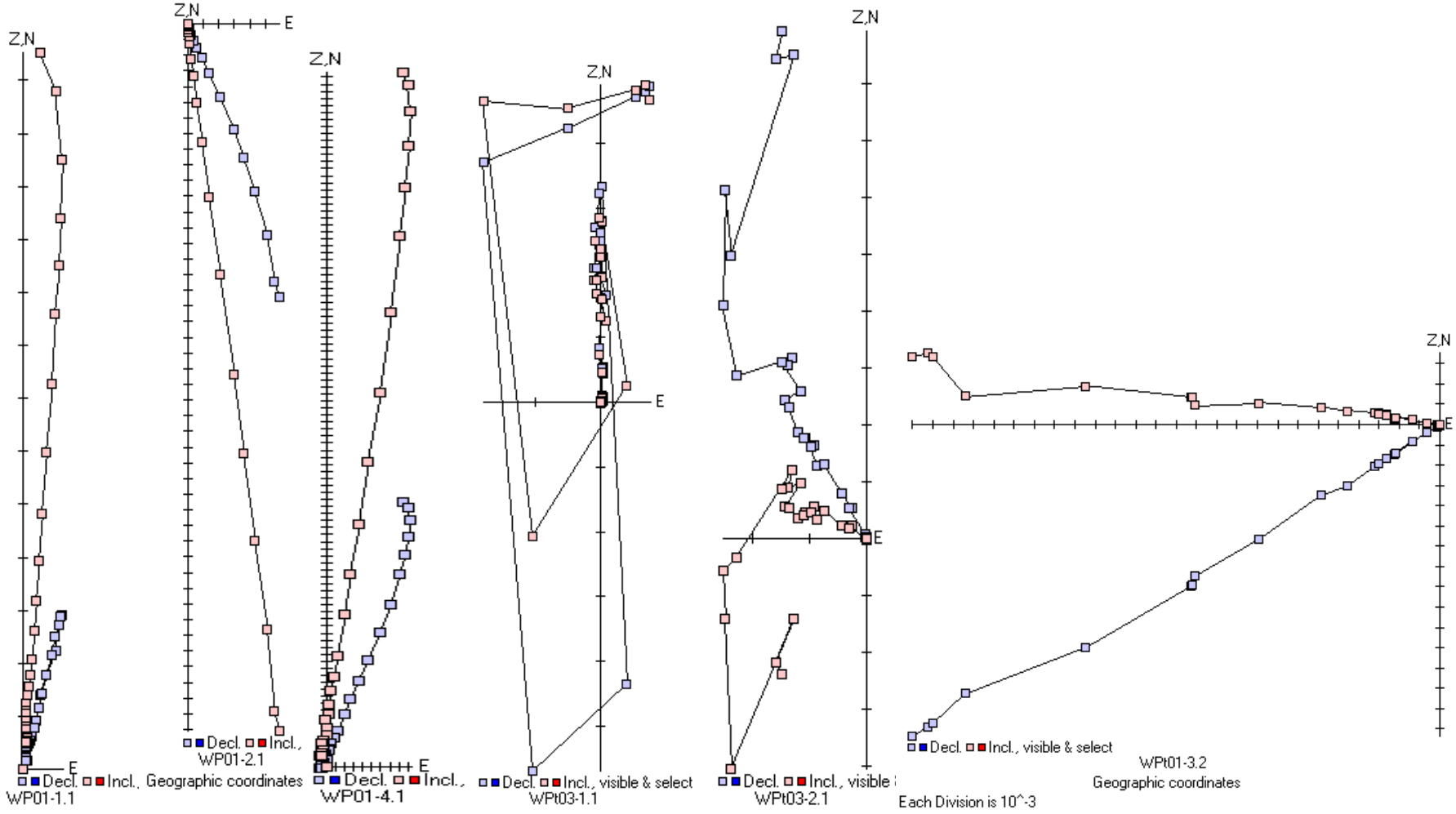

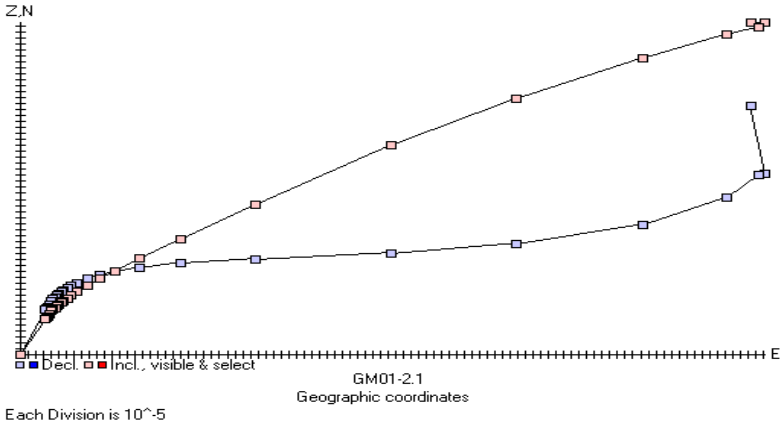

GM01-2.1
Geographic coordinates

Each Division is 10^-5

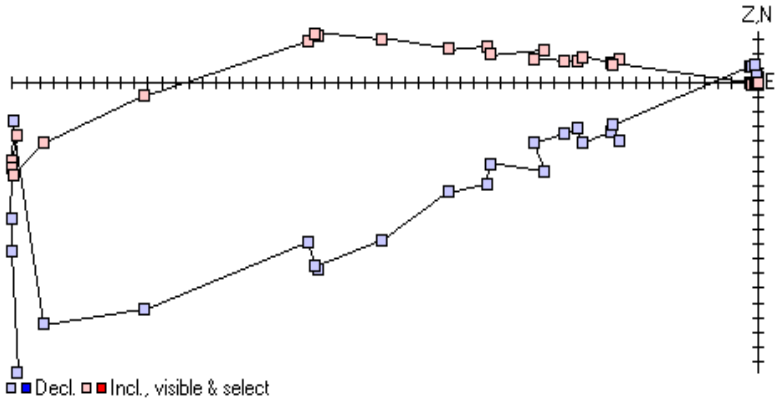

GMt01-4.2

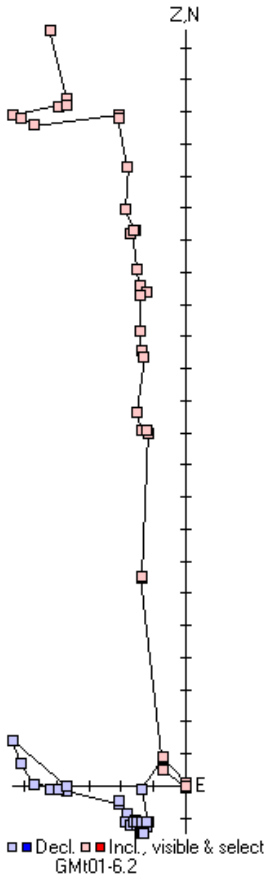

GMt01-6.2

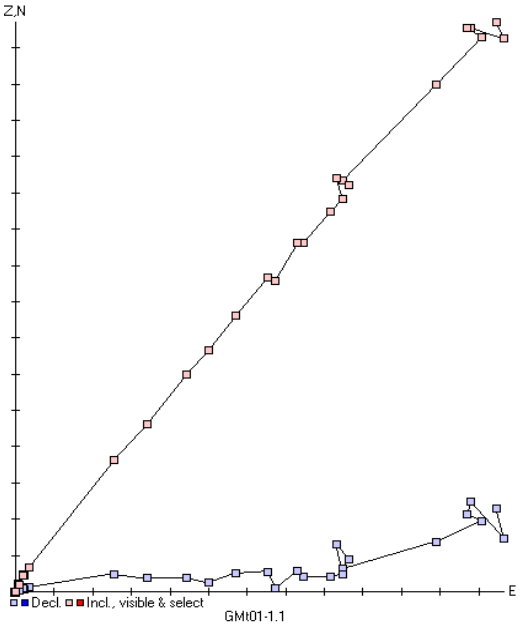

GMt01-1.1
Geographic coordinates
Division is 10^-4

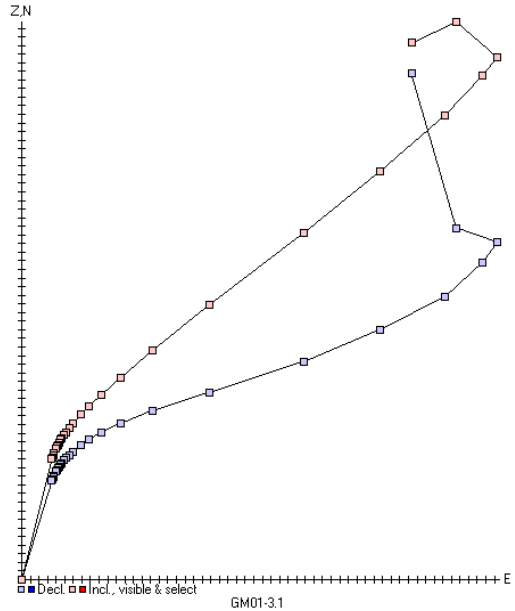

GM01-3.1
Geographic coordinates
Division is 10^-5

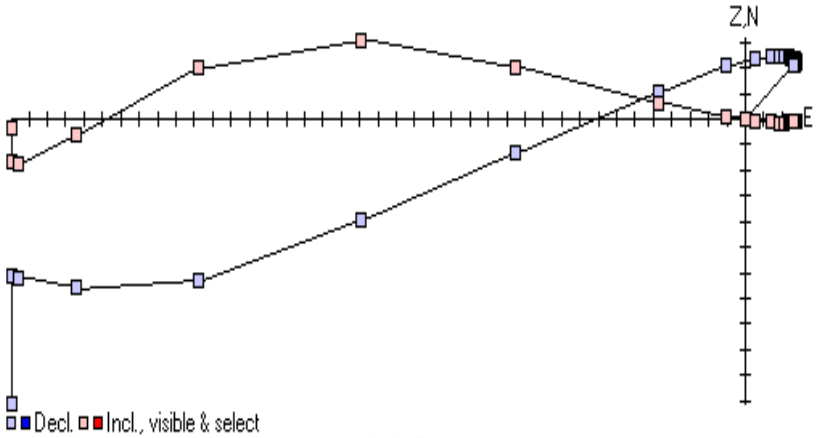

GM01-5.1

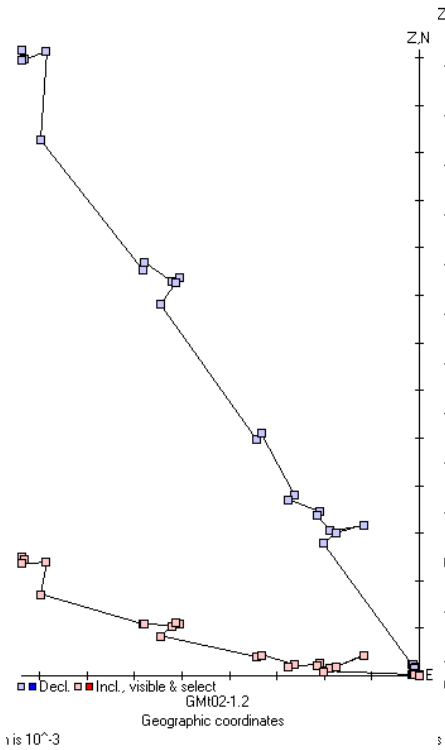
Z,N
E
Decl. Incl., visible & select
GMt02-1.2
Geographic coordinates
is 10^-3

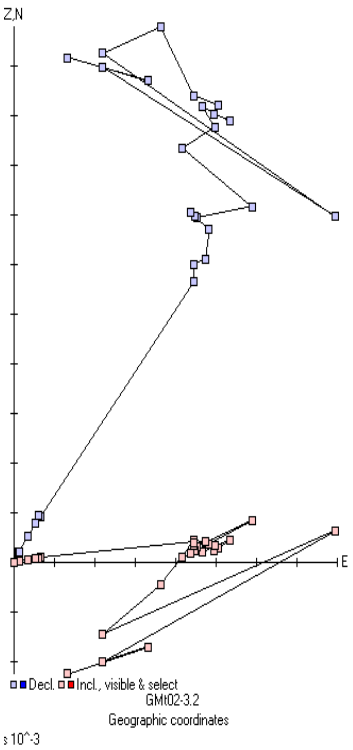
Z,N
E
Decl. Incl., visible & select
GMt02-3.2
Geographic coordinates
10^-3

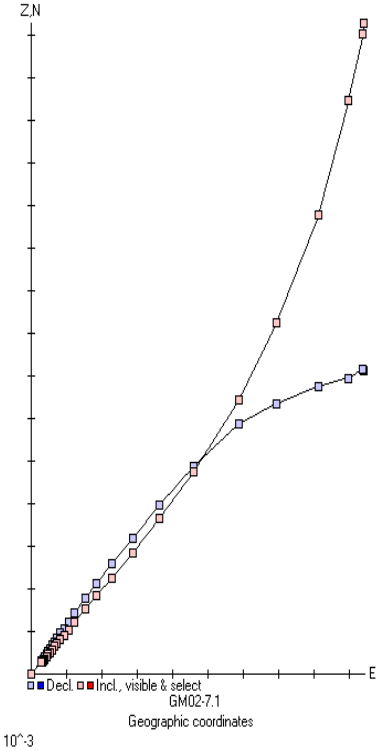
Z,N
E
Decl. Incl., visible & select
GM02-7.1
Geographic coordinates
10^-3

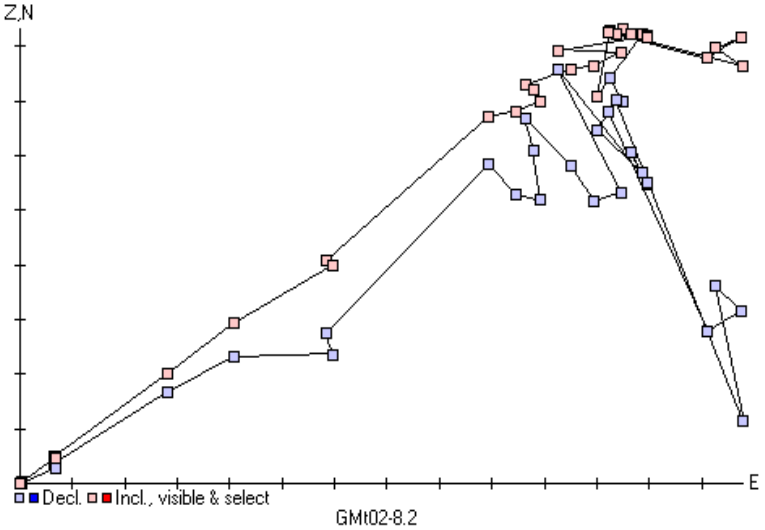
Z,N
E
Decl. Incl., visible & select
GMt02-8.2

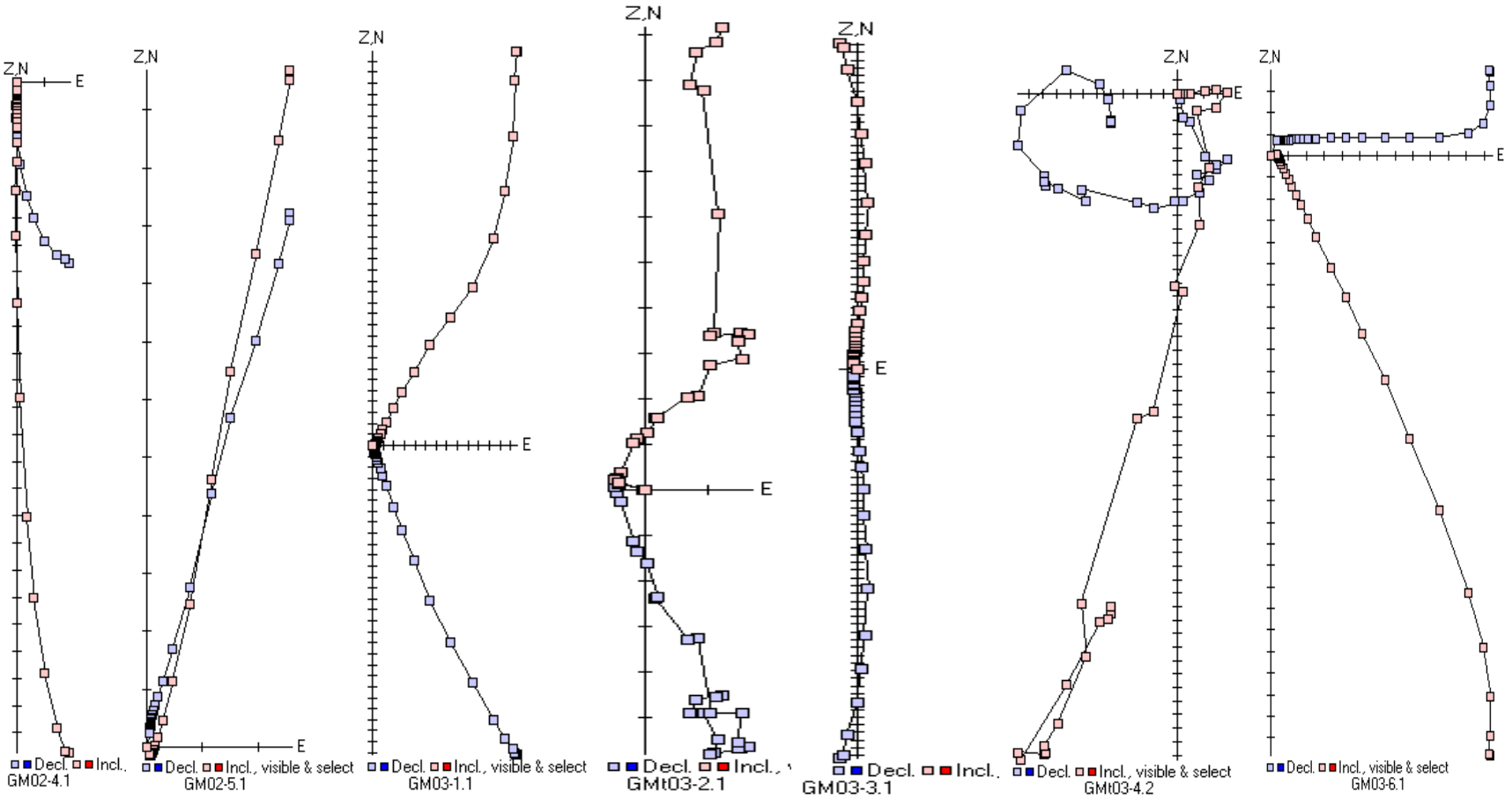
Z,N
E
Decl.
Incl.
GM02-4.1
Z,N
E
Decl.
Incl., visible & select
GM02-5.1
Z,N
E
Decl.
Incl., visible & select
GM03-1.1
Z,N
E
Decl.
Incl.,
GMt03-2.1
Z,N
E
Decl.
Incl.,
GM03-3.1
Z,N
E
Decl.
Incl., visible & select
GMt03-4.2
Z,N
E
Decl.
Incl., visible & select
GM03-6.1

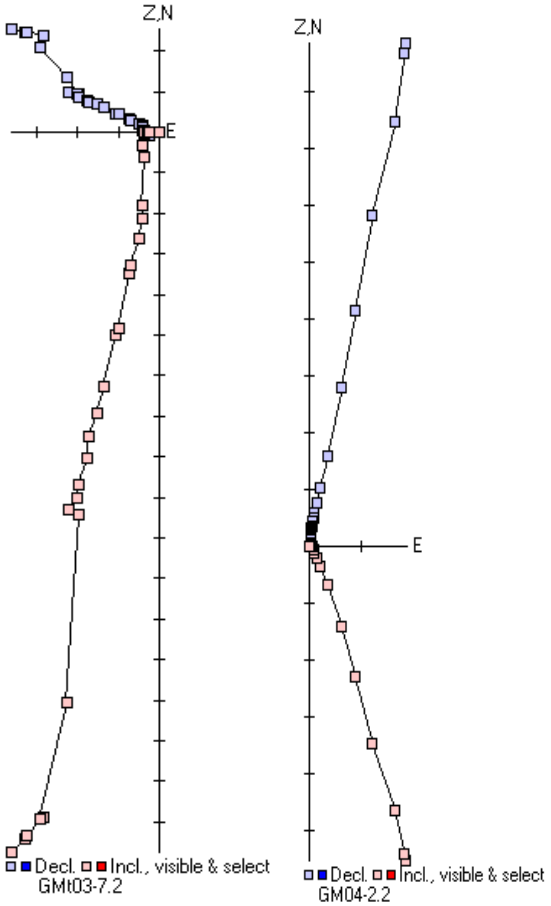

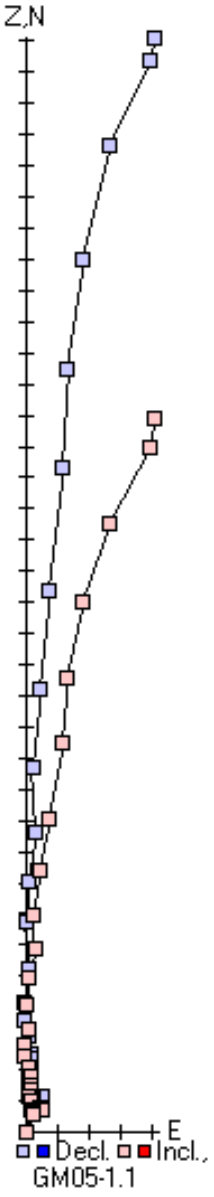

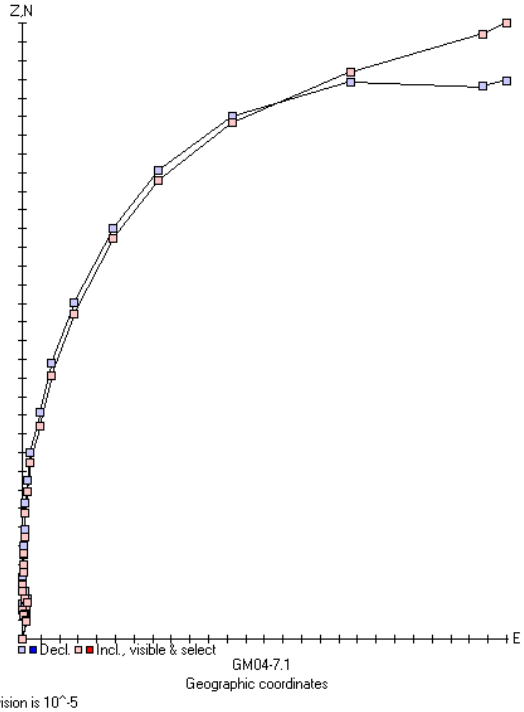

Division is 10^-5

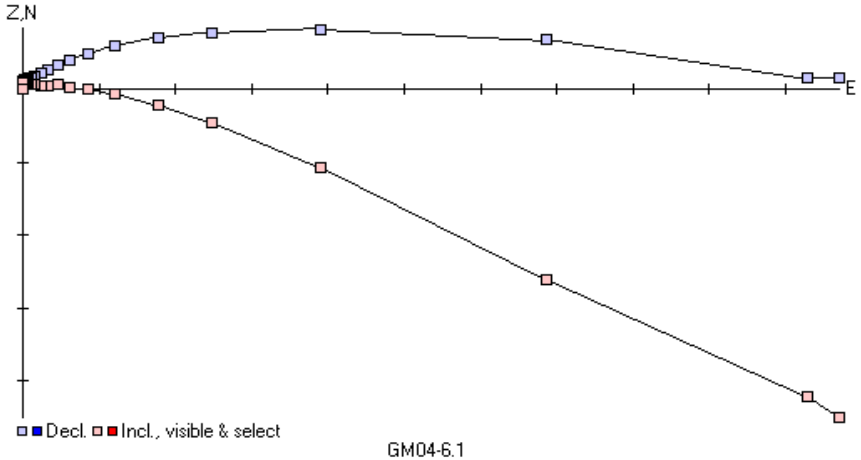

GM04-6.1
Geographic coordinates

Each Division is 10^-4

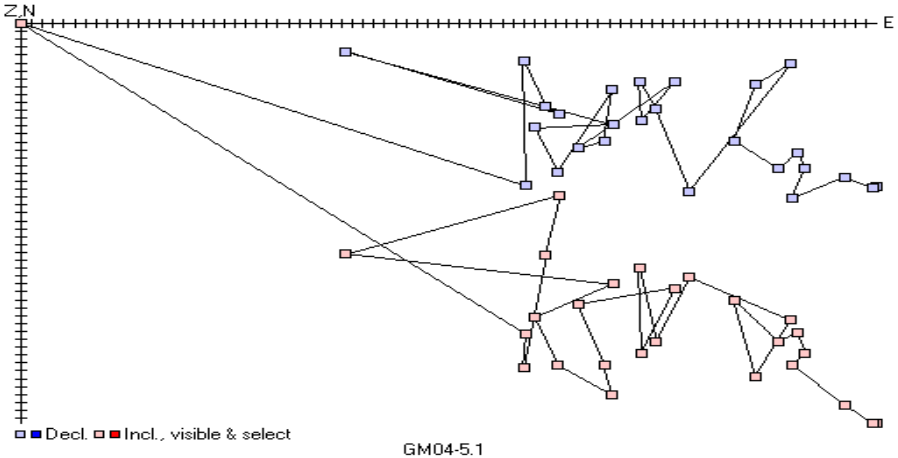

GM04-5.1
Geographic coordinates

Each Division is 10^-7

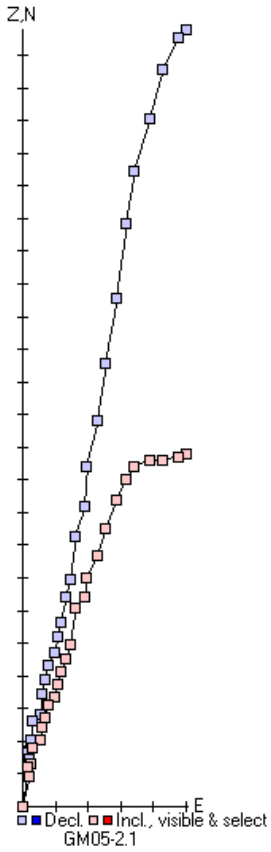

GM05-2.1

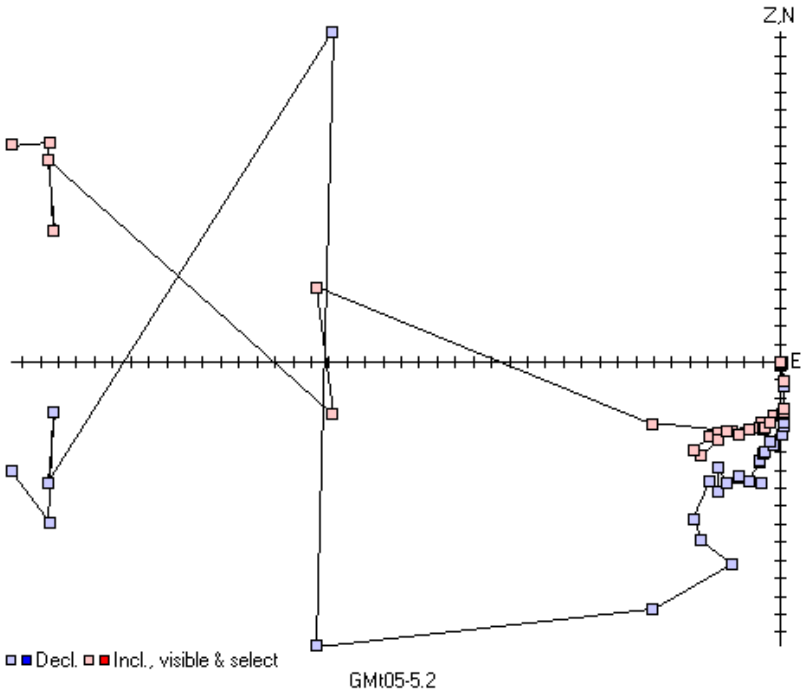

GMt05-5.2

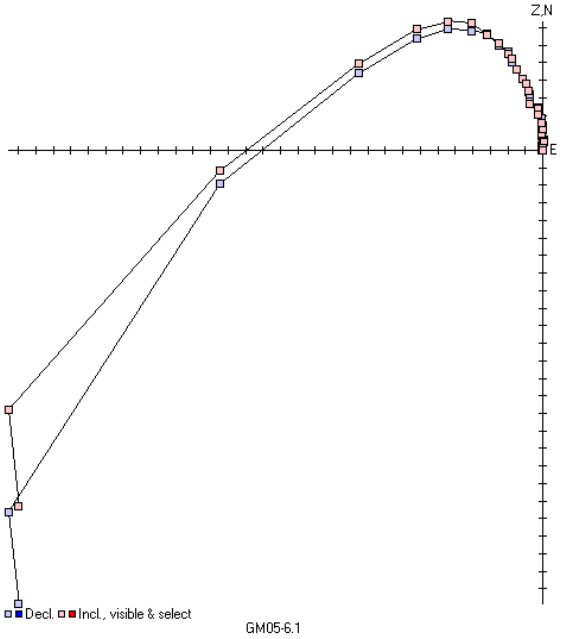

GM05-6.1

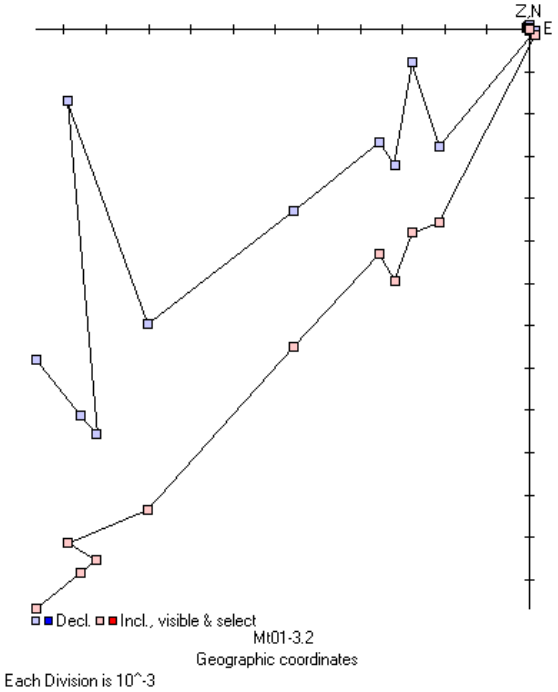
Z,N
E
Decl. Incl., visible & select
Mt01-3.2
Geographic coordinates
Each Division is 10^-3

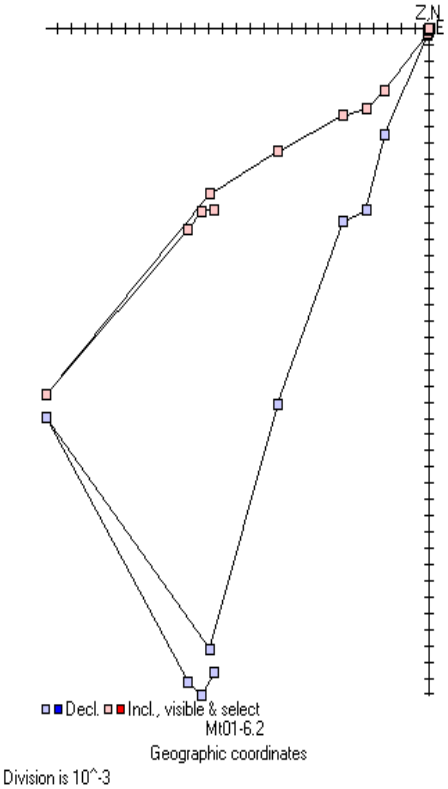
Z,N
E
Decl. Incl., visible & select
Mt01-6.2
Geographic coordinates
Division is 10^-3

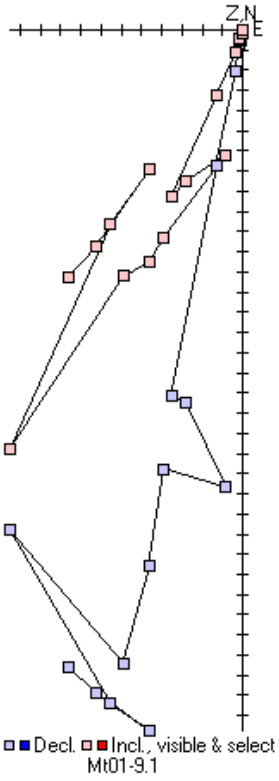
Z,N
E
Decl. Incl., visible & select
Mt01-9.1

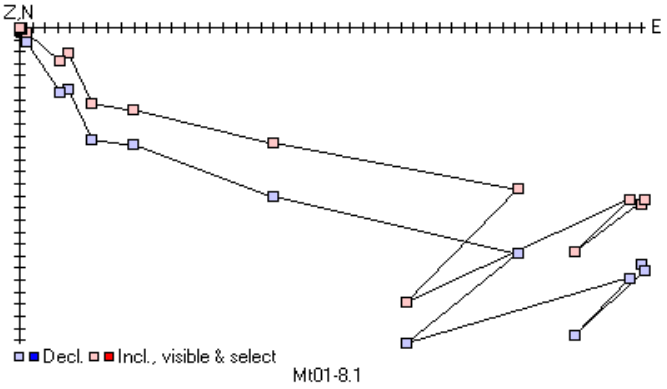
Z,N
E
Decl. Incl., visible & select
Mt01-8.1

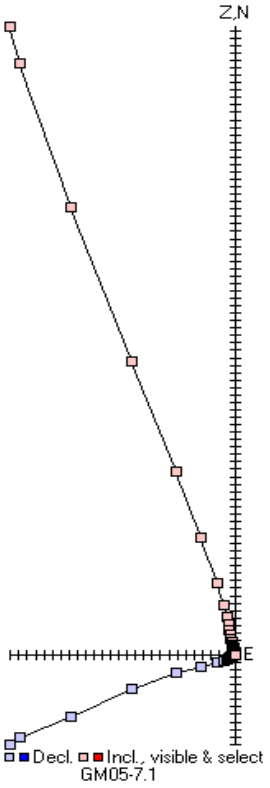
Z,N
E
Decl. Incl., visible & select
GM05-7.1

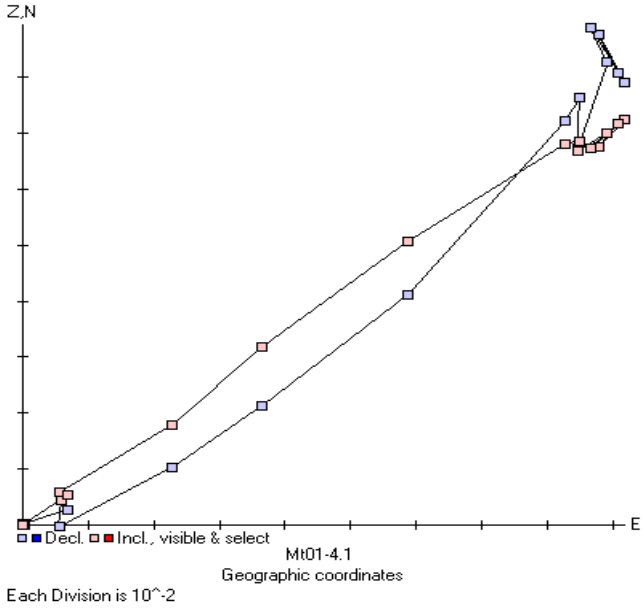
Z,N
E
Decl. Incl., visible & select
Mt01-4.1
Geographic coordinates
Each Division is 10^-2

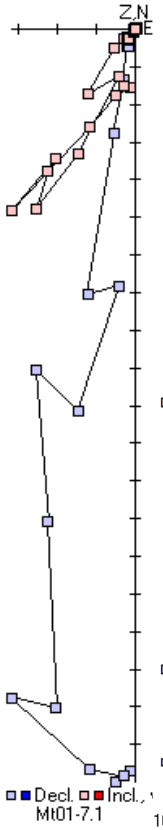
Z,N
E
Decl. Incl.,
Mt01-7.1

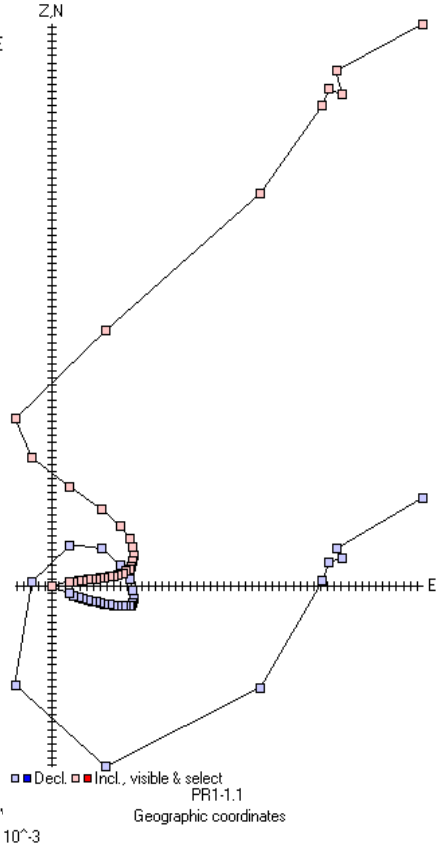
Z,N
E
Decl. Incl., visible & select
PR1-1.1
Geographic coordinates
10^-3

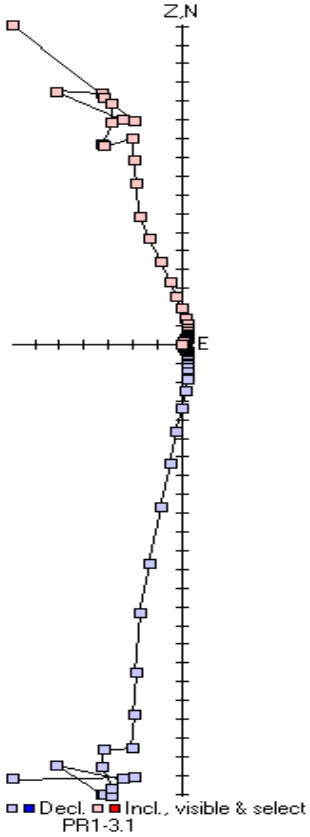
Z,N
E
Decl. Incl., visible & select
PR1-3.1

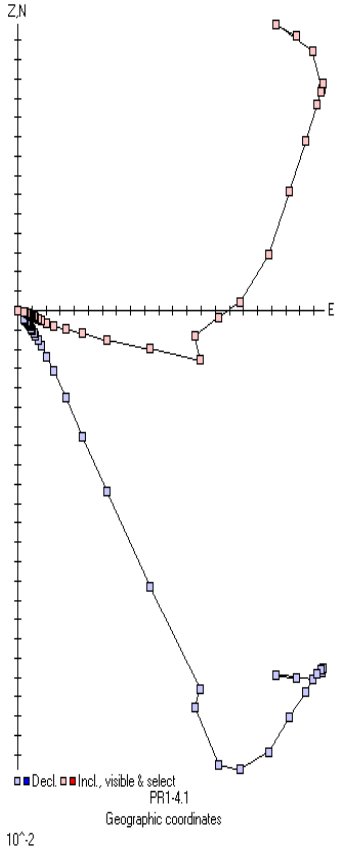
Z,N
E
Decl. Incl., visible & select
PR1-4.1
Geographic coordinates
10^-2

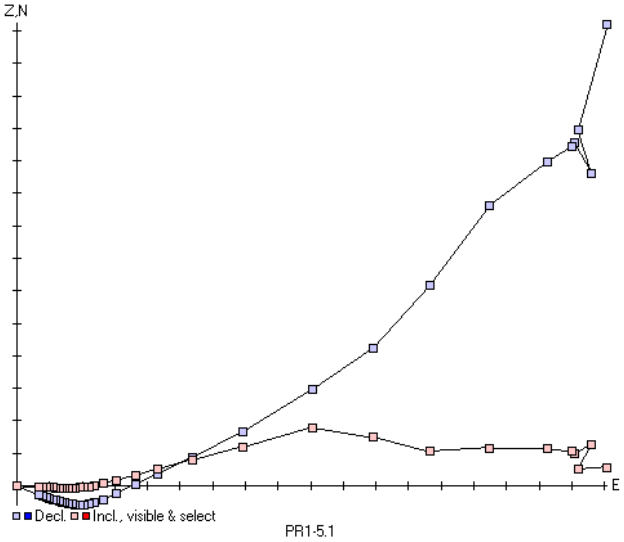
Z,N
E
Decl. Incl., visible & select
PR1-5.1

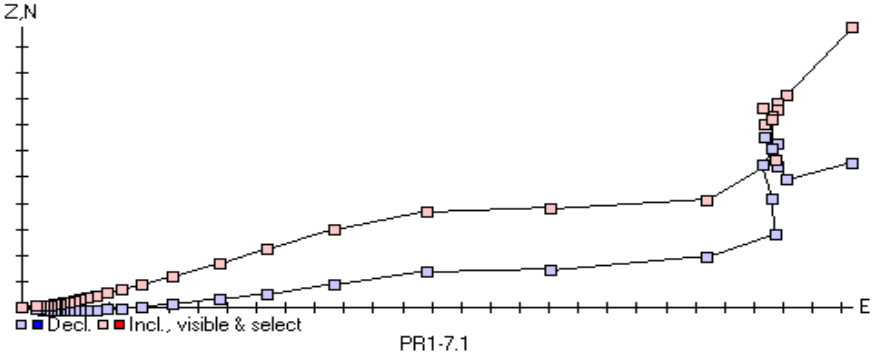
Z,N
E
Decl. Incl., visible & select
PR1-7.1

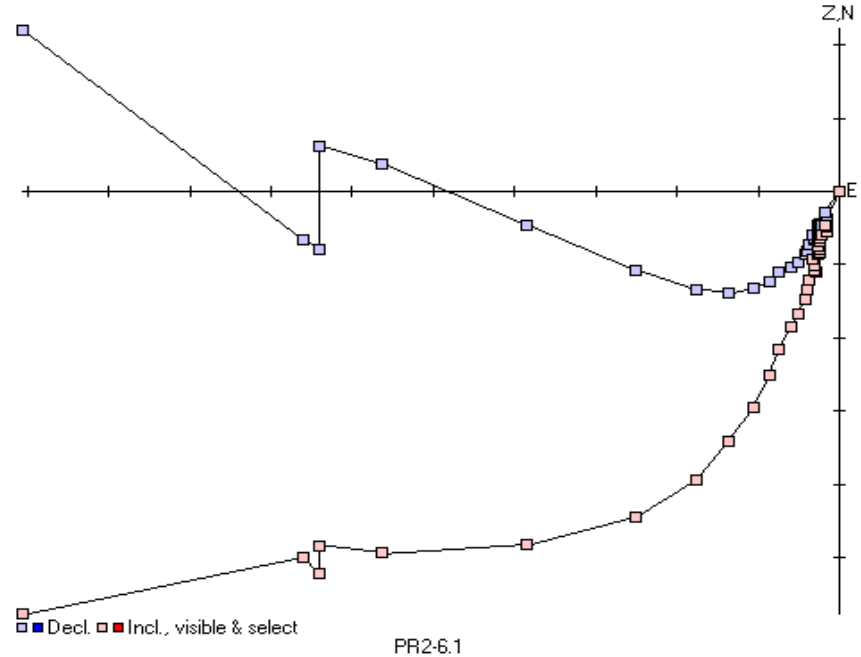

PR2-6.1
Geographic coordinates

Each Division is 10^-3

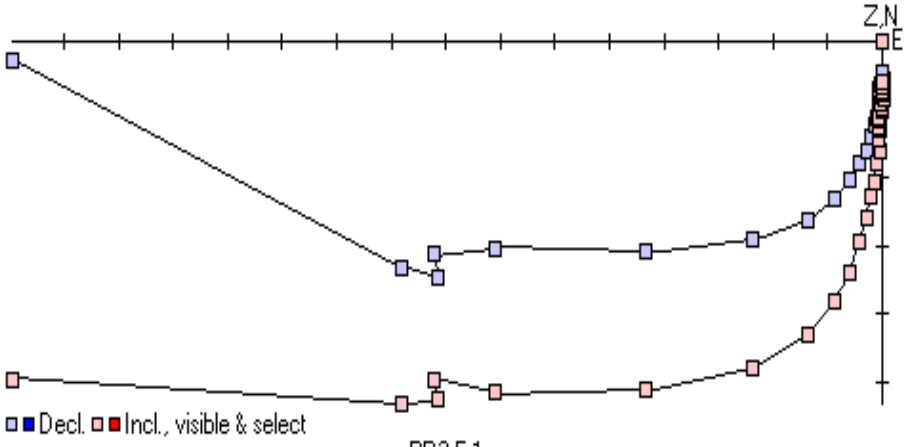

PR2-5.1
Geographic coordinates

Each Division is 10^-3

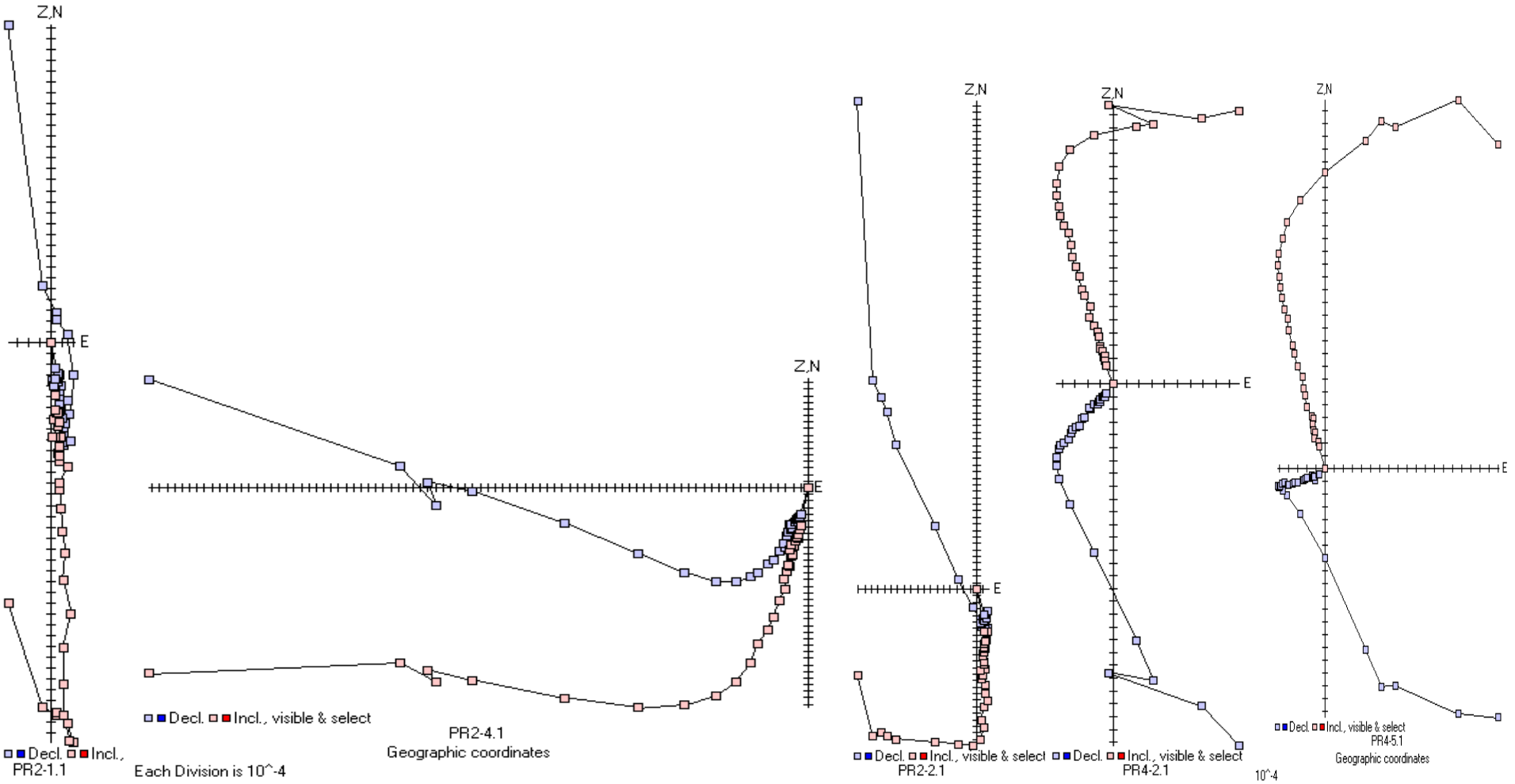
Z,N
E
Decl.
Incl.,
PR2-1.1
Each Division is 10^-4
Z,N
E
Decl.
Incl., visible & select
PR2-4.1
Geographic coordinates
Z,N
E
Decl.
Incl., visible & select
PR2-2.1
Z,N
E
Decl.
Incl., visible & select
PR4-2.1
Z,N
E
Decl.
Incl., visible & select
PR4-5.1
Geographic coordinates
10^-4

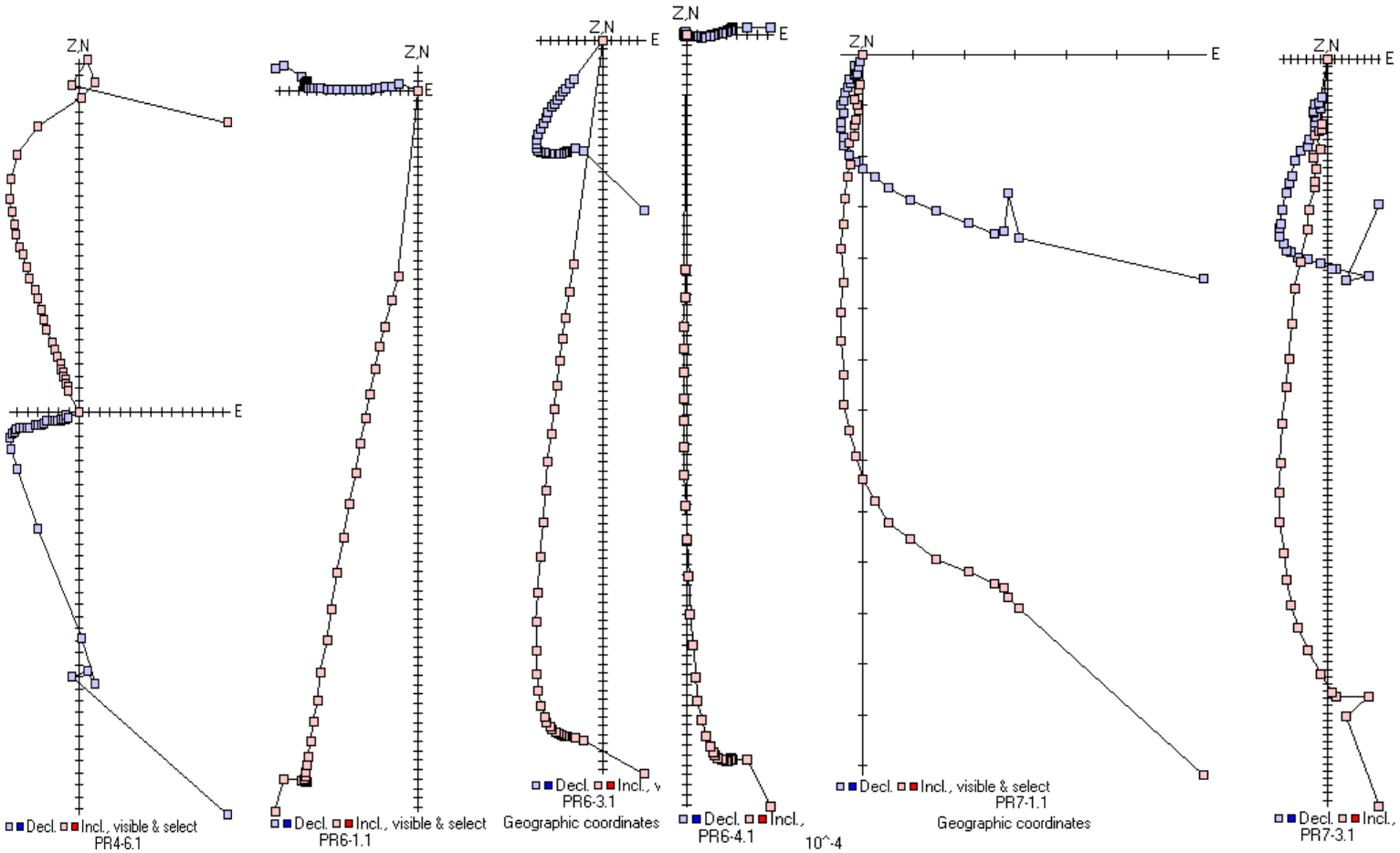
Z,N
E
Decl. Incl., visible & select
PR4-6.1
Z,N
E
Decl. Incl., visible & select
PR6-1.1
Z,N
E
Decl. Incl., v
PR6-3.1
Geographic coordinates
Z,N
E
Decl. Incl.,
PR6-4.1
10^-4
Z,N
E
Decl. Incl., visible & select
PR7-1.1
Geographic coordinates
Z,N
E
Decl. Incl.,
PR7-3.1

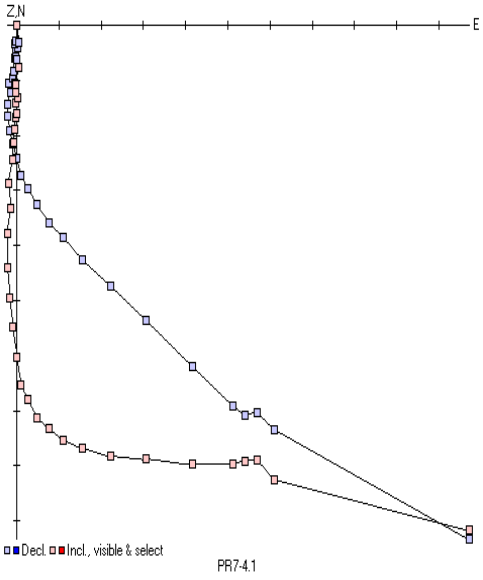
Z,N
E
Decl. Incl., visible & select
PR7-4.1

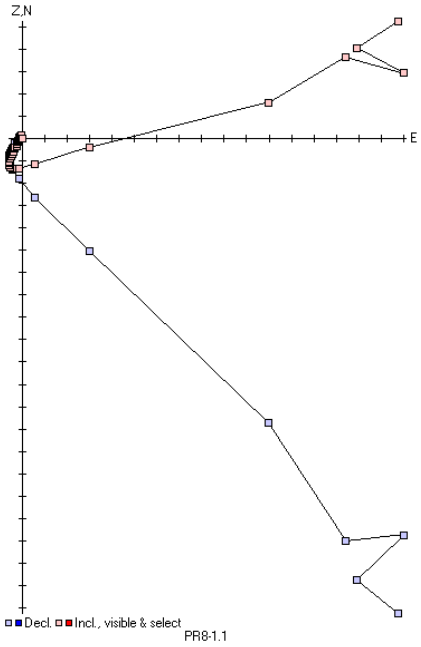
Z,N
E
Decl. Incl., visible & select
PR8-1.1

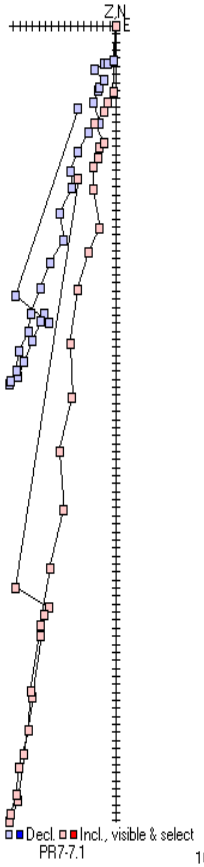
Z,N
E
Decl. Incl., visible & select
PR7-7.1

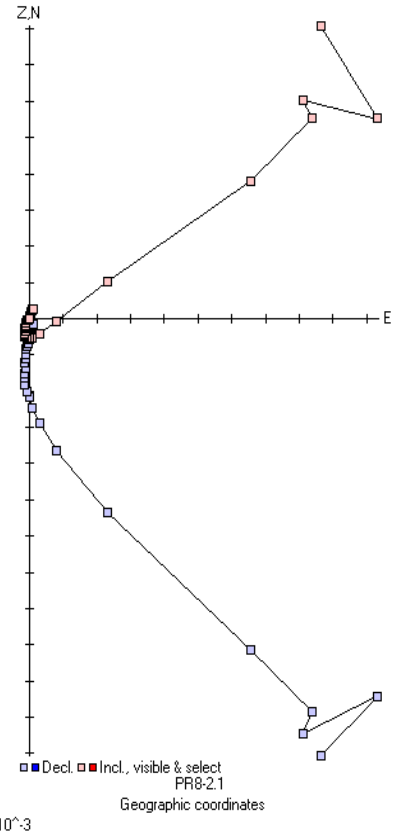
Z,N
E
Decl. Incl., visible & select
PR8-2.1
Geographic coordinates
10^-3

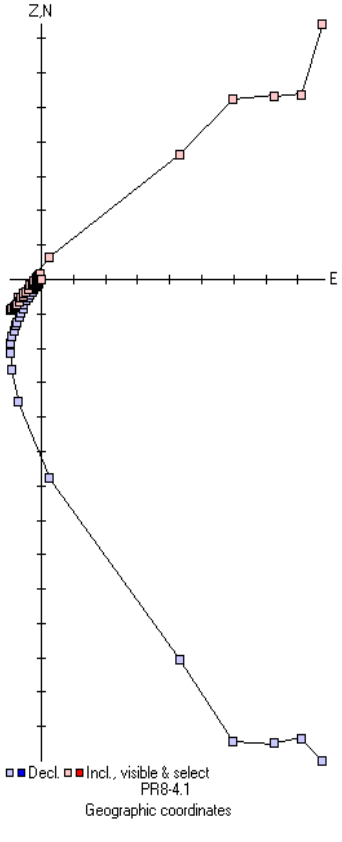
Z,N
E
Decl. Incl., visible & select
PR8-4.1
Geographic coordinates
10^-3

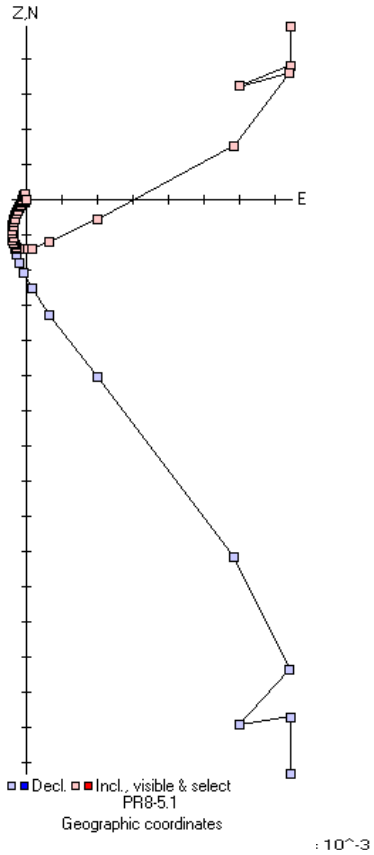

: 10^-3

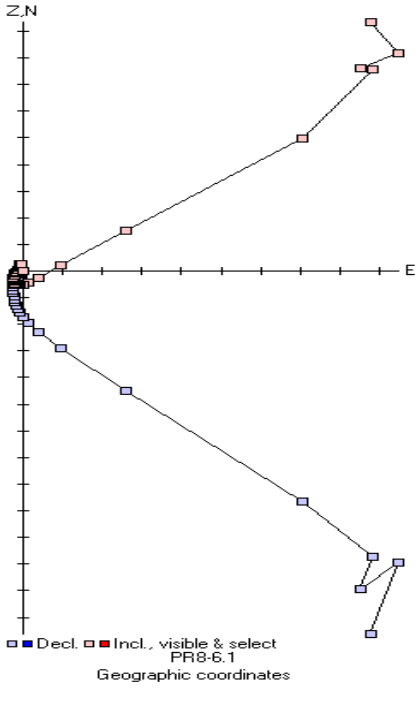

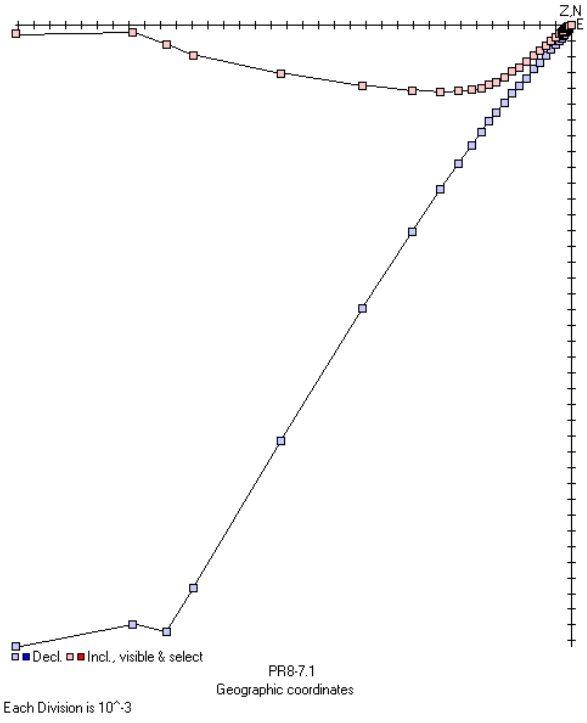

Each Division is 10^-3

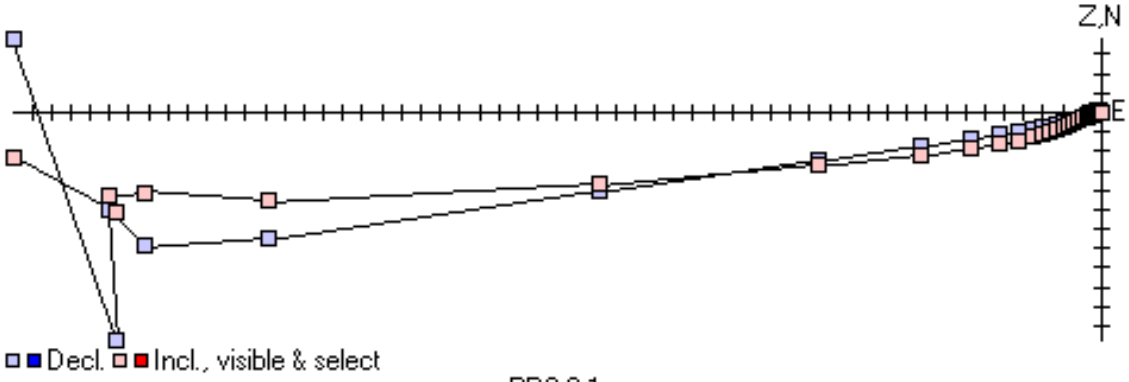

PR8-8.1
Geographic coordinates

Each Division is 10^-3

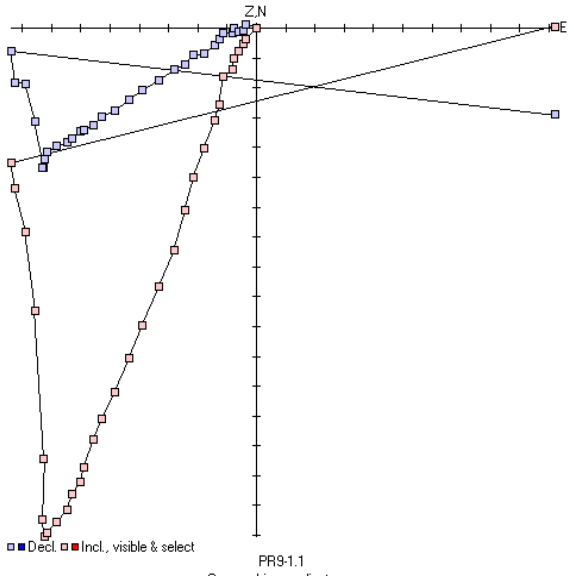

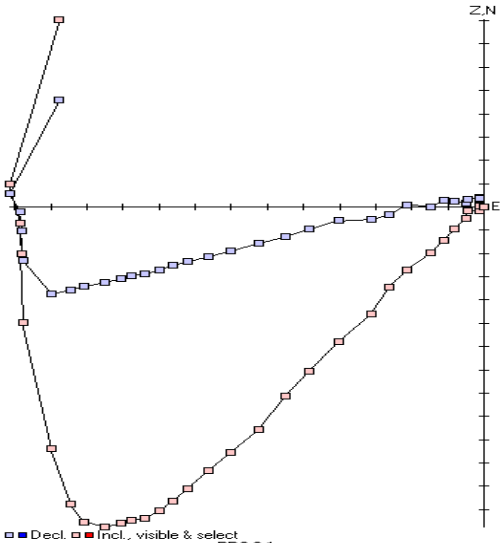

is 10^-4

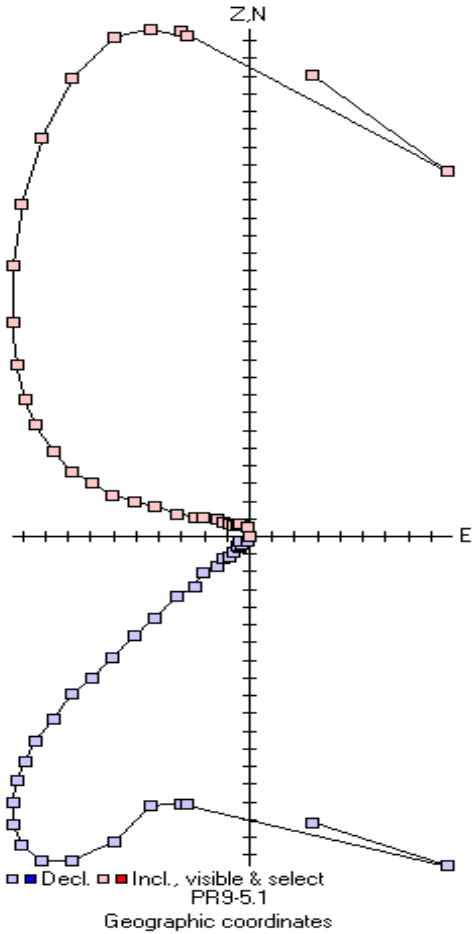

PR9-5.1

Geographic coordinates

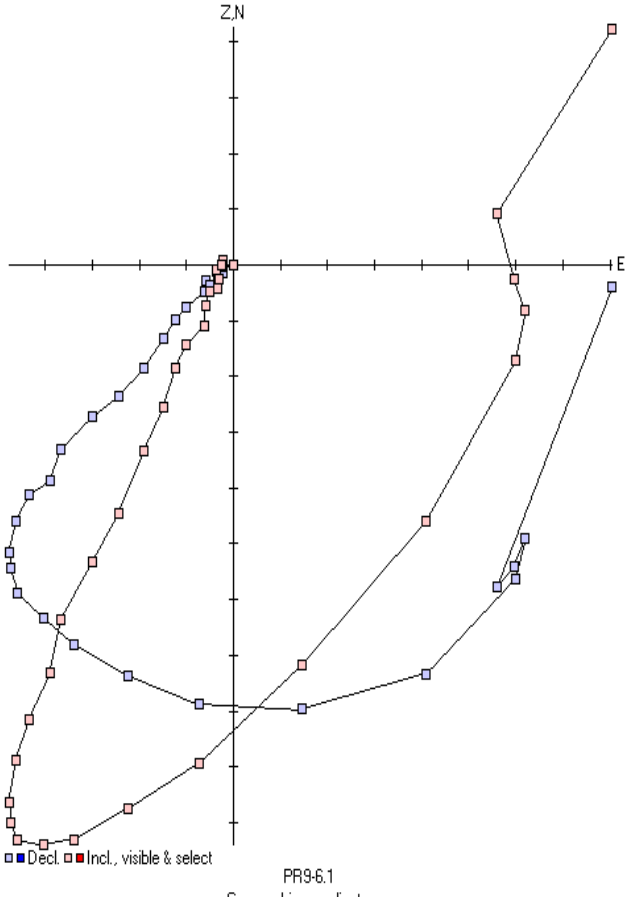

PR9-6.1

12.6 Tweed

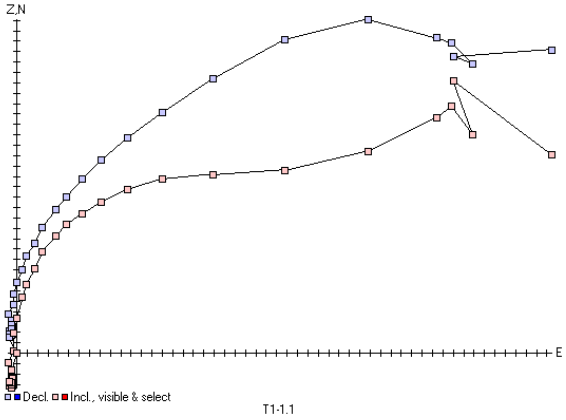
Z,N
E
Decl. Incl., visible & select
T1-1.1

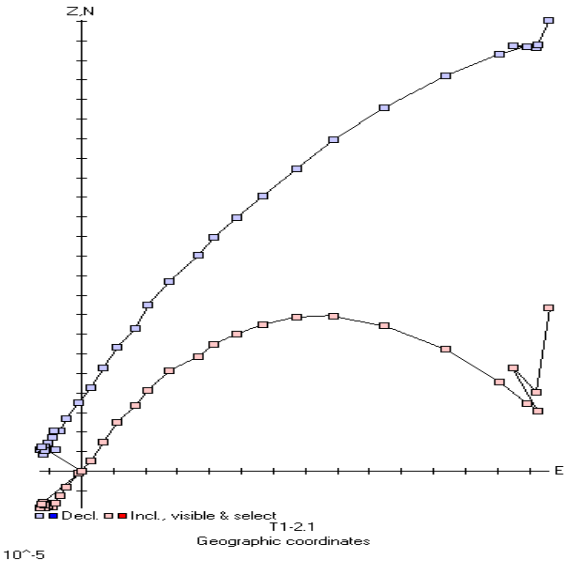
Z,N
E
Decl. Incl., visible & select
T1-2.1
Geographic coordinates
10^-5

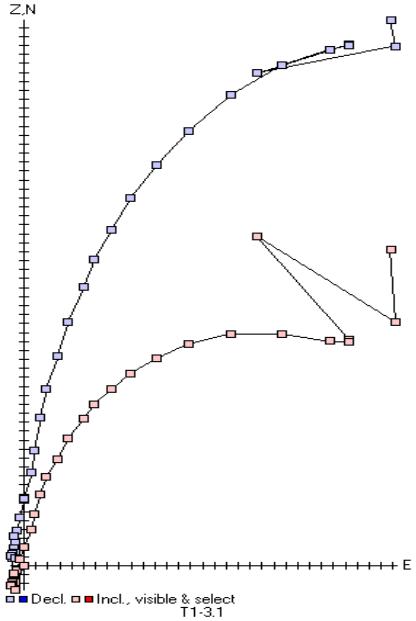
Z,N
E
Decl. Incl., visible & select
T1-3.1

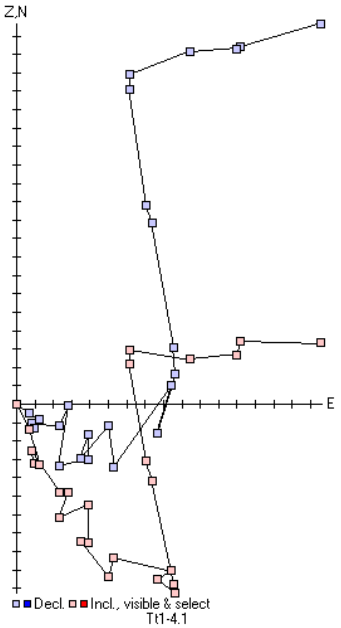
Z,N
E
Decl. Incl., visible & select
Tt1-4.1

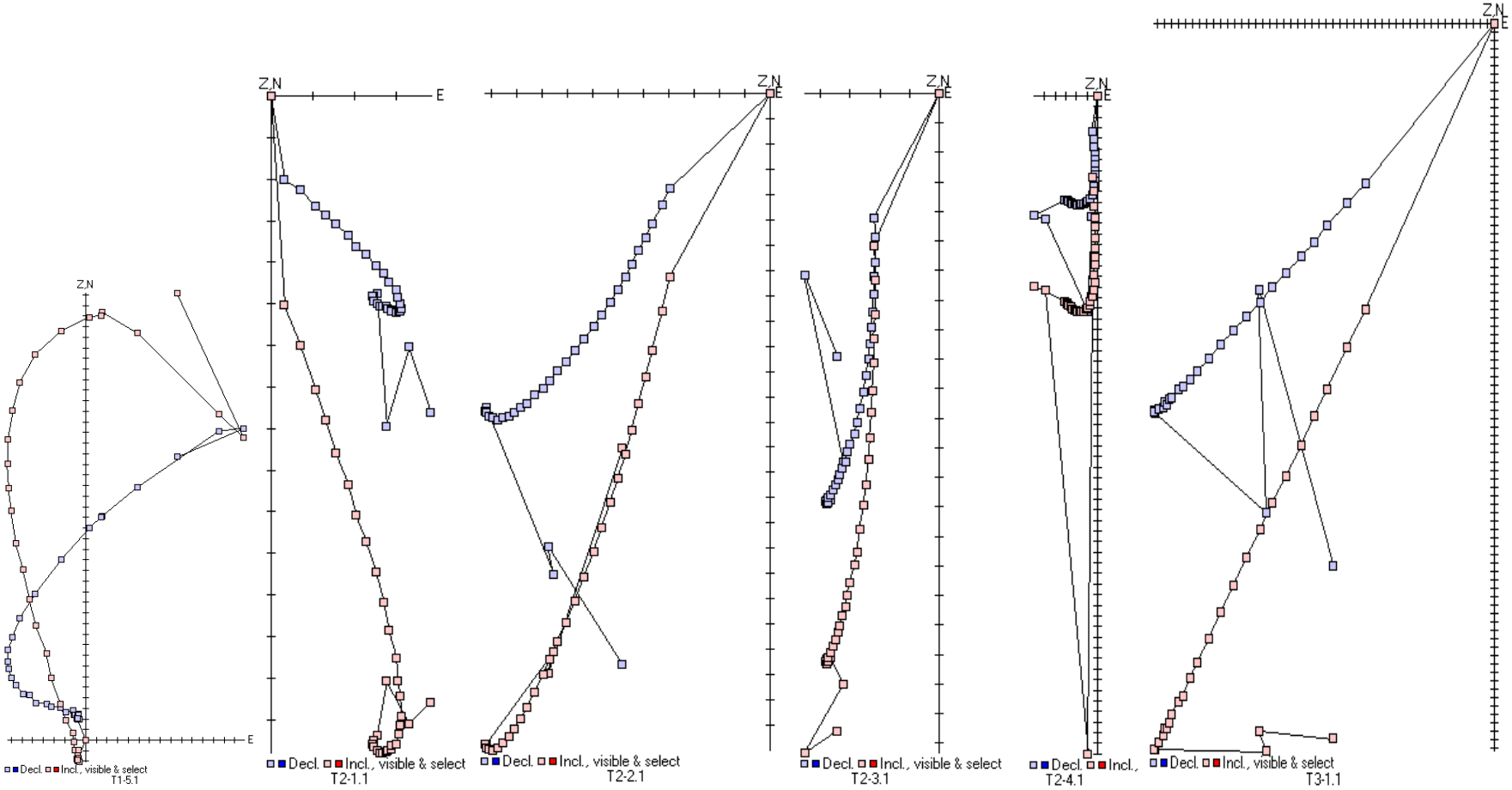
Z,N
E
Decl.
Incl., visible & select
T1-5.1
T2-1.1
T2-2.1
T2-3.1
T2-4.1
T3-1.1

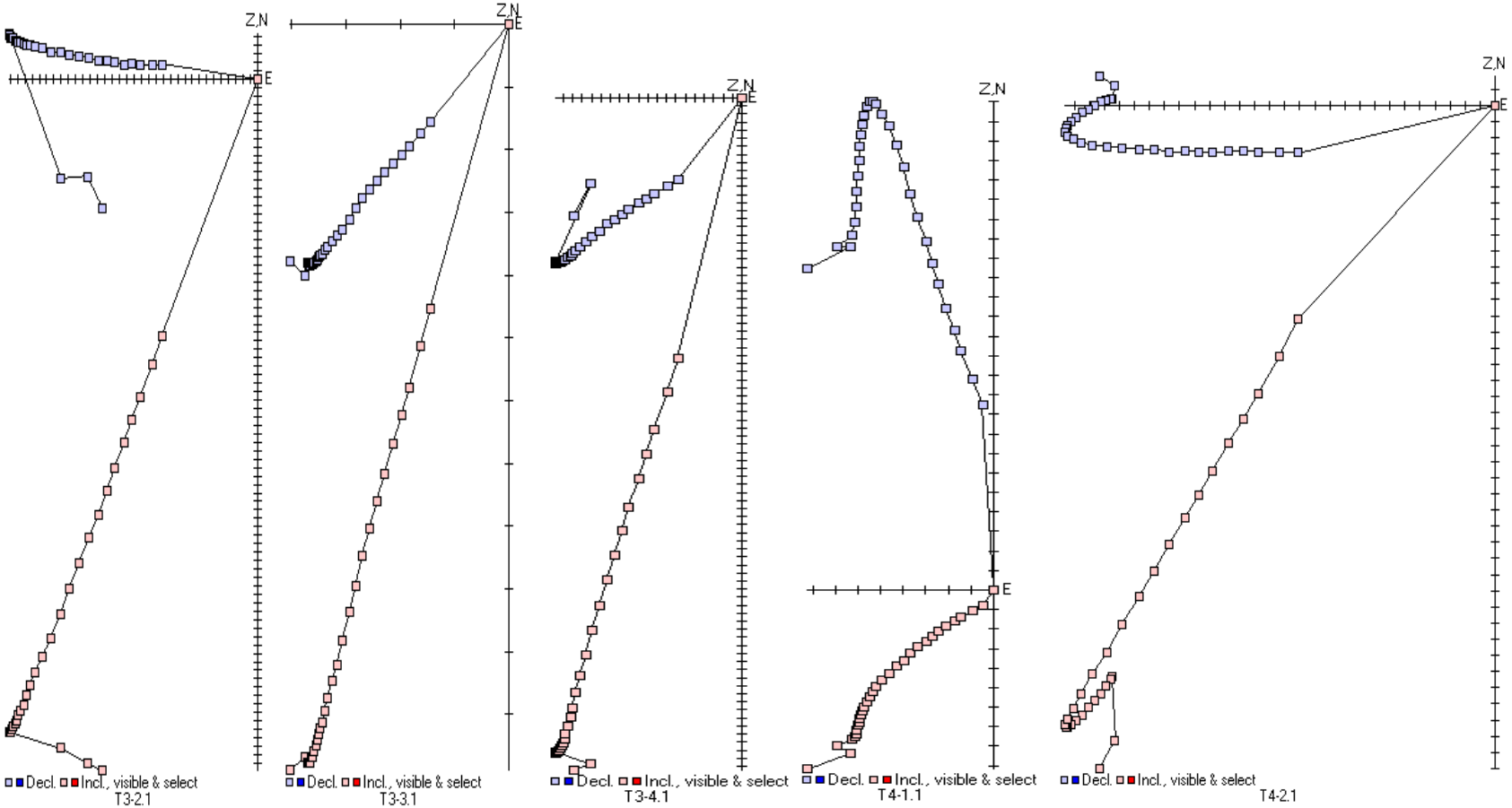
Z,N
E
Decl. Incl., visible & select
T3-2.1
Z,N
E
Decl. Incl., visible & select
T3-3.1
Z,N
E
Decl. Incl., visible & select
T3-4.1
Z,N
E
Decl. Incl., visible & select
T4-1.1
Z,N
E
Decl. Incl., visible & select
T4-2.1

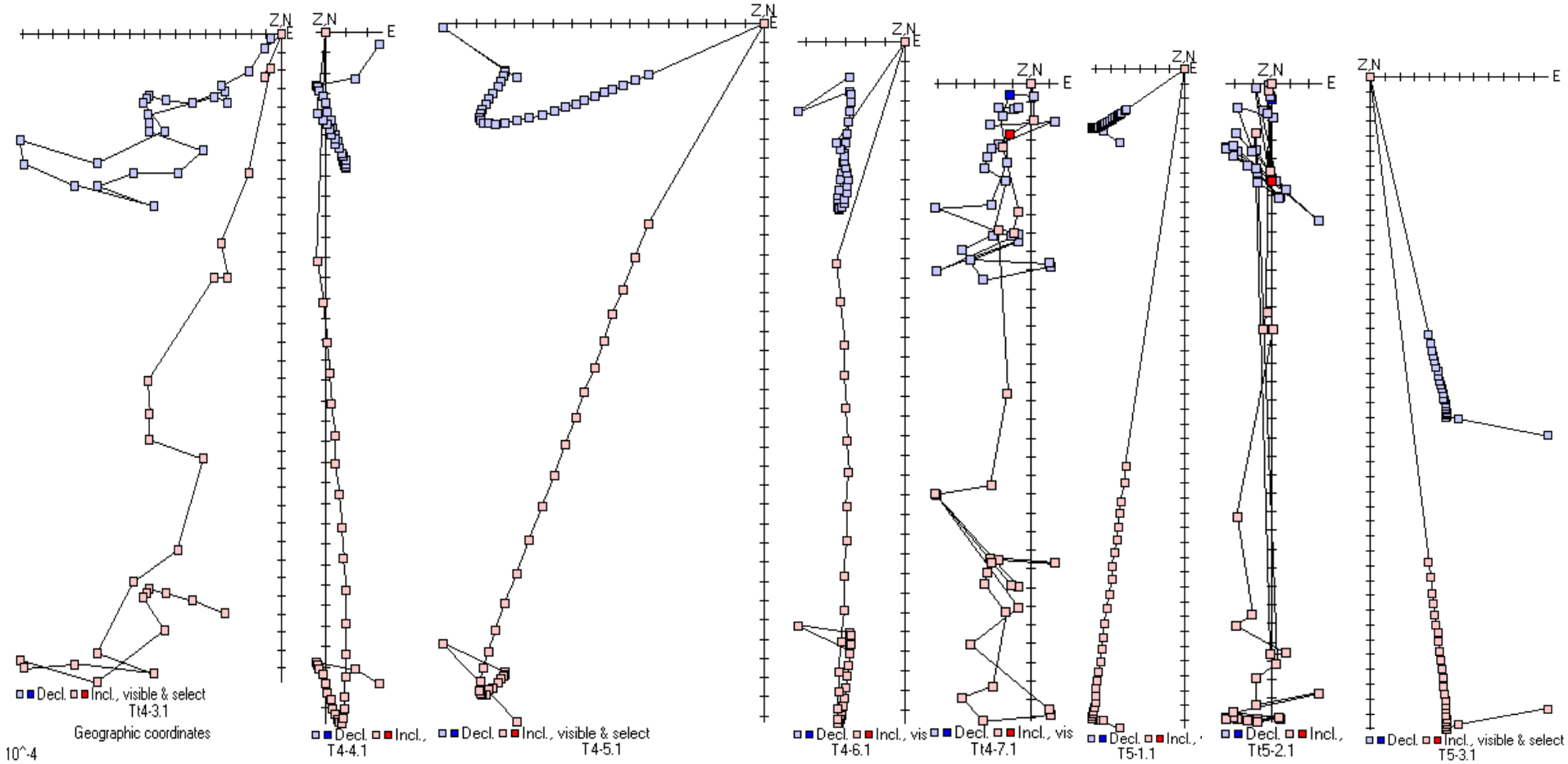
Z,N
E
Decl. Incl., visible & select
Tt4-3.1
Geographic coordinates
10^-4
Decl. Incl.,
T4-4.1
Decl. Incl., visible & select
T4-5.1
Decl. Incl., vis
T4-6.1
Decl. Incl., vis
Tt4-7.1
Decl. Incl.,
T5-1.1
Decl. Incl.,
Tt5-2.1
Decl. Incl., visible & select
T5-3.1

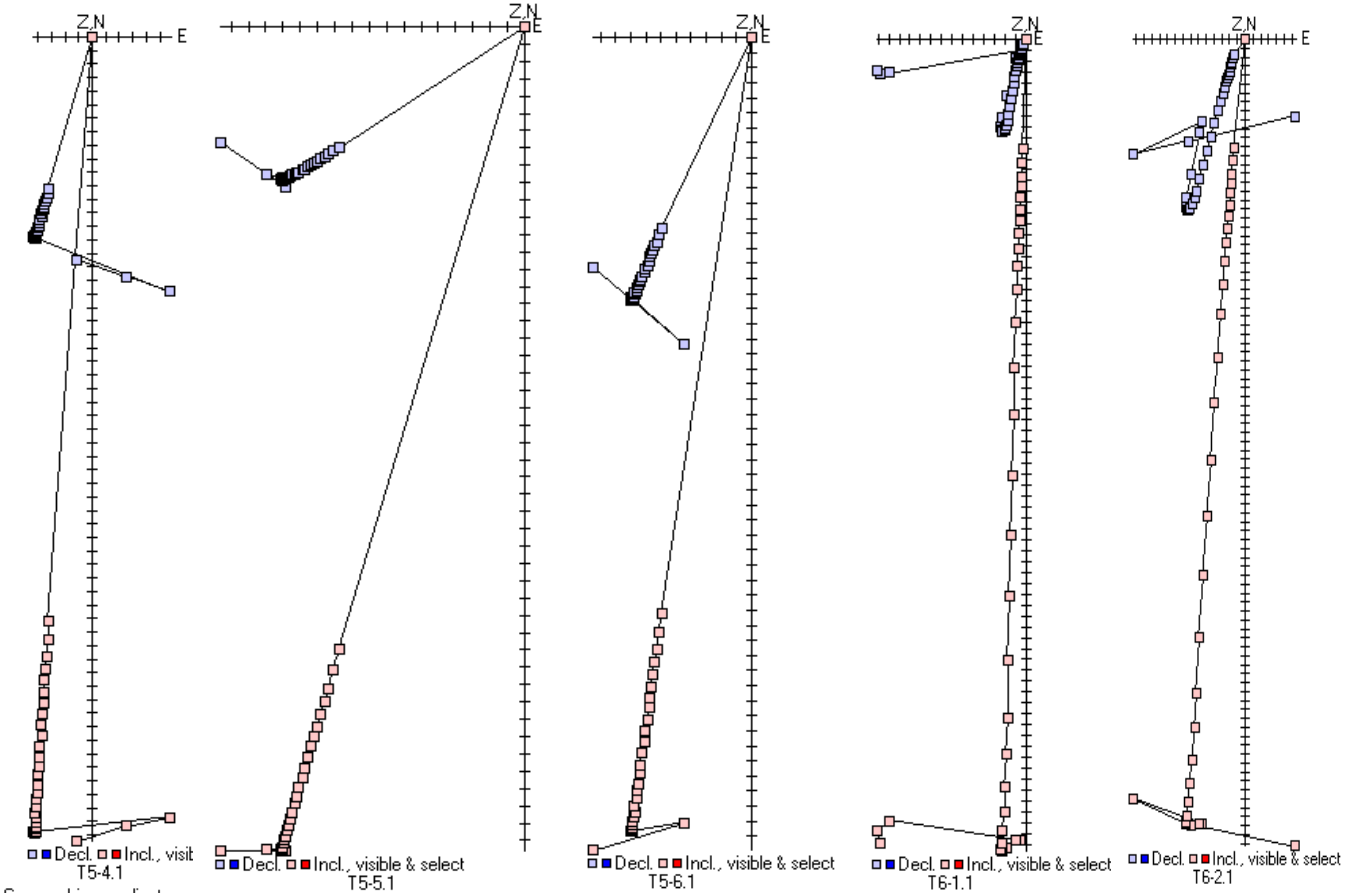
Z,N
E
Decl.
Incl., visit
T5-4.1
Z,N
E
Decl.
Incl., visible & select
T5-5.1
Z,N
E
Decl.
Incl., visible & select
T5-6.1
Z,N
E
Decl.
Incl., visible & select
T6-1.1
Z,N
E
Decl.
Incl., visible & select
T6-2.1

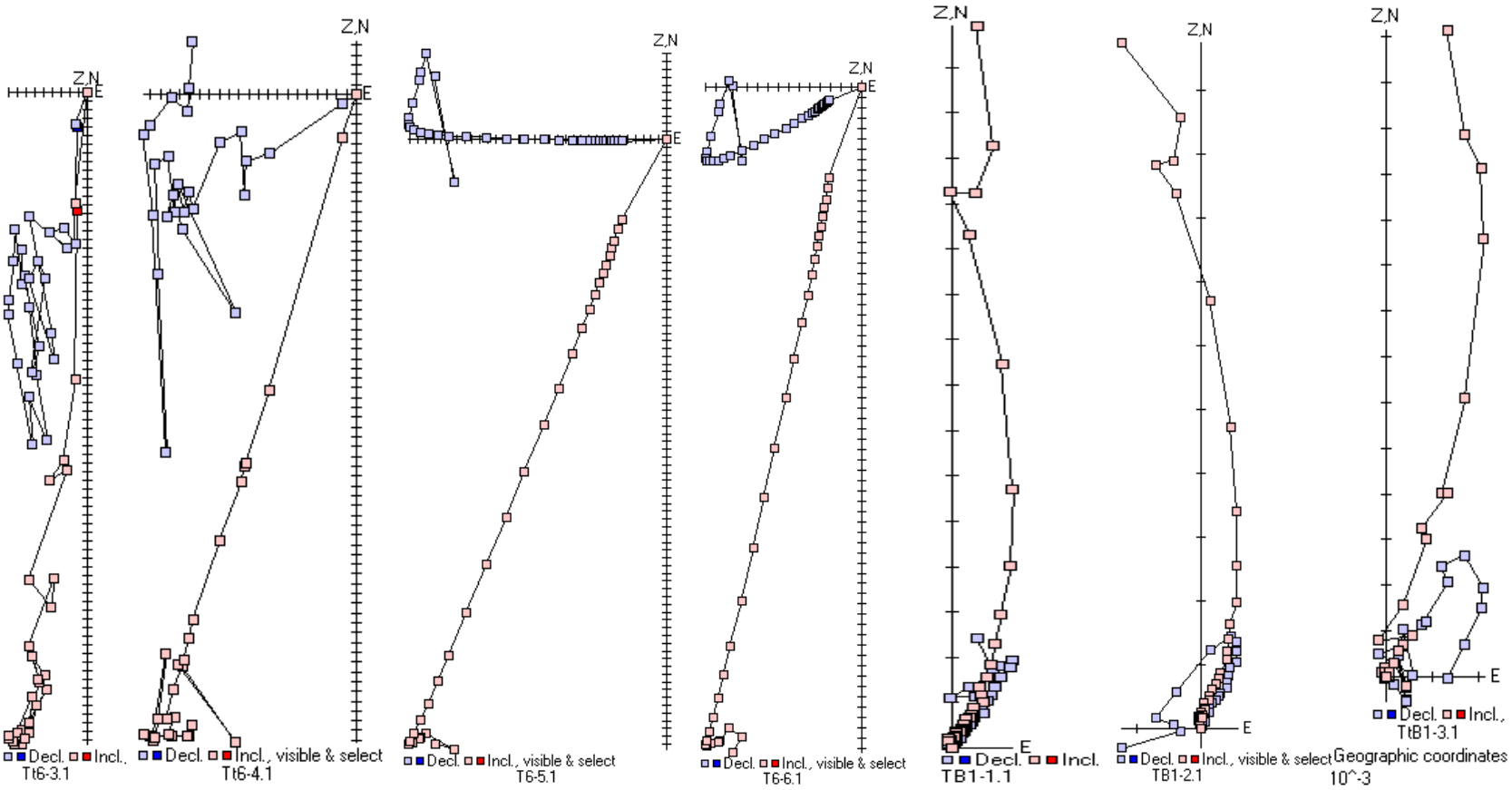
Z,N
E
Decl.
Incl.
Tt6-3.1
Z,N
E
Decl.
Incl., visible & select
Tt6-4.1
Z,N
E
Decl.
Incl., visible & select
T6-5.1
Z,N
E
Decl.
Incl., visible & select
T6-6.1
Z,N
E
Decl.
Incl.
TB1-1.1
Z,N
E
Decl.
Incl., visible & select
TB1-2.1
Z,N
E
Decl.
Incl.,
TtB1-3.1
Geographic coordinates
10^-3

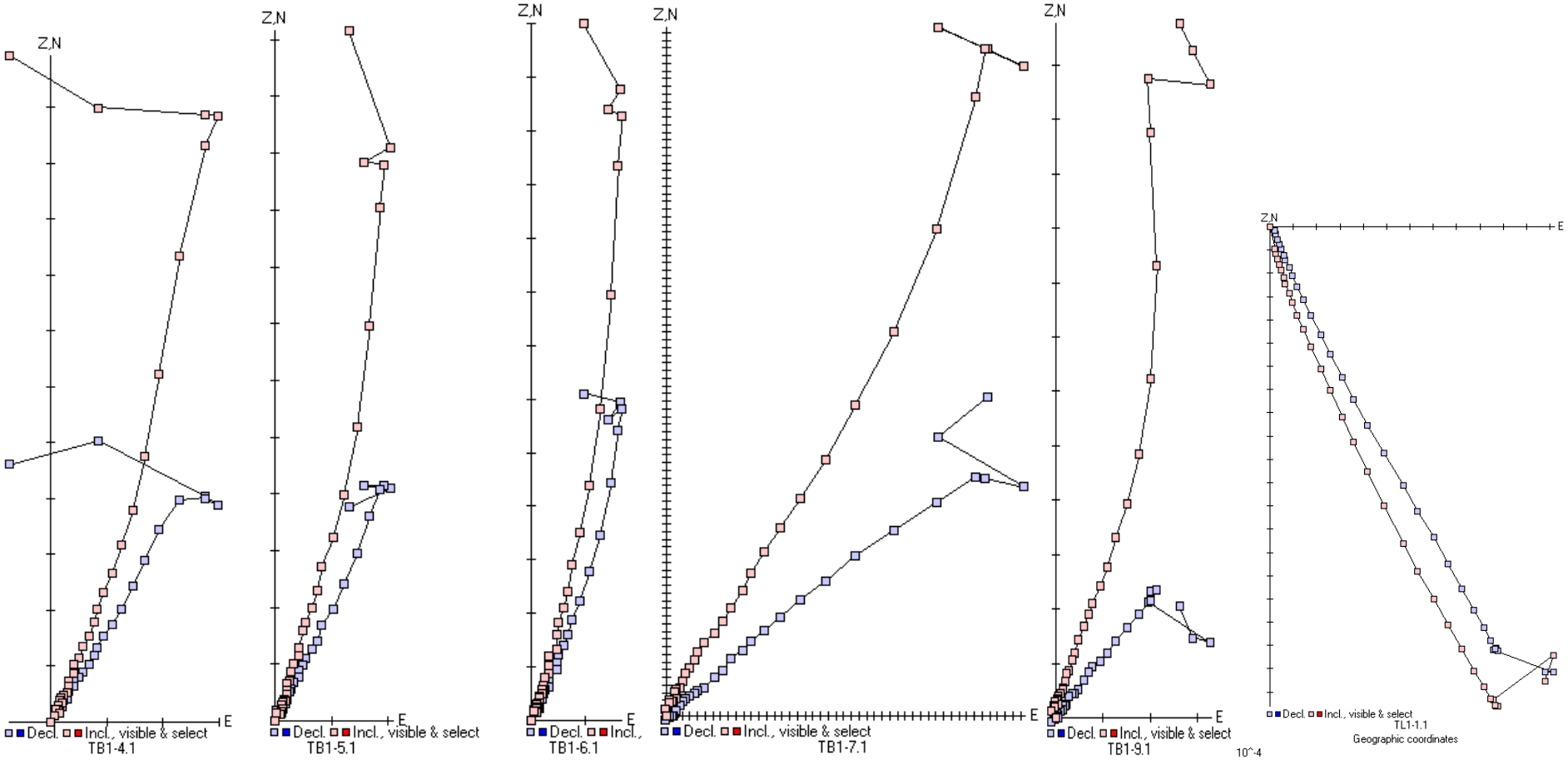
Z,N
E
Decl.
Incl., visible & select
TB1-4.1
TB1-5.1
TB1-6.1
TB1-7.1
TB1-9.1
10^-4
TL1-1.1
Geographic coordinates

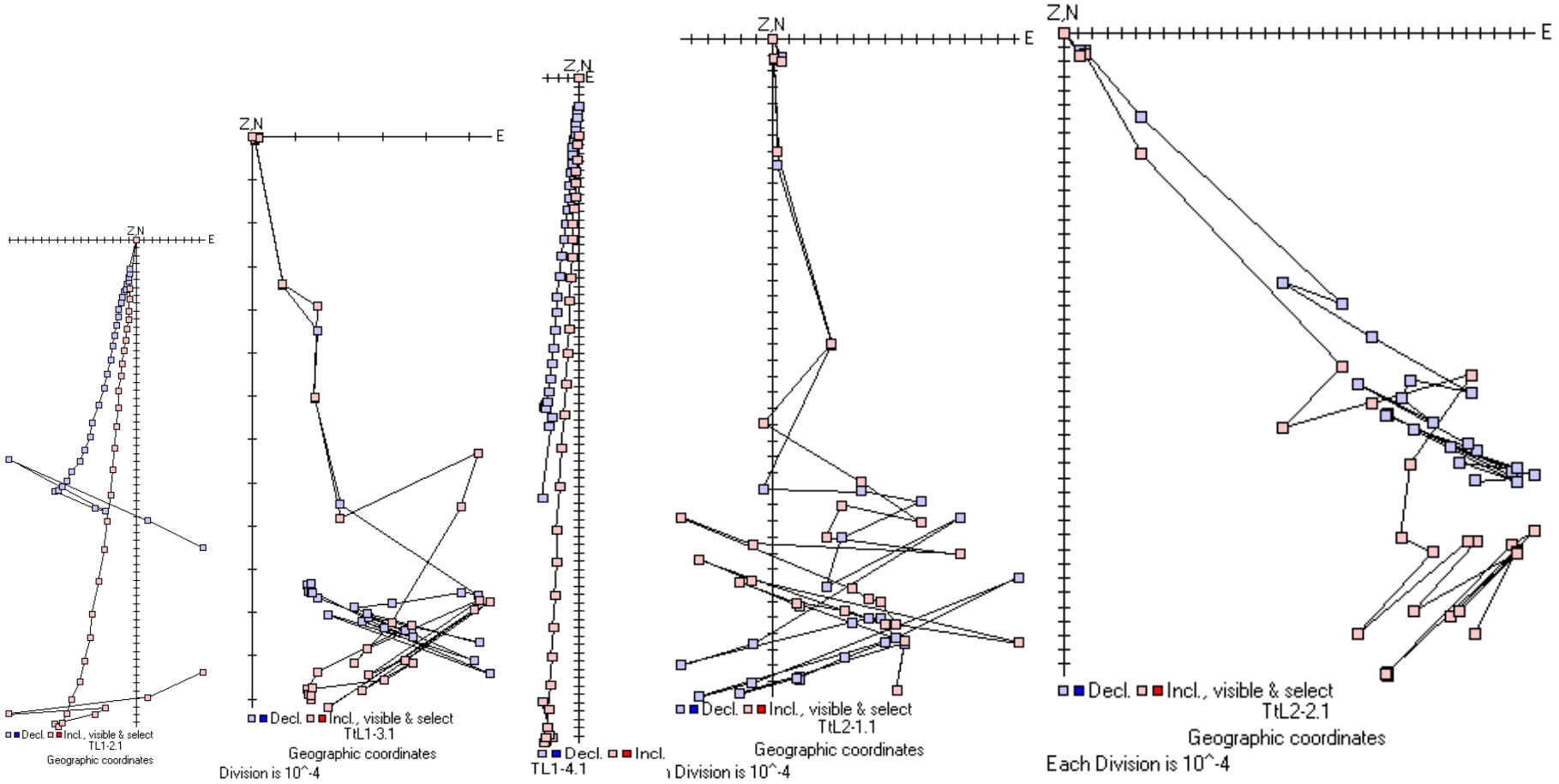
Z,N
E
Decl.
Incl., visible & select
TL1-2.1
Geographic coordinates
Z,N
E
Decl.
Incl., visible & select
TtL1-3.1
Geographic coordinates
Division is 10^-4
Z,N
E
Decl.
Incl.
TL1-4.1
Z,N
E
Decl.
Incl., visible & select
TtL2-1.1
Geographic coordinates
Division is 10^-4
Z,N
E
Decl.
Incl., visible & select
TtL2-2.1
Geographic coordinates
Each Division is 10^-4

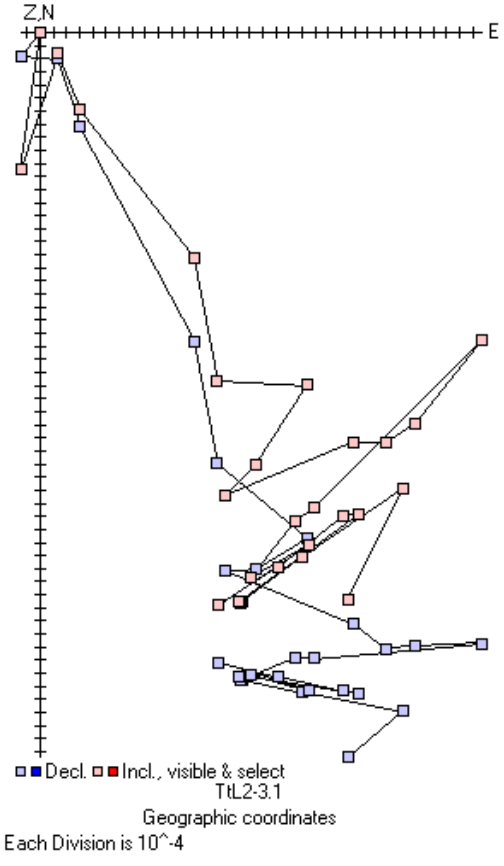
Z,N
E
Decl. Incl., visible & select
TtL2-3.1
Geographic coordinates
Each Division is 10^-4

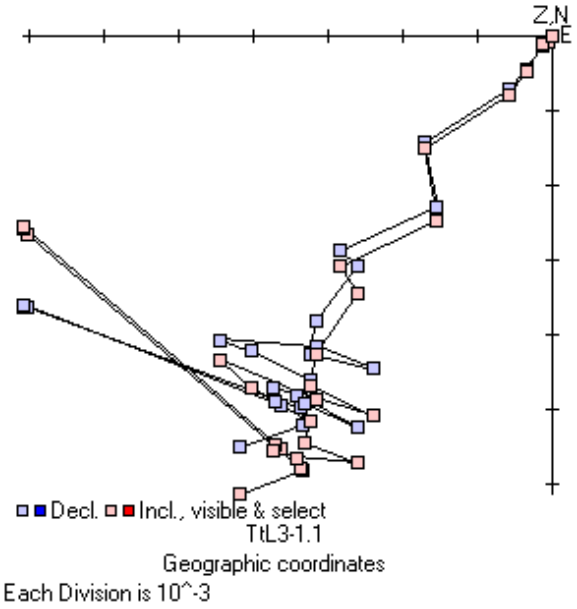
Z,N
E
Decl. Incl., visible & select
TtL3-1.1
Geographic coordinates
Each Division is 10^-3

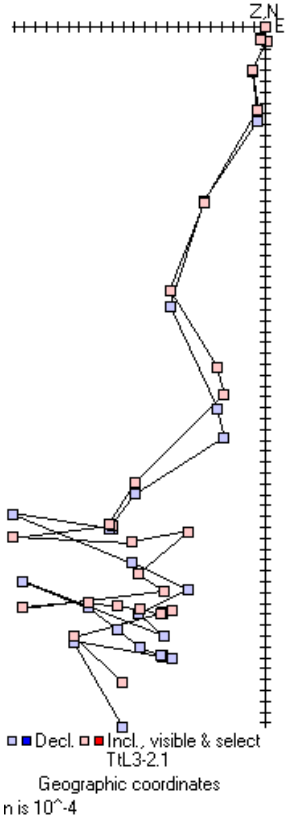
Z,N
E
Decl. Incl., visible & select
TtL3-2.1
Geographic coordinates
n is 10^-4

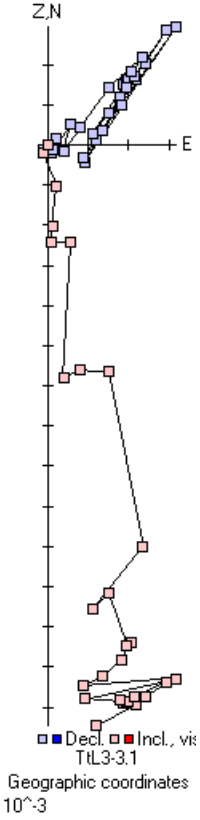
Z,N
E
Decl. Incl., vis
TtL3-3.1
Geographic coordinates
10^-3

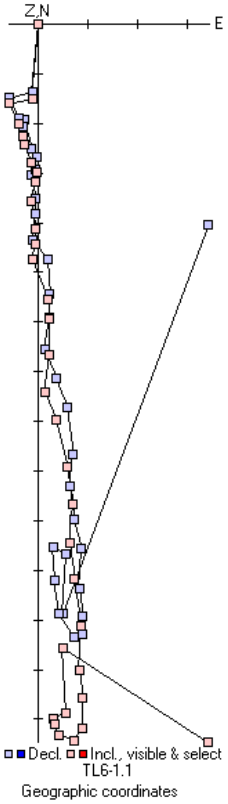
Z,N
E
Decl. Incl., visible & select
TL6-1.1
Geographic coordinates

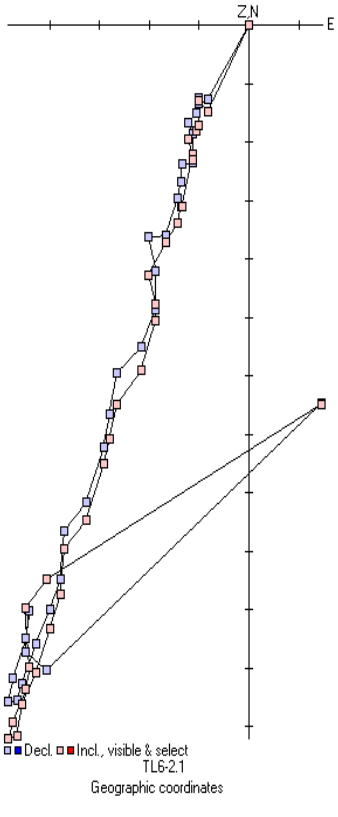

10^-4

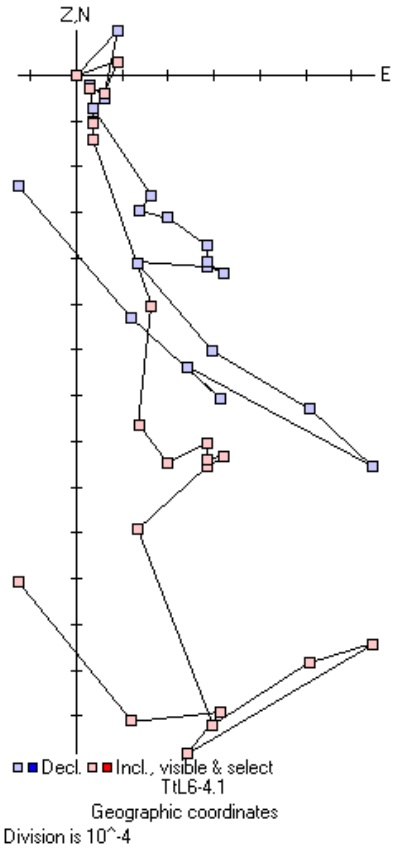

Division is 10^-4

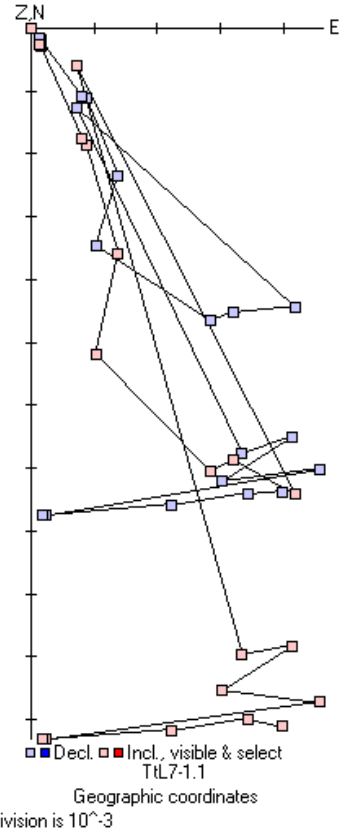

Division is 10^-3

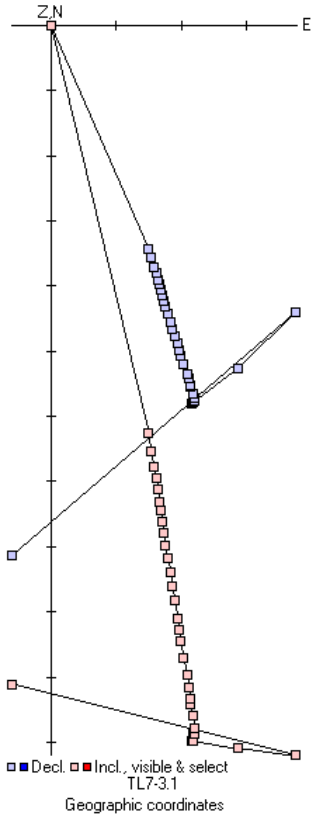

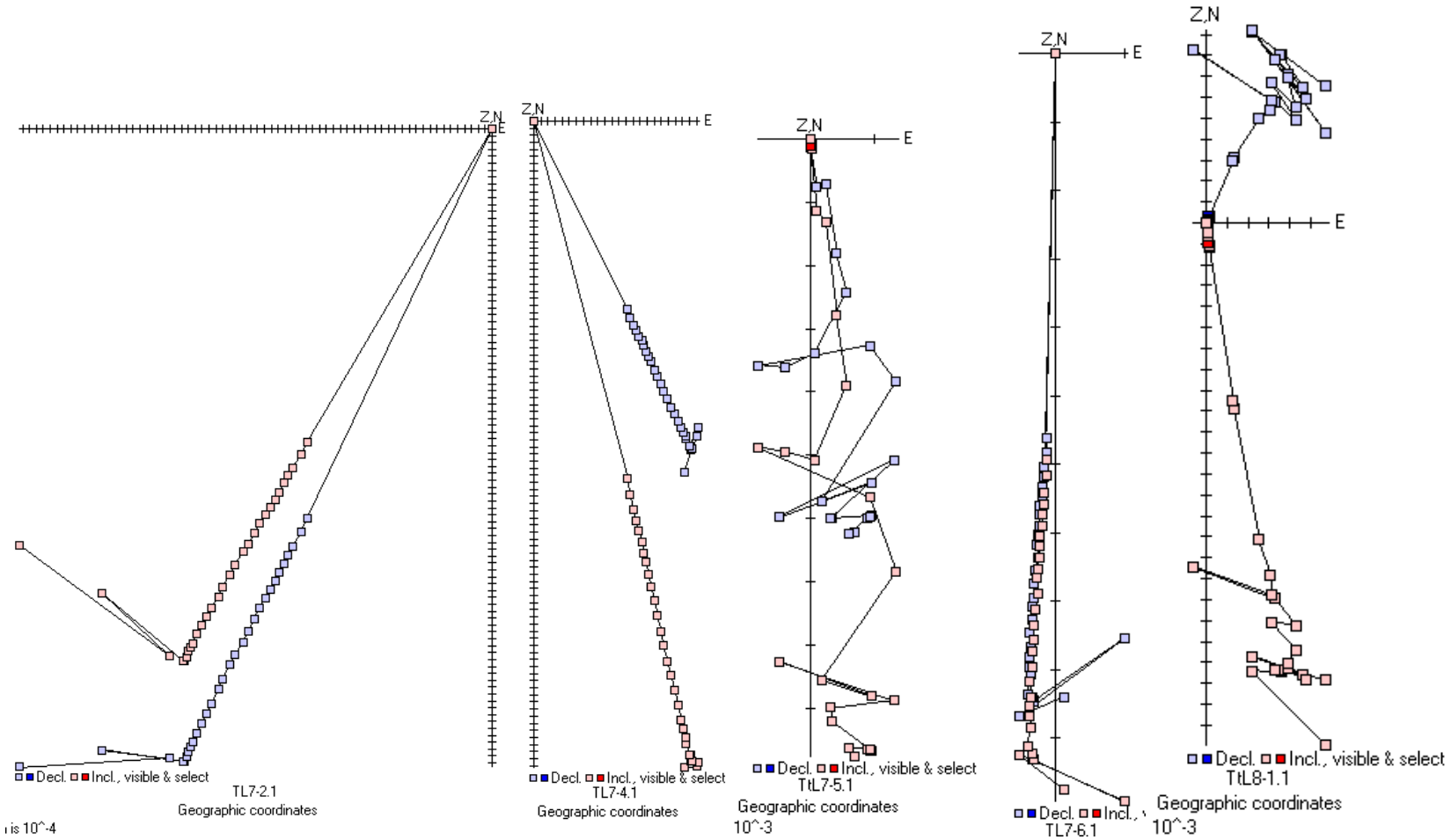
Z,N
E
Decl. Incl., visible & select
TL7-2.1
Geographic coordinates
is 10^-4
Z,N
E
Decl. Incl., visible & select
TL7-4.1
Geographic coordinates
Z,N
E
Decl. Incl., visible & select
TtL7-5.1
Geographic coordinates
10^-3
Z,N
E
Decl. Incl.,
TL7-6.1
Z,N
E
Decl. Incl., visible & select
TtL8-1.1
Geographic coordinates
10^-3

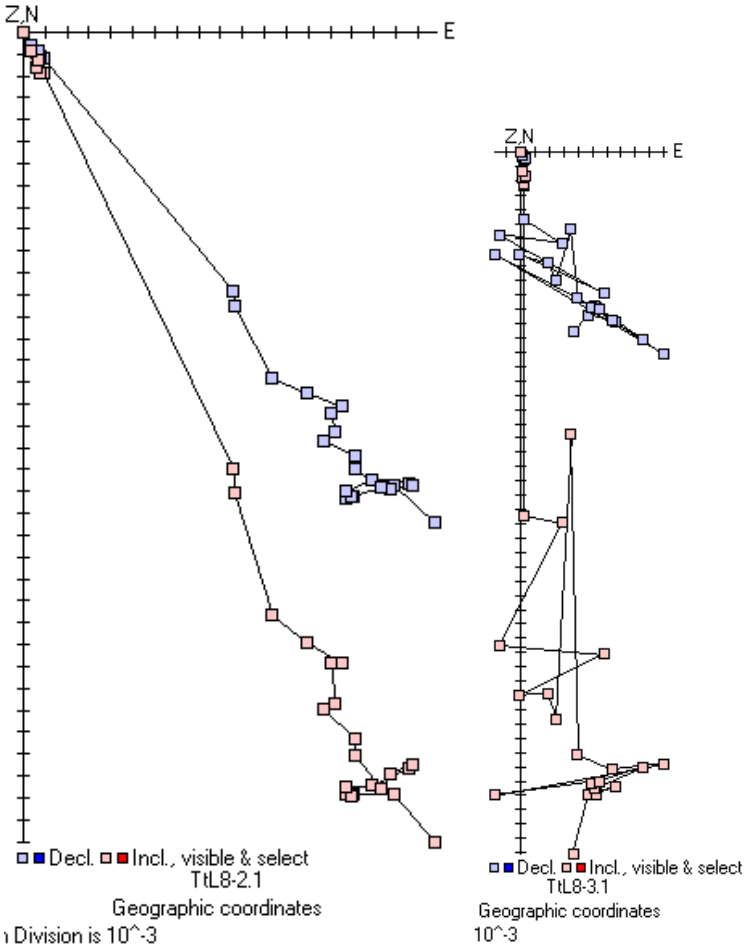
Z,N
E
Decl.
Incl., visible & select
TtL8-2.1
Geographic coordinates
Division is 10^-3

Z,N
E
Decl.
Incl., visible & select
TtL8-3.1
Geographic coordinates
10^-3

12.7 Warrumbungles

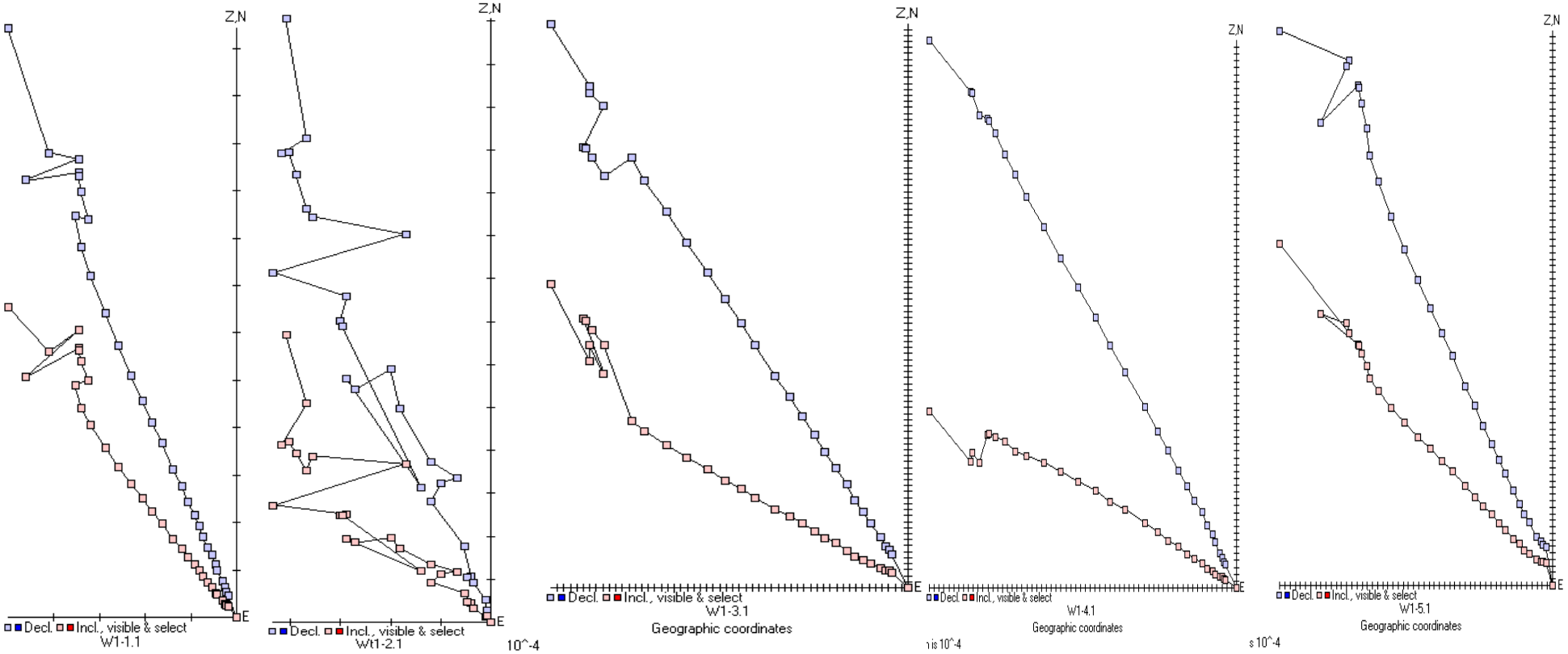

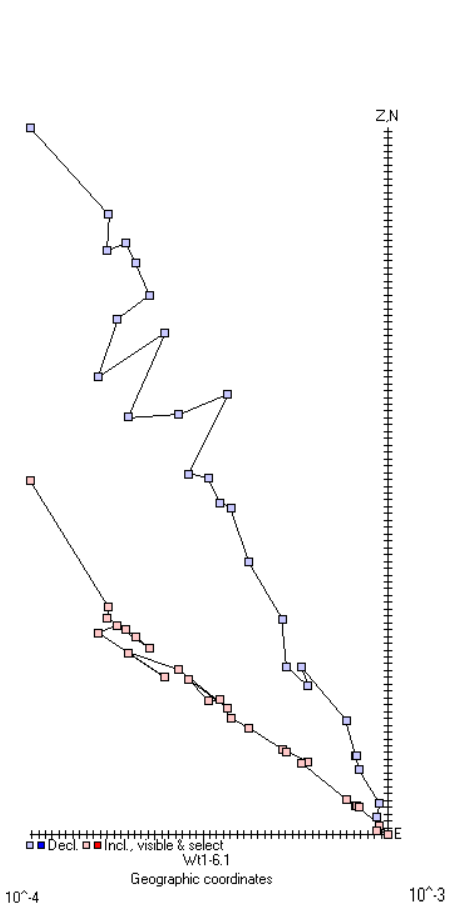
Z,N
E
Decl.
Incl., visible & select
Wt1-6.1
Geographic coordinates
10^-4
10^-3

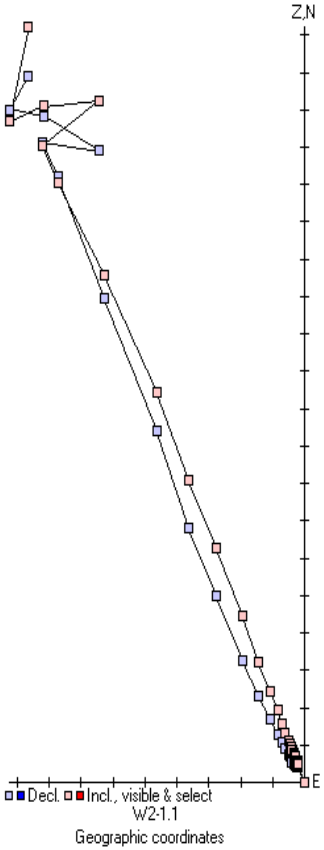
Z,N
E
Decl.
Incl., visible & select
W2-1.1
Geographic coordinates

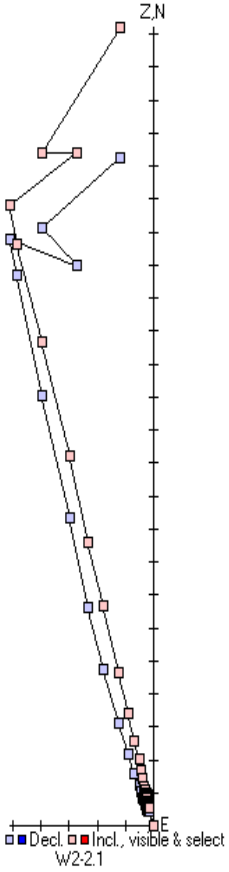
Z,N
E
Decl.
Incl., visible & select
W2-2.1

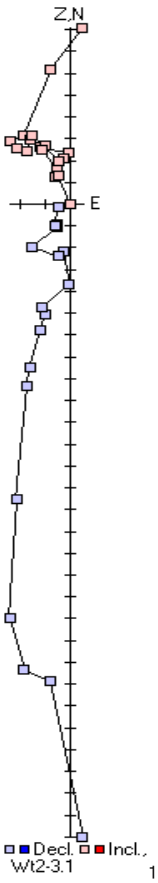
Z,N
E
Decl.
Incl.,
Wt2-3.1

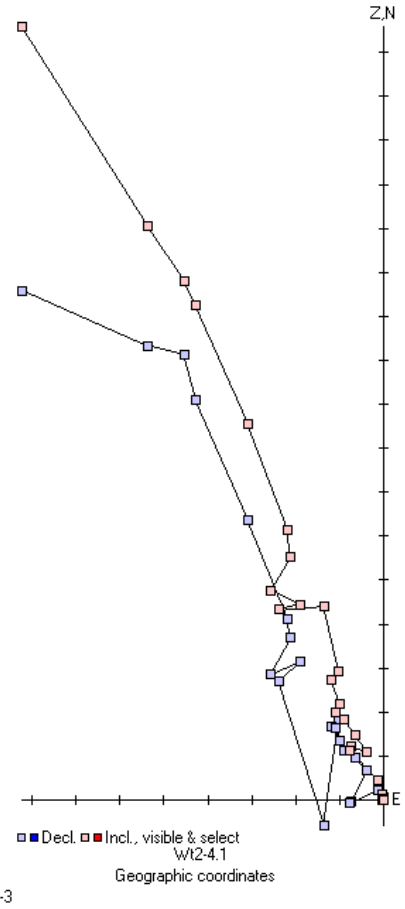
Z,N
E
Decl.
Incl., visible & select
Wt2-4.1
Geographic coordinates
10^-3

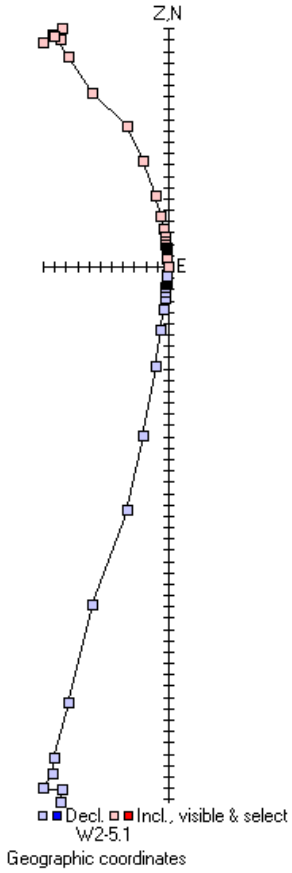

W2-5.1
Geographic coordinates

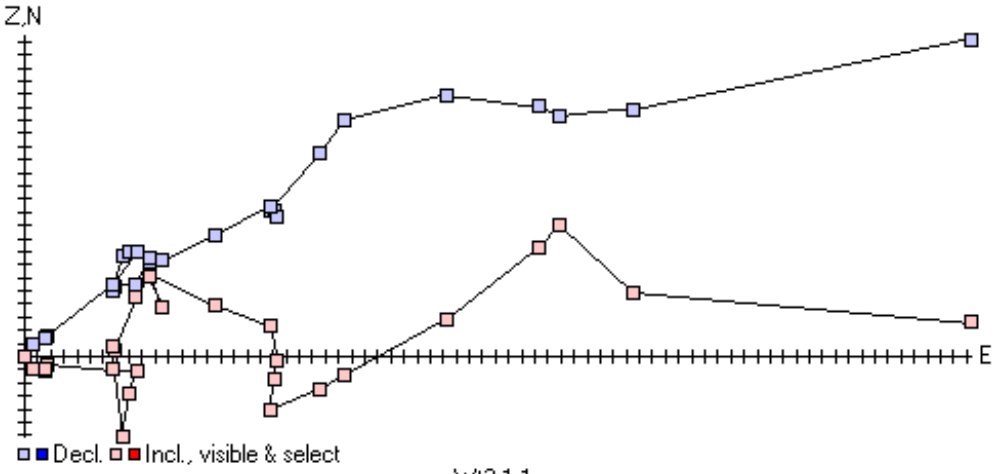

Wt3-1.1
Geographic coordinates

Each Division is 10^-4

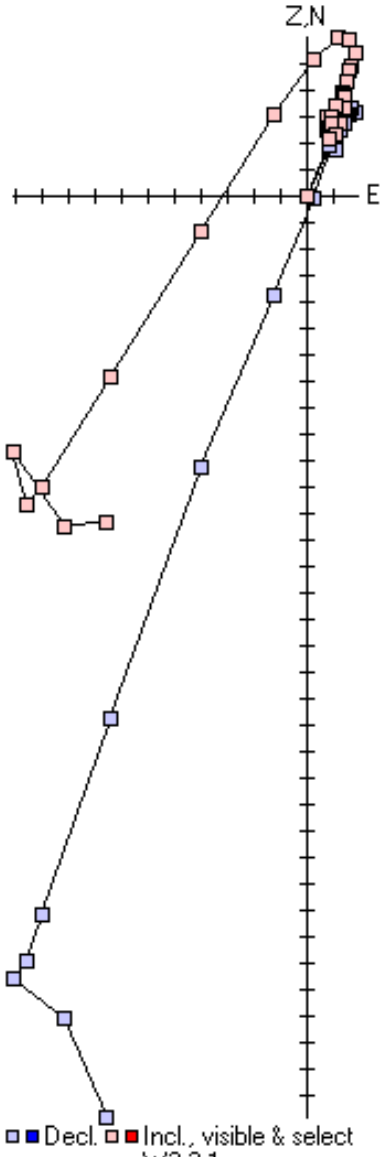

W3-2.1
Geographic coordinates

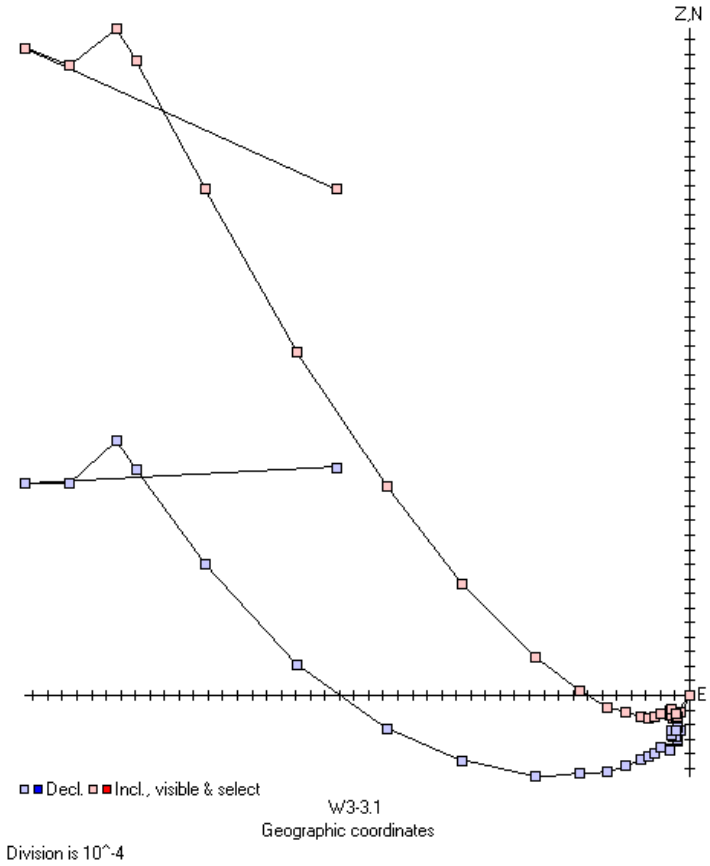

W3-3.1
Geographic coordinates
Division is 10^-4

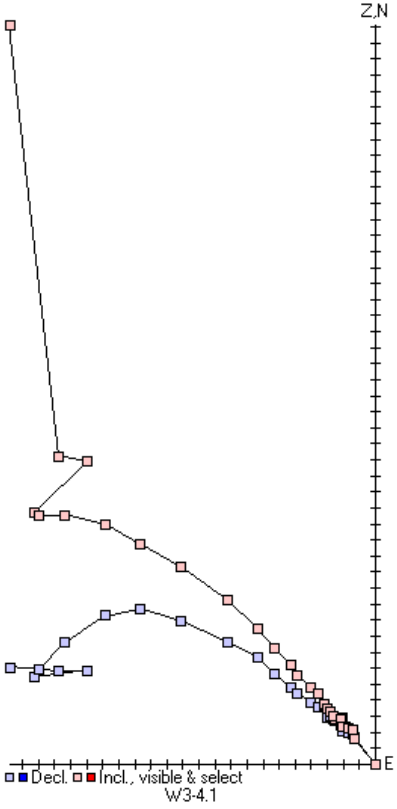

W3-4.1

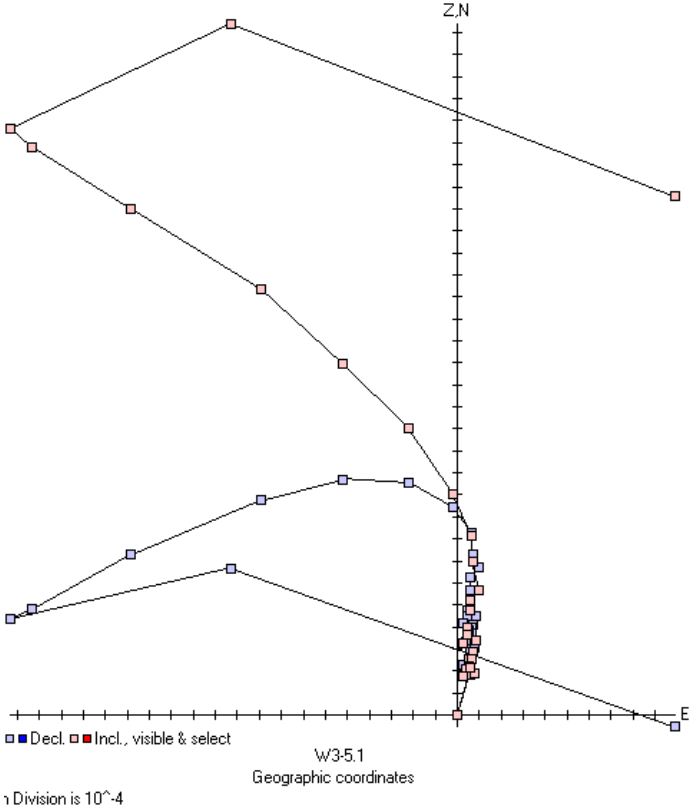

W3-5.1
Geographic coordinates
Division is 10^-4

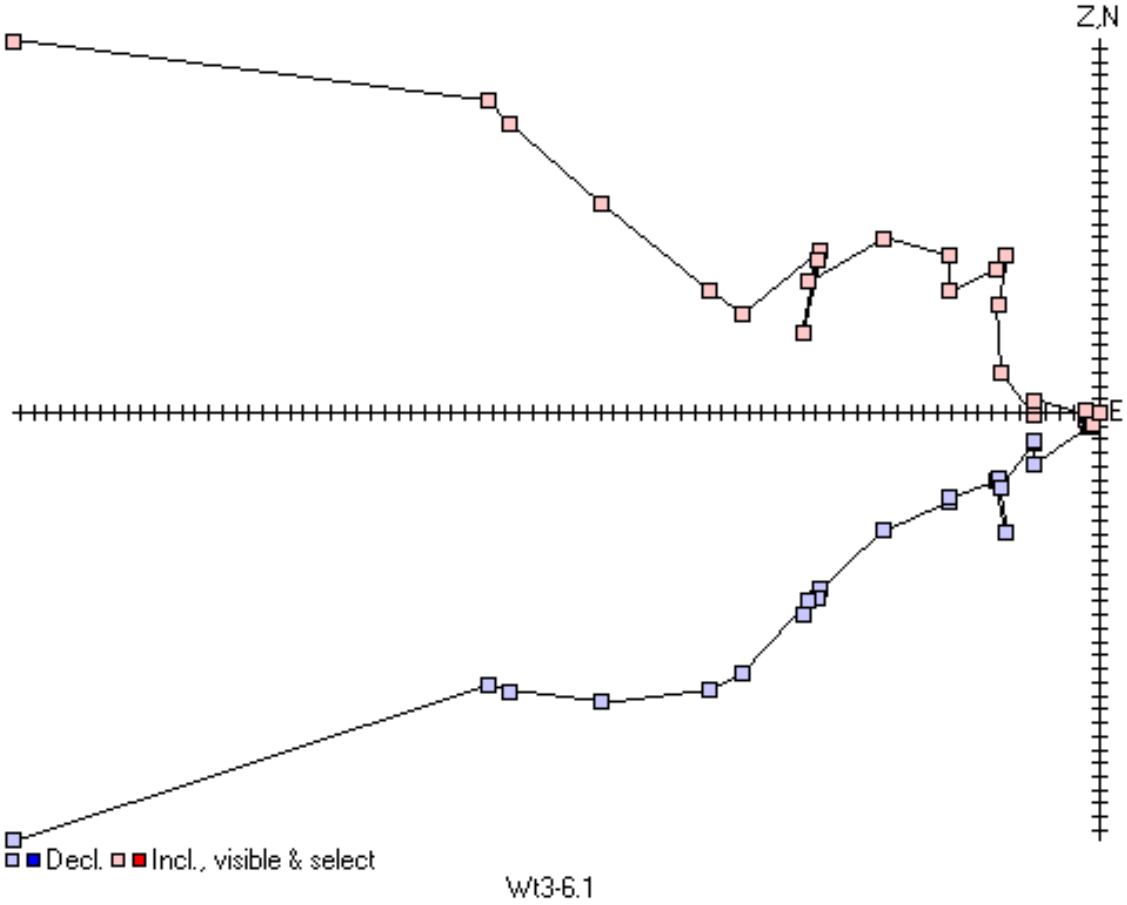
Z,N
E
Decl. Incl., visible & select

Wt3-6.1

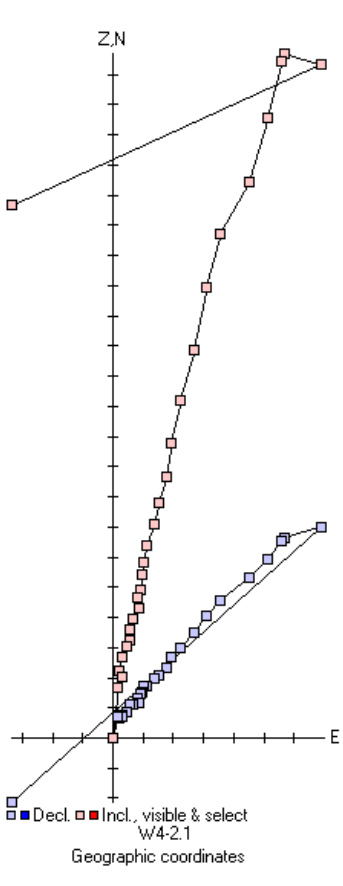
Z,N
E
Decl. Incl., visible & select
W4-2.1
Geographic coordinates

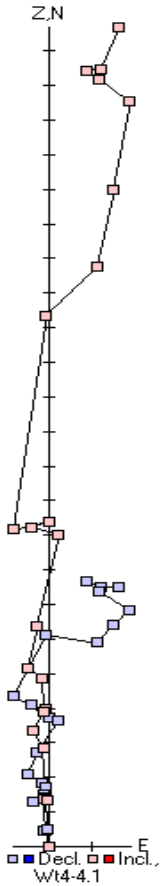
Z,N
E
Decl. Incl.,
Wt4-4.1

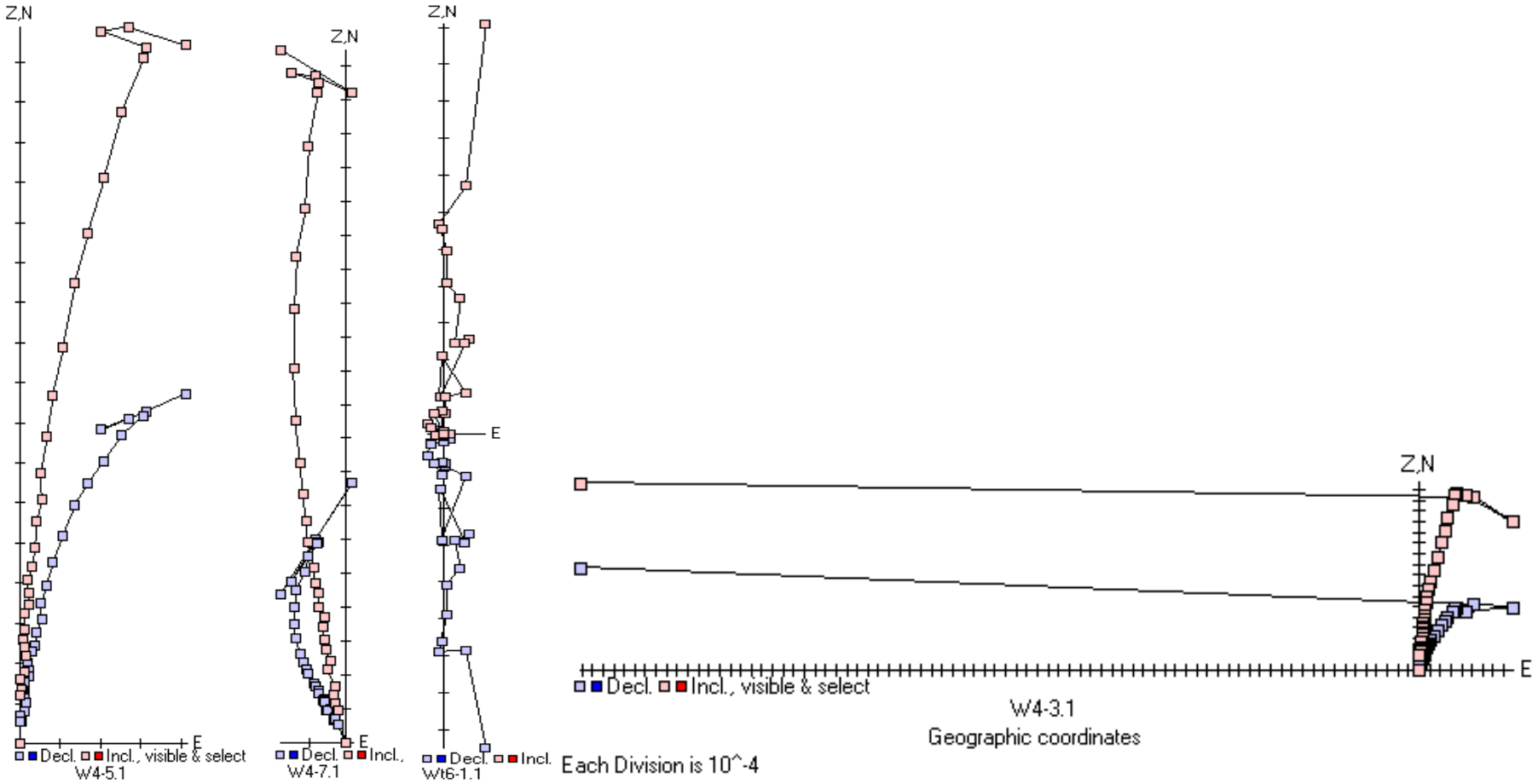
Z,N
E
Decl.
Incl., visible & select
W4-5.1
Z,N
E
Decl.
Incl.,
W4-7.1
Z,N
E
Decl.
Incl.
Wt6-1.1
Each Division is 10^-4
Z,N
E
Decl.
Incl., visible & select
W4-3.1
Geographic coordinates

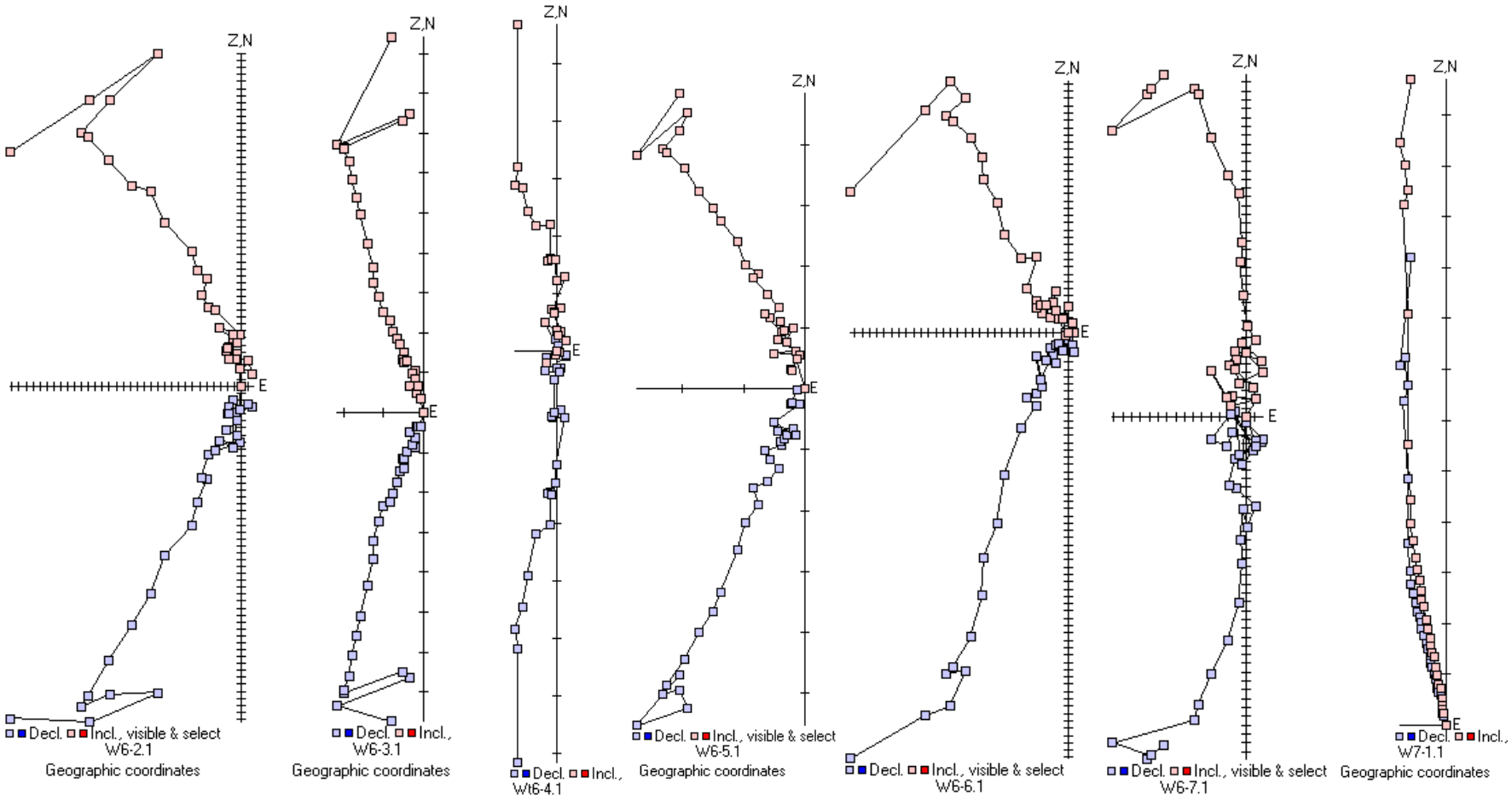
Z,N
E
Decl.
Incl., visible & select
W6-2.1
Geographic coordinates
Z,N
E
Decl.
Incl.,
W6-3.1
Geographic coordinates
Z,N
E
Decl.
Incl.,
Wt6-4.1
Z,N
E
Decl.
Incl., visible & select
W6-5.1
Geographic coordinates
Z,N
E
Decl.
Incl., visible & select
W6-6.1
Z,N
E
Decl.
Incl., visible & select
W6-7.1
Geographic coordinates
Z,N
E
Decl.
Incl.,
W7-1.1
Geographic coordinates

10^-5

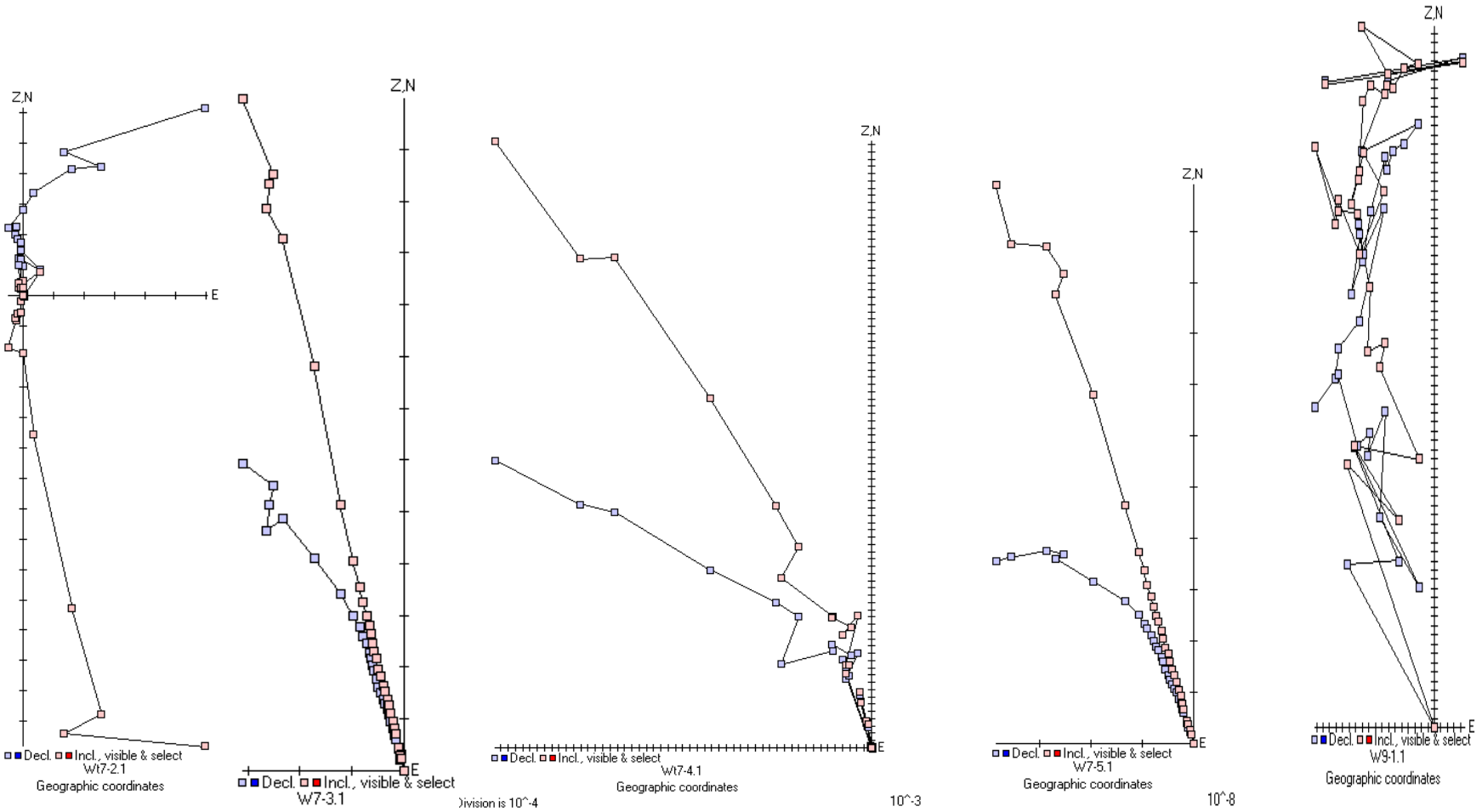

10^-3

Division is 10^-4

10^-3

10^-8

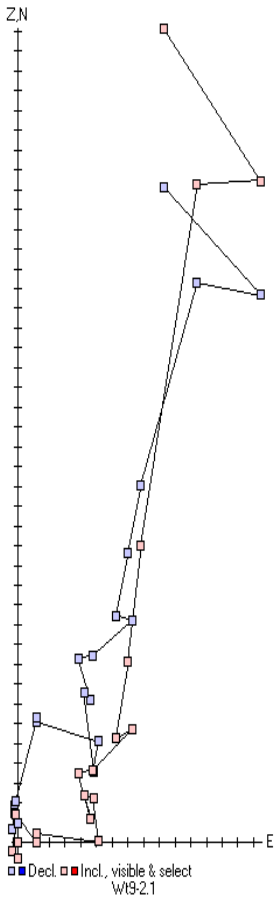

10^-7

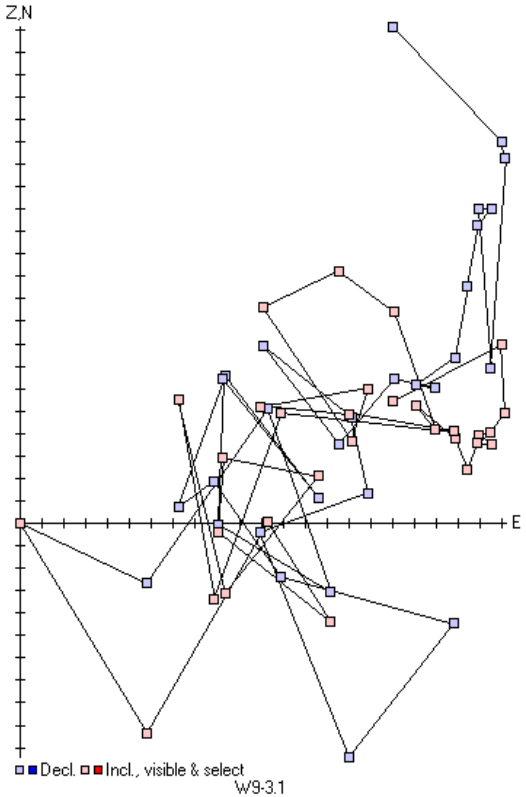

10^-8

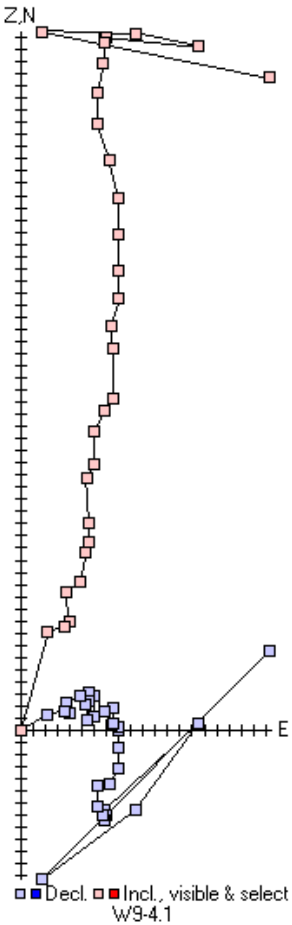

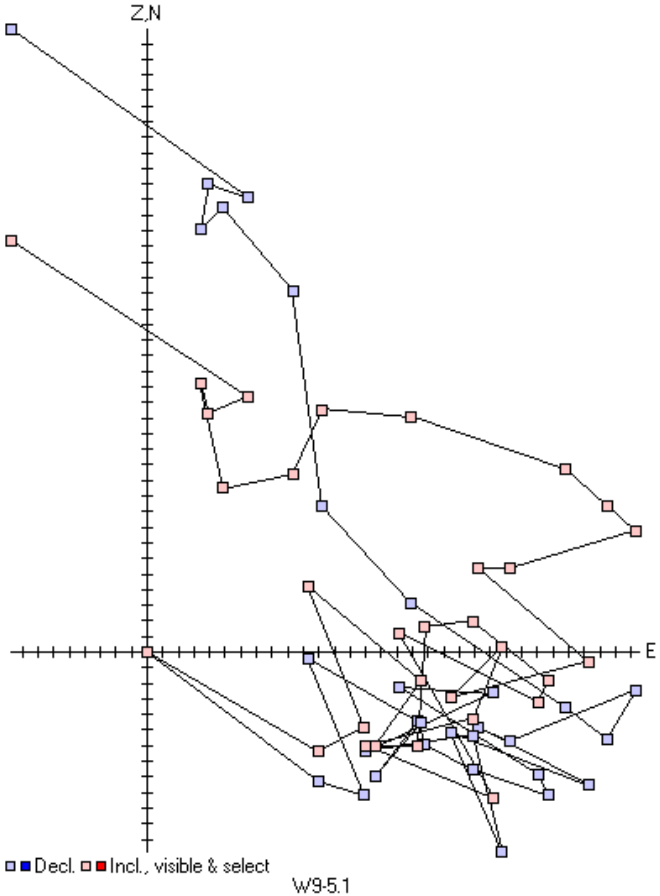

is 10^-8

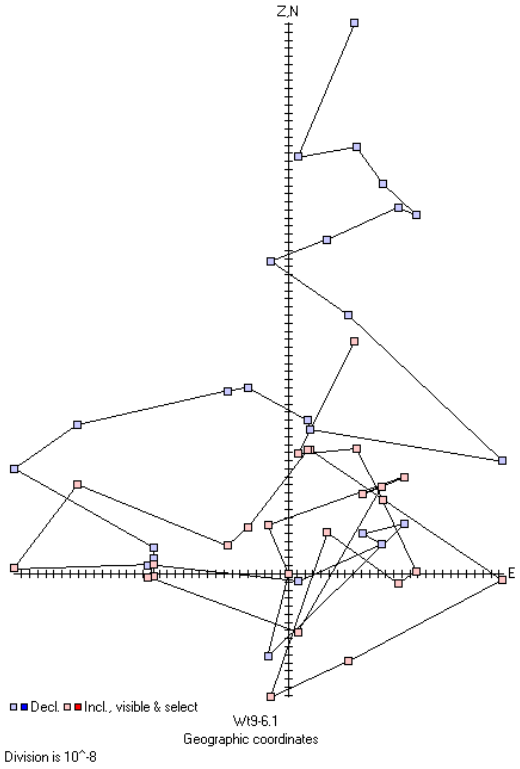

Division is 10^-8

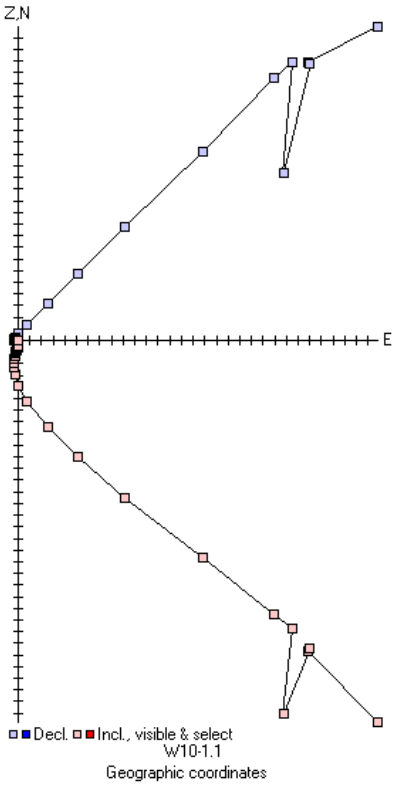

10^-3

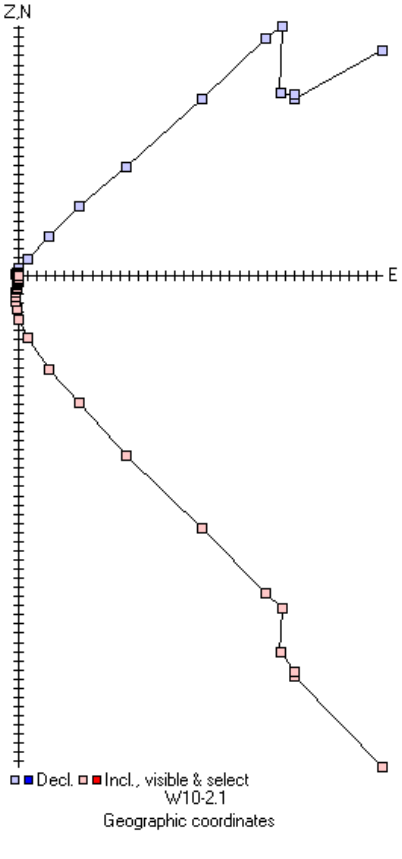

10^-3

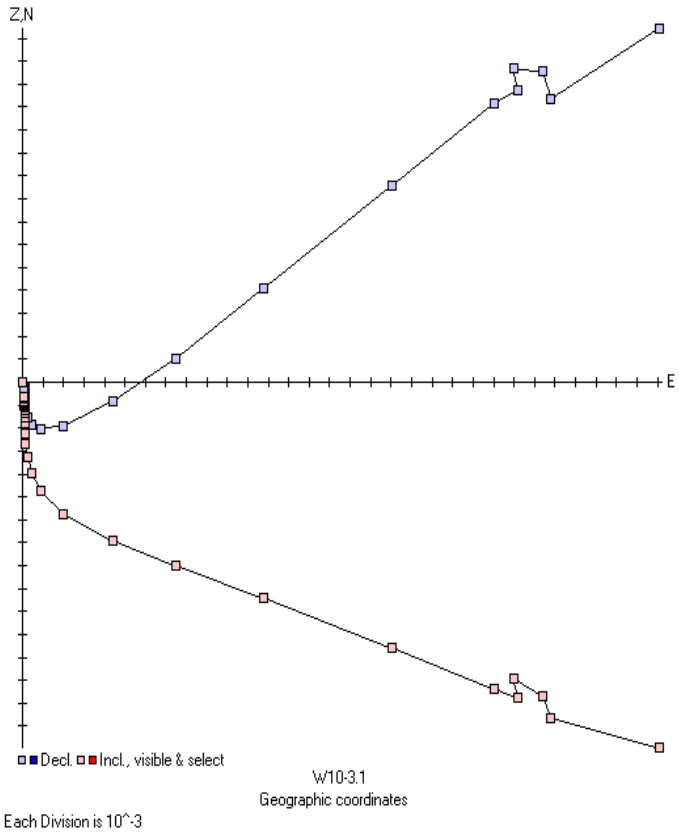

W10-3.1
Geographic coordinates

Each Division is 10^-3

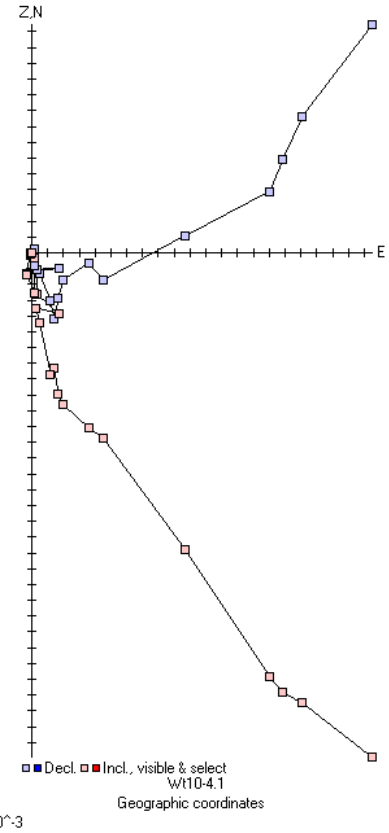

W10-4.1
Geographic coordinates

10^-3

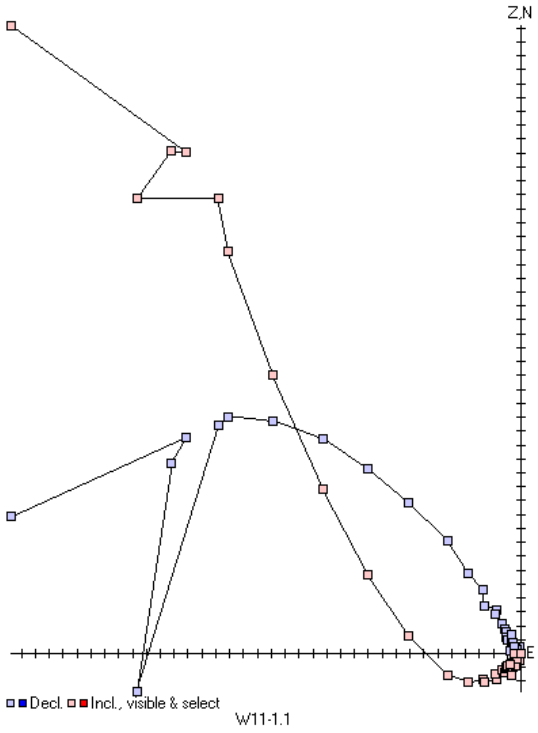

W11-1.1

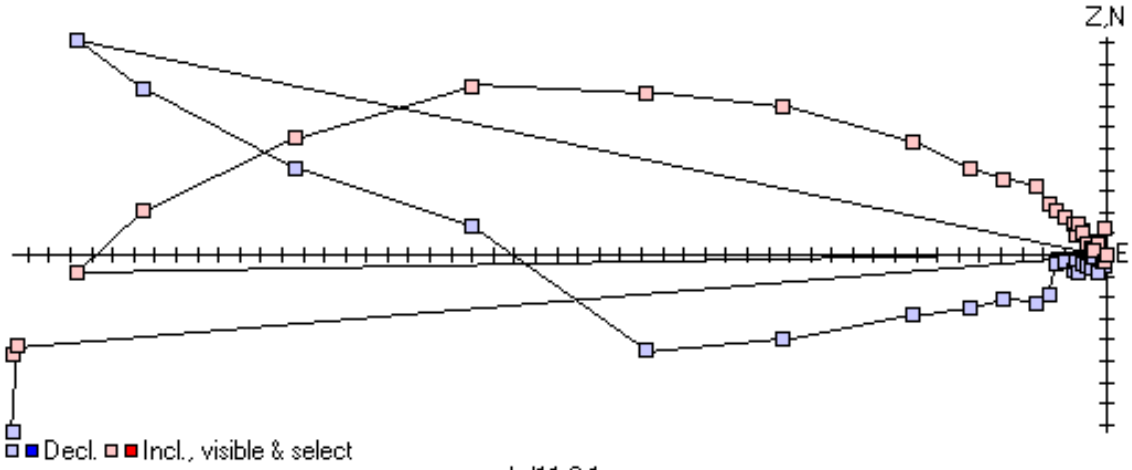

W11-2.1

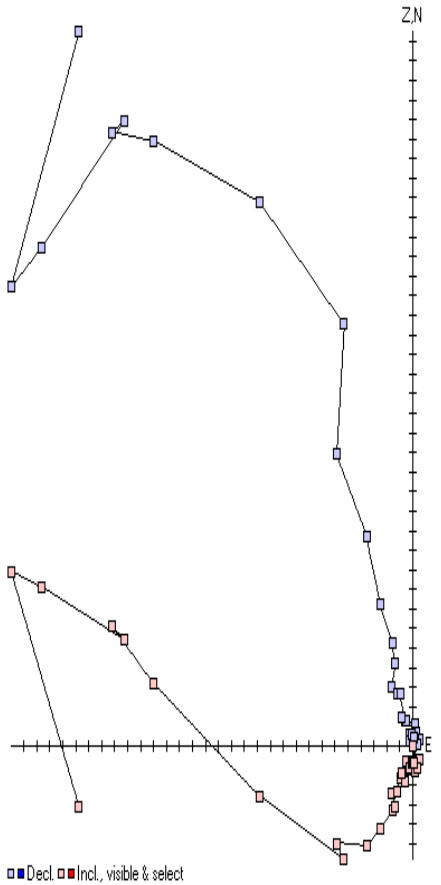

W11-3.1

Geographic coordinates

is 10^-4

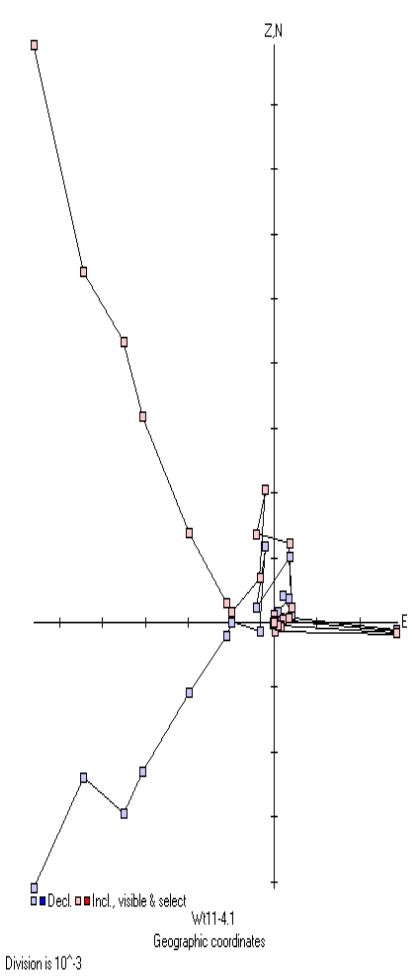
Z,N
E
Decl. Incl., visible & select
W11-4.1
Geographic coordinates
Division is 10^-3

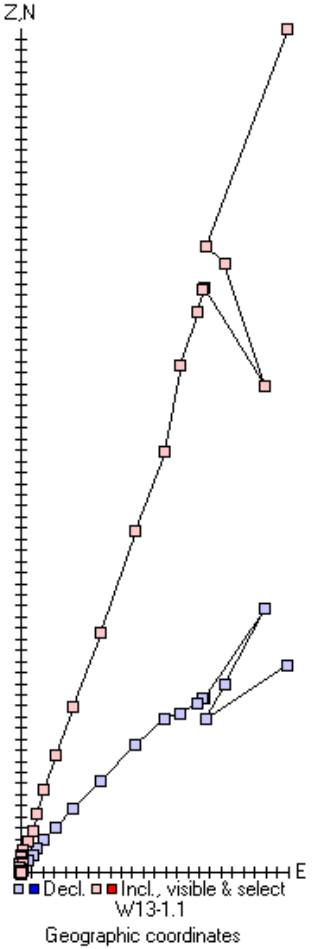
Z,N
E
Decl. Incl., visible & select
W13-1.1
Geographic coordinates

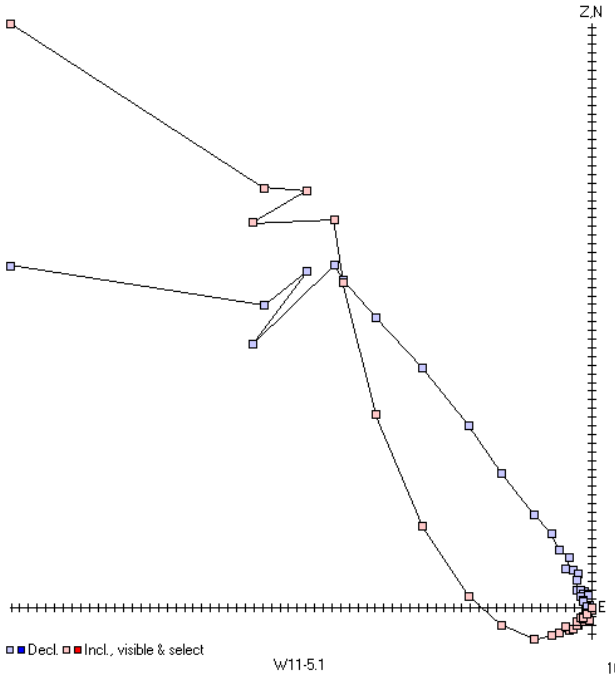
Z,N
E
Decl. Incl., visible & select
W11-5.1

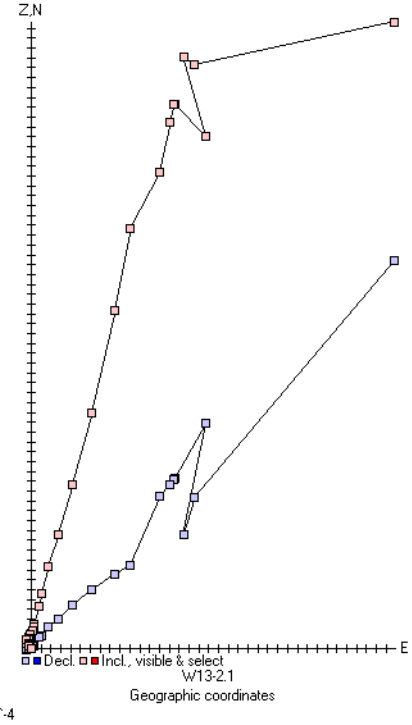
Z,N
E
Decl. Incl., visible & select
W13-2.1
Geographic coordinates
10^-4

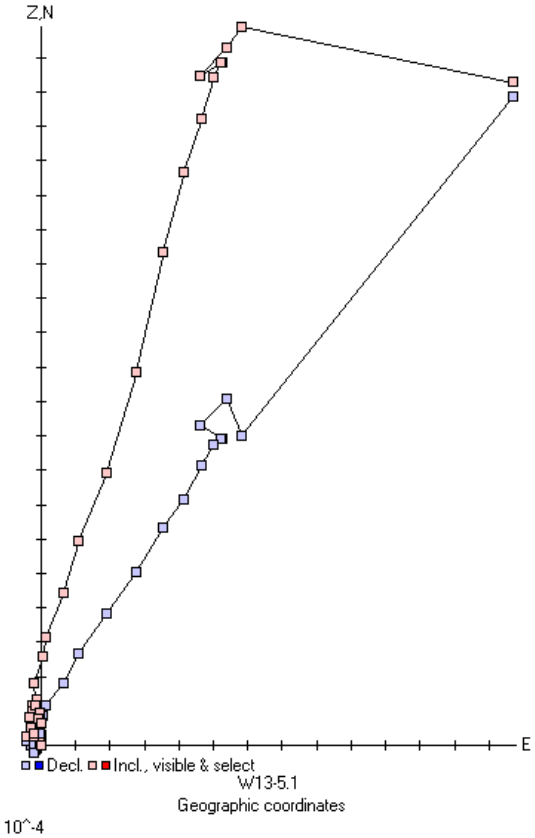
Z,N
E
Decl. Incl., visible & select
W13-5.1
Geographic coordinates
10^-4

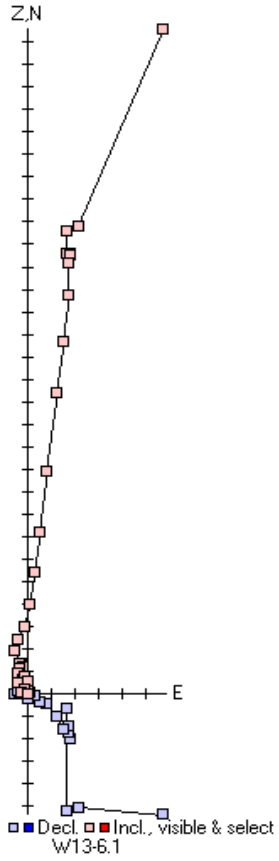
Z,N
E
Decl. Incl., visible & select
W13-6.1

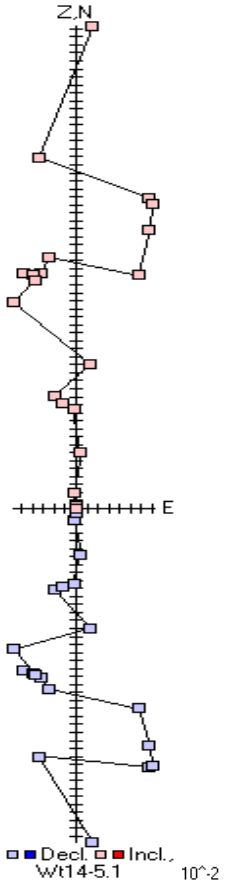
Z,N
E
Decl. Incl.,
Wt14-5.1
10^-2

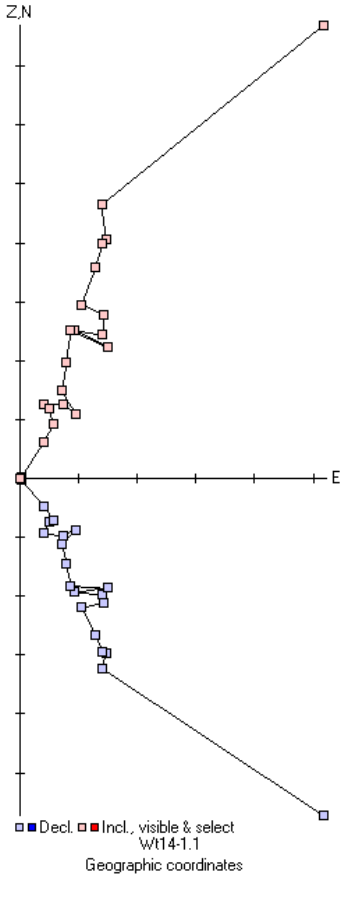
Z,N
E
Decl. Incl., visible & select
Wt14-1.1
Geographic coordinates

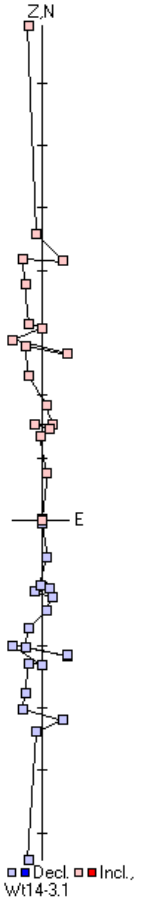
Z,N
E
Decl. Incl.,
Wt14-3.1

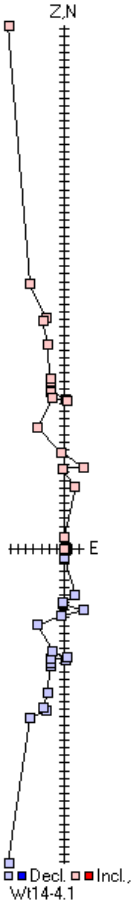
Z,N
E
Decl. Incl.,
Wt14-4.1

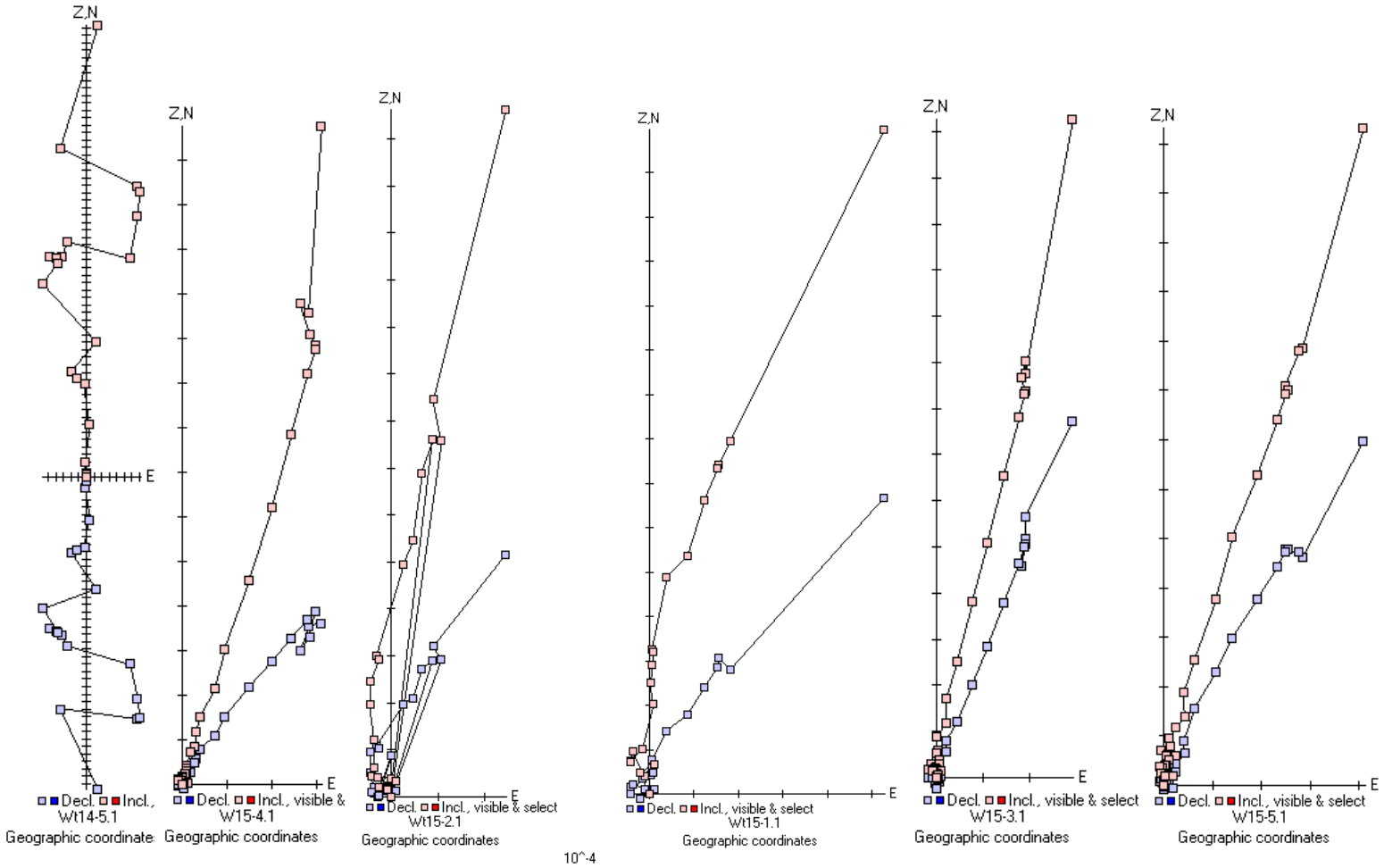
Z,N
E
Decl.
Incl.,
Wt14-5.1
Geographic coordinate
Z,N
E
Decl.
Incl., visible &
W15-4.1
Geographic coordinates
Z,N
E
Decl.
Incl., visible & select
Wt15-2.1
Geographic coordinates
Z,N
E
Decl.
Incl., visible & select
Wt15-1.1
Geographic coordinates
Z,N
E
Decl.
Incl., visible & select
W15-3.1
Geographic coordinates
Z,N
E
Decl.
Incl., visible & select
W15-5.1
Geographic coordinates
10^-4

12.8 Undara

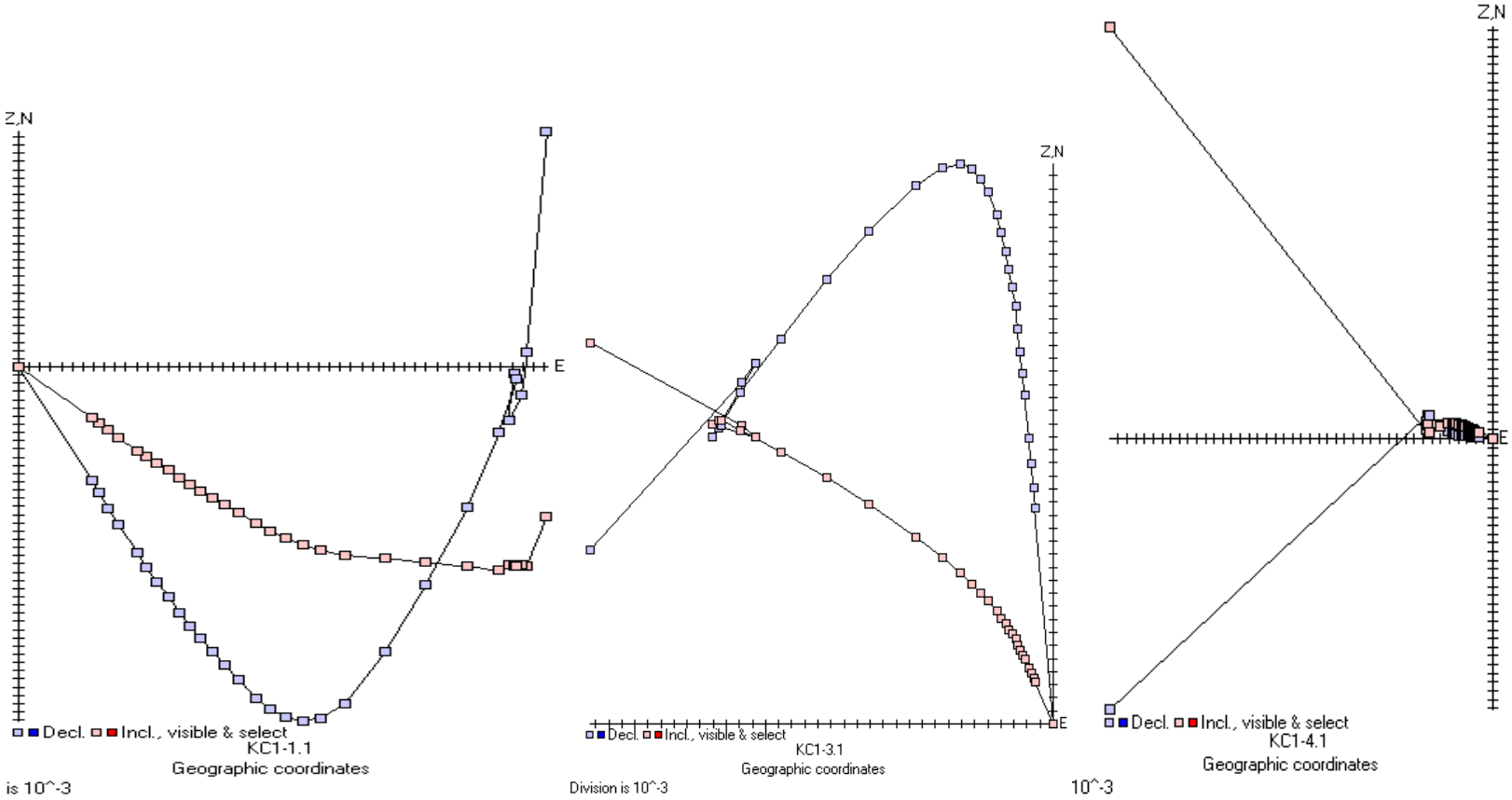
Z,N
E
Decl. Incl., visible & select
KC1-1.1
Geographic coordinates
is 10^-3
Z,N
E
Decl. Incl., visible & select
KC1-3.1
Geographic coordinates
Division is 10^-3
Z,N
E
Decl. Incl., visible & select
KC1-4.1
Geographic coordinates
10^-3

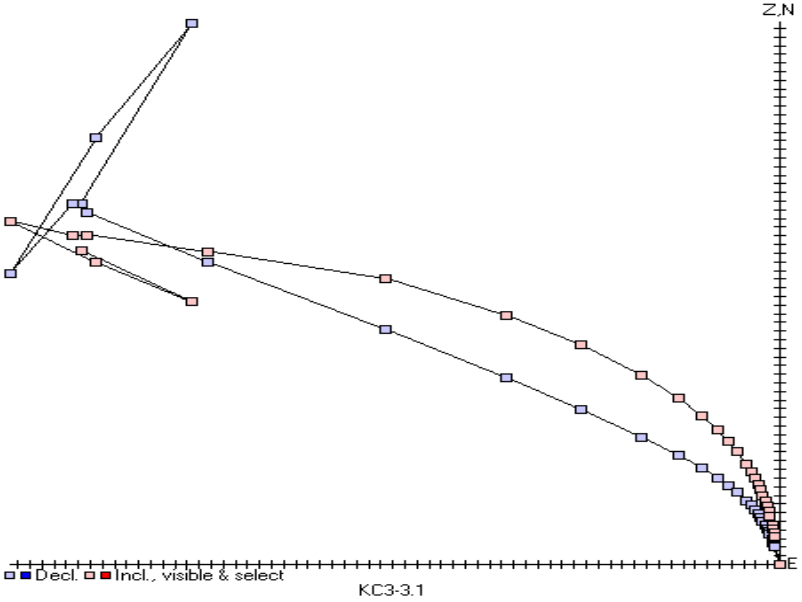

KC3-3.1

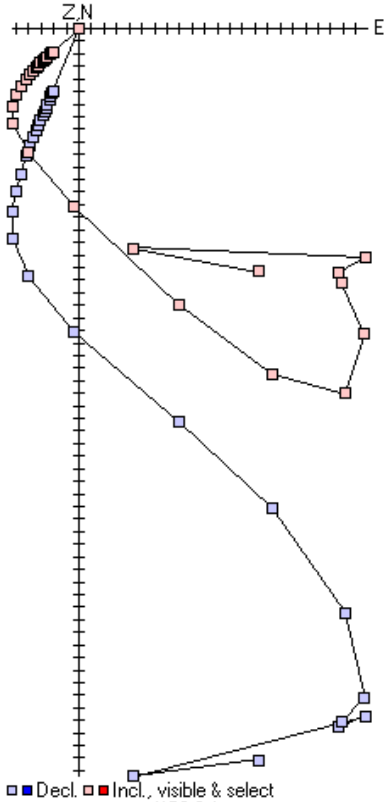

KC2-2.1

Geographic coordinates

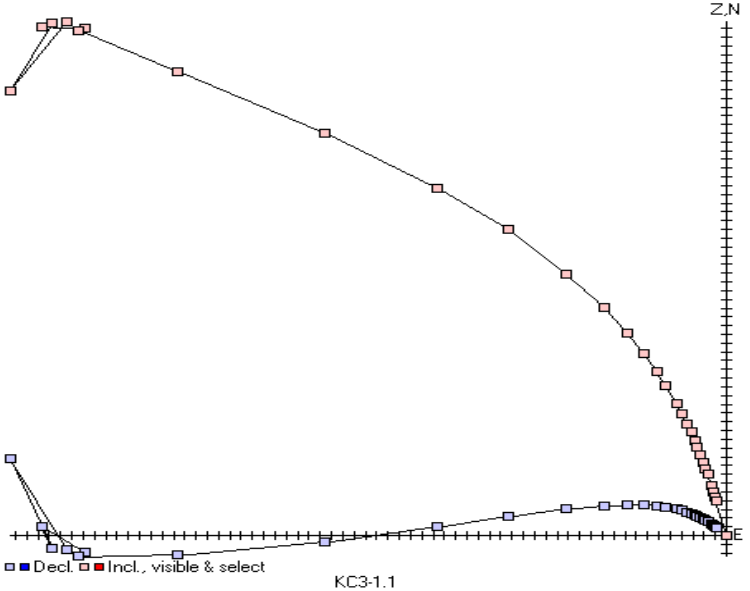

KC3-1.1

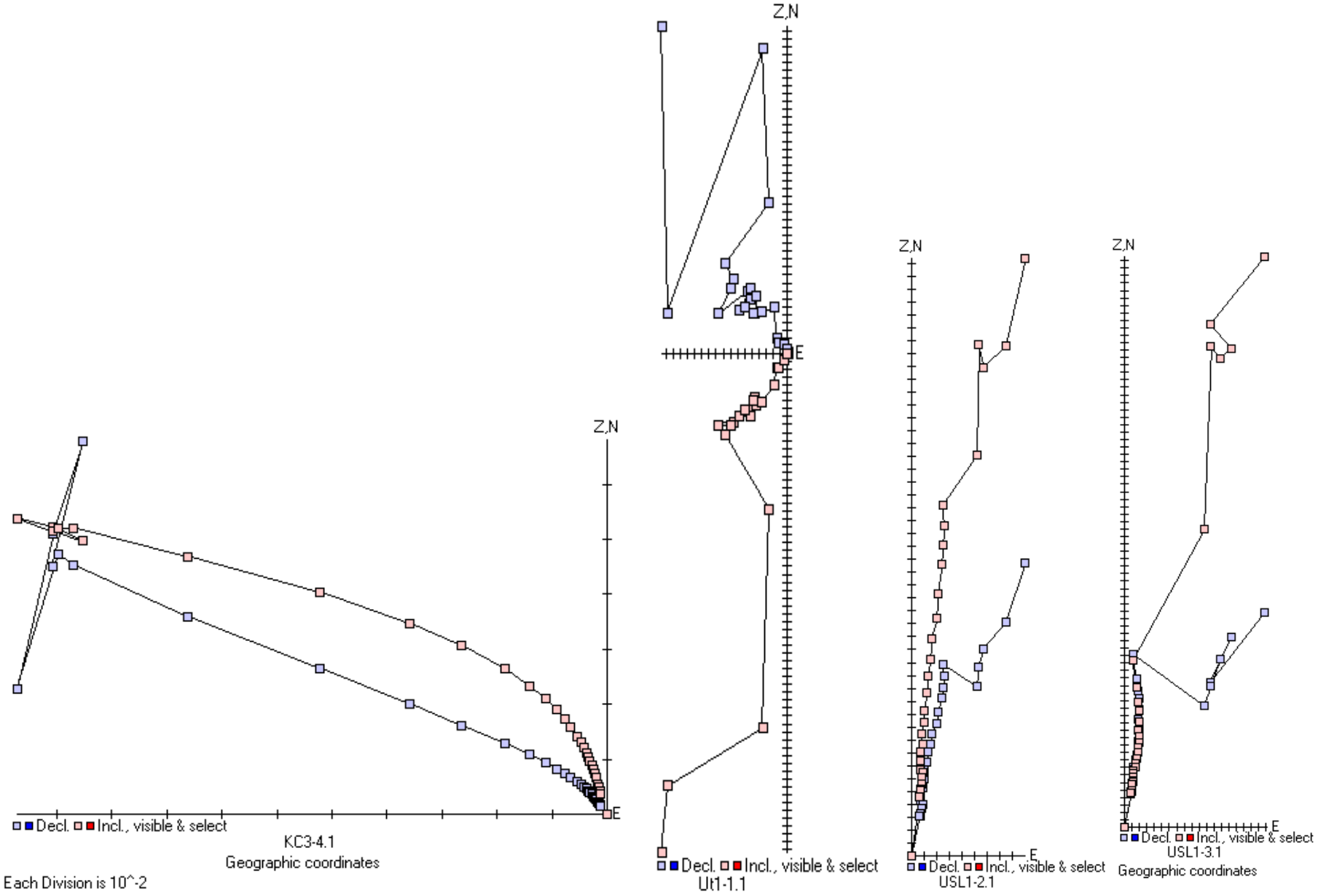
Z,N
E
Decl. Incl., visible & select
KC3-4.1
Geographic coordinates
Each Division is 10^-2
Z,N
E
Decl. Incl., visible & select
Ut1-1.1
Z,N
E
Decl. Incl., visible & select
USL1-2.1
Z,N
E
Decl. Incl., visible & select
USL1-3.1
Geographic coordinates

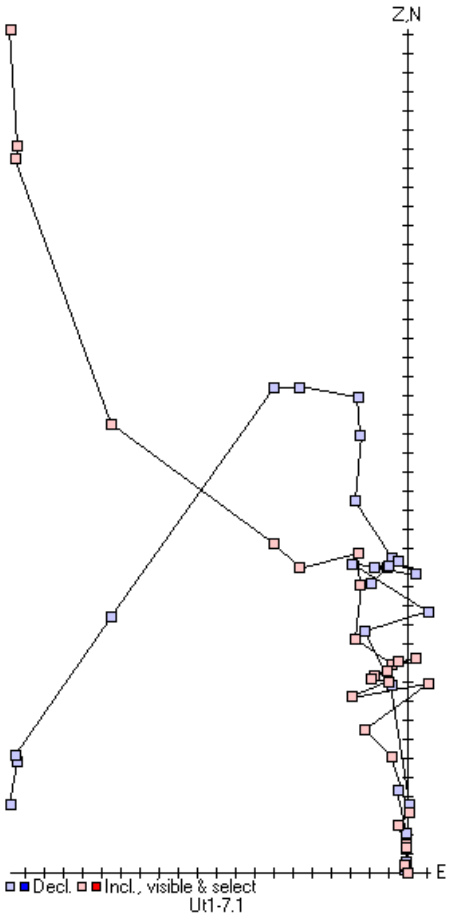

Ut1-7.1

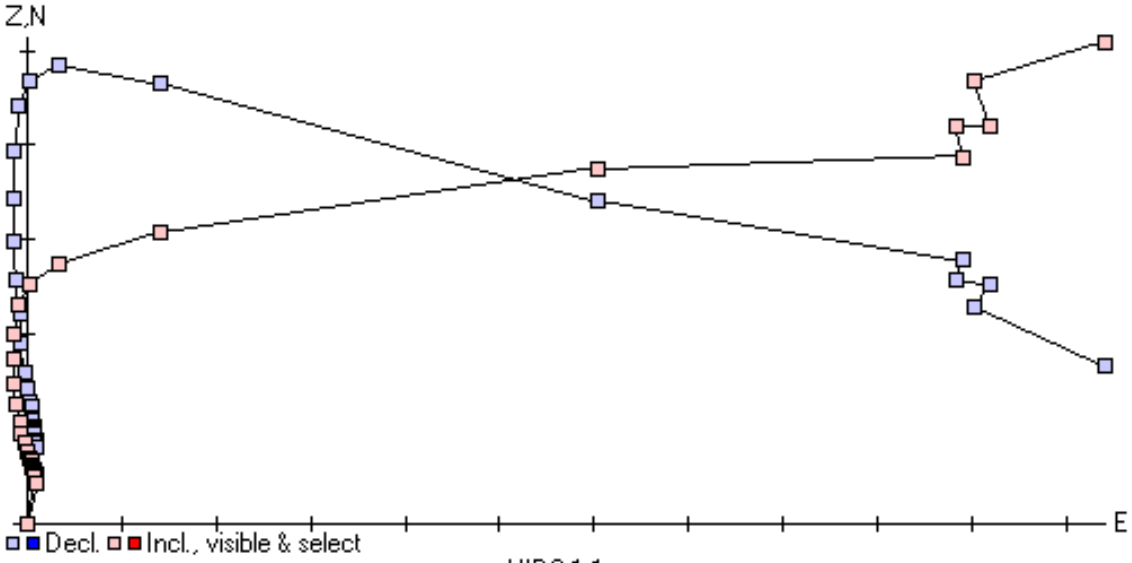

UID2-1.1

Geographic coordinates

Each Division is 10^-3

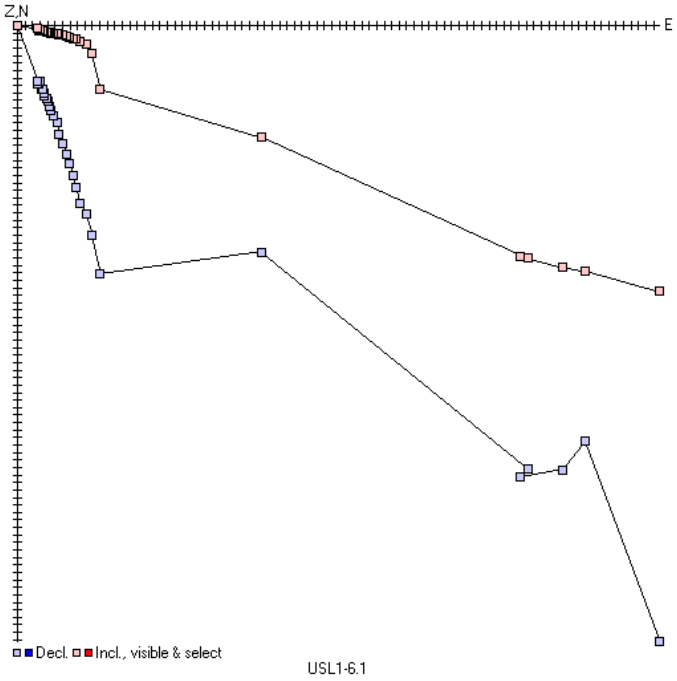

USL1-6.1

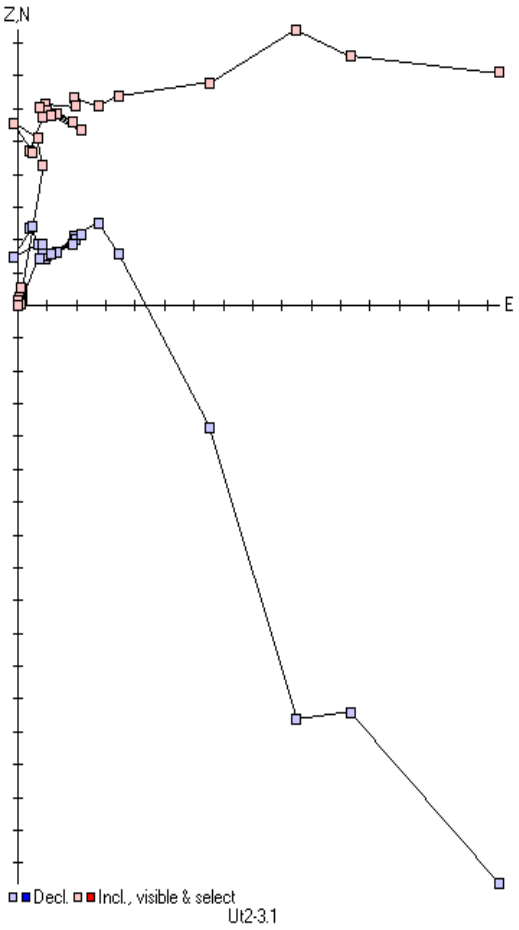

Ut2-3.1

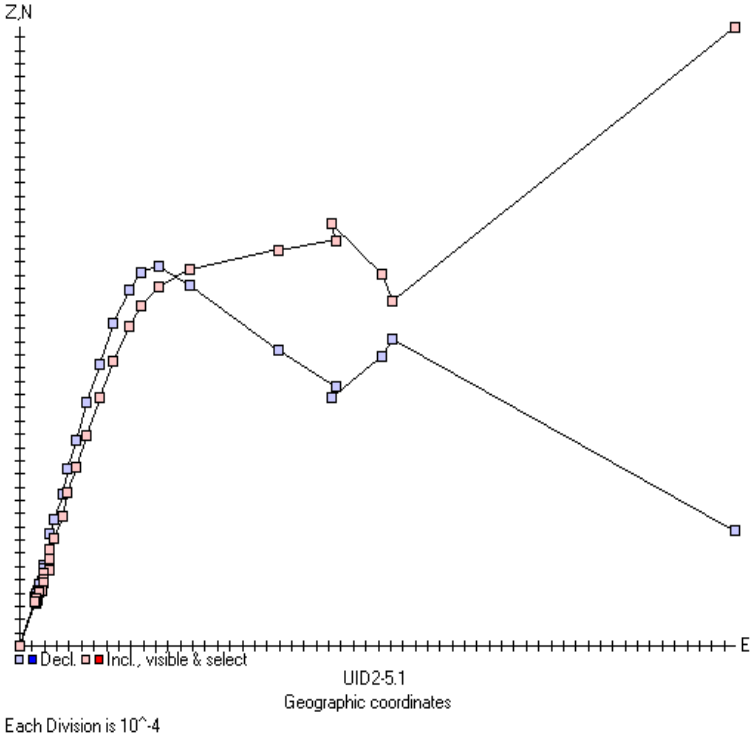

UID2-5.1

Geographic coordinates

Each Division is 10^-4

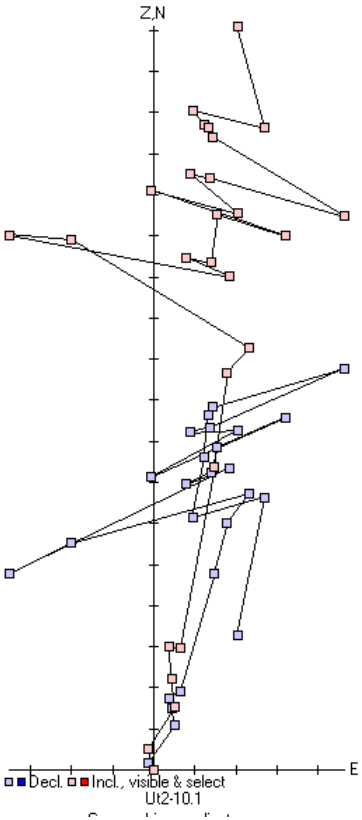

Ut2-10.1

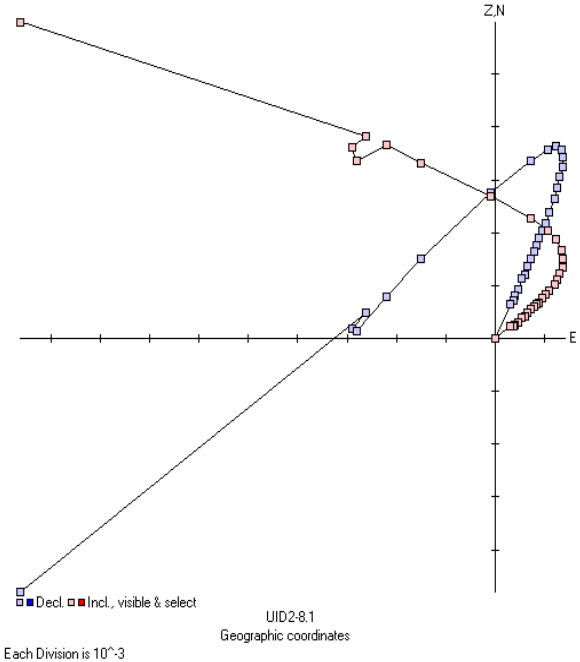

UID2-8.1
Geographic coordinates
Each Division is 10^-3

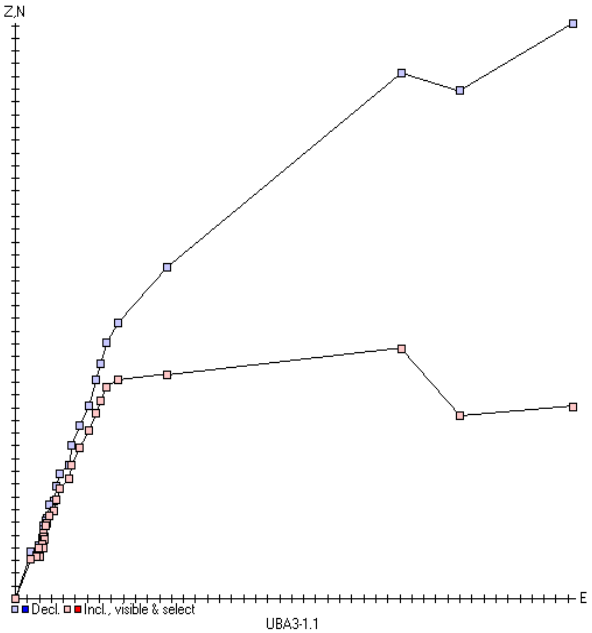

UBA3-1.1

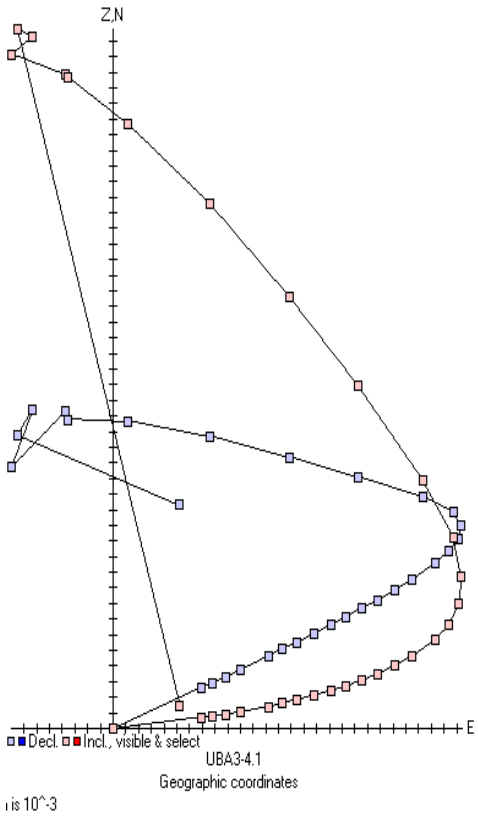
Z,N
E
Decl. Incl., visible & select
UBA3-4.1
Geographic coordinates
is 10^-3

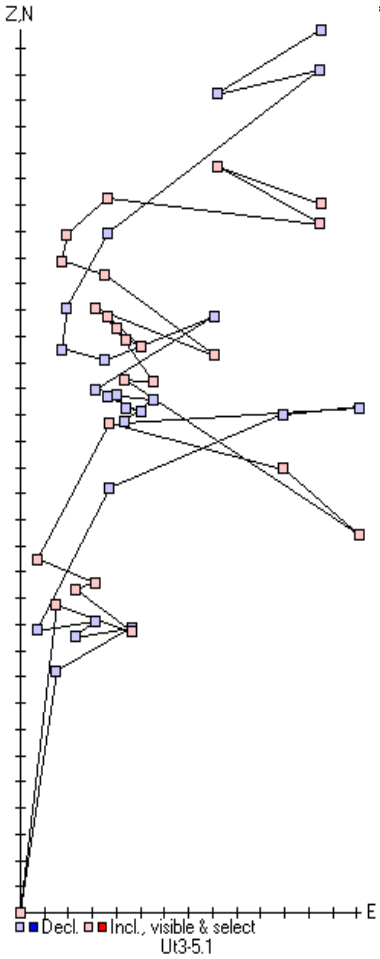
Z,N
E
Decl. Incl., visible & select
Ut3-5.1

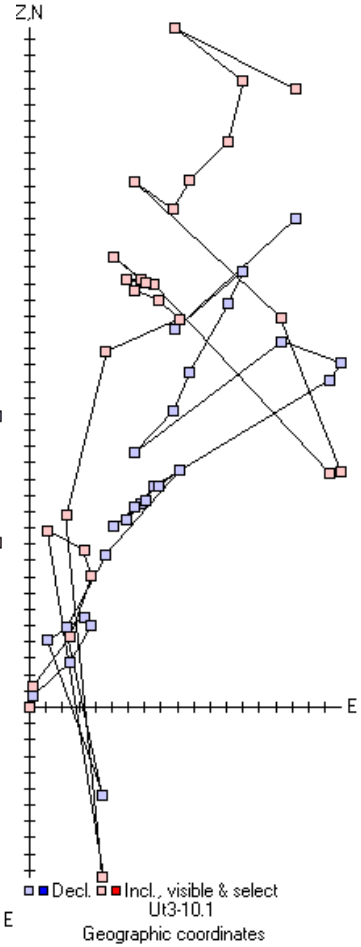
Z,N
E
Decl. Incl., visible & select
Ut3-10.1
Geographic coordinates

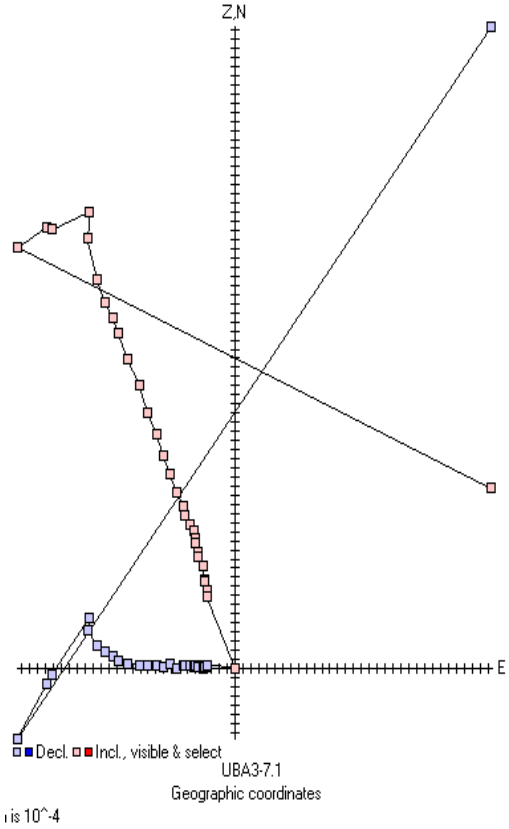
Z,N
E
Decl. Incl., visible & select
UBA3-7.1
Geographic coordinates
is 10^-4

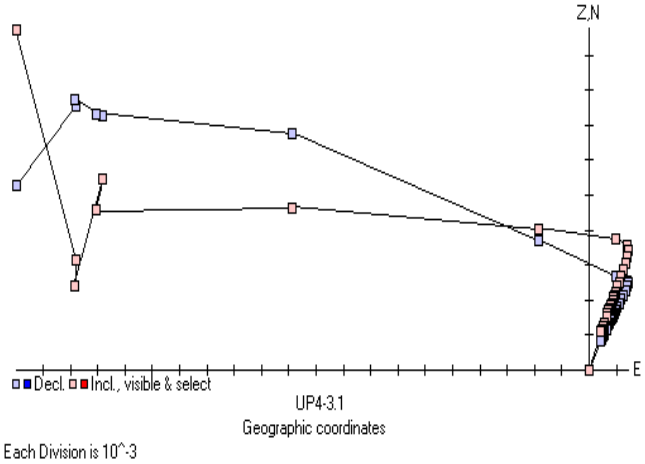

UP4-3.1
Geographic coordinates

Each Division is 10^-3

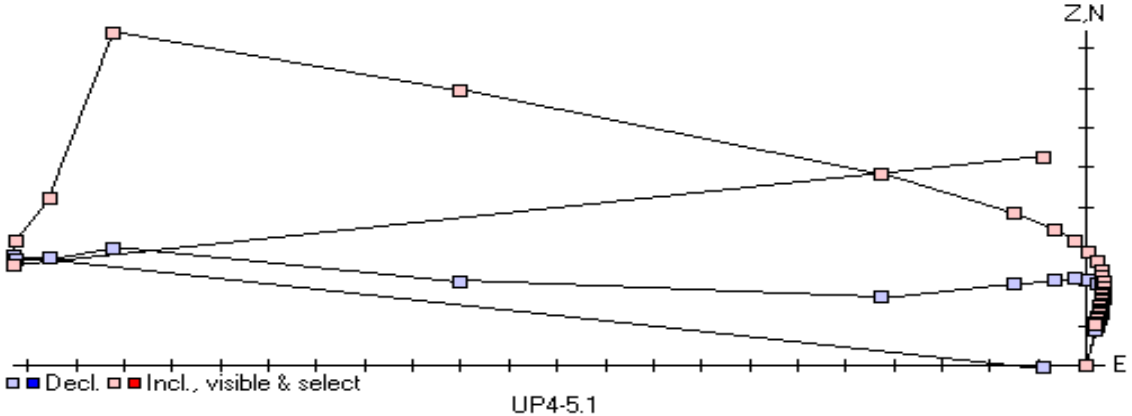

UP4-5.1
Geographic coordinates

Each Division is 10^-3

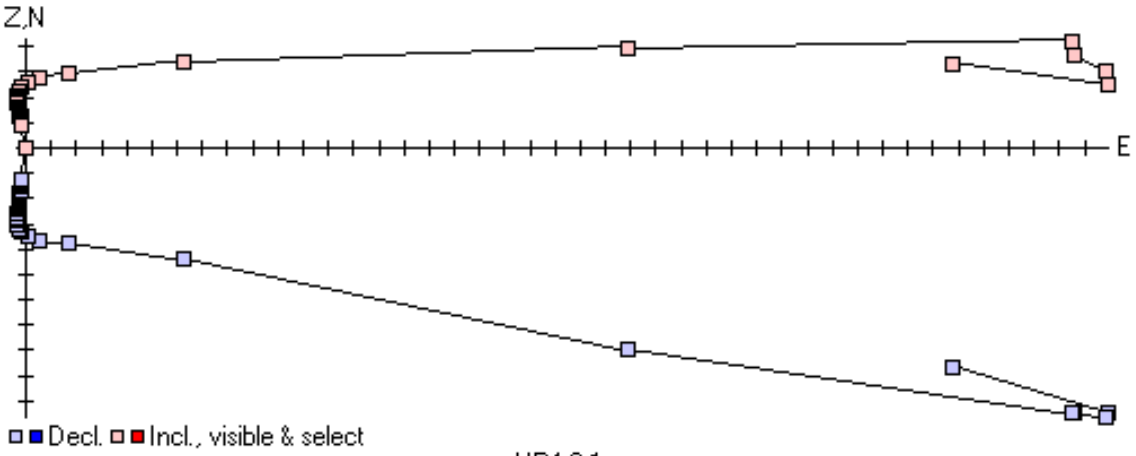

UP4-6.1

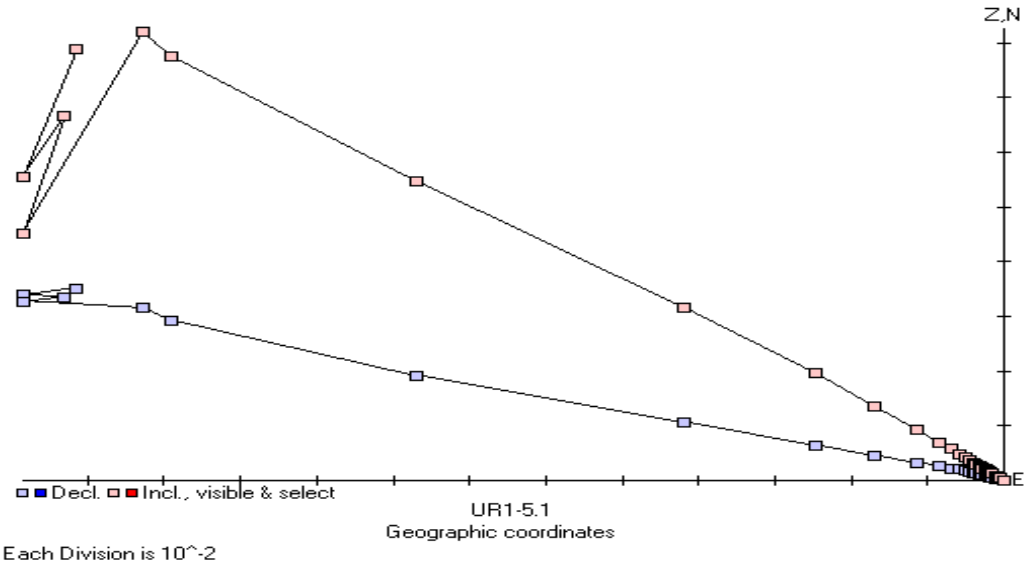
Z,N
E
Decl.
Incl., visible & select
UR1-5.1
Geographic coordinates
Each Division is 10^-2

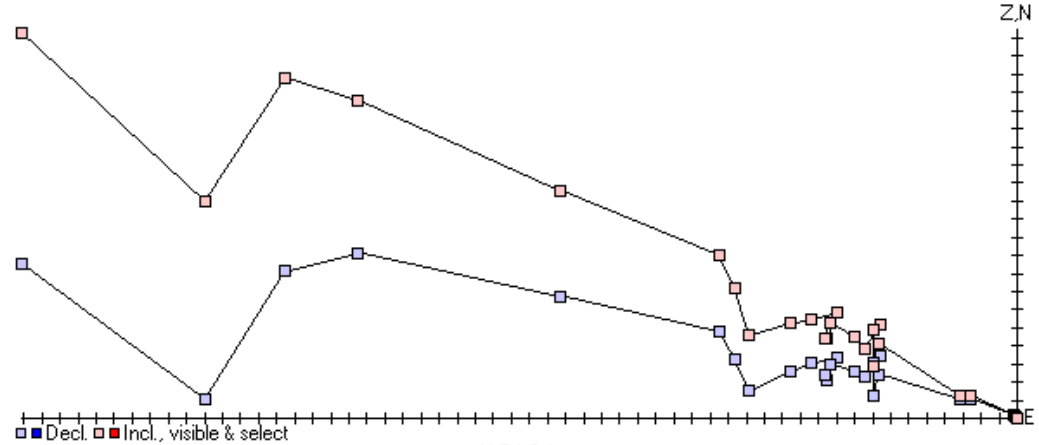

UtR1-6.1
Geographic coordinates

Each Division is 10^-3

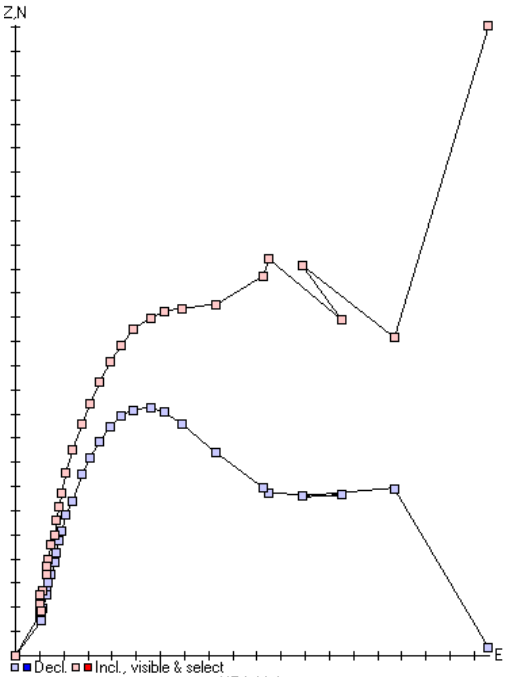

UR1-11.1
Geographic coordinates

is 10^-4

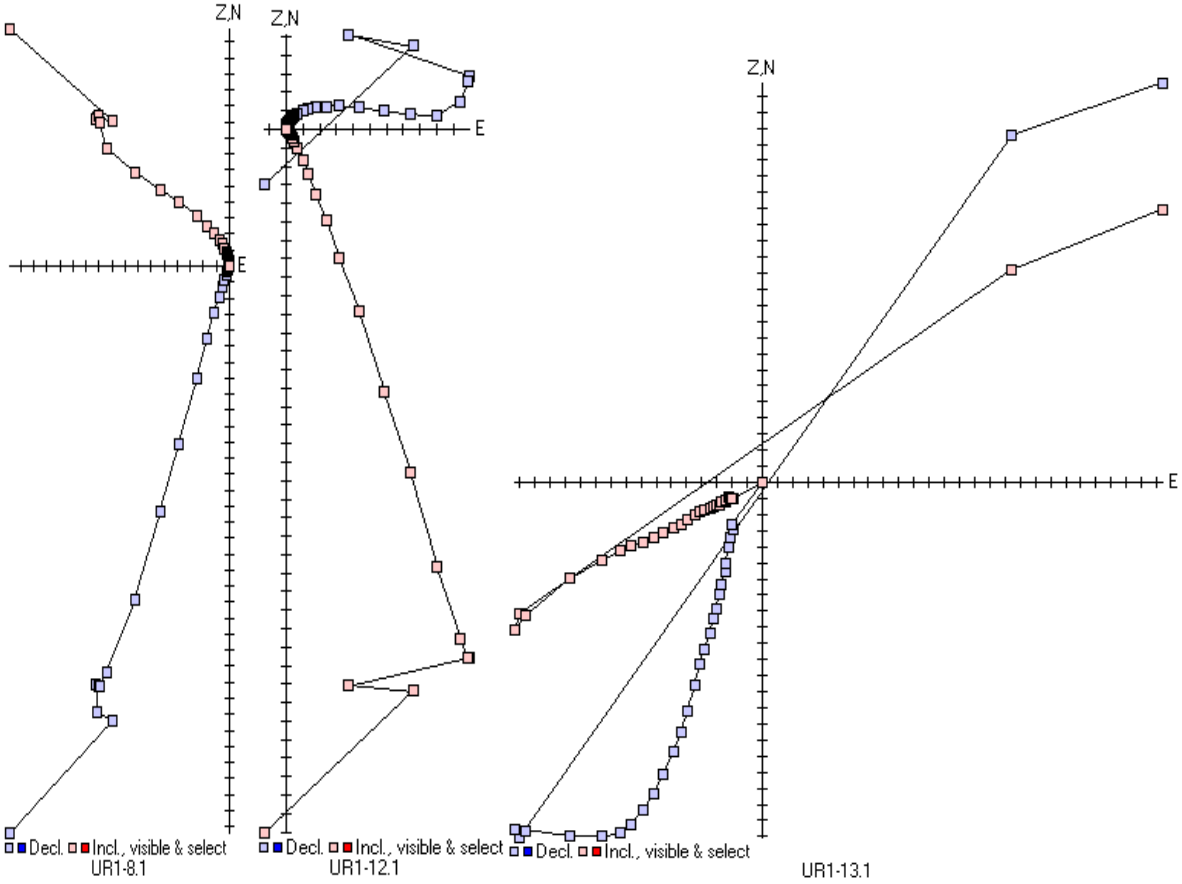
Z,N
E
Decl.
Incl., visible & select
UR1-8.1
Z,N
E
Decl.
Incl., visible & select
UR1-12.1
Z,N
E
Decl.
Incl., visible & select
UR1-13.1

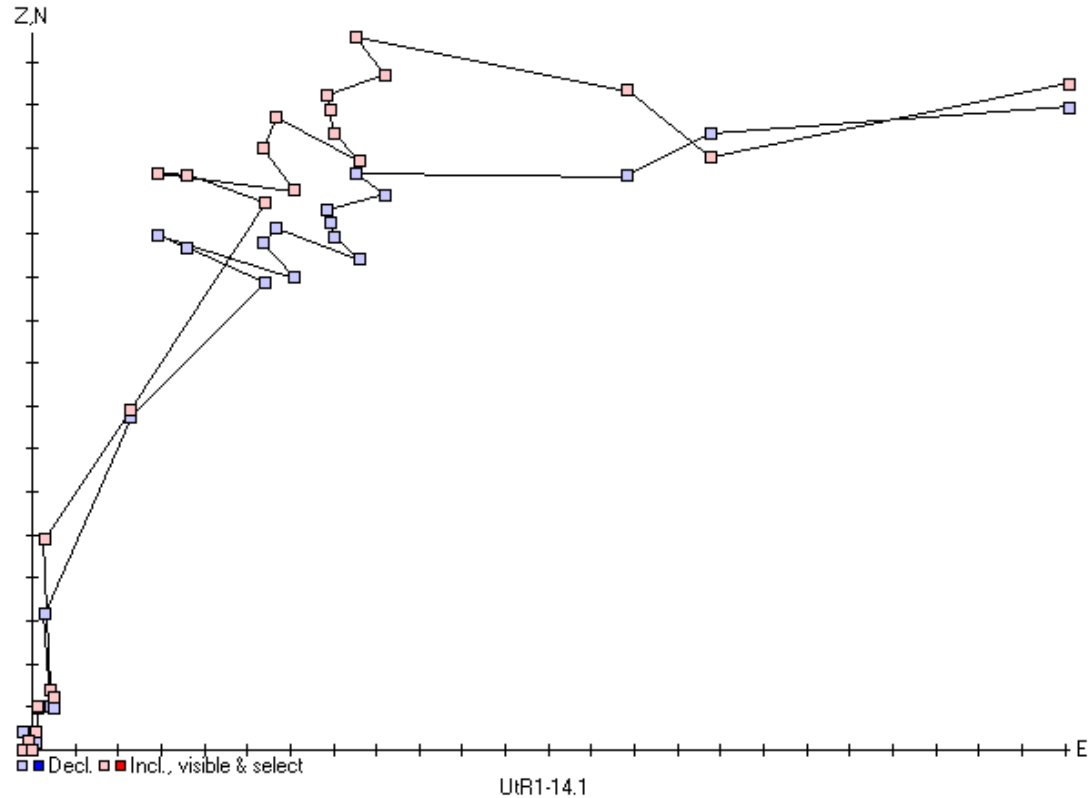

UtR1-14.1
Geographic coordinates

Each Division is 10^-4

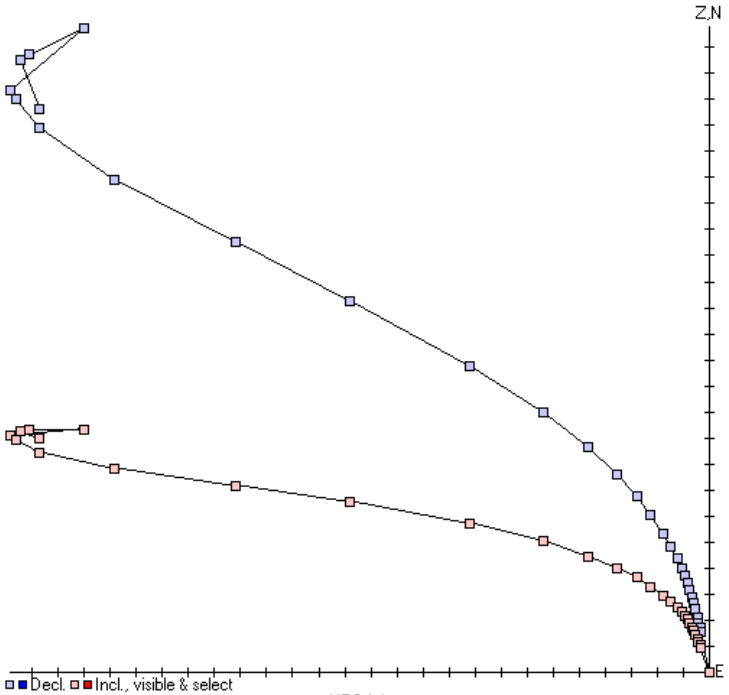

UR2-1.1
Geographic coordinates

Each Division is 10^-3

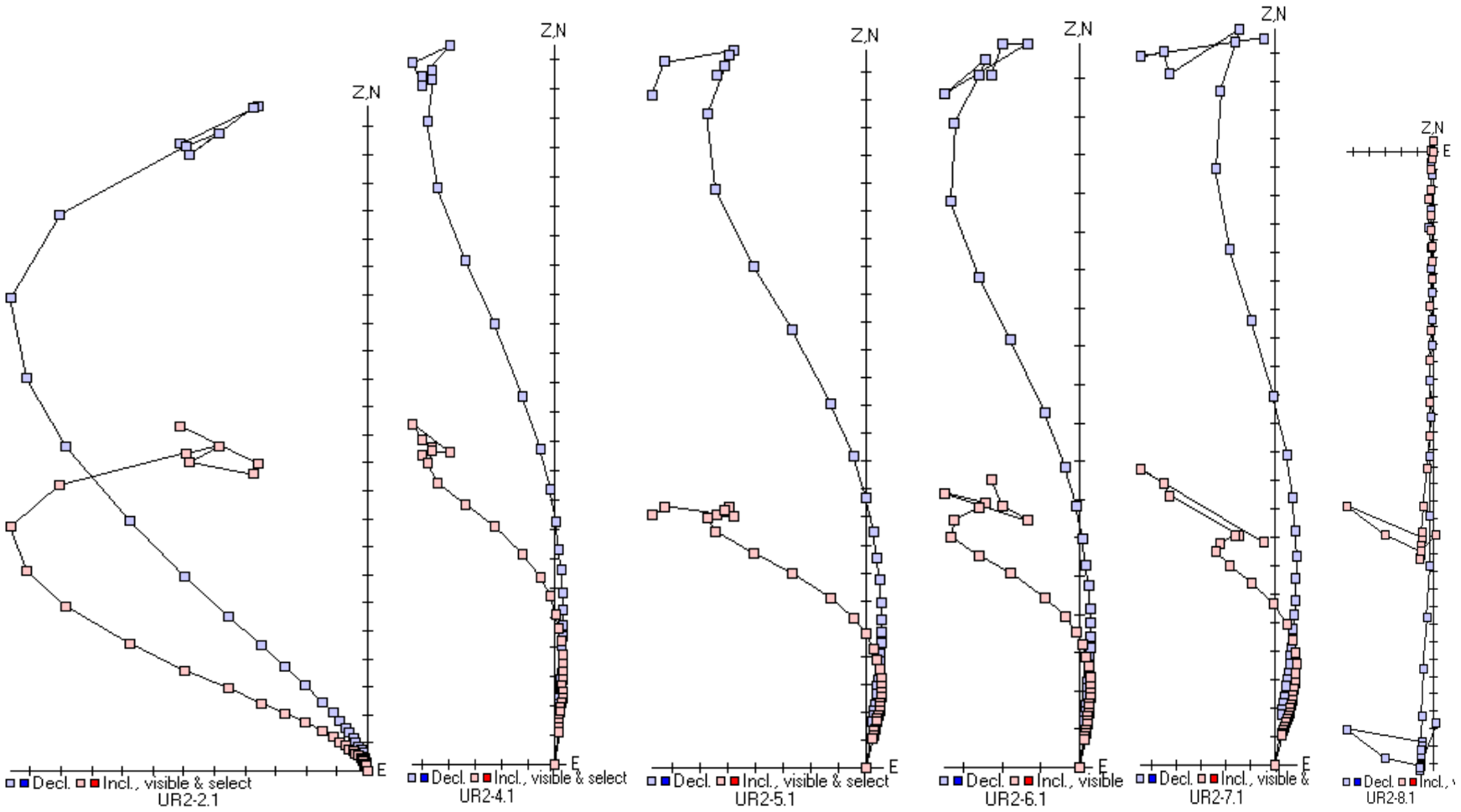
Z,N
E
Decl.
Incl., visible & select
UR2-2.1
Z,N
E
Decl.
Incl., visible & select
UR2-4.1
Z,N
E
Decl.
Incl., visible & select
UR2-5.1
Z,N
E
Decl.
Incl., visible
UR2-6.1
Z,N
E
Decl.
Incl., visible &
UR2-7.1
Z,N
E
Decl.
Incl.,
UR2-8.1

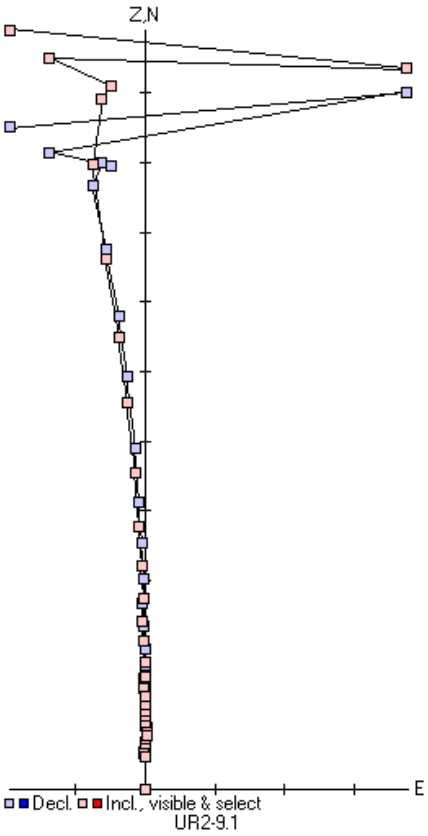

UR2-9.1

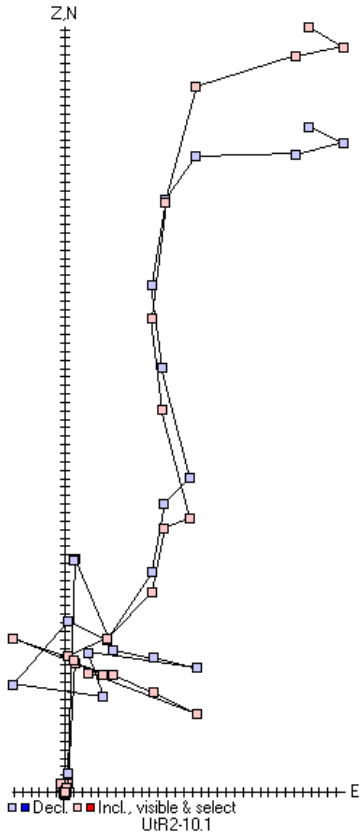

UtR2-10.1

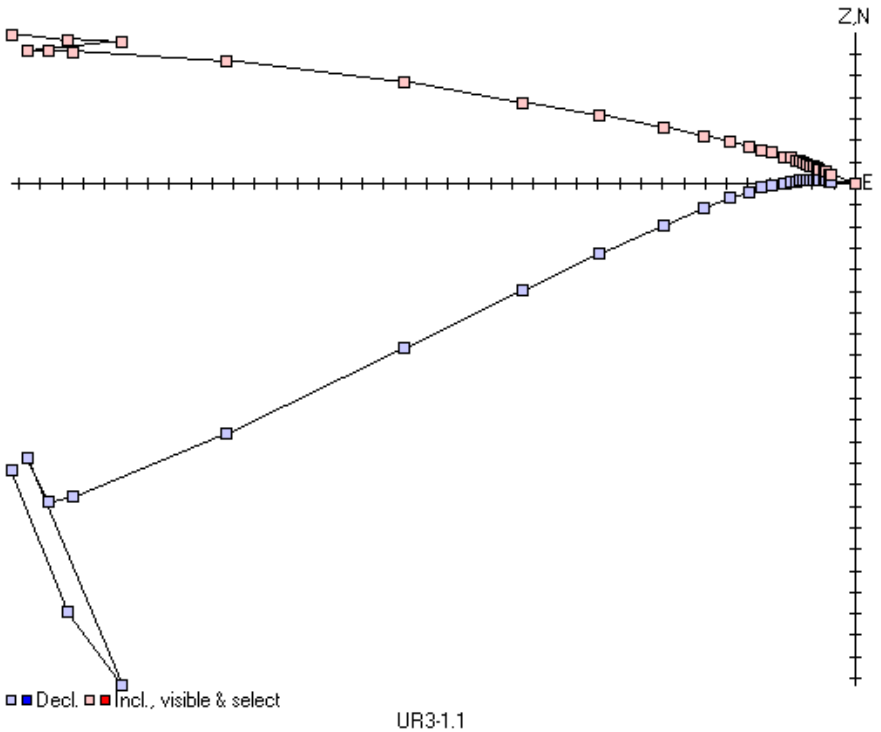

UR3-1.1
Geographic coordinates

Each Division is 10^-3

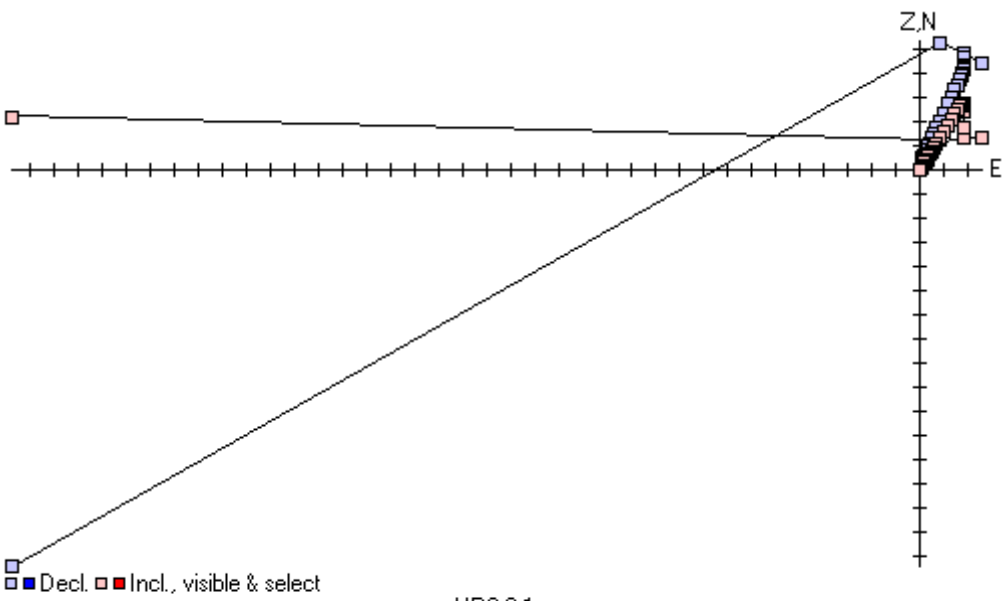

UR3-2.1
Geographic coordinates

Each Division is 10^-3

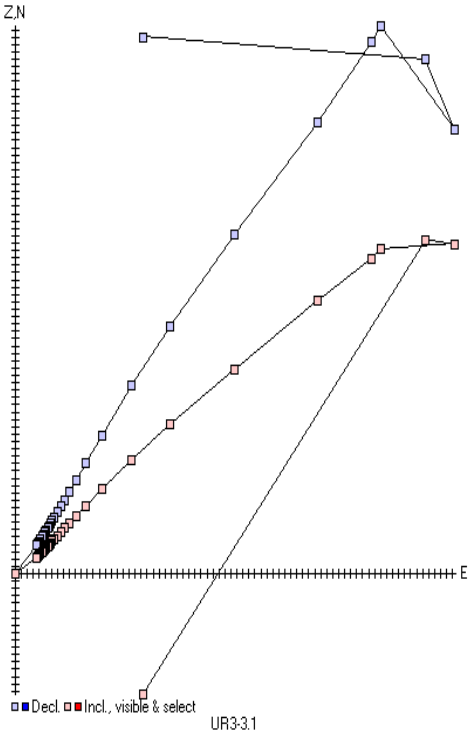

UR3-3.1

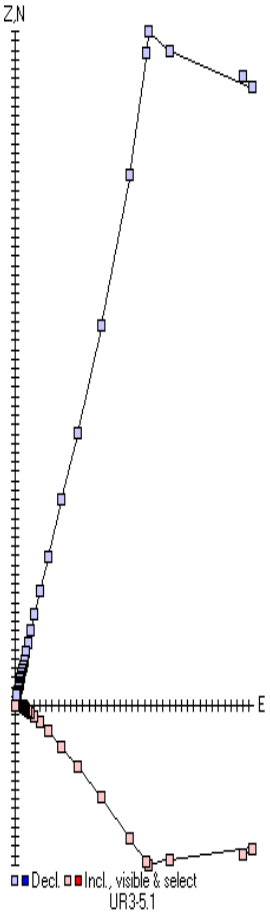

UR3-5.1

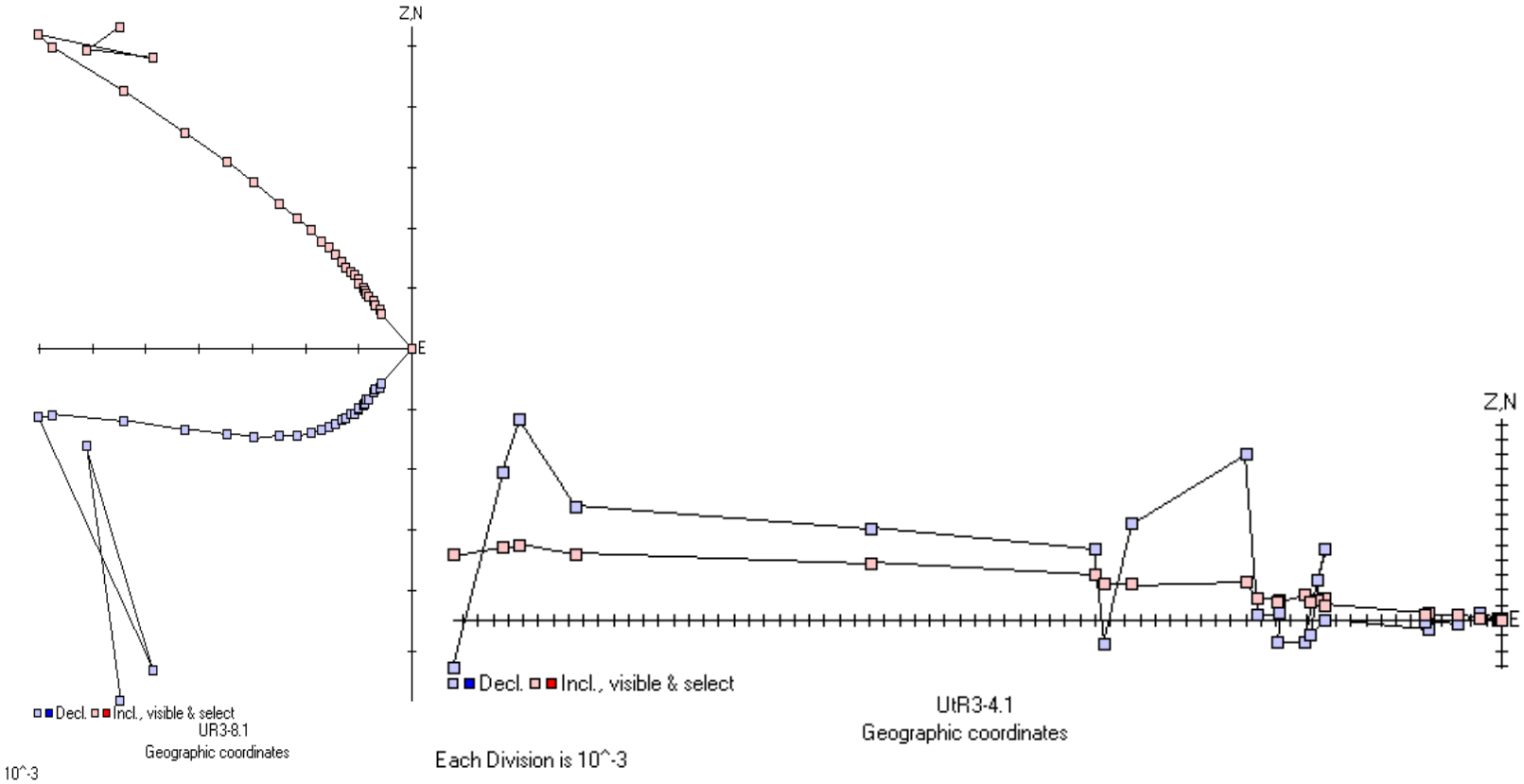
Z,N
E
Decl. Incl., visible & select
UR3-8.1
Geographic coordinates
10^-3
Z,N
E
Decl. Incl., visible & select
UtR3-4.1
Geographic coordinates
Each Division is 10^-3

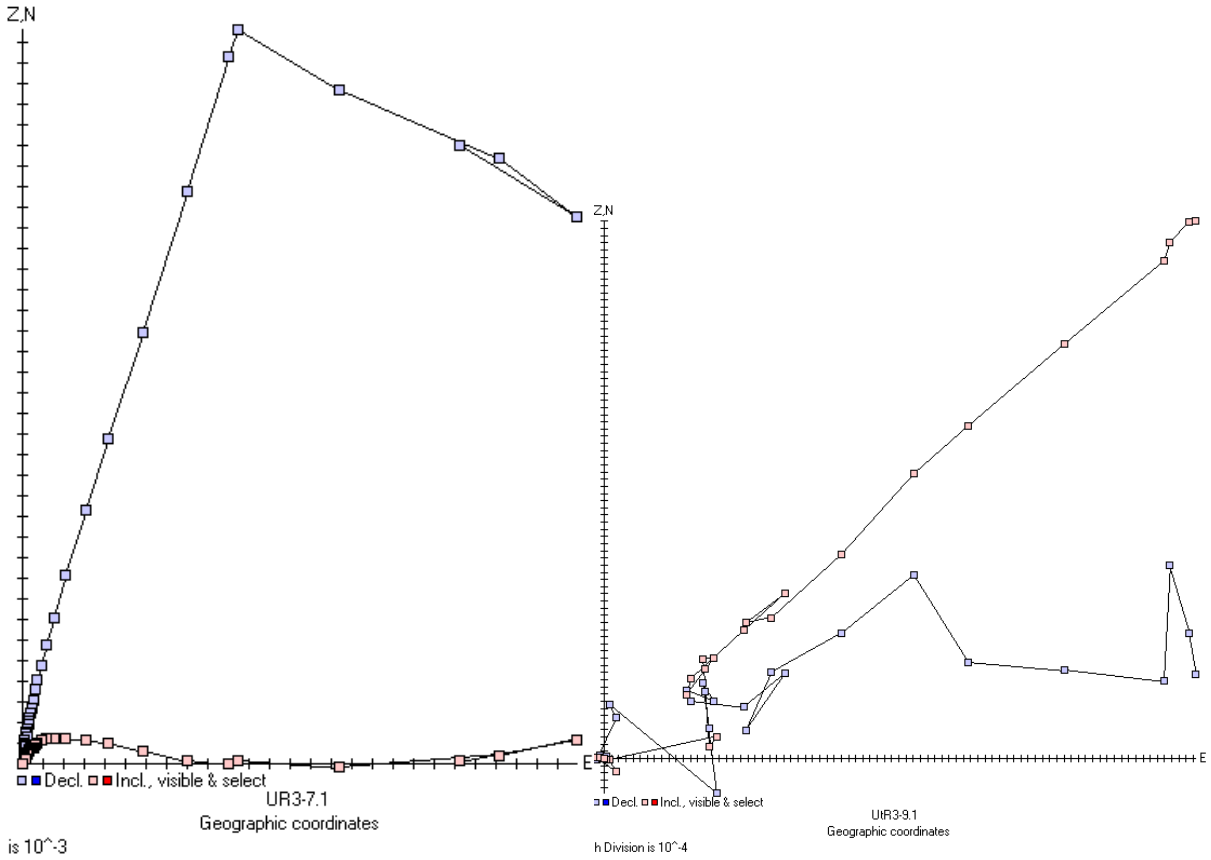
Z,N
E
Decl. Incl., visible & select
UR3-7.1
Geographic coordinates
is 10^-3
Z,N
E
Decl. Incl., visible & select
UtR3-9.1
Geographic coordinates
h Division is 10^-4

12.9 Policeman’s knob

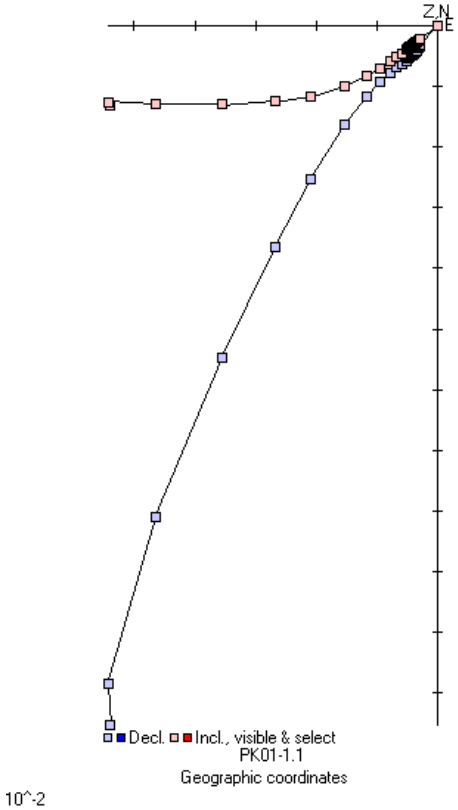

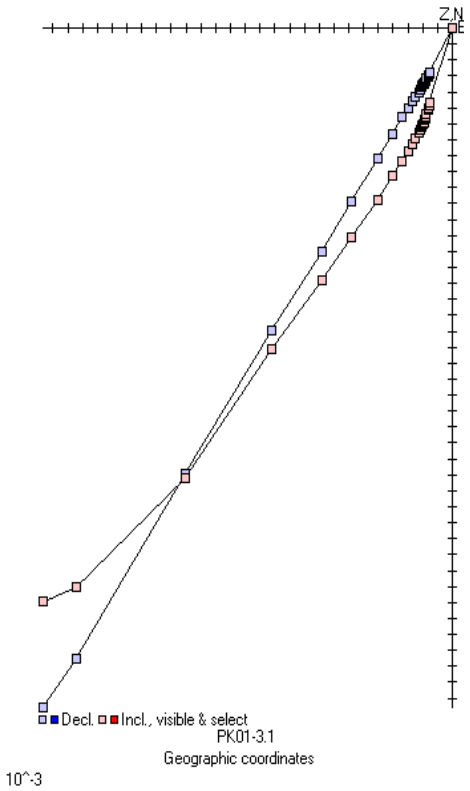

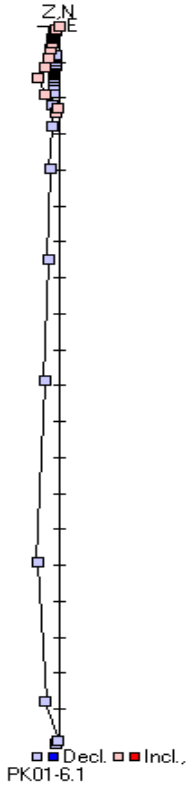

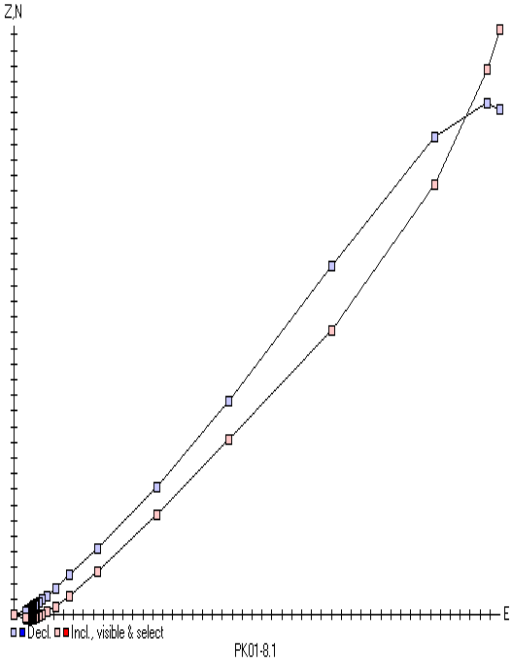

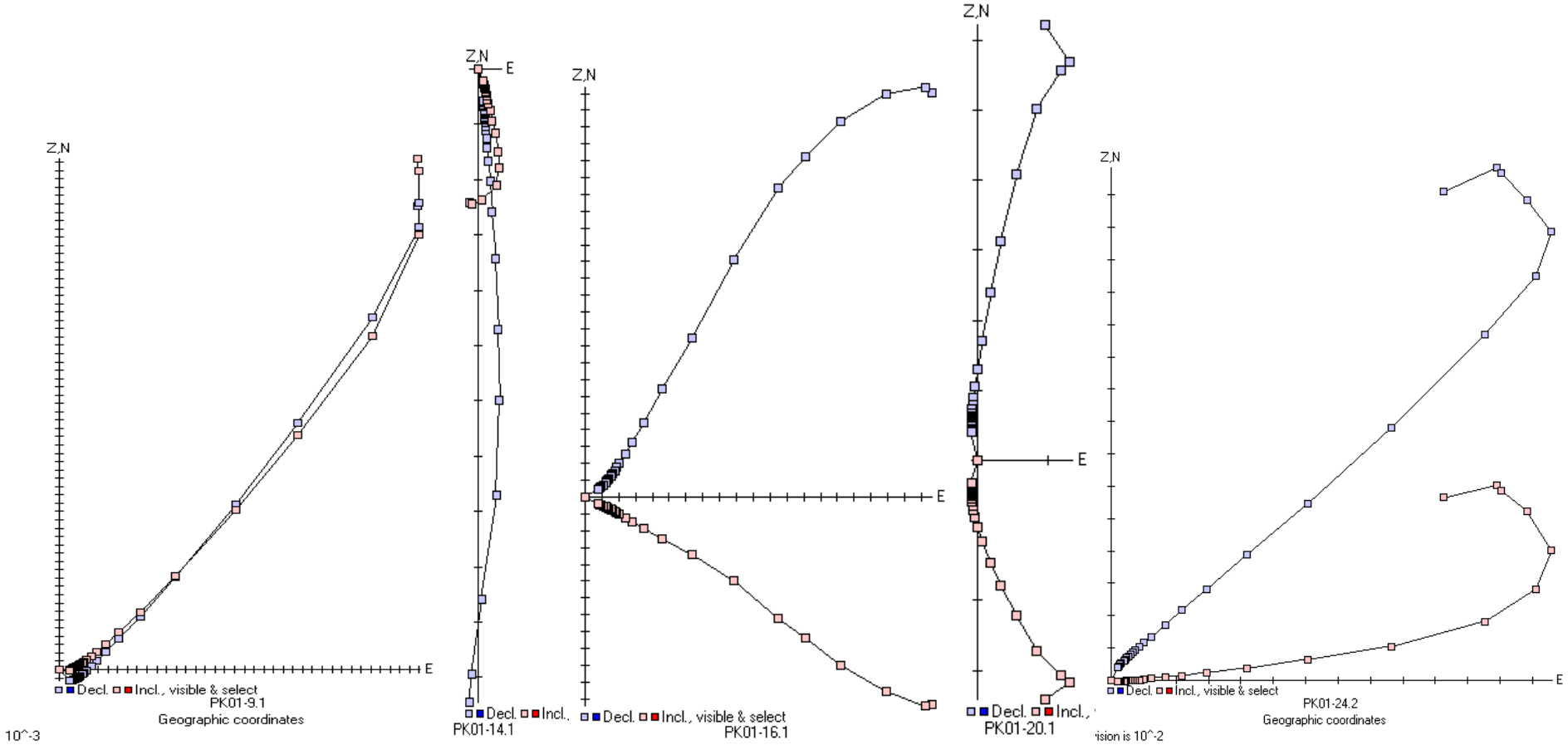
Z,N
E
Decl. Incl., visible & select
PK01-9.1
Geographic coordinates
10^-3
Z,N
E
Decl. Incl.,
PK01-14.1
Z,N
E
Decl. Incl., visible & select
PK01-16.1
Z,N
E
Decl. Incl.,
PK01-20.1
Z,N
E
Decl. Incl., visible & select
PK01-24.2
Geographic coordinates
ision is 10^-2

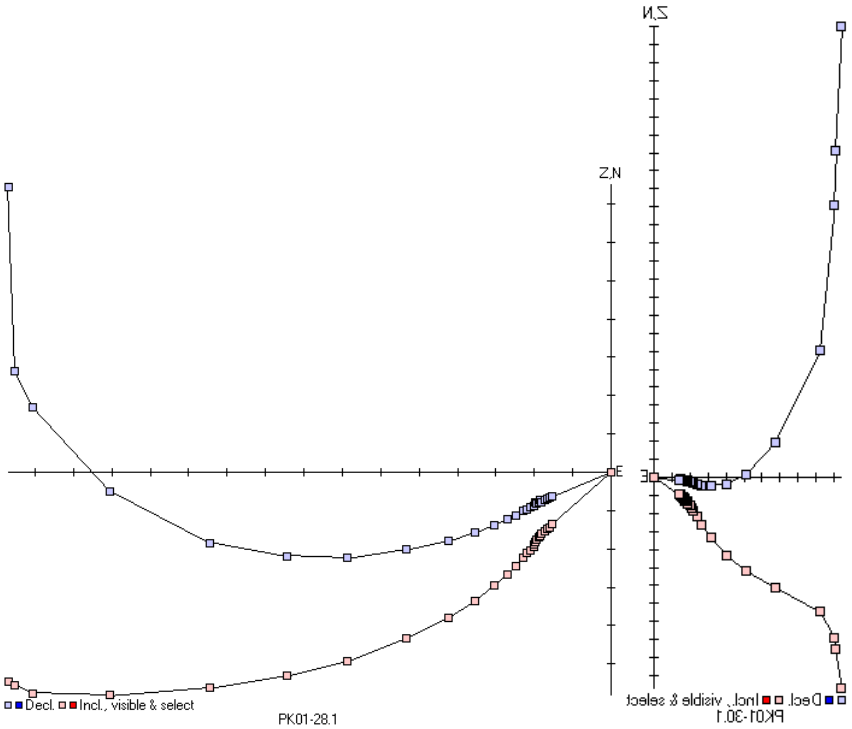
Z,N
N,S
E
Decl. Incl., visible & select
PK01-28.1
Decl. Incl., visible & select
PK01-30.1

12.10 Mitchell

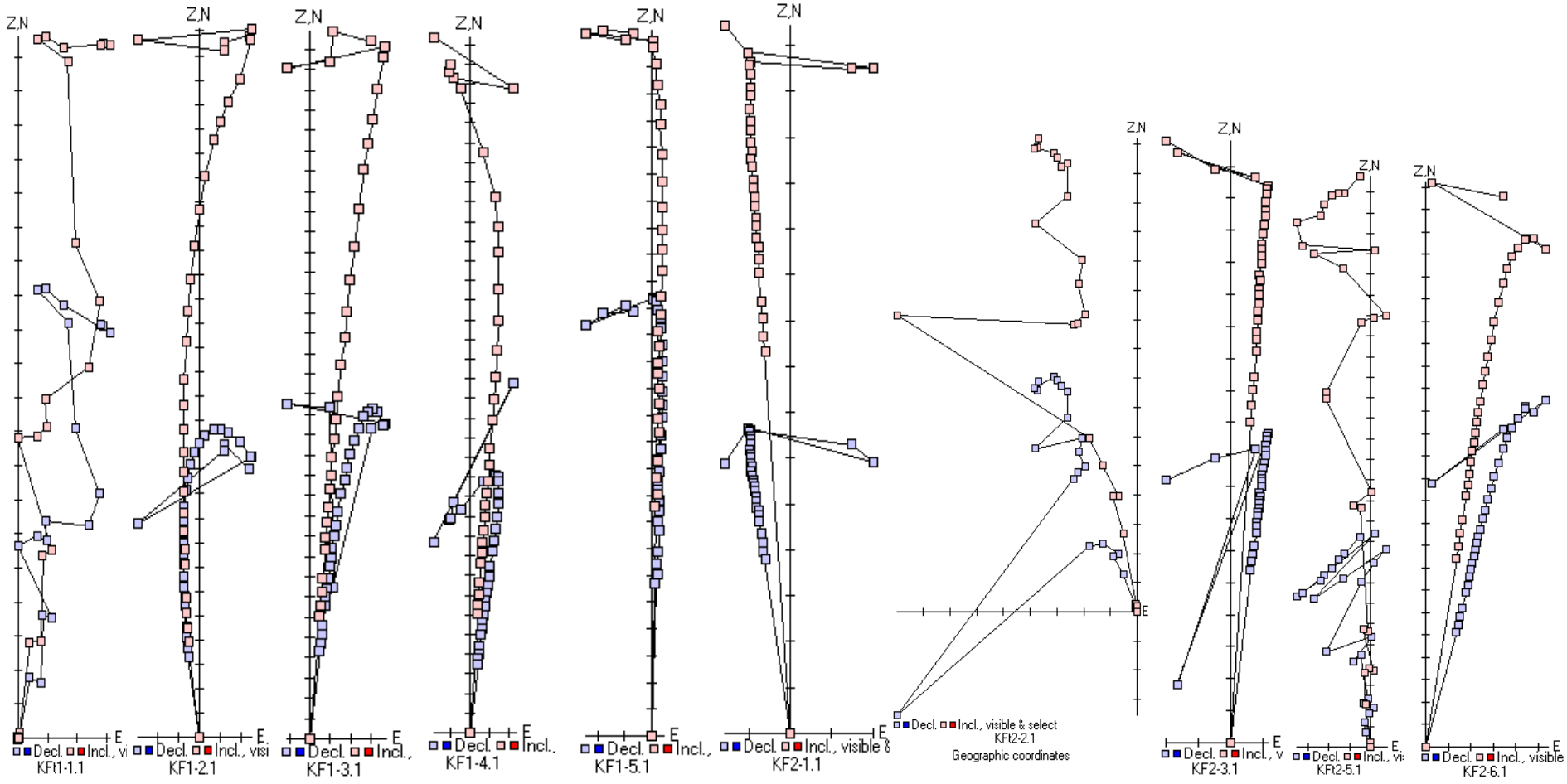

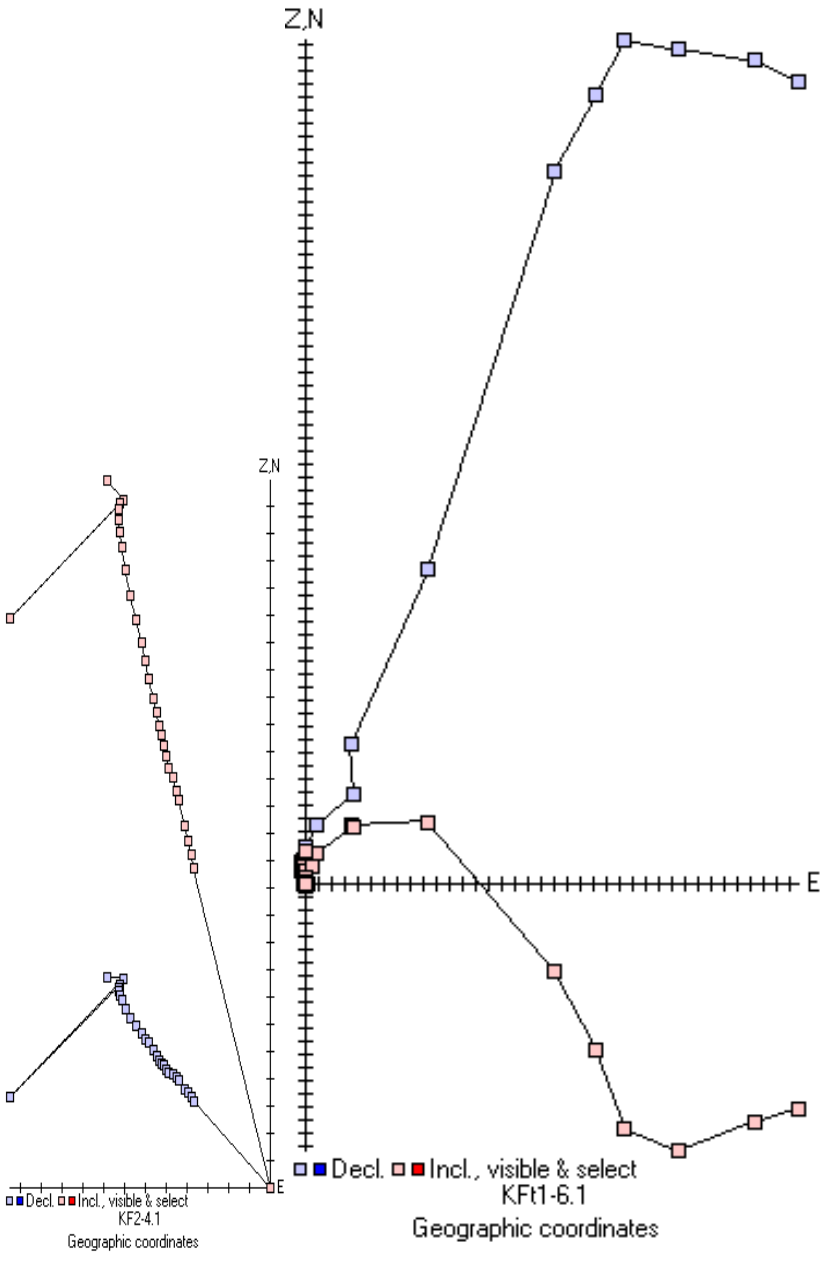
Z,N
E
Decl. Incl., visible & select
KFt1-6.1
Geographic coordinates
Z,N
E
Decl. Incl., visible & select
KF2-4.1
Geographic coordinates
10^-3